PREDICTION, CONTROL, AND REHABILITATION OF IRON ENCRUSTATION IN WATER SUPPLY BOREHOLES, WESTERN CAPE, SOUTH AFRICA: A GEOCHEMICAL APPROACH

MERIS SMITH

B. Sc. (Hons) (Geology) (Wits)

M. Sc. (Environmental Geochemistry) (UCT)

SUBMITTED IN FULFILMENT OF THE REQUIREMENTS FOR THE DEGREE OF DOCTOR OF PHILOSOPHY

in the

Department of Geological Sciences

Faculty of Science

University of Cape Town

Supervisor: Dr A. N. Roychoudhury

April 2006

Abstract

Boreholes in the Table Mountain Group (TMG) fractured and the Sandveld primary unconfined aquifers suffer from iron clogging resulting in low water yields. A comprehensive field and laboratory approach was used to search for biogeochemical controls on iron mobilisation and precipitation, and improved rehabilitation of boreholes for better management of wellfields. Lithological and redox characteristics of groundwater played the dominant role in iron mobilisation. The extent of iron mobilisation from aquifer rocks was proportional to amorphous iron oxide content which was greatest in iron-poor arenaceous rocks. In more iron rich argillaceous formations, iron release was inhibited because of clay minerals that buffer the pH (>5.7) and inhibit the catalytic leaching of iron by natural organic acids.

A flow through column was designed to determine the rate of iron oxidation and precipitation at low pO_2. The measured rate of Fe^{2+} oxidation was significantly greater than predicted by homogenous oxidation kinetics. The amount of iron retained within the column varied between 5% and 100% of the input at pH 5 and 7 respectively. Inoculation of the column with encrustation material from a Sandveld borehole resulted in growth of *Gallionella*, despite iron bacteria not being detected in the encrustations.

Precipitates observed in field samples consisted of 2-line ferrihydrite, 6-line ferrihydrite, goethite and schwertmannite. Dissolution experiments suggest that the reactivity of synthetically produced iron oxides was less than chemically precipitated iron oxides, and microbially precipitated iron oxides were the most reactive. The reactivity of oxides was a function of impurities, related to the chemistry of the groundwater.

The extent of adherence of iron precipitates was independent of the materials that are widely used for borehole/screen construction, but the construction material did play a role in the removal of the iron oxides. The rate and extent of iron dissolution in commonly used rehabilitation chemicals was related to mineral reactivity and reagent type. 0.1 M Na-dithionite buffered at pH 4.8 was found to be the most effective rehabilitation agent. Field observations suggest that physical rehabilitation methods may be as effective as chemical dissolution, but physicochemical dispersion methods used in the laboratory were not effective and were able to remove only 30% of the precipitated iron.

Extended abstract

Iron oxide precipitation within boreholes of the Klein Karoo and Atlantis Water Supply Schemes has caused economic and distribution problems for the wellfields. Severe water shortages experienced in the Western Cape has resulted in intended increased exploitation of the TMG aquifer, and necessitates an improved understanding of iron oxide encrustation in the wellfields. A comprehensive field and laboratory study was undertaken in order to identify controls on the mobilisation and precipitation of iron within an aquifer, aiming to predict sites prone to iron clogging, investigate the conditions under which iron oxidation and precipitation are promoted, and improve borehole rehabilitation procedures.

Iron encrustation occurs in both a primary unconfined aquifer (Sandveld, Atlantis) and a secondary fractured-rock aquifer (TMG, Klein Karoo). Groundwater chemistry of affected sites has variable pH (range 4.2 – 7.5), EC (27.8 – 105 mS/m) and organic carbon contents (<0.1 to 7.5 mg/L), but has in common low dissolved oxygen (DO) contents (< 5 mg/L) and detectable total iron concentrations (0.01 – 43.3 mg/L). Low pH and low DO conditions which favour iron mobilisation are likely to be associated with older waters from which DO has been removed by oxidation of organic carbon or Fe^{2+}-bearing minerals along the flow-path of groundwater. Batch dissolution tests revealed that the greatest extent of iron mobilisation (30 – 35 mmol Fe^{2+}/kg rock) is from iron-poor (< 75 mmol/kg Fe) arenaceous TMG rocks under anaerobic conditions. The amount of iron leached is proportional to the amorphous iron oxide fraction in the rock. Natural organic acids were found to catalyse iron mobilisation from arenaceous rocks at pH 5. The leaching of iron from more iron rich (344 – 854 mmol/kg) argillaceous rocks is limited to <10 mmol/kg by the presence of less amorphous iron oxide, pH buffering (pH 5.7) by clay minerals, and clay mineral inhibition of organic acid catalysis. The iron content of the water can be predicted by understanding the hydrogeology of the aquifer and by using DO measurements, but not by the total iron content of the rocks.

Iron clogging was initiated by oxidation and precipitation of the dissolved Fe^{2+} in groundwater. Iron oxidation occurred at rates well in excess of pure homogenous oxidation in a low DO (0.2 – 2.4 mg/L) laboratory column experiment. The presence of ferrihydrite within the column and increasing pH were found to greatly increase the rate of iron oxidation. The proportion of iron permanently retained within the column increased from 5% of the input at pH 5, to 100 % at pH 7. Growth of *Gallionella,* an

iron oxidizing bacteria, was observed when the flow-through column (pH 6) was inoculated with fresh iron oxide material from the Atlantis wellfield, although no *Gallionella* was observed in the field collected samples. Encrustations collected from low temperature surface environments were affected by bacteria other than *Gallionella* and by extra-cellular polymers. Heterogeneous iron oxidation and adsorption to ferrihydrite were unable to completely explain the observed iron flow-through results, and the role of microbes will require further investigation, both by sampling of deeper, less accessible parts of the well, and by further column studies. The occurrence of iron oxidation and precipitation is likely to be stratified within the borehole, with chemical precipitation in shallower more oxygenated parts of the borehole, but microbially mediated oxidation and precipitation possible in deeper, less aerobic parts of the borehole. pH was identified as the variable with the most potential for controlling iron oxidation.

In the absence of control methods, rehabilitation is required. The two methods currently used for chemical rehabilitation in South Africa, i.e., Blended Chemical Heat Treatment (BCHT) and Radical Water Treatment (RWT), have improved water yields in treated boreholes, but it is believed that some of the improvement was due to mechanical dislodging of precipitates. Problems identified with the BCHT method include contamination of the aquifer due to long residence times (> 36 hours) and density differences between the concentrated chemicals and the water; corrosion of well equipment; and the hazard to workers. Rehabilitation chemicals need to be effective at low concentration, have a high iron oxide dissolution rate, low corrosivity, high degradability, and low ecotoxicity.

Dissolution rates of natural and synthetic iron oxide minerals in a set of currently used and potential rehabilitation chemicals including acids (sulfamic acid, sulphuric acid, hydrochloric acid, phosphoric acid, acetic acid), and reductants combined with complexing agents (Na dithionite, hydroxylamine hydrochloride, ascorbic acid, ammonium oxalate) were affected both by the mineral properties and the dissolution reagent. Natural iron oxides, consisting of 2-line ferrihydrite, 6-line ferrihydrite, schwertmannite and goethite, were more reactive and less crystalline than synthetic iron oxides of the same mineralogy, and dissolved more rapidly in dissolution reagents. Reducing agents were more effective at dissolving oxides than acids at any given concentration and reductive dissolution was equally rapid for all minerals. The rate of dissolution of natural oxides in acid was proportional to structural disconformities probably caused by the incorporation of impurities from the

groundwater. The comparative dissolution rate of any specific mineral in different acids was controlled by the pH of the solution. An optimisation matrix was developed to assist wellfield managers to identify suitable rehabilitation chemicals. 0.1 M dithionite and 0.05 M ascorbic acid were optimal in terms of their effectiveness with minimal environmental impact.

The materials used in the construction of boreholes are believed to affect the degree of encrustation and the ease of rehabilitation. The adherence of natural and synthetic iron oxide minerals to smooth stainless steel surfaces was greatest near the PPZC (pristine point of zero charge; pH 5-6), whereas adherence to the rough PVC surface increased with decreasing pH below pH 7. The point of zero charge (PZC) of the substrate tended towards the PPZC of the coating material with increasing coverage of the substrate surface area, which occured more rapidly on smooth substrates with lower the surface areas. 2-line ferrihydrite was more easily dissolved from PVC than from stainless steel, but stainless steel was easier to clean by dispersive techniques. Complete removal of encrustation material from surfaces appeared to be impossible, and remaining encrustation would likely catalyse further oxidation.

Acknowledgements

The following people and organisations are thanked for their invaluable contributions to this thesis:

Dr Alakendra Roychoudhury for providing supervision and constructive criticism of drafts of this thesis.

The Thuthuka Program of the National Research Foundation and the University Research Council for providing generous funding for this project.

The following people for logistical assistance, access to sites, and great enthusiasm for the project:

Johan Uys (Klein Karoo Rural Water Supply Scheme)
Lucas Smith (DWAF) and all at Radical Waters
Rodney Bishop (City of Cape Town)
Edwin Fontein (Atlantis Water Supply Scheme)
The management of the Warmwaterberg and Calitzdorp Spas

The UCT support staff and postgraduate students for being so ready to assist with laboratory analyses:

Helen Divey and Stef (AA, BET)
Patrick Sieas (IC and general laboratory assistance)
Assoc. Prof Dave Reid and Ernest Stout (XRF)
Andreas Späth and Fayroosa Rawoot (ICP-MS)
Dr Jodie Miller (Stable isotopes)
Miranda Waldron (SEM)
Prof John Moss and Henri Chirriri (FT-IR)
Daniel Folefoc (general laboratory assistance)
David Wilson (Thin sections)
Victor Moisey, John Harrison, Ivan Wilson and Bruce Cairns (Workshop)

Outside of UCT, Dr Giovanni Hearne (WITS) conducted Mössbauer Spectroscopy analyses and Heather Sessions (Department of Marine and Coastal Management) completed all CHN analyses at no cost.

The following people assisted through useful discussions and suggestions:

Prof. Martin Fey (University of Stellenbosch)

Dr Gideon Tredoux, Lisa Cavé, Sumaya Clarke, Ross Campbell, Ashton Maherry, John Weaver, Dr Pannie Engelbrecht and Louise Fraser, all at the Environmentek, Council for Scientific and Industrial Research in Stellenbosch

Ruth Mitchell for the work she put into the initial stages of this project

Gavin Becker for providing PVC disks

Spatial Dimension for providing access to DEM data and use of excellent computing facilities

Toby Mills for being my No.1 HBRC, as well as for computer trouble-shooting, figure drafting and unfailing moral support without which I would never have made it through 5800 iron analyses.

Table of Contents

List of figures

List of tables

List of Abbreviations

AWSS	Atlantis Water Supply Scheme
BCHT	Blended Chemical Heat Treatment
CMC	Cape Metropolitan Council
CSIR	Council for Scientific and Industrial Research
DO	Dissolved oxygen
DWAF	Department of Water Affairs and Forestry
EC	Electrical conductivity
ECP	Extra cellular polymers
FH2	2-line ferrihydrite
FH6	6-line ferrihydrite
Gt	Goethite
IRB	Iron related bacteria
KKRWSS	Klein Karoo Rural Water Supply Scheme
PPZC	Pristine point of zero charge
PVC	Polyvinyl chloride
PZC	Point of zero charge
PZSE	Point of zero salt effect
RW	Radical Waters
SFB	Slime forming bacteria
SRB	Sulphate reducing bacteria
SST	Stainless steel
TMG	Table Mountain Group

1 Introduction

1.1 Motivation

South Africa is one of the twenty most water-stressed countries in the world, a fact that may considerably hamper its future development (Braune, 2000). The government is currently encouraging exploitation of groundwater in preference to already well-utilised surface water resources (Meyer, 2000). Groundwater in South Africa is found predominantly in fractured sedimentary terrains, with minor carbonate terrain and some unconsolidated porous sands in the western half of the country (Colvin *et al.*, 2004; Figure 1.1).

Two important aquifers that are currently being used for municipal water supply are the Table Mountain Group and the Sandveld Group (Figure 1.2). The extensive Table Mountain Group (TMG) fractured quartzite aquifer is one of the most promising potential sources of water in the Western and Eastern Cape Provinces. The City of Cape Town has already invested a substantial amount of money in investigating the TMG aquifer as an additional water source for Cape Town (CMC, 2001; Bishop and Killick, 2003). Many rural communities and farms currently rely on TMG groundwater, and the Eastern Cape regional government intends to increase by 80% the number of communities supplied with groundwater, mostly from the TMG (Braune, 2000). The unconsolidated to partially consolidated sands of the Tertiary Sandveld Group on the western coast of South Africa are currently exploited for domestic and industrial water supply to the town of Atlantis, which is partially reliant on this source of water (Tredoux and Cavé, 2002). Although hydrogeologically distinct, these aquifers have in common that they are seriously affected by precipitation of iron oxide minerals within the boreholes, leading to encrustation of borehole equipment, such as pumps, screens and pipes, and a dramatic decrease in water yield and quality (Engelbrecht and Jolly, 2000; Tredoux and Cavé, 2002).

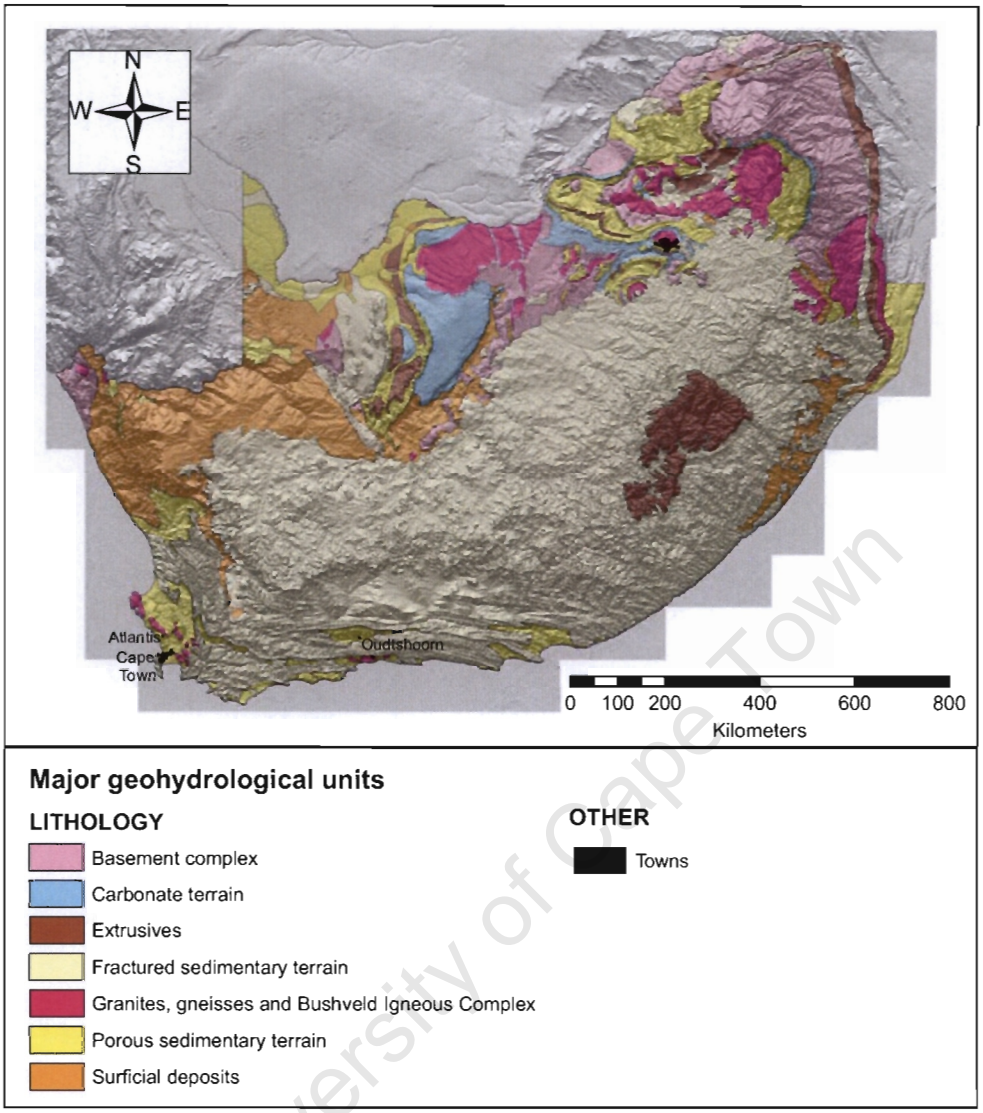

Figure 1.1. General hydrogeological terrains in South Africa (after Vegter, 1995)

The rural town of Dysselsdorp receives its water from the Klein Karoo Rural Water Supply Scheme (KKRWSS), a small-scale scheme that targets the TMG aquifer in the Klein Karoo region of the Western Cape. This scheme has been beset by problems of iron clogging almost since inception. Eight of the 17 wells have been chemically rehabilitated on more than one occasion at a cost of R70 000 (approx. US$10 000) per borehole (J. Uys, Overberg Water, pers. comm.). The Atlantis Water Supply Scheme (AWSS), which supplies water to the town of Atlantis from the Sandveld aquifer, has also been dogged by problems of iron encrustation.

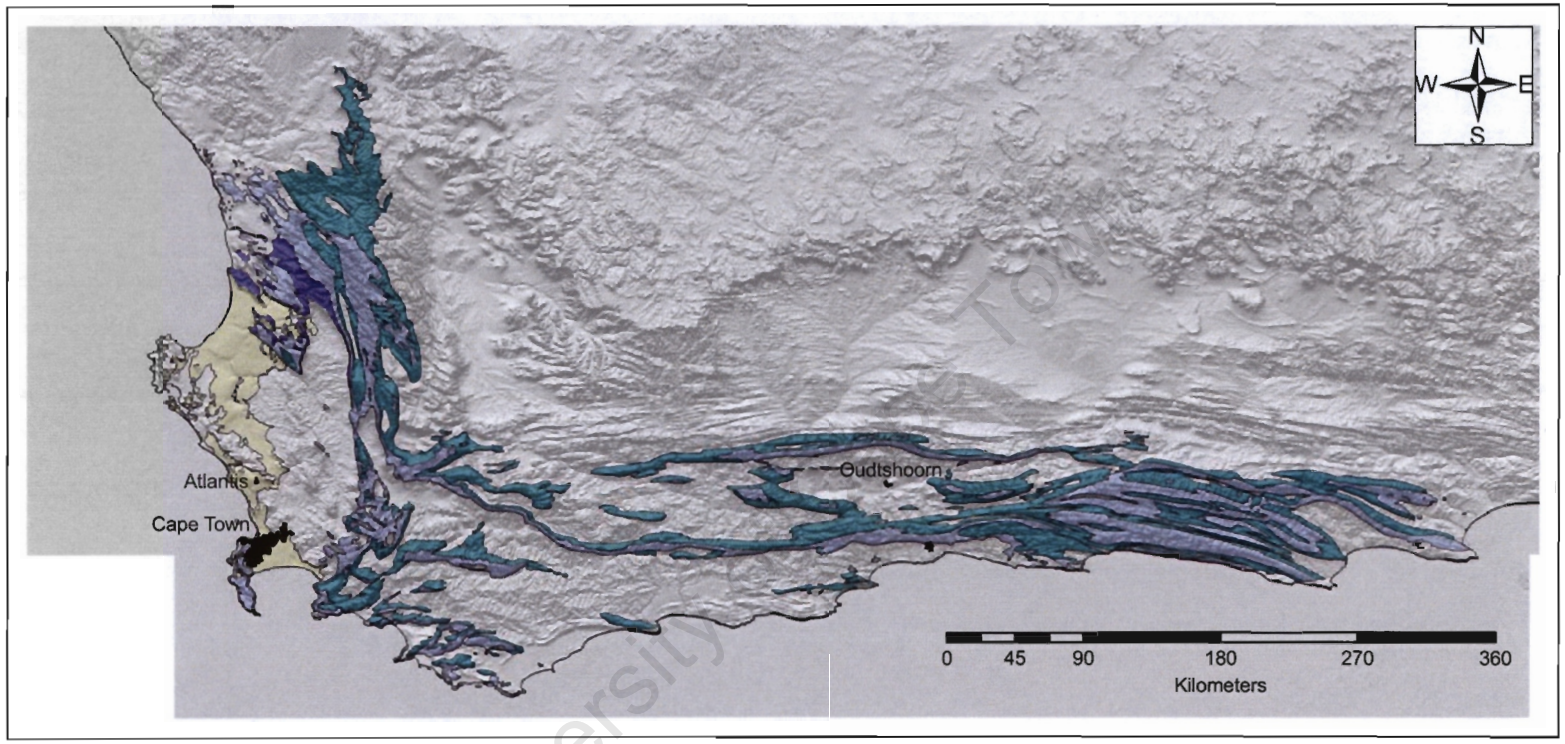

Figure 1.2. Areal extent of the Table Mountain Group and Sandveld Group Aquifers

Boreholes in the AWSS have had to be reconstructed and 28 boreholes were chemically rehabilitated in 2000 (Tredoux and Cavé, 2002; More Water cc; 2002). While these are the most prominent cases, iron-related problems appear widespread and have been encountered in boreholes drilled in the TMG at Bot River, Hermanus, Plettenberg Bay, St Francis Bay, Citrusdal and other sites in the Western and Eastern Cape (L. Cavé, CSIR, pers. comm.; Dr. C. Hartnady, Umvoto, pers. comm.; Meyer, 1999), as well as in Botswana (Riekel and Hintze, 2002). One drilling company estimates that they mechanically clean more than 60 boreholes annually that are affected by iron oxide encrustation (Myburg Drillers, pers. comm.). Iron oxide encrustation is clearly a costly problem that is poorly understood in a South African context.

Iron oxide encrustation of boreholes is a world-wide phenomenon with cases reported in the USA (Walter, 1997, Mansuy *et al.*, 1990; Smith and Tuovinen, 1985), Germany (Houben, 2003a; Kuntze, 1982), Canada (Gehrels and Alford, 1990; Rohde and Keevill, 1990; Cullimore and McCann, 1978), Scandinavia (Carlson *et al.*, 1980; Tuhela *et al.*, 1992), the UK (Tyrrel and Howsam, 1997) and Australia (McLaughlin and Knight, 1989). All these studies report iron oxide encrustation of wells combined with reduced yields and corrosion, and all suggest the influence of bacteria. The problem is often seen as a biological one rather than a chemical one, and most rehabilitation strategies focus on sterilisation of bacteria. Although iron oxide precipitates have been widely sampled and analysed, no studies have been able to elucidate the importance of bacteria in the precipitation of iron oxides in groundwater. Rehabilitation strategies targeted at bacteria have been imported to South Africa, and implemented without investigation of the local problem, and little knowledge of the degree of involvement of bacteria in the iron precipitation process in a South African context. It is imperative to study iron oxide encrustation in South Africa to gain an improved understanding of the sites likely to be prone to encrustation, the biogeochemical controls on iron oxide precipitation, mechanisms of formation of iron oxides, and optimal management and treatment strategies for iron encrusted boreholes and wellfields. In an international context, debates about the role of bacteria in

iron oxidation and the type of precipitate that forms by bacterial oxidation of iron need to be addressed.

1.2 Objectives of the study

The purpose of this research is to gain an improved understanding of the biogeochemical controls on iron oxyhydroxide precipitation within the Atlantis and Klein Karoo wellfields, with the aim of identifying methods to predict and prevent iron encrustation and rehabilitate encrusted wells.

The research objectives are to develop methods to:

- Predict likely sites of iron encrustation in the TMG by investigating the potential sources and mobility of iron.
- Prevent iron oxide encrustation by identifying the biogeochemical controls on iron behaviour at a redox interface, and by investigating the effect of materials used in borehole construction on the degree of encrustation.
- Rehabilitate encrusted boreholes by investigating the dispersability and solubility of natural iron oxide encrustations

The experimental work performed in this thesis will also address current debates on:

- The role of natural organic acids in mobilising metals, in this case iron.
- The role of microbes in iron oxidation at low partial pressures of O_2
- Chemical, mineralogical and solubility differences between synthetic, abiotically precipitated and biotically precipitated iron oxide minerals

1.3 Structure of this thesis

Chapter 1 and 2 set the scene for the thesis, describing the geohydrology of the affected aquifers, and providing a brief literature review on the biogeochemistry of iron in groundwater. More detailed literature review is included in specific chapters where required. Chapter 3 investigates the extent of iron mobilisation from rock formations of the TMG in the Kammanassie Mountains under different conditions of redox and pH, and in the presence and absence of natural organic acids, with the aim of identifying

ways to predict the likelihood that a borehole will develop iron encrustation problems. In Chapter 4, the controls on iron mobility and solubility at a redox boundary will be investigated using a flow-through column packed with aquifer sand with and without fresh iron encrustation material from an actively clogging well. The objective of this chapter will be to identify the rate and extent of iron oxidation and precipitation in a dissolved oxygen (DO) gradient. Chapter 5 discusses the crystallinity, mineralogy and chemistry of iron oxide minerals collected from encrusted boreholes, and the role of microbes and groundwater chemistry in determining oxide reactivity. The effectiveness of current rehabilitation methods is investigated in Chapters 6 and 7. These chapters describe the rate and extent of chemical dissolution of natural and synthetic iron oxide minerals, both in suspended form and attached to artificial materials as found in a borehole. The results of the research are compiled in the conclusions, Chapter 8.

1.4 The TMG aquifer in the Klein Karoo

1.4.1 The Klein Karoo Rural Water Supply Scheme (KKRWSS)

The KKRWSS supplies water to rural residents of the Klein Karoo, a semi-desert basin about 450 km east of Cape Town, and 50 - 100 km inland (Figure 1.2, 1.3). The scheme was commissioned in 1985 to improve water supply to the southern half of the Klein Karoo. 40 000 people and 180 000 livestock receive water through the KKRWSS (Weaver and Talma, 1999).

Water is obtained from 17 boreholes in the TMG aquifer: 12 in the Eastern Sector in the Kammanassie Mountains near Dysselsdorp, and 5 in the Western Sector in the Rooiberg Mountains near Calitzdorp (Jolly and Kotze, 2002; Figure 1.3-1.5). The 12 boreholes in the Eastern Sector are found in 5 different wellfields: Varkieskloof (DP10, DP29), Bokkraal (DP15, DP25 and DP28), Olifants River (alluvial – DP18), Droëkloof (DG110) and Vermaaks River (VG3, VR6, VR7, VR8 and VR11). There are just 2 wellfields in the Western Sector: Danielskraal (DL13, DL15, DL16 and DL17) and Kleinberg (KG1) (Kotze and Rosewarne, 1999). Although the scheme was designed to supply 4.7 x 10^6 m^3/a of purified water, current groundwater abstraction is just 1.0 x 10^6 m^3/a. The specific capacity of half of the boreholes dropped by 10-

30% between 1995 and 1998 (Jolly and Kotze, 2002; Jolly *et al.*, 2001). A number of factors contribute to poor wellfield performance, including limited understanding of the groundwater flow regime and water balance, poor borehole construction and pumping practices, and clogging of borehole screens with iron oxide precipitates. The expense of rehabilitation is just one consequence of deteriorating wellfield performance. High yielding trouble-free boreholes, such as those in the Vermaaks River wellfield, are increasingly relied upon to make up the deficit from poorly performing wells. The Vermaaks River boreholes are situated within the Kammanassie Mountain Nature Reserve and conservation officials are concerned that overpumping will lead to springs drying up and reduced groundwater contribution to baseflow (Yeld, 2002).

The KKRWSS was chosen as a study area for a number of reasons. Firstly, water chemistry has been monitored since 1993 and there is a considerable amount of historical data. Secondly, there have been a number of studies on the hydrogeology of the aquifer, particularly in the Kammanassie Mountains (Jolly and Kotze, 2002; Kotze, 2001; Greef and Hälbich, 2000; Kotze *et al.*, 2000; Kotze and Rosewarne, 1999; Weaver and Talma, 1999; Hälbich and Greef., 1995), and on the iron clogging problems (Jolly *et al.*, 2001; Engelbrecht and Jolly, 2000; Jolly, 2000; Miller, 2000). Finally, the boreholes are readily accessible and the officials of the supply scheme have been able to offer laboratory facilities close to the site.

1.4.2 Physiography, climate and land use

The Klein Karoo basin is about 150 km long and 20-40 km wide, and has an average altitude of approximately 500 m (Figure 1.3). The basin is enclosed by the Swartberg-Baviaanskloof mountain range to the north, which reaches a maximum altitude of 2300 m. To the east are the Kammanassie Mountains (1950 m), to the west the Rooiberg-Sandberg range (1400 m) and to the south the Outeniqua-Tsitsikamma Mountains (1800 m) (Kotze and Rosewarne, 1999). The Klein Karoo is drained by the westward-flowing Olifants River, which is dammed for irrigation and domestic water supply (Jolly and Kotze, 2002).

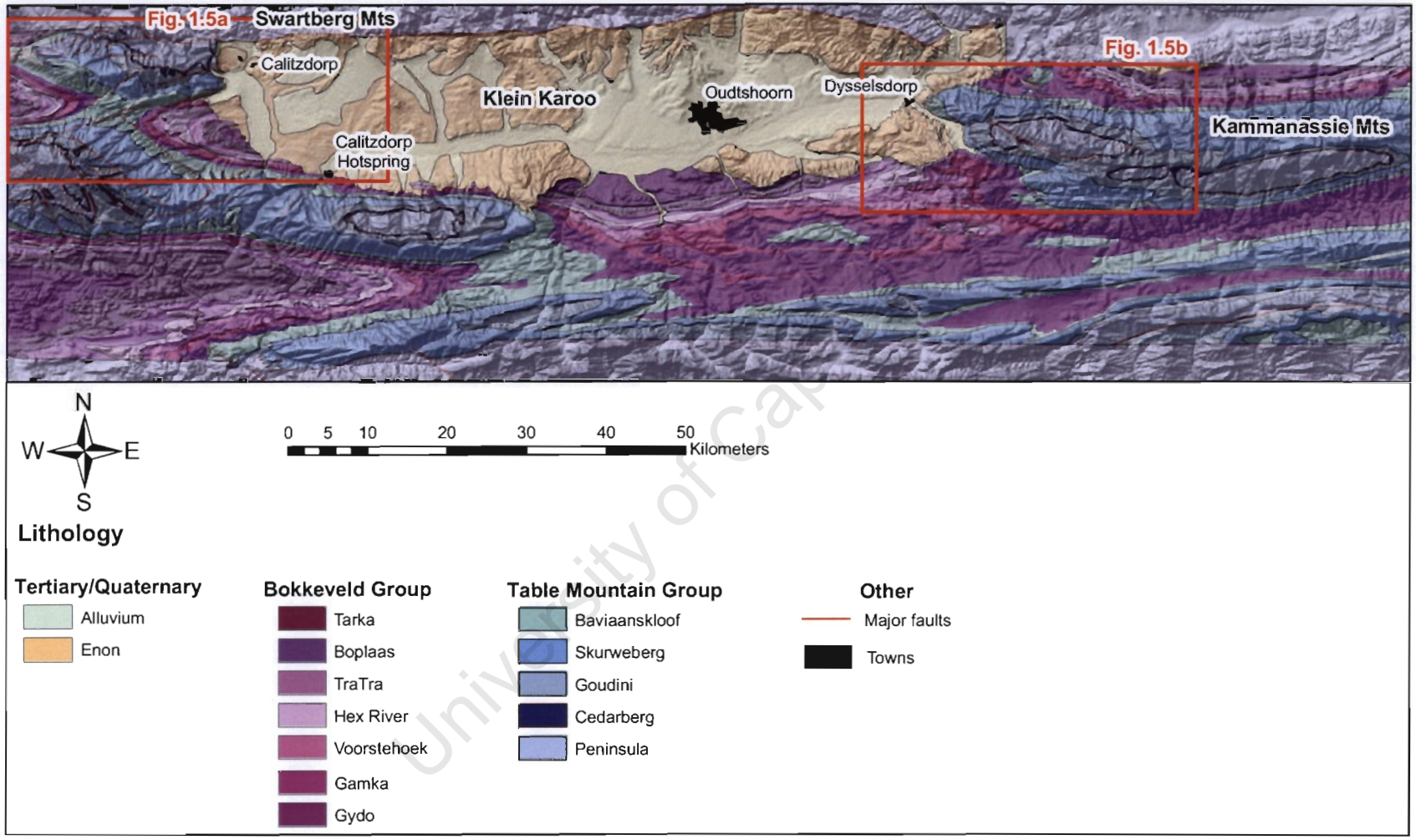

Figure 1.3. Physiography, geology and structure of the Klein Karoo region

The Klein Karoo has a semi-desert climate (Meyer, 1999). It receives rainfall all year round, in summer as thunder showers and in winter as frontal systems (Weaver and Talma, 1999). Mean annual precipitation is strongly controlled by topography and distance from the coast. Towns within the Klein Karoo valley receive on average between 199 and 329 mm/a, whereas precipitation of up to 2000 mm/a has been recorded in the mountains (Jolly and Kotze, 2002; Kotze and Rosewarne, 1999). A significant proportion of the precipitation in the mountains is snow (Kotze, 2001). Total annual evaporation is about 2000 mm/a, and is 50% higher in the summer months from October to March. Average daily temperatures in summer range from a minimum of 15°C to a maximum of 32°C, whilst in winter temperatures average between 5 and 18°C (Weaver and Talma, 1999).

Farming is the predominant industry in the Klein Karoo and the area is famous for ostriches and port. Viticulture is limited to the western end of the Klein Karoo around Calitzdorp. Most of the land and resources are owned by few people and the majority of the population is relatively poor, particularly the inhabitants of the village Dysselsdorp, who are employed as seasonal farmworkers and do not have a secure income (Tapscott and Ellis, 1999).

1.4.3 Regional geological setting

The arenaceous Table Mountain Group (TMG) is the oldest unit of the predominantly siliciclastic Cape Supergroup, which was deposited in an E-W oriented shallow inter-cratonic basin in a fairly stable continental shelf environment between 500 and 340 million years ago (de Beer, 2002 Kotze and Rosewarne, 1999). Stratigraphically above the TMG are the argillaceous Bokkeveld and arenaceous Witteberg Groups. The TMG is made up of 8 formations, although not all formations are present in all areas (Table 1.1). Between 280 and 220 million years ago, the collision of Africa and Antarctica crumpled these sedimentary rocks into an extensive orogenic belt, the Cape Fold Belt. Throughout its 900 km outcrop length along the western and southern coasts of South Africa, the Cape Supergroup is folded into coast-parallel anticlines and synclines that define the topography of the region (Figure 1.2).

Table 1.1: Lithostratigraphy of the Cape Supergroup. Highlighted formations are not present in the study area (modified from Weaver and Talma, 1999)

Age	Group	Subgroup	Formation	Thickness	Lithology
Carbon-iferous (300-360 Ma	WITTEBERG	Lake Mentz	Waaipoort	50	Shale
			Floriskraal	60	Shale/sst[a]
			Kweekvlei	130	Shale
			Witpoort	310	Sst
			Swartruggens	450	Shale/sst
		Weltevrede	Blinkberg	80	Sst
			Wagen Drift	70	Shale/sst
	BOKKEVELD	Bidouw	Karoopoort	50	Shale
			Osberg	55	Sst
			Klipbokkop	170	Shale
			Wuppertal	65	Sst
			Waboomberg	200	Shale
			Boplaas	30	Sst
			Tra-Tra	85	Shale
Devonian (360-408 Ma)		Ceres	HexRiver	100	Sst
			Voorstehoek	115	Shale
			Gamka	135	Sst
			Gydo	160	Shale
	TABLE MOUNTAIN	Nardouw	Rietvlei / Baviaanskloof		Sst
			Skurweberg	500	
Silurian (408-438 Ma)			Goudini		
			Cedarberg	120	Shale
			Pakhuis	40	Sst
Ordovician (438-500 Ma)			Peninsula	1550	Sst
			Graafwater	440	Sst/Shale
			Piekenierskloof	800	Cong[b]/sst

a. Sst = sandstone; b. Cong = conglomerate

The resistant arenaceous units of the TMG form most of the major mountain ranges in the Western Cape. Older rocks, such as the Neoproterozoic Malmesbury Group are sometimes exposed in the core of anticlines, and the younger Bokkeveld Group is often found in the core of synclines. Because these argillaceous units are less resistant to weathering than the TMG, the cores of synclines and sometimes anticlines define broad fertile valleys flanked by the resistant TMG fold limbs, although anticlines usually expose the resistant quartzites and form rugged, upstanding topography (Kotze and Rosewarne, 1999).

The Klein Karoo basin is the core of a syncline, which has been filled with Jurassic-Cretaceous sediments of the Enon Formation, and Tertiary alluvial and aeolian deposits (Kotze and Rosewarne, 1999; Figure 1.3; 1.4). The basin is flanked on the southern, eastern and western sides by anticlinal structures of predominantly TMG sediments.

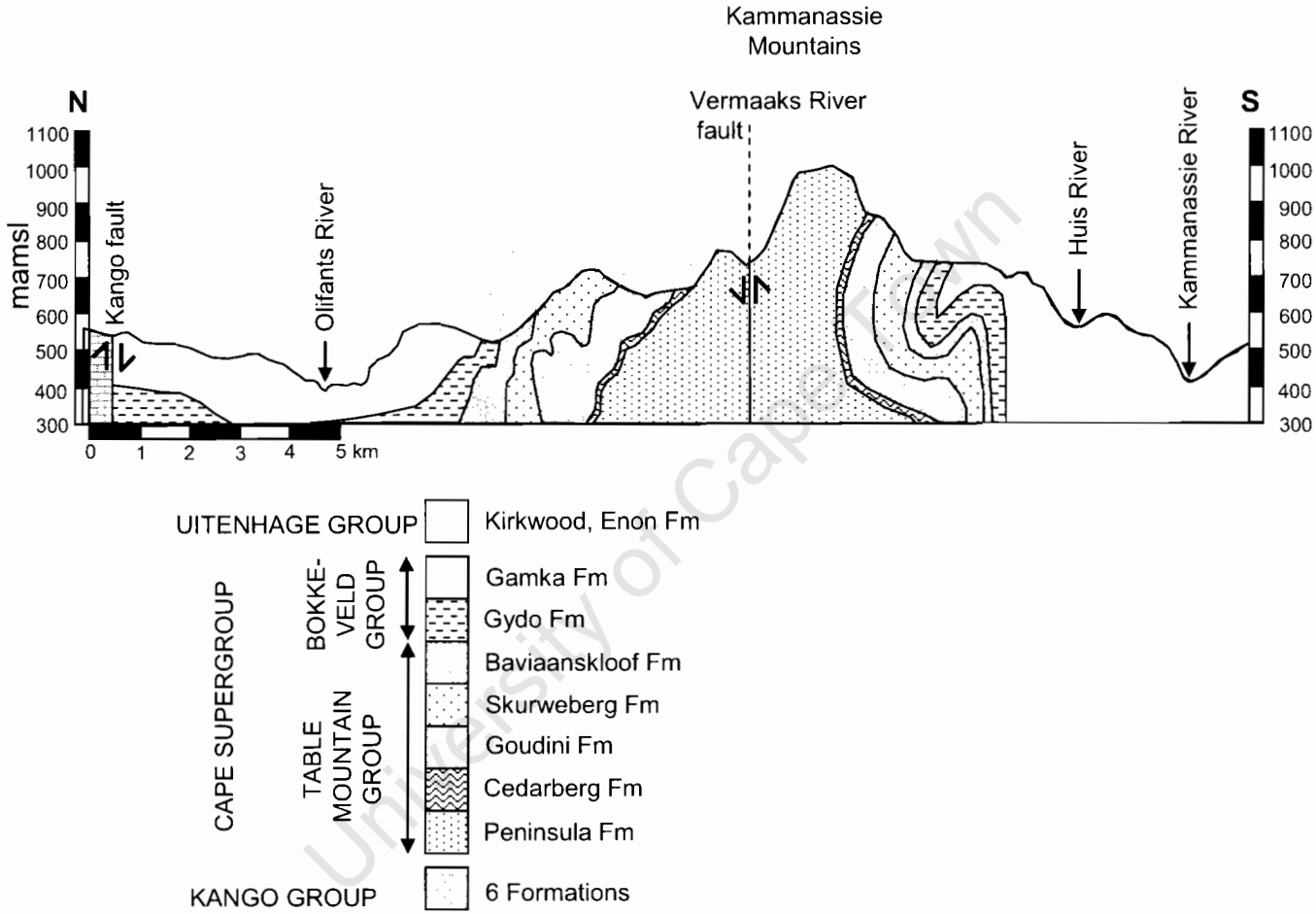

Figure 1.4. Schematic geological cross section of the Kammanassie Mountains (adapted from Weaver and Talma, 1999)

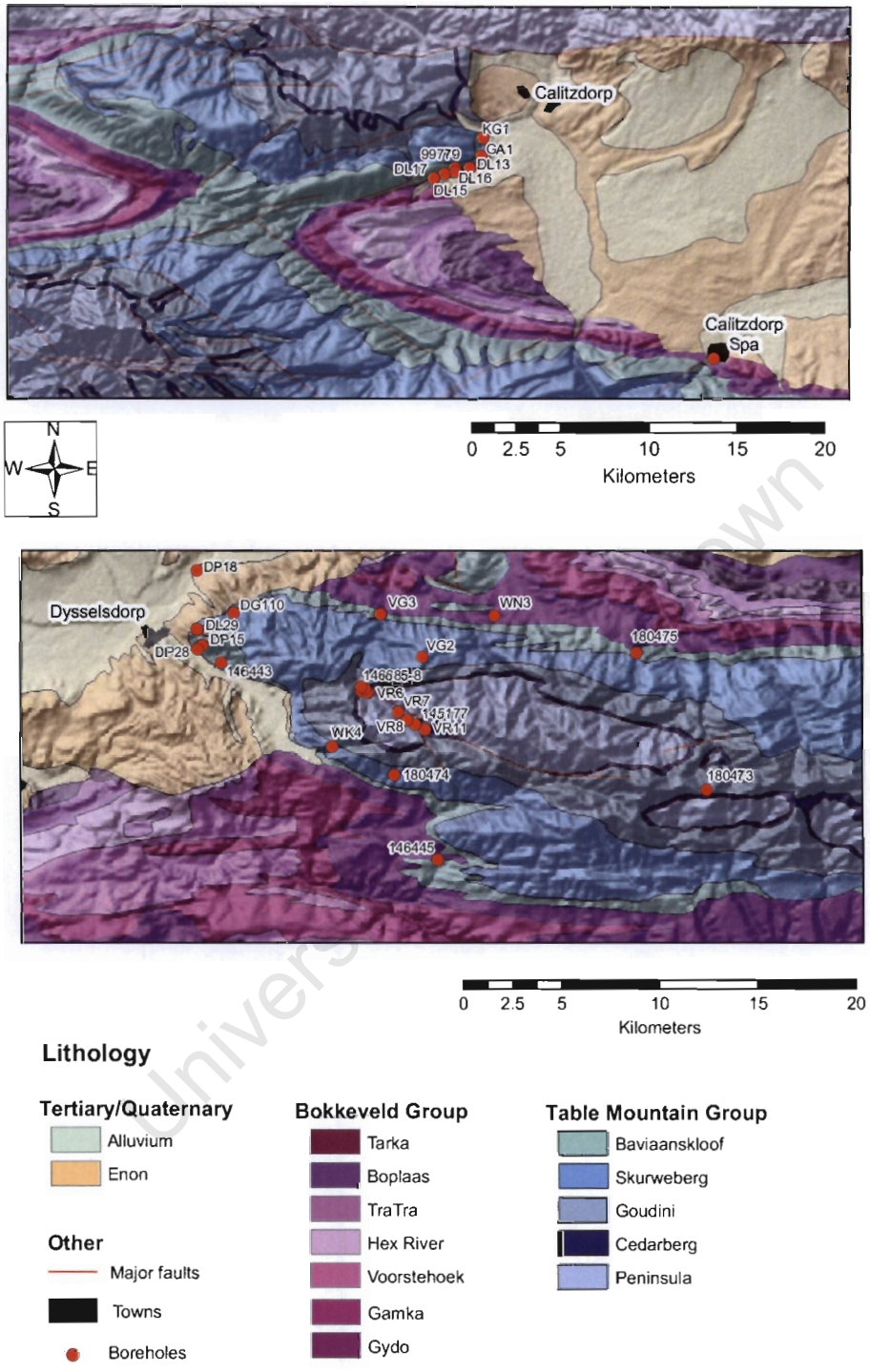

Figure 1.5. Location of boreholes at the a) Calitzdorp and b) Dysselsdorp wellfields

The northern boundary of the basin is formed by the extensive Cango thrust fault which has a throw of almost 7000 m, and exposes the Cango Supergroup basement. KKRWSS boreholes target narrow fault controlled valleys in the anticlinal structures adjacent to the Klein Karoo valley (Kotze, 2001; Figure 1.4, 1.5).

1.4.4 Lithostratigraphy

The Piekenierskloof, Graafwater and Pakhuis Formations are not present in the study area (de Beer, 2002). The basal Peninsula Formation is a white, coarse-grained quartz arenite containing scattered vein quartz pebbles and occasional conglomerate beds. The thickness of the unit is difficult to determine due to the unknown amount of thickening caused by folding and thrusting, but it is estimated at 1500 m (de Beer, 2002). An important marker bed, the Cedarberg Shale Formation (CS), unconformably overlies the Peninsula Formation, separating it from the Nardouw Subgroup. The CS coarsens upwards from a black silty shale at the base, through a brownish siltstone and into a fine sandstone at the top. Although no more than 120 m thick, the CS is continuous throughout the entire outcrop area of the TMG (de Beer, 2002).

The Nardouw Subgroup is subdivided into the Goudini, Skurweberg and Baviaanskloof Formations (Table 1.1). Resistant white to brown quartzitic sandstone with subordinate lenticular grey-black silty shale units is the predominant lithology (Malan and Theron, 1989). The Goudini Formation is finer grained and has thinner bedding than the overlying Skurweberg Formation, resulting in lower resistance to weathering. It is notable that the Goudini Formation contains higher iron and manganese contents than other formations in the TMG (Malan *et al.*, 1989). The Skurweberg Formation consists of medium-coarse grained cross-bedded quartzose sandstone with just 0-1% interbedded shale (Theron *et al.*, 1989). High feldspar contents and finer grain size characterise the Baviaanskloof Formation. The Kareedouw Member, which comprises more than half the thickness of the Baviaanskloof Formation, is a light-grey quartzitic sandstone unit (Hill, 1991; de Beer, 2002). The TMG is overlain by the Bokkeveld Group, dominated by shale rocks.

1.4.5 Structure

The hydrogeological potential of the TMG is derived almost exclusively from its structural characteristics. Two major tectonic events are primarily responsible for the current structural characteristics of the TMG. These are the Permo-Triassic Cape Orogeny, which tectonically thickened the sequence by N-S, NW-SE, NE-SW and E-W thrusts, and the Mesozoic fragmentation of southwestern Gondwana, which caused E-W oblique extensional faulting (Chevallier *et al.*, 1998). The western and southern branches of the Cape Fold Belt responded differently to the tectonic events. The study area is in the southern branch of the TMG, which has northerly-verging, often overturned first order folds sliced by thrusts and normal faults. The intensity of structural deformation increases from north to south across the Cape Fold Belt and has been divided into zones of similar deformation (Hälbich, 1983). The Kammanassie Mountains are situated within Zones 5 and 6, characterised by intense axial plane cleavage, crenulation cleavage, annealed quartz grains, and metamorphic grade ranging from epizonal to epimetamorphic greenschist facies (300-350°C; de Beer, 2002).

The intense structural deformation experienced by the TMG has destroyed the primary hydraulic conductivity of the sandstones. However, opening of fractures during structural deformation has generated secondary porosity and permeability. Well-developed breccia zones within major faults are often the best aquifers, but fold hinges with strongly developed fracture cleavage, joint sets and axial planar faults also bear water (de Beer, 2002). Rejuvenation of boundary faults suggests that the area is still under a NNE-SSW extensional regime (Hattingh and Goedhart, 1997). Structural features perpendicular to the direction of extension are more likely to be groundwater rich (Kotze, 2001). Vertical fractures are important for recharge, but groundwater movement within the aquifer is controlled by both vertical and horizontal fractures. Groundwater storage is primarily within micro-fractures rather than macro-fractures (Kotze, 2001).

1.4.6 Aquifer characteristics

1.4.6.1 Aquifer parameters

The hydraulic conductivity, transmissivity and storativity of the TMG are strongly influenced by the degree of fracturing of the rock and can vary significantly from site to site (Hartnady and Hay, 2002). Calculated hydraulic conductivity values range from 2 x 10^{-3} m/d to 2 m/d while storativity values range from 0.001 to 0.1 (Kotze and Rosewarne, 1999). Secondary porosity is estimated to be between 0.1 and 5% in the Kammanassie Mountains and is associated with weathering and microfracturing (Kotze, 2001).

Three major hydrogeological units can be defined in the Klein Karoo region – the Nardouw Aquifer, the Cedarberg Aquitard and the Peninsula Aquifer. The Peninsula Aquifer has greater permeability and higher yields than the Nardouw Aquifer due to its greater competence which results in more open fractures. The Peninsula aquifer also receives greater recharge because it forms the high lying ground where rainfall is higher. However, the Peninsula Aquifer is quite inaccessible as it forms rugged mountains, and most water supply boreholes are located in the poorer quality Nardouw aquifer (Kotze and Rosewarne, 1999). The Cedarberg Aquitard limits the movement of water between the Peninsula and the Nardouw Aquifers. Springs often develop on the Peninsula-Cedarberg contact (Kotze and Rosewarne, 1999; Weaver and Talma, 1999).

1.4.6.2 Groundwater circulation and recharge

Recharge occurs dominantly in mountainous regions where rainfall is high and thin (< 5m) coarse-grained quartz-rich soils results in high recharge potential (Weaver and Talma, 1999). Snow that falls annually on many of the mountain ranges also increases recharge potential due to the slow release by melting. Estimates of recharge to the TMG vary from 5% to as high as 50% of mean annual precipitation. The Nardouw Aquifer is recharged by direct rainfall, slow movement of water across the Cedarberg Aquitard, springs overflowing at the Peninsula-Cedarberg contact and water moving through transmissive fractures transecting the Cedarberg shale (Kotze and Rosewarne, 1999). Because the Nardouw Aquifer tends to outcrop at lower altitude than the

Peninsula Aquifer, less recharge is received into the Nardouw Aquifer (Hartnady and Hay, 2002).

Although the TMG is a secondary aquifer in which water movement is in structural features, the flow is often constrained by the stratigraphy because joints perpendicular to the stratigraphy do not cross less competent shale intercalations, for example the CS. Groundwater seeps are found above many shale intercalations within the TMG (Hälbich and Greef, 1995). Occasional disruption of the Cedarberg Shale Formation by keystone block-style faulting results in development of "TMG Window" areas, where water from the Peninsula Formation can mix with water in the Nardouw subgroup. TMG windows are favourable for groundwater exploitation (Kotze, 2001).

It has recently been shown using stable isotope studies of springs and borehole waters that the TMG is a regional aquifer, with 3 scales of flow system:

1. Local flow: Indicated by episodic seeps of water from small fractures and joints, evident only after rainy spells (Meyer, 2002)
2. Intermediate flow: Identified by lithologically controlled shallow circulating springs due to the presence of an aquitard unit such as the Cedarberg or Bokkeveld shales (Meyer, 2002). Temperatures of groundwater (22.9°C) from the KKRWSS boreholes indicate that water has circulated to a minimum depth of 330 m (Weaver and Talma, 1999), and tritium results indicate that the waters are older than 100 years (Greeff and Hälbich, 2000).
3. Regional flow: Hot springs, which are controlled by major faults and are associated with active deep fractures, bring up deep-circulating groundwater (Meyer, 2002; Kotze, 2001). Because of the folded nature of the Cape Fold Belt, the TMG sub-outcrops in the cores of synclines, beneath younger, more argillaceous, less porous material. Water that recharges in the mountains can flow down the fold limbs within the TMG to great depths, and return to the surface due to a large fault, or other such structure. Water emerging at hot springs, such as those found at Brandvlei and Calitzdorp, have been shown to originate at

high elevation and have residence times of 20 000 to 30 000 years (Harris and Diamond, 2002; Hartnady and Hay, 2002; Meyer, 2002; Kotze *et al.*, 2000; Kotze and Rosewarne, 1999; Weaver and Talma, 1999). Hot spring temperatures of on average 43°C indicate a minimum circulation depth of 1350 m (Weaver and Talma, 1999). Groundwater in the TMG aquifer of the Uitenhage Artesian Basin, approximately 300 km to the east of the Klein Karoo, has been dated at between 1500 and 28 000 years, and groundwater temperatures suggest circulation depths of 185 to 1330 m (Maclear, 2001).

1.4.7 Groundwater quality

Generally TMG water has low salinity with electrical conductivity (EC) between 4 and 100 mS/m and pH < 5.5 due to the quartzitic and poorly buffered nature of the aquifer lithologies (Weaver and Talma, 1999; Meyer, 1999). The water is considered corrosive to concrete and it requires treatment with lime before entering reticulation systems. The water is generally Na-Cl dominated due to the proximity of the mountain ranges to the coast (Hartnady and Hay, 2002; Maclear, 2001). High iron and manganese concentrations (>1 mg/L) are a common feature of TMG groundwater (Smart and Tredoux, 2002).

Although the poorly buffered nature of the groundwater and high recharge potential suggest that the aquifer should be vulnerable to pollution, the inaccessibility of outcrop provides some measure of protection to the aquifer. Groundwater contamination is occurring in areas where the TMG is close to development (Hartnady and Hay, 2002).

1.5 The Sandveld Aquifer at Atlantis

1.5.1 The Atlantis Water Supply Scheme

The AWSS has supplied high quality domestic and industrial water to the town of Atlantis, 50 km north of Cape Town, since 1976. Two wellfields, the Witzand and Silwerstroom, target quartz sands of marine and aeolian origin. The groundwater potential of the combined wellfields has been estimated at between 3.9 and 12.2 x 10^6 m^3/a (Tredoux and Cavé, 2002; Flower and

Bishop, 2003).. Natural recharge is supplemented by diversion of stormwater and treated domestic wastewater into detention and retention ponds, resulting in artificial recharge to the aquifer. Encrustation of boreholes with iron oxide material was first identified in 1991 (Tredoux and Cavé, 2002; Flower and Bishop, 2003).

1.5.2 Physiography and climate

Atlantis is located about 10 km from the western coastline of South Africa and is separated from the sea by a dunefield (Figure 1.2 & 1.6). The topography is low-lying and undulating with minimal non-perennial surface drainage. Atlantis lies approximately 100 m above sea level and the land slopes away to the sea in the west. The coastal lowlands experience a moderate Mediterranean climate. Summers, from October to March, are hot, dry and windy, the prevailing summer wind arriving from the south. On average, rainfall is 449 mm/a, mostly associated with winter frontal systems, between April and October. Atlantis was declared a deconcentration point and developed as an industrial node under the apartheid government. As a result, the town is economically poorly off, with most residents employed as labourers in the local industries (Tredoux and Cavé, 2002; Visser and Schoch, 1973).

1.5.3 Geological setting

Atlantis is located on the coastal plain between the mountains of the Cape Supergroup and the sea. The oldest rocks in the area are the Proterozoic Malmesbury Group meta-sediments, consisting of mica schists, fine-grained quartzites, and quartz schists with dolomite and limestone lenses (Hartnady *et al.*, 1974; Figure 1.6). The relatively flat topography defined by the Malmesbury rocks is broken by plutons of the 550 Ma Cape Granite Suite (Scheepers, 1995). Deeply weathered Malmesbury Group rocks are overlain by a succession of Cenozoic sediments making up the Sandveld Group. Four formations have been identified in this succession, the Elandsfontyn, Saldanha, Varswater and Bredasdorp Formations (Rogers, 1982). The stratigraphy, environment of deposition and ages of the formations are

summarised in Table 1.2. The Sandveld Group extends from Cape Town to Saldanha Bay (Meyer, 2001).

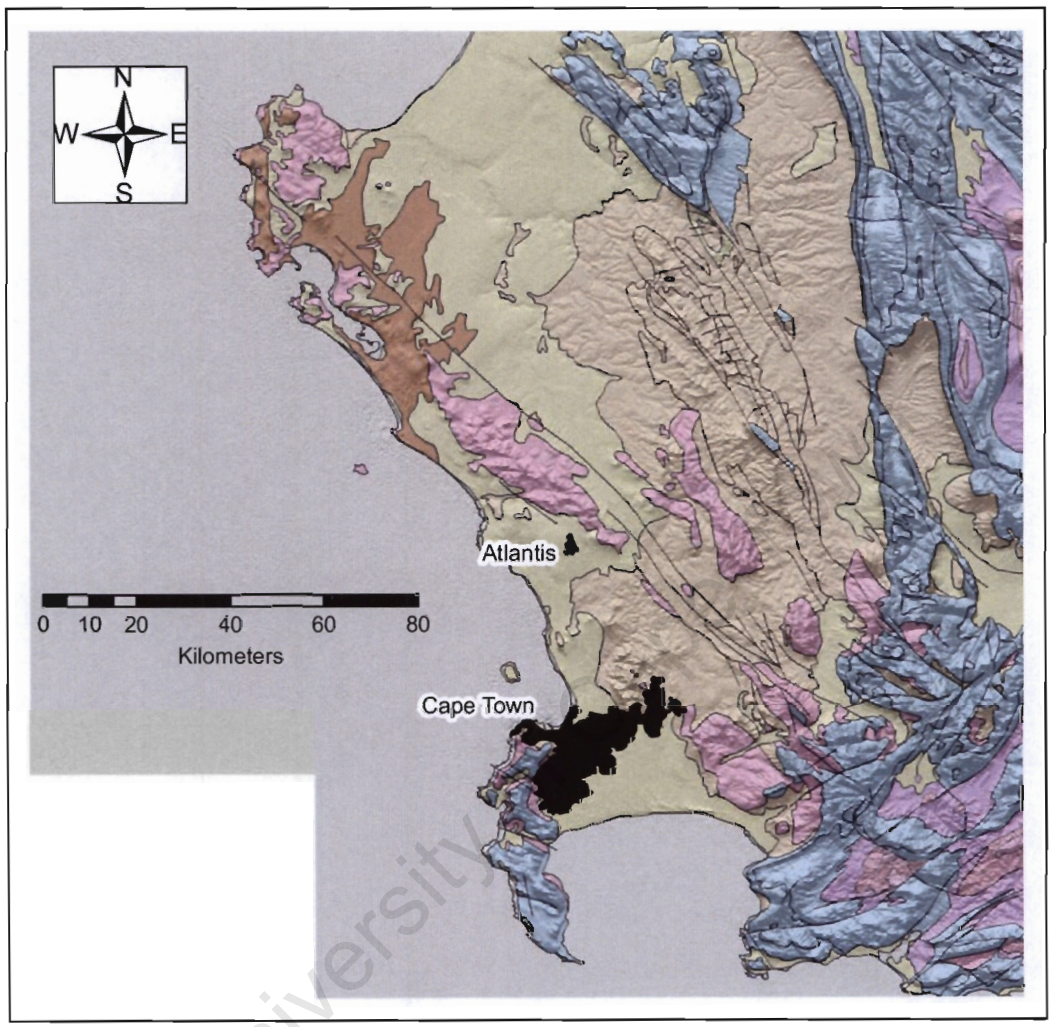

Figure 1.6. Regional geological setting of the Sandveld aquifer

Table 1.2. Stratigraphy, environment of deposition and age of formations in the Sandveld Group (Rogers, 1982; Tredoux and Cavé, 2002)

Formation	Member	Lithology	Environment of deposition	Probable age
Bredasdorp	Witzand	Calcareous qtz sand with shell fragments, calcrete	Inner shelf – beach – barrier dune – dune plume	Early Pleistocene - Holocene
	Mamre	Uniform windblown sands with fine organic matter		
	Springfontein	Peaty sand at base, mostly well sorted fg-cg qtz sand		
Varswater	Duynefontein	Slightly muddy well sorted qtz sands with no shelly material	Inner shelf and estuary	Early Pliocene
	Silwerstroom	Poorly sorted qtz sands, shell and phosphate-rich.		
Saldanha			Beach and lagoon	Late Miocene
Elands-fontein			Meandering fluviatile environment in tropical to subtropical climate	Miocene

1.5.4 Geohydrology

The Sandveld Group aquifer is divided into four spatially separate hydrogeological units: the Cape Flats Unit, the Silwerstroom-Witzand Unit, the Grootwater Unit and the Berg River Unit (Meyer, 2001). The AWSS exploits the Silwerstroom-Witzand unit where water is stored in the Varswater and Bredasdorp Formations, which form a primary unconfined aquifer. The maximum saturated thickness of the aquifer at Atlantis is 35 m and the water table is 4 to 7 m below ground level (Colvin *et al.*, 2004). Bedrock highs further compartmentalise the Silwerstroom-Witzand unit, although flow between adjacent compartments can occur when the water table rises above bedrock highs. Groundwater flows from W to SW, discharging to the sea (Tredoux and Cavé, 2002). Recharge to the aquifer is of the order of 15-35% and transmissivity measurements have obtained variable results of between 50 and 1300 m^2/day due to aquifer heterogeneity (Meyer, 2001).

1.5.5 Groundwater Quality

The chemistry of water in the aquifer is dependent on the lithology in which the water is held. Water in the calcareous formations has a Ca-HCO_3 character whereas water in quartz sands is Na-Cl dominated. Water is fresh

to brackish, with greatest salinity found where the aquifer is thinnest i.e. adjacent to bedrock highs, and where the aquifer sands pinch out laterally. Treatment of hardness is required before the water can be used for domestic supply (Tredoux and Cavé, 2002). The groundwater has a significant organic carbon content (0.6 – 7.5 mg/L) due to the presence of peat layers and a measurable iron concentration (0.05-0.2 mg/L; Flower and Bishop, 2003).

Due to its unconfined nature, limited buffering capacity and rapid infiltration and flow rates, the aquifer is highly susceptible to surface pollution from the nearby urban and industrial sites. In addition, proximity of the aquifer to the sea renders it prone to saline intrusion (Tredoux and Cavé, 2002).

1.6 Summary

Iron oxide encrustation of two important aquifers in South Africa is a costly problem which threatens to become more prevalent as the country moves towards greater use of groundwater. Few studies have been done on iron oxide encrustation in South Africa and overseas solutions have been implemented without proper investigation of the local problem. Currently just one method is used for treatment of boreholes in the two aquifers despite the significant differences in their geohydrology. The Table Mountain Group is a vast fractured rock aquifer which is still relatively unexploited and poorly understood, while the Atlantis aquifer is a much smaller primary unconfined aquifer which has been more thoroughly investigated. This thesis aims to explore iron encrustation from a water supply point of view, looking at practical aspects of avoiding and managing the problem, partly to provide wellfield managers with a tool to go forward with, and partly to dispel existing myths of iron oxide encrustation. In particular, the following points will be considered:

- potential sources and mobility of iron in the TMG in order to predict likely occurrences of iron encrustation
- the biogeochemical controls on iron behaviour at a redox interface to identify ways to prevent encrustation
- the similarities and differences between iron encrustations at different sites to determine if the current uniform treatment approach is valid

- the advantages/disadvantages of using different materials in the construction of boreholes in terms of rate of encrustation and ease of cleaning

2 The Biogeochemistry of Iron in Aquifers: A Review

2.1 Introduction

Iron is ubiquitous in the environment, and for the most part does not cause serious problems. However, the concentration of large amounts of iron in a borehole can lead to encrustation of the borehole with iron oxide minerals, with associated reduced yields and water quality. The understanding of iron biogeochemistry is fundamental to understanding the processes involved in iron encrustation of boreholes. This review will look at the aqueous geochemistry of iron and the role of microbes in iron cycling within groundwater, focussing particularly on iron behaviour at a redox front in a borehole, and the role of bacteria in clogging of boreholes. Currently employed management and rehabilitation procedures will also be discussed.

2.2 Aqueous geochemistry of iron

2.2.1 Iron solubility

Iron is a transition metal with a molecular mass of 55.847. Iron can occur in three oxidation states, Fe^{o}, Fe^{2+} and Fe^{3+}, but only Fe^{2+} and Fe^{3+} are stable at earth surface conditions. Fe^{2+} is soluble under reducing conditions, and oxidizes to Fe^{3+} in the presence of an oxidant, while Fe^{3+} is soluble only at low pH and becomes insoluble with increasing pH, although solubility can increase again at high pH. Iron is therefore found in solution in reducing conditions or in water of pH < 3, and occurs in the solid phase in all other environments. Iron solubility is affected by pH dependent hydrolysis and oxidation-reduction reactions (Schwertmann and Taylor, 1992). Hydrolysis is the reaction of iron with water to form pH-dependent hydroxyl complexes (Drever, 1997):

$$Fe^{3+} + H_2O \leftrightarrow Fe(OH)^{2+} + H^+ \qquad K_1 = 10^{-2.2} \qquad (2.1)$$

$$Fe(OH)^{2-} + H_2O \leftrightarrow Fe(OH)_2^{-} + H^+ \qquad K_2 = 10^{-3.5} \qquad (2.2)$$

$$Fe(OH)_2^{+} + H_2O \leftrightarrow Fe(OH)_3 + H^+ \qquad K_3 = 10^{0.8} \qquad (2.3)$$

$$Fe(OH)_3 + H_2O \leftrightarrow Fe(OH)_4^{-} + H^+ \qquad K_4 = 10^{-16.7} \qquad (2.4)$$

$$Fe^{2+} + H_2O \leftrightarrow FeOH^+ + H^+ \qquad K = 10^{-9.5} \qquad (2.5)$$

Hydrolysis of iron occurs because Fe^{3+} has a strong affinity for the -OH ligand. The formation of the negatively charged hydroxyl complex $Fe(OH)_4^-$ increases the solubility of iron at high pH, while the formation and precipitation of $Fe(OH)_3$ causes insolubility of Fe^{3+} at neutral pH. The hydrolysis reaction is difficult to reverse and pH < 2 is required to dissolve precipitated $Fe(OH)_3$ (Drever, 1997; Appelo and Postma, 1996).

Oxidation and reduction reactions also affect the solubility and mobility of iron. Reductive dissolution of iron oxides is more effective than reverse hydrolysis at remobilising iron (Schwertmann and Taylor, 1992):

$$Fe(OH)_3 + e^- + 3H^+ = Fe^{2+} + 3H_2O \qquad K_{eq} = 10^{17.9} \qquad (2.6)$$

The stability boundaries of iron species and minerals under variable pe and pH conditions are illustrated in Figure 2.1 (Faure, 1992; Appelo and Postma, 1996). Iron oxidation is a kinetically controlled reaction. The rate of iron oxidation is second order with respect to pH and first order with respect to dissolved oxygen concentration above pH 5 (Davison and Seed, 1983):

$$-\frac{d[Fe^{2+}]}{dt} = (k \cdot [Fe^{2+}] \cdot [OH^-]^2 \cdot pO_2) \qquad (2.7)$$

where k is the rate constant $(8.0(\pm 2.5) \cdot 10^{13}$ $min^{-1}.atm^{-1}.M^{-2})$, square brackets indicate molar concentrations and pO_2 is the partial pressure of dissolved oxygen in atmospheres. The pH-dependence of the iron oxidation rate becomes first order with respect to Fe^{2+} below pH 5, and is pH-independent below pH 3. The rate of oxidation of iron through the full pH range is (Stumm and Sulzberger, 1992):

$$-\frac{d[Fe^{2+}]}{dt} = (k_0 \cdot [Fe^{2+}] + k_1 \cdot [Fe(OH)^+] + k_2 \cdot [Fe(OH)_2] \cdot pO_2) \qquad (2.8)$$

where k_0 is the rate constant at pH < 3; k_1 for 3 < pH < 5, and k_2 for pH > 5. Substances which form stable complexes with ferric iron, e.g., fluoride, phosphate, colloidal iron oxide and natural organic matter, tend to increase the rate of iron oxidation, while elements which complex ferrous iron, such as sulphate, chloride, nitrate and bromide, result in a decrease in the rate of iron oxidation. Temperature has little effect on the rate of iron oxidation between

5° and 35°C (Walter, 1997). Under conditions of high pH and dissolved oxygen concentration, the half-life of Fe^{2+} can be as little as 2 minutes, whereas in low pH environments with no dissolved oxygen, the half-life of Fe^{2+} can be up to 2 700 days (Walter, 1997).

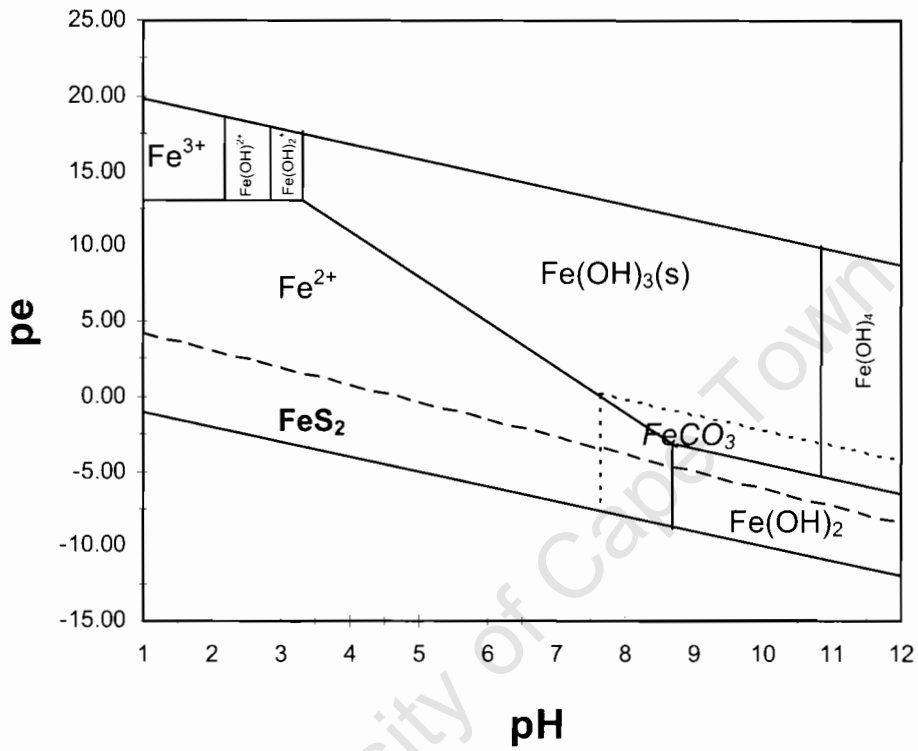

Figure 2.1. pe-pH stability diagram of iron species in equilibrium with $Fe(OH)_3(s)$ in water at a temperature of 25°C, assuming Fe^T concentration of 10^{-5}M. Dotted lines and italics delimit the siderite stability field ($pCO_2 = 10^{-2}$) and dashed line and bold represents the pyrite stability field ($SO_4^{2-} = 10^{-4}$ M).

2.2.2 Cycling of Fe within aquifers

Iron is cycled between sources and sinks within an aquifer as pH and redox conditions change. Iron is sourced from minerals within the aquifer, and is mobilised under reducing conditions or at low pH. The introduction of oxygen or an increase in pH in the system can cause iron to precipitate within the aquifer.

Source minerals of iron in groundwater depend on the aquifer rock-type. In crystalline rocks, most iron is present as Fe^{2+} in mafic minerals, such as amphiboles, pyroxenes, olivine, and biotite. Mafic minerals are not in

equilibrium with earth surface conditions, and weather incongruently to form clay minerals such as kaolinite. During the weathering reaction, Fe^{2+} present in the mafic mineral is oxidised and precipitates as an iron hydroxide mineral (Appelo and Postma, 1996; Schwertmann and Taylor, 1992):

$$2K(Mg_2Fe)(AlSi_3)O_{10}(OH)_2 \text{ (biotite)} + 10H^+ + 0.5O_2 + 7H_2O$$
$$= Al_2Si_2O_5(OH)_4 \text{ (kaolinite)} + 2K^+ + 4Mg^{2+} + 2Fe(OH)_3 + 4H_4SiO \qquad (2.9)$$

Iron can be present in sedimentary rocks as Fe^{2+}-bearing oxides (magnetite, ilmenite), sulphides (pyrite), and carbonates (siderite), or Fe^{3+}-bearing oxides (e.g. haematite, goethite, ferrihydrite, lepidocrocite), depending on the redox environment of deposition of the sedimentary rock (Faure, 1992). Iron can also be a constituent of clay minerals. Chlorite and glauconite contain iron as part of their structural formula, but iron can be substituted into clay mineral lattices such as smectite and illite. Iron in silicate minerals has been found in some cases to be a more important source of iron than iron oxide minerals such as ilmenite and magnetite (Hansel *et al.*, 2003).

Iron sinks are generally more important for controlling iron concentrations in groundwater than the source minerals of iron. Under oxidizing conditions, Fe^{2+} oxidised during weathering of unstable silicate minerals precipitates as amorphous iron hydroxide, which recrystallizes and 'ages' to more stable phases with time. The order of increasing stability of iron oxides is from amorphous (ferrihydrite) to lepidocrocite, maghemite, goethite and finally haematite. Groundwater is often found to be in equilibrium with an iron oxide phase. In a reducing aquifer, Fe^{2+} containing minerals such as siderite and iron sulphides control iron solubility. Siderite is likely to only be important where sulphate concentrations are low. In aquifers with available organic carbon and sulphate, sulphate reduction can occur, resulting initially in formation of H_2S and later in precipitation of iron sulphide minerals, such as marcasite or pyrite (Appelo and Postma, 1996).

The cycling of iron between sources and sinks in an aquifer is often controlled by the degree of oxygenation of groundwater. Recharge to the aquifer is

oxygenated, but oxidation of organic carbon within the water and organic carbon encountered along the flow path consume the oxygen in the water (Walter, 1997; Figure 2.2). Some oxygen is also consumed in weathering reactions (White and Yee, 1985). Once oxygen is depleted, organic carbon oxidation reactions require alternate electron acceptors. Electron acceptors are utilised in order of decreasing energy released, i.e. NO_3, MnO_2, $Fe(OH)_3$, SO_4, CO_2 and finally H_2. Reduction of iron in Fe^{3+}-bearing minerals to release Fe^{2+} into groundwater is commonly coupled with oxidation of dissolved organic carbon (DOC) by bacteria, in a process known as dissimilatory iron-reduction (Hansel *et al.*, 2003; Kostka and Nealson, 1995; Schwertmann and Taylor, 1992):

$$24FeOOH + C_6H_{12}O_6 + 42H^+ \rightarrow 24Fe^{2+} + 6HCO_3^- + 36H_2O \quad (2.10)$$

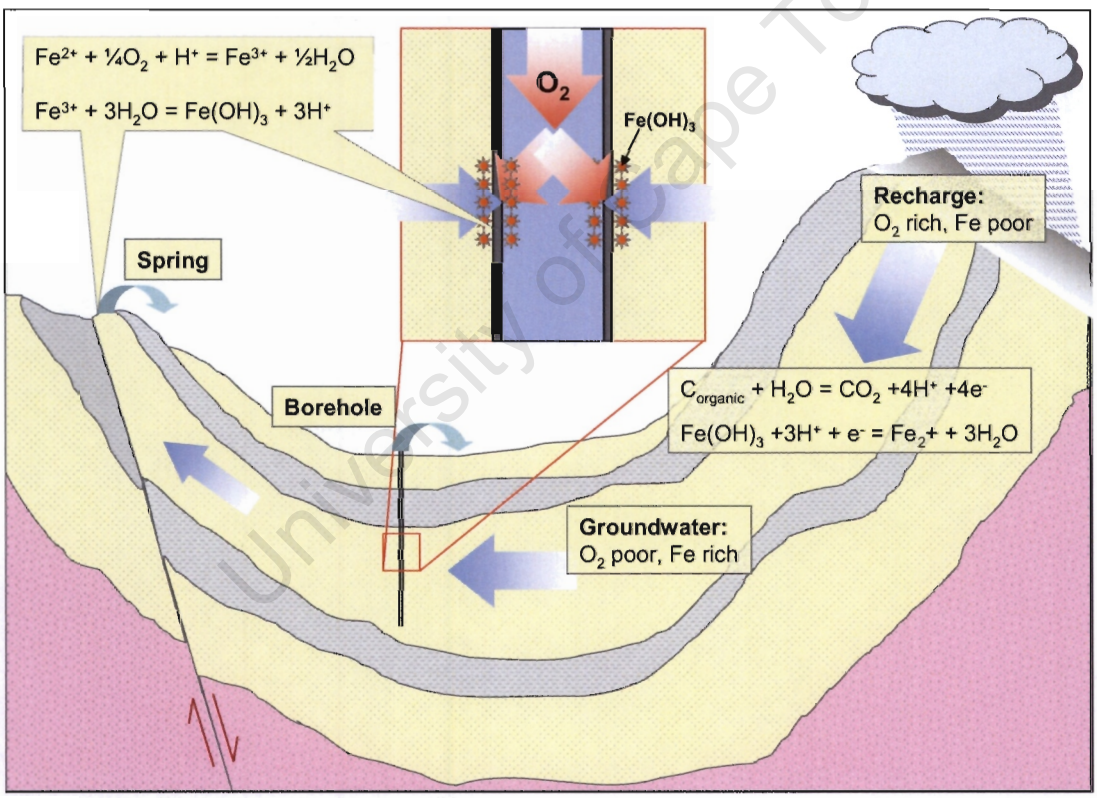

Figure 2.2. Schematic illustration of iron cycling within an aquifer

A redox gradient develops away from the recharge zone, resulting in zones of different reactions that are not mutually exclusive and can shift with time. A similar redox zonation can develop at an aquifer discharge point where oxygen can diffus into the aquifer to a limited extent. In the presence of oxygen, soluble Fe^{2+} is oxidized to Fe^{3+} and precipitates as $Fe(OH)_3$. Over

short time periods in a redox boundary area, mobilisation and immobilisation of iron can be cyclic, determining the spatial patterns of iron distribution (Schwertmann and Taylor, 1992).

2.3 Iron encrustation of boreholes

2.3.1 Introduction

Iron encrustation occurs at the anoxic-oxic boundary formed by introduction of oxygen into groundwater via a borehole. Just as at any other groundwater discharge point, the introduction of oxygen into the groundwater results in the oxidation of Fe^{2+} to Fe^{3+}. Fe^{3+} is insoluble under near-neutral pH conditions and precipitates as an iron oxyhydroxide mineral (hereafter referred to as iron oxides for the sake of brevity). Iron oxide minerals can fill the pores of the aquifer surrounding the borehole, or encrust equipment inserted into the hole for water extraction, such as pumps, pipes and well screens. The process of oxidation and precipitation leads to a decrease in borehole yield and ultimately costly cleaning and rehabilitation of the borehole is required to recover the lost yield. In order to correctly manage and treat the encrusted well, it is important to understand the processes by which mineral encrustation occurs, and the chemistry and mineralogy of the iron encrustations.

2.3.2 Process of iron encrustation

Iron encrustation occurs in boreholes in aquifers with near neutral pH (6.3 – 6.8) groundwater and iron concentration greater than 0.1 mg/L. The borehole is a fundamental part of the process because it introduces oxygen into the groundwater by the following processes:

- The borehole exposes the water column to atmospheric conditions, resulting in penetration of dissolved oxygen into the well and diffusion into the groundwater, as well as degassing of CO_2 leading to an increase in pH, further enhancing iron precipitation
- The borehole forms a "short-circuit" between oxidized water in the upper formations and reduced water in the lower formations of an aquifer, potentially resulting in mixing of these waters and aeration of water by physical cascading of water from higher levels to lower levels

(Houben, 2003a; Baveye *et al.*, 1998; Taylor *et al.*, 1997; Chapelle, 1993).

The introduction of oxygen into anoxic groundwater results in the formation of a redox gradient, affecting all redox-sensitive species in the water. The most important redox reactions in the iron clogging system are (Kuntze, 1982):

$$4Fe^{2+} + 10H_2O + O_2 = 4Fe(OH)_3 + 8H^+ \quad (2.11)$$

$$2HCO_3^- + H_2S = 2CH_2O + SO_4^{2-} \quad (2.12)$$

$$2FeOOH + 3HS^- = 2FeS + S^0 + H_2O + 3OH^- \quad (2.13)$$

Iron oxidation occurs in the suboxic zone of the redox gradient while sulphide oxidation will occur in the adjacent anoxic zone. Iron and sulphur cycling are often closely interlinked (McBride, 1994) and changes in sulphate concentration are commonly associated with well encrustation (Walter, 1997), possibly because iron sulphide minerals in the aquifer are oxidized. Infilling of joints and fractures with iron sulphides has been observed in borehole cores from the TMG (Meyer, 1999). The oxidation of iron sulphide due to influx of oxygen releases sulphate into solution (Drever, 1997):

$$FeS_2 + 3.5O_2 + H_2O = Fe^{2+} + 2SO_4^{2-} + 2H^+ \quad (2.14)$$

This reaction generates acid, as is well documented in acid mine drainage (AMD) literature, and can increase the corrosiveness of the water (Engelbrecht and Jolly, 2000). Rapidly increasing SO_4 concentrations and falling pH, symptoms usually associated with AMD, have been observed in boreholes in the TMG, indicating that sulphide oxidation may be occurring (Smart and Tredoux, 2002).

Within the suboxic zone in the borehole, Fe(II) is oxidized and precipitates as Fe oxyhydroxide (Taylor *et al.*, 1997). However, at the low concentrations of dissolved oxygen in the borehole, the rate of chemical iron oxidation is expected to be far slower than what has been observed. Calculations using known Fe oxidation rates indicate that the accumulation of iron oxide minerals in boreholes is more rapid than can be explained by chemical oxidation of iron and precipitation of iron oxides alone. Using equation 2.7, at an Fe(II) concentration of 10 mg/L, a pO_2 of 0.05 atm and a pH of 6, it would take 2000 days to produce 5g of Fe^{3+} (Ralph and Stevenson, 1995). Microaerobic batch

experiments inoculated with sludge from a borehole have been used to show that there is a considerable increase in the oxidation rate if bacteria are introduced into an iron oxidation system (Ralph and Stevenson, 1995). Biological oxidation/precipitation appears to be about 1000 times faster than chemical oxidation (Søgaard *et al.,* 2000). Microbially catalysed precipitation of iron oxyhydroxides from groundwater has often been observed (Ferris *et al.*, 2000; Brown *et al.*, 1999; Armon *et al.*, 1998; Taylor *et al.*, 1997; Tuhela *et al.*, 1997; Ralph and Stevenson, 1995; Carlson *et al.*, 1980). In the literature, iron encrustation is invariably linked to the process of biofouling, the formation of mineral depositing sessile colonies of bacteria (biofilms) within the well (Flower and Bishop, 2003; Smith 2002; Walter, 1997). Biofouling is thought to be the cause of iron encrustation in the TMG and Atlantis aquifers (Bishop and Killick, 2003; Jolly, 2000; Meyer, 1999).

2.3.3 Encrustations

Encrustations found in water wells include iron hydroxides, manganese oxides, iron sulphides and iron carbonates (Houben, 2003a; Walter, 1997). Iron hydroxides are by far the most common form of encrustation, although there is considerably variation in their mineralogy, crystallinity and chemistry. Commonly reported encrusting iron hydroxide minerals are ferrihydrite, goethite and haematite (Table 2.1; Houben, 2003a; Tuhela *et al.*, 1997; Walter, 1997; Tuhela *et al.*, 1992; von Gunten and Schneider, 1991; Vuorinen *et al.*, 1988; Carlson and Schwertmann, 1987). While lepidocrocite, maghemite and magnetite are also found in natural environments, they have not been reported from encrusted boreholes.

Natural iron oxides tend to be less crystalline than synthetic iron oxides (Schwertmann and Taylor, 1992). The crystallinity, chemistry, particle size, morphology, colour and surface properties of natural iron oxides are affected by the properties of the solution from which the oxide precipitates, in particular, the Fe^{3+} and Fe^{2+} concentrations, temperature, ionic strength, pH, Eh and ionic composition (Lo *et al.*, 1996; Schwertmann and Taylor, 1992). The ions in the precipitating solution can exchange and adsorb onto charged

iron oxide surfaces, and can substitute into the Fe-oxide framework (Cornell, 1988). Thermodynamic data for iron oxides are dependent on particle size and content of foreign ions (Schwertmann and Taylor, 1992). Under aerobic earth surface conditions, goethite should be the favoured iron oxide, however, slow transformations from metastable less crystalline phases into stable phases result in discrepancies between thermodynamically predicted and observed stable phases. Metastable phases, such as ferrihydrite and lepidocrocite, often control the activity of Fe in soil solutions (Schwertmann and Taylor, 1992).

Table 2.1. Physical characteristics of common iron oxide minerals (Schwertmann and Taylor, 1992)

	Goethite	Lepido-crocite	Ferrihydrite	Maghemite	Haematite	Magnetite
Chemical formula	α-FeOOH	$\tilde{\gamma}$-FeOOH	$5Fe_2O_3 \cdot 9H_2O$	γ-Fe_2O_3	α-Fe_2O_3	Fe_3O_4
Colour	Yellowish-brown	Orange	Reddish-brown	Red to brown	Bright red	Black
Crystal morphology	Needles, laths	Elongated serrated plates	Spherical	Cubic	Hexagonal	Cubes
Surface area (m^2/g)	60-200		200-500		50-120	
Conditions for formation	Low temp., OC, Fe^{2+}, Fe^{3+}, Al	Fe^{2+}, no Al, low pCO_2	Rapid oxidation Fe^{2+} in presence of OC, Si	Oxidation of magnetite		Lithogenic

Ferrihydrite (FH) forms in environments where Fe^{2+} is rapidly oxidized in the presence of high concentrations of organic matter or silicate (Schwertmann and Taylor, 1992). FH forms directly from Fe^{3+} in solution. Precipitation of Fe^{2+} directly from solution would form the mineral green rust, rather than FH (Taylor and Schwertmann, 1974). The crystallinity of FH varies and is determined by the number of peaks in an XRD scan, from six-line (most crystalline) to two-line (least crystalline) FH (See Figure D.6, Appendix D; Schwertmann and Taylor, 1992). The two forms of FH form under different conditions and 2-line FH does not become more ordered with time (Cornell and Schwertmann,1996). Synthetic 6-line FH particles (4-6 nm) have been found to be hexagonal and about twice as big as spherical 2-line FH particles (2-3 nm). The 2-line FH particles are usually heavily aggregated making distinction of individual particles difficult (Cornell and Schwertmann, 1996).

Microbially precipitated FH occurs as 0.5 to 2 μm spherical aggregates of 2 – 3 nm particles (Schwertmann and Taylor, 1989; Søgaard *et al.* 2000).

FH is usually the first oxide to precipitate from solution, and recrystallises with time to goethite, a thermodynamically more stable mineral with smaller surface area and lower solubility than FH (Houben, 2003a; Loewenthal *et al.*, 1986). The rate of conversion of FH to goethite is greater at higher pH, and is significantly slowed by the presence of contaminants, such as phosphate, divalent metals (Cu, Zn, Ni and Co) or silica (Houben, 2003a; Cornell and Schwertmann, 1996; Schwertmann and Taylor, 1992; Cornell, 1988). Conversion of FH to goethite involves dissolution of FH before goethite crystallises from solution. Contaminants form strong complexes with Fe, stabilising FH, and significantly slowing the rate of dissolution, thereby slowing the rate of conversion of FH to goethite (Cornell, 1988). In a groundwater environment, the conversion of FH to goethite is expected to take several years (Houben, 2003a). Goethite can also form by nucleation and crystal growth from solution, especially at low temperatures and high DOC concentrations (Schwertmann and Taylor, 1992). Al, Mn, Cr and V can substitute for Fe in goethite (Cornell and Schwertmann, 1996).

Minerals less commonly associated with borehole encrustations include haematite, lepidocrocite, maghemite and magnetite. Haematite can form by aggregation, dehydration and internal structural rearrangement of FH. Lepidocrocite forms from Al-free, Fe^{2+}-containing solutions with high pCO_2. The presence of Al and Fe^{3+} in solution favours the formation of goethite over lepidocrocite, while the presence of Si and DOC favour precipitation of FH rather than lepidocrocite. Because Al, Si and DOC are rarely absent from groundwater it is unlikely that lepidocrocite will be found in boreholes. Magnetite does not form under low temperature, low pressure earth surface conditions. It is easily converted to maghemite by partial or complete oxidation of Fe^{2+} to Fe^{3+}. Maghemite, an isomer of magnetite, can also form by dehydration of lepidocrocite at high temperatures (Schwertmann and Taylor, 1992).

2.4 Biofouling

2.4.1 Characteristics

Biofouling is the clogging of a borehole due to accumulation of bacterial cell bodies, formation of extra-cellular polymers (ECP; slimes) and microbially catalysed oxidation leading to precipitation of iron oxides in the borehole and the pores of the aquifer (Armon *et al.*, 1998; Baveye *et al.*, 1998; Cullimore and McCann, 1978). The microorganisms attach to submerged surfaces in a layer called a biofilm, a complicated heterogeneous assemblage of cell clusters, extra-cellular polymers, pores and conduits (Lee and Beveridge, 2001; Baveye *et al.*, 1998). The lifecycle of a biofilm begins with colonisation of surfaces by non-filamentous bacteria, providing an organic substrate for the growth of filamentous iron bacteria (Walter, 1997). Maturation of the biofilm into a consortium of species of bacteria follows, with different bacterial species arranged within the biofilm so that the different metabolic types contribute most efficiently to the overall ecosystem (Brown *et al.*, 1999). Localised micro-environments can develop within the biofilm, for example, reducing conditions suitable for the growth of sulphate-reducing bacteria such as *Desulfovibrio desulfuricans* can develop in the centre of the biofilm (Figure 2.3). These bacteria can corrode stainless steel by coupling oxidation of solid iron (Fe^0) to Fe^{2+} with the reduction of sulphate to sulphide. Biocorrosion, electrochemical corrosion induced or enhanced by the activity of biofilms, is a common side-effect of biofouling (Tyrrel and Howsam, 1997). Through-out its lifecycle, the biofilm is subject to periodic sloughing events for unknown reasons (Baveye *et al.*, 1998; Cullimore, 1992).

Iron biofouling of boreholes is favoured under the following conditions:

- High concentrations of Fe^{2+}, phosphorus and other nutrients, and organic substrates (Brown *et al.*, 1998; Walter, 1997).
- Water velocities of approximately 1 m/s, which enhance nucleation and precipitation of iron and nutrient uptake, but also limit scouring of the biofilm (Tyrrel and Howsam, 1997).
- pH in the near-neutral range (Søgaard *et al.*, 2000; Walter, 1997)

- Presence of a steep redox gradient and a boundary between oxic and anoxic water, as observed within boreholes (Emerson, 2000; Walter, 1997; Chapelle, 1993). Iron oxidising bacteria are most commonly found where anoxic water containing high levels of Fe^{2+} approaches an area with higher DO, such as an outflow of a spring or a borehole (Søgaard *et al.*, 2000; Walter, 1997).

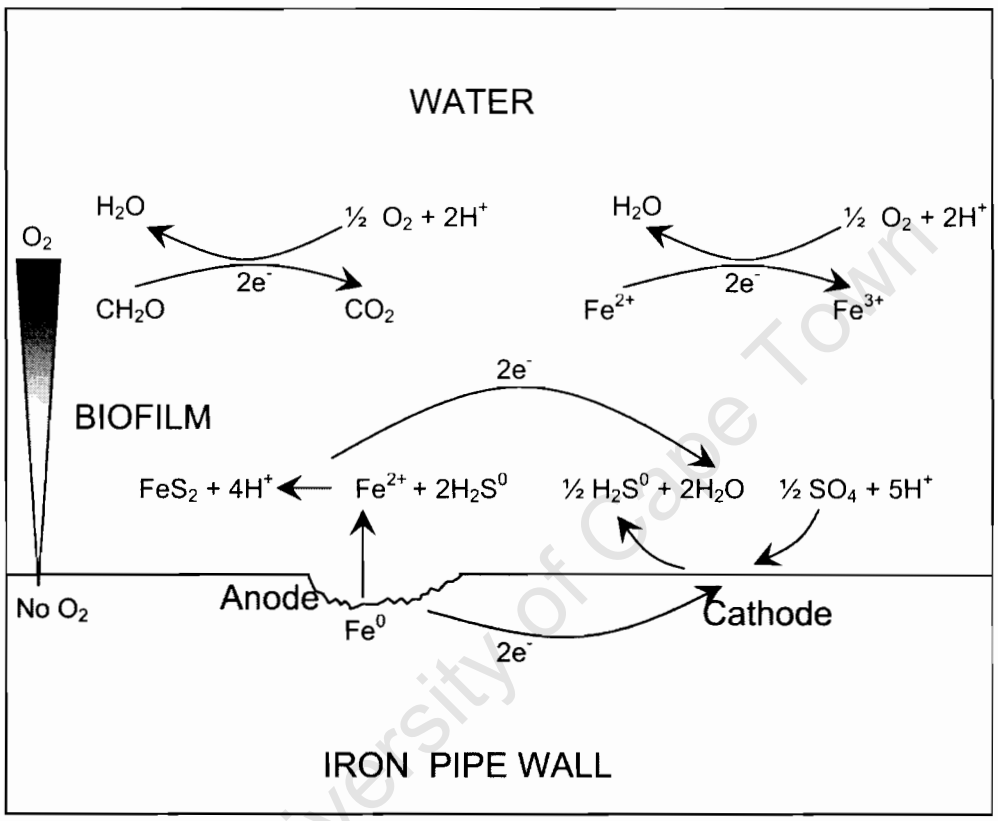

Figure 2.3. Schematic illustration of chemical reactions involved in a biofilm (adapted from Loewenthal, 1986)

Although biofouling is often blamed for iron encrustation problems, the link between cause and effect has yet to be conclusively proven because chemical oxidation of iron is rapid under the near-neutral pH conditions that the organisms appear to favour. Microbially mediated iron oxidation tends to occur under conditions where chemical oxidation is thermodynamically favoured but kinetically limited e.g. *Thiobacillus ferrooxidans* oxidizes iron at pH < 5 in acid mine drainage systems or *Gallionella ferruginea* which is believed to oxidize iron at low dissolved oxygen levels (Walter, 1997). Under conditions where abiotic oxidation is rapid it is virtually impossible to

distinguish microbially mediated from pure chemical oxidation (Tuhela *et al.*, 1997; Ralph and Stevenson, 1995; Schwertmann and Taylor, 1992; Smith and Tuovinen, 1985).

2.4.2 Organisms involved

A great diversity of bacteria are associated with water wells in which iron encrustation occurs, and they can be divided into three main groups: iron related bacteria (IRB), slime forming bacteria (SFB), and sulphate reducing bacteria (SRB). SFB are ubiquitous, and generate large volumes of extra-cellular polymers (ECP). SRB are found in more reducing areas of the aquifer i.e. further away from the source of oxygen and common genii are *Desulfovibrio* and *Desulfotomaculum* (Engelbrecht and Jolly, 2000). Organisms are considered to be IRB if they either catalyse the oxidation of ferrous iron or change the water chemistry of the well to favour iron oxidation (Ghiorse, 1984). No comprehensive study on the bacterial ecology in the TMG has been done, but initial investigations by Engelbrecht and Jolly (2000) indicate high concentrations of bacteria occur in clogged holes, consisting of mixtures of SRB, IRB and SFB.

Metabolic characteristics and habitat requirements differ within the IRB group, but all are associated with iron oxidation (Tyrrel and Howsam, 1997). IRB occur naturally in aquifer sediments and are capable of shedding extra-cellular material and moving through aquifers as small (0.1 - 0.3 μm), inactive cells that attach and grow only when conditions are favourable (Walter, 1997). Some of the most common IRB genera found in water wells at circumneutral pH are *Gallionella, Crenothrix*, *Sphaerotilus*, *Leptothrix* and *Metallogenium* (Baveye *et al.*, 1998; Table 2.2), while at low pH (<5), the well known iron oxidizing acidophiles *Thiobacillus ferrooxidans* and *Leptospirillum ferrooxidans* occur (Baveye *et al.*, 1998; Tyrrel and Howsam, 1997).

Gallionella spp. are probably the most well known of the iron-oxidising bacteria, and are easily recognized by their kidney shape and helical stalks which are composed largely of iron oxides (Walter, 1997). *G. ferruginea* is an autolithotroph or chemolithotroph, i.e., it utilises the energy obtained from

oxidation of iron to reduce inorganic carbon (HCO_3^-/ CO_2) to biomass (Emerson, 2000; Hanert, 1989; Ghiorse, 1984):

$$4Fe^{2+} + CO_2 + 11H_2O = 4Fe(OH)_3 + (CH_2O) + 8H^+ \quad (2.15)$$

Table 2.2. Characteristics of common iron-related bacteria (Tuhela *et al.*, 1997; Hanert, 1989; Mulder, 1989; Hanert, 1981; Mulder and Deinema, 1981)

	Gallionella	*Leptothrix*	*Sphaerotilus*	*Thiobacillus*
Cell width (μm)	0.5 -0.7	0.6 - 1.4	1.2 - 2.5	
Length (μm)	0.8 - 1.8	1 - 12	2 - 10	0.5 - 1.0
Shape	Kidney	Rod	Rod	Rod
Distinguishing characteristics	Spiral twisted stalk structure (<400 μm length)	Rough sheath	Smooth sheath	
C-source	CO_2	Glucose, sucrose, glycerol	Glucose, sucrose, glycerol	CO_2
Optimum pH	6.0 - 7.6	6.5 - 7.5	6.5 - 7.5	1.3 - 4.5
Flagella	Y	Y	Y	Y
Environment	Pure, Fe^{2+} bearing waters with <12 mg/L organic material. Redox gradient. Microaerobic	Unpolluted, flowing ditch, river or pond water	Flowing water polluted with sewerage and waste water	Aerobic, acidophile.

Lithotrophic bacteria tend to predominate in environments with little organic matter and high concentrations of Fe^{2+} (Emerson, 2000). *G. ferruginea* thrives in microaerophilic environments (0.1-1.0 mg/L DO) which have slightly acidic to near-nuetral pH, redox potentials between 200 and 320 mV (pe 7.7 to 9.8 at 25°), temperatures between 4 and 25.6°C, Fe^{2+} concentrations between 0.1 and 10 mg/L, but no more than 25 mg/L, and CO_2 concentrations greater than 150 mg/L (Søgaard *et al.* 2000; Walter, 1997; Hanert, 1989). The low energy yield of the iron oxidation reaction requires *G. ferruginea* to process large amounts of Fe, producing 350 g $Fe(OH)_3$ or 890 g FeOOH for every gram of cellular material produced (Walter, 1997). Under optimum conditions, the bacteria can consume 150 g Fe(II) per gram of dry weight per day (Hanert, 1989).

Leptothrix are gram-negative rod-shaped bacteria. The cells form chains which are encased in a sheath, a tubular structure composed of a protein-polysaccharide-lipid complex which can become encrusted in layers of iron oxides. The amount of iron deposited on the sheaths increases with increasing solution iron concentration. The sheath enables bacteria to attach to solid surfaces, and protects the cells from becoming encrusted in iron

oxides (Mulder, 1989; Mulder and Deinema, 1981; Ghiorse, 1984). *Leptothrix* are found in slowly running, unpolluted, fresh, iron-containing, ditch, river or pond water (Mulder and Deinema, 1981). *Leptothrix ocracea* and *L. discophora* are heterotrophic organisms i.e., utilize organic carbon as their carbon source and grow optimally between 10 - 35°C, pH 6.5 - 7.8, with low pO_2 and a source of organic carbon (Mulder, 1989; Mulder and Deinema, 1981). It is not know whether the organisms actively oxidize iron, or passively accumulate iron oxides because oxidation of iron does not appear to be of any benefit to the organism (Emerson, 2000; Tyrrel and Howsam, 1997; Walter, 1997; Mulder, 1989).

2.5 Management and treatment of iron encrustation

2.5.1 Wellfield management strategies

Regardless of the mechanism of formation of encrusting material, the outcome is the same - a borehole with significantly reduced yield. Prevention of biofilm development or clogging is desirable, and careful borehole management can greatly reduce the rate of clogging (Engelbrecht and Jolly, 2000). Most of the management strategies currently employed at wellfields assume that the problem is biofouling, rather than chemical iron oxidation. Strategies include management of oxygen concentrations in the borehole and borehole construction, as well as continuous monitoring of the wellfield.

Because iron oxidation requires the presence of oxygen, most wellfield management strategies are developed to reduce oxygenation of groundwater. There are a number of ways this can be done, namely:

- Minimize drawdown by reducing pumping rates and extending pumping times (Engelbrecht and Jolly, 2000). Reduced pumping rates also limit the supply of nutrients to organisms and can result in depletion of oxygen in water if organisms are using oxygen as an electron acceptor (Loewenthal *et al.*, 1986).
- Prevent mixing of anoxic and oxic waters from two different horizons within the well by sealing off oxygenated water strikes (Engelbrecht and Jolly, 2000; Tyrell and Howsam, 1997).

- Avoid pumping the water level to below the top of the screen, by correct screen placement and not overpumping the well (Tyrell and Howsam, 1997).
- Installing systems to prevent oxygen entering the hole at all, for example keeping the hole filled with nitrogen gas (Engelbrecht and Jolly, 2000).

There are suggestions that the design and construction of the borehole can influence the rate at which it clogs. The correct placement of screens is important in minimizing oxygen introduction into the well (Tyrell and Howsam, 1997). The borehole construction material may influence the rate of encrustation, as well as the ease of cleaning (Mogg, 1972). Stainless steel screens are believed to foul up more rapidly than PVC screens (Engelbrecht and Jolly, 2000) but they are thought to be easier to clean than slotted PVC screens. Stainless steel wedge-wire screens (Johnson screens) maintain an even laminar flow regime, limiting the turbulence with which biofilms are associated. Use of geotextiles surrounding the screens has been found to enhance clogging (Flower and Bishop, 2003). Sterilisation of tools, equipment and drilling tools is recommended prior to drilling a new well to minimise the chances of contamination by bacteria from another site (Mogg, 1972).

Another important process in management of iron oxide encrustation is monitoring parameters that can predict the onset of biofouling, such as the concentrations of iron and nutrients in the borehole. Monitoring of bacterial populations (by heterotrophic plate counts) and dissolved oxygen concentrations on a regular basis are also recommended, and down-hole video cameras have been found to be useful in determining the extent of iron clogging (Engelbrecht and Jolly, 2000; Tyrell and Howsam, 1997; Howsam and Tyrrel, 1989).

A completely different approach employed in Europe is to pre-empt iron oxidation by pumping oxygenated water into the well, or into boreholes surrounding the main supply well. Iron oxidation and precipitation occurs within the aquifer away from the borehole and iron-free water is pumped from

the borehole. The permeability of the aquifer has been found to only reduce slightly because the volume of aquifer affected by injecting oxygenated water is large (Hallberg and Martinell, 1976).

Once a borehole is clogged, neither management of pumping rates nor monitoring of well chemistry will improve the situation, at which point rehabilitation procedures must be implemented.

2.5.2 Rehabilitation

Biofilms and clogged boreholes are difficult to treat. Both mechanical and chemical methods are currently used, but there are no 100% effective rehabilitation methods (Armon *et al.*, 1998). Mechanical methods involve breaking the iron oxide precipitates from the borehole walls by wire brushing, water jetting to wash off loose deposits, surge and purge procedures using water or gases like carbon dioxide, steam cleaning to obtain well water temperatures of 60°-70°C, or using a sonar jet, a vibratory explosive. In some extreme cases, it has been known to place calcium hypochlorite in the borehole, and then throw in a stick of dynamite! (Flower and Bishop, 2003, Cullimore and McCann, 1978).

Chemical rehabilitation utilizes chemicals to sterilize the well and dissolve the iron encrustations. There are different groups of chemicals (Houben, 2003b; Engelbrecht and Jolly, 2000; Baveye *et al.*, 1998; Walter, 1997):

- Strong oxidizing agents are used to mineralise organic matter e.g. hydrogen peroxide (Houben, 2003b):

  $$C(H_2O) + 2H_2O_2 = CO_2 + 3H_2O \qquad (2.16)$$

  Other examples are sodium hypochlorite, calcium hypochlorite, chlorine dioxide, chlorine gas and potassium permanganate (Cullimore and McCann, 1978). The disadvantages of these chemicals are that they will oxidise Fe^{2+}, and Cl containing oxidizers e.g. hypochlorite could combine with dissolved organics to form chlorinated hydrocarbons (Houben, 2003b). Recently "electrochemically activated" water has been tested on boreholes in South Africa and Botswana. This

sterilizing solution consists of powerful oxidants with biocidal effects at a pH of 2-8.5 (Riekel and Hintze, 2002; Smith, 2002).

- Inorganic and organic acids e.g. hydrochloric, citric, acetic, sulphamic, and sulphuric acids dissolve Fe oxide minerals by the process of proton assisted dissolution (Houben, 2003b):

  $$FeOOH + 3H^+ = Fe^{3+} + 2H_2O \quad (2.17)$$

  Acid dissolution reactions are optimised at pH <<2. Acids are required to be neutralised after rehabilitation to prevent corrosion (Houben, 2003b).
- Complexing agents e.g. oxalate by the process of ligand controlled dissolution. Organic molecules have the disadvantage that they may lead to secondary microbial pollution (Houben, 2003b).
- Reducing agents e.g., ascorbic acid, sodium dithionite, which bring insoluble Fe^{3+} into solution by the process of reduction (Houben, 2003b):

  $$2FeOOH + Na_2S_2O_4 + 4H^+ = 2Fe^{2+} + 2Na^+ + 2HSO_3^- + 2H_2O \quad (2.18)$$

  Na-dithionite and oxalic acid are effective reducing agents able to dissolve both ferrihydrite and goethite relatively quickly (Houben, 2003b, Cornell and Schwertmann, 1996).

Combinations of reducing and complexing agents increase the effectiveness of rehabilitation. Many chemicals effectively dissolve ferrihydrite but have limited success with goethite (Houben, 2003b). Some authors believe that regular bacterial disinfection (by e.g., sodium hypochlorite) can slow down biofouling by retarding bacterial growth (Engelbrecht and Jolly, 2000).

Mechanical and chemical treatments are commonly combined, such as the Blended Chemical Heat Treatment™ (BCHT) which is used in South Africa (More Water cc, 2002). The treatment involves application of at least two heated chemical blends to shock, disrupt and disperse the clogging material, as well as brushing and/or high pressure jetting of the inside of the casing and screens. A heated alkali and surfactant solution shocks the biofilm, followed by disruption with a heated (65-95°C) chlorinated sulfamic acid solution with a dispersant chemical blend, and finally, the material is dispersed mechanically

using high pressure jetting, surging and brushing (Flower and Bishop, 2003; Chapelle, 1993).

None of these methods is effective in all cases and it is important to understand the causes and types of encrustation before attempting rehabilitation (Houben, 2003b). Encrustation also often recurs soon after rehabilitation, and management options are likely to be more effective and cheaper in the long run.

2.6 Summary

Iron occurs as two redox species in the groundwater environment, Fe^{2+} and Fe^{3+}. At redox boundaries, such as found in boreholes, soluble Fe^{2+} can be oxidized to Fe^{3+} which then precipitates as an iron oxide mineral. The oxidation reaction can be microbially catalysed by bacteria like *Gallionella sp.* These bacteria utilise the energy from iron oxidation to survive in microaerophilic near-neutral environments, but they have to compete with chemical iron oxidation which is rapid at near-nuetral pH. Commonly observed iron oxides in boreholes are ferrihydrite and goethite. The minerals precipitate within well screens, pump intakes, pipes and aquifer pores, resulting in reduced borehole yields, and costly rehabilitation procedures. Iron oxidation can be slowed by careful management of pumping and borehole construction, but once the yield has declined, rehabilitation is required. Both mechanical and chemical rehabilitation have been used to remove encrustations from wells, but chemical rehabilitation is focussed on sterilisation and control of bacterial populations within the borehole.

3 Iron mobility within the TMG aquifer in the Kammanassie Mountains, Klein Karoo

3.1 Introduction

The Klein Karoo Rural Water Supply Scheme (KKRWSS) has been hampered by problems of iron encrustation of water supply wells for many years. Employees of the well scheme have noted higher Fe concentrations and worse encrustation problems in boreholes drilled in particular lithologies, namely the Nardouw Subgroup quartzites adjacent to the Cedarberg and Bokkeveld shale contacts (Engelbrecht and Jolly, 2001). Nardouw Subgroup rocks are visibly more iron-rich, and geohydrologists now avoid drilling boreholes in these lithologies (C. Hartnady, Umvoto Groundwater Consultants, pers. comm.). No geochemical or hydrochemical study has ever been done to confirm these observations. The presence of dissolved iron at concentrations greater than 0.1 mg/L is fundamental to the formation of iron encrustations (Walter, 1997). A number of characteristics of TMG groundwater have been identified as important for potentially mobilising iron.

- pH: The TMG aquifer is poorly buffered and pH of 3 to 4 is often measured in groundwater (Meyer, 1999).
- Redox: Low concentrations of dissolved oxygen (DO) are commonly measured in groundwater.
- Lithology: Certain formations are visibly more iron rich than others
- Presence of organic acids: Dissolved organic acids in surface waters have been implicated in the mobilisation of iron during recharge.

It is hypothesised that understanding the lithological distribution of iron and conditions required for mobilisation of dissolved Fe in the TMG aquifer will allow for targeted drilling and screening of boreholes so as to avoid iron encrustation problems. This chapter will investigate the distribution of soluble iron in the TMG in the Klein Karoo, using field measurements of groundwater chemistry from selected boreholes combined with historical groundwater quality data. An attempt will be made to correlate the water chemistry with

iron concentration data for the main lithologies of the TMG in the Kammanassie Mountains. In addition, the potential for mobilisation of iron from different formations under different chemical conditions and in the presence and absence of natural organic acids will be investigated using batch leaching experiments. Although Fe encrustation is problematic in many aquifers, this Chapter focuses specifically on Fe mobility in the TMG of the Kammanassie Mountains, with the aim of identifying conditions and processes important to Fe mobilisation that can then be investigated in other aquifers.

3.1.1 Mobilisation of iron into groundwater

Iron is released from rock by the process of chemical weathering, the dissolution of minerals by water and solutes within water (Schnoor, 1990). Chemical weathering involves the attachment of a reactant in solution, e.g. H^+, to a surface species, forming a complex on the mineral surface. The complex polarizes, weakens and breaks the metal-oxygen bonds between the surface species and the surrounding mineral and results in slow detachment of the metal into solution (Brantley, 2003). Three types of dissolution occur: pH controlled, ligand promoted and reductive dissolution. All of these reactions are controlled by interaction between the reactant and the surface. In reality, the different types of dissolution are often interlinked e.g. reductants can act as ligands, and the three types of dissolution can occur simultaneously (Biber *et al.*, 1994). pH-dependent dissolution occurs due to the adsorption of protons onto an oxide surface, which polarizes metal-oxygen bonds and weakens them. Protonation of the surface also imparts surface charge to iron oxide minerals. Dissolution is expected to be slowest where the pH equals the point of zero charge (PZC) of the mineral (Brantley, 2003; Biber *et al.*, 1994).

3.1.1.1 Ligand promoted dissolution, especially by organic compounds

Ligands can both enhance and inhibit mineral weathering. Ligand promoted dissolution of iron oxide minerals occurs when ligands replace surface hydroxyl groups and weaken the bonds holding Fe^{3+} to the surface, such that Fe^{3+} slowly detaches (Sulzberger *et al.*, 1989). The type of surface complex that forms is important. Some studies have found that bidentate or multidentate polynuclear complexes at the surface are more effective than

monodentate complexes (Drever and Stillings, 1997), while others note that monodentate complexes have little effect on dissolution rate, bidentate complexes enhance dissolution rate and polynuclear complexes inhibit dissolution of minerals (Ochs, 1996). Another mechanism by which ligands enhance dissolution is by complexing metals in solution, thus reducing the activity of the metal in solution and promoting further dissolution. In the same way, the presence of ligands can affect the redox environment of the solution, by complexing Fe^{2+}, thereby changing the redox potential of the Fe^{3+}/Fe^{2+} couple in water (Stumm and Morgan, 1996).

A common source of ligands in natural systems is soluble organic compounds, which have been found to both promote and inhibit mineral dissolution (Brantley, 2003). Complexing of iron in minerals by fulvic acid destabilises the minerals and promotes weathering (Schnitzer and Kodama, 1976), but humic acid molecules can inhibit mineral dissolution by blocking surface sites and preventing detachment of metals (Ochs, 1996). Organic compounds also affect mineral dissolution by complexing and transporting Fe^{3+} away from the mineral surface, and complexing dissolved Fe^{2+}, inhibiting oxidation and precipitation. The Fe^{3+}-organic complex is unstable and Fe^{3+} is reduced by the organic compound. This process can continue until the organic compound is oxidized to an inert form (Theis and Singer, 1974):

$$Fe^{3+}\text{-humic complex} = Fe^{2+} + \text{oxidized humic} \qquad (3.1)$$

Organic acids can also affect the dissolution rate of silicate minerals by affecting the pH (Drever and Stillings, 1997).

3.1.1.2 Reductive dissolution

Reductive dissolution is special form of ligand-promoted dissolution where the ligand is a reductant and facilitates transfer of electrons from the solution to the oxide surface (Biber *et al.*, 1994). The ligand binds rapidly to the metal at the surface and exchanges electrons with the Fe^{3+} surface site, resulting in an oxidized ligand and an Fe^{2+} ion, which is more easily detached from the surface than an Fe^{3+} ion (Wieland and Stumm, 1992; Sulzberger *et al.*, 1989). To maintain the charge balance on the surface and in solution, a cation needs to be transferred from the surface to the solution. At pH > 3.0, the Fe^{2+} freshly

released into solution can oxidize and precipitate as an iron oxide mineral (White and Yee, 1985). Reductive dissolution of iron occurs predominantly in oxic-anoxic boundary layers where there are surface-coordinating organic compounds. Reductants forming inner-sphere complexes are most effective (Sulzberger *et al.*, 1989). Dissolution rates of silica minerals are considerably faster under anoxic than oxic conditions. This is because under oxic conditions, Fe^{2+} released from the mineral is rapidly oxidized to an insoluble Fe^{3+} form, coating the mineral with a layer of iron oxide which inhibits further dissolution by diffusion control. Reductive dissolution of FeOOH minerals can be quite rapid, and the presence of organic ligands can accelerate the process. Natural organic compounds such as phenols, tannic acid and cysteine are able to reduce Fe-oxide (Appelo and Postma, 1996).

3.1.1.3 Microbial iron reduction

A range of microorganisms, e.g. *Shewanella putrefaciens*, are able to couple reductive dissolution of Fe-oxides to oxidation of organic matter (Appelo and Postma, 1996; Reaction 2.10). Microbes are capable of reducing Fe^{3+} in amorphous Fe^{3+}-hydroxides (Brown *et al.*, 2000), magnetite (Kostka and Nealson, 1995); Fe^{2+}-rich clay minerals (Kostka *et al.*, 1999; Zachara *et al.*, 1998), and goethite (Liu *et al.*, 2001). Many characteristics of microbial reduction of iron minerals are similar to chemical dissolution i.e., it is surface controlled (Zachara *et al.*, 1998; Roden and Zachara, 1996), can be inhibited by precipitation of surface coatings on the mineral (Liu *et al.*, 2001; Urrutia *et al.*, 1999), and is promoted by the presence of organic ligands (Kostka *et al.*, 1999).

3.2 Methodology

3.2.1 Sample collection and analysis

3.2.1.1 Water samples

Groundwater from selected boreholes of the KKRWSS was sampled during August 2002 and August 2003 (Figure 1.3 and 1.5; Table 3.1). To ensure proper purging of the boreholes, water was only collected from boreholes that had been pumping for 24 hours prior to sampling (approximately 20 – 30 well volumes). Sampling taps were allowed to run for 10 minutes before sampling

in order to flush out stagnant water in the pipes. During 2002 a flow-through cell was used to obtain readings for pH, DO and EC, which were measured only once the readings had stabilised. No Eh meter was available at the time of the field work, but downhole logging data from the boreholes (See Appendix I) indicate a linear relationship between Eh and DO in the groundwater. Because of the limited availability of Eh data, DO is used as an indicator of redox potential in the field samples. Unfortunately the flow through cell and probes became coated in iron oxide precipitates, affecting the measurements, and in 2003 these parameters were measured immediately following collection of the water from the sampling tap.

Table 3.1. Boreholes sampled during 2002 and 2003 field work

Borehole	Sector	Formation	Wellfield
DL13	E	Baviaanskloof	Daniëlskraal
DL16	E	Baviaanskloof	Daniëlskraal
DL17	E	Baviaanskloof	Daniëlskraal
DP15	W	Baviaanskloof	Bokkraal
DP28	W	Baviaanskloof	Bokkraal
DP29	W	Baviaanskloof	Varkieskloof
VG3	W	Baviaanskloof	Voorzorg
CHS		Skurweberg	Hotspring
DG110	W	Skurweberg	Droëkloof
KG1	E	Skurweberg	Kleinberg
Spring	W	Peninsula-Cedarberg	Spring
VRNotch	W	Peninsula	Surfacewater
VR6	W	Peninsula	VermaaksRiver
VR7	W	Peninsula	VermaaksRiver
VR8	W	Peninsula	VermaaksRiver
VR11	W	Peninsula	VermaaksRiver

Iron concentrations were determined in the field in both filtered (0.45 μm) and unfiltered samples using the ferrozine method (Viollier *et al.*, 2000; To *et al.*, 1999). In both cases, a known volume of sample was added to pre-measured aliquots of ferrozine reagent. For determination of Fe^{2+} the reagent was 0.4 mM ferrozine in 50 mM HEPES buffer adjusted to pH 7. A mixture of 0.14 M hydroxylamine and buffered ferrozine solution was used for Fe^{T} determination. The ferrozine-sample mixtures were analysed colorimeterically (562 nm) within 8 hours of collection. Standards were prepared at the same time as samples to counter colour degradation with time. However, the colour of standards was found to degrade by no more than 5% over the 8 hour

period. The stability of iron in groundwater was tested in a sample collected from borehole DL17. The sample was allowed to stand for an hour during which time filtered subsamples were periodically taken and analysed for iron content.

During the 2002 sampling period, alkalinity was measured colorimetrically (Sarazin *et al.*, 1999) but these results were discarded because the alkalinity was found to decrease significantly before analysis. For subsequent sampling, alkalinity (pH > 4.5) or acidity (pH < 4.5) was determined by potentiometric field titration with 0.01 M HCl or 0.01 M NaOH respectively following Standard Method 2320 (Eaton *et al.*, 1995). Additional samples were collected and stored at <4°C for later analysis. Water for major cation analysis was filtered (0.45 μm membrane filter) and water for trace element analysis was filtered (0.45 μm) and acidified to pH < 2 with double distilled HNO_3. Samples for stable isotope analysis were neither filtered nor acidified, but the sampling container was filled to the brim to minimise headspace, and tightly sealed to prevent evaporation from affecting the isotope ratio.

Anions (Cl^-, SO_4^{2-}) were analysed using a Dionex DX500 ion chromatograph (IC) with an HPIC-AS4A exchange column and HCO_3^-/CO_3^{2-} eluent, while cations (Na^+, K^+, Ca^{2+}, Mg^{2+}) were measured with a Varian SpectraAA-30 atomic absorption spectrometer. Trace elements were determined using an ELAN 6000 inductively coupled plasma mass spectrometer (ICP-MS). Samples for stable oxygen and hydrogen isotope analysis were prepared following the method of Coleman *et al.* (1982) for deuterium and Socki *et al.* (1992) for ^{18}O and analysed on a Finnegan MAT252 mass spectrometer. Isotope ratios in the sample are reported relative to the international standard SMOW (Standard Mean Ocean Water). Si concentrations in the water were determined using the heteropoly blue spectrophotometric method (Standard Method 4500-SiO2; Eaton *et al.*, 1995). The colorimetric analysis of Fe was repeated in the laboratory on filtered unacidified and acidified samples. Duplicates were analysed for all methods, and external standards were analysed where possible

3.2.1.2 Rock samples

Two to five 2-3 kg rock samples were collected from outcrops of each formation of the Table Mountain Group from a number of sites in the Kammanassie Mountain Nature Reserve during August 2003 (Table 3.2). The weathered edges of the sample were broken from the rocks with a splitter, the fresh portion of the rock crushed in a jaw crusher and then milled in a Sieb mill (Mitchell, 2005).

Table 3.2. Description and locality of TMG lithology rock samples from the Kammanassie Mountain Nature Reserve (adapted from Mitchell, 2005)

Formation	Sample	Comments
Peninsula	P1	E side of the Kammanassie Mountains.
	P2	Near the Peninsula Cedarberg contact, W side of the Mountains.
	P3, P4	Weathered colour rusty to yellow, fresh sample whitish grey.
	P5, P6	E side of Kammanassie Mountains
Cedarberg	C1	Weathered. Collected adjacent to Cedarberg Goudini contact
	C4	Weathered. More resistant shale midway through Cedarberg formation
	C5	Sampled adjacent to Cedarberg -Peninsula contact.
	C2	Highly weathered soft Cedarberg shale with orange yellow colour
	C3	Fresh sample from road cutting. Bedding structures were visible. Dark grey green colour
Goudini	G1	Sampled in a riverbed along the Vermaaks River fault. Iron oxide banding within white-grey sandstone.
	G2	Sampled along the eastern side of the mountains.
	G3	Sampled adjacent to the Cedarberg Goudini contact
	G4	Sampled along the Vermaaks River. Weathered dark red/brown.
Skurweberg	S1	Clean white sandstone, resistant to weathering.
	S2	Sampled near borehole VG3. Orange brown weathered, grey to white fresh samples.
	S3	Sampled near borehole DG110.
Baviaanskloof	B4, B6	Weathered.
	B7, B8	From near to borehole DP15. Weathered and dark in colour.
Bokkeveld	B1, B2	Sampled near borehole DL16 near Calitzdorp.

Mineralogy was determined using a Philips PW 1390 XRD with a Cu K-α X-ray tube (λ=1.542Å) set at 40 kV and 25 mA. Many iron bearing minerals are ferromagnetic or paramagnetic, allowing them to be separated from the bulk of the rock by magnetic separation (Rosenblum and Brownfield, 1996). A 1-2 mm size fraction of crushed Peninsula rock was passed through a Frantz magnetic separator in an attempt to isolate iron containing minerals. The magnetic separate was also analysed by XRD. Thin sections of the rocks were examined with a light microscope and some sections were analysed using a Cameca Camebax electron microprobe instrument. Scanning

electron microscopy energy dispersive spectroscopy (SEM-EDS) microanalysis was performed using a Leica Stereoscan 440 SEM. Samples for SEM-EDS analysis were prepared by sprinkling the dry rock powder onto a stub coated with carbon-based glue, and coating with carbon, allowing EDS semi-quantitative spot analysis of the sample. For both the electron microprobe and SEM, it was difficult to distinguish matrix material from quartz grains, and most spot analyses are likely to be mixtures of minerals due to small grain sizes. The total carbon content of the rocks was analysed using a Leco 932 CHNS elemental analyser at Marine and Coastal Management in Cape Town on samples prepared by milling in an automated agate mortar and pestle.

The iron content of a number of different fractions in the rock was determined, namely total iron, iron redox speciation, crystalline reactive iron and hydrous reactive iron. Total iron (Fe^T) present in the rock was measured using a Philips 1480 "X'Unique" Side Window Wavelength Dispersive Spectrometer (XRF). Fusion disks were prepared for analysis by XRF using Sigma Flux (57 Li Tetraborate: 43 Li Metaborate; Mitchell, 2005). Relative proportions of Fe^{2+} and Fe^{3+} were determined for a few samples by Mössbauer spectroscopic analysis in the Department of Physics, University of the Witwatersrand. Mössbauer spectroscopy investigates the hyperfine interactions between the nucleus of the ^{57}Fe isotope and the electrons surrounding it and can distinguish between different redox states and iron in different minerals. A full report of the Mössbauer analyses is given in Appendix C.

Crystalline reactive iron and hydrous reactive iron were determined by chemical extraction. Crystalline reactive iron (Fe^X), including iron in goethite and haematite, was extracted using a buffered solution consisting of 0.29 M sodium dithionite, 0.2 M sodium citrate and 0.35 M acetic acid (pH 4.8; Roychoudhury *et al.*, 2003; Canfield, 1989). 10 mL of solution was added to 100 mg of powdered rock in a 15 mL centrifuge tube and placed on a reciprocating shaker for 3 days before the extract was filtered (0.2 μm membrane filter) and analysed for Fe^T and Fe^{2+}. Although Kostka and Luther (1994) noted no effect on the HEPES-buffered ferrozine standard curve when

measuring Fe concentrations in dithionite extracts, in this study a distinct discolouration of samples was observed. Iron concentrations in dithionite solution were instead determined using the phenanthroline method (Method 3500-Fe, Eaton *et al.*, 1995). The results of the dithionite extraction are affected by the amount, type and crystallinity of the sample, as well as the amount and pH of the extractant and extraction temperature (van Oorschot and Dekkers, 1999). All samples were run simultaneously using consistent rock:extractant ratios and one batch of reagent, so that the results should be comparable to each other.

Hydrous iron oxides were extracted from the rock samples using an ascorbic acid reagent (0.11 M ascorbic acid, 0.17 M sodium citrate, 0.60 M sodium bicarbonate in 200 mL distilled water (Roychoudhury *et al.*, 2003)), also using a 100mg:10mL rock:extractant ratio. The iron concentration in the filtered extracts was determined using ferrozine colorimetry and no interference was noted. Silica concentration was measured in both the ascorbic acid and dithionite iron extracts using the heteropoly blue spectrophotometric method (Standard Method 4500-SiO_2; Eaton *et al.*, 1995) to establish whether silicate minerals were dissolved by the reagents.

The surface area of the powdered rock samples was measured by the BET method in the Department of Chemical Engineering, UCT using a TriStar 3000. The monolayer capacity of adsorption and surface area can be calculated from the linear relationship between the extent of adsorption of N_2 on the solid and the relative vapour pressure at 77K (Brunauer *et al.*, 1938). The samples were first dried and outgassed to remove adsorbed water. Limitations of this method are that outgassing may alter the surface area of the solid, and N_2 is a large molecule which may not be able to enter small pores, especially in aggregated particles. In addition, grinding the sample can affect the measured surface area (Cornell and Schwertmann, 1996). However, the surface area must be known in order to normalise the calculated kinetic variables to surface area.

3.2.2 Historical groundwater chemistry data

Historical chemical data for TMG groundwater in the Klein Karoo were collated from 7 sources (DWAF, 2004; Kotze, 2001; Kotze *et al.*, 2000; Miller, 2000; Kotze and Rosewarne, 1999; Weaver and Talma, 1999; Kotze and Rosewarne, 1996). The database consists of 263 records, of which 84 have associated iron concentrations. Also included are samples collected and analysed by the author during the current study.

3.2.3 Leaching experiments

Leaching experiments were carried out to assess the potential for mobilisation of iron from common aquifer lithologies under different hydrochemical conditions. Initial batch leaching experiments were performed by Mitchell (2005), but these lasted just 3 days, a time period that does not equate with the residence time and flow rate of water in the aquifer (Kotze and Rosewarne, 1999). The leaching tests in this study were continued until the concentration of Fe in solution in most leaches reached a stable value.

The leaching tests were designed to test the effect of pH, availability of O_2, presence of humic acids and amount of iron present in the rock on the mobility of iron in groundwater. 1 g of crushed rock from each formation was placed in a 50 mL centrifuge tube, and 50 mL of leachate was added. Three natural water leachates were used:

- Water from borehole DL17, buffered at pH 5 using 0.1 M acetic acid
- Organic-rich stream water from a site in the Western Cape buffered at pH 5 with 0.1 M acetic acid
- Organic-rich stream water buffered at pH 3 with 0.1 M phosphoric acid

The pH of the waters was adjusted to the correct value by addition of small amounts of 0.1 M HCl or 0.1 M NaOH. Two separate sets of samples were leached in the dark at room temperature. One set remained under aerobic conditions in the laboratory, while the second set was prepared and extracted under anaerobic conditions within a Coy anaerobic chamber (80% N_2, 10% H_2, 10% CO_2). No attempt was made to sterilise the samples or leachate solutions. The samples were leached for a total of 16 weeks during which time 2 mL subsamples were removed from the centrifuge tubes at set

intervals, filtered through 0.2 μm filters and analysed for Fe by ferrozine colorimetry, and the pH and Eh of the leachate were also determined. 9 samples in each set were leached in duplicate. Following the leachate experiments, the remaining leachate was filtered and analysed for major cations by AA (except Na and Cl which were added to the sample in NaOH and HCl). The leached rock was washed with distilled water, dried and viewed using a Leica S440 SEM.

3.2.4 Geochemical modelling

Geochemical modelling was done using Phreeqc Interactive (Phreeqci) version 2.11.0.148 (Parkhurst and Appelo, 1999). Phreeqci is a computer program for performing low-temperature aqueous geochemical calculations, including speciation, saturation indices, batch reaction and 1-dimensional transport calculations. Phreeqci can account for aqueous, mineral, gas, solid solution, surface complexation and ion exchange equilibria, as well as kinetic reactions (Parkhurst and Appelo, 1999). Phreeqci is used here in conjunction with the Wateq4f thermodynamic database (Ball and Nordstrom, 1991). Saturation indices and pe values were calculated for the historical groundwater quality data, as well as the final leach extracts.

3.3 Results

3.3.1 Water chemistry

3.3.1.1 Field data

Results of field and laboratory chemical analysis of samples collected from boreholes during 2002 and 2003 are presented in Tables 3.3 to 3.6. The sample identifier is the borehole name followed by a number which represents the record number for that particular borehole in the historical groundwater quality database (Table A.1., Appendix A). pH is generally near-neutral but values as low as 3.6 were measured. The EC of the water ranged from 8.8 to 95 mS/m and the water is Na-Cl dominated, although borehole DP15 has high concentrations of SO_4. None of the DO concentrations were in equilibrium with atmospheric O_2 pressures, but the concentrations varied considerably (Table 3.3). Nitrate concentrations were generally at or below detection limits and have not been listed here.

Table 3.3. Field results and major ion data for water samples collected from boreholes in 2002/2003

Borehole	Year	T	DO	EC	pH	Na	Mg	Ca	K	Cl	SO_4	Si	TAL
		°C	mg/L	mS/m		mg/L	mg/L	mg/L	mg/L	mg/L	mg/L	mg/L	mg/L $CaCO_3$
CHS-1	2002	52.0	nd	19.6	6.8	16.3	2.8	10.0	8.9	32.0	5.3	18.5	nd
DG110-4	2002	nd	nd	18.9	4.8	20.8	3.4	3.6	1.7	nd	nd	4.8	nd
DL13-3	2003	16.6	7.5	95.0	7.5	173.1	40.1	37.3	26.4	nd	nd	3.1	nd
DL13-4	2002	24.7	<0.1	27.4	6.4	57.5	7.2	11.8	14.5	86.0	18.9	5.2	nd
DL16-6	2003	19.0	3.5	48.0	6.2	63.5	11.7	10.6	14.8	nd	nd	3.4	20.2
DL16-7	2002	22.8	0.6	52.2	6.3	54.4	8.5	13.7	14.7	90.6	18.9	5.6	nd
DL17-5	2003	20.3	4.5	56.6	7.2	62.2	17.2	17.8	17.1	nd	nd	3.3	nd
DL17-6	2002	22.5	<0.1	58.2	6.1	30.6	21.9	28.9	7.5	73.7	27.2	6.4	nd
DP15-3	2003	22.2	6.1	25.5	3.6	22.6	3.7	2.9	2.7	nd	nd	2.2	nd
DP15-4	2002	19.5	0.1	22.9	4.1	22.3	3.5	4.0	2.9	38.1	41.8	6.0	10.0
DP15-5	2002	18.5	2.7	19.8	4.3	22.9	3.6	3.7	2.9	34.6	38.2	6.0	10.0
DP28-6	2002	18.5	2.9	19.1	5.4	21.8	2.4	2.4	2.3	37.4	8.9	5.0	22.4
DP29-4	2003	20.8	1.5	18.4	6.7	25.3	3.8	4.3	3.4	nd	nd	1.8	16.8
DP29-5	2002	19.2	3.1	22.6	5.5	25.8	3.5	5.7	2.9	40.8	19.6	5.4	30.0
KG1-4	2003	21.5	3.2	43.9	6.1	44.7	10.8	11.7	10.1	nd	nd	1.0	24.3
KG1-5	2002	24.2	2.3	32.0	5.9	36.3	9.0	15.6	10.7	85.7	48.8	5.2	nd
Spring	2002	nd	nd	14.1	5.9	20.1	2.4	2.1	0.6	32.0	6.1	4.7	nd
VG3-4	2003	16.5	5.9	21.0	5.3	33.6	4.1	1.9	0.9	nd	nd	0.1	9.10
VRNotch-1	2002	nd	nd	19.1	6.0	29.1	3.4	2.6	0.4	42.4	8.9	5.6	nd
VR11-5	2003	16.7	0.5	27.1	6.2	nd	nd	nd	nd	nd	nd	nd	12.7
VR6-5	2003	16.1	<0.1	8.9	5.8	14.3	1.4	1.2	0.3	nd	nd	1.8	6.5
VR6-7	2002	nd	nd	10.0	4.3	11.8	1.3	1.6	0.7	21.8	1.8	4.1	nd
VR7-5	2002	nd	nd	8.8	4.2	10.5	1.2	1.6	0.5	18.8	1.5	4.1	nd
VR8-4	2002	nd	nd	9.4	3.7	8.4	1.0	1.3	0.5	17.3	2.4	4.3	nd

nd – no data

Iron concentrations measured in the field ranged from <0.01 to 18.4 mg/L. The iron concentration was found to decrease from the moment of sampling (Table 3.4, Figure 3.1). The decrease in concentration by almost 4 mg/L within an hour of sampling suggests that the time lag between sampling and filtering is critical, and may be one reason for the variability in iron concentrations in the historical groundwater quality data. Comparison of Fe measured in filtered samples compared to unfiltered samples show that up to 27% of the iron is removed by filtering (Table 3.5).

Table 3.4. Decay of iron concentration with time since sampling in borehole DL17

Time	Fe^{2+}	Fe^{T}	Time	Fe^{2+}	Fe^{T}
Min	mg/L	mg/L	Min	mg/L	mg/L
0	17.95	17.87	20	15.53	16.51
1	20.21	18.10	30	14.70	15.69
2	17.72	17.65	45	14.25	14.18
5	16.36	17.50	60	10.93	14.03
10	16.67	17.19			

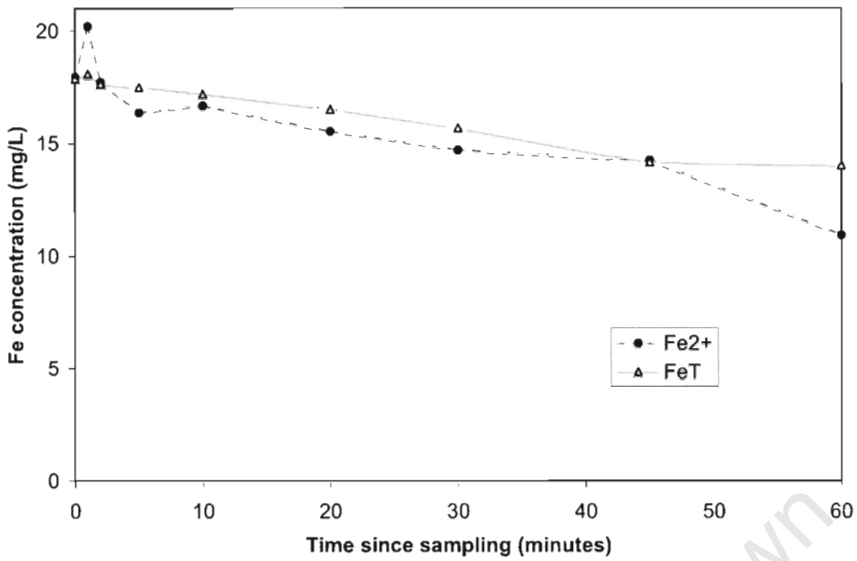

Figure 3.1. Decay of iron concentration with time following sampling from borehole DL17

Table 3.5. Filtered and unfiltered iron concentrations determined by colorimetry in the field and ICP-MS in the laboratory (all concentrations in mg/L)

Borehole	Year	ICP-MS	Field unfiltered		Field filtered		Fe^{2+}/Fe^{T} (Filt)	Fe^{T} filt / Fe^{T} unfilt	ICP-MS Zn (µg/L)
		Fe^{T}	Fe^{2+}	Fe^{T}	Fe^{2+}	Fe^{T}			
CHS-1	2002	0.87	0.69	1.11	0.65	0.83	0.78	0.75	nd
DG110-4	2002	8.89	nd	nd	nd	nd			23
DL13-3	2003	0.93	nd	nd	nd	nd			86
DL13-4	2002	3.56	5.39	6.55	4.53	4.79	0.95	0.73	23
DL16-6	2003	0.75	nd	nd	nd	nd			132
DL16-7	2002	0.26	5.41	5.97	5.01	6.12	0.82	1.03	24
DL17-5	2003	4.08	nd	nd	nd	nd			124
DL17-6	2002	13.03	12.29	14.25	10.75	14.12	0.83	0.91	73
DP15-3	2003	5.29	nd	nd	3.16	4.24	0.75		1715
DP15-4	2002	3.28	3.53	3.49	3.35	3.43	0.98	0.98	858
DP15-5	2002	2.94	2.80	3.28	2.80	3.10	0.90	0.94	980
DP28-6	2002	3.04	4.07	3.95	3.74	3.76	0.99	0.95	130
DP29-4	2003	1.26	nd	nd	1.39	1.67	0.83		71
DP29-5	2002	2.01	2.20	2.08	2.21	2.13	1.04	1.03	76
KG1-4	2003	5.37	nd	nd	nd	nd			302
KG1-5	2002	2.00	17.30	20.06	16.28	18.42	0.88	0.92	33
VG3-4	2003	<0.01	nd	nd	0.86	<0.01			58.4
VR6-7	2002	0.02	0.05	0.09	nd	nd			76
VR7-5	2002	0.01	<0.01	0.04	nd	nd			78
VR8-4	2002	nd	0.01	0.08	nd	nd			4

Stable isotope ratios are given in Table 3.6 and show little variation between boreholes. Duplicate analyses and analysis of external standards were used to quantify the error on the data. Uncertainties (precision plus bias) were generally high, possibly due to the low concentrations in the samples (Table B.1, Appendix B). A comparison of field and laboratory iron measurements is included in Table B.2 and Figure B.1. Because of the error on the analyses, the water chemistry measured during 2002 and 2003 were incorporated into the historical groundwater quality data to maximise the number of samples, thereby minimising errors in interpretation.

Table 3.6. Stable isotope results for boreholes sampled during 2002

Borehole	δD	$\delta^{18}O$	Borehole	δD	$\delta^{18}O$
DL13-4	-37	-6.8	**VR6-7**	-40	-7.4
DL17-6		-6.9	**VR7-5**	-42	-8.1
DP15-5	-42	-7.8	**DP28-6**	-42	-7.0
DP29-5	-45	-7.8	**KG1-5**	-39	-7.2
VR Notch-1	-43	-7.9	**DL16-7**	-40	-7.1

3.3.1.2 Historical groundwater chemistry data

The full historical groundwater chemistry dataset can be found in Table A.1, Appendix A, including samples collected and analysed during the current study. Water in the three aquifers is dominated by Na-Cl (Table 3.7). Charge balance values vary widely, but many of the samples lacked data for various elements, rendering the charge balance calculation useless. The data for each element were rather tested for normality within each aquifer group by the Shapiro-Wilks test using Statistica, a statistical computer package. All but temperature and dissolved oxygen data are normally distributed at the 99% confidence limit, and these two parameters are affected by their low n-value. The mean values of most chemical parameters from the Nardouw and Peninsula aquifers, namely EC, Na, Mg, Ca, Cl, SO_4, alkalinity, Si, K and Fe, are significantly different at the 95% confidence limit. The water in the Nardouw Subgroup and Bokkeveld Group has far more variable chemistry than the Peninsula Formation water, which has low standard deviations for most parameters.

Table 3.7. Average chemistry of the groundwater in TMG aquifers in the Klein Karoo region. Concentrations in mg/L unless otherwise stated.

	PENINSULA FORMATION						
	n	Mean	-95% CL	+95% CL	Min	Max	Std.Dev.
EC (mS/m)	77	11.8	10.3	13.3	2.6	48.5	6.5
pH	77				3.7	7.6	
Na	76	12.3	10.6	13.9	1.5	64.8	7.4
Mg	76	2.1	1.8	2.4	0.6	10.3	1.3
Ca	76	3.7	2.6	4.7	0.4	30.4	4.5
K	68	1.3	0.9	1.7	0.2	9.3	1.7
Cl	75	20.4	17.3	23.6	3.7	125.3	13.8
SO_4	70	8.0	5.2	10.8	1.0	96.9	11.7
Alkalinity	70	27.0	19.4	34.6	0.3	150.0	31.7
Si	72	4.4	3.7	5.1	0.7	15.5	2.9
Fe (µg/L)	18	270	84	459	50	1444	0.4
Al (µg/L)	2	40		486	2	73	0.1
Mn	24	0.3	0.1	0.5	<0.1	1.7	0.5
δD (‰)	50	-39.4	-41.9	-36.9	-52.7	-15.0	8.8
$\delta^{18}O$ (‰)	51	-6.76	-7.07	-6.46	-8.10	-3.6	1.1
DO	9	4.7	3.5	6.0	0.5	5.8	1.64
Temp (°C)	5	18.9	15.6	22.3	16.1	22.7	2.7
	NARDOUW SUBGROUP						
	n	Mean	-95% CL	+95% CL	Min	Max	Std.Dev.
EC (mS/m)	140	32.0	27.8	36.2	7.3	155.0	25.0
pH	140				3.1	8.3	
Na	140	33.5	28.1	39.0	7.2	232.8	32.6
Mg	140	6.5	5.3	7.7	1.0	43.1	7.0
Ca	140	9.9	8.0	11.9	0.9	73.4	11.8
K	133	5.9	5.0	6.9	<0.1	26.4	5.6
Cl	132	58.4	49.0	67.8	6.1	395.2	54.6
SO_4	128	31.2	20.5	42.0	3.0	548.0	61.5
Alkalinity	104	44.9	36.0	53.7	1.0	221.8	45.5
Si	124	6.0	5.3	6.7	0.1	21.4	4.1
Fe (µg/L)	58	5160	1960	8360	5.0	89100	12.2
Al (µg/L)	17	505	<1	1030	3.4	3670	1.0
Mn	63	1.4	1.1	1.8	0.1	7.2	1.4
δD (‰)	68	-42.2	-44.4	-40.0	-57.1	-19.0	9.1
$\delta^{18}O$ (‰)	70	-6.88	-7.13	-6.6	-8.10	-3.19	1.05
DO	28	2.6	1.9	3.3	0.1	7.0	1.8
Temp (°C)	22	21.7	18.5	24.9	15.0	52.0	7.2
	BOKKEVELD GROUP						
	n	Mean	-95% CL	+95% CL	Min	Max	Std.Dev.
EC (mS/m)	18	229.4	79.4	379.4	25.5	1350	301.7
pH	18				5.9	8.2	
Na	18	294.2	88.8	499.6	30.8	1792	413.1
Mg	18	69.4	9.8	129.0	4.1	533.0	119.8
Ca	18	126.6	53.7	199.5	2.9	662.0	146.6
K	18	9.5	5.1	13.9	0.8	31.7	8.8
Cl	18	509.2	88.6	929.7	51.0	3738	845.6
SO_4	18	310.9	59.0	562.8	5.6	2205	506.5
Alkalinity	18	272.2	169.2	375.2	12.7	764.4	207.2
Si	18	9.5	8.3	10.8	5.2	14.1	2.5
Fe (µg/L)	2	55.5		646.0	9.0	102.0	65.8
Al (µg/L)	1	59.0			59.0	59.0	
Mn	3	1.3			0.2	3.1	1.5
δD (‰)	2	-44.0			-49.5	-38.4	7.8
$\delta^{18}O$ (‰)	2	-6.28			-7.01	-5.55	1.03

There are a number of limitations to using data from varied sources. Firstly, no dataset contains the same selection of elements, for e.g. DO and Fe are not routinely measured. Secondly, sampling protocol and analytical methods used are not known for many of the data, in particular alkalinity, pH and iron. Alkalinity changes with time after sampling because the atmospheric concentration of CO_2 is lower than in the aquifer and the sample begins equilibrating with atmospheric pCO_2 by degassing immediately upon removal from the aquifer (Weaver, 1992). Degassing also affects the pH of the sample. Knowledge of whether alkalinity was determined in the laboratory or the field is required to have confidence in the alkalinity and pH data. Compounding this problem is uncertainty about the units of measurement. The unit used to report alkalinity in South Africa is generally mg/L $CaCO_3$ but some analysts use mg/L HCO_3^- and the actual unit used is often not stated. Samples for iron analysis require immediate filtering and analysis, or acidification for later analysis, to preserve the dissolved iron concentration in the water. During the 2002 and 2003 sampling trips, it was found that colloidal iron oxide material broken off from the clogged parts of the well was often collected in the sampling bottle. Without filtration, these particles could be included in analyses. The time period between collecting, filtering and acidifying the sample is also critical as was shown in the previous section (Figure 3.1). Pumping of fresh DO-poor water from the aquifer through the clogged screens and pump intakes may actually dissolve some iron from the encrustations. The range in concentrations of both alkalinity and iron in all three aquifers is large, probably in part due to different sampling and analytical protocols. Thirdly, few publications give any indication of the errors associated with the analyses. Finally, many of the boreholes were not adequately geologically logged, or logs have been lost, resulting in uncertainty about the origin of the waters. Waters may come from 2 or more separate aquifers, or only from one. It is virtually impossible to reconcile data with formations in hindsight.

The many limitations to the water chemistry data make it difficult to determine controls on iron distribution in the aquifer. Iron concentration, dissolved oxygen (DO) levels and alkalinity are a few of the most important parameters

in the understanding of cycling of iron within an aquifer, and the ones for which there is the least data. However, the major ion data can be used to gain an understanding of the regional chemistry of the aquifer and flow paths of groundwater.

3.3.1.3 Modelling results

Only historical groundwater quality samples with charge balances <10% (137 records) were used for Phreeqci modelling. Because of the poor alkalinity data, the average of all alkalinity records for the particular borehole was used in modelling calculations. Only 9 records with qualifying charge balance values had measured Al values, and aluminosilicate mineral saturation indices were calculated only from these samples. Saturation index calculations indicate that the system is closest to equilibrium with quartz and $Al(OH)_3$ (Table 3.8). The TMG groundwaters are on the whole undersaturated with respect to feldspar minerals and supersaturated with respect to kaolinite. Just 5 of all the records had measured both speciated iron and dissolved oxygen (DL16-7; DP15-5; DP29-5; KG1-5) allowing calculation of iron oxide saturation indices, and included only boreholes from the Nardouw Aquifer. The waters are closest to equilibrium with amorphous $Fe(OH)_3$ (Table 3.9), however there are few available datapoints.

Table 3.8. Saturation indices of some common silicate minerals for groundwaters of the TMG aquifer

Sample	Formation	pH	$Al(OH)_3$	Albite	Anorthite	Illite	Kaolinite	Quartz
DP28-7	TMG-N	4.1	-4.15	-8.04	-15.84	-8.40	-1.37	0.32
DP29-1	TMG-N	6.4	1.08	-0.52	-0.83	6.21	9.02	0.30
RF8	TMG-N	5.3	-1.37	-4.31	-8.35	-1.25	4.10	0.28
VG3-2	TMG-N	5.0	-2.31	-5.48	-10.87	-3.77	2.16	0.25
VG3-5	TMG-N	6.3	-0.50	-2.11	-4.48	2.19	5.94	0.34
VG3-6	TMG-N	5.4	-1.79	-4.36	-8.94	-2.06	3.30	0.31
YR2	TMG-N	5.6	-0.54	-2.90	-5.42	1.78	5.89	0.34
M-vnotch-3	TMG-S	6.1	0.20	-2.23	-3.85	2.77	6.98	0.15
VR Notch-4	TMG-S	6.5	0.82	-1.58	-1.98	4.39	8.05	0.07

Table 3.9. Saturation of TMG groundwaters with respect to some common iron minerals

Sample	pH	pe (Fe)	pe (DO)	Fe(2) µM	Fe(3) µM	$Fe(OH)_3$ SI	Gt SI	Ht SI	JarK SI	Mght SI	Mgt SI	Sid SI
DL16-7	6.3	5.53	14.20	89.7	19.9	2.38	8.19	18.38	0.66	8.15	19.00	-2.60
DP15-5	4.3	9.63	16.80	50.1	5.4	-0.08	5.58	13.13	-0.83	3.24	9.17	-3.38
DP29-5	5.5	-1.24	15.50	38.9	bdl	-7.23	-1.55	-1.12	-26.6	-11.07	-2.62	-1.88
KG1-5	5.9	6.07	14.60	292.0	37.6	2.25	8.11	18.23	2.21	7.90	18.61	-0.38
DP28-6	5.4	6.07	15.50	67.0	0.4	-0.12	5.59	13.16	-5.50	3.15	11.64	-2.12

Gt = goethite; Ht = haematite; JarK = K-Jarosite; Mght = maghemite; Mgt = magnetite; Sid = siderite

3.3.2 Aquifer lithology mineralogy and chemistry

3.3.2.1 Mineralogy

The TMG sedimentary rocks from the Kammanassie Mountains occur as three main lithologies: metaquartzites of the Peninsula and Skurweberg Formations, the more arkosic Goudini and Baviaanskloof Formations and shales of the Cedarberg and Bokkeveld Formations. Descriptions of mineralogy as determined by XRD and thin sections are given in Table 3.10. Microanalysis data from the electron microprobe and SEM were combined and are included in Table A.2, Appendix A. Photomicrographs are included in Figure 3.2.a-e and XRD scans in Appendix D.

The meta-quartzites are dominated by quartz with minor amounts of feldspar, muscovite and sericite in the Peninsula and Skurweberg Formations, while the arkosic Baviaanskloof Formation contains a significant amount of feldspar. The matrix of both rock types is very fine grained clay (Figure 3.2.a and b). A 7Å peak in many of the samples indicates that feldspar is weathering to kaolinite, and the 10Å peak of muscovite is present in all. The samples show varying degrees of recrystallisation in thin section, including annealing of quartz grains, microcrystalline quartz and crystalline muscovite (Figure 3.2 a, b, e.). The shale rocks are matrix supported and consist of small angular quartz grains in a very fine grained matrix of clay minerals. Cedarberg samples are dominated by large iron-rich chlorite grains (blue birefringence), which are sometimes associated with an opaque mineral, possibly ilmenite or magnetite (Figure 3.2.c).

Table 3.10. Description of rock samples collected from the Kammanassie Mountains used in leaching experiments

Sample	XRD mineralogy	Thin section description
B1	Quartz, feldspar, muscovite, kaolinite	Clast supported, angular fg quartz with sericitic matrix and muscovite leaves. Haematite veins with entrained quartz and muscovite
B2	Quartz, muscovite, feldspar	Matrix supported, dominance of sericitic matrix with no obvious Fe oxide veining. Mud clasts?
B4	Quartz, feldspar, muscovite, kaolinite	Recrystallised quartz and 30% rounded feldspar grains. Feldspar being weathered to kaolinite and Fe oxide.
B7	Quartz, K-feldspar, trace mica	Dominantly recrystallised quartz with minor amounts of matrix sericite and iron oxide. Significantly more Iron oxide between quartz grains in weathered edge.
S1	Quartz, trace muscovite, trace feldspar	Large intergrown quartz grains with traces of sericite between grains. Occasional larger clay particles – kaolinite/muscovite?
S2	Quartz, broad peak at 3.07 (pyrophyllite?)	Large intergrown quartz grains, more clay minerals between grains than S1.
G1	Quartz, muscovite, kaolinite, haematite, siderite?	Matrix supported quartzite with angular small quartz grains surrounded by sericite. Heavily banded with haematite stringers. Muscovite laths aligned with stringers.
G2	Quartz, trace mica	Clast supported, large rounded quartz grains with minor amounts of sericitic and iron oxide between grains.
C1	Quartz, muscovite, kaolinite	Matrix supported siltstone, weathered with overall red colouring, sericitic matrix, iron oxide bands
C2	Quartz, muscovite, chlorite, feldspar, siderite?	Vfg quartz grains (0.05 mm) in banded clay matrix with numerous muscovite laths. Also large rounded Fe-rich chlorite (0.2 mm) grains. Some chlorite intergrown with magnetite.
P1	Quartz, trace mica	Angular quartz grains (0.2-0.3 mm) with muscovite between grains. Occasional magnetite grains. At weathered edge muscovite is weathered to Fe oxide.
P3	Quartz	Intergrown quartz crystals (0.5 mm) with occasional feldspar(?) grains weathered to kaolinite. Magnetite and haematite stringers. Dark mineral inclusions – magnetite?

The metaquartzite rocks from the Skurweberg and Peninsula Formations have little obvious iron except for an unidentified opaque mineral which may be magnetite or ilmenite. However, these formations often have red weathered rims in the field, and in thin section this appears to be where iron in a matrix mineral has oxidised and reprecipitated as iron oxide between quartz grains (Figure 3.2.e). Microanalysis of matrix minerals in quartzites show that clay minerals have a measurable iron content, with muscovites containing 0.3 to 7.1 wt % Fe and chlorites containing 0.6 - 8.9 wt % Fe (Table A.2). Magnetic separation of Peninsula Formation rocks concentrated some muscovite and a 7Å peak, possibly due to an iron-rich chlorite (Scan MS, Figure D.1). Iron is more obviously present in finer grained rocks, e.g. G2, B1, B4 and B7 have thin stringers of an orange mineral, perhaps haematite or goethite (Figure 3.2.d). Haematite was only detected by XRD in sample G1. A single peak at 2.79Å in the XRD scan of C1, C2, G1 and B2 could be due to the presence of siderite, however this was not visible in thin section nor did the samples react to dilute acid.

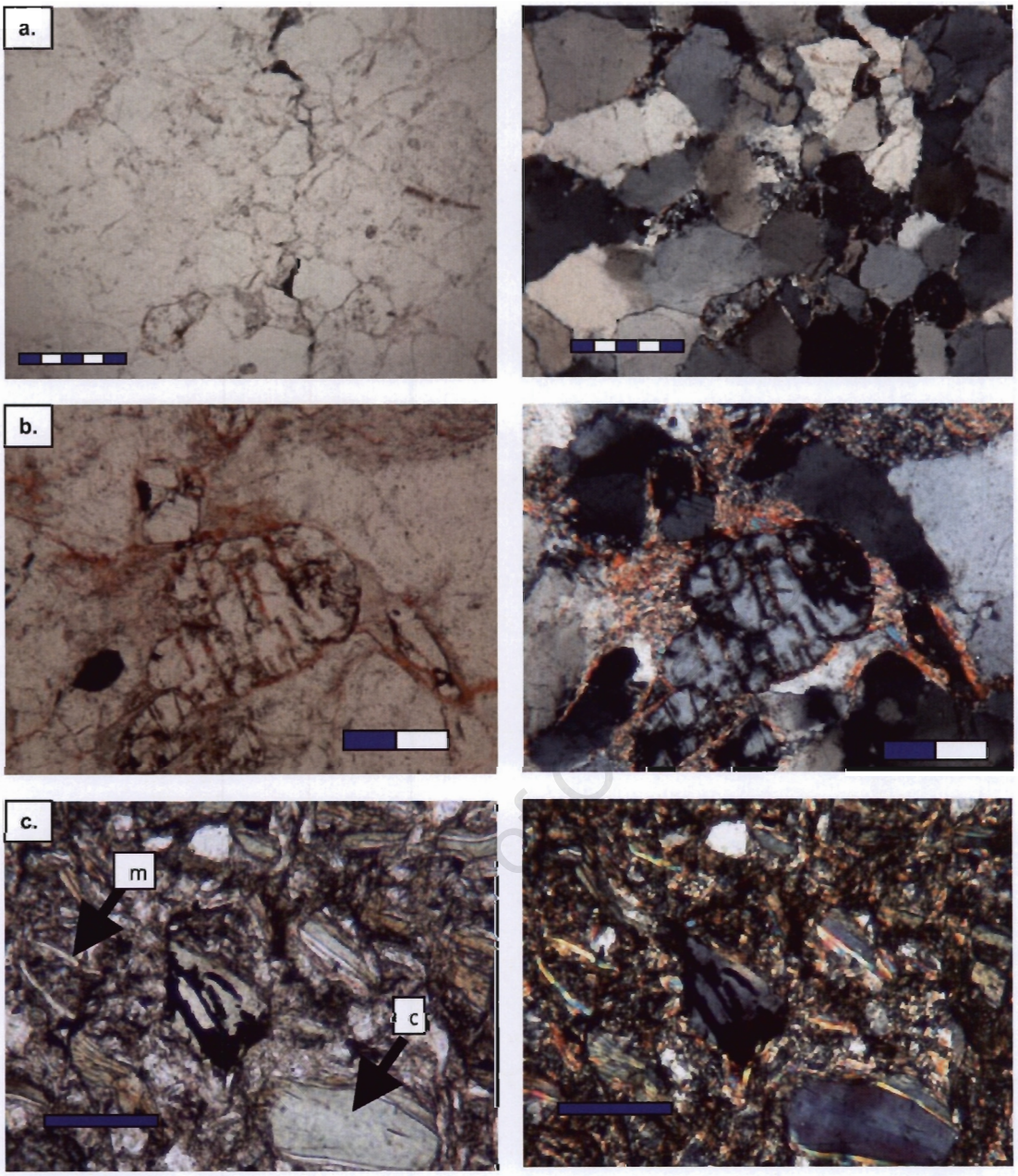

Figure 3.2. Photomicrographs of TMG aquifer rocks. Images on the right are under crossed nicols. Each segment on the scale bar represents 1 mm. a. Peninsula Formation (P3) quartzite showing quartz grain annealing, microcrystalline quartz and stringer of opaque mineral, b. Weathering feldspar grain in Baviaanskloof Formation (B4), showing iron oxide formation along twinning lamellae, c. Cedarberg Formation shale (C2) with large crystals of iron-rich chlorite (c), in some cases associated with opaque mineral. Matrix is sericitic with muscovite flakes (m).

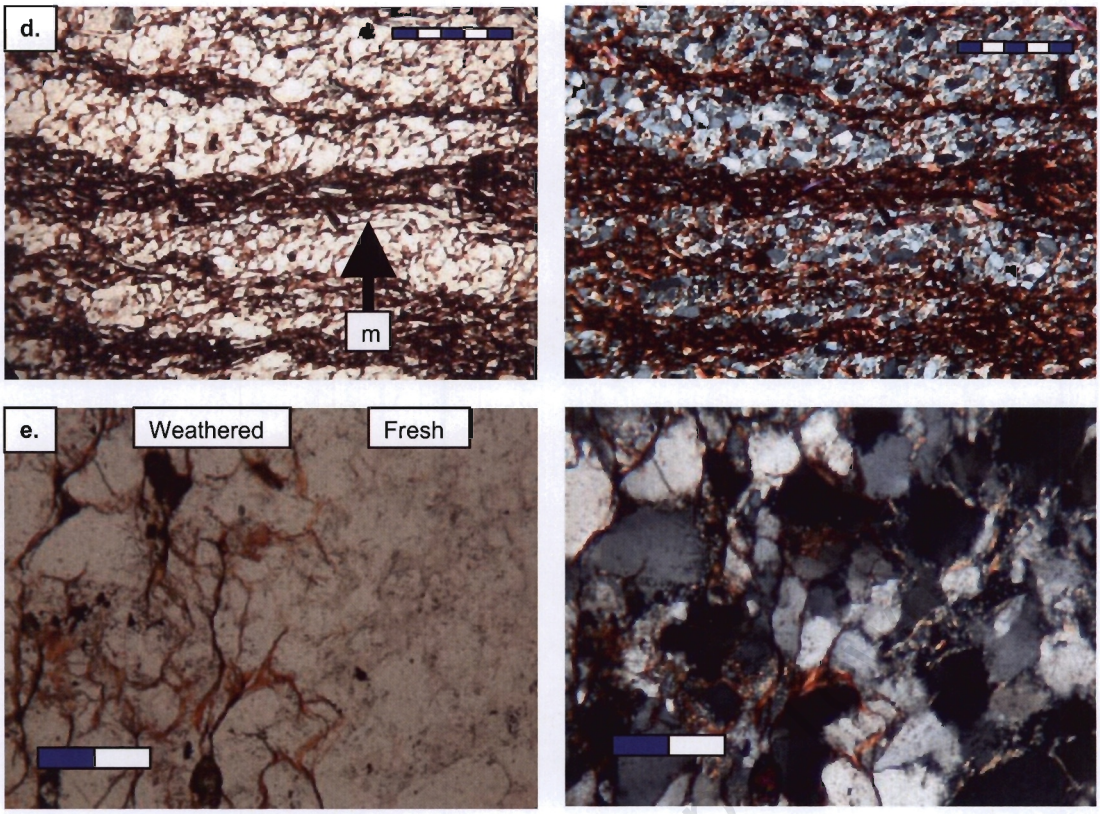

Figure 3.2. cont. Photomicrographs of TMG aquifer rocks. Images on the right are under crossed nicols. Each segment on the scale bar represents 1 mm. d. Iron oxide banding and associated muscovite (m) crystals in Goudini Formation (G1), e. Weathered rim of Peninsula Formation quartzite (P1) showing weathering of matrix minerals to release iron oxide minerals

3.3.2.2 Geochemistry

The average geochemistry of the TMG rocks reflects the mineralogy with a predominance of SiO_2 in the metaquartzitic rocks and significant amounts of Al and K due to aluminosilicate and clay minerals in the shales (Table 3.11). The full geochemical dataset is given in Table A.3 (Appendix A). The total carbon content of all the formations is low. The geochemistry of the rocks used in the leaching experiments is similar to the average rock chemistry for most samples (Table 3.12), although the Goudini Formation chemistry is quite variable. G1 is most similar in chemistry to the Cedarberg Formation, while G2 is more like the quartzitic Skurweberg and Peninsula Formations. The total amount of iron present in the rocks ranges from 49.0 mmol/kg to 854.3 mmol/kg, with highest concentrations in the shaly Cedarberg, Goudini (G1) and Bokkeveld rocks. The portion of iron in crystalline iron oxide phases is quite variable, whereas the amount present in amorphous iron phases is low and relatively constant across all samples. Mössbauer scans indicate that

most iron is present as Fe^{2+} in B4 and C2, and Fe^{3+} in P1 and G1. Although some of the Fe^{3+} is in haematite, the remainder is in an unidentifiable phase. The full Mössbauer report is given in Appendix C. Duplicate analyses of the total carbon, amorphous and oxide leaches can be found in Table B.3 and B.4 (Appendix B). The analyses were generally repeatable within 10 % relative standard deviation (RSD) although RSD > 10% where concentrations are low.

Table 3.11. Average chemistry of the TMG formations in the Kammanassie Mountains (all data except total carbon (TC) from Mitchell, 2005)

Average (wt. %)	Peninsula	Cedarberg	Goudini	Skurweberg	Baviaanskloof	Bokkeveld
SiO_2	96.21	61.74	80.01	96.31	90.94	69.48
Al_2O_3	1.83	17.86	9.62	1.86	4.87	15.25
TiO_2	0.13	0.89	0.60	0.16	0.17	1.06
Fe_2O_3	0.56	6.40	3.83	0.49	0.64	3.06
MnO	0.02	0.07	0.03	0.02	0.02	0.02
MgO	0.22	1.91	0.56	0.18	0.35	1.33
CaO	0.02	0.35	0.03	0.02	0.05	0.19
Na_2O	0.15	0.38	0.34	0.17	0.19	0.70
K_2O	0.45	4.67	2.63	0.30	1.48	4.86
P_2O_5	0.02	0.39	0.04	0.01	0.01	0.08
SO_3	0.01	0.01	0.01	<0.01	<0.01	0.01
Cr_2O_3	0.01	0.02	0.02	0.01	0.01	0.02
NiO	0.00	0.01	0.01	0.01	0.02	0.00
H_2O^-	0.05	0.56	0.09	0.05	0.12	0.69
LOI	0.31	4.23	1.81	0.34	0.90	3.22
Total	**99.98**	**99.49**	**99.60**	**99.93**	**99.78**	**99.97**
S (ppm)	7.73	60.69	79.66	64.61	34.07	258.30
TC	0.061	0.167	0.090	nd	0.136	0.088

Table 3.12. Chemistry of rock samples used in leaching experiments

	TC[a]	Al_2O_3	S	SA[b]	FeT[c]	FeA[d]	FeX[e]	Mossbauer		
	%	%	ppm	m^2/g	mmol/kg	mmol/kg	mmol/kg	$\%Fe_2O_3$	$\%Fe^{2+}$	$\%Fe^{3+}$
B1	-	13.82	4.1	6.71	423.3	11.9	231.5	-	-	-
B2	0.088	16.68	3.5	8.89	344.1	5.2	34.6	-	-	-
B4	0.093	6.18	49.8	1.39	74.6	19.5	27.5	bdl	60	40
B7	0.219	5.03	21.6	1.39	75.7	20.6	26.1	-	-	-
S1	-[f]	3.11	101.5	1.10	75.0	39.6	39.8	-	-	-
S2	-	1.67	1.6	1.23	53.7	36.0	50.0	-	-	-
G1	0.126	20.20	3.4	4.27	819.6	12.7	620.5	77	15	8
G2	0.057	1.06	136.9	1.50	83.6	23.3	92.6	-	-	-
C1	0.137	15.66	59.5	9.22	854.3	21.0	371.2	-	-	-
C2	0.177	19.03	29.1	6.38	807.1	20.7	77.4	bdl[g]	79	21
P1	0.073	1.27	426.4	1.48	49.0	32.6	46.3	16	44	40
P3	0.082	1.70	90.2	1.12	61.9	34.2	43.8	-	-	-

a. Total carbon, b. SA = surface area, c. determined by XRF, d. iron in amorphous oxide phases, determined by ascorbic acid extraction, e. iron in amorphous and crystalline oxide phases, determined by dithionite extraction, f. not done, g. below detection limits

3.3.3 Leaching experiment results

3.3.3.1 Leachate results with time

The chemistry of the leachate waters before buffering and degassing is given in Table 3.13. The organic fraction of the organic-rich water is thought to be fulvic acid dominated (Smit, 2002).

Table 3.13. Chemistry of natural leachate waters before buffering & degassing (concentrations in mg/L unless otherwise stated; some data from Smit, 2002)

	DL17		Organic	
	Average	Std dev	Average	Std dev
pH	6.5	0.6	3.9	0.2
EC (mS/m)	48.2	7.7	12.8	0.8
Na (mg/L)	43.9	2.2	14.5	1.0
K (mg/L)	15.9	2.1	0.6	0.1
Ca (mg/L)	22.1	0.2	1.4	0.4
Mg (mg/L)	13.2	0.2	0.6	0.5
Cl (mg/L)	91.6	6.7	26.3	3.5
SO_4 (mg/L)	23.4	4.1	2.6	0.5
Alkalinity (mg/L HCO_3)	37.0	8.9	0.5	0.3
DOC (mg/L)	<1		16	
Charge balance (%)	-8.7		2.4	

Raw iron concentration data in the leaches were corrected for the amount of solution removed from the centrifuge tube and recalculated normalised to the mass of rock used. Full data are given in Table A.4 and A.5 (Appendix A) and data quality in Table B.5 (Appendix B). Change in iron concentrations with time are given in Figures 3.3 to 3.8. The final equilibrium concentrations for all samples are summarised for aerobic conditions in Table 3.14 and for anaerobic conditions in Table 3.15. Results indicate higher iron concentrations at equilibrium under anaerobic conditions, ranging from 0.04 to 34.2 mmol/kg, compared to <0.01 to 2.49 mmol/kg under aerobic conditions. pH has little effect on iron concentrations under anaerobic conditions, but strongly affects iron concentrations in aerobic conditions. Iron is dominantly present as Fe^{2+}, except at pH 3 under aerobic conditions where Fe^{3+} dominates. Cations other than Fe are more strongly influenced by pH than by the presence or absence of oxygen. Leaches extracted in the presence of organics have marginally higher concentrations of iron under aerobic conditions but the amount of iron leached under anaerobic conditions is not affected by the presence of organic compounds.

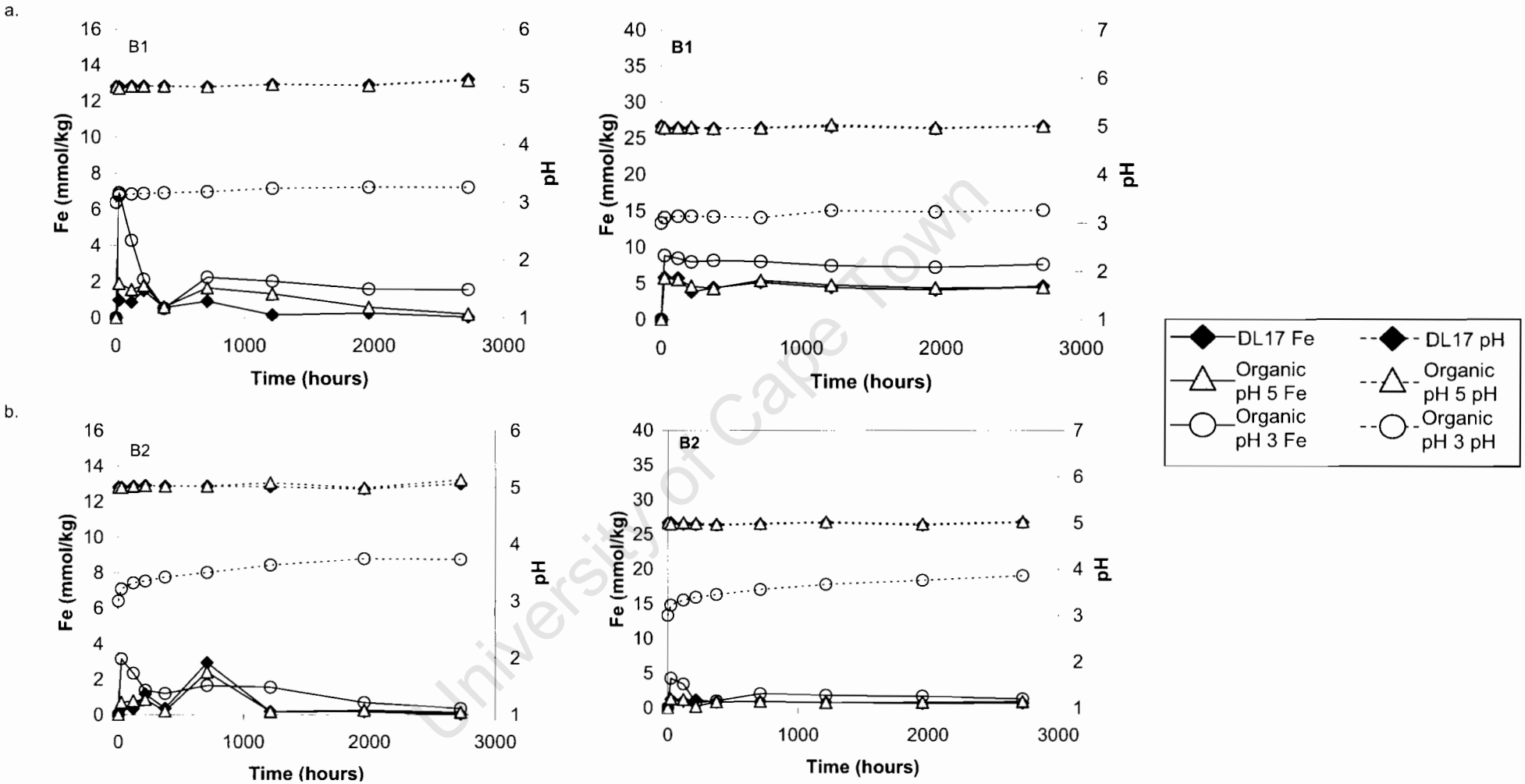

Figure 3.3. Iron release and change in pH with time in leaching experiments. Graphs on the left are under aerobic conditions and those on the right under anaerobic conditions. a. Sample B1, b. Sample B2

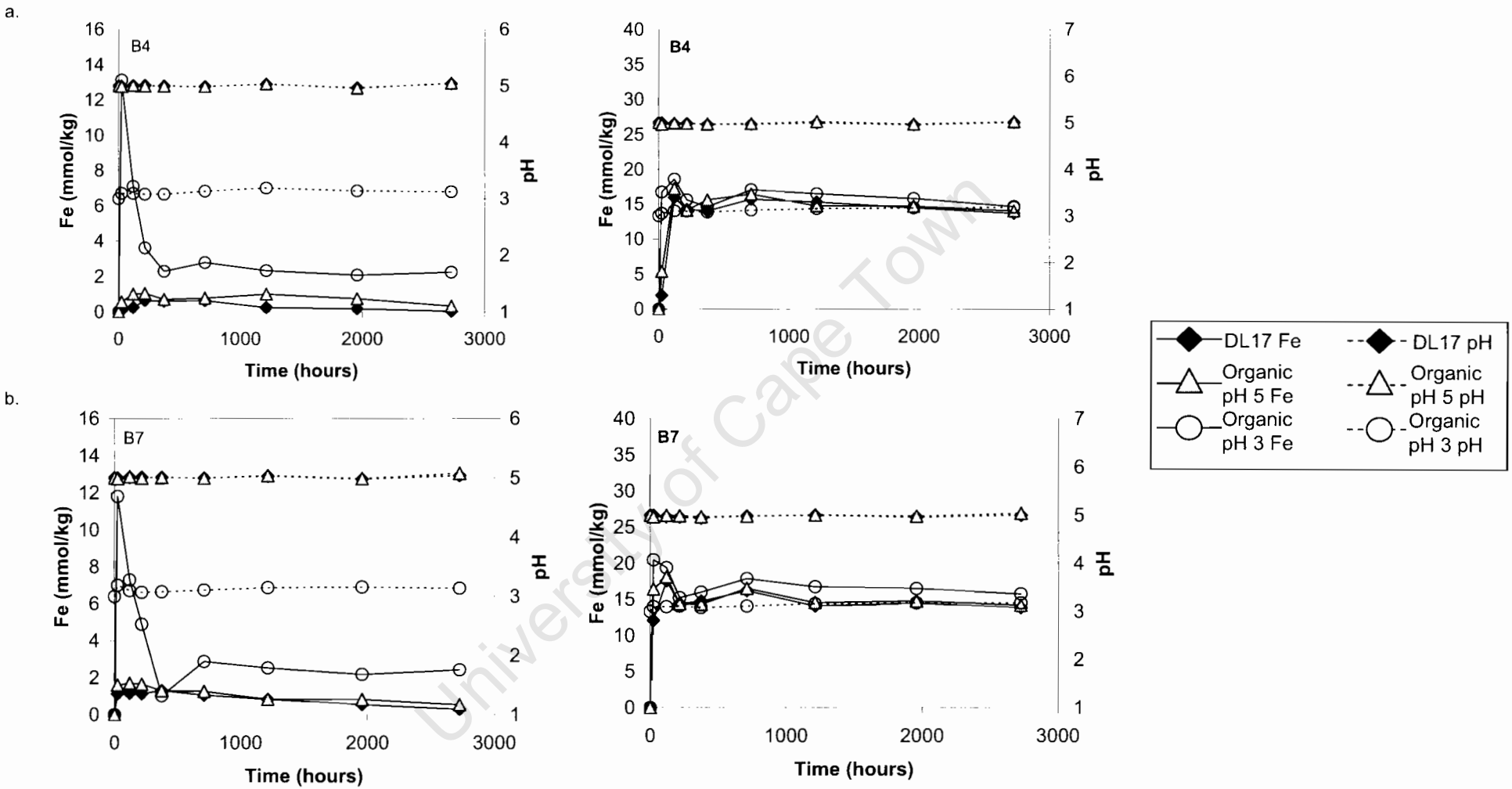

Figure 3.4. Iron release and change in pH with time in leaching experiments. Graphs on the left are under aerobic conditions and those on the right under anaerobic conditions. a. Sample B4 and b. Sample B7.

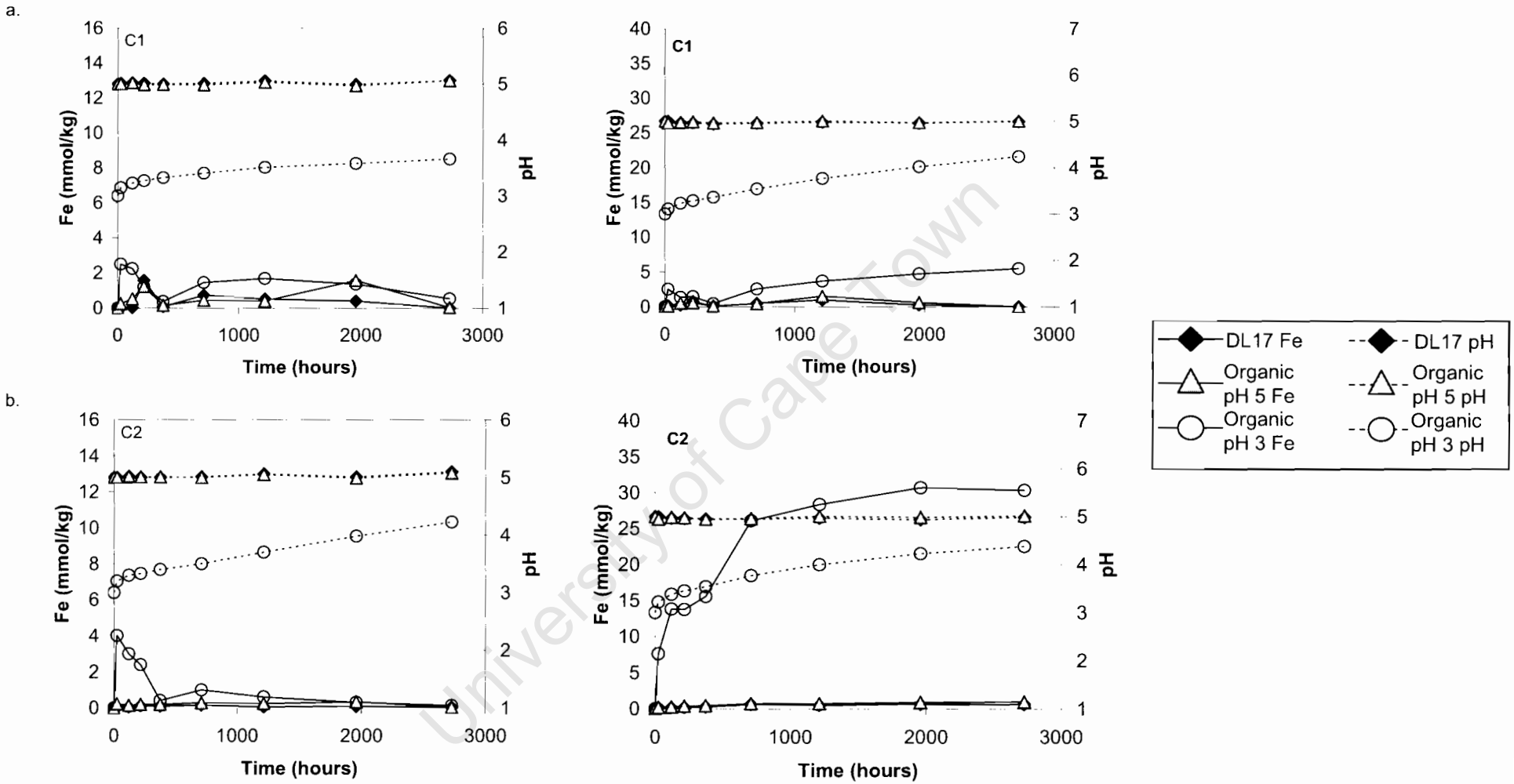

Figure 3.5. Iron release and change in pH with time in leaching experiments. Graphs on the left are under aerobic conditions and those on the right under anaerobic conditions. a. Sample C1, b. Sample C2

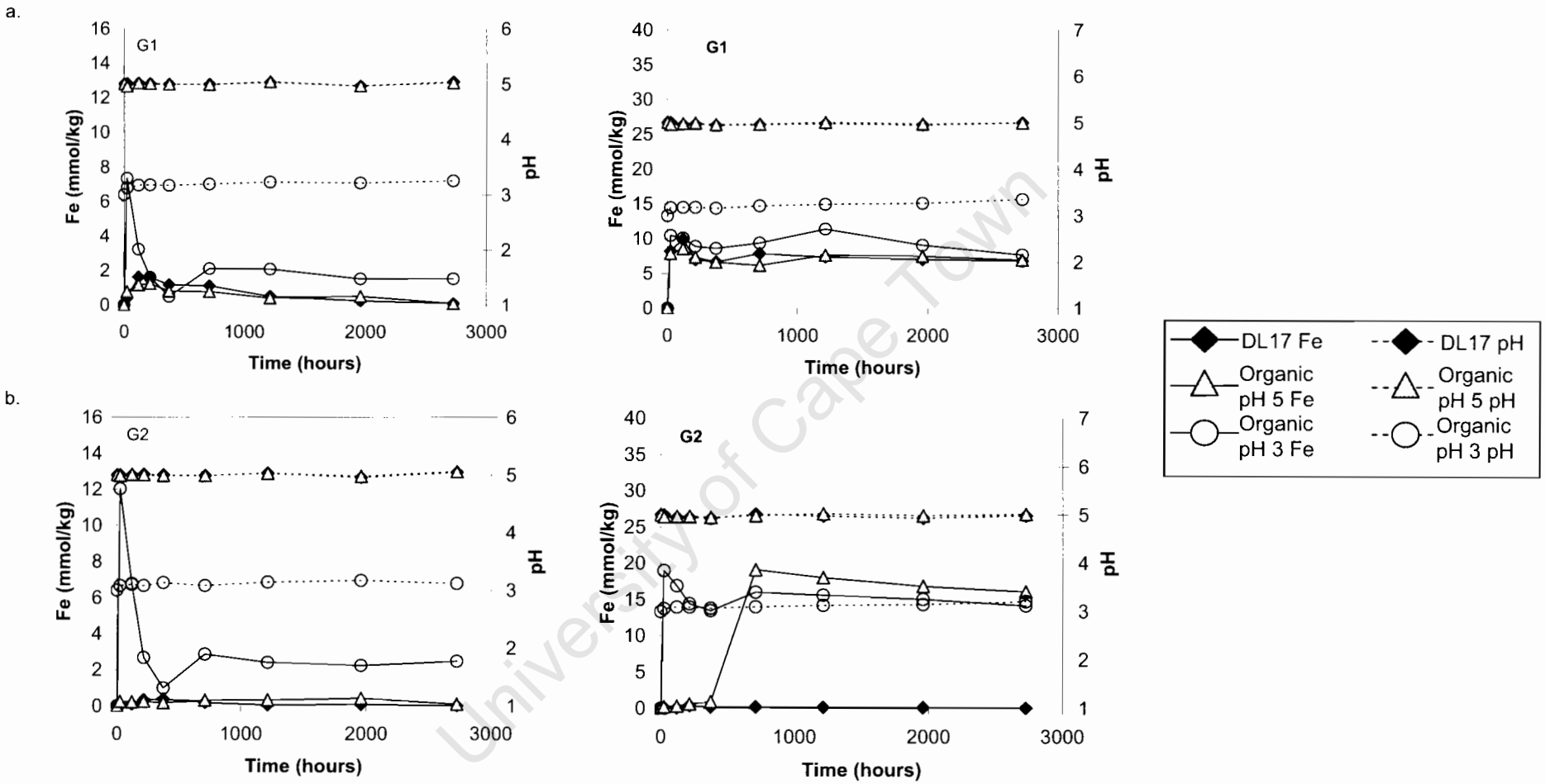

Figure 3.6. Iron release and change in pH with time in leaching experiments. Graphs on the left are under aerobic conditions and those on the right under anaerobic conditions. a. Sample G1 and b. Sample G2

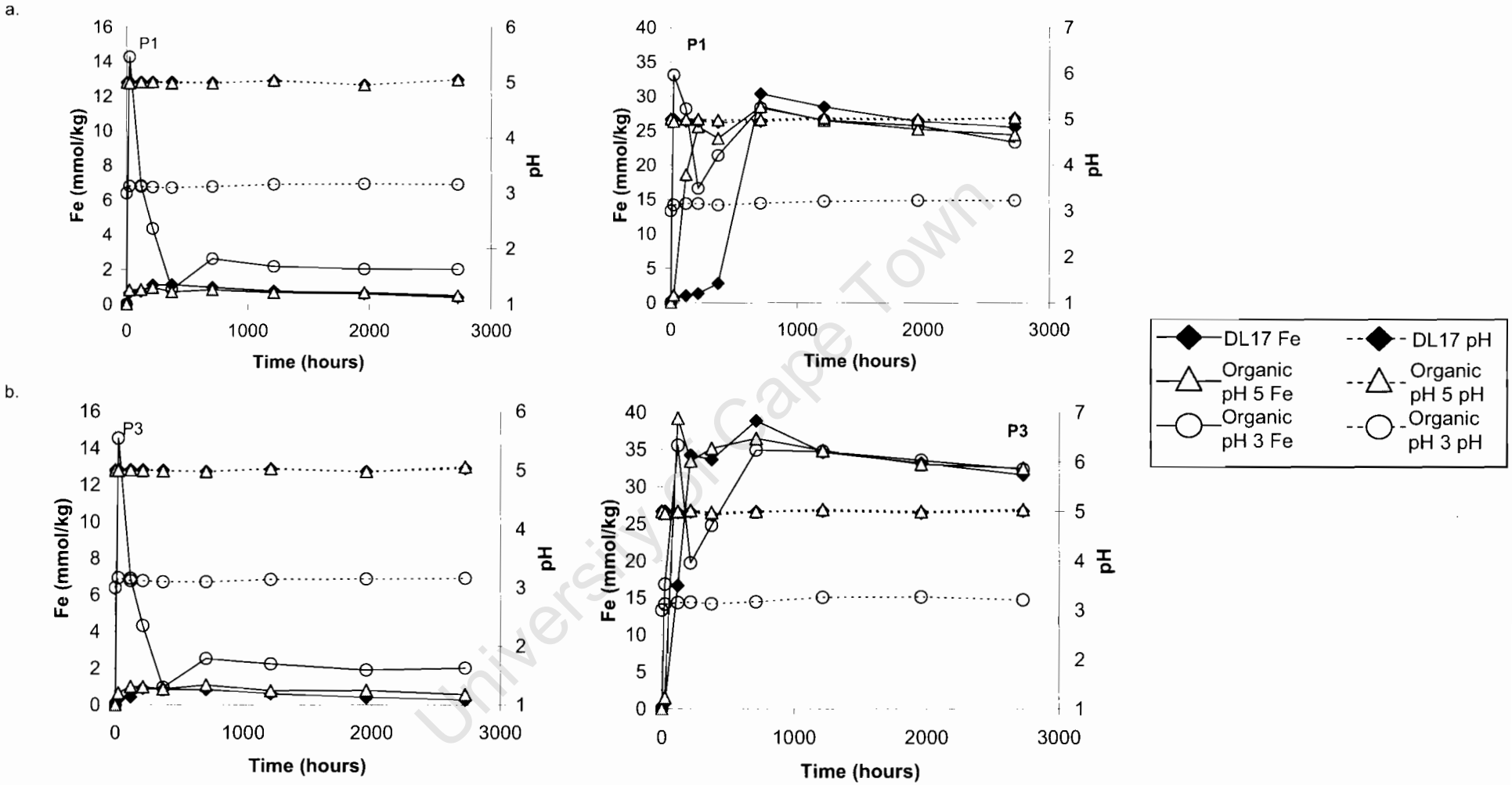

Figure 3.7. Iron release and change in pH with time in leaching experiments. Graphs on the left are under aerobic conditions and those on the right under anaerobic conditions. a. Sample P1, b. Sample P3

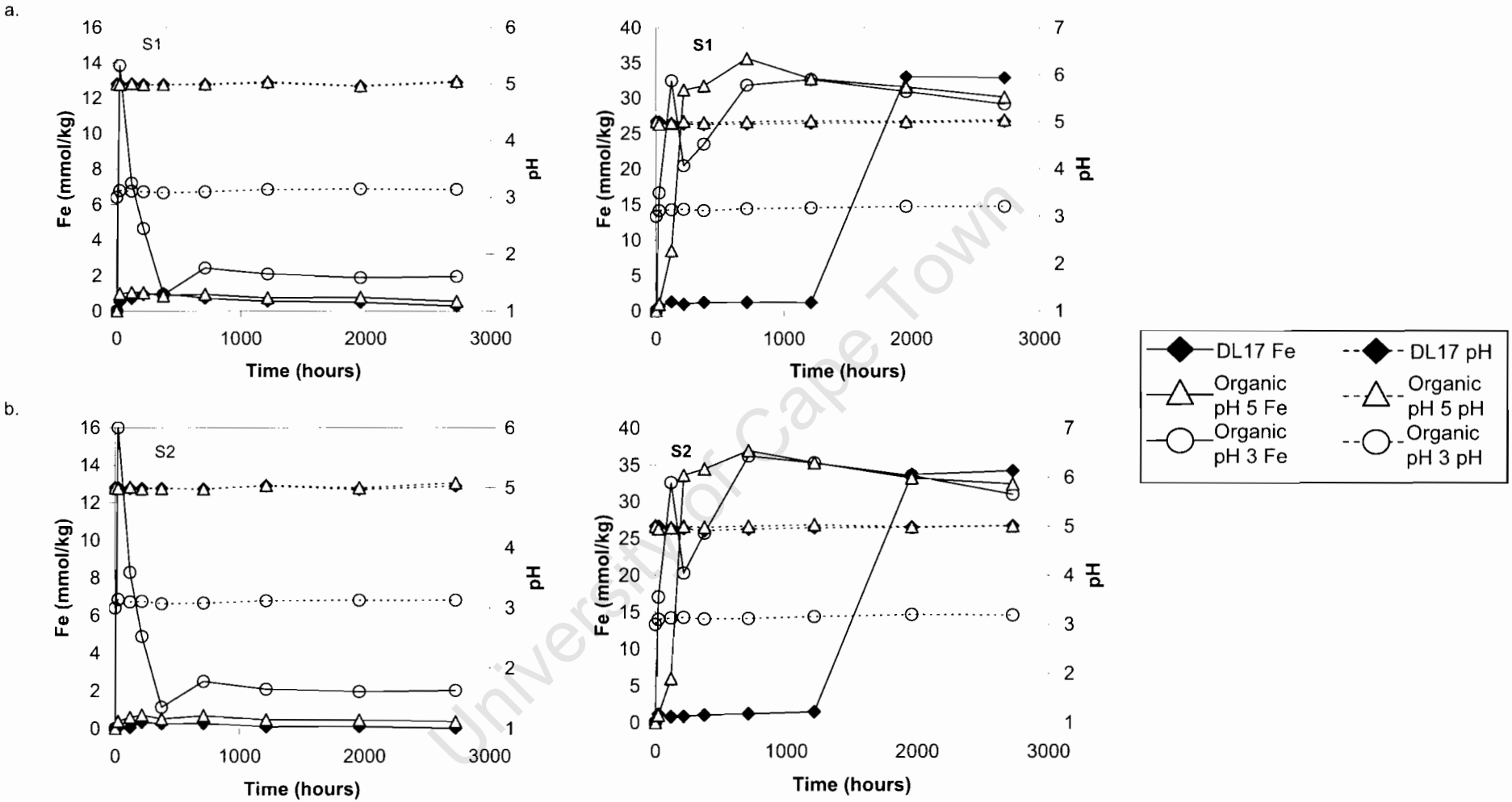

Figure 3.8. Iron release and pH change with time in leaching experiments. Graphs on the left are under aerobic conditions and those on the right under anaerobic conditions. a. Sample S1 and b. Sample S2

Table 3.14. Equilibrium concentrations (mmol/kg rock) of selected ions after 16 weeks in aerobic conditions

Organic pH 3	pH	pe	FeT	Fe^{2+}	Al	Si	K	Mg	Ca
Blank	3	-	0.19	-	0.05	2.03	bdl	0.59	1.00
B1	3.3	9.5	1.57	0.08	11.7	41.0	11.8	6.40	13.9
B2	3.7	8.8	0.35	0.09	9.56	74.3	23.8	50.5	22.5
B4	3.1	9.9	2.24	0.11	8.90	13.4	9.22	1.53	2.47
B7	3.1	9.4	2.43	0.15	8.10	13.2	8.04	1.70	3.54
S1	3.1	9.9	1.95	0.13	5.73	10.3	4.57	0.59	1.50
S2	3.1	10.1	2.02	0.13	11.8	7.56	4.89	1.97	2.21
G1	3.3	10.0	1.54	0.09	27.1	32.6	14.6	0.52	1.69
G2	3.1	10.0	2.49	0.10	7.55	13.0	6.25	1.42	1.85
C1	3.7	10.0	0.54	0.07	7.52	53.8	10.5	16.3	9.01
C2	4.2	9.1	0.15	0.07	2.19	63.4	7.24	8.49	1.77
P1	3.2	10.0	2.02	0.14	9.26	17.6	9.83	0.37	1.73
P3	3.2	10.2	2.00	0.22	6.14	12.0	6.17	2.05	1.66
Organic pH 5									
Blank	5.0	-	0.19	-	0.05	1.72	0.80	1.36	0.80
B1	5.1	8.7	0.21	0.21	1.43	14.2	10.2	7.55	11.7
B2	5.1	8.5	0.13	0.13	1.37	21.0	20.9	16.6	20.7
B4	5.1	8.7	0.33	0.32	1.60	7.35	5.77	3.50	2.10
B7	5.1	8.6	0.54	0.45	1.77	7.98	5.82	3.32	3.06
S1	5.1	8.7	0.55	0.46	1.70	7.68	4.10	2.69	1.26
S2	5.1	8.9	0.36	0.31	1.22	6.01	2.95	2.47	1.74
G1	5.0	8.9	0.09	0.14	1.57	12.4	11.9	2.99	1.33
G2	5.1	8.9	0.10	0.13	1.90	7.31	5.00	2.82	13.5
C1	5.1	9.0	0.04	0.12	0.97	6.82	7.98	9.38	8.08
C2	5.1	8.7	0.05	0.09	1.72	7.89	7.62	4.99	1.77
P1	5.1	8.7	0.50	0.37	2.23	10.4	6.42	1.82	1.61
P3	5.1	8.8	0.56	0.53	2.00	8.13	5.10	2.80	1.36
DL17 pH 5									
Blank	5.0	-	0.03	-	0.47	11.9	0.73	8.08	12.0
B1	5.1	8.5	0.05	0.15	0.83	18.7	21.2	-	-
B2	5.1	7.8	0.01	0.00	1.00	21.5	21.4	36.8	37.7
B4	5.0	8.5	0.04	0.10	1.7	12.9	19.0	26.6	19.6
B7	5.0	8.2	0.30	0.31	1.85	12.9	18.5	25.7	20.9
S1	5.0	8.7	0.29	0.30	0.37	12.0	16.8	25.3	19.0
S2	5.0	8.9	0.03	0.05	1.24	11.3	15.0	25.2	18.7
G1	5.0	8.7	0.10	0.16	1.61	17.9	24.2	14.1	19.1
G2	5.1	8.7	0.01	0.01	1.98	12.2	17.5	24.6	18.8
C1	5.1	8.8	0.01	0.04	0.64	12.1	18.4	18.2	23.4
C2	5.1	8.4	0.05	0.10	1.70	15.9	19.2	26.9	19.0
P1	5.1	8.7	0.40	0.36	2.31	16.4	18.6	26.5	19.2
P3	5.0	8.8	0.26	0.28	1.96	13.0	17.7	25.6	18.4

- = no data

Table 3.15. Equilibrium concentrations (mmol/kg rock) of selected ions after 16 weeks in anaerobic conditions

Organic pH 3	pH	pe	FeT	Fe^{2+}	Al	Si	K	Mg	Ca
Blank	-	-	0.19	-	0.05	2.03	0.80	0.59	0.75
B1	3.3	4.3	7.65	6.0	12.1	43.9	12.3	13.4	13.5
B2	3.9	3.5	1.32	1.25	6.09	79.3	24.3	45.7	22.8
B4	3.2	3.9	14.7	14.3	14.4	18.6	9.60	1.80	2.37
B7	3.2	5.3	15.8	15.0	12.8	15.7	10.4	1.90	3.50
S1	3.2	4.2	29.2	27.7	10.8	12.9	5.49	1.78	1.51
S2	3.2	3.0	31.0	31.2	7.0	8.67	4.22	2.65	1.95
G1	3.4	2.4	7.77	7.72	31.7	35.7	14.4	0.79	1.81
G2	3.2	4.1	14.2	12.2	9.36	12.7	7.65	1.88	1.71
C1	4.2	-1.6	5.50	5.36	2.62	74.3	12.	22.2	8.48
C2	4.4	-0.2	30.3	30.5	2.21	67.2	5.64	15.9	1.39
P1	3.2	4.1	23.3	23.8	19.2	21.1	8.94	1.56	1.72
P3	3.2	2.9	32.3	32.1	11.9	14.5	3.32	2.60	1.75
Organic pH 5									
Blank	-	-	0.19	-	0.05	1.72	0.80	1.36	0.80
B1	5.0	-3.5	4.46	4.67	0.74	16.3	9.69	9.42	12.1
B2	5.0	-3.3	0.93	0.94	1.10	18.5	10.8	17.8	7.92
B4	5.0	-3.4	14.1	14.1	8.20	7.72	8.11	4.06	2.24
B7	5.0	-3.4	14.2	14.3	1.72	7.17	5.68	3.50	3.12
S1	5.0	-3.5	30.2	30.4	1.51	9.47	4.19	3.20	1.42
S2	5.0	-3.5	32.4	32.6	1.12	6.26	2.92	3.33	1.89
G1	5.0	-3.5	7.01	7.10	1.25	13.3	11.6	3.45	1.65
G2	5.0	-3.5	16.1	16.4	1.64	6.11	5.75	3.61	1.73
C1	5.0	-3.5	0.04	0.05	0.79	7.46	8.43	11.4	8.21
C2	5.0	-3.5	0.98	0.99	1.55	8.81	7.81	5.03	1.49
P1	5.0	-3.5	24.4	24.6	2.11	11.4	6.73	3.30	1.39
P3	5.0	-3.5	32.5	33.0	1.52	10.2	6.12	3.53	1.43
DL17 pH 5									
Blank	-	-	0.03	-	0.47	11.9	0.73	8.08	11.5
B1	5.0	-3.5	4.64	4.66	0.87	20.0	20.6	30.5	29.6
B2	5.0	-3.4	0.72	0.70	0.91	22.0	19.6	35.7	37.8
B4	5.0	-3.5	13.7	13.9	1.40	13.7	17.8	24.6	18.5
B7	5.0	-3.5	13.9	13.9	1.70	12.3	16.3	23.2	18.8
S1	5.0	-3.4	32.9	33.1	1.84	16.1	16.5	28.5	19.4
S2	5.0	-3.5	34.2	34.7	1.18	13.1	14.9	24.8	18.0
G1	5.0	-3.5	6.89	6.92	1.49	17.4	26.7	25.7	18.6
G2	5.0	-3.4	0.06	0.04	1.74	12.3	18.0	24.6	18.8
C1	5.0	-3.4	0.04	0.03	0.62	12.9	19.1	31.0	23.8
C2	5.0	-3.4	0.63	0.63	2.16	14.9	19.2	26.5	18.7
P1	5.0	-3.5	25.5	25.7	2.36	17.1	18.1	26.0	18.0
P3	5.0	-3.5	31.6	27.5	1.77	15.8	17.6	26.4	19.5

- = no data

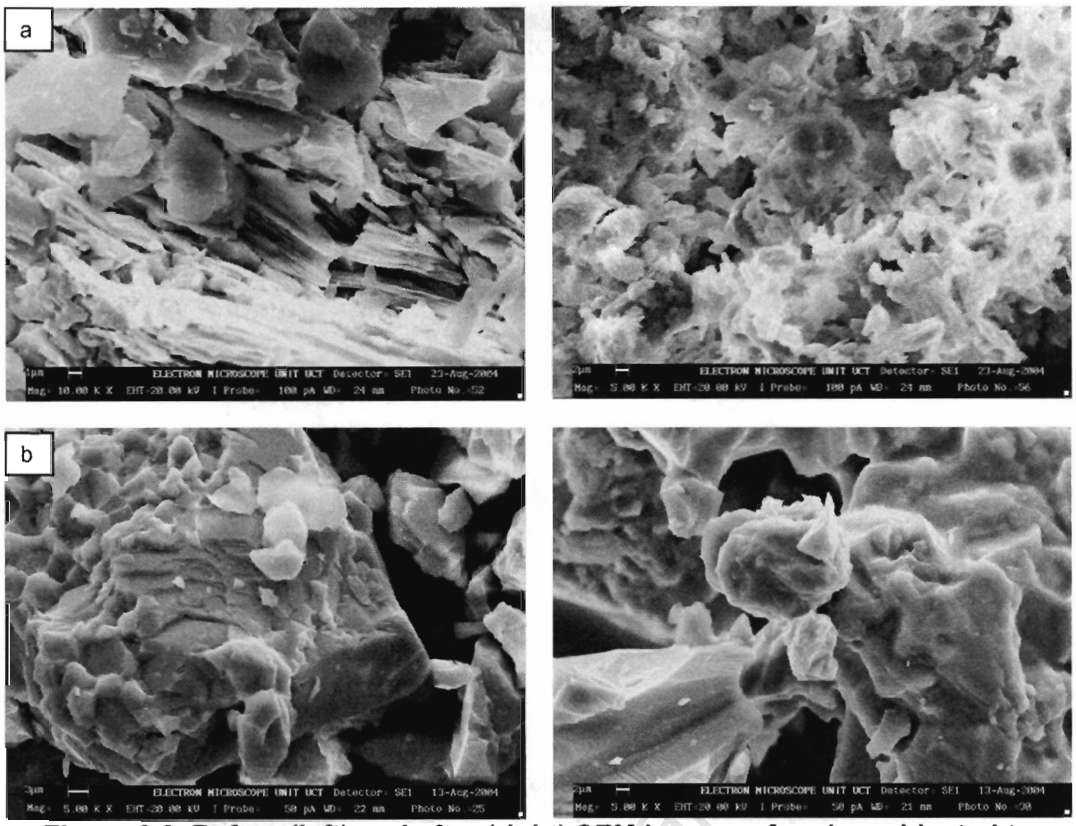

Figure 3.9. Before (left) and after (right) SEM images of rocks subjected to anaerobic leaching. a. C1 - note more rounded look to clay flakes and finer grained nature, b. B1 - slight rounding of quartz grain edges

The use of powdered rock samples for carrying out batch dissolution tests is problematic because of initial rapid dissolution of ultrafine particles and more reactive surface defects. The results obtained from the batch leaching tests on finely powdered rock cannot be directly extrapolated to the field situation where rock surface areas are significantly lower and reactions likely far slower (Brantley, 2003; Schnoor, 1990; Schott and Berner, 1983). Ions released during dissolution are not removed from the reaction site as they would be in an aquifer, and can precipitate on surfaces, preventing or limiting further reaction at that surface, such that the solution does not reach equilibrium with respect to the minerals present (Malmström *et al.*, 1996). Interpretation of the data can be complicated by the effect of buffer solutes in solution. Of the 192 duplicate analyses performed, 75% were found to have a relative standard deviation (RSD) of less than 10%. Only 12% of the duplicates exhibited a difference > 1 mmol/kg and just 4% were >2 mmol/kg different. SEM images of leached rocks reveal some rounding of mineral grains following 3 months of leaching (Figure 3.9) but on the whole there is little change.

3.3.3.2 Modelling results

Aerobic and anaerobic leachate solutions at pH 5 are close to equilibrium with respect to quartz, $Al(OH)_3$ and illite (Table 3.16). Aerobic leachates at pH 5 are at equilibrium with amorphous iron oxide but anaerobic leachates are closer to equilibrium with haematite, goethite and magnetite (Table 3.17). .

Table 3.16. Saturation index and speciation modelling for leach solutions under aerobic conditions

	pH	pe	Fe^{2+}	Fe^{3+}	$Al(OH)_3$	Ill.	K-m	Qtz	FeAm	Gt	Ht	Mgt	Pyt
Organic pH 3			µM	µM	SI	SI	SI	SI	SI	SI	SI	SI	SI
B1	3.3	9.5	48.6	0.3	-5.5	-10.3	-6.5	0.8	-3.2	2.6	7.1	1.2	-109.2
B2	3.7	8.8	10.0	0.0	-4.4	-6.2	-2.0	1.0	-3.4	2.4	6.8	0.9	-106.5
B4	3.1	9.9	66.3	0.5	-5.7	-12.8	-8.8	0.3	-3.1	2.7	7.4	1.4	-113.1
B7	3.1	9.4	71.1	0.2	-5.7	-13.0	-9.1	0.3	-3.6	2.2	6.4	0.5	-106.1
S1	3.1	9.9	57.9	0.4	-5.8	-13.9	-10.0	0.2	-3.1	2.6	7.3	1.2	-113.1
S2	3.1	10.1	56.3	0.7	-5.6	-13.7	-9.6	0.0	-3.0	2.8	7.6	1.6	-116.0
G1	3.3	10.0	43.2	0.6	-4.6	-8.9	-4.2	0.7	-2.6	3.2	8.4	2.6	-118.2
G2	3.1	10.0	71.7	0.7	-5.7	-13.2	-9.3	0.3	-3.0	2.8	7.7	1.7	-114.4
C1	3.7	10.0	15.5	0.8	-4.0	-5.8	-1.2	0.9	-1.8	4.0	9.9	4.5	-124.8
C2	4.2	9.1	4.60	0.2	-3.0	-2.9	2.3	1.0	-1.8	4.0	10.1	5.1	-120.6
P1	3.2	10.0	57.7	0.6	-5.2	-11.5	-7.1	0.4	-2.7	3.1	8.1	2.3	-117.3
P3	3.2	10.2	59.1	1.0	-5.4	-12.3	-8.2	0.3	-2.5	3.3	8.6	2.7	-120.1
Organic pH 5													
B1	4.9	9.2	3.80	2.3	-1.8	-2.0	4.4	0.3	0.0	5.8	13.6	9.7	-130.5
B2	4.9	9.0	2.90	1.1	-1.9	-1.1	5.2	0.5	-0.3	5.5	13.0	8.9	-127.9
B4	4.9	9.0	5.30	4.6	-1.1	-1.3	5.7	0.0	0.4	6.2	14.5	11.0	-131.2
B7	4.9	8.9	9.90	6.9	-1.1	-1.1	5.9	0.1	0.6	6.4	14.8	11.7	-129.4
S1	4.9	9.0	9.00	7.9	-1.0	-1.1	5.9	0.1	0.7	6.5	14.9	11.8	-130.8
S2	4.9	9.3	4.60	6.5	-1.3	-2.1	4.7	0.0	0.6	6.4	14.7	11.2	-134.2
G1	4.9	9.2	2.20	1.9	-1.3	-0.8	6.0	0.3	0.0	5.8	13.5	9.6	-132.5
G2	4.9	9.2	1.70	2.4	-1.0	-1.0	6.1	0.0	0.2	6.0	13.9	10.0	-134.3
C1	4.9	10.4	0.20	3.4	-1.4	-2.0	4.7	0.0	0.3	6.1	14.1	9.1	-151.3
C2	4.9	9.0	1.40	1.3	-1.1	-1.0	5.9	0.1	-0.1	5.7	13.3	9.3	-131.7
P1	5.0	9.0	7.60	7.1	-0.8	0.1	7.3	0.2	0.7	6.5	14.9	11.8	-131.7
P3	5.0	9.1	7.70	9.1	-0.8	-0.5	6.6	0.1	0.8	6.6	15.1	12.0	-133.2
DL17 pH 5													
B1	4.8	9.0	3.10	1.2	-2.2	-2.1	4.1	0.4	-0.3	5.5	13.0	9.0	-128.1
B2	4.8	8.3	0.30	0.0	-2.1	-1.5	4.6	0.5	-2.0	3.8	9.7	4.7	-119.3
B4	4.8	8.8	2.10	0.7	-1.3	-0.6	6.1	0.3	-0.5	5.3	12.7	8.6	-127.1
B7	4.9	8.5	7.50	1.3	-1.3	-0.5	6.2	0.3	-0.2	5.6	13.2	9.7	-122.3
S1	4.8	9.2	5.60	3.0	-2.2	-2.8	3.3	0.2	0.1	5.9	13.7	10.0	-130.3
S2	4.8	9.2	0.80	0.7	-1.5	-1.2	5.4	0.2	-0.5	5.3	12.5	8.1	-133.3
G1	4.8	9.0	2.90	1.6	-1.4	-0.1	6.6	0.4	-0.1	5.7	13.3	9.5	-129.7
G2	4.9	9.0	0.20	0.2	-1.0	0.2	7.1	0.2	-1.0	4.8	11.6	6.7	-132.6
C1	4.9	9.3	0.60	0.6	-1.7	-1.5	5.0	0.3	-0.5	5.3	12.6	8.0	-134.5
C2	4.9	8.7	2.00	0.8	-1.1	0.2	7.0	0.3	-0.3	5.5	13.0	9.1	-127.6
P1	5.0	9.0	5.60	4.9	-0.8	1.1	8.1	0.4	0.5	6.3	14.6	11.2	-132.1
P3	4.9	9.1	4.70	3.3	-1.1	-0.1	6.7	0.3	0.2	6.0	14.0	10.4	-131.9

Ill = illite; K-m = K-mica; Qtz = quartz; FeAm = Amorphous Fe(OH)3; Gt = goethite; Ht = haematite; Mgt = magnetite; Pyt = pyrite

Table 3.17. Saturation index and speciation modelling for leach solutions under anaerobic conditions

	pH	pe	Fe^{2+}	Fe^{3+}	$Al(OH)_3$	Ill.	K-m	Qtz	FeAm	Gt	Ht	Mgt	Pyt
Organic pH 3			µM	µM	SI	SI	SI	SI	SI	SI	SI	SI	SI
B1	3.3	4.3	216	0.0	-5.5	-10.4	-6.7	0.8	-7.8	-2.0	-2.0	-7.2	-35.7
B2	3.9	3.5	38.5	0.0	-4.0	-5.0	-0.5	1.1	-7.5	-1.7	-1.5	-6.3	-34.9
B4	3.2	3.9	420	0.0	-5.2	-11.2	-6.9	0.4	-8.0	-2.2	-2.4	-7.5	-30.0
B7	3.2	5.3	444	0.0	-5.2	-11.6	-7.3	0.3	-6.6	-0.8	0.4	-4.6	-49.6
S1	3.2	4.2	844	0.0	-5.3	-12.2	-8.0	0.3	-7.4	-1.6	-1.2	-6.0	-33.9
S2	3.2	3.0	898	0.0	-5.5	-13.2	-9.2	0.1	-8.6	-2.8	-3.6	-8.3	-17.1
G1	3.4	2.3	220	0.0	-4.3	-7.8	-2.9	0.7	-9.3	-3.5	-5.0	-9.9	-11.7
G2	3.2	4.1	403	0.0	-5.4	-12.2	-8.1	0.3	-7.8	-2.0	-2.1	-7.1	-32.7
C1	4.2	0.6	171	0.0	-3.0	-2.4	2.8	1.1	-8.8	-3.0	-4.0	-7.4	0.7
C2	4.4	0.7	1015	0.0	-2.5	-1.4	4.0	1.0	-7.4	-1.6	-1.2	-3.5	-2.7
P1	3.2	4.1	691	0.0	-5.0	-10.5	-6.1	0.5	-7.6	-1.8	-1.6	-6.4	-33.9
P3	3.2	2.9	922	0.0	-5.2	-11.8	-7.7	0.3	-8.7	-2.9	-3.8	-8.4	-16.8
Organic pH 5													
B1	4.8	-0.3	136	0.0	-2.4	-3.0	3.0	0.4	-8.2	-2.4	-2.8	-5.3	5.4
B2	4.8	-0.2	28.1	0.0	-2.3	-2.4	3.5	0.5	-8.8	-3.1	-4.2	-7.5	4.1
B4	4.9	-0.6	394	0.0	-0.4	0.5	8.0	0.0	-7.3	-1.5	-1.1	-2.6	5.7
B7	4.9	-0.5	413	0.0	-1.3	-1.9	4.9	0.0	-7.5	-1.7	-1.3	-3.0	5.6
S1	4.8	-0.5	939	0.0	-1.4	-1.6	5.1	0.2	-7.1	-1.4	-0.7	-2.1	6.3
S2	4.8	-0.5	928	0.0	-1.6	-3.0	3.5	-0.1	-7.2	-1.4	-0.8	-2.3	6.2
G1	4.8	-0.5	210	0.0	-1.5	-1.1	5.6	0.3	-7.8	-2.0	-2.0	-4.0	5.6
G2	4.8	-0.5	448	0.0	-1.4	-2.4	4.5	-0.1	-7.4	-1.7	-1.3	-3.0	6.0
C1	4.8	-0.5	1.40	0.0	-1.8	-2.7	3.7	0.0	-10.0	-4.2	-6.5	-10.7	3.4
C2	4.9	-0.5	32.6	0.0	-1.3	-1.1	5.7	0.2	-8.6	-2.8	-3.5	-6.3	4.9
P1	4.9	-0.6	706	0.0	-1.1	-0.6	6.3	0.2	-7.3	-1.5	-1.0	-2.4	6.1
P3	4.8	-0.6	924	0.0	-1.3	-1.4	5.4	0.1	-7.2	-1.4	-0.8	-2.2	6.1
DL17 pH 5													
B1	4.8	-0.3	134	0.0	-2.3	-2.2	3.8	0.5	-8.2	-2.4	-2.8	-5.3	5.4
B2	4.8	3.8	20.6	0.0	-2.3	-1.9	4.0	0.5	-4.8	1.0	3.9	0.6	-53.8
B4	4.8	-0.5	423	0.0	-1.4	-0.7	5.9	0.3	-7.5	-1.7	-1.5	-3.2	5.9
B7	4.9	-0.5	436	0.0	-1.3	-0.4	6.3	0.3	-7.5	-1.7	-1.4	-3.1	5.9
S1	4.8	-0.5	924	0.0	-1.3	-0.4	6.2	0.3	-7.2	-1.4	-0.8	-2.2	5.9
S2	4.8	-0.5	1069	0.0	-1.6	-1.1	5.4	0.3	-7.2	-1.4	-0.8	-2.2	6.2
G1	4.8	-0.5	200	0.0	-1.4	-0.2	6.4	0.4	-7.8	-2.1	-2.1	-4.2	5.6
G2	4.9	-0.5	1.10	0.0	-1.3	-0.6	6.1	0.2	-10.1	-4.3	-6.6	-10.9	3.0
C1	4.8	-0.4	1.10	0.0	-1.9	-1.8	4.5	0.3	-10.2	-4.4	-6.8	-11.2	2.9
C2	4.9	3.7	17.6	0.0	-1.2	-0.1	6.7	0.3	-4.6	1.2	4.3	1.2	-54.6
P1	4.9	-0.6	758	0.0	-1.0	0.6	7.4	0.4	-7.3	-1.5	-1.0	-2.4	6.1
P3	4.9	-0.6	793	0.0	-1.2	-0.1	6.6	0.4	-7.3	-1.5	-1.0	-2.4	6.0

3.4 Discussion

3.4.1 Major ion hydrochemistry

3.4.1.1 Controls on the major ion chemistry of the TMG aquifers in the Klein Karoo

In the Klein Karoo wellfield, boreholes in the Nardouw Subgroup are most affected by iron clogging (Jolly and Engelbrecht, 2001). Understanding the

controls on the groundwater chemistry of the Nardouw aquifer may help to understand reasons for the encrustation. Groundwater chemistry is determined by the chemistry of the recharge water i.e. precipitation, and the addition of solutes along a flow path by weathering reactions (White, 2003; Parkhurst and Appelo, 1999; Garrels and Mackenzie, 1967).

The pH of the groundwater in the Peninsula and Nardouw aquifers ranges from 3 to 9, and is indistinguishable between the two aquifers (Figure 3.10a). Weathering, biochemical and redox reactions would all be expected to affect the pH of the water. Low pH in waters from the TMG is normally associated with organic acids, although oxidation of pyrite known to be present in certain formations can also lead to a decrease in pH (Meyer, 2001). Strikingly, only water with Cl < 1.5 mmol/L has pH < 5.5, suggesting that increased buffering is associated with increased Cl concentrations, perhaps due to the presence of clay-rich shale formations formed in a marine system. The buffering effect may distinguish groundwater sourced from arkosic Baviaanskloof and Goudini Formations, from groundwater residing in the more quartzitic Skurweberg Formation. The relationship between buffering and higher clay contents is supported by observation of the increase in pH with time in a number of the pH 3 leachates (C1, C2 and B2) indicating that buffering is occurring (Figure 3.3-3.8). The change in leach pH was greatest in samples with the highest Al contents, i.e., those with higher concentrations of aluminosilicates, which react with hydrogen ions (Drever, 1997):

$$2KAlSi_3O_8 + 9H_2O + 2H^+ = Al_2Si_2O_5(OH)_4 + 2K^+ + 4H_4SiO_4 \quad (3.2)$$

An alternative buffering reaction is the hydrolysis of Al within aluminosilicates (McBride, 1994):

$$nH^+ + >Al\text{-}OH_2]^{-1/2} = Al^{3+} + H_2O \quad (3.3)$$

Al hydrolysis reactions buffer solution pH between 4.97 and 5.7 (McBride, 1994).

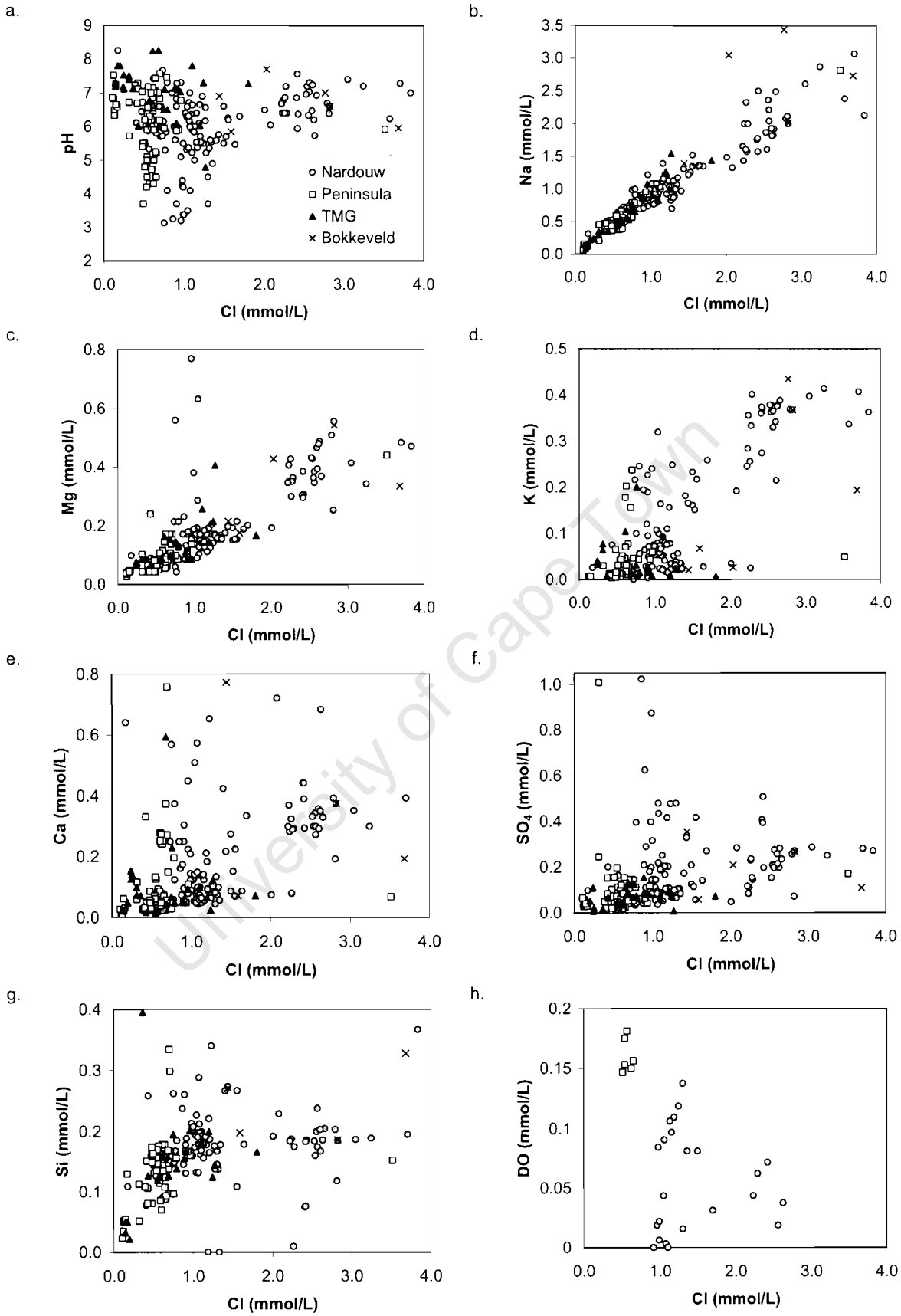

Figure 3.10. Relationship of groundwater parameters to Cl concentration. a. pH, b. Na, c. Mg, d. K, e. Ca, f. SO_4, g. Si, h. DO. TMG labelled samples are those for which the formation of origin is not known.

Plots of ions against conservative Cl can reveal relationships between the water in the different aquifers. Na behaves as conservatively as Cl in the aquifers, and there is a clear trend from the Peninsula into the Nardouw aquifer (Figure 3.10b). The slope of the Na-Cl relationship is 0.53 in the Peninsula aquifer, 0.56 in the Nardouw aquifer and 0.66 in the Bokkeveld aquifer. The ratio of Na:Cl in seawater is 0.56, similar to the ratio observed in the Peninsula and Nardouw aquifers, due to recharge by marine signature rainfall. Mg demonstrates a similar relationship with Cl, and the calculated slopes of 0.08 and 0.11 for the Peninsula and Nardouw aquifers agree well with the ratio of 0.07 in seawater (Figure 3.10c). Na and Cl were not measured in the leach extracts.

Relationships of Ca, SO_4 and K to Cl in groundwaters show a lot of scatter, more so in the Nardouw aquifer than the Peninsula aquifer (Figure 3.7d-f). The scatter in the Nardouw data reflects the greater variability in the chemistry and mineralogy of the Nardouw aquifer rocks compared to the Peninsula aquifer rocks. Concentrations of K are likely controlled by equilibrium with aluminosilicate minerals, such as illite. Above pH 6, the groundwater is in equilibrium with $Al(OH)_3$ and illite (Figure 3.11a). Below pH 5.5, the solution is undersaturated with respect to these minerals. pH 5.5 corresponds to the lower limit of the buffering range noted above for waters with Cl concentration above 1.5 mmol/L. The lack of equilibrium with respect to aluminosilicate minerals below pH 5.5 confirms the buffering effect of clay minerals in the aquifers, however, there are few datapoints. The relationship between pH and K (Figure 3.11b) supports the proposed buffering reactions as low pH waters contain only low concentrations of K, whereas K-liberating clay weathering reactions result in pH values above 5.5 (See Reaction 3.2).

a.

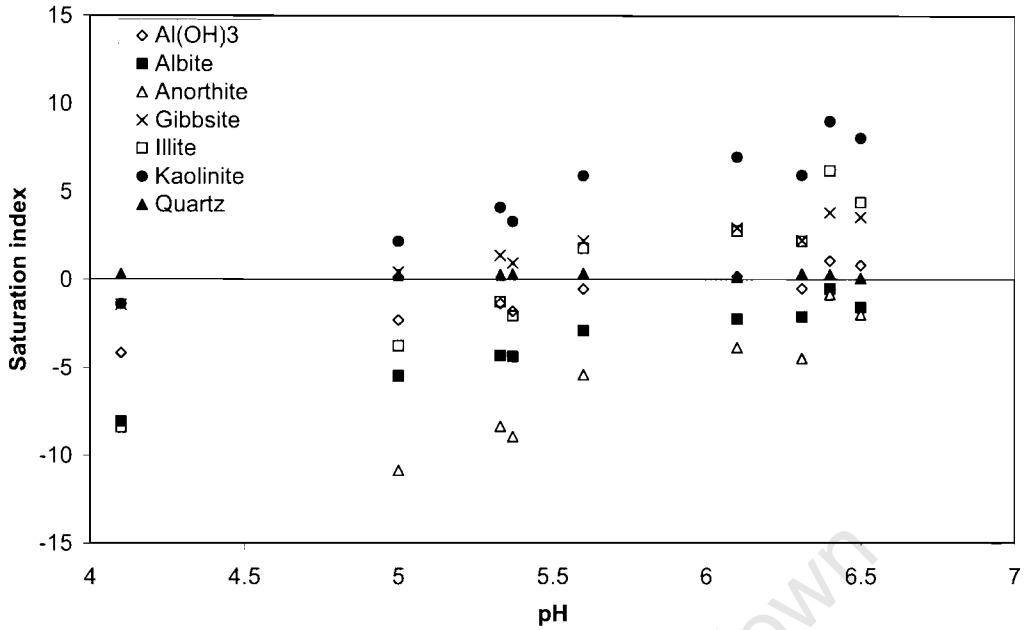

b.

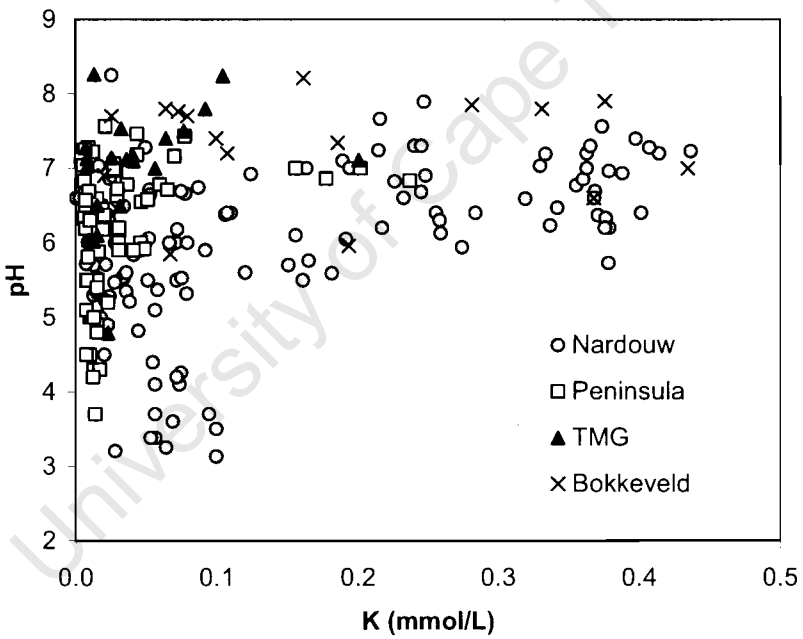

Figure 3.11. a. Saturation indices of common aluminosilicates in groundwater as calculated from the historical groundwater quality dataset, b. Relationship between K and pH in the groundwater

K, Mg and Ca were also measured in the final extract from the leaching experiments, and found to be highest in the pH 5 DL17 leachate. DL17 is drawn from a well in the KKRWSS and has much higher blank concentrations than the organic leachate. The greatest increase in concentrations of K, Mg and Ca from the blank to the final extract are in the Cedarberg and Bokkeveld Formation leaches.

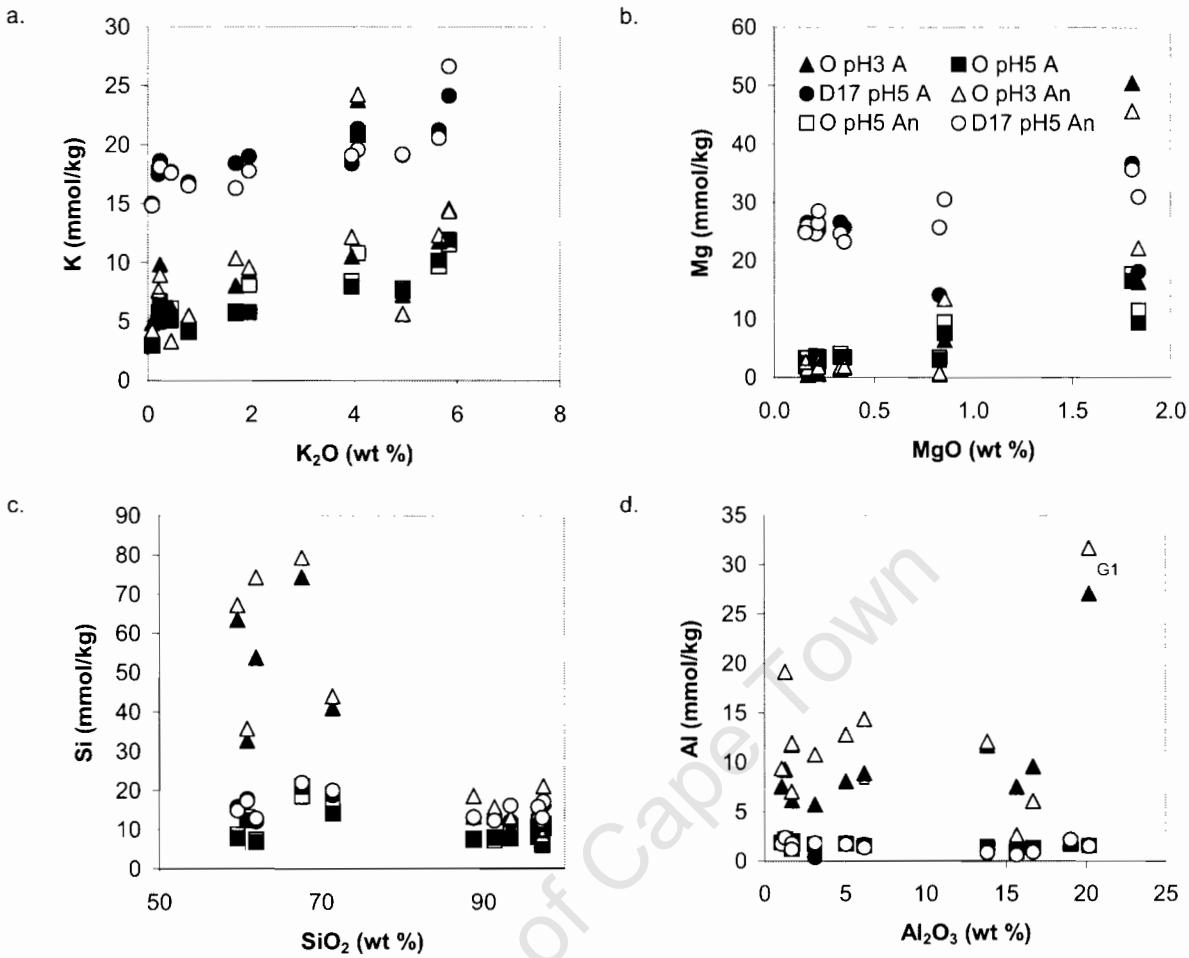

Figure 3.12. Relationship between concentrations of dissolved ions in leach with the content of the same ion in the rock a. K, b. Mg, c. Si, d. Al (O – organic; A – aerobic; An – anaerobic)

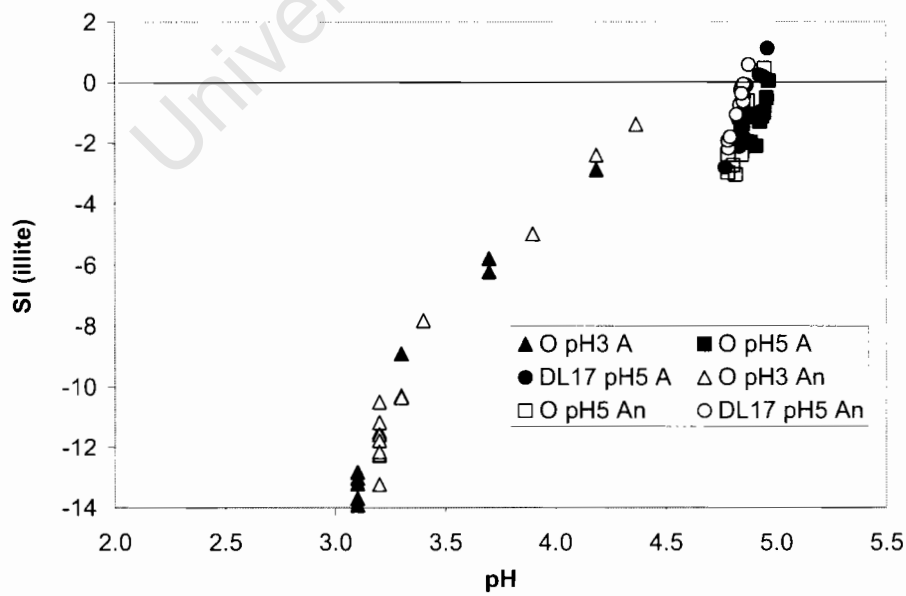

Figure 3.13. Saturation indices of illite in final extract from leaching experiment (O – organic; A – aerobic; An – anaerobic)

K, Mg and Ca all show broadly increasing leach concentrations with increasing amount of the element in the rock (e.g. K, Mg Figure 3.12 a-b), supporting the conclusion from field data that variability in concentrations of these ions in Nardouw aquifer groundwater is related to variability in the chemistry of the Nardouw aquifer rocks. Although the pH range of this analysis is not large, the leach data agree with the field data in that the saturation level of the solution with respect to illite is reached at pH 5 (Figure 3.13).

Si concentrations in groundwater increase with increasing Cl concentrations, but reach a plateau at about 5 mg/L (Figure 3.10g). Concentrations in the Nardouw and Peninsula aquifers are similar because they are both controlled by equilibrium with quartz. The average quartz saturation index of Nardouw waters is 0.11 (n=12), and for Peninsula Formation water is -0.12 (n=6). The different SI for quartz in the two aquifers may be a function of residence time. The Si concentrations in the leach experiments are relatively constant (Figure 3.12c). However, some of the clay rich samples (B1, B2, C1, C2 and G1), which have lower SiO_2 contents, have significantly elevated Si concentrations compared to all other samples, particularly at pH 3. These leachates are also oversaturated with respect to quartz indicating that quartz is not controlling Si solubility in these samples. The samples from which the most Si is leached are the finer-grained rocks rich in clay minerals and increased leaching could be due to the finer grain size i.e., increased surface area or the presence of more reactive aluminosilicate minerals. Little Si is leached from the samples highest in SiO_2 due to the occurrence of the silica in quartz, which has a low susceptibility to weathering (Faure, 1992).

Too few Al concentrations are available from the historical groundwater quality data to draw any conclusions regarding controls on Al behaviour in groundwater. In the leach experiments, Al concentrations are quite variable but elevated in the organic pH 3 leaches under both aerobic and anaerobic conditions, suggesting dissolution of aluminosilicate minerals at pH 3 (Figure 3.12d). Al and Si have an interesting relationship to each other in the pH 3

samples (Figure 3.14). Siliceous samples i.e. > 90% SiO_2, show a linear increase in Al with increasing Si in the leachates, whereas more aluminous rocks have elevated Si, relatively low Al and no linear relationship between the two variables. The limitation on Al solubility in more aluminous rocks could be due to a mineralogical control which is not present in great quantities in siliceous rocks, for example illite. Illite appears to control Al solubility at pH 5, resulting in low constant Al concentrations with increasing Al_2O_3 contents in the rock (Figure 3.14).

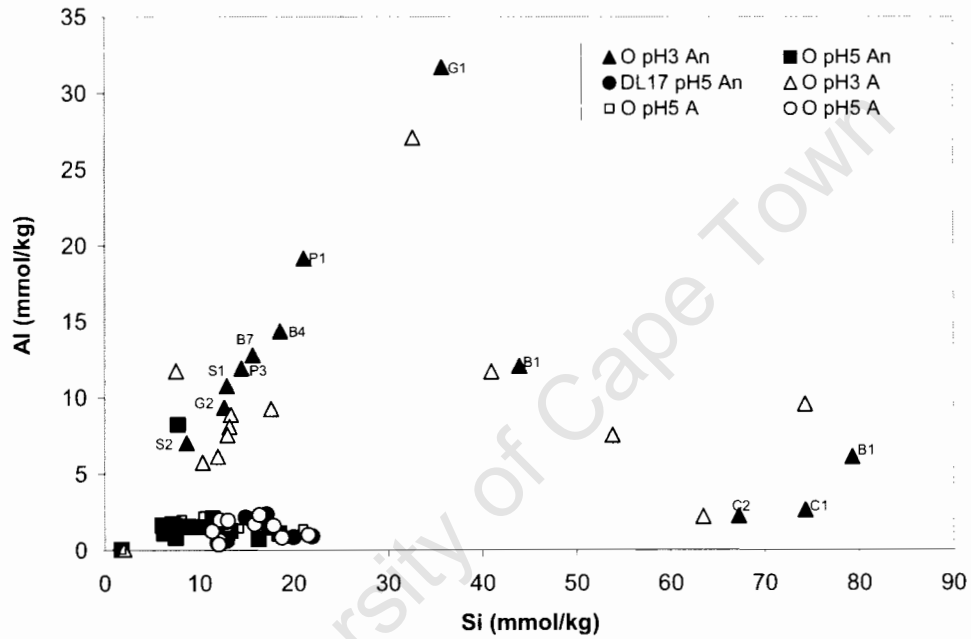

Figure 3.14. Relationship between concentration of Al and Si in final extracts from leaching experiments (A – Aerobic, An – anaerobic, O – organic)

The only parameter to show a decrease in concentration from the Peninsula to the Nardouw aquifer is DO (Figure 3.7g). DO in neither aquifer is at equilibrium with atmospheric pO_2, but Nardouw aquifer DO is significantly lower than Peninsula aquifer DO. DO is generally removed from water by biochemical respiration of organic carbon (Drever, 1997):

$$C_{106}H_{263}O_{110}N_{16}P + 138O_2 =$$
$$106CO_2 + 16NO_3^- + HPO_4^{2-} + 122H_2O + 18H^+ \qquad (3.4)$$

However, the TMG aquifers contain little organic carbon, and there must either be an alternative pathway for DO removal or the residence time of groundwater must be long. Oxidation of reduced Fe^{2+} in minerals in the

aquifer can also consume oxygen, for example (Grenthe *et al.*, 1992; Stumm and Sulzberger, 1992):

$$KMg_2Fe_2AlSi_3O_{10}(OH)_2 \text{ (biotite)} + \tfrac{1}{2}O_2 + 8H_2O + 3H^+ = Al(OH)_3 + 2Fe(OH)_3 + K^+ + Mg^{2+} + 3Si(OH)_4 \quad (3.5)$$

This reaction means that goethite and haematite coatings can be found on fractures under strongly reducing conditions and do not indicate that conditions are oxidizing (Grenthe *et al.*, 1992). Iron oxide coated fractures are observed in drill chips brought up from recently drilled boreholes in the Peninsula aquifer in the Vermaaks River valley (Figure 3.15). The lower DO would not affect the concentration of any of the major ions because the dissolution of silicates is not oxidation controlled (Siever and Woodford, 1979).

Figure 3.15. Iron oxide coated quartzite drill chips from a fracture in the Peninsula Formation, Kammanassie Mountains

3.4.1.2 Hydrogeochemical model for evolution of groundwater chemistry

The chemistry of Peninsula and Nardouw aquifer waters in the Klein Karoo appear to show an evolutionary pathway from the marine signature dominated rainfall recharge into the Peninsula aquifer, with ever more reactions with aquifer rocks leading to increased ion concentrations in the Nardouw aquifer. The greater variability in chemistry of Nardouw aquifer rocks leads to greater variability in Nardouw groundwater chemistry. Reaction with clay-rich formations could strongly affect the chemistry of the groundwater, as is observed in the leach experiments on the Cedarberg and Bokkeveld Formations. pH is buffered above 5.5 in rocks which have greater clay

content but in more quartzitic rocks, the pH can be affected by reactions such as iron hydrolysis, sulphide oxidation and the presence of organic acids. The concentration of Si is controlled by equilibrium with quartz, and the concentration of Al and K may be controlled by equilibrium with illite. The only parameter which has a higher concentration in the Peninsula than the Nardouw aquifer is DO.

The chemical data presented here support the hydrogeological model developed by Kotze (2001) and Weaver and Talma (1999) based on stable isotopic data and age dating of groundwater. The average isotopic ratio, and ranges of ratios in the Peninsula and Nardouw aquifers are almost identical, and have been used to argue that most recharge occurs at high-altitude (Weaver and Talma, 1999). Groundwater in the Nardouw aquifer has an age range of 1 000 to 10 000 years, whereas the Peninsula Aquifer has an age range of about 1000 years (Kotze, 2001). The hydrogeological model states that recharge occurs via precipitation at higher altitudes where the more competent Peninsula Formation outcrops and to a lesser extent at lower altitudes where the Nardouw Subgroup is present. Recharge is then transferred from the Peninsula to the Nardouw in a number of ways including flow through fractures and faults across the Cedarberg Shale aquitard (CS), overflow across the CS layer, flow along bedding planes, and leakage of groundwater through the CS aquitard. Poor fracture connectivity and low leakage through the CS aquitard lead to longer residence times along the flow path to the Nardouw Aquifer (Kotze, 2001; Weaver and Talma, 1999).

The hydrogeological model provides an explanation for the lower DO concentrations in the Nardouw aquifer compared to the Peninsula aquifer. More DO is likely to be removed during the longer residence time in the Nardouw aquifer, and recharge to the Nardouw through the more organic carbon rich Cedarberg Formation may also enhance DO removal from groundwater. The distribution of DO is likely to be fundamental to understanding the distribution of dissolved Fe because Fe has been shown to be strongly redox controlled in the leach experiments.

3.4.2 Iron geochemistry

Redox, pH, rock lithology, corrosion and the presence of organic acids in recharge water have been identified as important variables controlling the concentration of iron in groundwater.

3.4.2.1 pH

The concentration of Fe in groundwater of the Klein Karoo does not correlate with the pH in any aquifer (Figure 3.16a). The amount of iron present at steady state in both aerobic and anaerobic leaching experiments is also independent of pH, but under aerobic conditions, more iron is mobilised at pH 3 (Figure 3.16b). The rate and extent of initial iron release under both aerobic and anaerobic conditions is affected by pH, with iron being released most rapidly at pH 3. Under aerobic conditions, the Fe concentration decreases following the initial peak as iron oxide is precipitated, until a steady state concentration of Fe is reached that is determined by the pH. The sensitivity of iron solubility to pH in aerobic leaches is evident by the decrease in Fe concentration with time due to buffering of pH by dissolution of aluminosilicates in samples B1, B2, C1 and C2 (Figure 3.3-3.8). The anaerobic pH 3 iron concentrations also decrease following the initial spike, but then increase again to a steady state value independent of pH.

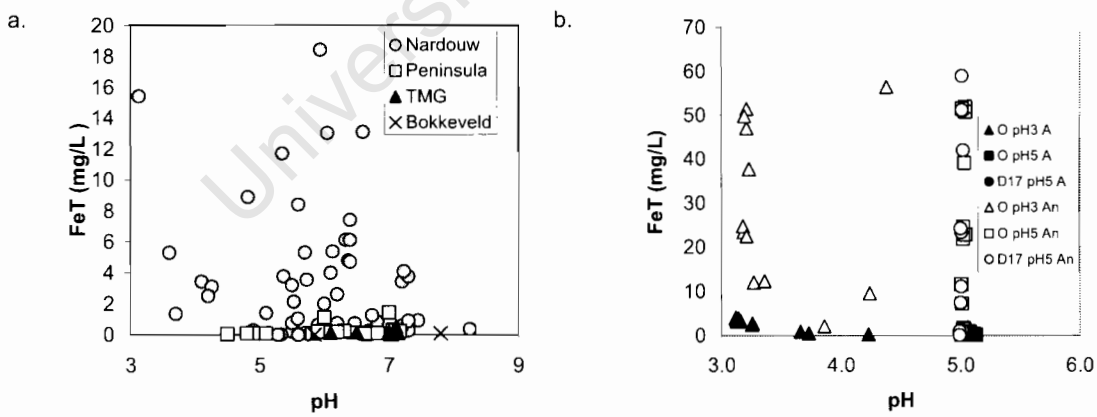

Figure 3.16. Relationship between total iron concentration and pH in a. the groundwater, b. the final extract from the leaching experiments (A – Aerobic, An – anaerobic, O – organic)

3.4.2.3 *Redox control on iron concentration*

The redox state of groundwater is an important control on iron behaviour within the aquifer as iron is soluble and more mobile in the reduced Fe^{2+} form than in the oxidized Fe^{3+} form (Drever, 1997). However, no correlation is

observed between iron concentration in groundwater and DO, and it is likely that Fe concentrations in groundwater are misleading due to the factors discussed in Results (Section 3.3). In the leach experiments, the strongest control on steady state Fe concentrations is the pO_2 of the atmosphere under which the leach was carried out. Similar experiments by Siever and Woodford (1979) show that the amount of dissolution of basalt increased by an order of magnitude from oxic to anoxic systems. In aerobic systems, following the initial pH-dependent iron release, iron is slowly removed from the system due to oxidation and precipitation as iron oxide. Comparable behaviour of iron has been observed by White and Yee (1985), during oxic dissolution of hornblende at neutral pH, and Siever and Woodford (1979), during dissolution of iron silicates between pH 4.5 and 5.5 in O_2 saturated environments.

The redox conditions of the aquifer can be further investigated using pe-pH diagrams. The pe of groundwater was calculated from historical groundwater quality data using three separate redox couples (Drever, 1997):

DO:	$pe = ½ \log Keq + ¼ \log pO_2 - pH$	(3.6)
Fe^{2+}-Fe^{3+}:	$pe = \log Keq + \log([Fe^{3+}]/[Fe^{2+}])$	(3.7)
$Fe(OH)_3$-Fe^{2+}:	$pe = \log Keq - 3pH - \log [Fe^{2+}]$	(3.8)

The variation in pe calculated by these three methods is considerable (Figure 3.17). If the sample is in redox equilibrium, pe calculated from all methods should be the same (Drever, 1997). Disagreement between pe calculated from a number of different redox couples is not uncommon, and reflects disequilibrium between various redox couples in solution due to different kinetics (Grenthe *et al.*, 1992; Langmuir, 1997). An alternative explanation for the lack of redox equilibrium is that anoxic Fe^{2+} rich water is mixing with oxic water within the borehole. Comparison of measured pe with pe calculated for each redox couple present in solution can allow identification of the redox pair responsible for determining the redox state of the system (Langmuir, 1997). Down-hole measurements in environments with dissolved $Fe>>10^{-7}$ M normally provide meaningful, stable readings (Grenthe *et al.*, 1992; Langmuir, 1997). Values of pe measured with a down-hole logger in some Klein Karoo boreholes plot along the Fe^{2+}-$Fe(OH)_3$ boundary suggesting that this reaction is buffering redox within the borehole system (Cavé and Smith, 2004;

Appendix E; Figure 3.17). The pe measured with the down-hole logger in the deepest parts of the boreholes indicates that groundwater is in the Fe^{2+} stability field in the aquifer. An increase in pH in the borehole, possibly due to degassing of CO_2, shifts the system onto the Fe^{2+}-$Fe(OH)_3$ boundary. The downhole data agree most with the calculated historical groundwater quality data pe calculated from the Fe^{2+}-$Fe(OH)_3$ couple. Walter (1997) and Applin and Zhao (1989) both found similar disequilibrium between pe calculated from DO and from the Fe^{2+}-$Fe(OH)_3$ redox couples, and Applin and Zhao (1989) also found measured pe to be controlled by equilibrium between Fe^{2+} and $Fe(OH)_3$. Based on the analysis of the pe values it is clear that pe values calculated from field DO measurements are misleading. The most accurate determination of field pe is with a down-hole probe, alternatively measurement of iron speciation in the field is required to allow calculation of pe using the Fe^{2+}-$Fe(OH)_3$ couple.

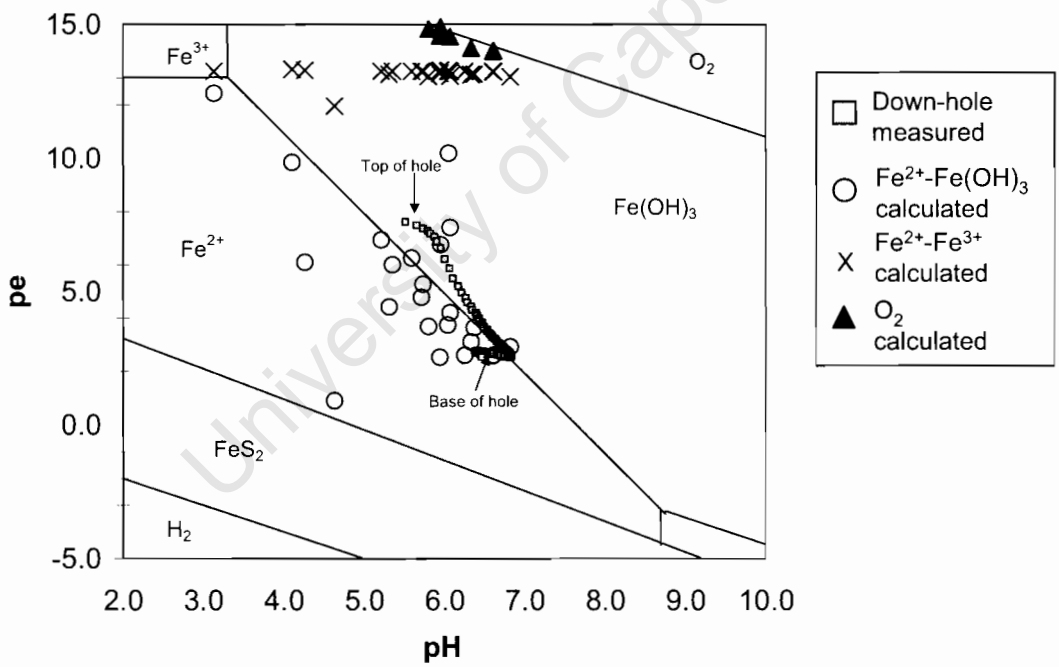

Figure 3.17. pe-pH diagram with points calculated from field data and with points measured by down-hole logger (See Cavé and Smith, 2004; Appendix E). Solid field boundaries for Fe concentration 10^{-5} M. dashed field boundaries for Fe concentration 10^{-3} M.

Values of pe measured under aerobic conditions during the leaching experiments vary, but at pH 5 appear to be controlled by the Fe^{2+}-$Fe(OH)_3$ equilibrium reaction and at pH 3 fall within the Fe^{2+} stability field (Figure 3.18).

Under anaerobic conditions, most points fall close to or within the FeS_2 field. Calculated SI for the final extract of the iron oxide leach support the measured pe in the pyrite stability field. Iron mineral solubility is redox controlled and saturation with respect to pyrite controls iron solubility under anaerobic conditions, while saturation with respect to amorphous iron oxide controls iron solubility under aerobic conditions (Figure 3.19).

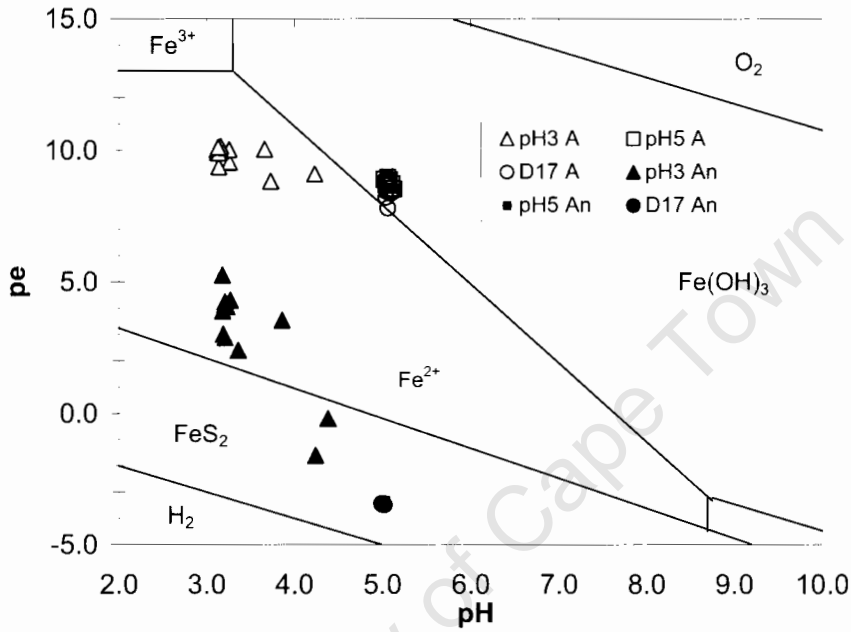

Figure 3.18. pe-pH diagram of points measured during leaching experiments. Solid field boundaries for Fe concentration 10^{-5} M. dashed field boundaries for Fe concentration 10^{-3} M (A – Aerobic, An – anaerobic, O – organic).

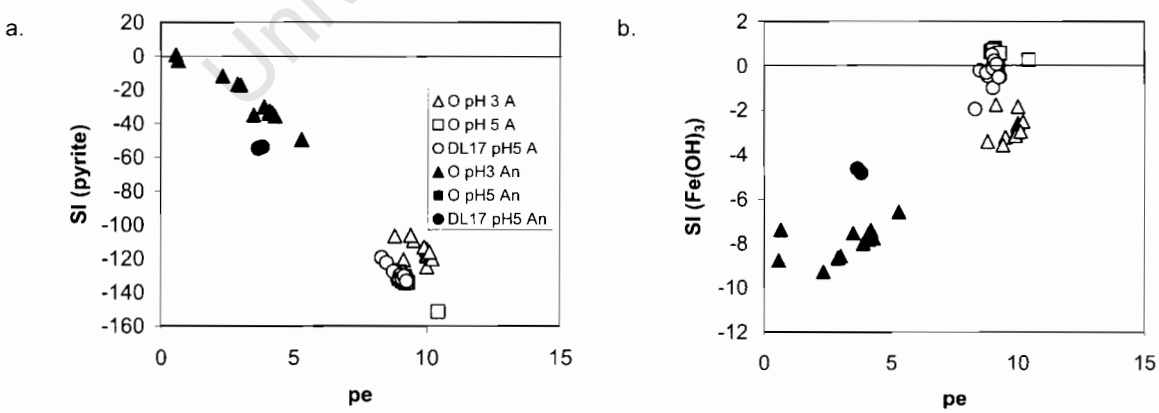

Figure 3.19. Saturation of the final leach solution with respect to a. pyrite and b. amorphous $Fe(OH)_3$ as a function of pe (A – Aerobic, An – anaerobic, O – organic).

3.4.2.2 *Lithological control on iron concentration in groundwater*

The average sandstone contains 0.98 % Fe (2.8 % Fe_2O_3) while shales contain on average 4.7% Fe (13.4% Fe_2O_3) (Faure, 1992). Relative to world averages, the TMG rocks have low iron contents yet groundwater contains measurable concentrations of soluble Fe (Tables 3.11 & 3.12). The Nardouw Subgroup rocks, in particular those from the Goudini Formation, do have higher iron contents than the other formations. Iron staining of weathered Goudini Formation rocks is common, and the formation is considered the most iron rich in the Nardouw Subgroup (Malan *et al.*, 1989). Based on the distribution of Fe in TMG rocks, the most Fe would be expected to leach from the Goudini and Cedarberg Formations, but the leaching experiment results indicate that most iron is leached from rocks with the lowest total iron content (Figure 3.20). The mineralogy of iron rather than the total iron content must be an important control on its mobility.

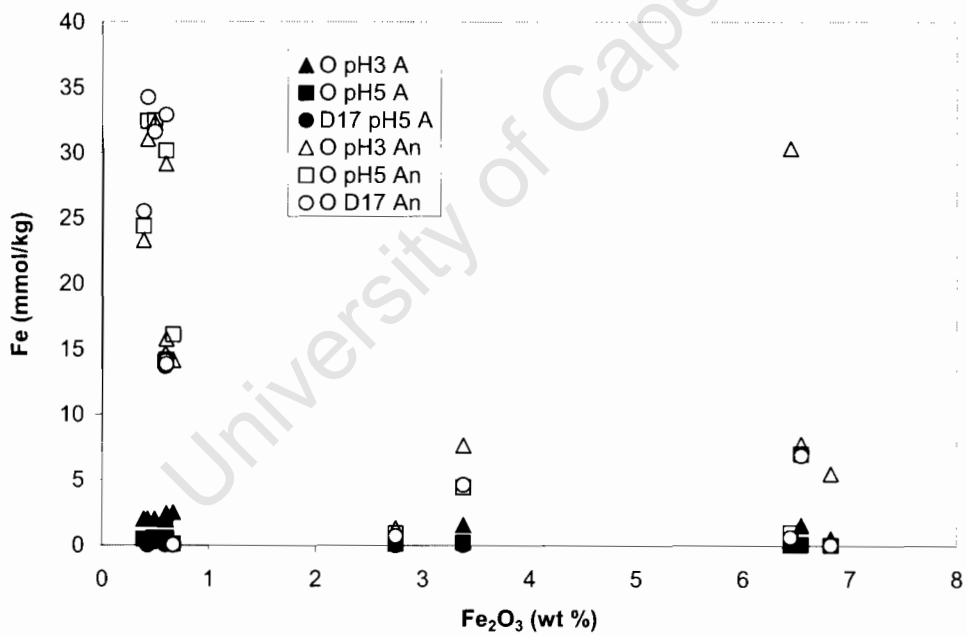

Figure 3.20. Relationship between Fe in final extract from leaching experiments and amount of Fe_2O_3 in the rock (A – Aerobic, An – anaerobic, O – organic).

Obvious potential iron source minerals include haematite and iron oxides in most of the sandstone rocks, and chlorite in the Cedarberg Formation. There has clearly been remobilisation of iron at some point in the geological history of these rocks because iron oxide minerals are often present in stringers and veins. Iron oxide stringers are commonly associated with authigenic muscovite, suggesting that iron remobilisation could have been concurrent

with the extreme diagenesis or greenschist metamorphism of the TMG in the Klein Karoo that resulted in growth of authigenic quartz, muscovite, chlorite, and pyrophyllite and sericitization of feldspar (de Swardt and Rowsell, 1974; Figure 3.2d). Along with iron present in oxide minerals, iron is substituted in clay minerals such as mica or illite. Microanalysis of clay minerals in rocks from this study revealed Fe contents of up to 8.9 wt % in clay minerals. Thamm (1988) also found concentrations of Fe up to 5 wt % in illites in TMG rocks from Clanwilliam and Piketberg. Weathering of quartzite rocks results in replacement of clay minerals by iron oxide phases suggesting that Fe is released from clays (Figure 3.2e).

The SO_4:Cl ratio of most groundwater from the TMG is greater than that of seawater, suggesting S is lithologically derived, possibly from oxidation of pyrite (Figure 3.21). No pyrite was observed in any of the rocks in this study, although pyrite veins are reported in other parts of the TMG (Meyer, 1999). Pyrite oxidation would be expected to be associated with low pH. A subset of samples from the Nardouw Subgroup groundwaters do show low pH and high SO_4:Cl ratio, but the samples that have the highest Fe concentrations are those with SO_4: Cl ratios closer to the seawater ratio. These observations indicate that pyrite is not likely to be the cause of the high iron concentrations observed, but do not discount the possibility that pyrite oxidation is contributing to the iron load in the groundwater.

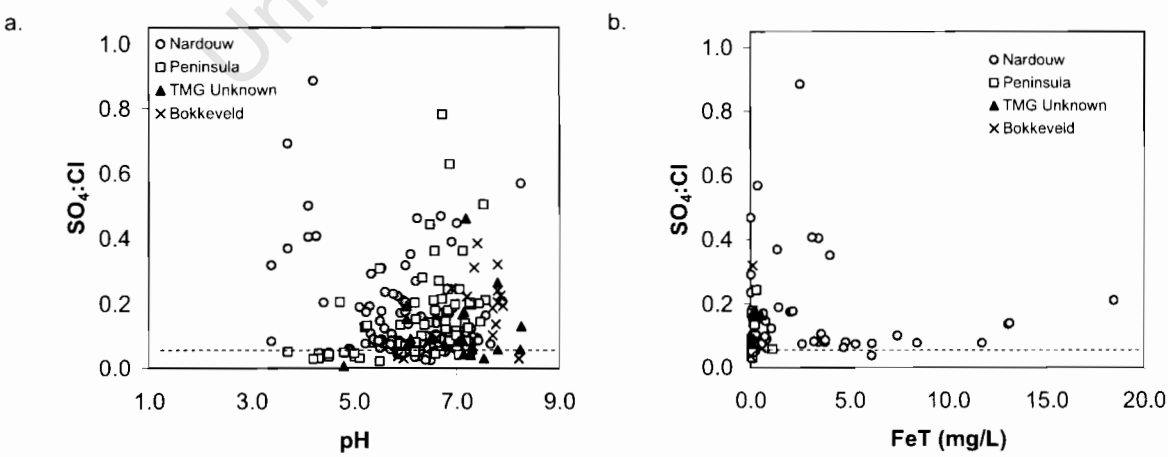

Figure 3.21. a. Relationship between the SO_4: Cl molar ratio and a. pH and b. FeT in groundwaters of the TMG. Dashed line represents seawater SO_4:Cl molar ratio.

Specific iron phase extractions were performed to identify the more mobile Fe phases in the rock, namely amorphous hydrous iron oxide, crystalline iron oxides including goethite and haematite, and other phases, including iron in aluminosilicate minerals (Figure 3.22). The percent of iron present in amorphous form is greatest in those rocks with the lowest total iron content, in particular siliceous rocks from the Skurweberg, Baviaanskloof and Peninsula Formations. Rocks from the Bokkeveld, Cedarberg and Goudini Formations have low contents of amorphous oxide phase iron. A significant additional amount of iron is leached from samples C1, B1 and G1 by the crystalline Fe-oxide extraction due to the presence of haematite and goethite as observed in thin section and detected by Mössbauer spectroscopy. C1 and B1 appear to be oxidized/weathered versions of C2 and B2, which are grey in colour. In C2, iron is predominantly present in chlorite grains, and in B2, iron may be in reduced form in the sericitic matrix and not readily leachable. Samples with high contents of amorphous iron oxide tend to have low crystalline iron oxide contents.

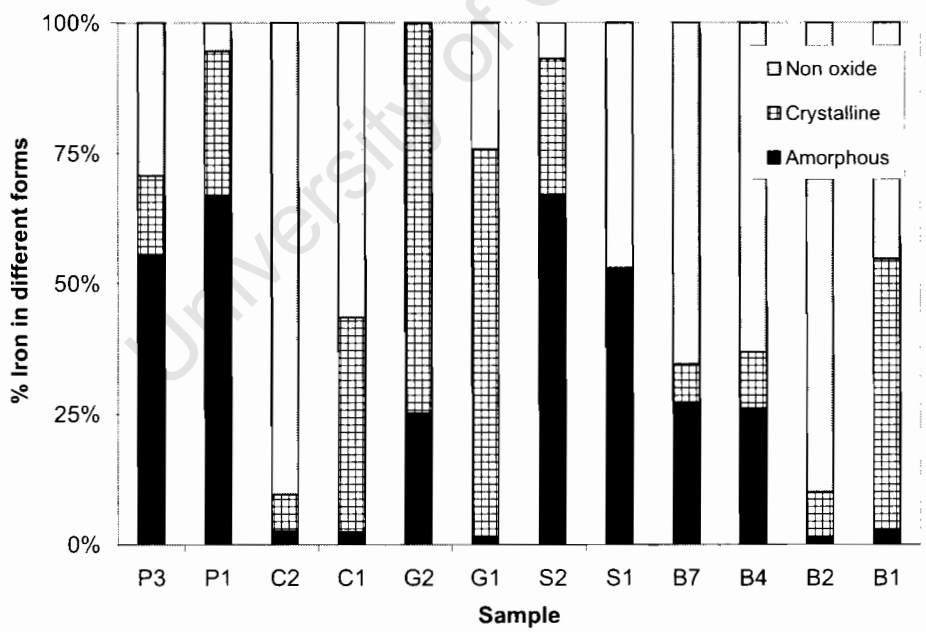

Figure 3.22. Distribution of iron between different phases in rock samples from the Kammanassie Mountains

Mössbauer spectroscopy analyses of a few of the rock samples correlate fairly well with the iron phase extractions and provide insight into the non-oxide forms of iron. Sample B4 contains about 37% of the total Fe in amorphous

and crystalline oxides, correlating well with the 40% as Fe^{3+} determined by Mössbauer spectroscopy. The remaining 60% is present as Fe^{2+} in an unknown mineral. Sample G1 has 74.2% Fe in crystalline oxides, corresponding well with the measured 77% as haematite using Mössbauer spectroscopy. The remaining 23% is present as 8% Fe^{3+} and 15% Fe^{2+}. A small amount of the Fe^{3+} is in amorphous form (1.5%) but 6.5% is in another form. Sample C2 has 21% as Fe^{3+}, of which only half is present as iron oxides. At least some of the 79% of Fe^{2+} is present in iron-rich chlorite, observed in thin section and in XRD scans. In sample P1, chemical extractions determined 67% of the iron to be in an amorphous phase, and a further 28% in the crystalline fraction, making a total of 95% expected as Fe^{3+}. However, the Mössbauer scan indicates that 44% of the iron is present as Fe^{2+}. This suggests that in sample P1 the ascorbate and dithionite leaches are extracting iron from other minerals besides oxides. Lack of obvious alternative sources of iron suggests that a fairly large proportion of the iron is present substituting as Fe^{2+} in a leachable aluminosilicate mineral. The magnetic separation of Peninsula rock concentrates a 7Å clay mineral, possibly chlorite, in the magnetic fraction. Further investigations will be required to see if this is the source of iron that is extracted by the dithionite and ascorbic leaches.

The amount of iron leached from rocks under anaerobic conditions correlates strongly with the proportion of iron present in amorphous oxide form (3.23a). Amorphous oxides are the form of iron that is most readily leachable, soluble and available to bacteria (Brown *et al.*, 2000; Canfield, 1989). There is no correlation between the crystalline iron oxide extract and the amount of iron leached from samples, indicating that the crystalline oxides are not readily weathered under the conditions used in these experiments (Figure 3.23b).

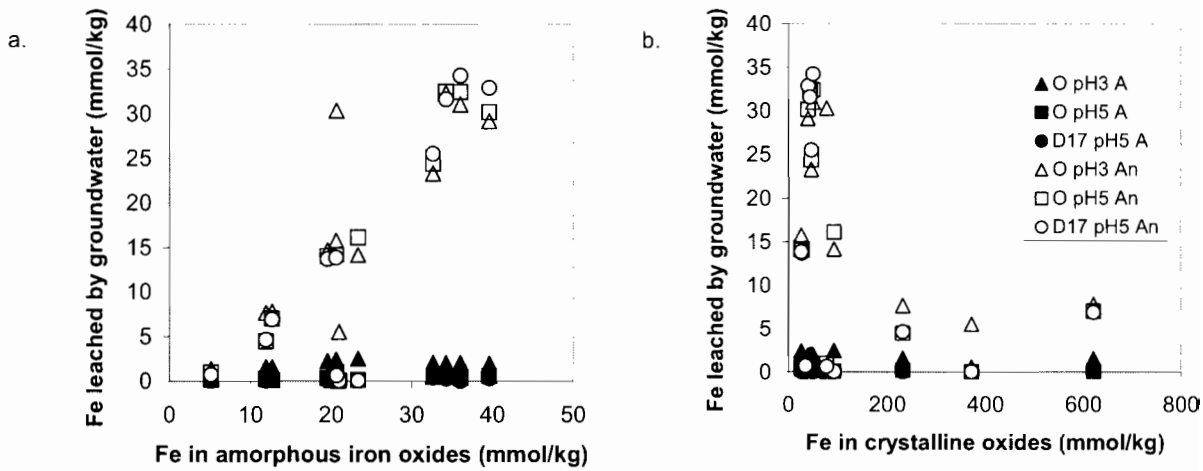

Figure 3.23. Relationship between Fe phases and Fe leached from rock samples by groundwater. a. relationship of Fe leached by groundwater to amount of Fe in amorphous oxide phase, b. relationship of Fe leached by groundwater to amount of Fe in crystalline oxide phase (A – Aerobic, An – anaerobic, O – organic).

3.4.2.3 Corrosion

While the background iron concentration of the groundwater is likely to be explained by iron silicate weathering reactions, measured concentrations of up to 16 mg/L Fe^{2+} could be due to corrosion of borehole equipment. Corrosion has not been reported as a problem in the Klein Karoo, probably because most material in the borehole is PVC and galvanised steel and therefore less susceptible to corrosion. Corrosion of galvanised steel would also liberate Zn. Zn concentrations are noted to be elevated in groundwater from boreholes KG1 and DP15 (Table 3.5), yet these groundwaters do not have the highest iron concentrations. Groundwater in borehole DP15 has particularly low pH and the elevated Zn concentrations are quite possibly due to steel corrosion. However, the near-nuetral pH and low Zn concentrations of groundwater in other boreholes, even those with elevated Fe concentrations, suggest that corrosion is not a major source of iron.

3.4.2.4 Effect of organic acids on iron concentration in groundwater

Fulvic acids have been found in other studies to be more effective than dilute HCl at mobilising Fe from minerals (Schnitzer and Kodama, 1976). Under aerobic conditions, the initial amount of iron leached by the organic pH 5 leachate is slightly higher than that leached by the DL17 pH 5 leach. The organic pH 5 iron concentration does not remain higher than the DL17 concentration in all samples for the full period of the leach, but this could be

due to analytical error at the low concentrations in the aerobic samples. Under anaerobic conditions, dissolution of arenaceous lithologies (P1, P3, S1, S2) in the organic acid rich leachate at pH 5 is faster than in DL17 water at pH 5 but the steady state concentration in both is the same. In more argillaceous rock types the presence of organic acids in the leaches has no effect on the rate of iron dissolution (e.g. B1, B2, B4, B7, C1, C2 and G1). Organic acids could be preferentially adsorbed onto clay particles in these argillaceous rocks, preventing the acceleration of iron reduction. The effect of humic acids at pH 3 could not be investigated because a non-organic leach was not done for comparison. However, the effect is expected to be less pronounced because humic acid adsorption to surfaces is more effective at higher pH (Ochs, 1996; van Hees *et al.*, 2002). Natural organic acids could result in greater mobilisation of Fe during recharge if the recharge is anaerobic, rapid and through arenaceous rocks. The longer the recharge water is in contact with the rock, the more likely that the steady state iron concentration will be reached.

3.4.2.5 Rate of iron dissolution

A rate constant could not be calculated for these leaching experiments because of insufficient time resolution and because there are likely to be too many reactions occurring simultaneously (Siever and Woodford, 1979). The behaviour of iron with time can however be qualitatively investigated. Under aerobic conditions all leaches and all lithologies follow a similar pattern with time i.e., an initial increase in iron concentration, particularly pronounced at pH 3, followed by a decline in Fe concentrations due to precipitation of iron oxide to a steady state concentration determined by the pH. The rapid initial Fe spike at pH 3 may reflect an initial desorption of iron from sorption sites on clay minerals in the rock (Siever and Woodford, 1979).

Under anaerobic conditions, three different dissolution behaviours with time are observed (Figure 3.3-3.8):

Type 1: Initial rapid increase in iron concentration, followed by slight decrease and then slight increase in iron concentration to a constant concentration e.g. B1, B2, B4, B7, G1. The initial maximum iron concentration is highest at pH 3

but steady state concentration is generally similar at both pH 3 and pH 5. The rate of initial iron dissolution is equally rapid at both pH 3 and 5, except in sample B4, where the pH 5 samples take slightly longer to reach maximum dissolution.

Type 2: Initial rapid increase, followed by a slight decrease and then continuous increase in iron concentration, never reaching steady state e.g. C1 and C2. The final iron concentration is significantly higher at pH 3 than pH 5. C1 and C2 were the only samples to contain authigenic iron-rich chlorite and it is probably slow dissolution of this mineral which is continuously releasing iron.

Type 3: The rate of iron release in the different leaches is different, but the steady state concentration is generally the same e.g. G2, P1, P3, S1 and S2. Iron is generally mobilised rapidly by the pH 3 leachate, although more slowly than in Type 1 behaviour. After reaching the initial maximum, the iron concentration drops rapidly and then increases rapidly again to the steady state concentration. The pH 5 leaches do not show such a dramatic fluctuation in iron concentration, but are slower to reach steady state. The presence of organics accelerates dissolution in the pH 5 organic leaches compared to the pH 5 DL17 leach.

These groupings correlate with the chemistry of the rocks. Type 3 occurs only in the arenaceous rocks with low Al and K concentration, indicative of low overall clay contents. Type 1 and Type 2 leach patterns are restricted to samples with significantly higher clay contents. The difference in behaviour of the three leach types therefore appears to be related to the clay content of the rock. Steady state is reached more rapidly in the Type 1 leaches than in the Type 3 leaches, possibly because of the iron source mineral in the sample, or the finer grain size. Samples P1, P3, S1, S2 and G2 are all similar in thin section, and would probably have similar Mössbauer spectrographs, suggesting that iron is not actually all in amorphous oxide form, but in a readily mobilisable alternative form of iron. This form of iron may not be as rapidly dissolved as amorphous iron oxide, leading to the delays in dissolution observed at pH 5.

Initial rapid dissolution observed in most leaches could be due to the rapid reaction of fine grained crushed material. The dissolution of iron minerals is a surface controlled reaction and the rate would be expected to be surface area controlled (Stumm and Sulzberger, 1992). In this study, leaching data normalised to surface area indicates that the amount of mineral dissolved appears to be greater in rocks with lower surface areas. The apparent contradiction is because the surface areas measured in this study are for the rock as a whole and not for the minerals of interest.

3.5 Conclusion

During the historical groundwater quality data analysis and leaching studies the following were identified as important parameters for the mobilisation of iron from aquifer rocks in the Kammanassie Mountains:

- Redox – anoxic conditions are the most important parameter determining the iron concentration of groundwater in equilibrium with aquifer rocks.
- Form of iron in the rock - iron was leached to some extent from all rocks under anaerobic conditions, but steady state concentrations were highest in those rocks which had the most extractable amorphous iron oxide.
- pH - Under anaerobic and aerobic conditions, pH determined the rate and extent of initial iron dissolution. Under aerobic conditions, this initial iron was removed from solution by precipitation of iron oxides until an equilibrium concentration of iron in solution was reached, which was pH dependent.
- Presence of organic ligands - Organic acids were found to increase the rate of iron dissolution in arenaceous rocks under anaerobic conditions, but did not increase the extent of dissolution.

The hydrogeological model and hydrochemistry of the waters can help identify sites at which the above parameters are most likely to be problematic. The most reducing waters are those with the longest residence times, and the slowest flow rates. In the Kammanassie Mountains, the low DO of the Nardouw aquifer is due to long reaction with organic carbon and Fe^{2+}-bearing

minerals in the rocks. The Nardouw rocks have been identified as the most problematic in terms of iron encrustation and the geohydrological model explains these observations. The potential for dissolution of iron due to low pH waters is greatest in arenaceous formations where water chemistry has low salinity and is poorly buffered against decrease in pH. All lithologies are capable of producing mobile iron under the right conditions, but under experimental low DO conditions, arenaceous Peninsula and Skurweberg Formations were found to release the most iron, correlating with high amorphous iron contents. In the field, the higher DO in the Peninsula aquifer limits Fe dissolution.

The prediction of the likelihood of a borehole in the Kammanassie Mountains being affected by iron clogging therefore requires prediction of the redox conditions in the aquifer, for which a knowledge of the residence times and evolutionary flow paths of water in the aquifer is needed. In addition, it would be useful to understand the distribution of the different phases of iron in the lithologies of the aquifer. Regardless of the lithology, in this study the most iron was released into groundwater under anoxic conditions. Atlantis aquifer groundwater is associated with Fe clogging and anoxic water. It is likely that low DO conditions in any aquifer should sound a warning note that Fe clogging may occur, and that further investigations should be carried out. In South Africa, there is rarely this level of knowledge about an aquifer, so it is unlikely that iron encrustation can be accurately predicted at this time. However, measurements of water chemistry, in particular DO and Eh in newly drilled boreholes will give some idea of the likelihood of the borehole becoming encrusted in the future. Although technically more difficult, a downhole Eh/pH/DO probe or measurements of Fe speciation on site will provide even better results.

4 Use of a flow-through column and geochemical modelling to assess controls on iron oxidation in low pO_2 groundwater environments

4.1 Introduction

Oxidation of iron and precipitation of iron oxide minerals within boreholes and aquifers adjacent to boreholes has caused borehole clogging problems at two wellfields in South Africa. Initial clogging took about 10 to 15 years to manifest, yet repeated rehabilitation of these wells with chemical treatments only manages to improve the situation for on average 3 months (Flower and Bishop, 2003; Tredoux and Cavé 2002; Weaver and Talma, 1999). An iron bacterial presence has been identified in the wells using BARTS tests and bacteria have been blamed for the severity of the problem. However, the role of bacteria in iron oxidation at circumnuetral pH is difficult to establish. Kirby *et al.* (1999) found no significant differences between iron oxidation in systems with or without bacteria above pH 6.4. Sø*gaard et al.* (2001) found that although bacteria initiated Fe oxidation at a rate 1000 times faster than chemical oxidation, as soon as some iron oxide had precipitated iron oxidation became autocatalytic. In addition, at high concentrations of iron, iron precipitated from a solution oversaturated with respect to ferrihydrite by a purely physico-chemical mechanism. Emerson and Moyer (1997) showed that iron bacteria do not alter the rate of iron oxidation in systems where concentrations of both iron and DO are diffusion limited. In a similar system, Sobolev and Roden (2001) proved that bacteria can catalyse iron oxidation at concentrations of DO below detection limits, and at DO levels lower than oxidation can occur in a purely chemical system. However, these bacteria secrete chelator molecules which slow the rate of iron oxide precipitation. Although many studies of borehole clogging focus on the bacterial nature of iron encrustation (e.g. Stuetz and McLaughlan, 2004; Walter, 1997; Tuhela *et al.*, 1992; Smith and Tuovinen, 1985; Carlson *et al.*, 1980; Cullimore and McCann, 1978), bacteria have been ruled out as a cause of encrustation at some sites, e.g., Applin and Zhao (1989).

This chapter investigates the use of a column reactor to assess the rate of iron oxidation in an aquifer at low pO_2. To assess the effects of the presence of iron oxide and possible bacteria on iron oxidation, the column sediment matrix was inoculated with iron encrustation material from a borehole in the AWSS. Column reactors have significant advantages over batch tests and take into account the effects of physical processes likely to occur in aquifers, such as dispersion and aggregation (Roychoudhury *et al.*, 1998). Column reactors have been used for many studies of the biogeochemical processes affecting iron in aquifers, e.g., Amirbahman *et al.* (2003), von Gunten and Furrer (2000), Roden *et al.* (2000), Furrer *et al.* (1996), and von Gunten and Zobrist (1993), but most studies focus on iron and sulphate reduction.

Geochemical modelling of groundwater systems has been used to understand processes controlling the concentration of iron in groundwater (e.g. Houben, 2004; Appelo and de Vet, 2003; Burke and Banwart, 2002; Appelo *et al.*, 1999; Boochs and Barovic, 1981). Transport modelling of the column was performed, both for comparison to actual results obtained from column experiments, and for assessing the usefulness of geochemical modelling for understanding iron clogging systems.

4.1.1 Pathways for iron removal from solution at a redox boundary

To investigate the behaviour of iron in a column reactor, the various pathways of iron removal at low DO need to be considered. The boundary between anoxic and oxic systems is defined as 1-5 x 10^{-6} M DO (0.03 – 0.16 mg/L). At such low concentrations of DO, homogenous iron oxidation is a slow process. Precipitating iron oxide material can become a catalyst for further iron oxidation by a heterogeneous mechanism. Adsorption of Fe^{2+} to oxide surfaces is required for heterogeneous oxidation, but adsorption of Fe^{2+} with no oxidation or precipitation can also slow down the movement of iron through the aquifer.

4.1.1.1 Homogenous oxidation

Homogenous oxidation was discussed in Section 2.2.1. In the presence of an oxidizing agent, Fe^{2+} is oxidized to Fe^{3+}:

$$Fe^{2+} = Fe^{3+} + e^{-} \qquad (4.1)$$

Fe^{3+} undergoes hydrolysis and at near neutral pH will precipitate as an iron oxide mineral. Above pH 5, the homogenous oxidation of iron is a kinetically controlled reaction which is second order with respect to pH and first order with respect to dissolved oxygen concentration (Reaction 2.7; Emerson, 2000). Between pH 3 and pH 5, the rate of oxidation becomes first order with respect to pH, and below pH 3, the rate of oxidation is independent of pH (Stumm and Sulzberger, 1992). Davison and Seed (1983) suggested a universal rate constant for Equation 2.7 of 2 x 10^{-13} M^{-2} atm^{-1} min^{-1} and Sung and Morgan (1980) showed the rate constant was not temperature dependent between 5° and 35° C.

The production of protons during the hydrolysis reactions following oxidation (Reactions 2.1 to 2.3) will cause the pH to decrease in unbuffered systems, resulting in slower iron oxidation, and even redissolution of precipitated iron oxide minerals (Appelo *et al.*, 1999). Although little work has been done on the rate of iron precipitation following oxidation, Applin and Zhao (1989) believe that the formation of $Fe(OH)_3(s)$ from $Fe(OH)_3^0$ is slower than the rate at which Fe^{2+} is oxidized.

4.1.1.2 Adsorption

Adsorption of Fe^{2+} to iron oxides has been found to remove Fe^{2+} from groundwater (Appelo *et al.*, 1999). Iron oxides have two types of sorption sites, strong sites (Hfos) and weak sites (Hfow) (Appelo *et al.*, 2002; Dzombak and Morel, 1990):

$$Hfo\_wOH + Fe^{2+} \rightleftharpoons Hfo\_wOFe^{+} + H^{+} \qquad \log K = -2.98 \quad (4.2)$$

$$Hfo\_wOH + Fe^{2+} + H_2O \rightleftharpoons Hfo\_wOFeOH + 2H^{+} \qquad \log K = -11.55 \quad (4.3)$$

$$Hfo\_sOH + Fe^{2+} \rightleftharpoons Hfo\_sFe^{+} + H^{+} \qquad \log K = -0.95 \quad (4.4)$$

One mole of ferrihydrite with a surface area of 600 m^2/g has approximately 0.2 mol of weak sites and 0.005 mol of strong sites (Appelo *et al.*, 2002).

Fe^{2+} sorbs rapidly to iron oxide, and the distribution coefficient is proportional to the amount of Fe^{3+} hydroxide and pH (Tamura *et al.*, 1976). For the reaction:

$$Fe^{2+} + Fe(OH)_3 \cdot H^+ \Leftrightarrow Fe^{2+}_{ad} \cdot Fe(OH)_3 + H^+, \quad (4.5)$$

the distribution coefficient is (Tamura *et al.*, 1976):

$$\frac{[Fe^{2+}_{ads}]}{[Fe^{2+}]} = \frac{K[Fe-oxide]}{H^+} \text{ where K = } 10^{-9.6} \text{ mol/mg.} \quad (4.6)$$

Sorbed Fe^{2+} can be oxidized and become incorporated into the iron oxide. Distinguishing between sorption and precipitation in a growing and reordering precipitate is difficult (Appelo and de Vet, 2003).

4.1.1.3 Autocatalysis

An increase in the rate of oxygenation of Fe^{2+} in the presence of a ferric hydroxide precipitate is due to heterogeneous oxidation. Catalysis of the iron oxidation reaction by the presence of Fe^{3+} oxide usually involves adsorption of reacting species onto the oxide surface. The observed reaction rate in the presence of iron oxides is the sum of the heterogeneous and homogenous reaction rates (Tamura *et al.*, 1976):

$$\frac{-d[Fe^{2+}]}{dt} = k([k_0] + [k' \cdot [Fe\text{-oxide}]]) \times [Fe^{2+}] \quad (4.7)$$

$$\text{where } k' = \frac{k_{s,0}[O_2]K}{[H^+]} \quad (4.8)$$

$$\text{and } k = k_0 [O_2][OH^-]^2 \quad (4.9)$$

k_0 (2.3×10^{14} $M^{-3}s^{-1}$) is the rate constant for the homogenous reaction, $k_{s,0}$ (73 M^{-1} s^{-1}) is the specific rate constant for the heterogenous reaction and K is the adsorption distribution coefficient ($10^{-9.6}$ $mol.mg^{-1}$; Tamura *et al.*, 1976).

The effect of autocatalysis is more pronounced at lower pH where homogenous oxidation is slow (Houben, 2004), although the sorption of Fe^{2+} is not promoted at low pH (Pullin and Cabaniss, 2003). Autocatalytic oxidation is found to be strongly inhibited by the presence of PO_4 and organics, which sorb to surfaces and block Fe sorption sites. Autocatalytic and homogenous oxidation compete for Fe^{2+}, and homogenous oxidation decreases with time as more surface area becomes available for catalysis (Wolthoorn *et al.*, 2004b). Heterogenous oxidation promotes the growth of colloids, so oxides formed by autocatalysis tend to be large, and plate shaped.

Small spheroidal colloids are found where autocatalysis is limited by PO_4 and fulvic acid interferences (Wolthoorn *et al.*, 2004a).

4.2 Methodology

4.2.1 Experimental design

4.2.1.1 Experimental set-up

A 28 cm long, 5 cm diameter, clear plastic column packed with aquifer material was used to simulate aquifer conditions for the flow-through experiments. The column was packed with sandstone collected from the Peninsula and Skurweberg Formations of the TMG, crushed and sieved to a grain size interval of 1 to 2 mm. Prior to packing the column, the material was repeatedly washed with hydrogen peroxide, to remove organic carbon contaminants, and HCl. Because hydrogen peroxide can result in Fe^{2+} oxidation, the column was extensively rinsed with deionised water. The sand was mixed into a slurry with deionised water and poured into the column with tapping to ensure complete settling of the grains. A frit was placed at the column inlet to spread the inflow. Details of the packed flow-through column are given in Table 4.1.

Table 4.1. Parameters for flow-through column

Parameter	Unit	Value
Length	cm	28.0
Internal diameter	cm	4.63
Cross sectional area	cm^2	16.8
Volume	cm^3	471
Porosity	%	45.3
Pore volume	cm^3	214
Bulk density	g/cm^3	2.18
Specific surface area of grains	m^2/g	0.250
Average grain size	cm	0.150

Influent solution was pumped from a reservoir into the base of the column using an Eyela MP3 Microtube peristaltic pump. The reservoir was set up to enable degassing with N_2 for Fe^{2+} oxidation experiments. The effluent solution emerging from the top of the column was directed to a Gilson FC203B fraction collector with 80 test tubes, which was programmed to collect approximately 8 mL fractions at intervals over the duration of the experiment. The experimental set-up is illustrated in Figure 4.1.

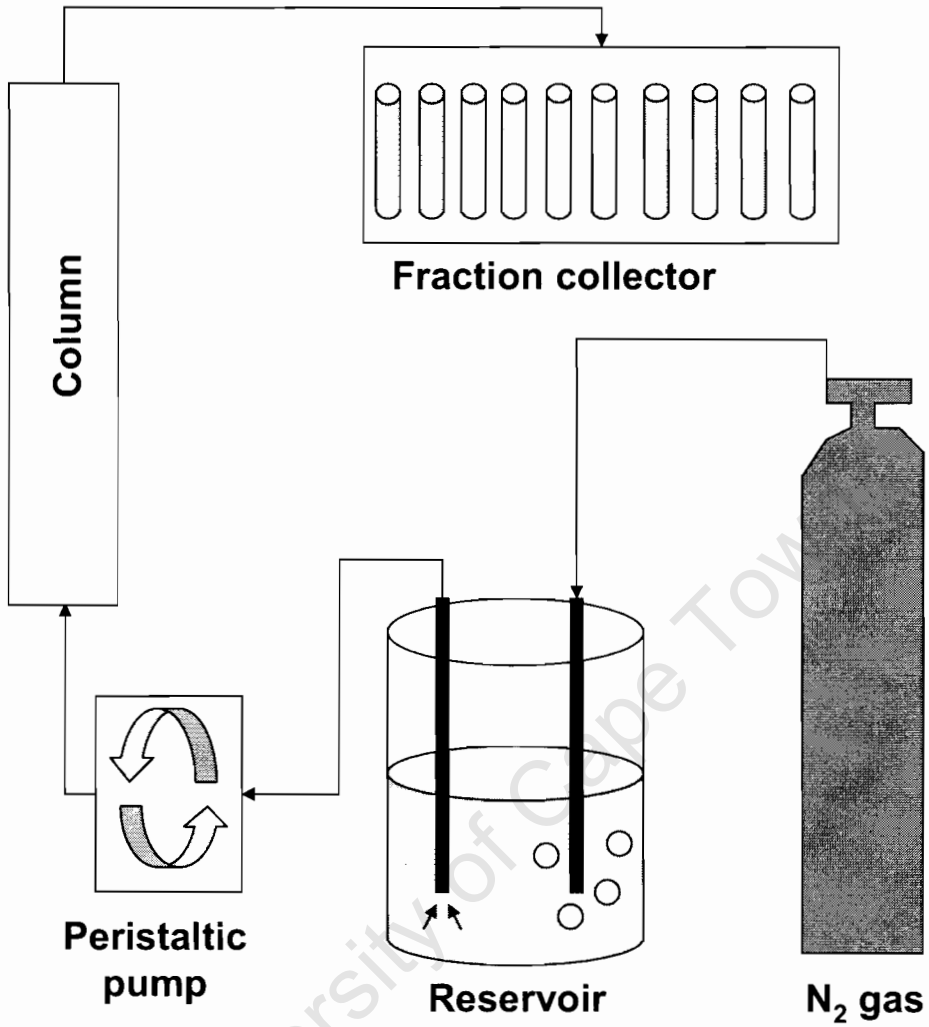

Figure 4.1. Experimental set-up for column flow-through experiments

The peristaltic pump has 10 flow rate settings ranging from 0.35 to 280 mL/minute. Choice of flow rate is important in determining the residence time of the solution in the column, which needs to be sufficiently long to allow a measurable change in concentration between the input solution and the output solution (Roychoudhury *et al.*, 1998). The residence time (τ) is related to the flow rate through the column (Q), the sediment porosity (ϕ) and the reactor volume (V):

$$\tau = \phi V/Q \qquad (4.10)$$

The residence time for each flow rate is given in Table 4.2.

Table 4.2. Residence time of fluid in column for each flow rate

Flow rate mL/hr	Residence time Hr
21	10.16
38	5.67
65	3.27
99	2.16
129	1.65
168	1.27
203	1.05
240	0.89
273	0.78
283	0.75

4.2.1.2 Breakthrough experiments

Breakthrough experiments involve measuring the change in the concentration of an inert tracer in the effluent, in this case Cl^-, in response to a step increase in the influent solution. The breakthrough curve can be used to calculate mean residence times and dispersivities, and the shape of the curve is also useful for identifying problems with the column such as channelling (Roychoudhury, 1998; Wen and Fan, 1975). 1M KCl was pumped through the column at different flow rates, and effluent was collected at set intervals. The KCl concentrations in the effluent were estimated using an EC meter.

4.2.1.3 Iron flow-through experiments

Experiments were repeated using two different carrier solutions: artificial groundwater synthesised using the method of Smith *et al*. (2002), and natural unfiltered groundwater collected in the field from borehole DL17. The chemistry of the artificial groundwater and DL17 water are given in Table 4.3.

Table 4.3. Aqueous chemistry of artificial groundwater and natural groundwater from borehole DL17 (concentrations in mg/L).

	Artificial	DL17
pH	7.3	7.2
Ca	9.3	22.1
K	4.7	15.9
Mg	0.6	1.2
Na	28.5	69.8
Cl	60.0	91.6
SO_4	30.0	23.4
HCO_3	91.8	146.0
Fe^T	<0.01	1.0

Four L of the carrier solution were first degassed in the influent reservoir by bubbling with N_2 until the measured DO was less than 0.20 mg/L. The solution was then buffered to the pH of the experiment (5.0, 6.0, 6.5 or 7.0)

using 12 g HEPES buffer (0.1 M) adjusted with 10 M NaOH or concentrated HCl. Other authors have found that HEPES buffer does not interfere with iron reactions (Pullin and Cabaniss, 2003). Two to three column volumes of buffered, degassed solution were pumped through the column prior to beginning the experiment to ensure the column was filled only with degassed water.

Flow-through experiments were conducted using a degassed ferrous ammonium sulphate ($Fe(NH_4)_2(SO_4)_26H_2O$) solution with a concentration of approximately 12.5 mg/L dissolved Fe^{2+}. The influent solution pH, DO, Fe^{2+} and Fe^T concentration were monitored for the length of the experiment by periodic sampling. Based on the homogenous oxidation rate of iron at 0.20 mg/L DO, the half-life of 12.5 mg/L of Fe^{2+} is 132 000 hours at pH 5 and 13.2 hours at pH 7 (Houben, 2004). Given these long half-lives, the lowest pump setting (flow rate of 21 mL/hour, residence time of approximately 10 hours) was chosen for the experiments to ensure a measurable difference between influent and effluent iron concentration. Alternate test tubes in the fraction collector were pre-acidified with 0.05 mL of concentrated HCl, allowing for measurement of pH (unacidified) and iron concentration and speciation (acidified) in the outflow. Experiments were performed over 2-5 days, until the effluent iron concentration became constant. Iron concentrations in the fractions were determined by ferrozine colorimetry as described in Chapter 3.

The experiments using artificial groundwater were performed first, in order of increasing pH. After the experiments with artificial groundwater were complete, the column was opened, the distribution of iron within the column noted and some iron oxide coated sand removed for SEM analysis. The column was then repacked with fresh sand and the experiments performed using DL17 groundwater, also in order of increasing pH. The only experiment that was performed out of increasing pH order was pH 5 DL17, which was performed after all other DL17 experiments.

4.2.1.4 *Effects of inoculation on iron oxidation*

The effect of iron oxides and possible microbial populations present in natural iron oxide encrustations on iron oxidation was tested by inoculating the column with iron oxide material from the field. Clean sand was mixed into a slurry with the soft fresh iron oxide precipitate collected from borehole W34020 at Atlantis. The slurry was packed into the column using the same method as previous experiments, and the experimental set-up remained the same. The experiment was repeated with $HgCl_2$ added to the influent solution to inhibit microbial reactions. $HgCl_2$ is highly bacteriocidal and operates by reacting with sulphide groups to inactivate proteins (Todar, 2002).

4.2.2 Geochemical modelling

The breakthrough curves and iron flow-through experiments were modelled using Phreeqci (Section 3.2.4, Chapter 3). The Phreeqci input files were developed with reference to Appelo *et al.* (1999) and Appelo and de Vet (2003), using iron oxidation kinetic equations from Tamura *et al.* (1976). Modelling was done using the Wateq4f thermodynamic database (Ball and Nordstrom, 1991) supplemented with additional information obtained from the references given above, which is listed in Appendix F.

Modelling of the flow-through column was performed using the TRANSPORT keyword, which simulates 1D transport processes with advection and diffusion. The calculations are based on a formulation from Appelo and Postma (1996), and require input of parameters for column length, dispersivity, boundary conditions, and solution chemistry for the solution in the column as well as the solution added to the column. The column is divided into equal sized cells and the solution in each cell is advected into the next cell after the given residence time. Dispersion effects are calculated, followed by kinetic calculations and chemical equilibration. Boundary conditions were set as flux at both ends of the column and flow through the column was in a forward direction. The total residence time in the column is the product of residence time in each cell and the number of cells (Parkhurst and Appelo, 1999). Modelling of breakthrough curves is relatively simple. The

breakthrough solution is entered as the influent solution and the concentration of the conservative ion calculated in the effluent solution at various time intervals. Full details and the input file for breakthrough curve calculations are given in Appendix F.

Iron flow-through modelling is more complex because it has to take into account changing chemical conditions along the length of the column as well as chemical reactions occurring in the column (Brantley, 2003). The modelling procedures used to account for changing conditions and chemical reactions are described below (full details and input files are given in Appendix F, more detail on the keywords can be found in Parkhurst and Appelo (1999)):

- **Increase in DO concentration along the column**: Although the change in DO concentration along the column was measured, the distribution of DO within the column was not directly measured. For the sake of simplicity, the increase in DO was assumed to be constant along the length of the column and the solution in each subsequent cell was equilibrated with a uniformly increasing pO_2 using the EQUILIBRIUM_PHASES keyword. Some modelling was also attempted by equilibrating the first cell in the column with pO_2 of atmospheric pressure.
- **Iron oxidation**: KINETICS and RATE keywords were used to calculate the amount of iron oxidation in the column. KINETICS calculates the change in moles from the rate equation for each time period, while RATE specifies how the rate equation will affect the solution chemistry. The kinetics of homogenous and heterogenous iron oxidation were compared using the equations of Tamura *et al.* (1976).
- **Iron oxide precipitation**: The EQUILIBRIUM_PHASES keyword was used to equilibrate the solution with an iron oxide phase, usually ferrihydrite, within each cell. Any Fe^{3+} generated by oxidation of Fe^{2+} was then immediately removed from solution as ferrihydrite. The amount of ferrihydrite available for dissolution was set at 0 or extremely

low levels (10^{-9} M) to prevent an increase in dissolved iron in the column due to the dissolution of ferrihydrite.

- **Adsorption:** The equilibrium constants of Dzombak and Morel (1990) for sorption on strong and weak sites on hydrous ferric oxide are incorporated into the Wateq4f database (Ball and Nordstrom, 1991). These were updated using the latest values determined by Appelo *et al.* (2002). The SURFACESPECIES keyword is used to define the equilibrium constants of the sites, and the SURFACE datablock instructs Phreeqci how to calculate the number of available sites, in this case based on the increasing amount of ferrihydrite as it precipitates in the column
- **Buffering**: To test the effect of buffering, each model was run first without buffering, and then with buffering. To model buffering, a FixpH parameter was included in the EQUILIBRIUMPHASES datablock to enable dissolution and precipitation of HCl to maintain a constant pH.

Hypothetical modelling was performed by varying the parameters individually to assess each ones effect on the outflow curve. All of the initial models were generated using the same DO gradient and the same input solution, namely the artificial groundwater solution containing 12.5 mg/L dissolved Fe^{2+}. A few additional models were generated using an initial DO influx at the column entrance, but the results were the same as observed with a DO gradient and are not reported here.

4.3 Results

4.3.1 Column experiments

4.3.1.1 Chloride breakthrough curves

Chloride breakthrough curves at various flow rates are shown in Figure 4.2. The cumulative age distribution (F-curve), exit age distribution function E(t), residence time (t-bar) and effective longitudinal dispersion co-efficient (D_T) were calculated following the method of Roychoudhury (1998; full calculations in Section A.3.1; Appendix A) and are summarised in Table 4.4.

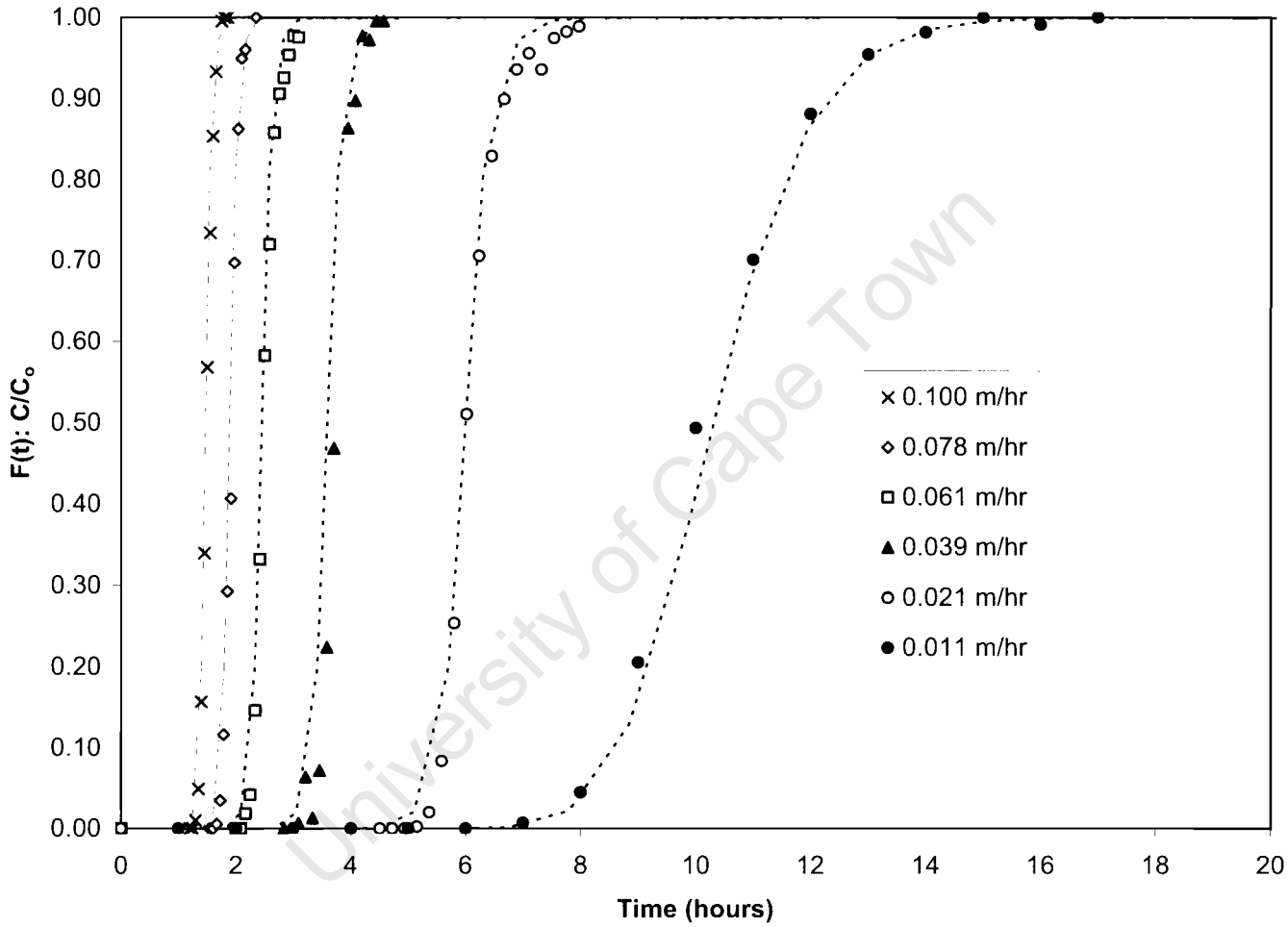

Figure 4.2. Chloride breakthrough curves for different flow velocities. Dashed lines represent fits calculated using Phreeqci.

Table 4.4. Calculated dispersion parameters for flow through column using method of Roychoudhury (1998)

Flow rate (Q) (mL/min)	Flow velocity (m/hr)	Mean residence time (hr)	Second moment	Longitudinal Peclet Number	Hydrodynamic dispersion (cm^2/s)	Dispersivity (m)
2.8	0.100	1.47	4.16×10^{-3}	239.9	3.09×10^{-4}	1.11×10^{-3}
2.2	0.078	1.89	3.58×10^{-3}	278.8	2.06×10^{-4}	9.65×10^{-4}
1.7	0.061	2.45	4.67×10^{-3}	213.8	2.08×10^{-4}	1.27×10^{-3}
1.1	0.039	3.59	4.60×10^{-3}	216.8	1.40×10^{-4}	1.30×10^{-3}
0.6	0.021	6.00	6.59×10^{-3}	151.2	1.20×10^{-4}	1.93×10^{-3}
0.3	0.011	10.77	5.10×10^{-3}	195.7	0.84×10^{-4}	1.69×10^{-3}

4.3.1.2 Iron oxidation curves

The average inflow and outflow pH and DO for each of the experiments is given in Table 4.5. Although the pH was buffered and initially adjusted with HCl or NaOH, it was found to drift slightly with time in the influent solution. Influent solution DO was less than 0.5 mg/L, but generally in the range 0.1 to 0.2 mg/L and increased by 5 to 10 times to 1.5 – 3 mg/L before exiting the column. Although the average concentration of DO in the effluent of the inoculated column at pH 6 is 1.98, on two occasions effluent DO was found to be lower than influent DO in this particular experiment. Fe^{2+} concentrations remained constant at most pH in the reservoir but oxidation occurred at pH 7 (Figure 4.3) and the values given for influent Fe concentration at pH 7 are initial Fe concentrations. Duplicate runs were performed for pH 6 and pH 6.5 with artificial groundwater and the relative standard deviation found to be within 10% for most repeats (Table B.6, Appendix B).

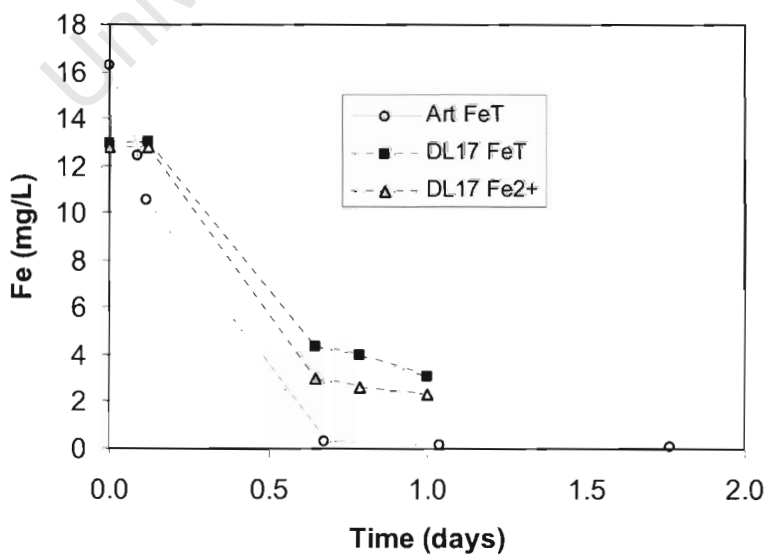

Figure 4.3. Decrease in iron concentrations with time in influent reservoir at pH 7 (Art – artificial groundwater, FeT – total iron concentration)

Table 4.5. Average influent and effluent solution chemistry for all flow-through experiments

		Average inflow concentrations				Average outflow	
		Fe^T	Fe^{2+}	pH	DO	pH	DO
		mg/L	mg/L		mg/L		mg/L
pH 5.0	DL17	13.18	nd[a]	5.00	0.15	nd	nd
	Art	12.57	12.57	5.15	0.44	4.93	2.30
pH 6.0	DL17	11.41	11.57	5.98	0.17	5.80	1.58
	Art	11.82	11.44	6.00	0.24	5.72	2.34
	Inoc	11.76	11.86	6.20	0.28	6.26	1.91
	Inhib	11.29	11.28	5.93	0.09	5.46	2.78
pH 6.5	DL17	12.83	13.45	6.52	0.13	6.30	3.00
	Art	10.68	10.42	6.50	nd	nd	nd
pH 7.0 (initial)	DL17	12.93	12.82	6.94	0.27	nd	nd
	Art	12.43	nd	6.96	0.35	6.90	1.88

a. Not determined

Iron oxidation curves at different pH are given in Figures 4.4 to 4.8. The full dataset is given in Section A.3.2 (Appendix A). Iron breakthrough is delayed at all pH relative to Cl breakthrough. Fe concentrations in the effluent increase constantly to a steady state after 24 - 36 hours. Fe^T eluting from the column at steady state decreases with increasing pH, from 90% in artificial solutions at pH 5 to below detection limits in both solutions at pH 7. The slope of the breakthrough curve also decreases with increasing pH. In general, steady state Fe^T is higher when DL17 water is used compared to artificial water, and the slope of the DL17 curve is steeper than the artificial water Fe curve at pH 6 and pH 6.5. More iron occurs as Fe^{3+} in artificial effluent than in DL17 effluent, and the proportion as Fe^{3+} decreases with increasing pH. The steady-state concentrations fluctuate, in some cases showing distinct oscillations, particularly at pH 5. The periodicity of oscillations at pH 5 is 7 to10 hours, at pH 6 oscillations are not rhythmic, and at pH 6.5, the periodicity is 5 hours. The Fe flow-through curves of the inoculated column both with and without microbial inhibition are quite different to the non-inoculated columns (Figure 4.8). Before inhibition, Fe concentrations in the effluent increase slowly and steadily without reaching a steady state value. The effluent Fe concentration at the beginning of the inhibition experiment was many times higher than measured in any other iron flow through experiment. With addition of $HgCl_2$ the amount of iron in the effluent rapidly decreased and remained <0.01 mg/L for the remainder of the experiment.

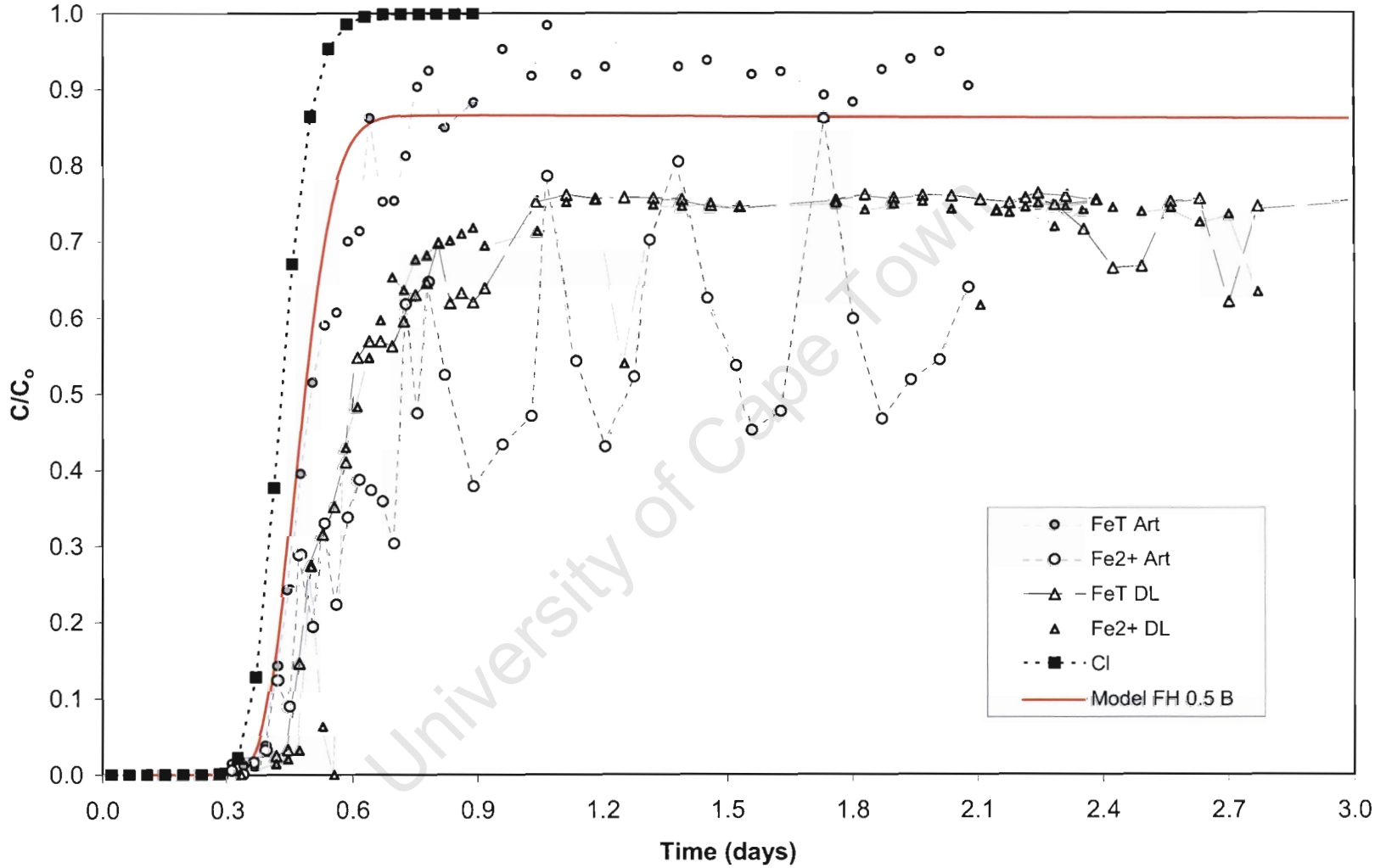

Figure 4.4. Iron concentrations in effluent solution as a function of time for pH 5 influent solution. Solid red line is transport model.

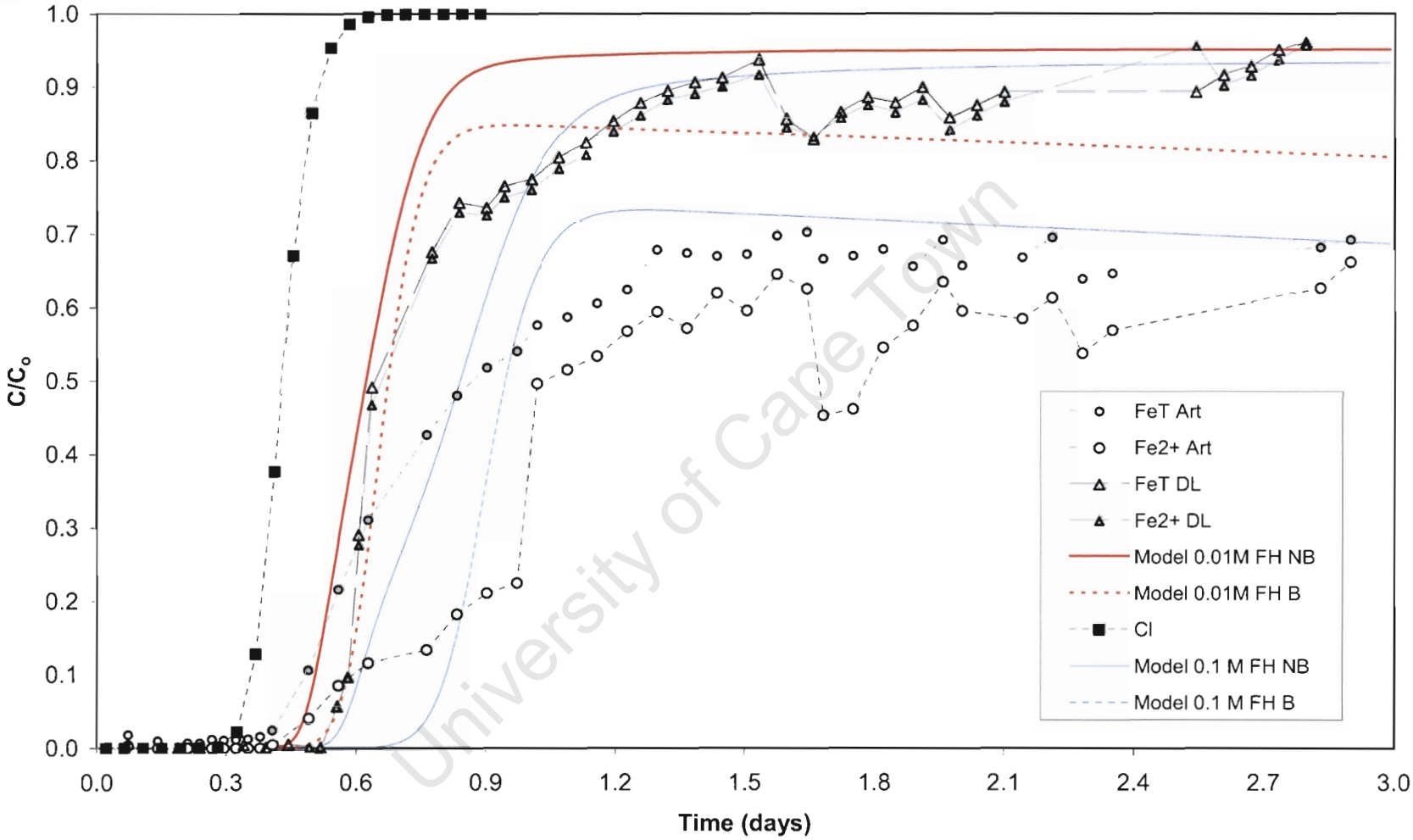

Figure 4.5. Iron concentrations in effluent solution as a function of time for pH 6 influent solution. Coloured lines are transport models

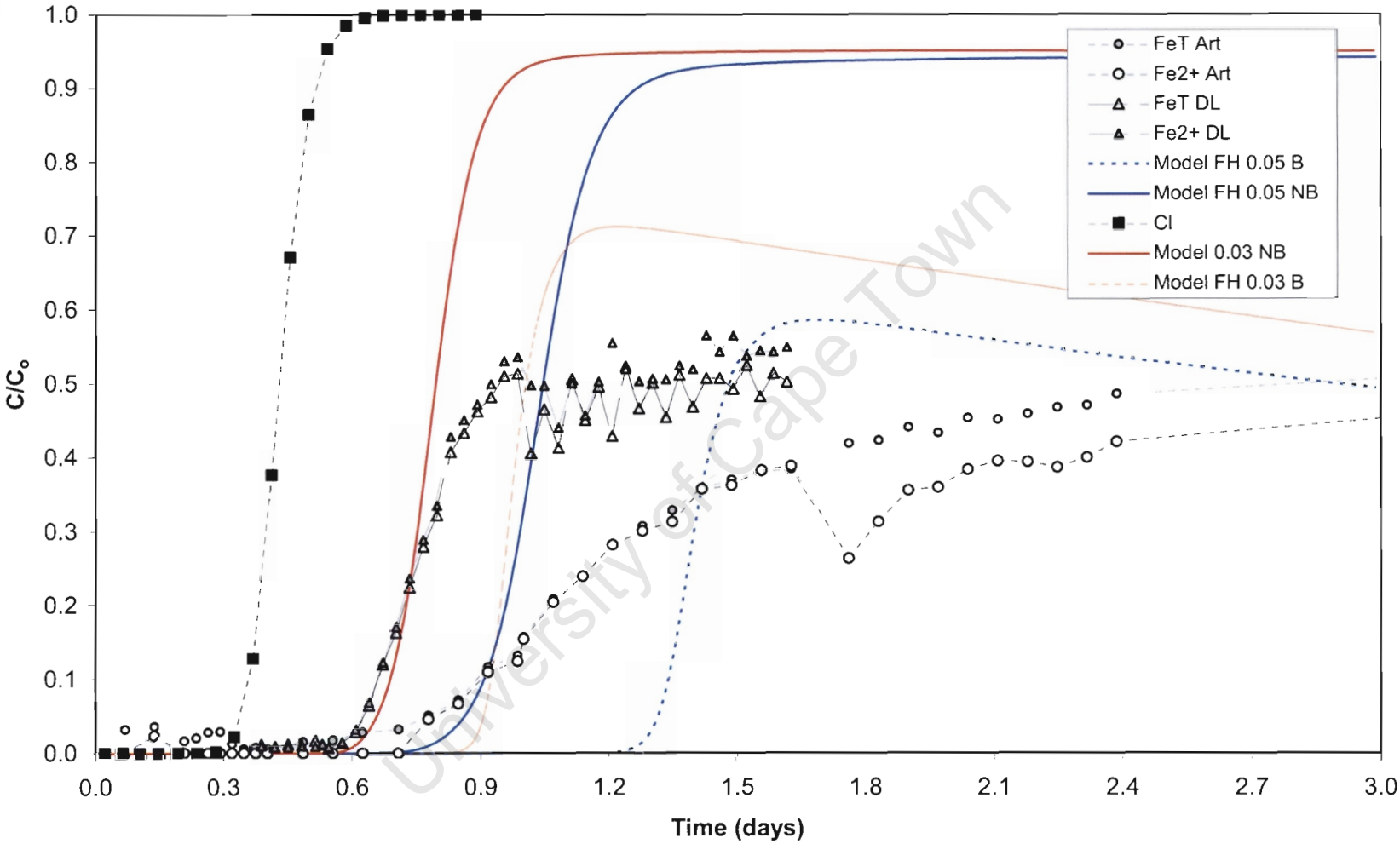

Figure 4.6. Iron concentrations in effluent solution as a function of time for pH 6.5 influent solution. Coloured lines are transport models

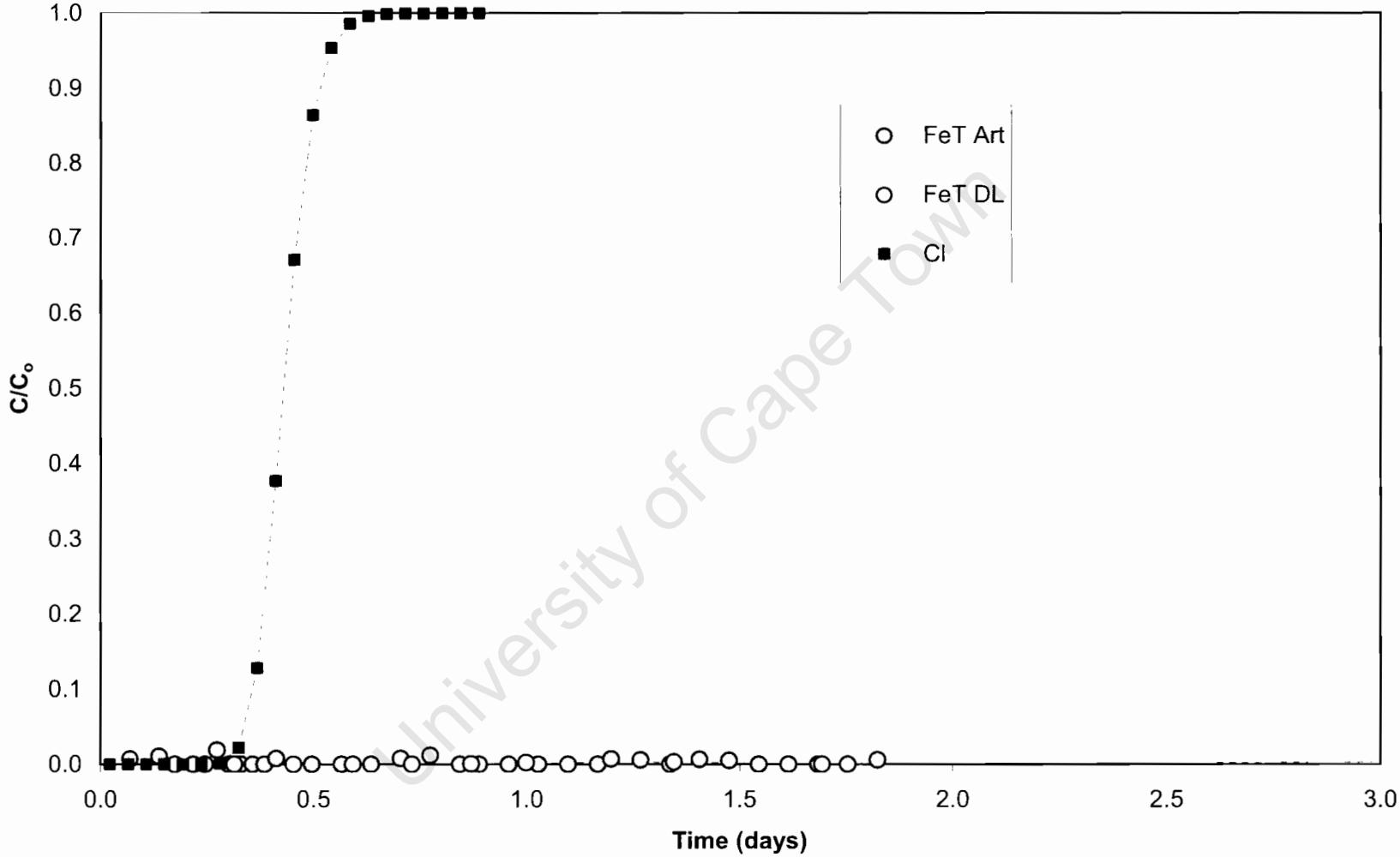

Figure 4.7. Iron concentrations in effluent solution as a function of time for pH 7 influent solution.

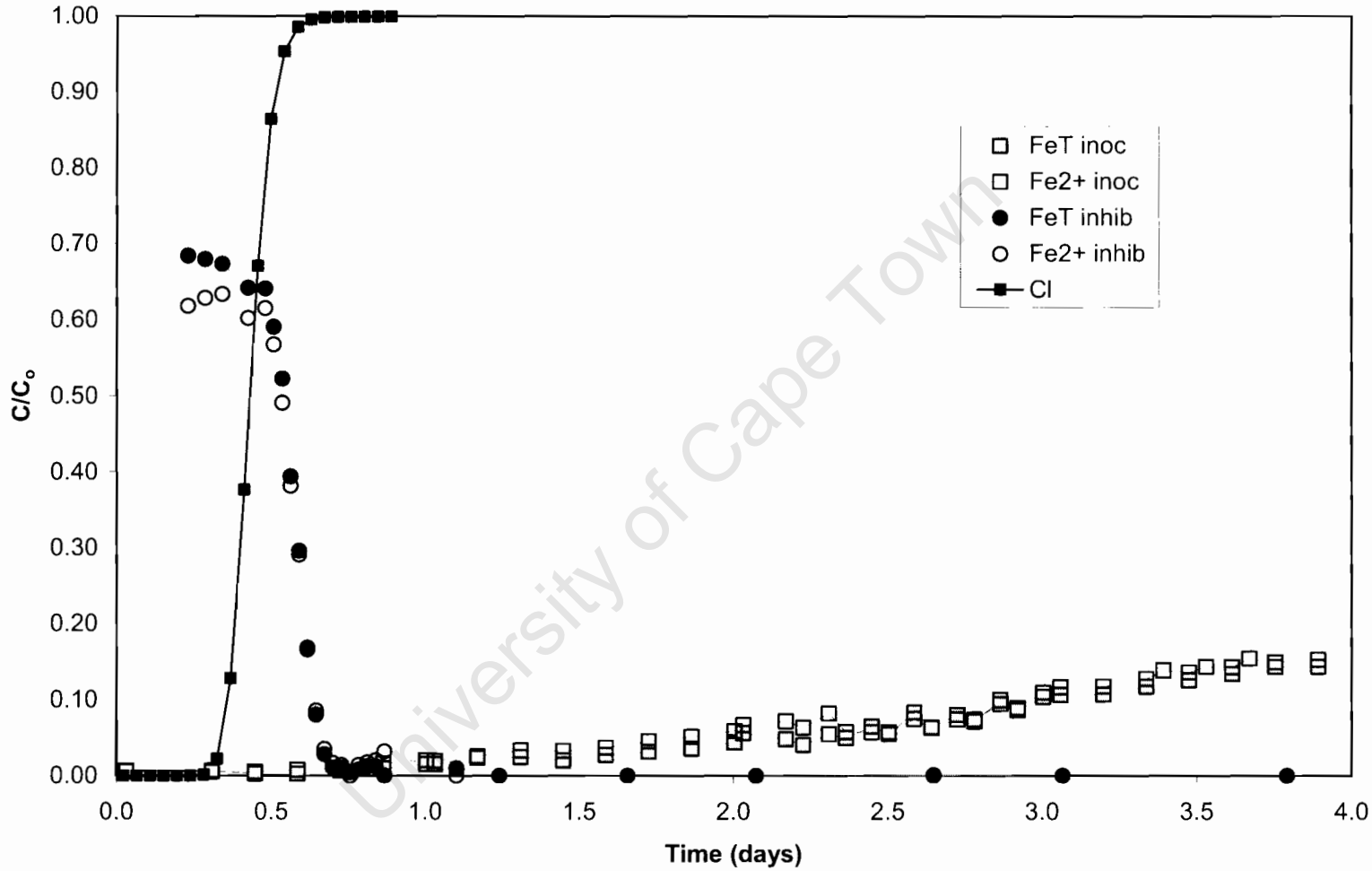

Figure 4.8. Iron concentrations in effluent solution as a function of time for pH 6 influent solution in the inoculated column with and without $HgCl_2$ inhibition.

On opening the column following the experiments, all precipitates were found within the first 5 cm of the inflow. XRD and SEM analysis of precipitates formed in the solution indicated that precipitates in DL17 solution are amorphous iron oxide, whereas precipitates formed from the artificial groundwater solution are needle-like lepidocrocite. The types of precipitates differ in appearance as can be seen in SEM images of iron oxides attached to sands (Figure 4.9-4.11). Oxides attached to the sand surfaces after the DL17 experiments are small, rounded aggregates, which do not appear to be as closely attached to the sand surface as precipitates from the artificial water (Figure 4.9). A single globular string precipitate was found, but it is probably material from the unfiltered groundwater solution, as it did not represent the bulk of the precipitates (Figure 4.9 c). In the artificial groundwater experiments, the precipitates form as small flat accretions on the smooth sand surface, or as aggregates of tiny needles on the rougher surfaces (Figure 4.10). Precipitates on the sand grains in the inoculated column were quite different, with clear evidence of the twisted stalks of *Gallionella* sp. bacteria. The cells at the apex of the stalks appeared to be attached to the sand surface, and the stalks were associated with smooth gelatinous masses, presumably ECP.

4.3.2 Modelling results

4.3.2.1 Chloride breakthrough curves

The modelled Cl breakthrough curves are given in Table F.3 (Appendix F) and the curves are illustrated in Figure 4.2. The breakthrough curves calculated by Phreeqci fit the measured data well when using dispersivities of 2.5×10^{-3} m for 0.11 m/hr, and 7×10^{-4} m for all other flow velocities. These dispersivities bracket the values calculated using the method of Roychoudhury (1998; Table 4.4) which range from 9.7×10^{-4} m to 1.9×10^{-3} m.

4.3.2.2 Iron flow-through curves

Iron flow-through curves are presented in Figures 4.12 and 4.13. For all iron flow-through modelling at the flow rate of 0.11 m/hr, the Phreeqci determined dispersivity of 2.5×10^{-3} is used. Results are summarised in Table 4.6 and Table 4.7.

a.

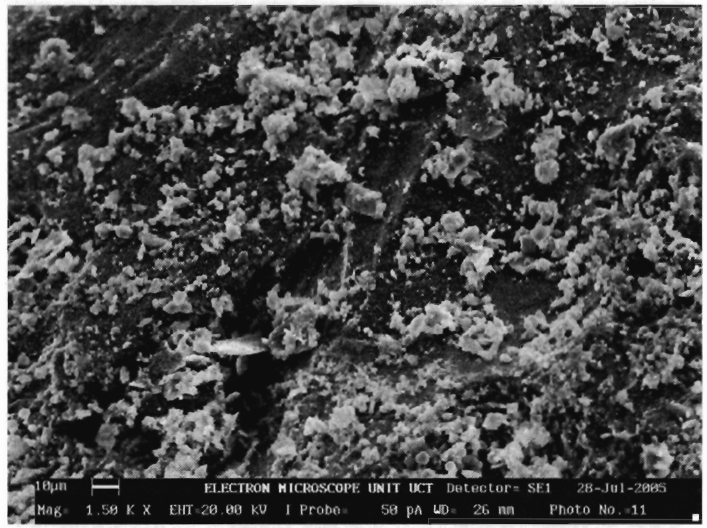

b.

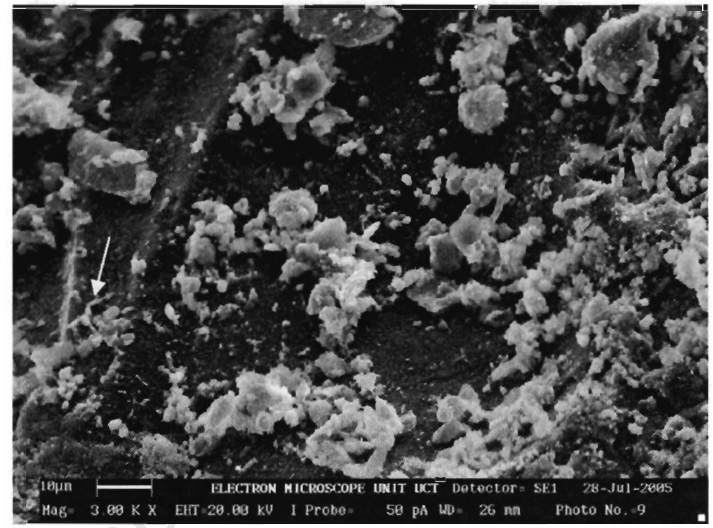

c.

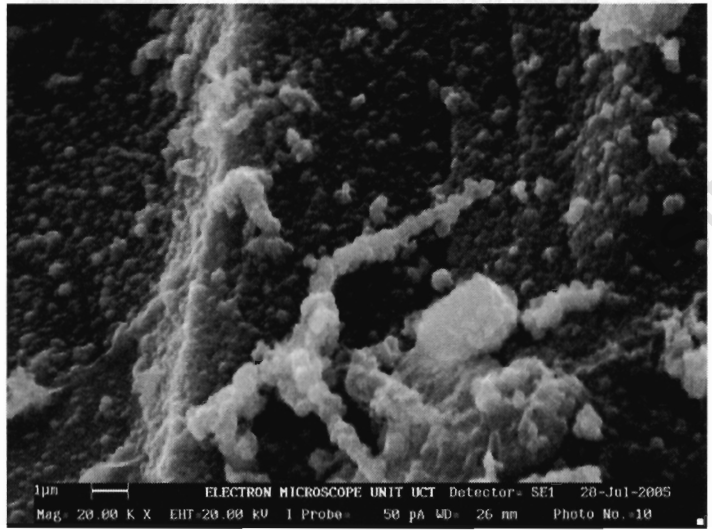

Figure 4.9. SEM images of iron oxides attached to sand grains sampled from the column after DL17 Fe flow-through experiments. a. 1500x; b. 3000x, arrow indicates precipitate shown at 20 000x magnification in c.

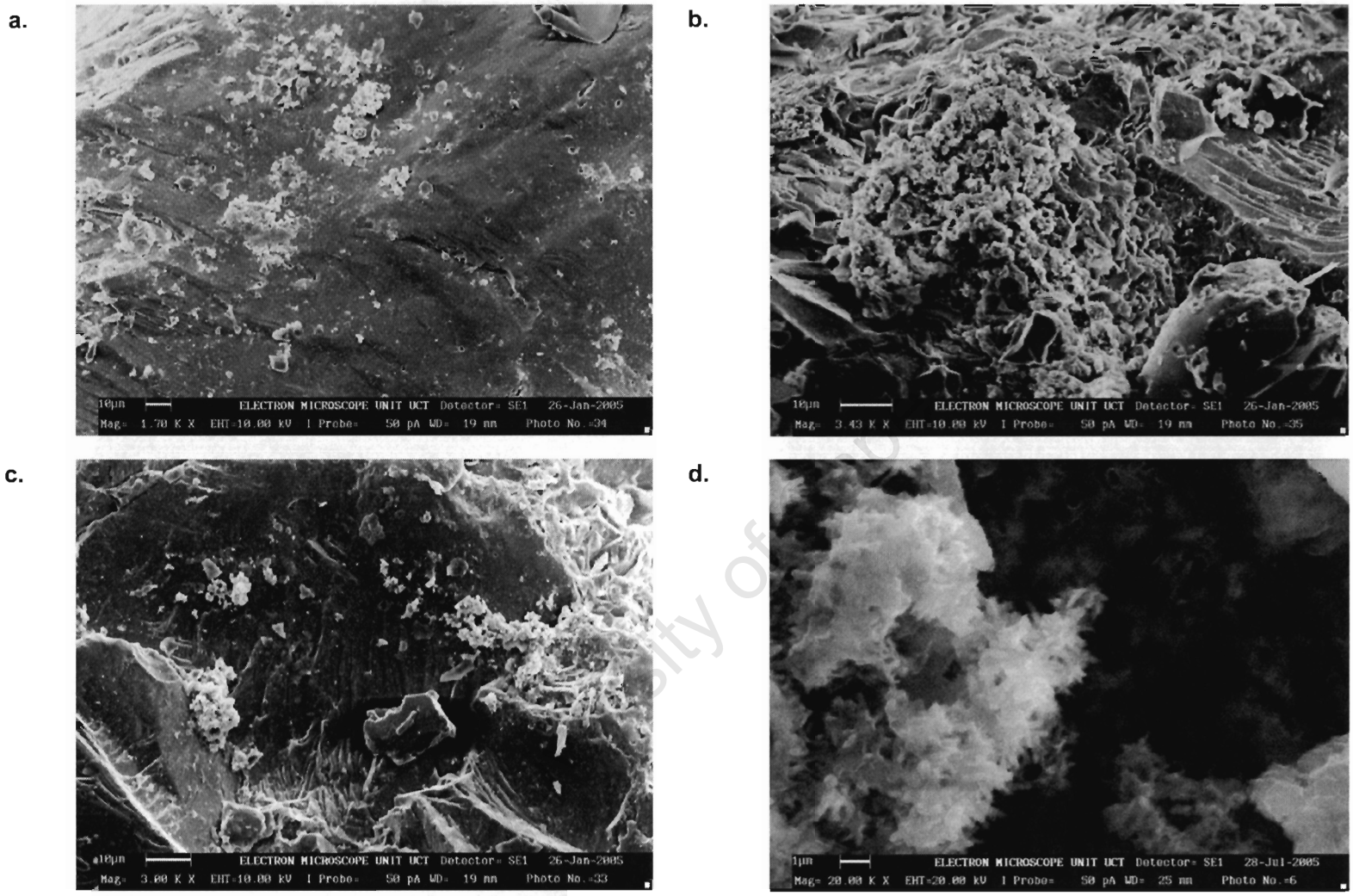

Figure 4.10. SEM images of iron oxides attached to sand grains sampled from the column after artificial groundwater Fe flowthrough experiments. a. Flat aggregates on smooth quartz surface, b. & c. More rounded aggregates on rougher surfaces and on quartz edges, d. Close up of lepidocrocite needles

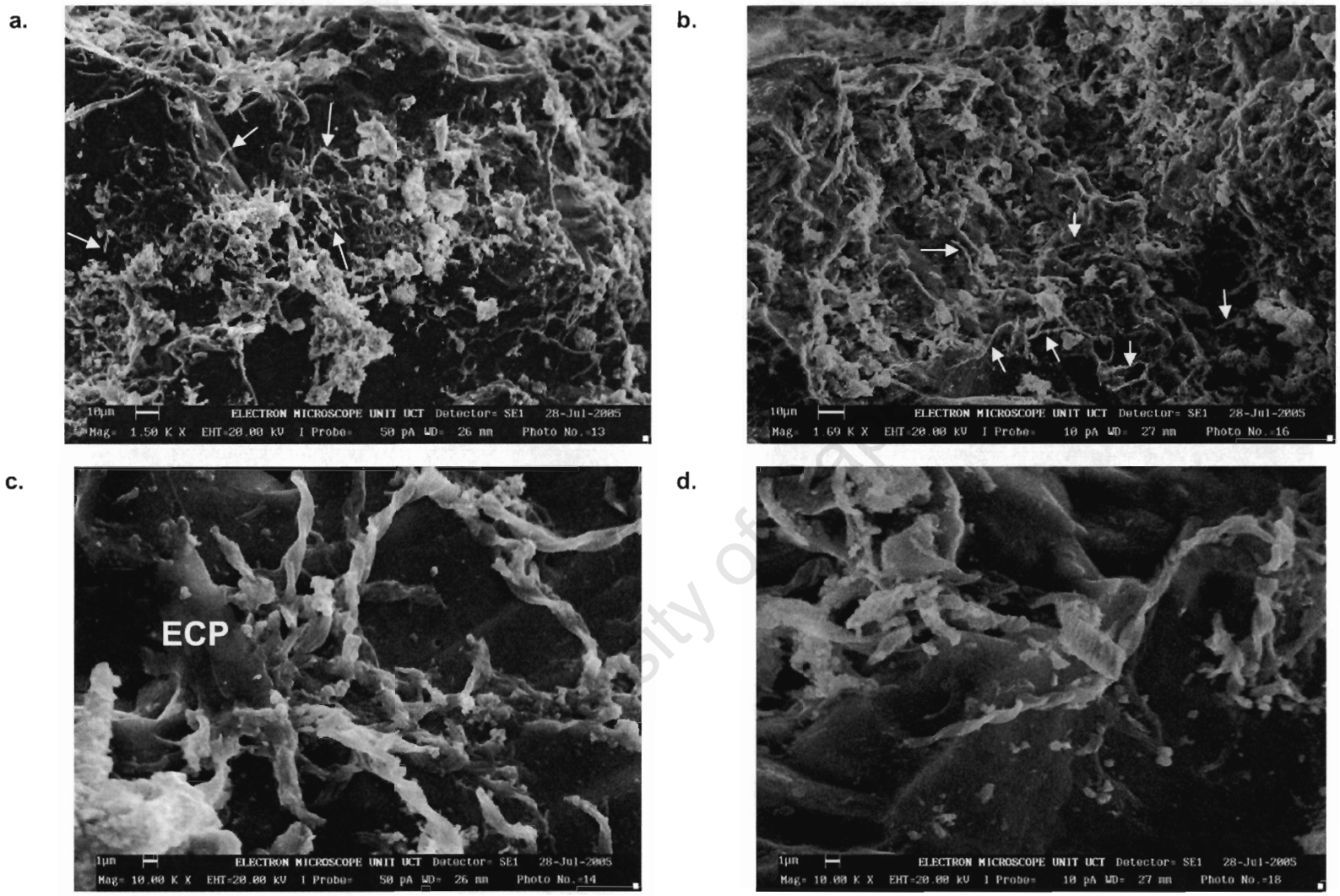

Figure 4.11. SEM images of iron oxides attached to sand grains sampled from the column after inoculated column Fe flowthrough experiments. a., b. Overview of precipitate with *Gallionella* stalks indicated by arrows, c., d. Close up of *Gallionella* stalks with amorphous ECP in c. (labelled)

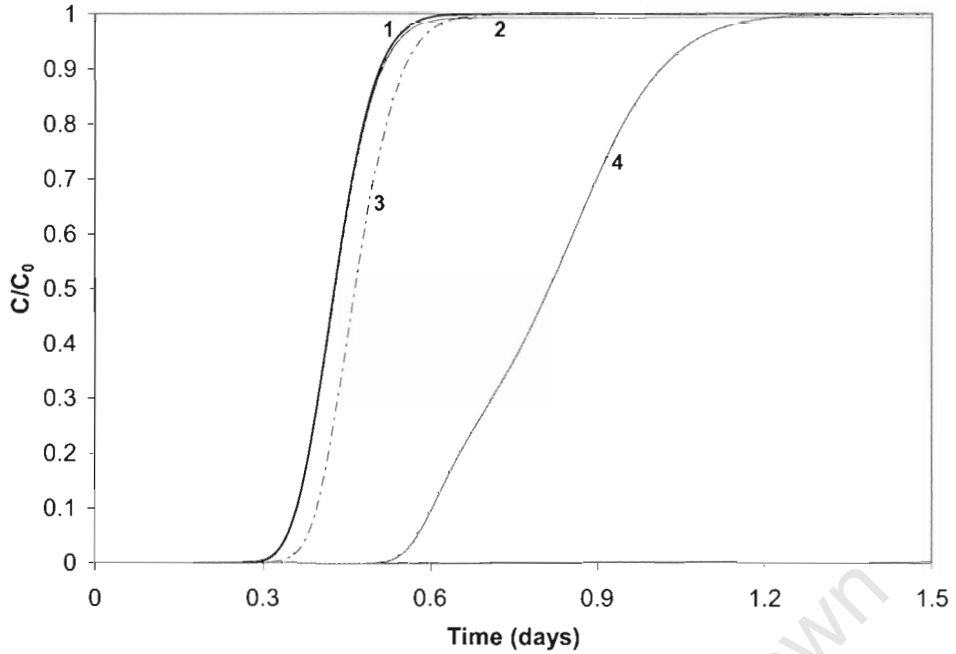

Figure 4.12. Modelled C/C_o values for Fe^T in the column effluent assuming homogenous oxidation at different influent solution pH, with and without adsorption. Curve 1: Homogenous oxidation at pH 5, no buffering and Cl^- breakthrough curve; Curve 2: Homogenous oxidation at pH 7, buffered; Curve 3: homogenous oxidation and adsorption at pH 6, no buffering, assuming initial amount of 0.01 M ferrihydrite/cell; Curve 4: homogenous oxidation and adsorption at pH 6, no buffering, assuming initial amount of 0.1 M ferrihydrite/cell.

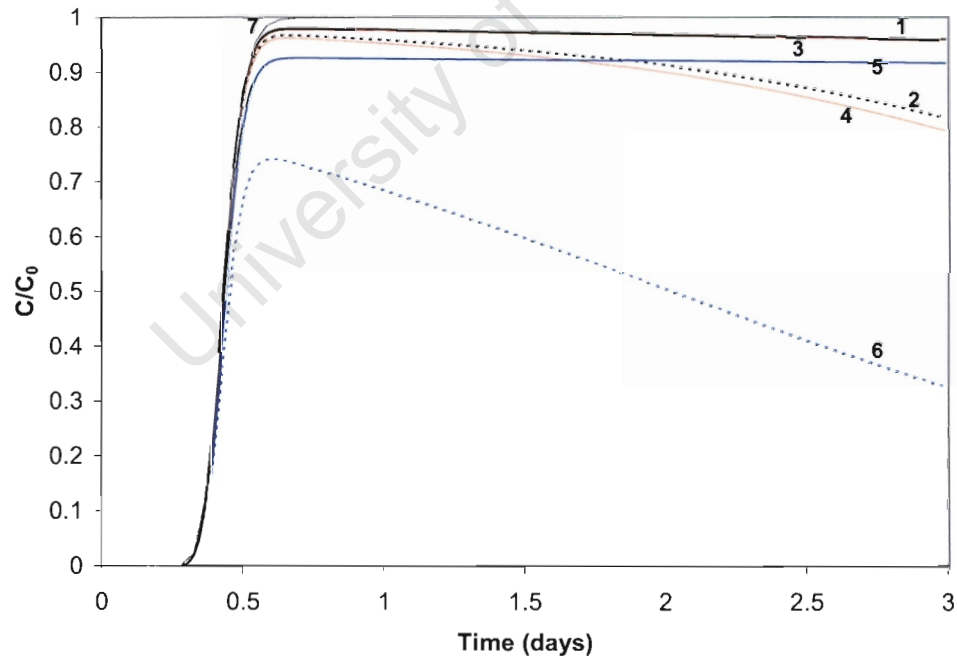

Figure 4.13. Modelled C/C_o values for Fe^T in the column effluent assuming homogenous and heterogeneous oxidation, at influent solution pH of 6.0, with and without buffering, with variable amounts of initial FH in the column. Curve 1: no initial FH, not buffered; Curve 2: no initial FH, buffered at pH 6; Curve 3 (red): $2x10^{-6}$ M FH initially in each cell, not buffered; Curve 4 (red): $2x10^{-6}$ M FH initially in each cell, buffered; Curve 5 (blue): $4x10^{-4}$ M FH initially in each cell, not buffered; Curve 6 (blue): $4x10^{-4}$ M FH initially in each cell, buffered; Curve 7: Cl breakthrough

Table 4.6. Summary of results of homogenous iron oxidation modelling at different pH

	Fe_{out}/Fe_{in}	
pH	Not buffered	Buffered
5	1.000	1.000
6	1.000	1.000
6.5	0.999	0.999
7	0.996	0.992

Table 4.7. Summary of results of heterogeneous iron oxidation and adsorption modelling at pH 6

	Adsorption (steady state)		Autocatalysis (after 3 days)	
Initial FH	Fe_{out}/Fe_{in}		Fe_{out}/Fe_{in}	
(M/cell)[a]	B[b]	NB[c]	B	NB
0	nd[d]	nd	0.817	0.961
1.0×10^{-9}	1.000	1.000	nd	nd
2.0×10^{-6}	1.000	1.000	0.792	0.958
4.0×10^{-4}	1.000	1.000	0.326	0.917
0.01	nd	0.999	nd	nd
0.1	nd	0.998	nd	nd

a.moles ferrihydrite/cell in model; b. Buffered; c. Not buffered; d. not done

Concentrations of Fe^{3+} in the outflow are extremely low (2.5×10^{-10}) because of the modelling set-up which forces Fe^{3+} to precipitate. In the following discussion, iron refers to the total Fe concentration of the effluent, consisting of >99.9% Fe^{2+}. At the low DO levels in the column, homogenous oxidation is extremely slow, and modelled outflow curves indicate that <1% of iron is retained within the column, regardless of the pH (Figure 4.12). Slightly more iron is retained at pH 7, and with buffering. The curves also show no retardation compared to the Cl breakthrough curves. The amount of iron in the effluent remained the same regardless of the iron oxide used as the sink for oxidized Fe^{2+}, e.g., goethite, amorphous iron oxide ($Fe(OH)_3(a)$), or ferrihydrite. Introduction of heterogeneous oxidation has a significant effect on the shape of the Fe_{out}/Fe_{in} curve, particularly when the column was modelled with pre-existing amounts of ferrihydrite (Figure 4.13). In a buffered heterogenous oxidation system, the amount of iron in the effluent initially increases similar to homogenous oxidation, but the concentration reaches a maximum and then begins to decline. In the non-buffered system, the decrease in Fe concentration is less pronounced. The greater the amount of ferrihydrite present before the experiment begins, the lower the maximum

Fe_{out}/Fe_{in} reached before the iron concentration in the effluent begins to decrease. Adsorption operating in conjunction with homogenous oxidation does not affect the steady state Fe_{out}/Fe_{in}, which increases to >99.9%, but at high enough initial ferrihydrite concentrations, retardation of the outflow curve is observed (Figure 4.12). The retardation effect becomes more pronounced the more ferrihydrite is present in the column.

Attempts to model the actual outflow curves are shown on the measured data graphs (Figure 4.4 – 4.6). The models used a combination of heterogeneous oxidation and adsorption, with and without buffering, and a varying amount of ferrihydrite in the column. No single model is able to replicate the curves observed. Only two variables can be modified at any particular pH, i.e., buffering versus no buffering and the amount of ferrihydrite present in the column at the beginning of the experiment. The modelled curve at pH 5 for heterogeneous oxidation and adsorption in a buffered system with an initial FH concentration of 0.5 M FH/cell follows the artificial groundwater Fe^T curve quite well, although the steady state level predicted is not as high as observed. The measured data indicate that a large proportion of the iron has oxidized and is present as Fe^{3+}, while the modelled data represent only Fe^{2+}, so the fit is actually quite poor.

At pH 6, the flow-through of Fe in DL17 water is best predicted by a model using a buffered inflow solution and assuming an initial FH concentration in the column of 0.01 M. However, the measured Fe breakthrough curve does not follow a single slope as predicted by the model, but has a steep initial slope which gradually shallows until steady state is achieved. The breakthrough time of the artificial groundwater Fe curve is predicted well by the 0.01 M initial FH non-buffered model, but the steady state concentration of the measured data is closer to what would be predicted by a model with 0.1 M initial FH per cell and a buffered inflow solution. At pH 6.5, modelled heterogeneous oxidation and adsorption with an initial FH of 0.03 M describe the breakthrough time of the measured data but the amount of precipitation is much greater than could be described except by a buffered system with 0.05 M of initial FH.

4.4 Discussion

4.4.1 Effectiveness of uninoculated column experiments

4.4.1.1 Water chemistry

The flow-through column was designed to replicate conditions experienced within an aquifer close to a discharge point, where chemical reactions occur due to diffusion of oxygen into the groundwater. Monitoring of changes in the chemistry of pH, pe and iron should aid in understanding the processes occurring within the DO gradient. The fraction of iron remaining in the column can be used to calculate the rate of clogging under different influent solution chemistry. The advantage of the column over monitoring of the natural system is that the chemistry of the influent solution can be properly quantified which, as established in Chapter 3, is difficult to do in a natural aquifer. The effectiveness of the column at replicating aquifer conditions close to the discharge point can be assessed by comparison of the chemical changes occurring in the column with chemical changes measured in a borehole using a down-hole chemical logger (Cavé and Smith, 2004; Appendix I).

The pH in down-hole logs was found to increase from the base of the borehole, from 6.2 to 6.8, but then in the upper 2/3 of the borehole, pH was found to decrease by 1.2 pH units (Cavé and Smith, 2004). In the column, a decrease of between 0.2 and 0.4 pH units was observed from the influent to the effluent solution, probably moderated by the buffering of the influent solution required to prevent a significant decrease in pH on addition of the ferrous ammonium sulphate solution. The decrease in pH observed in both the natural system and the column is due to iron oxidation and hydrolysis. Iron hydrolysis is a proton producing reaction, and causes a decrease in pH in a non-buffered system (Equations 2.1-2.5). The pH increase observed at the base of the boreholes could be due to CO_2 degassing (Deng, 1997), which is not replicated in laboratory experiments. The rate of iron oxidation is second order with respect to the concentration of OH^- ions (Davison and Seed, 1983), so the decrease in pH observed in both the natural system and the column would slow the rate of iron oxidation. The implication is that iron encrustation should be exacerbated in groundwater systems with natural buffering. The

absence of buffering in the Peninsula aquifer could be an explanation for the lower incidence of iron clogging compared to the Nardouw aquifer. The groundwater in Atlantis has a much higher alkalinity than water from the Klein Karoo, and coupled with the generally higher pH of the Atlantis groundwater, iron oxidation is expected to be rapid and sustained. Encrustation rates of cm's in a few months have been observed at Atlantis (E. Fontein, AWSS, pers. comm.), but it is not known how this compares to rates of iron accumulation in the KKRWSS.

The redox state of the column and the groundwater system are difficult to compare. The pe of the groundwater was measured with a down-hole logger (Cavé and Smith, 2004), whereas the pe of the column effluent solution is calculated from the Fe^{2+}/Fe^{3+} ratio using Phreeqci. The accuracy of the calculated pe is dependent on the accuracy of measurement of low concentrations of Fe^{3+} in the column outflow. The ferrozine method of determining Fe^{3+} by difference could not give accurate readings below 0.1 mg/L, so the pe of the effluent could not be accurately calculated. The outflow pe-pH values are plotted in Figure 4.14 and show a large amount of scatter.

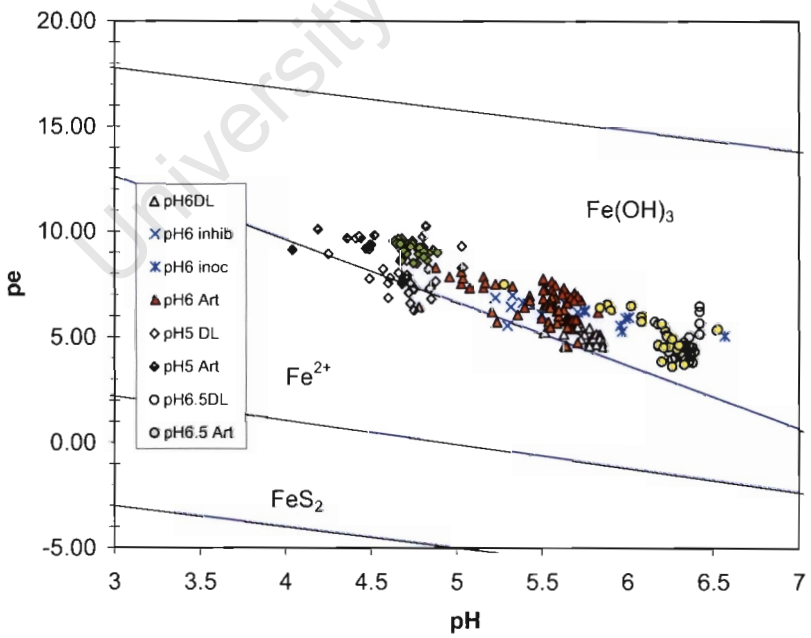

Figure 4.14. pe-pH diagram for column effluent. pe calculated by Phreeqci. Equilibrium lines on the graph are based on an iron concentration of 12.7 mg/L (DL – DL17, inhib – inhibited, inoc – inoculated, art – artificial groundwater).

However, they do define a trend parallel to the Fe^{2+}-$Fe(OH)_3$ equilibrium pe-pH relationship, as do the down-hole data measured by Cavéand Smith (2004; Figure 3.15). This trend is elevated compared to the equilibrium line for $Fe(OH)_3$ at 12.7 mg/L Fe^{2+}, suggesting that the form of $Fe(OH)_3$ formed has a higher K_{sp} than the K_{sp} for $Fe(OH)_3$ used by Phreeqci. The pe-pH relationships indicate that the pe in both the column and the groundwater system is buffered by oxidation and precipitation of Fe^{2+} in the form of an iron oxide mineral.

4.4.1.2 Iron oxide precipitation and mineralogy

Iron oxide precipitation within the aquifer and the flow-through column was noted to be localised in zones of change in flow regime. Observed iron oxide precipitation in the KKRWSS boreholes was just above or within the well screen zones, and at Atlantis, a large amount of encrustation was found on the pump inlet. Most oxide precipitation in the column occurred within the first 5 cm of the inlet, starting at the fritte, where DO concentrations are expected to be relatively low. Iron encrustation is commonly associated with zones of increased turbulence (Flower and Bishop, 2003). Turbulence will aid in mixing O_2 into the groundwater, and will also result in a greater number of collisions between Fe^{2+}, newly precipitated colloids, and surfaces, possibly increasing the rate of adsorption and precipitation. Once a single layer of iron oxide has formed, the rate of accumulation should increase dramatically due to heterogeneous oxidation and adsorption.

Observed iron oxide precipitates in boreholes of the KKRWSS include 2-line ferrihydrite, 6-line ferrihydrite, goethite and schwertmannite (Chapter 5). Two distinctly different precipitates formed in the columns. An amorphous iron oxide was found in the DL17 groundwater experiments, while lepidocrocite was found when using artificial groundwater. Lepidocrocite is a polymorph of goethite which forms by oxidation of Fe^{2+} in the absence of Al (Schwertmann and Taylor, 1989). The presence of Al in natural systems and the DL17 influent solution inhibits the formation of lepidocrocite. The iron oxide precipitated in the DL17 column is more amorphous than the precipitates sampled in the field which can clearly be identified as either 2-line or 6-line

ferrihydrite, and suggests either that the precipitates in the field have aged or that the conditions of precipitation in the column do not replicate those in the field. This highly amorphous precipitate is likely to be more soluble than more crystalline phases and as such would have a higher K_{sp} as discussed in the previous section.

The speciation of iron at different depths in the borehole was estimated using the measured pe, and used to calculate saturation indices of common iron minerals. The groundwater was found to be supersaturated with respect to all iron minerals, including $Fe(OH)_3$, in the upper parts of the borehole (Cavé and Smith, 2004). The saturation indices of $Fe(OH)_3$ calculated for the column indicate that the effluent solution is also supersaturated with respect to $Fe(OH)_3$ (by 0 to 2 times), so it appears that this mineral does not control the solubility of iron in the column (Figure 4.15). Goethite (5 to 8 times) and ferrihydrite (2.5 to 4.5 times) are also supersaturated in the column effluent solution. The detection of an extremely amorphous form of iron oxide in the DL17 column suggests that a mineral with a lower K_{eq} than $Fe(OH)_3$ controls the solubility of Fe. However, the saturation indices show a large amount of scatter due to the poor accuracy of Fe^{3+} measurements at such low concentrations, so it is difficult to draw any real conclusions from the data.

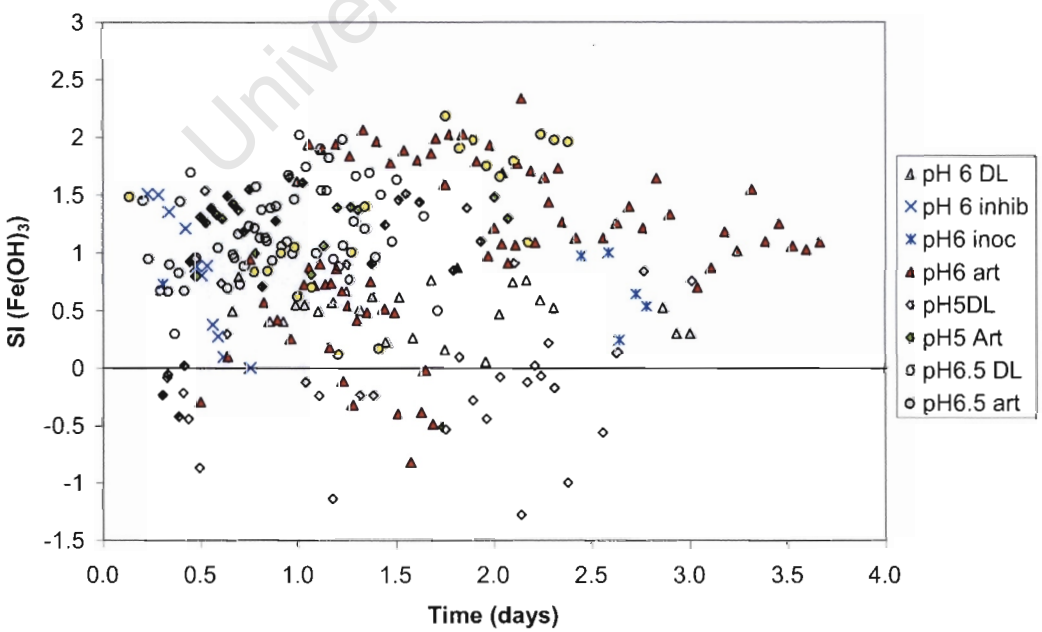

Figure 4.15. Saturation indices of $Fe(OH)_3$(a) for all flow through experiments.

4.4.2 Behaviour of iron in column experiments

The chemical conditions and mineralogy in the flow-through column have been shown to approximately replicate borehole conditions, suggesting that the behaviour of iron in the column should be a reasonable proxy of low pO_2 field conditions.

In all experiments, the effluent solution initially contains no Fe, after which the iron concentrations increase to a steady state level. The breakthrough of Fe occurs later than the breakthrough of Cl^-, and steady state $Fe_{out}/Fe_{in}<1$, indicating that some Fe remains in the column. Roychoudhury *et al.*, (1998) suggest that a delay in breakthrough relative to a conservative tracer represents reversible sorption, while a steady state concentration of $C_{out}/C_{in} < 1$ indicates irreversible removal from solution. Both adsorption and permanent removal are occurring in the column, and both processes increase with increasing pH. The more rapid breakthrough and higher steady state concentrations of iron in DL17 experiments compared to artificial groundwater experiments could be due to complexation of iron in a soluble form by a ligand not present in the artificial groundwater (Table 4.8). Further evidence for complexation is that all iron in the outflow from DL17 experiments is present as Fe^{2+} whereas a significant proportion of soluble iron is present as Fe^{3+} in the outflow of artificial groundwater experiments, signifying that oxidation of Fe^{2+} is slower in the DL17 experiments than in artificial groundwater.

Table 4.8. Differences in breakthrough and steady state concentrations of effluent from iron flow-through columns (approximate values)

	Breakthrough (days)		Steady state Fe_{out}/Fe_{in}		Steady state $Fe^{2+}{}_{out}/Fe_{in}$		Steady state $Fe^{3+}{}_{out}/Fe_{in}$	
pH	DL17	Artificial	DL17	Artificial	DL17	Artificial	DL17	Artificial
5	0.44	0.38	0.76	0.93	0.76	0.60	0	0.33
6	0.57	0.40	0.89	0.67	0.89	0.62	0	0.05
6.5	0.58	0.71	0.50	0.37	0.50	0.32	0	0.05

Most assessment of iron precipitation in boreholes assumes that iron oxidation is the limiting reaction in the precipitation of iron oxides from an Fe^{2+} rich solution. There has been a significant amount of work done on the kinetics of iron oxidation but there is virtually no literature on the kinetics of iron oxide precipitation. Applin and Zhou (1989) noted that iron precipitation did not occur immediately from a groundwater sample collected in the field. In

Chapter 3, results are presented for the change in iron concentration following sampling of groundwater from a borehole in the Klein Karoo. The proportion of Fe^{3+} in solution does not increase even though the Fe^{T} concentration is decreasing, indicating that any Fe^{3+} is immediately removed from solution as a precipitate and iron oxidation is indeed limiting at this pH. The iron precipitate material may not be easily visible, but is collected onto a 0.45 μm filter. However, during flow through experiments it was noted that the proportion of Fe^{3+} in the outflow from artificial groundwater experiments is greater than the proportion of Fe^{3+} in the outflow from DL17 groundwater experiments. The presence of Fe^{3+} in the outflow from artificial groundwater experiments suggests that oxidation is occurring without precipitation, or that precipitates are not filtered out. The proportion of Fe as Fe^{3+} increased at lower pH, suggesting that precipitation is slower at lower pH.

The data indicate that iron oxidation and precipitation at low levels of pO_2 are capable of removing a large proportion of iron from solution, but the degree of removal is dependent on the chemistry of the water, including the pH and the presence of complexing agents.

4.4.2.1 Comparison of measured to modelled iron behaviour

Sensitivity analysis of modelled flow-through curves at pH 6 was used to identify the effects of different chemical processes on the retardation and retention of iron within the column. Three processes were considered, homogenous oxidation, heterogeneous oxidation and adsorption (Figures 4.12 and 4.13). Results of the sensitivity analysis were used to formulate models to describe the measured data.

Homogenous oxidation modelling reveals that at the low pO_2 concentrations maintained in the column experiments, there should be hardly any retention of iron in the column at any pH, regardless of whether the influent solution is buffered or not (Figure 4.12; Table 4.6). Clearly additional processes are required to explain the observed flow-through curves for iron. Heterogeneous oxidation at pH 6 is more effective at removing iron from solution. The amount of iron modelled to be retained by the column increases with time due to the increasing amount of ferrihydrite in the system, particularly in the

buffered system (Figure 4.13; Table 4.7). Even more efficient iron removal from solution is predicted when the column is assumed to contain ferrihydrite at the start of experiment. Modelling of adsorption processes requires a significant initial amount of ferrihydrite to be present in the column before any effect is seen on the iron breakthrough curve. The number of sorption sites present has to be close to the same order of magnitude as the concentration of iron in solution before a retardation effect is noticed. Modelled adsorption processes cause a retardation effect, but do not affect the total amount of iron measured in the effluent solution at steady state compared to homogenous oxidation with no adsorption. The presence of clay in the column would also be expected to cause a retardation effect due to adsorption of Fe from solution, but clay minerals have fewer sorption sites than iron oxides and could not explain the degree of retardation observed.

Attempts to replicate the observed iron flow-through curves using transport modelling including the abovementioned three processes were not particularly successful, implying that important processes occurring in the column, and in boreholes, have been overlooked (Figure 4.4–4.6). Initial concentrations of between 0.01 M and 0.7 M FH per cell were required in all the models to generate a breakthrough curve delayed with respect to the Cl breakthrough curve, and with a steady state concentration closer to the observed steady state concentrations. There are two problems with this requirement. Firstly, the columns were sand filled with low concentrations of FH, so use of FH to achieve the observed results is incorrect. Secondly, the delay on Fe breakthrough and the steady state concentration in the model are linked because they are both controlled by the amount of FH present. A single initial FH content was not sufficient to explain both the observed breakthrough of retardation and the observed steady state concentration, for e.g. at pH 6.5, the breakthrough of Fe in DL17 groundwater is best described with a model assuming unbuffered influent solution and 0.03 M initial FH per cell, whereas the closest prediction of the measured steady state concentration of Fe is using a model assuming a buffered influent solution with 0.05 M initial FH per cell. The excess iron removal observed compared to what is predicted to be associated with a particular breakthrough time suggests that adsorption

processes and iron removal processes are not both related to the content of FH. The modelling results do show the sensitivity of the degree of iron retention to the amount of FH present, possibly explaining rapid re-encrustation of wells following rehabilitation.

The oscillations in the iron flow-through curves are also not explained by the modelled data. Oscillations on a 5 to 6 hour wavelength could be due to the growth dynamics of interacting populations of organisms (Roychoudhury *et al.*, 1998). The presence of microbes would not be expected when an artificial groundwater solution is pumped through aquifer sand that has been repeatedly washed in peroxide and acid, but as no specific precautions were taken to inhibit bacteria in most of the experiments, microbial action cannot be ruled out. SEM images of precipitates formed in the uninoculated experiments do not reveal any obvious iron bacterial presence, supporting the view that iron bacteria were not significantly involved in iron oxidation and precipitation in these experiments. If these oscillations do represent bacterial growth, then the bacterial effect is most pronounced on Fe^{2+} concentrations at pH 5, as this curve is most affected by oscillations (Figure 4.4).

The comparison of measured iron flow-through curves to modelled flow-through curves indicates that the degree of iron retention in a column designed to replicate a borehole can be greater than predicted by homogenous oxidation. The slow kinetics of homogenous iron oxidation has been used as an argument for the microbial mediation of iron oxidation (Ralph and Stevenson, 1995), but these results suggest that heterogeneous oxidation, adsorption and other as yet unidentified processes could account for some of the differences between observed and predicted iron oxidation rates and extent.

4.4.3 Effect of inoculation

The iron flow-through curves observed after inoculation of the column with material from an actively clogging well are quite different to flow-through curves from the uninoculated columns, possibly due to heterogeneous oxidation or microbial oxidation. The presence of large amounts of iron oxide

material would be expected to catalyse heterogeneous oxidation of iron, resulting in retention of iron within the column, and the presence of iron oxidizing microbes in the column should have a similar effect. However, the effluent from the inoculated column shows a slow linear increase in iron concentration with time with no oscillations. The DO and pH of the effluent from the inoculated column also differed from the other experiments. The DO concentrations in the effluent were found on 2 occasions to be lower than the concentration in the reservoir, and the difference in pH between inflow and outflow was less than in any other experiment, and in some cases the effluent pH was higher than the influent pH. The data suggest that in the inoculated column, rather than iron oxidation, iron reduction is occurring (Drever, 1997):

$$Fe(OH)_3 + C_{organic} + 8H^+ = CO_2 + 4Fe^{2+} + 10H_2O \qquad (4.11)$$

Iron reduction is a proton consuming reaction, unlike iron oxidation and precipitation. Similar iron flow-through curves to the inoculated column curves presented here were obtained by Roden *et al.* (2000) during studies on microbial reduction of synthetic goethite coated sand. Although the artificial groundwater does contain some HCO_3, no additional C source was added to the influent solution. The inoculating material from Atlantis consists of approximately 4 wt% organic carbon in the dry state (See Chapter 5), which may be used as a C source by iron-reducing bacteria. Introduction of a microbial inhibiting $HgCl_2$ solution results in an iron flow-through curve that is inverse to all other flow-through curves, i.e., starting with high iron concentrations before breakthrough, and decreasing to <0.01 mg/L. The results suggest that the $HgCl_2$ inhibits the iron reducing microbes, but does not affect heterogeneous iron oxidation or microbial iron oxidation.

Although the overall reaction in the column on inoculation with iron oxide material from the field appears to be iron reduction, iron oxidizing bacteria were observed by SEM in the first few cm of the column. The unmistakable helical stalks of *Gallionella sp.* are clearly visible in Figure 4.11 a-d. These bacteria were not observed in any sample collected from the field (See Chapter 5), or in the uninoculated columns. The bacteria appeared to be attached to surfaces and are associated with stringy gelatinous masses, presumably extra-cellular polymers. The appearance of *Gallionella* in the

column when it was not observed in field samples from the same site suggests that, although the bacteria are present, field conditions do not support the growth of the stalks. Conditions under which *Gallionella* do not grow stalks, i.e. CO_2 as a carbon source and FeS as an electron donor (Hallbeck and Pedersen, 1990; Lüters-Czekalla, 1990), do not equate with conditions in the aquifer and the absence of *Gallionella* stalks in field samples may indicate that *Gallionella* are not actively involved in iron oxidation.

The presence of iron-oxidizing bacteria at the column inlet and the overall iron reduction reaction are not mutually exclusive. Iron oxidation may occur at the column inlet, but as organic carbon is oxidized and the little O_2 removed from the system, iron reduction can occur. Emerson and Moyer (1997) observed close association of iron oxidizing and iron reducing bacteria and suggested that bacterial Fe^{2+} oxidation may promote Fe^{3+} reduction by producing amorphous/poorly crystalline iron oxides which are readily available for Fe^{3+} reducing bacteria. The interface between microbial iron oxidation and microbial iron reduction is probably controlled by the rate of supply of DO. At slow rates of supply, oxidation of organic carbon can consume most O_2, and iron reduction will predominate. In a system where supply of DO exceeds consumption, iron oxidation will predominate. In the column this interface is controlled by the flow rate and the rate of oxygen supply. The results indicate that the niche area for microbial iron oxidation is limited by high pH and DO, where chemical iron oxidation takes over, and by low DO and high organic carbon, where iron reduction can occur.

Further experiments will be necessary to fully understand the results from the inoculated and inhibited column flow-through experiments, but the growth of *Gallionella*, the differences between the inoculated and inhibited experiments, and the apparent iron reduction observed all indicate that the flow-through column experimental approach could be useful to gain an understanding of microbial involvement in iron oxidation at low pO_2.

4.4.4 Rate and extent of iron precipitation

The steady state Fe_{in}/Fe_{out} values do not reach unity in any of the column experiments, indicating that some iron remains in the column. The amount of iron retained in the column increases with increasing pH, and virtually all the iron is retained in the column at pH 7. The actual amount of ferrihydrite that is precipitated per time period at steady state can be calculated for each pH level, and ranges from 0.82 mg (pH 6 artificial water) to 11.65 mg (pH 7) ferrihydrite per day (24 hours). At a density of 1.5 g/cm^3 (assuming extremely hydrous precipitates as observed at Atlantis (Chapter 5)), 11.65 mg of ferrihydrite will occupy a volume of 7.8 μL. The pore volume of the column is 214 mL, so to clog the entire column will take approximately 75 years. The flow rate used in this experiment was to ensure measurable changes in reactants between the inflow and outflow, and is not representative of a borehole. The residence time of a borehole water column 200 m high, with a diameter of 20 cm being pumped at 300 L/minute is about 20 minutes, compared to 10 hours in the column.

Initial clogging took years to manifest at both the KKRWSS and Atlantis wellfields, but repeat episodes occur in a short time following rehabilitation. The volume of a hydrous precipitate (density = 1.5 g/cm^3) required to clog a Stevenson screen of 100 slots (assuming slots of 0.5 cm height, 20 cm diameter and 0.5 cm depth) is 795 mL. The mass of precipitate is then 1190 g. For ferrihydrite, this equates to 623 g of Fe. At an iron concentration of 5 mg/L, 125 000 L of water is required if all iron is removed from groundwater, which would take 7 hours to precipitate if pumping at an average of 300 L/minute. This calculation shows that iron encrustation of boreholes can be extremely rapid if complete oxidation and precipitation of iron occur in the well. The calculation assumes that precipitation is highly localised, as observed during down-hole video logging. The same volume of precipitate spread over a wider area is unlikely to be problematic. Both Hallberg and Martinell (1976) and Appelo *et al.* (1999) have found no significant reduction in borehole yield following years of inducing iron oxide precipitation in aquifers by pumping oxygenated water into the aquifer (the Vyredox method), because the iron precipitation is spread over a wide area. The Vyredox method is effective

where groundwater pH is greater than 6, no sulphides are present in the aquifer, and the aquifer is relatively homogenous. These conditions are satisfied at the AWSS, but not at the KKRWSS. The rapid reclogging of boreholes observed at both Atlantis and Klein Karoo wellfields following chemical rehabilitation is most likely due to incomplete removal of iron oxide material in the well and aquifer, which can catalyse further oxidation and result in more rapid encrustation of wells.

The flow rate and residence time of the water in the borehole may be immaterial as both Walter (1997) and Applin and Zhou (1989) came to the conclusion that most iron oxide precipitation occurs during standing water times. However, allowing the inoculated column to stand for several days resulted in an increase in soluble iron concentrations in the column due to iron reduction. The DO concentration of two standing water columns determined by down-hole logging was found to be lower in the water column that had been standing for a longer period of time, although the depth of diffusion of oxygen from the water table was greater in this borehole (Cavé and Smith, 2004). Although oxidation and precipitation is likely to be high when pumping is initially stopped, it appears that oxidation of iron and organic carbon in water and precipitates removes oxygen from water, and the system may become reducing. Localisation of precipitation in areas of high turbulence, as observed in this study and others (e.g. Houben, 2004) suggests that pumping may promote precipitation.

4.5 Conclusion

The near borehole environment of a sandstone aquifer was successfully replicated by building a flow-through column with a buffered (pH 5 – 7), low DO, high Fe^{2+} influent solution. An increase in O_2 in the column resulted in iron oxidation and precipitation within the column. Processes likely to be occurring in the column include adsorption of Fe^{2+} onto surfaces, resulting in retardation of the Fe breakthrough curve compared to a conservative tracer, and oxidation of iron by both homogenous and heterogeneous oxidation reactions, followed by precipitation of Fe^{3+}, resulting in retention of a proportion of the influent iron within the column. Iron precipitates were found

to be amorphous iron oxide in the presence of Al, or lepidocrocite in the absence of Al, and no evidence of bacteria was observed by SEM. The degree of iron removal from the flow-through solution is in excess of the degree of removal predicted by transport modelling of simple homogenous oxidation. Incorporation of buffering, heterogenous oxidation and adsorption into the flow-through model improved the correspondence between measured and modelled flow-through curves, but modelling clearly does not account for all the processes occurring in the column. Observation of maximum iron precipitation at the inlet to the column where flow dynamics change, and in high turbulence regions of boreholes indicates that flow dynamics play a role in localising iron precipitation.

Inoculation of the column resulted in the growth of *Gallionella* near the column inlet, but the observed slow increase in Fe concentration in the effluent suggest that elsewhere in the column iron reduction was occurring. Iron oxidizing and iron reducing bacteria survive in only marginally different niche environments, and iron oxidizing bacteria have to not only compete with chemical iron oxidation in neutral pH environments, but also with iron reducing bacteria in low DO environments with the presence of organic carbon, such as stagnant zones in boreholes. A large body of evidence associating iron clogging with the occurrence of iron-oxidizing bacteria suggests that the bacteria do play a role in borehole clogging, but the tiny niche environment in which they can survive may limit the spatial extent of their involvement in iron clogging, perhaps localising their occurrence to narrow zones within the borehole in which the right conditions exist.

5 A geochemical investigation of iron oxyhydroxide encrustations precipitated from two aquifers

5.1 Introduction

Two lithologically distinct wellfields in South Africa are affected by problems of iron oxyhydroxide encrustation of wells. The Klein Karoo Rural Water Supply Scheme (KKRWSS) sources water from deep boreholes within the structurally controlled Table Mountain Group aquifer, whereas the Atlantis Water Supply Scheme (AWSS) taps water from shallow boreholes in an unconfined sandy aquifer that is being artificially recharged. In both cases, the encrustation problem is ongoing and is an economic drain to the well scheme managers. Treatment processes in both wellfields have so far been only chemical rehabilitation, using a combination of heated bases, acids and oxidizing agents of differing volumes but similar concentrations. Although some analyses of the encrusting material have been performed, there is little basis to the rehabilitation treatments other than that they are effective in the short term. Groundwater practitioners place a heavy emphasis on the bacterial nature of the encrustations, referring to them as biofilms, yet there is no clear evidence that the deposits are due to bacteria. It is clear that a better understanding of the encrustating material is needed. In addition, there is debate in the recent literature regarding the differences between natural and synthetic iron oxide minerals, particularly ferrihydrite, and the role of bacteria in their formation (Rancourt *et al.*, 2005; Gloter *et al.*, 2004; Janney *et al.*, 2001; 2000 a, b). The current study provides a good opportunity to compare naturally precipitated iron oxides to synthetically prepared samples.

Questions to be answered in this chapter include:

- Are the encrustations from the two wellfields the same?
- What affects the mineralogy/crystallinity of the samples?
- How do natural precipitates compare with synthetic precipitates?
- Can bacterially precipitated iron oxides be distinguished from chemically precipitated iron oxides?

5.2 Methodology

5.2.1 Sample collection

5.2.1.1 Natural samples

Samples of iron encrustations were collected from accessible components of borehole equipment, such as riser pipes, wellheads and submersible pumps at both the KKRWSS and the AWSS (Table 5.1; Figure 5.1). A summary of the average water chemistry of the two aquifers is given in Table 5.2. All the KKRWSS samples are from boreholes in the Nardouw Subgroup, and all the Atlantis samples are from the Witzand Formation. Details of the water chemistry of the specific boreholes and hotsprings from which the samples were obtained can be found in the hydrocensus (Table A.1) in Appendix A (KKRWSS).

Table 5.1. Naming convention and description of synthetic and natural samples analysed in this study

	Sample ID	Borehole	Sampling point	Date	Comments
SYN-THETIC	FH2				2-line ferrihydrite
	FH6				6-line ferrihydrite
	Gt				Goethite
	Sch				Schwertmannite
ATLANTIS	A1	W34012	Flowmeter	2003/11/04	Dry at collection
	A2	W34020	Flowmeter	2003/11/04	Slimy and ridged perpendicular to flow direction. About 2-3 mm thick only 1 month after previous service.
	A3	W34020	Top of riser pipe	2003/11/05	Wet at time of collection
	A4	W34020	Orifice plate	2003/11/05	1.5 cm thick coating on orifice plate strongly resembling lab-prepared FH2. Lost 80% of mass on air-drying.
	A5	W34032	Top of riser pipe	2003/11/05	Wet at time of collection
	A6	W34032	Pump	2003/11/05	Wet at time of collection
KKRWSS	K1	DL16	Top of riser pipe	2002/07/30	Dry at collection
	K2	DP28	Well head	2003/08/12	Dry at collection
	K3	GA1	Borehole pump (standing next to hole)	2003/08/13	Dry at collection
	K4	DG110	Well head	2003/08/12	Dry at collection
	K5	DP10	Well head	2003/08/12	Dry at collection
HOT-SPRING	H1	Warmwater-berg	Overflow spillage	2003/08/08	Flaky clods
	H2	Calitzdorp Hot spring	Overflow point	2003/08/14	Flaky clods
COLD-SPRING	S1	Dyss	Dysselsdorp Water Treatment Works	2003/08/10	Contains hard white nodules
	S2	HERMANUS	Hermanus artesian borehole	2003/09/20	Wet and slimy

a.

b.

c.

d.

e.

Figure 5.1. Sampling sites for natural iron oxide encrustations: a. Overflow pipe at Calitzdorp hotspring (H2); b. Warmwaterberg hotspring (H1); c. Iron coated flow meter from borehole W34020 in the AWSS (A2); d.Top of riser pipe of borehole DL16 in the KKRWSS (K1); e. Pump from borehole GA1 coated in thin layer of dry iron oxides in the KKRWSS (K3)

Table 5.2. Average water chemistry for the Nardouw Subgroup of the TMG (from Hydrocensus, Appendix A) and Atlantis groundwater (from Tredoux and Cavé, 2002). All results in mg/L unless otherwise indicated.

	NARDOUW SUBGROUP			WITZAND FORMATION ATLANTIS		
	Mean	-95% CL[a]	+95% CL	Mean	-80% Qt[b]	+80% Qt
EC (mS/m)	32.0	27.8	36.2	85	65	105
pH	6.05	5.88	6.23	7.5	7.2	7.9
Na	33.5	28.1	39.0	70	40	110
Mg	6.50	5.33	7.68	9	6	13
Ca	9.92	7.95	11.9	90	65	100
K	5.94	4.98	6.90	1.9	1.0	2.8
Cl	58.4	49.0	67.8	130	80	180
SO_4	31.2	20.5	42.0	40	22	55
Alkalinity (mg/L $CaCO_3$)	44.9	36.0	53.7	200	135	300
Si	5.99	5.27	6.71	4.42	1.8	7.4[c]
Fe (µg/L)	5160	1960	8360	3810	10	43300[c]
Al (µg/L)	505	<1	1030			
DOC (mg/L)	<0.1			3.3	0.6	7.5[c]
DO	2.59	1.88	3.30			
Temp (°C)	21.7	18.5	24.9			

a CL = confidence limit
b Qt = quartile
c Information for Atlantis based on few samples because these variables are not routinely analysed. For these variables, low and high values represent minima and maxima, rather than interquartile ranges.

Most KKRWSS samples were dry at the time of sampling because many of the holes were out of commission and borehole equipment had been left standing near the hole. In contrast, most AWSS samples were collected while still wet. The samples were scraped from the surface into a sampling bag using a wooden spatula. In addition, samples from four surface water sites were collected for comparison to groundwater samples. Calitzdorp Spa and Warmwaterberg are two hot springs originating from the TMG aquifer in the Klein Karoo area. The precipitate occurs as a hard flaky mass in the outflow (Figure 5.1a and b) and material was chipped from the centre of the outflow. A sample was obtained from a TMG artesian borehole near Hermanus on the south coast, and a sample was obtained from the KKRWSS groundwater treatment plant at Dysselsdorp for comparison to the material formed in the boreholes. All the samples were air dried and gently disaggregated using an agate mortar and pestle prior to analysis. Only small amounts (<1 g) were collected from some sites, limiting the amount of analytical work that could be performed.

5.2.1.2 Synthetic samples

Synthetic samples of common iron oxide minerals found in encrustations were produced in the laboratory following the methods of Cornell and Schwertmann (1996). Goethite (Gt) was prepared by aging ferrihydrite at 70°C for 60 hours. The ferrihydrite for goethite preparation was synthesised by adding 180 mL 5 M KOH to 100 mL 1 M $Fe(NO_3)_3$ solution. 2-line ferrihydrite (FH2) was prepared by gradually adding approximately 330 mL 1 M KOH to 500 mL 0.1 M $Fe(NO_3)_3$ solution, and 6-line ferrihydrite (FH6) was formed by heating a $Fe(NO_3)_3$ solution at 75°C for a few minutes, followed by rapid cooling in ice water. Schwertmannite was synthesised by adding $FeCl_3 \cdot 6H_2O$ and Na_2SO_4 to deionised water at 60°C and keeping at that temperature for 12 minutes. Following preparation, all samples were centrifuged and dialysed before freeze-drying. After freeze-drying, the samples were disaggregated using an agate mortar and pestle.

5.2.2 Sample characterisation and analysis

5.2.2.1 Mineralogy

The mineralogy of the samples was characterised by x-ray diffraction (XRD) using a Philips PW 1390 XRD with a Cu K-α X-ray tube (λ=1.542Å) set at 40 kV and 25 mA. The samples were scanned from 10° to 70° 2θ at a step-width of 0.05° and a time per step of 10s. Sample powders were pressed into aluminium sample holders for analysis. Samples for which there was only a small available mass were spread thinly over a glass slide and lightly compacted before analysis. Although this is not an ideal method, the XRD scans from these samples are similar to scans using standard sample holders. The mineralogy of iron oxides was also investigated with Fourier transform infra-red spectroscopy (FT-IR). Infra-red (IR) spectroscopy measures the excitation of iron oxides with electromagnetic radiation of wavelength 1 – 300 m, resulting in stretching and bending deformations of interbond angles. FT-IR provides increased resolution by averaging a large number of spectra. The method can provide information on the crystal morphology, degree of crystallinity and extent of metal substitution (Cornell and Schwertmann, 1996). Before analysis, samples were dried for 1 hour at 40°C to rid them of any non-structural water and then stored in a dessicator.

Samples were prepared for analysis by mixing 2 mg of sample with 200 mg of oven-dried KBr, grinding to a fine powder and pressing in a dye under 10 t of pressure for 1 minute. The discs were analysed with a Perkin-Elmer Spectrum One FT-IR from 4000 to 450 cm^{-1}, at a step rate of 4 scans per 4 cm^{-1}.

5.2.2.2 Physical parameters

The surface areas of samples for which there was sufficient mass were measured by the BET method in the Department of Chemical Engineering UCT using a TriStar 3000 (Section 3.2.1.2). The morphology of iron oxide encrustations was investigated using a Leica Stereoscan 440 SEM. Samples were prepared by sprinkling the dry iron oxide powder onto a stub coated with carbon-based glue, and coating with gold for improved visual resolution. The SEM was operated with a tungsten filament allowing a resolution of 100 nm. Normal preparation for biological samples involves dehydration with ethanol and fixing in gluteraldehyde to prevent breakdown of soft biological tissues, but due to the precipitation of iron onto bacterial surfaces, air-dried samples should still show the characteristics of the bacteria, as has been observed by Søgaard *et al.* (2000) and Kim *et al.* (2002).

5.2.2.3 General chemical parameters

The total carbon content of the samples was analysed using a Leco 932 CHN at the government Department of Marine and Coastal Management in Cape Town. A small amount of sample (5-9 mg) was weighed into an Al boat for analysis. Organic carbon was also analysed on those samples for which there was sufficient mass. Two methods were used for comparison. The first method involved pretreating the sample with 50% HCl at 60°C to remove any carbonates, washing the dried sample in ammonium formate and then filtering the residue for analysis with the CHN analyser in the same way as the total carbon content. This method was problematic as the iron was dissolved in the strong acid solution, resulting in loss of sample which was difficult to quantify. The second organic carbon method used was the Walkley-Black method. Dichromate added to the sample oxidizes organic carbon to CO_2 and is itself reduced to chromic ions (Cr^{3+}). The amount of dichromate reduced can be calculated by titration of the remaining dichromate with a ferrous solution and

corresponds to the amount of organic carbon oxidized. The method does not effectively oxidize all organic carbon and an empirical correction factor is added to the calculation to account for organic carbon not oxidized (Baker, 1976).

The point of zero salt effect (PZSE) of the samples was determined using an approach similar to that of Hunter (1981). The surfaces of iron oxide minerals are amphoteric and can adsorb H^+ or OH^- ions, depending on the pH of the solution, resulting in a positively or negatively charged surface. The pH at which the amount of positive charge and negative charge on the surface is equivalent is called the point of zero charge (PZC; Schwertmann and Taylor, 1992). The PZC can be estimated by titrating the oxide surface with acid and base in solutions of different ionic strength to obtain a variable called the point of zero salt effect (PZSE). Increasing ionic strength increases the activities of the base and acid in solution and causes the equilibrium of the adsorption reaction at the surface to shift to consume more acid or base, resulting in increased charge on the surface (McBride, 1994). At the PZSE, the ionic strength has no effect on the net adsorption of potential determining ions, and an intersection point of titration curves at varying ionic strength is observed (Appel *et al.*, 2003).

Six 10 mg aliquots of an iron oxide sample were placed in 15 mL centrifuge tubes, to which 10 mL of 1 M KCl solution was added. The pH of these mixtures was adjusted using a known volume of 0.1 M HCl or 0.1 M NaOH to obtain pH in the range between 3 and 9. The solutions were allowed to equilibrate on a reciprocating shaker for 24 hours and the final pH measured. This process was repeated for iron oxide aliquots in 0.1 M and 0.01 M KCl. The volume of acid or base required to reach the same pH in a pure KCl solution of the same concentration was subtracted from the volume of acid or base added to the sample. The PZSE is determined from the crossing over point of these titration curves (McBride, 1994). Problems were experienced with pH measurement of the suspension as these measurements did not stabilise at near-neutral pH. Drifting pH could be due to slow exchange of protons within the interior of the oxide particles (Dzombak and Morel, 1990).

5.2.2.4 Bulk and iron chemistry of precipitates

Total iron and other major elements present in the sample were measured using a Philips 1480 "X'Unique" Side Window Wavelength Dispersive Spectrometer (XRF) on fusion disks prepared using Sigma Flux (57 Li Tetraborate : 43 Li Metaborate). The samples were prepared by initially drying overnight at 100°C to determine the free water content of the sample, followed by overnight roasting at 850°C to burn off any remaining water or volatile material. The loss in mass on roasting is termed the loss on ignition (LOI). The samples were cooled in a dessicator. Fusion disks were prepared by weighing out 0.7000 g of sample, mixing with 6.000 g of dried lithium tetraborate flux, and then melting in a Claisse Fluxy. Samples for which there was limited available mass were diluted with acid-washed quartz sand, and the measured concentrations corrected after analysis.

Three different chemical iron extractions were performed on the iron oxide minerals:

- Oxalate-extractable iron (poorly crystalline iron oxides, predominantly ferrihydrite) was determined by reaction of 10 mg of sample with 25 mL of 0.2 M ammonium oxalate at pH 3 (Schwertmann and Taylor, 1992).
- Ascorbic acid-extractable iron, also in hydrous iron oxides, was dissolved from 10 mg of sample using a 25 mL solution of 0.11 M ascorbic acid, 0.17 M sodium citrate and 0.60 M sodium bicarbonate (Roychoudhury *et al.*, 2003; Canfield, 1989).
- Dithionite-soluble iron in crystalline iron oxides was extracted from 10 mg of sample with 25 mL of 0.29 M sodium dithionite in a 0.2 M sodium citrate + 0.35 M acetic acid buffer (pH 4.8; Roychoudhury *et al.*, 2003).

Although these extractions are usually performed for a fixed length of time, the oxalate extract was monitored over 3 days to determine the standard 2-hour concentration as well as the steady state concentration. The ratio of oxalate- to dithionite-soluble Fe is useful in quantifying the more and less active fractions of Fe-oxide (Schwertmann and Taylor, 1992). Iron concentrations in dithionite solution were determined using the phenanthroline method (Method 3500-Fe, Eaton *et al.*, 1995) but the ferrozine method was used for measuring iron in the oxalate and ascorbic acid extracts (Viollier, 2000).

5.3 Results

5.3.1 Mineralogy and morphology of iron oxides

Mineralogy as determined by XRD and FTIR, as well as morphology determined by SEM are summarised in Table 5.3. XRD scans are included in Figures D.6-D.8 (Appendix D), FTIR scans in Figures H1-H5 (Appendix H) and SEM images in Figure 5.2. XRD and FTIR confirm the mineralogy of the synthetic samples (Jambor and Dutrizac, 1998). Gt has sharp, narrow XRD peaks and is distinctly more crystalline than FH2, FH6 and Sch. SEM images confirm the XRD scans as FH6, FH2 and Sch appear amorphous and homogenous, while Gt occurs as acicular crystals of about 5 μm in length, aggregated into flat plates. The homogenous appearance of FH6, FH2 and Sch is probably because the reported grain size for these minerals is less than 10 nm, which is below the resolution ability of the SEM (Cornell and Schwertmann, 1996). Goethite has distinct FT-IR OH-bending bands at 882 and 796 cm^{-1}, while ferrihydrite is characterised by FT-IR bands at 690, 530 and 450 cm^{-1} (Cornell and Schwertmann,1996). Characteristic schwertmannite FT-IR bands are at 1110-1140, 1040-1070 and 970 -980 cm^{-1} (Bigham *et al.*, 1990).

The KKRWSS samples are mixtures of FH2, FH6 and Gt. The colours are mostly yellowish red except for K5 which is distinctly yellow. A broad FT-IR band between 950 and 1050 cm^{-1} in K1, K4 and K5 could be due to the inclusion of Si bonded to Fe (Schwertmann and Thalmann, 1976). Although schwertmannite was not detected in any samples by XRD analysis, FT-IR analysis of samples K2 and K3 reveal bands at 1110, 1040 and 980 cm^{-1} which suggest the presence of schwertmannite (Bigham *et al.*, 1990). SEM analyses of the samples reveal some interesting structures. Most samples are aggregates of fine-grained (0.5 μm) spheres, but samples K4 and K5 have distinctly biological structures of rods and globular chains (K4; Figure 5.3 d & e).

Table 5.3. Summary of mineralogy and morphology of iron oxide samples from XRD, FTIR and SEM analysis

	Sample	Mineralogy (XRD)	Mineralogy (FTIR)	Colour	SEM comments
Syn	FH2	Ferrihydrite 2-line	Ferrihydrite 2-line	5YR 3/4 Dark reddish brown	Irregular amorphous fragments
	FH6	Ferrihydrite 6-line	Ferrihydrite 6-line	5YR 3/4 Dark reddish brown	Irregular amorphous fragments
	Gt	Goethite	Goethite	2.5Y 7/8 Yellow	20-50 μm plates made up of fine needles of goethite
Atlantis	A1	2L FH with unidentified additional peaks	Has 650 cm^{-1} FH peak, but other FH peak shifted (540 to 515). Additional intense peak 1032-1085 similar to Sch but slightly shifted (985-1045). Strong peak at 1390 due to organic carbon?	7.5YR 4/6 Strong brown	Irregular amorphous platy fragments (20-50 μm) coated in small amount of vfg particles
	A2			7.5YR 4/6 Strong brown	Irregular amorphous platy fragments (20-50 μm) coated in vfg particles
	A3	2L FH with unidentified additional peaks		10YR 5/6 Yellowish brown	Irregular amorphous platy fragments (20-50 μm) coated in large amount of vfg particles. One possible tube
	A4	2L FH with unidentified additional peaks		7.5YR 4/6 Strong brown	Irregular amorphous fragments
	A5	2L FH with unidentified additional peaks		7.5YR 5/8 Strong brown	Very small <0.1 μm grains, formed into aggregates.
	A6	Goethite and 2L FH with unidentified additional peaks		7.5YR 5/8 Strong brown	Very small <0.1 μm grains, formed into aggregates.
KKRWSS	K1	6L FH	FH with adsorbed Si (970 cm^{-1})	5YR 5/8 Yellowish red	Uniformly 0.5 μm spherical grains, no evidence of bacteria.
	K2	6L FH with minor goethite and quartz	FH with Gt and Sch	5YR 4/6 Yellowish red	Irregular amorphous platy fragments (20-50 μm) coated in small amount of vfg particles
	K3	6L FH + distinct goethite	FH with Gt and Sch	7.5YR 5/8 Strong brown	Very small <0.1 μm grains, formed into aggregates.
	K4	2L FH	FH with adsorbed Si (970 cm^{-1})	7.5YR 6/8 Reddish yellow	Aggregates made up of spherical grains 0.5 μm diameter and occasional elongated tubes 1 μm diameter, 15-20 μm length. Tubes curved, different from S2
	K5	2L FH + trace quartz	Main FH peak (650 cm^{-1}) missing. Adsorbed Si (990 cm^{-1})?	2.5YR 8/6 Yellow	More angular small grains (0.5-1 μm) cemented together plus definite elongated structures
Springs	H1	2L FH	FH with adsorbed Si (920 cm^{-1})	10YR 5/8 Yellowish brown	Irregular shaped fragments of various sizes aggregated into rounded balls.
	H2	2L FH	FH with adsorbed Si (920 cm^{-1})	7.5YR 6/8 Reddish yellow	Very small <0.1 μm grains, formed into aggregates.
	S1	6L FH with minor goethite and quartz	FH with adsorbed Si (990 cm^{-1})	5YR 5/8 Yellowish red	Aggregates made up of spherical grains 0.5 μm diameter and elongated bumpy (not smooth) tubes 1 μm diameter, 15-20 μm length. Tubes look like spherical aggregates stuck together.
	S2	2L FH and quartz	FH with weak adsorbed Si peak (920 cm^{-1}) plus strong 1370 cm^{-1} peak due to organic carbon?	7.5YR 5/6 Strong brown	Very fg aggregates, but also Fe-oxide coated tubes 2 μm diameter, up to 20 μm long, with straight sides

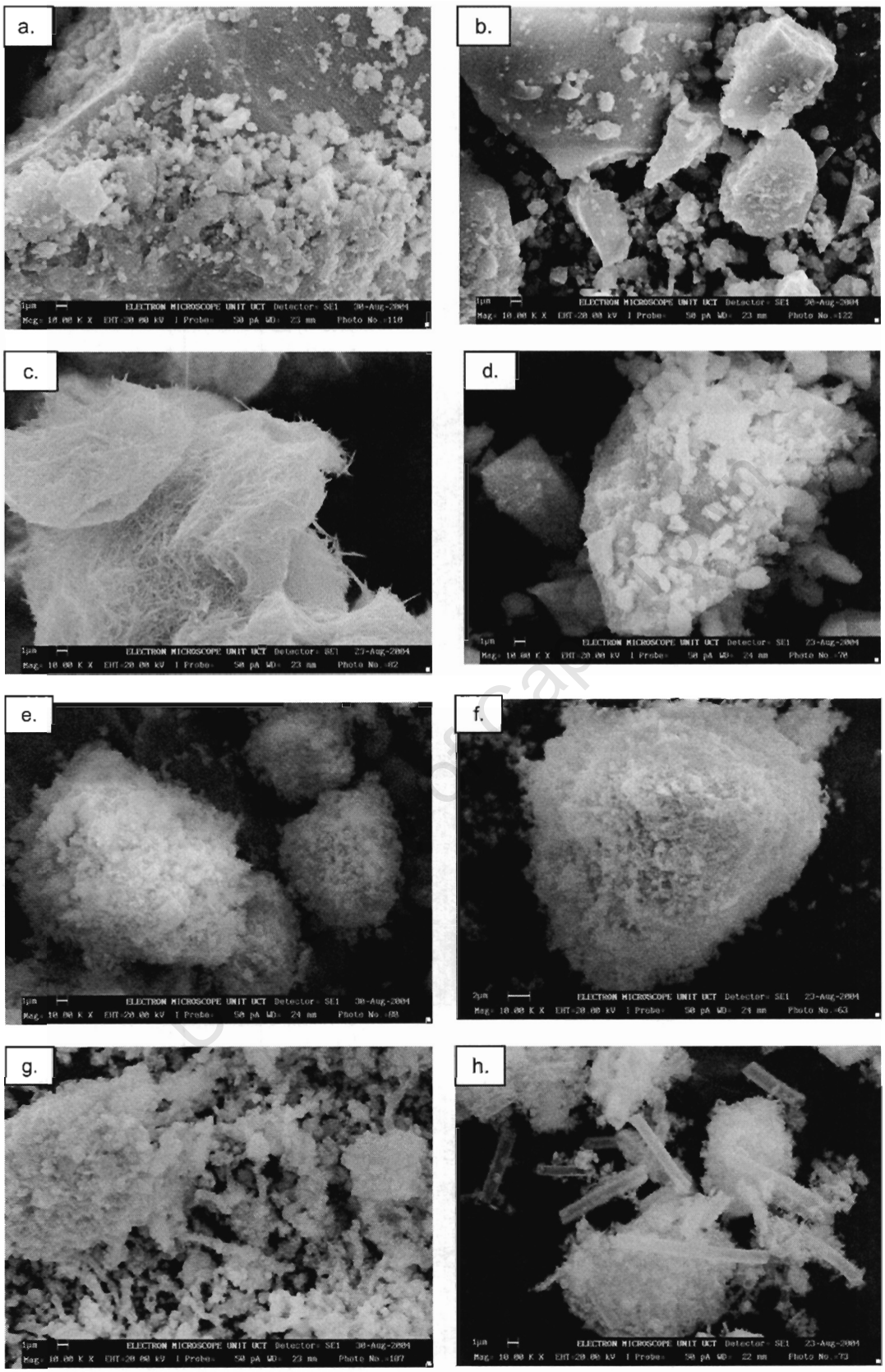

Figure 5.2. SEM images of synthetic iron oxide samples and samples from the hotsprings. a. FH2, b. FH6, c. Gt, d. Sch, e. H1, f. H2, g.S1, h.S2

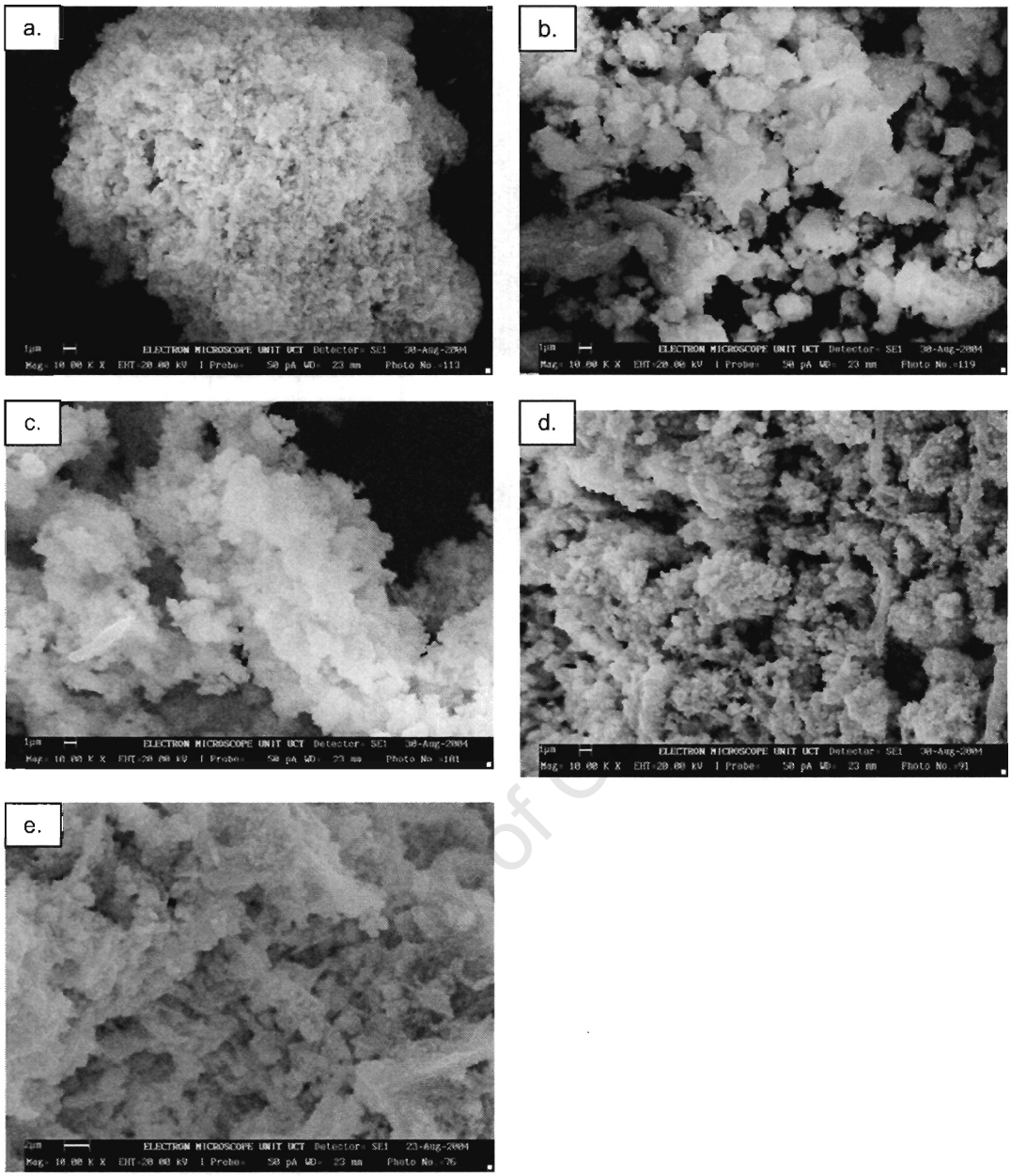

Figure 5.3. SEM images of iron oxide encrustation samples from the KKRWSS a. K1, b. K2, c. K3, d. K4, e. K5

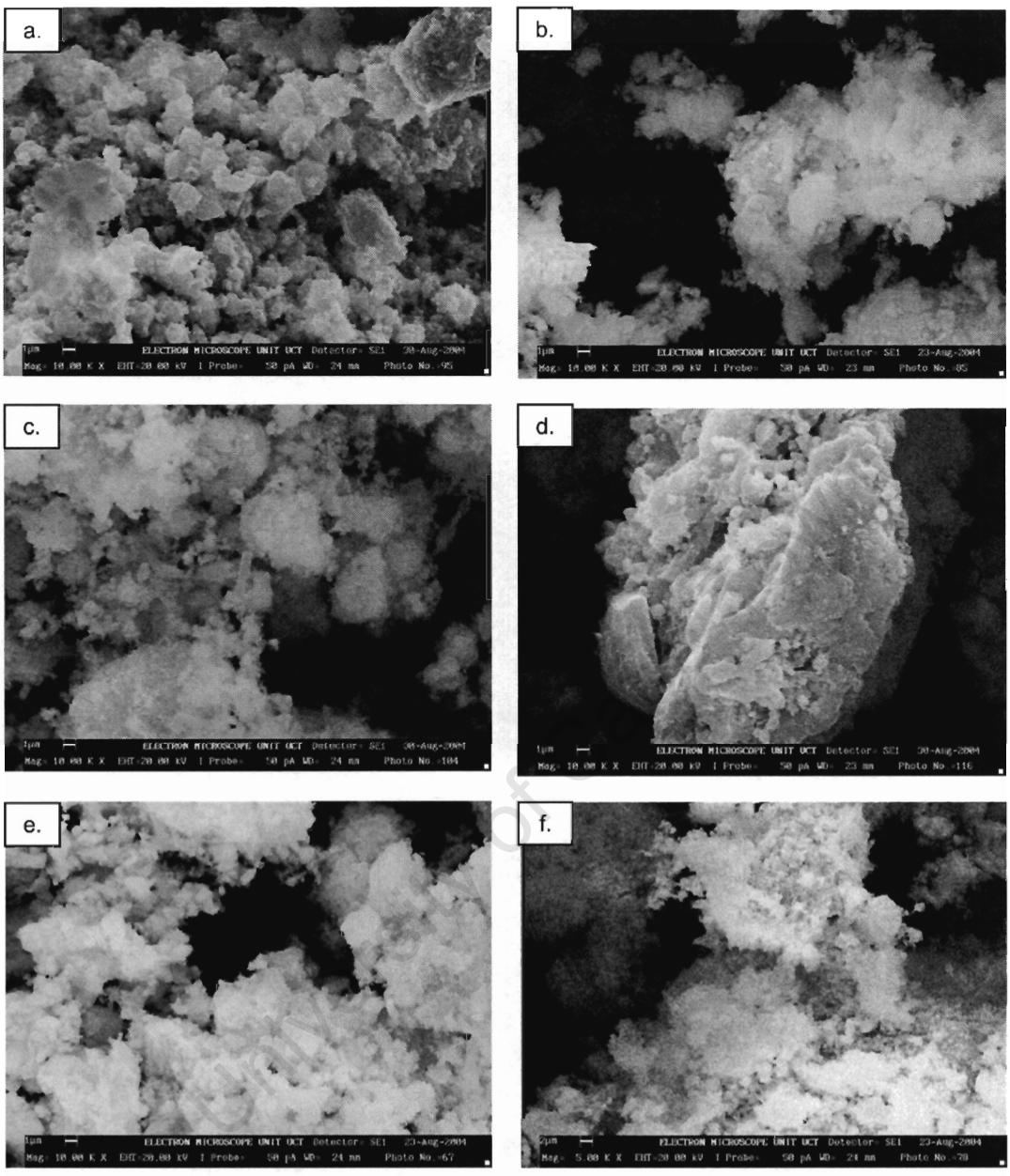

Figure 5.4. SEM images of iron oxide encrustation samples from the AWSS a. A1, b. A2, c. A3, d. A4, e. A5

The samples from the springs and hotsprings have variable colours. Samples H1, H2 and S2 are FH2, and S1 can be designated 4-line ferrihydrite. These samples all have a broad Si-adsorption FTIR band due to entrained quartz in S1 and S2, but due adsorbed Si in the hotspring samples. The hotspring samples consist of aggregates of fine-grained (nm-scale) particles when viewed under SEM, whereas S1 and S2 have more defined structures including sheaths and globular chains, showing clear evidence of bacteria.

AWSS samples are generally browner than the KKRWSS samples. Sample A5 from Atlantis appears to be a 3-line ferrihydrite, with trace amounts of quartz. The remaining samples from Atlantis have thus far not been identified, although they do appear similar to FH6. FT-IR scans also resemble the KKRWSS samples with some stronger bands (500 cm^{-1}, 1400 cm^{-1}) and some more complex bands (950-1050 cm^{-1}). Viewed with the SEM, samples from Atlantis consist of aggregates of tiny particles < 0.1 μm in diameter, considerably smaller than those observed in the KKRWSS samples. There are no signs of bacterial presence. Gel-like samples collected from the orifice plate and the pump inlet at Atlantis (A2, A4) were found to be extremely hydrous, containing up to 80% water by mass. The sample could be dehydrated by drying at room temperature, but drying was slow, taking up to a week to dry a few grams (dry weight) of sample. Once dehydrated, the sample could not be rehydrated. Water contents of 85 – 97 % were found in iron biofouling deposits by McLaughlan (2002).

5.3.2 General chemical characteristics of encrustations

pH(KCl), pH of host water, PZSE, total carbon (TC) content, organic carbon (OC) content, and surface area measurements are included in Table 5.4. The unit pH change is the amount of acid plus base required to effect a change in pH from 6 to 7, determined during the 1 M KCl PZSE titration. Particle diameter was calculated using the surface area, assuming spherical particles with a mineral density of 3.96 g/cm^3 (Jambor and Dutrizac, 1998).

The PZSE graphs are given in Appendix G. The PZSEs of the synthetic ferrihydrite samples are close to neutral, whereas the PZSE of goethite is quite alkaline. The PZSE pH values determined for the KKRWSS and spring samples are well below neutral and much lower than the PZSE values of the synthetic samples. PZSE values could not be determined for the Atlantis samples because the curves show considerable scatter in the pH 6.5-7.5 region, no distinct crossover point, and at lower pH the order of the curves is not what is expected i.e. the 0.01 M KCl curve occurs at the highest pH, suggesting that the samples are still above the PZC. The amount of acid plus base required to achieve a change in pH from 6 to 7 was greatest for Atlantis samples.

Table 5.4. Various parameters for iron oxide encrustation samples.

	ID	pH (1M KCl)	Water pH	PZSE	Unit pH change (μmol/g)	TC (wt %)	OC (wt %)	Surface area (m^2/g)	Particle diameter (nm)
Syn	FH2	6.9	-	6.9	60	<0.10	nd	314	2
	FH6	6.6	-	6.4	50	<0.10	nd	197	4
	Gt	7.6	-	9.0	8	<0.10	nd	29.1	26
Atlantis	A1	7.0	7.4	6.8	75	4.70	3.78	157	5
	A2	nd	7.5	nd	nd	5.36	nd	nd	nd
	A3	6.5	7.5	none	80	4.70	3.80	176	4
	A4	6.7	7.5	none	150	3.93	3.37	227	3
	A5	7.2	7.2	none	140	5.01	3.95	nd	nd
	A6	7.0	7.2	none	100	4.80	4.48	nd	nd
KKRWSS	K1	5.5	6.5	5.1	45	0.82	0.66	288	3
	K2	nd	4.2	nd	nd	1.47	nd	nd	nd
	K3	nd	5.5	nd	nd	1.49	1.01	nd	nd
	K4	4.6	5.7	3.6	40	0.69	0.12	92	8
	K5	nd	nd	nd	nd	0.32	0.31	nd	nd
Springs	H1	6.5	7.3	<4.6	30	0.18	<0.10	31	24
	H2	5.5	6.8	3.6-4.1	15	0.29	<0.10	171	4
	S1	5.6	nd	<5.0	70	1.17	0.92	225	3
	S2	nd	nd	nd	nd	8.58	0.32	nd	nd

nd = not determined

Samples from Atlantis have higher total and organic carbon content than samples from the KKRWSS and springs (except for sample S2). The organic carbon data from CHN analysis agree with Walkley-Black data to within 10% at concentrations greater than 3 wt % but repeatability is poor at low concentrations (Table B.3 and B.7, Appendix B). The data from the two methods is averaged. The TC content is predominantly made up of OC, but all samples contain some inorganic carbon. The difference between TC and OC could be due to analytical problems with OC determination as no

carbonate minerals were detected, nor did the samples react to dilute HCl. BET measured surface areas are variable, covering a range of 31 - 314 m^2/g. Particle sizes calculated for spherical particles with these surface areas are between 2 and 8 nm, with the exception of goethite and sample S2.

5.3.3 Chemistry of encrustations

Results of XRF analysis of iron oxide encrustations are given in Table 5.5, with duplicate analyses in Table B.8 (Appendix B). The repeatability of Fe analyses is excellent (<1% RSD), but the low concentrations of most other elements results in variable RSD (<0.1 to 136.4%), although absolute concentration differences are small (<0.87 wt%). Dilution did not affect the measurement of concentrations in the samples. Iron is the dominant element present in all samples. The Atlantis samples have the lowest average but the most consistent iron content of all the groups. The iron content of the KKRWSS and spring samples is quite variable, but closer to the values found in the synthetic samples. Atlantis samples have relatively high proportions of Ca compared to KKRWSS samples, and a consistently high concentration of P. Only two KKRWSS samples have high P, K4 and K5.

All natural samples contain some Si, with the highest concentrations found in the hotsprings. Quartz was only detected by XRD in a few samples (A1, A5, K2, K5, S1 and S2), and in most of these at trace level so the Si detected in the encrustations could be an adsorbed phase. The high concentration of Si in the hotsprings reflects the increased solubility of Si in the high temperature water, whereas in the cold springs, it is probably due to entrained quartz. Other constituents present in significant concentrations are Al and Na. Mn, which is commonly associated with iron oxide encrustations, is present only in small amounts, except in the hotspring samples. The low S concentration measured for schwertmannite ($Fe_{16}O_{16}(OH)_y(SO_4)_z \cdot nH_2O$) by XRF indicates that S is lost as SO_2 during the roasting phase of sample preparation. S data from SEM are included in the table for comparison, although the repeatability of these analyses is poor. The expected ratio of Fe:S in schwertmannite is 8, and in this analysis a value of 7 was obtained. The high concentrations of S in samples K2 and K3 support the identification of schwertmannite by FT-IR in

these samples. Cu and Zn were detected at levels up to 6000 mmol/kg in Atlantis samples by SEM but were not analysed by XRF. SEM data are not included because of the high variability and poor repeatability.

Table 5.5. Composition of iron oxide encrustations (in mmol/kg on an H_2O free basis, calculated from oxide wt %)

	Sample	Si	Al	Ti	Mn	Mg	Ca	Na	K	P	S	Fe	S (SEM)
Synthetic	FH2	102	60.0	5.46	4.50	44.3	5.80	129	118		4.29	10837	<100
	Gt	34.9	55.5	4.44	3.37	47.0	8.21	72.0	93.1		3.10	10660	<100
	Ht	8.29	48.7	4.64	5.87	37.6	3.53	41.3	0.86		5.71	12390	nd
	Sch	41.1	93.2	6.25	3.81	62.2	21.0	46.4	3.54	6.97	2.47	8795	10190
Atlantis	A1	931	380	8.37	15.1	66.2	891	244	17.7	515	16.0	7365	520
	A3	530	103	5.30	5.11	63.0	943	547	7.70	634	12.1	7431	520
	A4	509	75.0	4.42	4.86	68.4	746	341	5.71	448	13.6	8061	350
	A5	847	228	8.84	4.80	74.3	1077	375	15.0	624	33.3	7055	<100
	A6	920	156	14.6	11.6	112	1022	93.0	12.6	555	41.7	7289	2145
KKRWSS	K1	767	82.0	5.38	20.7	46.3	48.1	44.8	13.3	367	1.33	9880	395
	K2	310	300	26.3	11.5	120	18.5	138	29.2	279	2.80	9197	3010
	K3	501	249	11.3	5.97	69.2	14.4	91.9	20.4	306	2.88	8172	5995
	K4	233	55.4	4.51	12.2	42.7	11.9	54.4	3.63	1147	2.25	8868	<100
	K5	450	215	11.7	14.0	60.9	52.6	72.4	69.9	1894	2.89	6816	1035
Springs	H1	2318	63.5	5.83	446	70.7	324	44.2	20.4	243	3.37	8350	<100
	H2	1736	48.3	4.21	173	51.7	77.2	35.3	5.59	241	2.27	9137	<100
	S1	1395	153	10.3	71.8	72.9	93.0	47.1	44.7	288	23.8	9451	675
	S2	2857	125	9.12	85.6	74.0	517	50.0	24.4	50.4	53.7	6486	2180

5.3.4 Forms of iron in iron oxide minerals

Results of iron determination by oxalate-extraction, ascorbate-extraction, dithionite-extraction, as well as by XRF are given in Table 5.6. Data quality is given in Table B.4 (Appendix B). In most cases, the difference between total iron determined by XRF and dithionite extraction is less than 5%. An XRF value greater than a dithionite value could be explained by the presence of iron in a form not readily dissolvable by dithionite e.g. a silicate mineral, but the XRF value only exceeds the dithionite value in samples A4 and S1, within the margin of error. In the remainder of the samples, dithionite-extracted Fe exceeds XRF Fe, in general by <10% except K5 and S2 which differ by 10.7 and 21.5 % respectively. It appears that the dithionite method over-estimates the iron content of samples by on average 3 %. The Atlantis samples have the lowest total iron content while the synthetic samples have the highest total iron content.

The ascorbate method is expected to extract all amorphous oxide phases, including FH2 and FH6, but not Gt. The reaction time used was clearly insufficient to completely extract the synthetic ferrihydrite minerals, but extracted >80% of the natural samples. The ascorbate method extracted more iron from the natural samples than the oxalate method, but the oxalate method was more effective at extracting the synthetic iron oxides.

Table 5.6. Iron contents of encrustation as determined by chemical extractions and XRF

	ID	Fe^{a} (wt %)	Fe^{o2} (wt %)	Fe^{oe} (wt %)	Fe^{X} (wt %)	Fe^{x} (wt %)	Fe^{T} (wt %)	Fe^{a}: Fe^{T}	Fe^{o2}: Fe^{T}	Fe^{o2}: Fe^{oe}
Syn	FH2	25.6	31.0	37.5	50.0	49.4	49.7	0.52	0.62	0.83
	FH6	6.3	29.0	52.3	57.1	Nd	57.1	0.11	0.51	0.56
	Gt	0.1	<0.1	<0.1	61.5	60.4	60.9			
Atlantis	A1	31.2	23.4	25.9	36.5	34.4	35.4	0.88	0.64	0.90
	A2	35.0	nd	nd	36.9	Nd	36.9			
	A3	29.7	21.0	22.6	32.2	31.4	31.8	0.93	0.65	0.93
	A4	32.9	16.1	27.8	34.5	34.8	34.7	0.95	0.47	0.58
	A5	30.3	21.1	23.3	32.6	31.3	31.9	0.95	0.65	0.91
	A6	27.9	20.1	25.2	35.5	34.0	34.7	0.80	0.57	0.80
KKRWSS	K1	39.7	30.8	40.1	48.8	47.4	48.1	0.83	0.63	0.77
	K2	30.5	33.5	35.1	48.1	45.5	46.8	0.65	0.70	0.95
	K3	34.4	25.0	33.3	43.2	40.4	41.8	0.82	0.58	0.75
	K4	40.2	29.4	32.3	43.1	41.3	42.2	0.95	0.68	0.91
	K5	32.7	22.3	24.4	35.4	31.8	33.6	0.97	0.63	0.92
Springs	H1	26.4	21.0	39.9	44.7	42.7	43.7	0.60	0.47	0.53
	H2	41.0	32.8	39.4	50.0	46.0	48.0	0.85	0.66	0.83
	S1	34.4	28.3	42.8	46.7	47.1	46.9	0.73	0.61	0.66
	S2	35.0	23.7	25.3	37.0	29.9	33.4	1.05	0.64	0.94

a = ascorbate extraction, o2 = 2 hour oxalate extraction, oe = equilibrium oxalate extraction; X = dithionite extraction; x = XRF; T = average dithionite and XRF

5.4 Discussion

5.4.1 Mineralogy and crystallinity of iron oxide encrustations

The mineralogy and crystallinity of the iron oxide encrustations is expected to have important implications for rehabilitation of clogged wells, as more crystalline minerals could be more difficult to physically and chemically treat. The assemblage of minerals found in the samples is similar to those found in other studies of borehole environments (e.g. Houben, 2003a; Tuhela *et al.*, 1997; Walter, 1997), i.e. primarily ferrihydrite with lesser amounts of crystalline iron oxide, including goethite. A trace amount of schwertmannite is observed in samples K2 and K3. During a similar study of iron encrustations in Klein Karoo boreholes, Miller (2000) found 6-line ferrihydrite and goethite in

most samples. Lepidocrocite, maghemite, magnetite, siderite and haematite are minerals found in other studies that were not observed here (Walter, 1997; Houben, 2003a). Mn encrustations and sulphides form under different redox conditions than iron oxide minerals but have been found in boreholes in Germany (Houben, 2003a). Black material observed at the base of borehole KG1 in downhole video logs could not be sampled but appeared sulphidic suggesting that the deeper parts of the well are quite reducing (Figure 5.5).

Figure 5.5. Sulphidic material observed in the base of borehole DL15 by downhole video logging (Courtesy of J. Uys, KKRWSS and B. Venter, DWAF)

Ferrihydrite is the dominant mineral found in many of the encrustations examined in this study. Ferrihydrite is a common natural iron oxide, and forms by rapid oxidation of Fe^{2+} in an environment with high concentrations of organic matter, phosphate or silicate (Schwertmann and Taylor, 1992). The International Mineralogical Association defines ferrihydrite as a mineral with six broad XRD peaks at d-spacings of 2.53, 1.97, 1.72, 1.51, 1.47 and 2.2Å (Janney *et al.*, 2000a). However, the term ferrihydrite is used in the literature to describe minerals which display between 2 (2.53 and 1.51Å; FH2) and six (FH6) peaks (Janney *et al.*, 2000a; Tuhela *et al.*, 1992). In this study both end-members of the ferrihydrite range, as well as examples between the two end-members, were observed in encrustations. The relative crystallinity of ferrihydrite can be determined from the number and positions of XRD peaks. Six-line ferrihydrite is the most crystalline, with the d-spacing of the main peak at 2.53Å. With decreasing crystallinity, the lines weaken, broaden and begin to disappear, starting with 1.97 and 1.72Å, then 1.51Å and 1.47Å merge into a single peak at 1.50Å. Finally, peak 2.2Å disappears and the main peak shifts

to higher d-spacing, resulting in two-line ferrihydrite (Janney *et al.*, 2001; 2000a, b; Tuhela *et al.*, 1992).

Using this information, the relative crystallinity of each group of samples can be determined. In the Klein Karoo, crystallinity decreases in the order K3>=K1>K2>K4>K5. K1, K2 and K3 are all distinctly FH6, whereas K4 and K5 are FH2. The spring samples have the following order of decreasing crystallinity: S1>S2>=H2>H1. Goethite, a more crystalline, less hydrous, iron oxide is found along with ferrihydrite in a few samples from these two environments (K2, K3 and S1). Goethite is commonly associated with more crystalline FH6 as is observed here (Carlson and Schwertmann, 1981). Schwertmannite (Sch) has a similar diffractogram to FH6, but the chemical formula of schwertmannite contains S, allowing easy distinction from FH6 on a chemical basis (Bigham *et al.*, 1990). K2 and K3 have high concentrations of sulphur and may contain some schwertmannite, as the broad XRD peak at 3.34Å and FT-IR bands correspond to schwertmannite.

The majority of the Atlantis samples are of unknown mineralogy. Although the peaks on the diffractograms appear similar to FH6, there are a few distinct differences. There is a peak at 3.3Å which is not characteristic of FH6 and the 2.53Å peak is broad and appears to be two converged peaks, one at 2.53Å, and the second at 2.36Å. In addition, the peaks at 1.72Å and 2.20Å are missing, although the 1.97Å peak is present. The 1.97Å peak normally disappears first as ferrihydrite decreases in crystallinity (Carlson and Schwertmann, 1981). A plateau at d-spacing just before the main peak, corresponding to the observed peak at 3.3Å, has been observed in natural organic C-rich FH precipitates but the reason for the effect is not known (Tuhela *et al.*, 1992). Ferrihydrite can be confused with schwertmannite, hisingerite, which has almost equal iron and silica contents, and julgoldite, which contains Ca, Si and mixed valence iron (Gloter *et al.*, 2004) but the observed peaks match none of these minerals. Sample A6 clearly contains goethite. The relative crystallinity of the samples can be classified by assessing the number and sharpness of peaks, and is in the order A6>A4>=A1>A5>A3.

Ferrihydrite is not stable under groundwater conditions and is expected to recrystallise to the more stable goethite. The encrustations containing goethite could have formed by "aging" of ferrihydrite, or by simultaneous precipitation of the two minerals (Schwertmann and Taylor, 1992). The small amount of goethite observed in the encrustations could be due to a short time period between formation of FH and sampling, or because the aging process is retarded by adsorbed species, such as phosphate, silica and organic carbon (Mayer and Jarrell, 1996; Schwertmann and Taylor, 1992; Tuhela *et al.*, 1992; Carlson and Schwertmann, 1981).

The order of crystallinity suggested by the oxalate:total and ascorbic:total ratios is:

Ascorbic:	Oxalate:
A6>A1>A3>A4>=A5	A3>=A6>=A1>A5>A3
K2>K3>=K1>K4>K5	K3>K1>=K5>K4>K2
H1>S1>H2>S2	H1>S1>H2>S2

The oxalate ratio is closer to what is observed than the ascorbic ratio but it predicts that K2, which is composed of FH6, is less crystalline than K4 and K5, which are FH2. These ratios are a better indication of reactivity than crystallinity. A variable which was found to agree with the order of crystallinity is the ratio of oxalate extracted after 2 hours to oxalate at equilibrium. All the natural samples are more reactive than the more crystalline synthetic analogues. Preparation of synthetic iron (III) hydroxides in the laboratory does not follow pathways found in natural systems and synthetic samples are not a good natural analogue (Deng, 1997).

5.4.2 Effect of impurities on crystallinity and reactivity

The impurities present in iron oxide samples reflect the chemistry of the groundwater from which they are precipitated, and consist predominantly of Si, Al, Mg, Ca, Na, P and S (Figure 5.6). Atlantis samples precipitate from more saline water and contain more impurities, in particular Na, Ca and organic carbon, than KKRWSS which are precipitated from the less saline TMG groundwater.

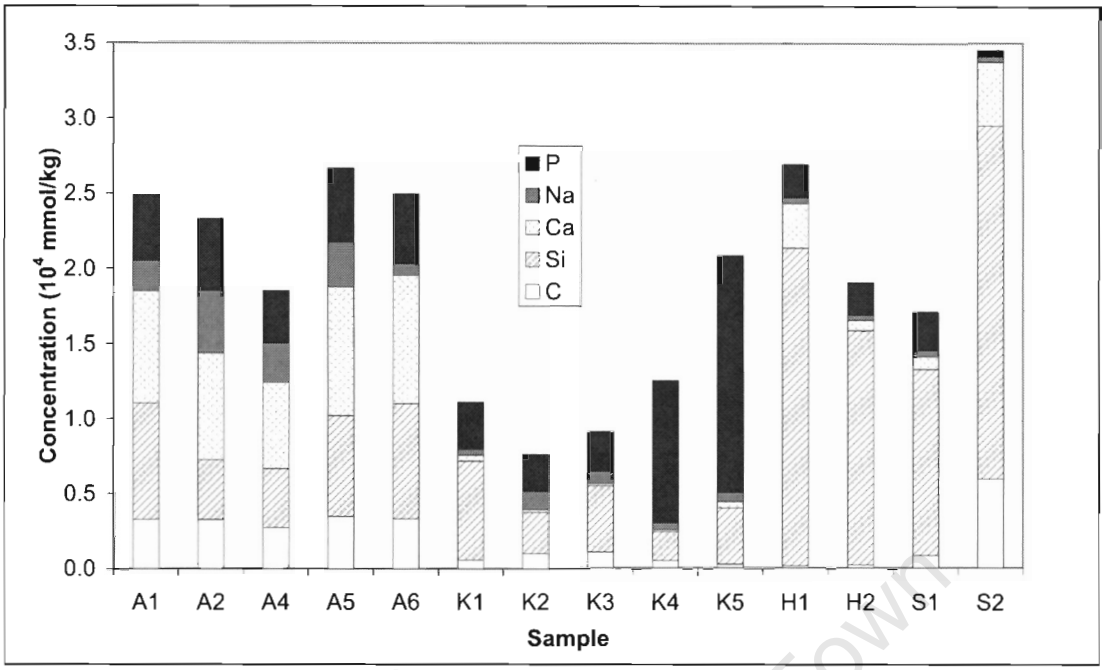

Figure 5.6. Summary of impurities present in iron exide encrustations

The degree of crystallinity does not correlate with any of the impurities present in the samples. However, the total amount of Fe present in the sample does support the suggested order of crystallinity, with samples A6, A4 and A1 having a greater total amount of iron than A3 and A5, and K1 and K2 containing more iron than less crystalline K4 and K5. Chemically adsorbed ions are generally found to suppress the ordering of ferrihydrite and therefore affect their reactivity (Carlson and Schwertmann, 1981). There is a distinct negative correlation between the total iron content of the sample and the ascorbate:total Fe ratio i.e. more reactive samples contain less total iron, or inversely, more total non-iron species (Figure 5.7). The reason for the lower iron content of Atlantis samples is probably the presence of more impurities than the KK samples, reflecting the different groundwater chemistry of the aquifer. The inverse relationship between total iron and the sum of non-iron species is to some extent an inherent artefact of normalising the data to 100%, but also indicates that the varying iron content of the natural samples does not reflect mineralogical differences as is the case with synthetic samples, but instead indicates the degree of impurity present in the iron oxide sample. It is difficult to know if these impurities are adsorbed to the surface of the iron oxide, or if they are incorporated into the mineral structure. The authors of the German study concluded that a high ratio of elements,

particularly PO_4 and Ca, to Fe (>0.34) in iron oxide minerals from aquifers indicate that the elements are part of the colloid and not only sorbed to the surface (Wolthoorn *et al.*, 2004a). Ratios of impurities to Fe in this study were not nearly so high (< 0.15), but were found to affect the reactivity of the oxide minerals.

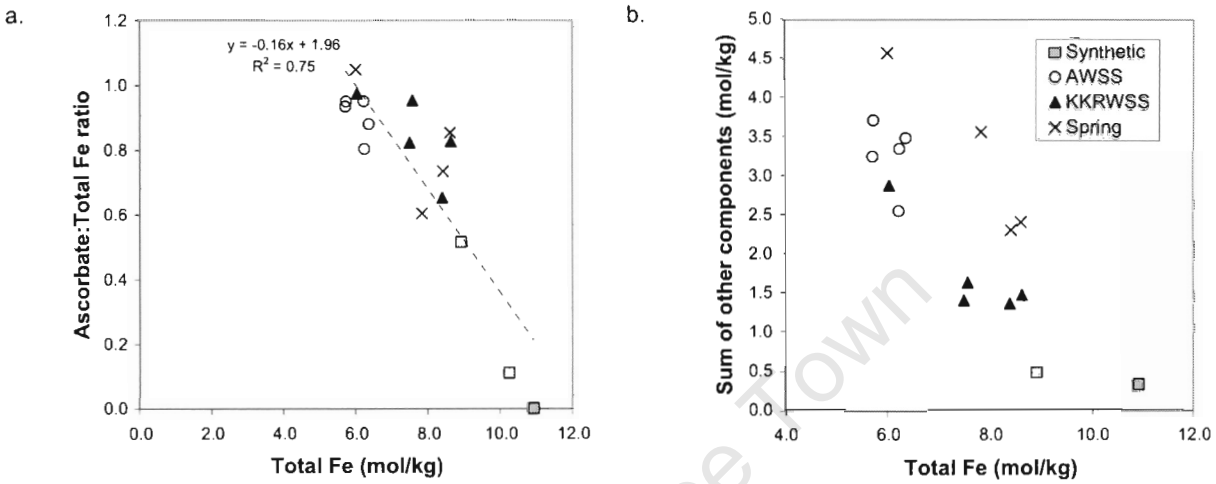

Figure 5.7. a) Relationship between ascorbate:total iron ratio and total Fe content of iron encrustations, b) Relationship between non-iron species present in iron encrustations and total iron content

A few samples contain high levels of P, S and Si. The high concentrations of S in the Klein Karoo encrustations K2 and K3 are thought to be in the form of the mineral schwertmannite, and are found in boreholes with low pH (5.5 and 4.2). The low pH and high S concentrations could be due to oxidation of sulphide within the aquifer in a process analogous to acid mine drainage, or could be a side-effect of rehabilitation procedures which introduce strong sulphur based acids into the groundwater. Si is commonly associated with natural iron oxide minerals and research has been done to assess if the Si is bonded to iron in the oxide (e.g. Mayer and Jarrel, 1996; Carlson and Schwertmann, 1981). Some of the silica, i.e., in samples S1, S2, K3 and A5, can be attributed to the presence of quartz within the sample, but the FT-IR peak at around 970 cm^{-1} indicates that silica is adsorbed to the surface.

Phosphate adsorption onto iron oxide can be calculated for samples with known surface area. The amount of P adsorbed varies from 1.2 to 12.4 $\mu mol/m^2$ in this study, similar to the 1.9-9 $\mu mol/m^2$ determined for natural ferrihydrite samples from Germany (Houben, 2003a). The amount of P in the

Klein Karoo samples correlates inversely with crystallinity suggesting that P may play a role in retarding recrystallisation of the minerals. The high concentrations of P in precipitates K4 and K5 are unexpected as the natural PO_4 concentration of the groundwater is low. K5 has a P concentration almost double any of the other samples, making up nearly 30% of the molar mass of the sample, which may account for the samples anomalous yellow colouring. Deng (1997) noted that slow oxidation of Fe(II) in the presence of P (in the ratio P(V):Fe(II) = 0.4) resulted in the formation of an unidentifiable yellow precipitate, and Wolthoorn *et al.*, (2004a) also noted differently coloured precipitates forming in the presence of P. The concentration of so much P in the precipitates suggests that the precipitate has been exposed to the groundwater for long periods. Precipitation of 1 g of iron oxide containing 9000 mmol/kg Fe from water with an iron concentration of 10 mg/L and a PO_4 concentration of 0.01 mg/L requires 900 L of water. For that iron encrustation to contain 2000 mmol/kg of P, all the PO_4 would have to be removed from 200 000 L of water. It would be expected that precipitates exposed to groundwater for the extended period required to accumulate this amount of PO_4 would begin to age, but PO_4 retards the aging process and results in formation of small colloids (<0.2 microns; Wolthoorn *et al.*, 2004a).

5.4.3 Presence of bacteria

Precipitation of iron from groundwater in water wells is often ascribed to bacterial mediation, because the rate of precipitation is believed to be too rapid to explain by chemical oxidation alone. The rate of biological oxidation is about 1000 times faster than chemical oxidation (Ralph and Stevenson, 1995; Søgaard *et al.*, 2001). However, distinguishing the two processes is difficult, especially as bacteria can mediate oxidation by actively metabolising iron or by passively sorbing iron (Rancourt *et al.*, 2005).

SEM images of encrustations from the KKRWSS show a clear biological influence in sample K4, and possibly in K5, but not in any other sample (Figure 5.3). *Gallionella*, one of the most commonly observed and easily identified bacteria in groundwater systems, was not observed here. Similar results were obtained by Miller (2000) who also found no evidence of bacterial

precipitation of iron oxides in the Klein Karoo, except in one borehole. The lack of visible bacterial evidence is supported by the results of BARTS tests that were performed on the groundwaters of the KKRWSS by Engelbrecht and Jolly (2000) and Smith (2002; Table 5.7). BARTS tests are field tests for microbial activity in groundwater and consist of a test tube containing a growth medium specific to the bacteria of interest. In this case two reactors were used, one specific for iron related bacteria (IRB) and one for sulphate-reducing bacteria (SRB). Water is added to the reactor and the appearance of the reactor is monitored over a period of time. Different bacterial populations cause different visible changes to the reactor and can be classified following a simple visual scheme. The time required for the reaction to develop gives an idea of the aggressivity of the microbial population (Engelbrecht and Jolly, 2000; Mansuy *et al.*, 1990).

Table 5.7. Microbial populations found in boreholes of the KKRWSS (from Engelbrecht and Jolly, 2000; Smith, 2002).

Sample	Borehole	IRB[1]	SRB[2]
K1	DL16	Moderate (10 000 cfu) mixed aerobic and anaerobic bacteria dominated by psuedomonads	Moderate (150 cfu) anaerobic slime formers incorporating SRB
K2	DP28	Variable from no bacteria to 10 000 cfu psuedomonads	Variable from none to <100 cfu anaerobic slime formers
K3	GA1	Moderate (10 000 cfu) mixed aerobic and anaerobic bacteria dominated by psuedomonads	Variable from none to <100 cfu anaerobic slime formers incorporating SRB
K4	DG110	Moderate to high (10 000 -30 000 cfu) mixed aerobic and anaerobic bacteria dominated by psuedomonads with some IRB	None to background levels of deep seated anaerobic bacteria dominated by *Desulfovibrio*
K5	DP10	nd[3]	nd

1. Iron related bacteria 2. sulphate reducing bacteria 3. no data

Low to moderate populations of both psuedomonads and SRB are found in most boreholes, but IRB are only detected in DG110, from which sample K4 was collected. K4 is the only groundwater sample to show obvious bacterial presence by SEM. Virtually no bacteria of any kind were detected in borehole DP28 (sample K2) on two sampling occasions and this may be related to the low pH of the groundwater (4.2). Interestingly, boreholes from the Vermaaks River wellfield, which are not prone to clogging, have similar IRB populations to the boreholes that are known to clog (Engelbrecht and Jolly, 2000).

Sheathed bacteria e.g. *Lepthothrix* and *Sphaerotilus* are associated with large amounts of precipitated iron, and occur in groundwater as large iron-stained

amorphous flocs which float in the water column (Cullimore, 1992). Flocs have been observed during down-hole camera logging of boreholes in the KKRWSS (Figure 5.8a), even in boreholes in which low bacterial presence was detected, suggesting that either the bacterial tests are not effective, or that the flocs are not always associated with bacteria. There are distinct differences in the appearance of encrustations with depth in the borehole, from the dry iron-rich precipitates collected in the field at the top of the borehole, to the orange neutral-density flocs associated with well screens in the middle of the borehole, to a white-grey dense overgrowth on the basal screens (Figure 5.8b), and sulphidic material at the base of some holes (Figure 5.5). Sampling of each of these zones would be necessary to adequately describe the bacterial influence on borehole clogging.

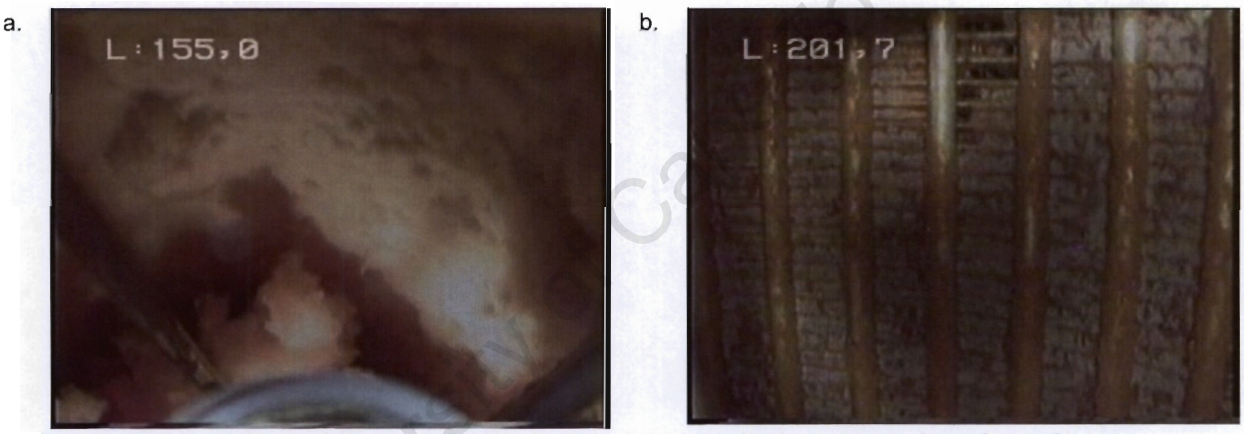

Figure 5.8. a. Flocs observed in water column during down-hole logging of borehole DP28, b. Grey-white overgrowth of deep screens in borehole DP28 (L is depth in m; Courtesy of J. Uys, KKRWSS and B. Venter, DWAF)

The Klein Karoo samples with bacteria have the highest P of all samples and the highest 2 hour oxalate:equilibrium oxalate ratio of the KK samples, corresponding with the low crystallinity determined by XRD. The organic carbon content of these samples is low (<2 wt %). Biologically precipitated encrustations are not necessarily associated with high concentrations of organic carbon because, e.g., *Gallionella* is capable of oxidizing 350 g $Fe(OH)_3$ or 890 g FeOOH for every gram of celluiar material produced (Walter, 1997). However, other studies have found organic carbon contents of 10 – 18 wt % (McLaughlan, 2002) and 35 wt % (Martinez *et al.*, 2003) in bacteriogenic iron oxides

No bacteria were observed in any of the samples from Atlantis, even those collected from the pump, despite the presence of higher concentrations of nutrients in the Atlantis groundwater (Figure 5.4). No BARTS tests have been performed at Atlantis, so data cannot be compared to KKRWSS data. The average pH of Atlantis groundwater in the sampled boreholes is 7.4. According to Kirby *et al.* (1999), above a pH of 6.4 iron oxidizing bacteria are unable to compete with chemical precipitation, so it is not surprising that no bacteria were observed at Atlantis. The high OC of the Atlantis samples does not appear to be bacterial, and could be due to adsorption of OC from the OC-rich groundwater. The organic carbon content of iron oxides in Finland was related to the organic carbon content of the source water, and an increased OC content correlated with decreased crystallinity (Carlson and Schwertmann, 1981; Carlson and Schwertmann, 1987).

Samples from the hotsprings were also devoid of bacteria (Figure 5.2e and f), and in terms of mechanism of formation are probably most similar to synthetic samples, i.e., precipitating from a rapidly oxidizing, cooling solution. Sample H1 has a low surface area and low 2 hour oxalate: equilibrium oxalate Fe ratio despite being FH2, suggesting that it is quite unreactive. Samples S1 and S2 from surface sites show the clearest evidence of bacteria in SEM images (Figure 5.2g and h). The rough globular tubes in S1 appear similar to precipitates collected by Hanert (2002) in shallow waters in the Aegean Sea. Hanert (2002) postulates that the globular tubes are strands of ECP that have become encrusted with iron oxides, and that these strands have exceptional catalytic properties for oxidizing iron. The larger, smooth sheaths in S2 are likely to be from the genus *Sphaerotilus,* which thrives in slowly running waters polluted with organic nutrients (Mulder and Deinema, 1981). S2 was collected from an artesian borehole in the vicinity of a waste disposal site and the groundwater may be polluted. The cold spring samples have a more crystalline mineralogy than the hotspring samples, yet the oxalate:total Fe ratio indicates that the cold spring samples are more reactive possibly due to the presence of bacteria or the large amount of impurities.

It is generally believed that the association of 2-line ferrihydrite and bacteria is due to the bacteria providing a nucleation site for precipitation. The adsorption of iron to bacterial surfaces increases the rate of precipitation, but only in systems undersaturated with respect to chemically precipitated iron oxides (Wightman and Fein, 2005). Ferrihydrite precipitated in the presence of bacteria has been found to be different to chemically precipitated ferrihydrite. Biologically precipitated ferrihydrite is denser, with smaller particle sizes (1-5nm), a less ordered structure than colloidal chemical ferrihydrite, and sometimes contains Fe^{2+} (Rancourt *et al.*, 2005; Søgaard *et al.*, 2001). The smaller particle size of biologically precipitated ferrihydrite is thought to be due to poisoning of the iron oxide surface by adsorption of organic molecules excreted by bacteria (Rancourt *et al.*, 2005). Ferrihydrite from this study is found to have small particle sizes (3-8 nm) of the same order of magnitude as expected from biologically precipitated ferrihydrite. The small particle size of all samples (except H1) and the high reactivity compared to synthetic samples suggests that bacteria may be involved in precipitation even when they are not evident in the sample. Of interest is that sample S1, which has clearly been affected by biological mediation of precipitation, is actually 6-line ferrihydrite, challenging the notion that bacteria precipitate only 2-line ferrihydrite.

Although not conclusive, these results suggest that bacteria do not play a significant role in directly precipitating iron oxides in boreholes of the KKRWSS and AWSS, although they may well be involved indirectly as described by Rancourt *et al.* (2005). The low organic carbon contents of most precipitates compared to iron content also suggests that rehabilitation methods developed to destroy the bacterial component of encrustations will be less than effective. An interesting observation from samples with clear evidence of bacteria is that the presence of bacteria results in the precipitation of more reactive forms of ferrihydrite

5.4.4 Oxide surface chemistry

The surface chemistry of iron oxide minerals will determine the degree of aggregation compared to dispersion, the characteristics of the interaction of

the oxide with the solution phase, and the interaction of colloidal iron oxides with surfaces. All these effects are important to consider when investigating the likelihood and extent of iron clogging occurring in a well.

Measured PZSEs of synthetic samples correspond to literature values of between pH 7 and 9 for synthetic ferrihydrite (Grantham *et al.*, 1997; Schwertmann and Taylor, 1992), and 7.9 for goethite (Appel *et al.*, 2003, Scheidegger *et al.*, 1993). The lower PZSE measured for the KK (3.6 - 5.1) and spring (3.6 - 5) samples is due to the presence of anions sorbed to the oxide surface, such as phosphate, silica and organic molecules. The anions are sorbed to balance the net charge the natural samples carry in the groundwater environment (Schwertmann and Taylor, 1992; Carlson and Schwertmann, 1987). The pH of the water from which the KKRWSS and spring samples were precipitated exceeds the PZSE, indicating that these samples will have a negatively charged surface in the groundwater environment and will be prone to dispersion rather than flocculation and aggregation. However, aggregation is enhanced in less crystalline and higher surface area iron oxides (Grantham *et al.*, 1997; Schwertmann and Taylor, 1992). The difficulties experienced in obtaining PZSEs for the Atlantis samples may be due to the high levels of organic carbon in these samples. Adsorbed organics can affect the surface charge of the iron oxide, making the surface more negative (Schwertmann and Taylor, 1992). Titration curves that do not intersect can be explained by asymmetrical binding to the surface of the cation and anion in the added neutral salt due perhaps to the presence of negatively charged organic C (Sverjensky, 2005). Martinez *et al.* (2003) found that bacteria in a bacteriogenic iron oxide contributed acidic sites but that the overall surface charge on iron oxides was dominated by contributions from the oxide reactive groups. Surface charge density appears to be greater on Atlantis samples as a more acid/base was required to be added to the Atlantis than KKRWSS samples to achieve a change in pH from 6 to 7.

BET-measured surface areas of synthetic minerals correspond well to published values. Ferrihydrite is expected to be between 163 and 560 m^2/g (Carlson and Schwertmann, 1981; Carlson and Schwertmann, 1987;

Schwertmann and Taylor, 1992; Houben, 2003a), and goethite should be between 20 and 112 m^2/g (Houben, 2003a). The results for natural precipitates in this study largely fall within the range expected for synthetic ferrihydrite, but some surprisingly low surface areas were recorded for K4 and H1, two of the least crystalline and most reactive samples. Poorly ordered ferrihydrite is densely aggregated and homogenous, limiting the accessibility of gases to the interior when doing surface area measurements, resulting in poorly reproducible and low readings (Carlson and Schwertmann, 1981; Dzombak and Morel, 1990).

The negative surface charge held by the iron oxide in the near-neutral aquifer waters indicates that they will likely remain dispersed and not aggregate, and that they will attach to positively charged surfaces. Most bacteria have negatively charged surfaces at circumneutral pH due to acidic functional groups (Glasauer *et al.*, 2001). The surface chemistry of iron encrustations from natural systems does not correspond to observed behaviour and suggests that measurement of PZC and surface area are not worthwhile for the development of rehabilitation strategies.

5.5 Conclusion

Iron encrustation samples precipitated from TMG aquifer groundwater are predominantly ferrihydrite with some goethite. Samples precipitated from the Atlantis aquifer are so far of unknown mineralogy. Bacteria clearly play a role in formation of some precipitates but it is not known to what extent they are involved in the formation of the majority of the samples. Precipitates from Atlantis show no evidence of bacterial influence in their formation. The following conclusions are important considerations for designing a rehabilitation strategy:

- Wet samples collected from Atlantis lost over 80% of their mass when dried at room temperature. If this is an indication of clogging problems generally (very rare to source still wet samples) then only a small amount of iron is required to generate voluminous clogging deposits.
- Predictions of iron oxide behaviour from surface properties i.e., that they should be dispersed and are unlikely to adhere to bacterial cells,

do not correspond with observed behaviour and can not be used to assist in developing a rehabilitation strategy.

- Naturally precipitated iron oxides are less crystalline and more reactive than synthesised iron oxides, and will most likely behave quite differently during chemical rehabilitation. Of the natural samples, those precipitated in association with bacteria are more reactive. Synthetic iron oxides are not a good analogue for natural iron oxides.
- The crystallinity and reactivity of natural iron oxides appears to be strongly dependent on the presence of impurities co-precipitated or adsorbed onto the iron oxides, which is in turn a function of the chemistry of the groundwater. No one ion appears to determine the reactivity, but rather the sum of all ions other than iron in the sample. The chemistry of the groundwater could be used to qualitatively predict the reactivity of precipitated iron oxides.
- The amount of organic carbon present in samples with obvious biological influence is generally low (with the exception of S2) compared to the amount of iron present. Chemical rehabilitation methods targeting organic carbon on the assumption that the precipitate is biological in nature (i.e. oxidizing agents) are therefore unlikely to be effective.
- The samples analysed in this study reflect only the material that was accessible for sampling. Down-hole video logs indicate variability of encrustation types with depth in the borehole, and these should be sampled to determine the bacterial influence at different depths in the boreholes.

In answer to the questions asked at the beginning of the chapter, natural iron oxides appear to be hugely variable in chemistry and mineralogy depending on the groundwater chemistry from which they are formed, and the degree to which bacteria are involved in their precipitation. The more impurities included in the oxide, the more reactive the oxide, and oxides associated with bacteria appear be the most reactive. Synthetic precipitates are more crystalline and less reactive than natural precipitates and are therefore not a good analogue for natural iron oxides. At this stage, bacterial iron oxides can

only be distinguished from chemical iron oxides if bacteria are detected during microscope analysis. Oxides precipitated in the obvious presence of bacteria appear to be more reactive than those with no apparent bacterial presence, but the absence of bacteria in SEM images does not mean that they were not involved in oxide precipitation.

6 Rehabilitation of iron encrusted wells: Field and laboratory investigations

6.1 Introduction

Wells affected by iron oxide encrustation in South Africa are commonly chemically rehabilitated. The effectiveness of rehabilitation is assessed by measuring the yield of the borehole before and after treatment. Although yield improvements are noticed with most treatments, the chemical treatment methods have never been optimised, and the same chemicals are used for all aquifers and encrustations. The concentration of the reagents is high (10 %) and the environmental impact of these chemicals has not been adequately considered. Synthetic minerals are generally used to study the dissolution behaviour of iron oxide minerals in chemical reagents (Houben, 2003b; Cornell and Giovanoli, 1993, 1988; Sidhu *et al.*,1981). Results from Chapter 4 show that synthetic iron oxides are poor analogues for natural iron oxides, and that there are distinct differences between encrustations from different aquifers, suggesting that the one size fits all' approach, although effective, is not optimal. The aim of this chapter is to identify shortcomings of current rehabilitation methods and to use laboratory tests to investigate the potential for using alternative reagents or different reagent concentrations to optimise the rehabilitation process.

6.1.1 Chemical rehabilitation Methods

6.1.1.1 Introduction

The aim of chemical borehole rehabilitation is to dislodge, disperse and dissolve the encrusting material and to sterilize the borehole. Many methods focus on sterilization and removal of organic deposits even though the encrustation is dominantly iron (Engelbrecht and Jolly, 2000; Chapter 5). As discussed in Chapter 3, dissolution of iron can be achieved by 3 mechanisms, proton promoted dissolution, reduction and ligand promoted dissolution. Most reagents in use for chemical borehole rehabilitation can be classified based on the mechanism of iron dissolution (Houben, 2003b; Cornell and Schwertmann, 1996):

- Proton promoted dissolution – Mineral and organic acids are used to dissolve iron encrustations e.g. HCl:

  $$3HCl + Fe(OH)_3 = Fe^{3+} + Cl^- + 3H_2O \qquad (6.1)$$

  Strong mineral acids can cause corrosion, and organic acids are associated with secondary microbial pollution (Houben, 2003b).
- Reduction - reducing agents are used on their own or combined with complexing agents e.g. Na dithionite:

  $$2FeOOH + Na_2S_2O_4 + 4H^+ = 2Fe^{2+} + 2Na^+ + 2HSO_3^- + 2H_2O \quad (6.2)$$

  Reduction has been found to be the most effective dissolution mechanism in terms of rate, particularly when aided by complexing agents (Cornell and Schwertmann, 1996).
- Ligand promoted dissolution - Complexing agents are used to accelerate dissolution rates e.g. NH_4 oxalate (Cornell and Schwertmann, 1996):

  $$(NH_4)_2C_2O_4.H_2O + Fe(OH)_3 + 3H^+ = (NH_4)_2C_2O_4.H_2O\text{-}Fe^{3+} + 3H_2O \quad (6.3)$$

6.1.1.2 Chemical rehabilitation in South Africa

The treatments used at the KKRWSS and AWSS are Blended Chemical Heat Treatment™ (BCHT) and the Radical Waters treatment method (RWT). Because these methods are proprietary, scant information is available on the chemicals used and mechanism of dissolution. Information presented here is gleaned from discussions with the rehabilitation experts (C. Less, More Water CC., pers. comm.; J.J. Viljoen & S. Rawhani, Radical Waters, pers. comm.; L. Smith, DWAF, pers. comm.), and the few technical reports prepared for the respective water supply schemes (Flower and Bishop, 2003; More Water cc, 2002; Riekel and Hintze, 2002; Smith, 2002). Both treatment methods are developed on the premise of the clogging material being a biofilm.

BCHT involves a 3 day process of pumping mixtures of heated acids, oxidizing agents and bases into the borehole combined with physical cleaning mechanisms. The procedure as applied in the KKRWSS is as follows:

1. Down-hole video logging and step test to determine the pre-treatment state of the borehole. A step test involves measuring the drawdown in the borehole as the pumping rate is stepped up, and then monitoring water level recovery. The results of the step test can be used to calculate the borehole yield, i.e., the flow rate of water the borehole can sustain without being pumped dry.
2. A solution of 8% NaOH prepared from groundwater is pumped into the borehole with physical brushing and jetting of the inside walls of the borehole.
3. The NaOH solution is left in borehole for 18 hours
4. A mixture of 10% sulfamic acid and HTH™ (calcium hypochlorite) heated to 60°C is pumped into the borehole with physical brushing and jetting of the inside walls of the borehole.
5. The sulfamic acid-calcium hypochlorite solution is left in borehole for 18 hours
6. Purge borehole by pumping until the pH and EC in the outflow water return to pre-rehabilitation values
7. Repeat of down-hole video logging and step test to determine post-treatment state of the borehole.

Volumes of reagents vary according to the depth and diameter of the well but are typically of the order of 10 000 L for the Klein Karoo boreholes. Although not explicitly stated, it is believed that the initial high pH phase is aimed at dispersing the attached material, the sulfamic acid lowers the pH to dissolve the iron phases, and the Ca hypochlorite is intended to oxidise organic matter. According to Cullimore (1992), rapid changes in pH and high pH gradients are the only effective rehabilitation mechanism to penetrate biofilm organisms before they can initiate stress-survival mechanisms.

The RWT was developed to clear biofilms from pipelines, and involves the use of an electrochemically generated strongly oxidizing solution to destroy cellular and organic carbon material (Riekel and Hintze, 2002). To generate the treatment solution, groundwater is pumped from the borehole into a holding tank and a small quantity of NaCl is added to the water. The Na-Cl solution passes through an electrochemical cell in which the anode and

cathode are separated by a membrane, splitting the solution into two streams, an oxidizing high pH "anol yte" and a reducing low pH "catholyte". The anolyte, containing oxidants including O_3, H_2O_2, hypochlorite and OH radicals, is pumped into the well with jetting and brushing, while the catholyte is discarded. Because of the rapid decomposure of these oxidants, no purge phase is practised, although pre- and post-treatment step-tests are performed to determine the improvement in yield.

6.1.1.3 Rate models for dissolution of iron oxide minerals

The effectiveness of a chemical rehabilitation reagent can be assessed by the rate and extent of encrustation dissolution. A number of models have been developed to describe the dissolution behaviour of iron oxide minerals (Postma, 1993; Cornell and Schwertmann, 1996). Dissolution is normally measured by monitoring the concentration of Fe in solution, and rate equations express dissolution in terms of Fe in solution rather than the reduction in the remaining solid $Fe(OH)_3$. The extent of dissolution is described using the amount of Fe in solution at time t (C) as a proportion of the total amount of solid phase iron available to dissolve (C_0):

$$\alpha = C/C_0 \qquad (6.4)$$

The fraction of Fe dissolved can be linearly or non-linearly related to the time elapsed. Linear dissolution behaviour indicates that dissolution is a function only of time and not solute or mineral concentration:

$$\alpha = kt \qquad (6.5)$$

where k is the apparent rate constant (because amounts are not normalised to surface area) and t the elapsed time. Often a linear rate law will only describe part of the experiment, because dissolution slows with time, resulting in a deceleratory curve (Houben, 2003b). The initial rapid dissolution is of particles with high surface area, surface defects (dissolution cavities, edges, corners) and impurities, but with time the particles that remain are harder and slower to dissolve and the rate of dissolution decreases, resulting in a non-linear relationship between α and time. Non-linear dissolution behaviour is more pronounced in natural samples due to their heterogeneity (Dold, 2003; Postma, 1993; Borggaard, 1991). Slower dissolution at the beginning and

end of a dissolution experiment will result in a sigmoidal relationship between α and t. The initial slower dissolution is possibly due to the time needed for the sample to properly disperse, or for all surfaces to become saturated with the dissolution reagent (Houben, 2003b), or it could indicate that particles are breaking up during dissolution (Dold, 2003).

Deceleratory and sigmoidal models commonly used to describe dissolution of iron oxide minerals are based on two premises, one is the changing geometry of the dissolving solid, and the other is the nucleation of dissolution sites at the solid surface (Dold, 2003; Cornell and Schwertmann, 1996). In both cases dissolution is surface controlled i.e., the chemical reaction at the solid-solution interface is rate-determining, and the rate of dissolution is proportional to the surface area of the solid. The models described below are illustrated in Figure 6.1. Fitting a geometrical model to data implies that the dissolving solid is shrinking at a constant rate. The surface area decreases as the solid shrinks resulting in deceleratory behaviour. Two geometrical models are the square root law and the cube root law. The square root law describes dissolution of a shrinking disc (Dold, 2003; Cornell and Schwertmann, 1996):

$$1-(1-\alpha)^{1/2} = kt \qquad (6.6)$$

The cube root law describes a shrinking sphere (Cornell and Giovanoli, 1988):

$$1-(1-\alpha)^{1/3} = kt \qquad (6.7)$$

Dissolution of oxides in reducing agents has been found to follow a cubic rate law, i.e., the rate is proportional to the instantaneous surface area (Segal and Sellers, 1980).

Nucleation models describe dissolution that is controlled by the rate at which the dissolution reagent attaches to reaction sites on the iron oxide surface. Random nucleation assumes that the binding strength of the reagent to all surface sites is equal. The rate of dissolution decreases because the number of binding sites decreases with decreasing surface area. Random nucleation gives a first order rate equation (Cornell and Schwertmann, 1996):

$$(1-\alpha) = e^{-kt} \qquad (6.8)$$

Random nucleation of the reagent on reaction sites can also be modelled by the Avrami-Erofejev (A-E) equations which describe nucleation on a disc or sphere. The two dimensional A-E equation is (Cornell and Schwertmann, 1996):

$$(-\ln(1-\alpha))^{1/2} = kt \qquad (6.9)$$

and the three dimensional A-E equation is (Cornell and Schwertmann, 1996):

$$(-\ln(1-\alpha))^{1/3} = kt \qquad (6.10)$$

These dissolution curves are sigmoidal.

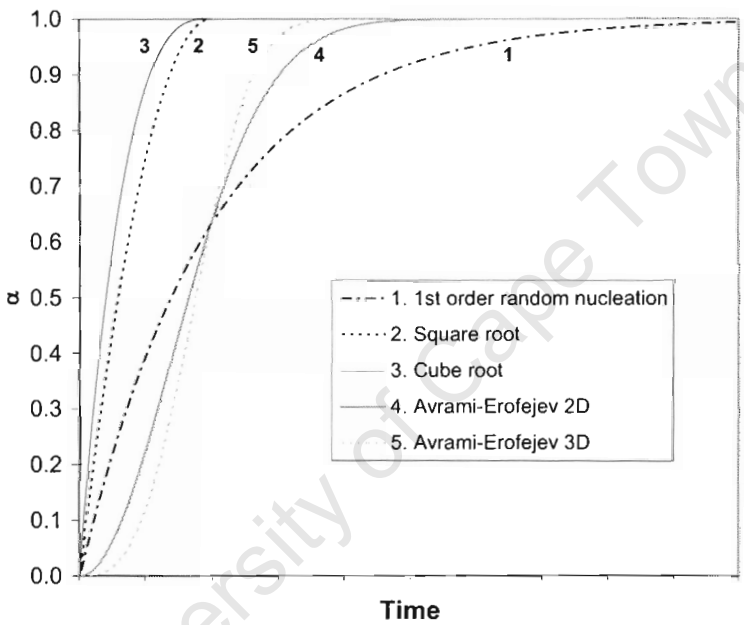

Figure 6.1. Shapes of iron oxide dissolution curves

Dissolution data are often hard to fit to a particular model, or are found to deviate from a model at the beginning or end of dissolution. In such instances, the Kabai model is useful for summarising rate data although it does not describe a physical dissolution process (Cornell and Schwertmann, 1996):

$$1-\alpha = e^{-(kt)^{\beta}} \qquad (6.11)$$

β is a fitting variable with no physical explanation. For $\beta>1$, dissolution is sigmoidal, and for $\beta<1$ dissolution is deceleratory (Dold, 2003; Cornell and Schwertmann, 1996). If the exponent β is 1, the equation reduces to first order random nucleation; for $\beta=2$, to the Avrami-Erofejev 2D law; and for $\beta=3$, to the Avrami-Erofejev 3D law.

6.2 Methodology

6.2.1 Field measurements

Chemical rehabilitation was carried out by the Department of Water Affairs and Forestry (DWAF) on 3 boreholes in the KKRWSS during July and August 2002. Boreholes KG1 and DL16 were initially treated by BCHT, and borehole DP28 and DL16 were treated by RWT in a follow up visit. During the pumping phases of the rehabilitation procedure, this author periodically monitored and sampled the groundwater. Analytical techniques as described in Chapter 3 were used to determine pH, DO, EC, Fe^{2+}, and Fe^{T} (colloidal and dissolved) of the pumped water in the field, and samples were collected for later analysis of major and trace elements.

6.2.2 Batch dissolution experiments

The dissolution rate of synthetic and natural iron oxide minerals was tested in a number of reagents using batch dissolution experiments (Table 6.1). Experiments were carried out at room temperature (20 to 25°C) under artificial lighting in the laboratory. To maintain conditions similar to those expected during field rehabilitation, reagents were not degassed. Approximately 10 mg of powdered mineral was placed in a 50 mL centrifuge tube, to which 25 mL of reagent was added. To ensure that dissolution is independent of the concentration of the reagent, <1-5% of the reagent should be consumed during dissolution (Cornell and Schwertmann, 1996; Postma, 1993). The percentage of reagent estimated to be consumed during the dissolution reaction based on a 10 mol Fe/kg iron oxide is given in Table 6.1. Note that most oxide samples contain less than 10 mol/kg iron, and that the calculation for acids is based on formation of Fe^{3+} and not $Fe(OH)_x^{3-x}$ species, so these values are maximum possible reagent consumption. Even so, most are close to or less than 1% consumption. The tubes were placed on a reciprocating shaker, to ensure sufficient agitation to transport the reagent to the solid/solution interface (Cornell and Schwertmann, 1996). 1 mL subsamples were taken periodically, filtered (0.2 μm membrane filter) and analysed for iron concentration by ferrozine colorimetry for all reagents except dithionite, which was determined by phenanthroline colorimetry (see Chapter 3).

The reactions were continued until either the iron concentration reached steady state or for 48 hours to obtain as complete a dissolution curve as possible. Often dissolution at the beginning of an experiment does not represent the behaviour of the bulk oxide, because initial dissolution is of iron oxide made more soluble by impurities in natural oxides, and surface defects in synthetic oxides (Cornell and Schwertmann, 1996). The pH of the mixture was measured before and after dissolution and was found to remain constant. Most of the batch dissolution experiments were performed on a selection of samples including the synthetic samples FH2, FH6 and Gt, and natural samples K1, K4, A2 and A4. For selected reagents (dithionite, oxalate, ascorbic acid and sulfamic acid) all the synthetic and natural iron oxides from the Klein Karoo and Atlantis sites were used. At least one sample was reacted in duplicate for each reagent.

Table 6.1. Reagents used in batch dissolution experiments.

Reagent	Chemical formula	Conc. (M)	pH	Mech.[a]	Cons. (%)[b]	Buffer/ Complexant
Sulfamic acid	NH_2SO_3H	0.1	1.2	P	1.2	
Sulfamic acid	NH_2SO_3H	0.4	0.6	P	0.3	
Ascorbic acid	$C_6H_8O_6$	0.05	7.6	R, C	0.8	Na citrate ($C_6H_8O_7Na_32H_2O$) / $NaHCO_3$
Hydrochloric acid	HCl	0.1	1.1	P	1.2	
Sulphuric acid	H_2SO_4	0.1	1.0	P	0.6	
Acetic acid	CH_3COOH	0.1	2.8	P	1.2	
Hydroxylamine hydrochloride	$NH_2OH.HCl$	0.1	3.9	R	0.1?	
Sodium dithionite	$Na_2S_2O_4$	0.1	4.8	R, C	0.2	Sodium citrate/acetic acid
Sodium dithionite	$Na_2S_2O_4$	0.01	5.2	R, C	2	Sodium citrate/acetic acid
Sodium hydroxide	NaOH	2	13.8	P	0.02	
Ammonium oxalate	$(NH_4)_2C_2O_4H_2O$	0.2	3.0	C		
Phosphoric acid	H_3PO_4	0.1	1.6	P	0.4	
Mixture sulfamic acid and NaOH	NH_2SO_3H, NaOH	0.4, 2	13.3	P	1.2,0.02	

[a]Mechanism of dissolution P = proton promoted; R = reductive; C = complexation; O = oxidation

[b]Estimated percentage reagent consumed on dissolution of 10 mg 10 mol Fe/kg iron oxide in 25 mL of solution.

6.3 Results

6.3.1 Field rehabilitation

Complete monitoring results for both BCHT and RWT rehabilitation treatments of boreholes KG1, DP28 and DL16 are included in Tables A.17 – A.22 (Appendix A). Data are presented in Figures 6.2 to 6.4. Note that due to the long time periods involved, the abscissa is not on a time scale. The timing of sampling is given in Appendix A.

The water chemistry at the end of the initial pump test can be taken as the backgroundwater chemistry of the aquifer at that site. BCHT affects the chemistry of the groundwater in boreholes KG1 and DL16, causing marked decrease in pH to about 2 and increase in EC and DO (Figure 6.2 and 6.4). The iron pumped out of the borehole during the purge phase is predominantly dissolved, with about 80% in borehole KG1 and 50% in DL16 as Fe^{2+}. Zn and Mn concentrations in the purged water are an order of magnitude greater than background concentrations, and Si concentrations are trebled. The origin of Zn is believed to be from galvanised steel borehole components, and a brass jetting hose damaged during the rehabilitation procedure. The reagents added to the borehole are detected in the outflow, with high Na concentration from NaOH, and sulfamic acid represented by N and S compounds including NO_2^-, NO_3^-, NH_4^+ and SO_4^{2-}. The increased Ca and Cl concentrations are due to the small amount of calcium hypochlorite added to the sulfamic acid. RWT of DL16 and DP28 affects the pH and EC but not to the same extent as BCHT, and the values return to background levels quickly during the post-treatment step test (Figure 6.3 and 6.4). Na and Cl are part of the RWT solution so the concentration of these ions is high in the waste water, but other ions are only marginally affected. Iron is pumped from the borehole initially primarily in colloidal form but in concentrations only slightly above background.

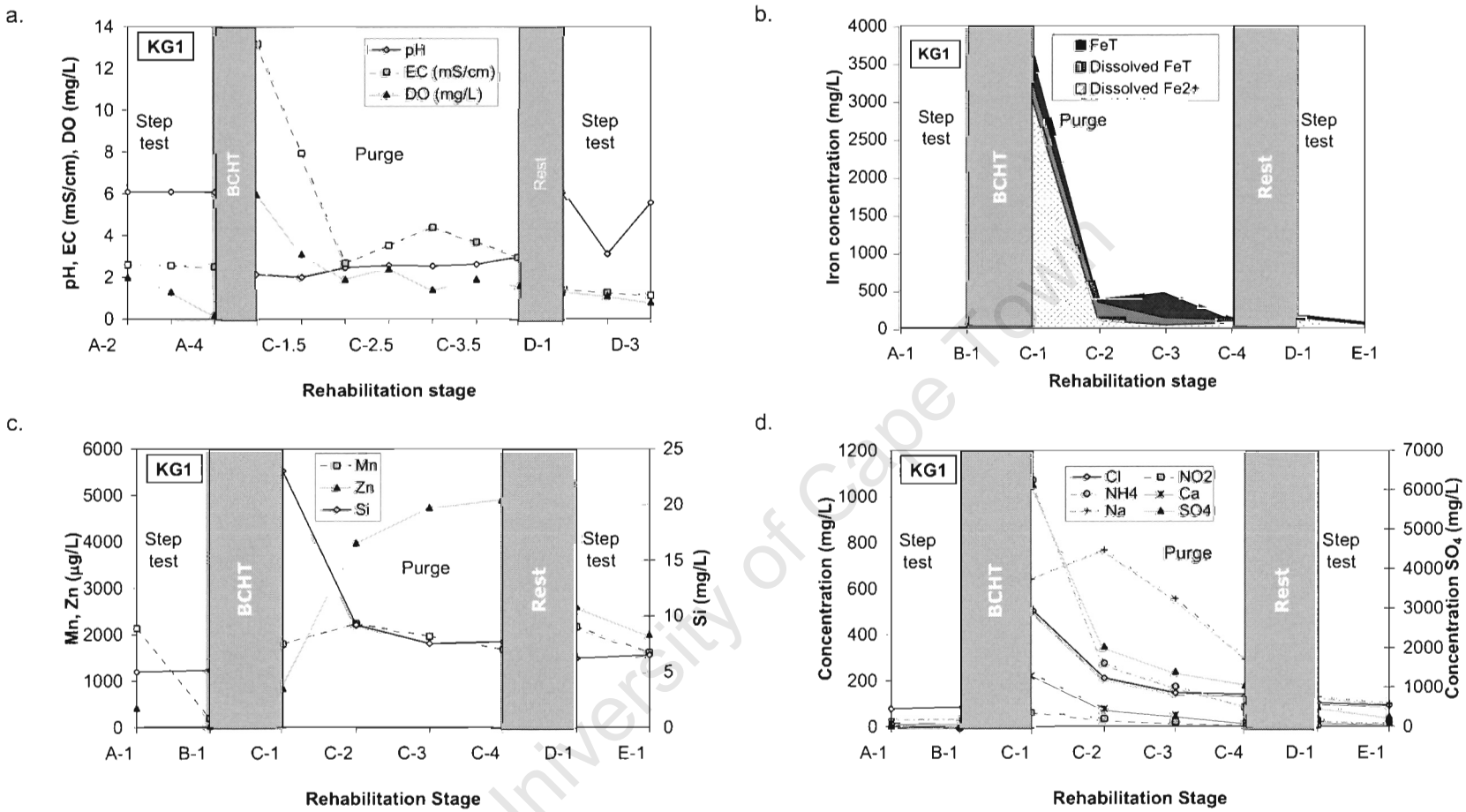

Figure 6.2. Changes in variables with time before and after rehabilitation for borehole KG1, which was treated by BCHT. Abscissa is not on a time scale, and letters refer to stage in rehabilitation (A. Calibration step test, B. Step test, C. Purge, D. Final step test). Vertical grey bars represent times during which there was no pumping from the well, so no samples could be obtained. a) pH, EC and DO, b) Proportions of iron in different fractions, c) Metals, including Si, d) Species present due to the rehabilitation chemicals.

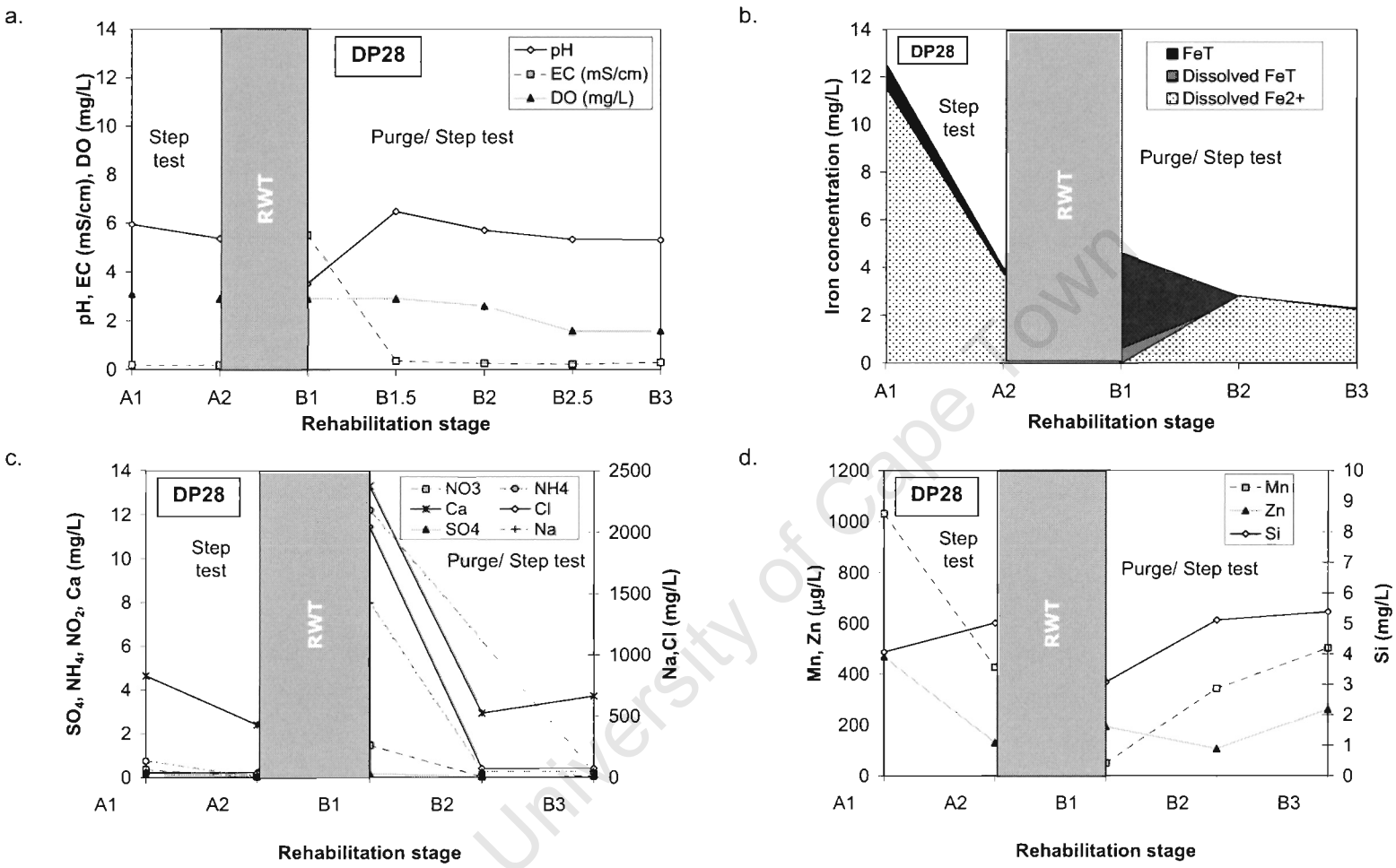

Figure 6.3. Changes in variables with time before and after rehabilitation for borehole DP28, which was treated by RWT. a) pH, EC and DO, b) Proportions of iron in different fractions, c) Metals, including Mn, Zn and Si, d) Species present due to the rehabilitation chemicals. Stages in rehabilitation A. Step test, B. Final step test

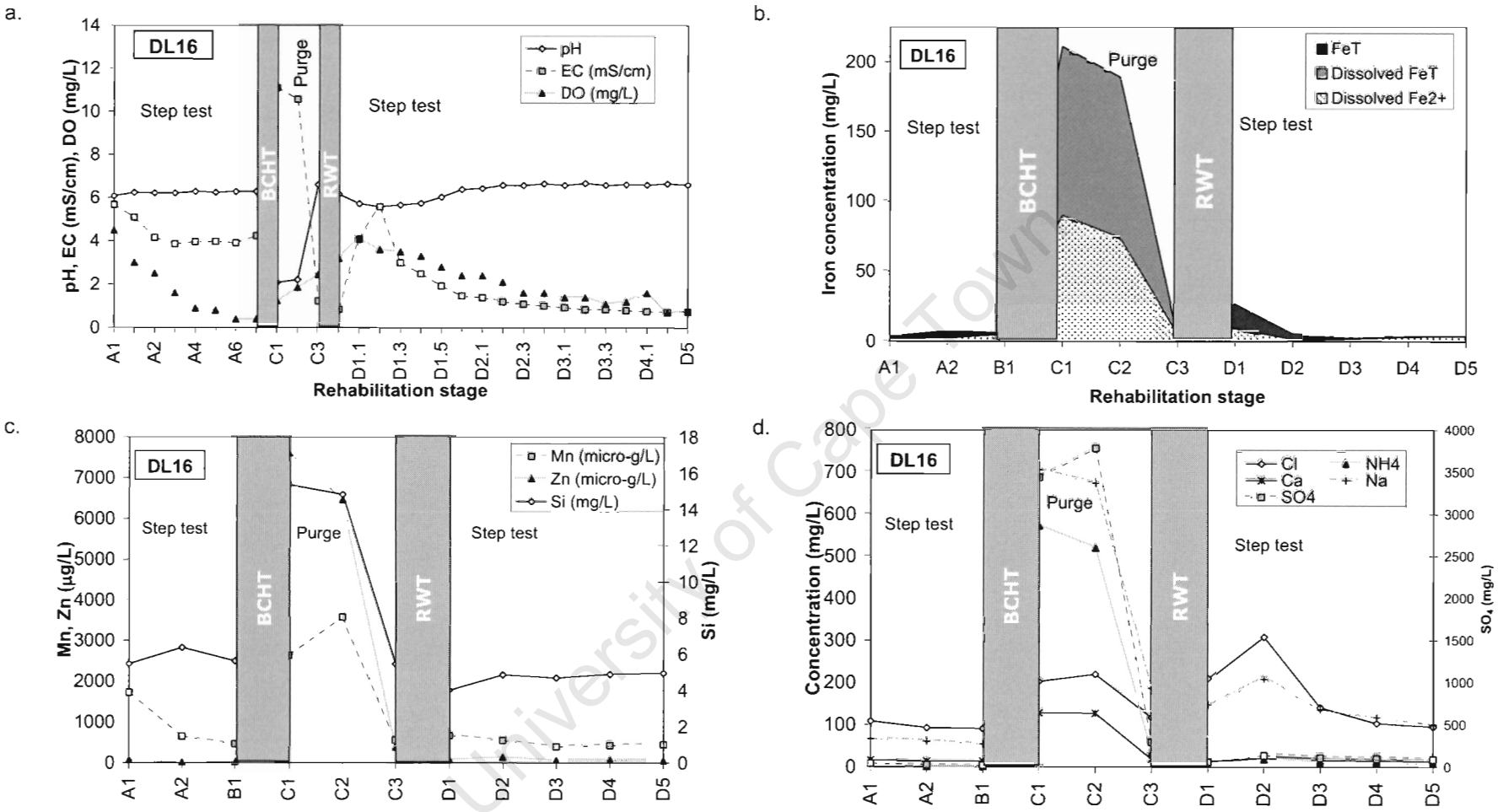

Figure 6.4. Changes in variables with time before and after rehabilitation for borehole DL16, which was first treated by BCHT followed by RWT. a) pH, EC and DO, b) Proportions of iron in different fractions, c) Metals, including Mn, Zn and Si, d) Species present due to the rehabilitation chemicals. Stages in rehabilitation are A. Calibration step test, B. Step test, C. Purge, D. Final step test

6.3.2 Batch dissolution of iron oxides

The full dataset of batch dissolution results is given in Tables A.23 to A.32 (Appendix A). The data are summarised in Figures 6.5-6.6, using only representative samples from Atlantis (A3, A4), the Klein Karoo (K1, K4) and synthetic samples. Dissolution of all samples for 0.1 M dithionite, 0.2 M oxalate and 0.4 M sulfamic acid are shown in Figure 6.7-6.10, grouped by sampling site. The measured iron concentrations were corrected for the volume of solution removed from the batch reactor during sampling, normalised to the mass of sample used and recalculated as a proportion of the total iron present in the undissolved sample (α).

Iron concentrations were below detection limits during dissolution of samples using a mixed sulfamic acid-NaOH reagent, and the RWT 'Anolyte"reagent, and data for these experiments are not presented. Repeatability of duplicates for all reagents except ascorbic acid is within 10% relative standard deviation (RSD; Table B.9 to B.12, Appendix B). The lines on the graphs are the Kabai fit to the data (see discussion). Most of the curves show initial rapid dissolution slowing down as equilibrium is approached, i.e., deceleratory curves, except NH_4 oxalate which has a distinctly sigmoidal curve. NH_4 oxalate can be decomposed to form a reductant in the presence of light, which can reduce the iron oxides to Fe^{2+}. The presence of Fe^{2+} catalyses further iron oxide dissolution, resulting in a steepening of the dissolution curve with time. In general, the Atlantis samples dissolve the most rapidly, followed by the Klein Karoo samples, then FH2, FH6 and Gt. In many cases the Atlantis samples are fully dissolved in 48 hours, but the synthetic and Klein Karoo samples lag behind. FH2 often dissolves at a similar rate to the Atlantis and Klein Karoo samples. 0.1 M dithionite results in complete dissolution of all samples within 5 hours. Gt is only dissolved in dithionite. Qualitatively, the effectiveness of the reagents decreases in the order dithionite, strong acids (HCl, H_2SO_4, sulfamic, H_3PO_4), NH_4 oxalate, ascorbic acid, hydroxylamine HCl and least effective reagent is acetic acid.

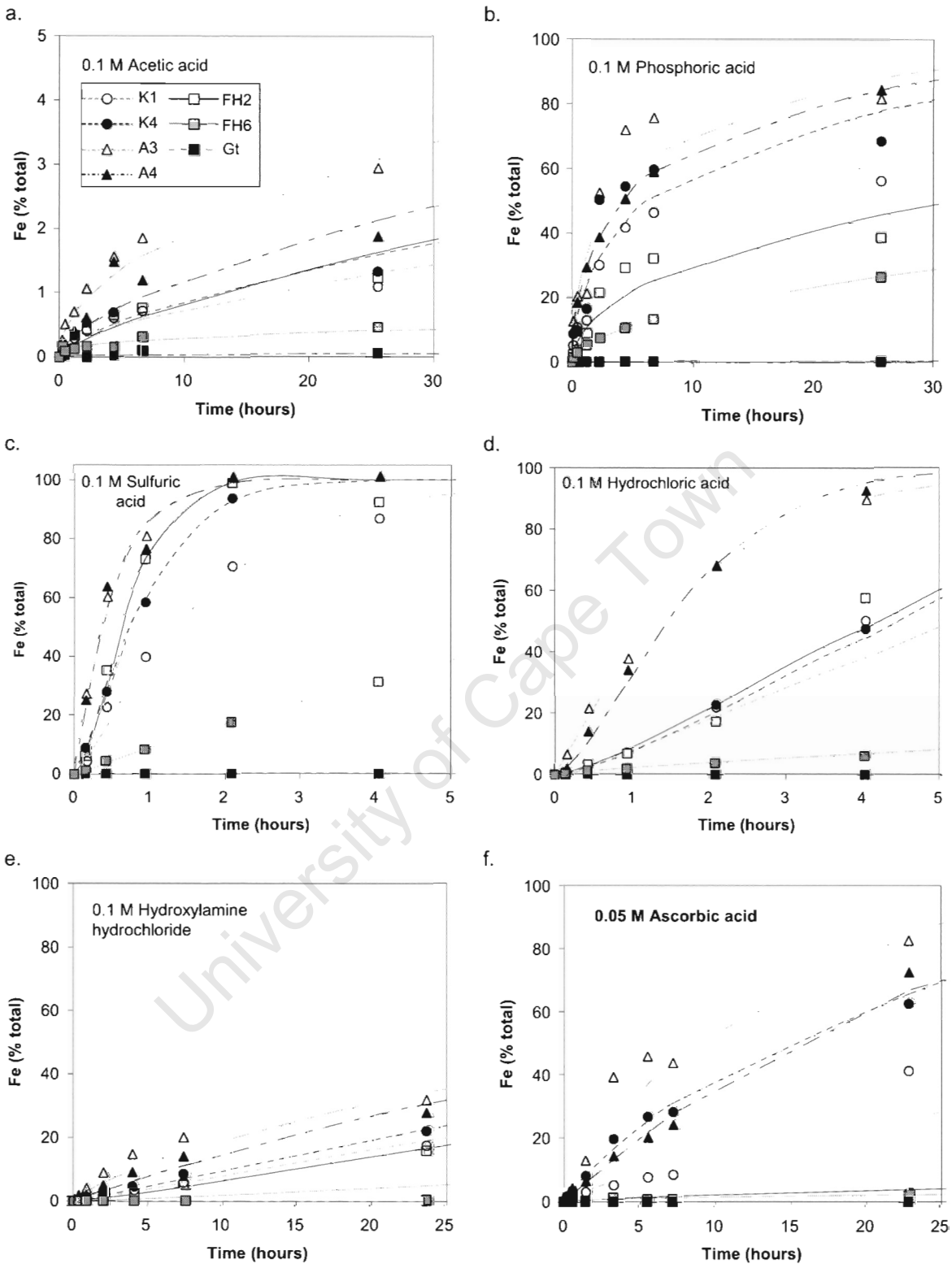

Figure 6.5. Percent of total iron content of iron oxides dissolved with time. Lines on the graphs are Kabai fits (for fit parameters see Table 6.2). a. 0.1 M acetic acid, b. 0.1 M phosphoric acid, c. 0.1 M sulphuric acid, d. 0.1 M hydrochloric acid, e. 0.1 M hydroxylamine hydrochloride, f. 0.05 M ascorbic acid

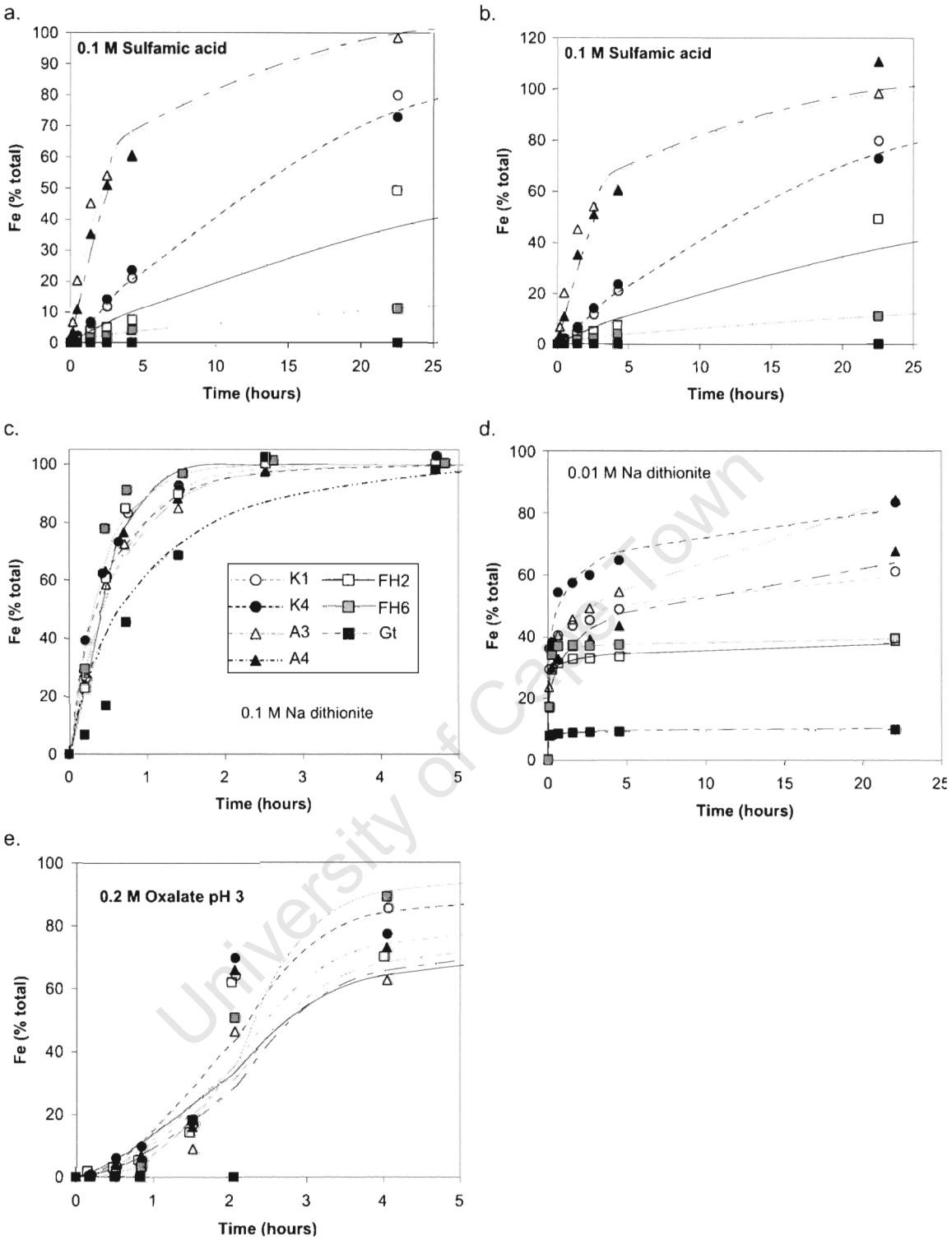

Figure 6.6 Percent of total iron content of iron oxides dissolved with time. Lines on the graphs are Kabai fits (for fit parameters see Table 6.2). a. 0.4 M sulfamic acid, b. 0.1 M sulfamic acid, c. 0.1 M dithionite, d. 0.01 M dithionite, e. 0.2 M oxalate

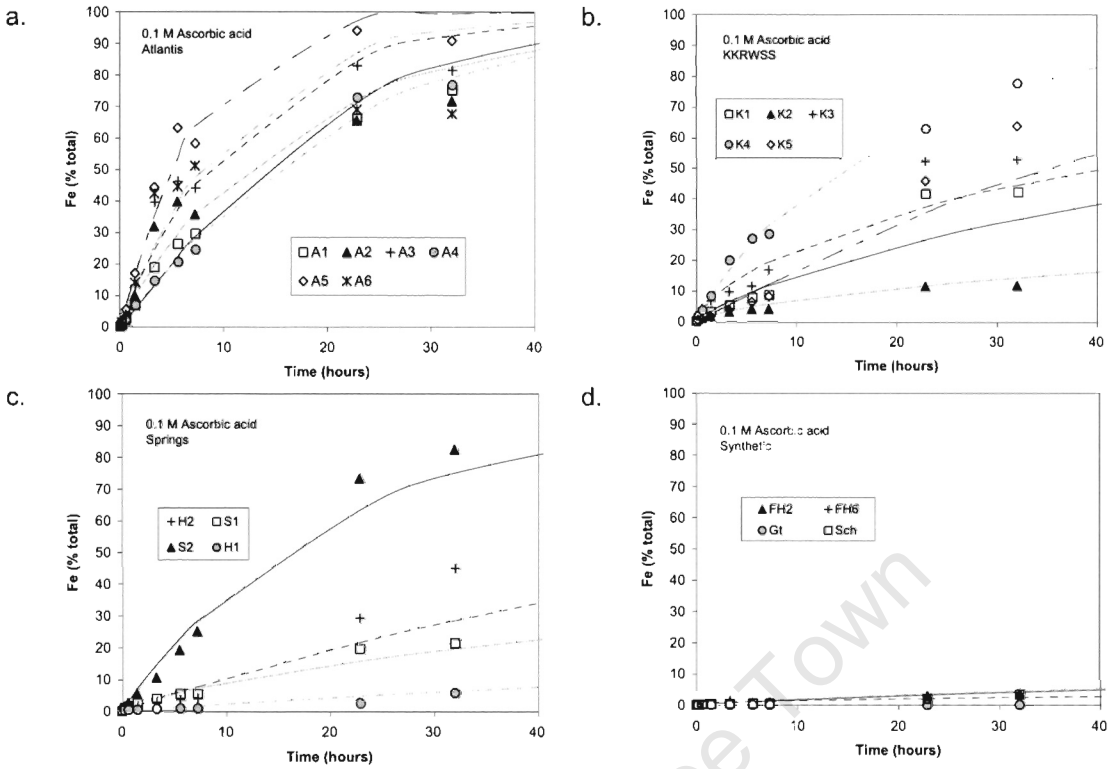

Figure 6.7. Dissolution of all samples in 0.1 M ascorbic acid. Lines are the Kabai fit (for fit parameters see Table 6.2). a) Atlantis, b) KKRWSS, c) Springs, d) Synthetic samples

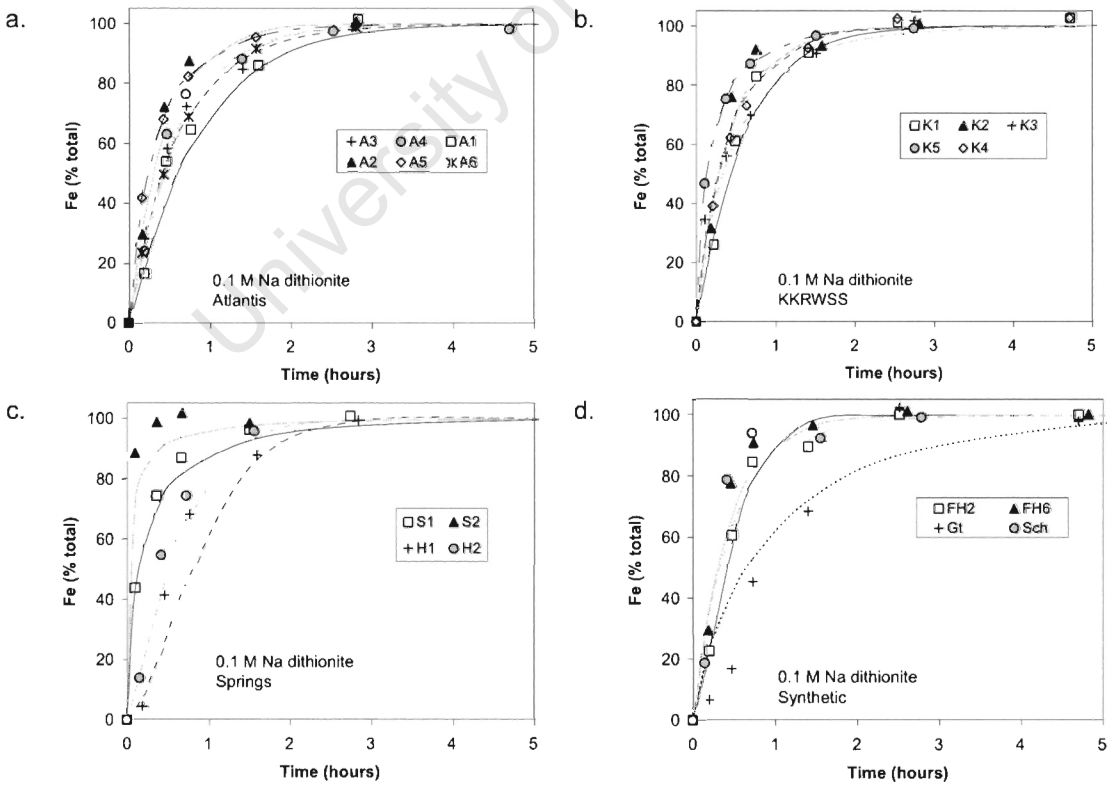

Figure 6.8. Dissolution of all samples in 0.1 M dithionite. Lines are the Kabai fit (for fit parameters see Table 6.2). a) Atlantis, b) KKRWSS, c) Springs, d) Synthetic samples

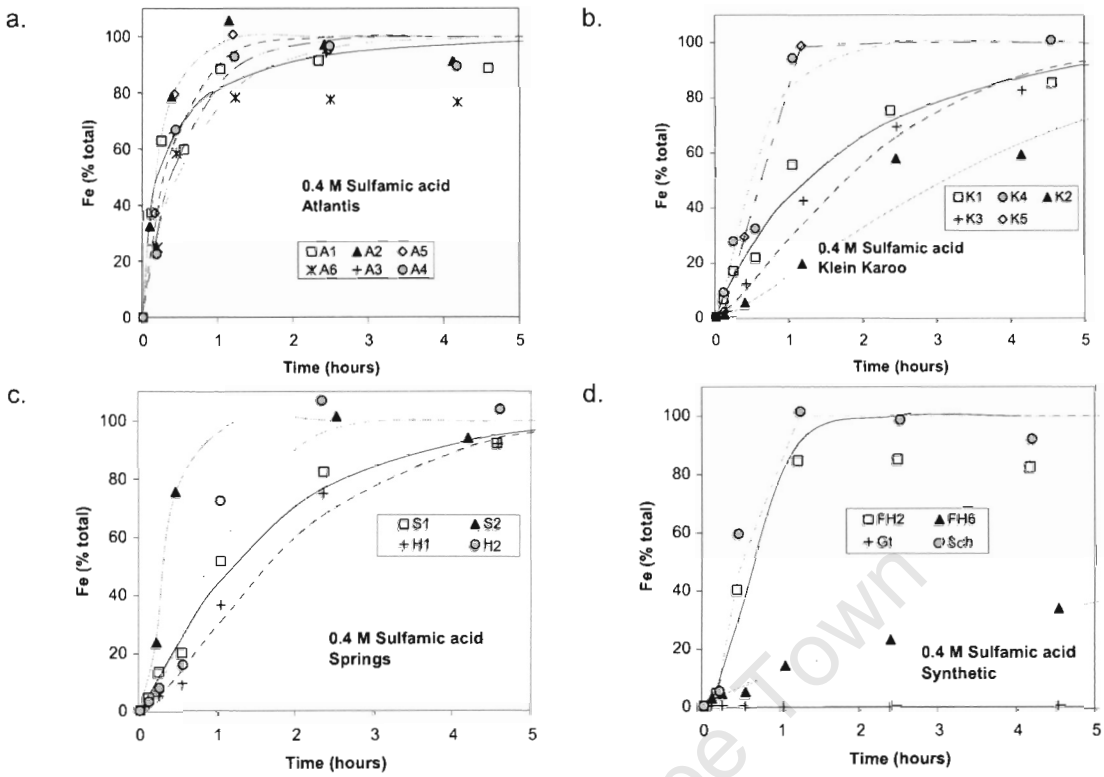

Figure 6.9. Dissolution of all samples in 0.4 M sulfamic acid. Lines are the Kabai fit (for fit parameters see Table 6.2). a) Atlantis, b) KKRWSS, c) Springs, d) Synthetic samples

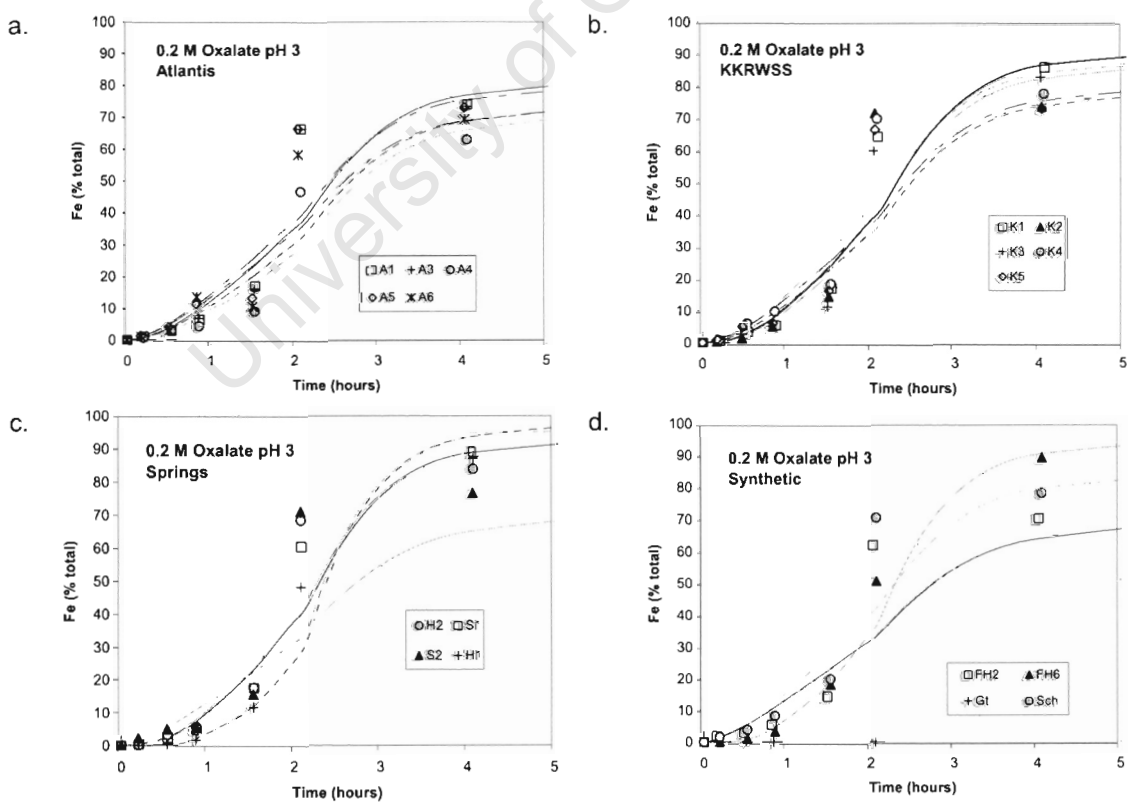

Figure 6.10. Dissolution of all samples in 0.2 M oxalate. Lines are the Kabai fit (for fit parameters see Table 6.2). a) Atlantis, b) KKRWSS, c) Springs, d) Synthetic samples

6.4 Discussion

6.4.1 Assessment of current rehabilitation methods

Rehabilitation of KKRWSS boreholes by the BCHT and RWT appears to have been effective. Improvements in yield following rehabilitation are 64.4% for KG1, 14.7% for DL16 and 31.6% for DP28 (Smith, 2002). Comparison of the effectiveness of the two methods is difficult because a number of factors, e.g., borehole construction, type of encrustation material etc., could influence the improvement in yield. Based on visual improvements, the methods appear to be equally effective (Figure 6.11). Although effective, these chemical methods, particularly the BCHT, suffer from a number of drawbacks, including potential for groundwater pollution, corrosion, and being a hazard to the health of rehabilitation workers.

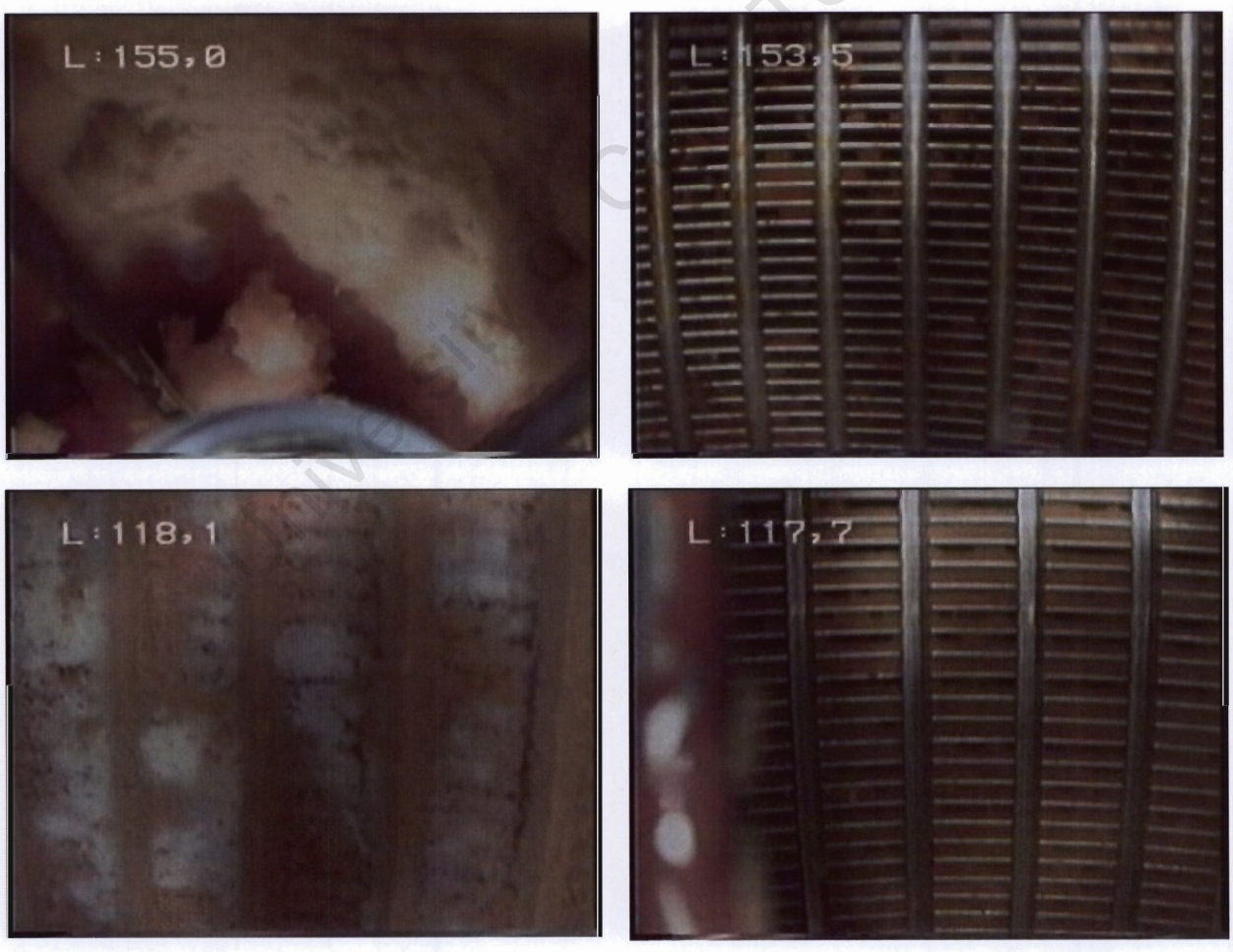

Figure 6.11. Improvement in well screens before (left) and after (right) rehabilitation for boreholes DP28 (top) and KG1 (bottom) (Courtesy of J. Uys, KKRWSS; B. Venter, DWAF)

Pumping a chemical into a borehole could result in groundwater pollution if the chemical is not completely removed. Evidence from monitoring of the groundwater chemistry during the purge and post-treatment step tests suggests that not all the chemicals are removed from the borehole. Firstly, the acidic pH measured during both KG1 and DL16 purge phases was unexpected, because equal volumes of 8% NaOH and 10% sulfamic acid were added to the borehole. Laboratory mixtures of these reagents became acidic only when sulfamic acid constituted more than 80% of the mixture. The NaOH is in the well for 18 hours prior to addition of the sulfamic acid, and has had the opportunity to migrate away from the well. An increase in pH is not detected in the outflow, suggesting that the bulk of the NaOH is not pumped out. A simple mass balance calculation indicates that 460 000 g of Na are added to the borehole, yet pumping out purge water of 0.7 g/L Na (maximum measured concentration of Na in KG1 purge water) at 5 L/s for 24 hours only accounts for 259 200 g of Na, so a significant proportion of the NaOH is lost to the aquifer. Secondly, although the purge phase continues until pH and EC values return to pre-rehabilitation values, a drop in pH is noted during the final step test at borehole KG1 suggesting that pockets of low pH water remain. In addition, the concentration of ions due to the added reagents, i.e., Ca, Cl (from Ca hypochlorite), Na (from NaOH), nitrogen species (NO_2, NH_4, NO_3) and sulphate (from sulfamic acid) are still slightly elevated during the final pump test, indicating that not all of the reagent has been removed from the borehole. Finally, during down-hole chemical logging of an Atlantis borehole that had been rehabilitated many months before, purged, but not subsequently put back into production, a pH of 1.6 was detected at the base of the borehole (L. Cavé CSIR, pers.comm). The concentrated chemicals used for rehabilitation are denser than the water and may not readily mix, sinking to the base of the borehole or the aquifer, from where they are difficult to pump out. These observations suggest that the aquifer is being polluted with the rehabilitation chemicals.

Apart from groundwater pollution, the BCHT chemicals are a hazard to the borehole equipment, to the workers who are involved in rehabilitation and to the environment. The sulfamic acid completely corroded and destroyed the

jetting tool during rehabilitation at the KKRWSS, and stainless steel screens are also believed to be in danger of corrosion. The sulfamic acid solution mobilised metals by corrosion of stainless steel and dissolution of metal rich precipitates, resulting in high concentrations of metals in the purge water which was disposed into a drainage ditch. Addition of Ca hypochlorite to heated sulfamic acid has the danger of violent reaction and generation of chlorine gas, posing a health risk (Mallinckrodt Baker, Inc., 2003a).

The RWT method has far fewer negative consequences compared to the BCHT method. However, its effectiveness is questionable as the iron concentration in the step test is hardly above background levels. The encrustations are predominantly iron, which is not soluble in the neutral pH oxidizing 'Anolyte'. Despite these reserv ations, the improvement in well yield and visual improvement observed by down-hole camera are significant (Figure 6.11), suggesting that the dispersing effect of the reagent along with physical jetting and surging is sufficient to dislodge many of the encrustations.

6.4.2 Rate of iron oxide dissolution

Dissolution of natural samples in this study clearly shows non-linear behaviour. Dissolution apparent rate constants (k) and other fitting parameters (β) were calculated for the experimental data with equations 6.6 to 6.11. The k and β values were determined from the slope and intercept values of linear regressions of rate equations. Values at steady state were excluded from the calculations to improve the fits, and the final point included in the calculation of models is the highest concentration reached. Data points with $\alpha>1$, i.e., the measured concentration exceeded the expected maximum concentration were omitted from rate calculations using natural logs because calculation resulted in a negative log. Iron concentrations in some reagents appeared to be particularly over-estimated, resulting in poor modelling. Because the differences between measured and expected concentrations were small in the case of 0.1 M dithionite, the C_o value was adjusted to the highest value determined in the batch experiment so that more points could

be included in the model. This modification was not performed for any other reagent.

Theoretical dissolution curves were calculated by substituting the calculated apparent rate constant back into the rate equation. The optimal model was chosen based on the correlation coefficient (r^2) between the measured data and the modelled data (Cornell and Schwertmann, 1996). The k, β and r^2 values for each model, each sample and each reagent are given in Tables A.33 to A.35 (Appendix A), with the highest r^2 for each sample in each reagent highlighted. Rate equations often only describe the initial or final parts of the dissolution curve, and sometimes a number of different models describe the data equally well (Cornell and Schwertmann, 1996), as is observed here. The first order random nucleation model (Equation 6.8), and the Kabai model (Equation 6.11) demonstrate the best fits to the data. As the only model for which measured and modelled data are consistently well correlated, the Kabai fit was chosen to summarise all the data so as to allow comparison of rates between different reagents (Figure 6.5 – 6.10; Table 6.2). However, the β value of many samples for many reagents approaches 1, suggesting that the random nucleation model probably best describes the mechanism of dissolution (Figure 6.12).

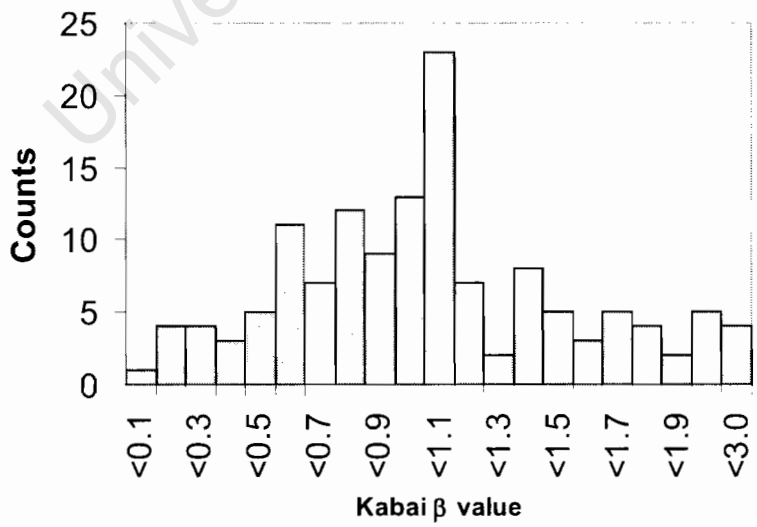

Figure 6.12. Histogram of Kabai β values for all samples and reagents

Table 6.2. Apparent rate constants calculated using the Kabai equation

	Sample	r^2	k (per hr)	β	r^2	k (per hr)	β	r^2	k (per hr)	β	r^2	k (per hr)	β	r^2	k (per hr)	β
		0.4 M Sulfamic acid			0.1 M Sulfamic acid			0.05 M Ascorbic			0.1 M Dithionite			0.2 M Oxalate		
Syn	FH2	0.933	1.28	1.880	0.972	1.93×10^{-2}	0.889	0.846	3.97×10^{-4}	0.703	0.990	1.88	1.373	0.839	0.380	2.500
	FH6	0.937	6.99×10^{-2}	0.774	0.998	2.00×10^{-3}	0.685	0.968	1.26×10^{-5}	0.474	0.980	2.36	0.981	0.982	0.306	1.741
	Gt	0.828	3.17×10^{-6}	0.558	0.850	2.05×10^{-19}	0.169	0.619	7.21×10^{-27}	0.127	0.943	0.963	1.804	0.863	bdl	
Atlantis	Sch	0.955	1.86	2.812	0.998	0.101	1.319	0.824	5.07×10^{-4}	0.772	0.937	2.09	0.888	0.834	0.255	1.463
	A1	0.914	2.59	0.542	0.889	0.100	0.764	0.955	5.34×10^{-2}	1.138	0.988	1.15	1.041	0.771	0.345	2.031
	A2	0.925	4.01	1.001	0.976	0.196	0.736	0.904	5.75×10^{-2}	0.920	0.962	2.33	0.955	0.929	0.327	2.028
	A3	0.947	2.36	1.002	0.988	0.272	0.804	0.953	8.17×10^{-2}	0.983	0.994	1.62	0.918		0.297	1.700
	A4	0.908	1.81	0.976	0.986	0.267	1.076	0.964	4.76×10^{-2}	1.059	0.984	1.70	0.971	0.808	0.350	1.761
	A5	0.929	3.51	1.352	0.955	0.823	1.055	0.939	0.140	1.094	0.980	2.77	0.772	0.891	0.308	1.624
KKRWSS	A6	0.897	1.48	0.886	0.906	8.95×10^{-2}	0.480	0.878	8.94×10^{-2}	1.004	0.976	1.57	1.001	0.918	0.339	3.166
	K1	0.966	0.542	0.911	0.982	6.04×10^{-2}	1.058	0.903	9.75×10^{-3}	0.786	0.988	1.64	1.037	0.823	0.274	1.501
	K2	0.960	0.243	1.279	0.998	1.77×10^{-2}	1.043	0.964	1.60×10^{-3}	0.629	0.978	2.47	0.896	0.887	0.306	1.586
	K3	0.962	0.429	1.302	0.992	2.39×10^{-2}	1.058	0.885	1.37×10^{-2}	0.672	0.982	2.37	0.879	0.869	0.254	1.413
	K4	0.924	1.53	1.325	0.998	6.04×10^{-2}	1.079	0.945	4.69×10^{-2}	0.916	1.000	1.91	0.807	0.834	0.349	2.512
	K5	0.933	1.60	2.274	0.992	6.68×10^{-2}	1.350	0.891	1.96×10^{-2}	1.060	0.978	4.53	0.644	0.968	0.308	1.624
Springs	H1	0.974	0.463	1.372	0.992	4.08×10^{-2}	1.099	0.826	1.33×10^{-3}	0.851	0.962	0.978	1.531	0.912	0.269	1.666
	H2	0.949	0.867	1.608	0.968	4.95×10^{-2}	1.083	0.933	1.01×10^{-2}	0.953	0.992	1.47	1.197	0.962	0.257	1.733
	S1	0.960	0.599	1.101	0.986	2.89×10^{-2}	0.943	0.982	4.35×10^{-2}	0.962	0.998	3.82	0.552	0.766	0.331	1.633
	S2	0.914	2.54	2.157	0.974	0.165	1.032	0.733	3.57×10^{-3}	0.702	0.984	21.9	0.379	0.839	0.352	2.188
		0.1 M Phosphoric			0.1 M Acetic			0.1 M HCl			0.1 M H2SO4			0.1 M Hydroxylamine Hydrochloride		
Syn	FH2	0.887	1.61×10^{-2}	0.539	0.924	1.25×10^{-4}	0.720	0.978	0.182	1.411	0.990	1.22	1.666	0.970	1.03×10^{-2}	1.189
	FH6	0.974	5.20×10^{-3}	0.555	0.933	2.15×10^{-9}	0.327	0.978	1.05×10^{-2}	0.857	0.956	9.83×10^{-2}	1.037	0.970	3.13×10^{-3}	1.129
	Gt	0.982	2.09×10^{-13}	0.554	0.236	9.57×10^{-19}	0.203	0.966	1.08×10^{-12}	0.347	0.982	9.47×10^{-7}	0.589	0.434	5.76×10^{-31}	0.123
Atl	A3	0.931	0.158	0.573	0.980	4.41×10^{-5}	0.506	0.996	0.537	1.081	0.996	1.84	1.099	0.937	1.43×10^{-2}	0.795
	A4	0.908	0.121	0.222	0.876	7.98×10^{-5}	0.623	0.994	0.525	1.486	0.988	1.84	1.115	0.966	1.50×10^{-2}	0.982
KK	K1	0.935	3.76×10^{-2}	0.534	0.939	2.95×10^{-5}	0.603	1.000	0.138	1.261	0.968	0.531	1.179	0.992	9.66×10^{-3}	1.088
	K4	0.910	8.19×10^{-2}	0.560	0.922	6.76×10^{-5}	0.654	0.859	0.172	1.457	0.996	0.974	1.339	0.949	1.16×10^{-2}	1.089

Although there is some variation between reagents, in general the samples from Atlantis are the most quickly dissolved, followed by the samples from the KKRWSS and FH2 (Figure 6.13). FH6 dissolves more slowly than any of the natural samples, and goethite is virtually insoluble in all reagents except dithionite.

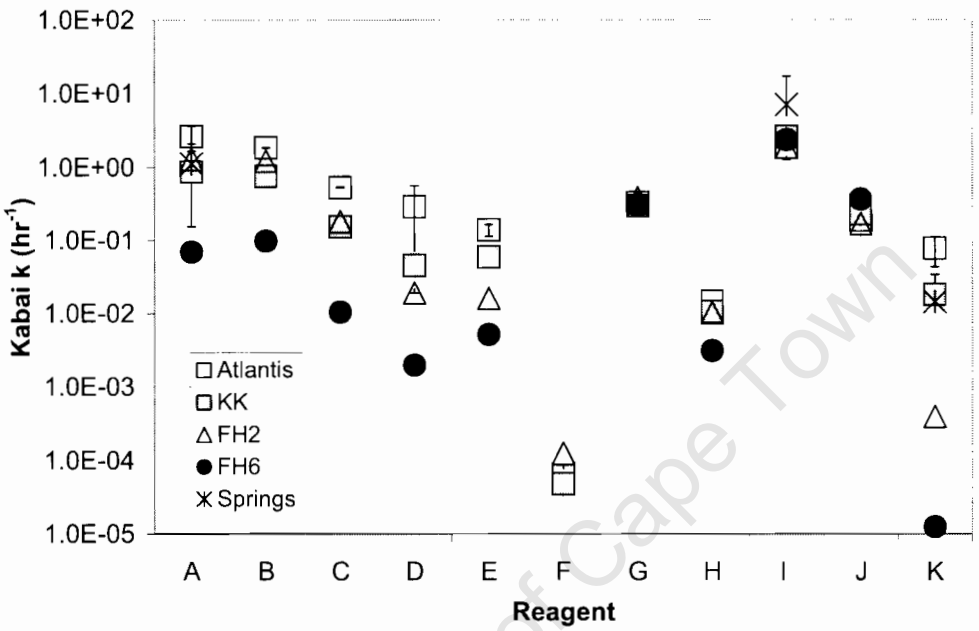

Figure 6.13. Average Kabai k values for dissolution of iron oxides (excluding Gt) in a number of reagents. Reagents are arranged in order of increasing pH. Reagents are: A. 0.4 M sulfamic acid, B. 0.1 M sulphuric acid, C. 0.1 M hydrochloric acid, D. 0.1 M sulfamic acid, E. 0.1 M phosphoric acid, F. 0.1 M acetic acid, G. 0.2 M oxalate, H. 0.1 M hydroxylamine hydrochloride, I. 0.1 M dithionite, J. 0.01 M dithionite, K. 0.05 M ascorbic acid. Error bars indicate standard deviation of average Kabai k values for each group.

Comparison of dissolution rates measured in this study to literature values is difficult because different authors use different rate equations and different units of dissolution. The most consistently used method of calculating the apparent rate constant is to fit a straight line to the first part of the dissolution curve. Linear dissolution apparent rate constants from the literature are given in Table 6. 3. The linear apparent rate constants calculated in this study are of a similar order of magnitude to those published in the literature, and differences are probably due to experimental setup. An exception is the apparent rate constant of 72 hr^{-1} for dissolution of 2-line ferrihydrite in ammonium oxalate, but this value could be erroneous due to possible

incorrect assumptions during recalculation from the units given in the paper (Borggaard, 1991). Qualitative comparison of ascorbic acid dissolution to results obtained by Larsen and Postma (2001) show that in this study FH6 is dissolved to a lesser extent. However, in the Larsen and Postma (2001) study, the ascorbic acid solution was degassed, allowing reductive dissolution, so the rates are not directly comparable.

Table 6.3. Comparison of linear apparent rate constants (hr^{-1}) from this study to literature values for dissolution of synthetic minerals.

Reagent	Mineral	This study	Literature	Reference
0.1 M HCl	FH2	0.14	0.060	Houben (2003b)[a]
	FH6	0.010	0.024	Houben (2003b)
0.1 M H_2SO_4	FH2	0.48	0.32	Houben (2003b)
0.1 M Sulfamic acid	FH2	0.022	0.046	Houben (2003b)
0.1 M NH_4 oxalate (pH 3)	FH2	0.90	72	Borggaard (1991)[b]
	FH2	0.20	0.36	Dold (2003)[c]
	FH6	0.24	0.11	Dold (2003)
0.5 M HCl	Gt	-	1.4	Sidhu *et al.*, (1981)

a. Rate constants in Table 2 of Houben (2003b) were recalculated to hr^{-1} assuming they were given in $\%.min^{-1}$ as suggested by the slopes of the graphs, rather than in s^{-1} as indicated in Table 2.
b. Recalculated from rate constant given in µmole/day
c. Calculated from data given in Table 3 of Dold (2003)

6.4.3 Controls on dissolution of iron oxides

Factors influencing the rate of dissolution are the overall system properties (temperature, UV light), composition of the solution phase (pH, redox potential, concentrations), and properties of the oxide (mineralogy, grain size, stoichiometry, substitution within the lattice, crystal chemistry, habit and defects, surface area). Each crystal face should have its own dissolution rate, resulting in shape-preserving dissolution, but microheterogeneities such as point defects, dislocations, microfractures, kinks, domain boundaries, corners, ledges and edges result in different dissolution behaviour (Cornell and Schwertmann, 1996; Postma, 1993). The overall system properties, although not strictly controlled, did not change significantly during the batch experiments. Variations in the dissolution rates are due to the oxide mineralogy, crystallinity and composition, including surface area, and chemical properties of the dissolution reagent, including pH and redox potential.

6.4.3.1 Properties of the iron oxide

The difference between the dissolution rates of minerals in a reagent is due to properties of the oxide, such as surface area, mineralogy and crystallinity

(Cornell and Schwertmann, 1996). No significant relationship is observed in this study between dissolution rate and surface area (Figure 6.14), although deceleratory dissolution models are commonly observed to be related to the surface area of the mineral (Houben, 2003a, Cornell and Schwertmann, 1996; Borggaard, 1991). Surface area may not have been accurately determined because the BET method of surface area measurement is not effective for iron oxide minerals (See Section 5.2.2.2).

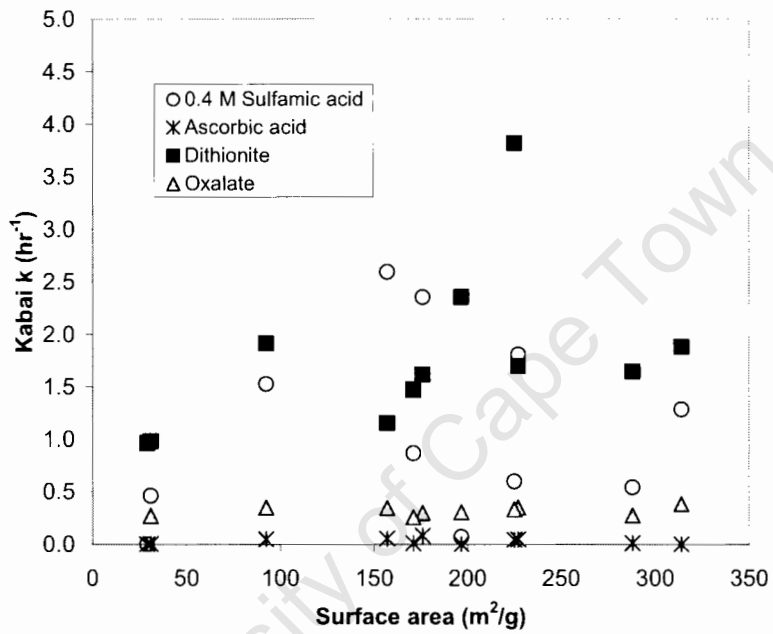

Figure 6.14. Relationship between Kabai k values and surface areas of samples dissolved in a selection of reagents

The mineralogy of the samples has a significant effect on the rate of dissolution. FH6 and FH2 dissolved many orders of magnitude faster than Gt in most reagents, although only 2- 4 times faster in dithionite. Ferrihydrite has been found to dissolve a factor of 1000 times faster than other iron oxide minerals, which is faster than would be expected based on surface area. The greater solubility of FH compared to other oxides is possibly due to decreased bond energies with decreased crystallinity (Cornell and Schwertmann, 1996; Borggaard, 1991). Synthetic FH2 dissolved slower than natural 2-line ferrihydrite (K4, K5, H1, H2, S2), and Atlantis samples, but dissolved more rapidly than 2-line ferrihydrite from the hotsprings in most reagents. Synthetic FH2 also dissolved more slowly than natural FH6 in 0.1 M sulfamic acid, ascorbic acid, 0.1 M dithionite and hydroxylamine hydrochloride. Natural

ferrihydrites have also been found to dissolve faster than synthetic ones, and dissolution rates reflect the rate of precipitation, i.e., more rapidly precipitated ferrihydrite dissolves more rapidly (Dold, 2003).

The presence of impurities within natural iron oxide samples affects the rate of iron oxide dissolution in acid reagents (sulfamic acid, hydrochloric acid, phosphoric acid, sulphuric acid, and acetic acid). A marked negative correlation is observed between the total iron content of the sample and the acid dissolution Kabai k value, or inversely, a positive correlation between the sum of non-iron ions and the k value (Figure 6.15). The increased rate of dissolution with decreasing iron content agrees with observations in Chapter 4 on the reactivity of samples. Substitution of impurities into the oxide crystal structure may result in crystal strains and defects, rendering the mineral more easily soluble than a pure phase. Cornell and Giovanoli (1993, 1988) found that the crystal morphology of haematite and goethite affects the acid dissolution rate, and that strained areas of haematite crystals and surface imperfections in lepidocrocite crystals are particularly susceptible to dissolution.

Adding to this argument is the observation that samples K4 and K5, with high phosphate contents (Table 5.5), have the highest dissolution rates of the KK samples. Proton-assisted, ligand controlled and reductive dissolution are all surface controlled reactions and should be inhibited by the presence of ligands, such as phosphate, which can block surface sites, (Houben, 2003b; Biber *et al.*, 1994; Borggaard, 1991). However in this study it is clear that dissolution of oxides in acids is enhanced, and reductive dissolution is unaffected by the presence of impurities, including phosphate. These results suggest that the impurities are substituted within the crystal structure, rather than being present on the surface, and result in a greater number of structural defects than in less contaminated samples. Saleh and Jones (1984) noted that while the dissolution rate of Si-containing ferrihydrite in oxalate decreased at low concentrations of added Si (Si:Fe < 0.02), as the Si content of the ferrihydrite (Si:Fe>0.04) increased the ferrihydrite became more soluble. This was attributed to a possible disordering of the ferrihydrite structure by large

numbers of silanol groups (Saleh and Jones, 1984). Iron is more easily detached from these structural defects thus dissolution is more rapid.

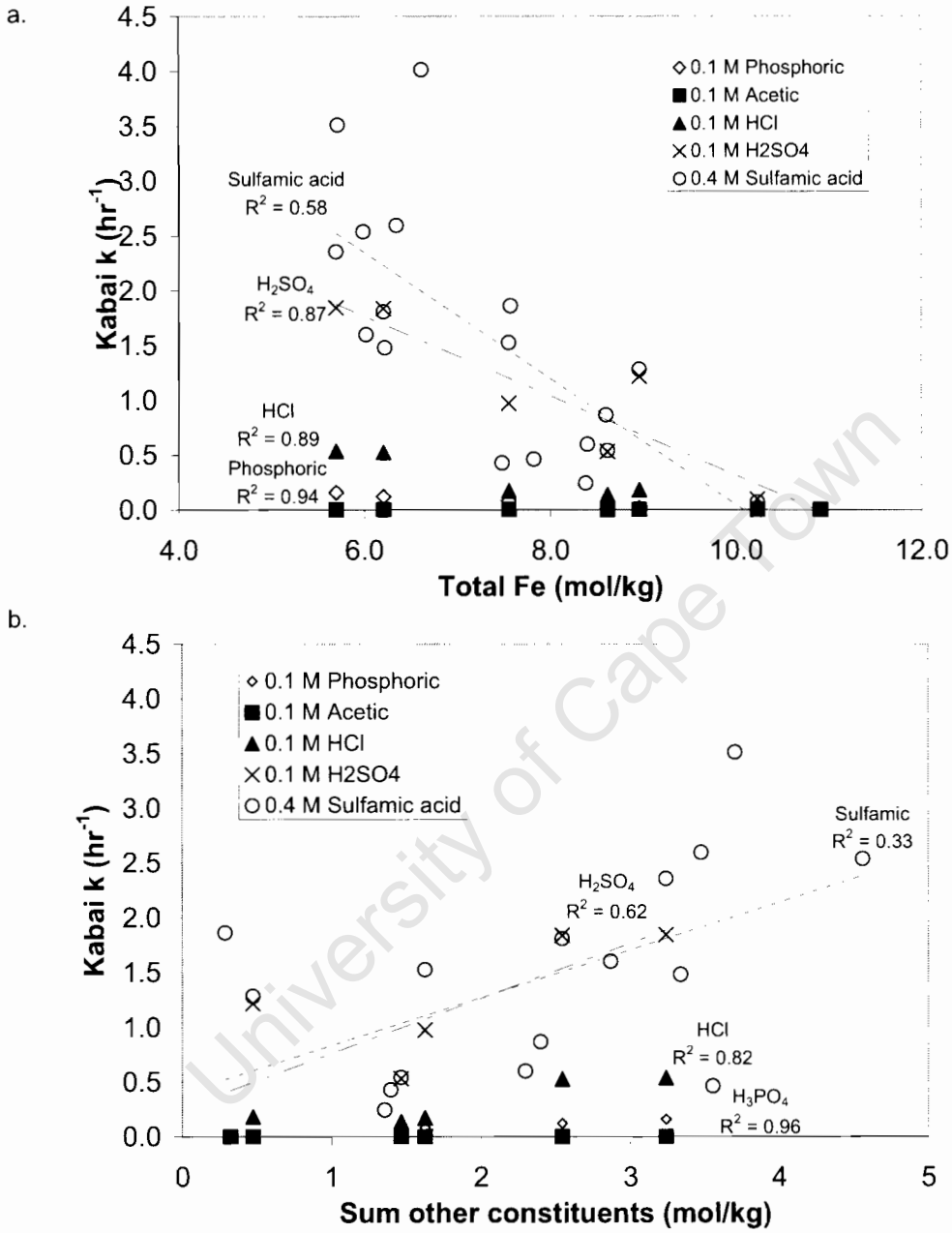

Figure 6.15. Relationship between a. the total iron content and b. the non-iron content of iron oxide encrustations and the Kabai k value

6.4.3.2 Properties of the reagent

The difference in reaction rates between reagents is related to the chemical mechanism of dissolution. The rate of acid dissolution is controlled by protonation and can usually be described by (Cornell and Schwertmann, 1996):

$$k = b[H^+]^n \qquad (6.12)$$

where n and b are constants, and 0<n<1. Plotting log Kabai k for acid reagents against pH gives a negative correlation, significant at the 95% confidence level for each sample group, which can be used to calculate b and n values (Figure 6.16; Table 6.4). The value n is calculated as greater than 1 but this could be because the Kabai k value is used for the rate.

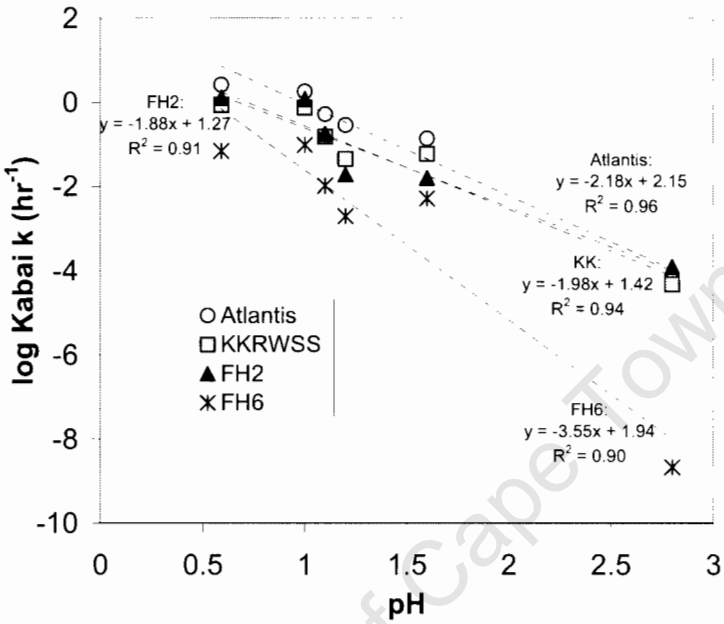

Figure 6.16. Relationship between pH of reagents and acid dissolution rates (log Kabai k) for various sample groups

Table 6.4. Calculated constants for the control of pH on dissolution rate of iron oxides in acids

	Atlantis	KK	FH2	FH6
n	2.18	1.98	1.88	3.55
b	2.14	1.42	1.26	1.94

The rate of protonation is controlled not only by the pH, but also by the presence of sites for protonation on the mineral surface. The rapid dissolution of Atlantis samples in acid suggests that there are more surface sites available to protonate on these samples. Atlantis samples have a higher surface charge density than the other iron oxide samples (Section 5.44) and are also found to dissolve at the greatest rate in acids.

Reductive dissolution will occur in reducing agents Na dithionite and hydroxylamine hydrochloride. Reductive dissolution is found to be more

effective than acid dissolution in agreement with other studies (Cornell and Schwertmann, 1996). A notable difference between iron oxide dissolution in acids and reductants is that the k-values for the different sample groups for any one acid reagent vary over a significant range, whereas reductant k-values are more similar for all samples, i.e., dissolution rates in reducing agents are more consistent (Figure 6.13). In addition, there is no relationship between dissolution rate and iron content for the reducing agents, which have a constant k value for all samples (Figure 6.17). Reductive dissolution is more complex than ligand-controlled and proton-assisted dissolution due to electron transfer processes. Although Fe detachment is expected to be rate limiting as is the case with acid dissolution, the electron transfer reaction may be rate-limiting. The pH of the reducing solution might affect the rate of dissolution because the reducing ligand is often a charged species, and pH will affect the extent to which it sorbs to surfaces (Cornell and Schwertmann, 1996), but, except for hydroxylamine hydrochloride, pH was optimised using buffers. The differences observed between controls on acid compared to reductive dissolution suggest a different reaction mechanism or different rate controlling step.

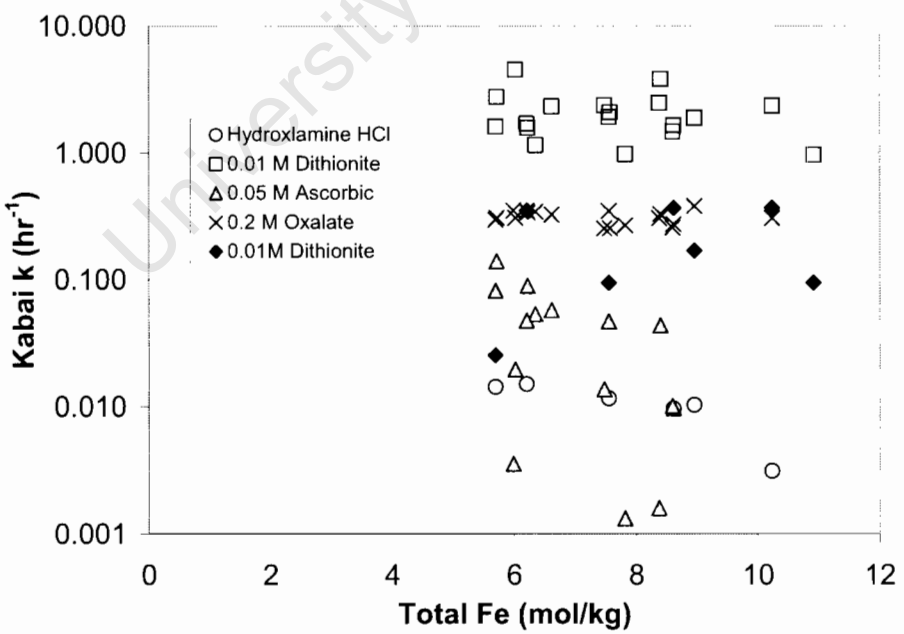

Figure 6.17. Relationship between Kabai k value of reducing reagents and total iron concentration of iron oxides

6.4.4 Optimisation of rehabilitation

6.4.4.1 Purpose

Wellfield managers and most practitioners implementing chemical rehabilitation procedures are not chemists, and have little knowledge to assist them in designing a rehabilitation strategy. With this in mind, the important characteristics of rehabilitation chemicals are identified, and a tool is developed to help wellfield managers assess the usefulness of rehabilitation chemicals.

6.4.4.2 Dissolution rate and reagent concentration

The choice of reagent for chemical rehabilitation should be guided by the dissolution rate and by the minimum concentration required to achieve optimal dissolution. Dissolution rate determines the length of time the reagent is left in the borehole and the distance it can travel from the borehole. Concentrated reagents are a hazard to workers, and are denser than water, sinking to the bottom of an aquifer from where they are more difficult to pump out. From an environmental point of view, a concentrated reagent will require greater dilution before returning to undetectable concentrations. It would be worthwhile to investigate the effective concentration of the reagents in the borehole during rehabilitation, because this work has shown that a solution of 0.4 M sulfamic acid is able to completely dissolve natural iron oxides within 5 hours, whereas the concentration of sulfamic acid used in the field is 1 M for 18 hours. Na dithionite was shown to be even more effective at concentrations of just 0.1 M, achieving complete dissolution of natural samples in under 3 hours. 0.1 M sulphuric acid and 0.2 M oxalate were also more effective than 0.1 M sulfamic acid. The long time periods for which the reagents are left in the well do allow penetration of the reagent into the aquifer around the borehole, dissolving any oxide material clogging pores. However, this time period should be calculated for each aquifer based on aquifer hydraulic characteristics.

6.4.4.3 Environmental considerations

The environmental impacts of the reagent should be considered. Although the borehole is pumped until pH and EC return to background levels following rehabilitation, it is likely that some reagent will still leak into the aquifer.

Workers implementing rehabilitation are also at risk from the chemicals used. Significantly altering the pH of the groundwater can also have knock-on effects e.g., dissolution of aquifer minerals, release of toxic elements from aquifer minerals, corrosion of the borehole equipment etc. For these reasons, pH, toxicity and degradability of the reagent are important considerations

6.4.4.4 Optimisation matrix

Reagents are classified according to their suitability for rehabilitation by use of a matrix. Each reagent is given a score in a number of categories, with 1 being poor and 5 being good. The sum of scores allows the choice of reagent, with high scores identifying suitable reagents. The criteria for scoring are given in Table 6.5 and the classification matrix is given in Table 6.6.

Table 6.5. Criteria for assessing suitability of reagent for borehole chemical rehabilitation

Parameter	Criterion	1	2	3	4	5
Rate	No. hrs taken to reach 50% dissolution	>20	10-20	5-10	2-5	<2
Extent	% dissolution after 10 hours	<40	>40	>60	>80	100
Concentration	M	>2	1 - 2	0.5 – 1.0	0.1 – 0.5	< 0.1
Aquatic toxicity	LD_{50} (96 hours)[a]	Toxic at trace conc.	Toxic at low conc.	Toxic at mod conc.	Toxic at high conc.	Non-toxic
pH	Difference between aquifer pH and reagent pH	>4	3-4	2-3	1-2	<1
Corrosivity	MSDS[b] Rating	Severe		Slight		None
Degradability	Reaction	Does not degrade	Slow degradation to less toxic	Rapid degradation to less toxic	Slow degradation to non-toxic	Rapid degradation to non-toxic

a. Concentration at which 50% of organisms are dead after 96 hours. Concentration used should be for the most vulnerable species on record. Not all reagents have been tested for aquatic toxicity.
b. Material data safety sheet

Table 6.6. Assessment of suitability of reagents tested in this study for chemical rehabilitation of iron oxide encrusted boreholes

Reagent	Reaction	Rate[a]	Extent	Concen-tration	Aquatic Toxicity	pH	Corrosivity	Degrad-ability	SUM
0.4 M sulfamic acid	$3NH_2SO_3H + Fe(OH)_3 = 3NH_2SO_3^- + Fe^{3+} + 3H_2O$	A – 5 K – 5	A – 5 K – 5	4	4	A – 1 K – 1	1	3	A – 23 K – 23
0.1 M sulfamic acid		A – 4 K – 2	A – 4 K – 2	4	4	A – 1 K – 1	1	3	A – 21 K – 17
0.1 M H_2SO_4	$H_2SO_4 + Fe(OH)_3 + H^+ = Fe^{3+} + SO_4^{2-} + 3H_2O$	A – 5 K – 5	A – 5 K – 5	4	4	A – 1 K – 1	1	3	A – 23 K – 23
0.1 M HCl	$3HCl + Fe(OH)_3 = Fe^{3+} + 3Cl^- + 3H_2O$	A – 5 K – 4	A – 5 K – 5	4	4	A – 1 K – 1	1	3	A – 23 K – 22
0.1 M H_3PO_4	$H_3PO_4 + Fe(OH)_3 = Fe^{3+} + 3PO_4^{3-} + 3H_2O$	A – 4 K – 2	A – 3 K – 2	4	4	A – 1 K – 1	1	2	A – 19 K – 16
0.05 M ascorbic acid	$C_6H_8O_6 + 2Fe(OH)_3 = 2Fe^{2+} + 6CO_2 + 6H^+$	A – 2 K – 1	A – 2 K – 1	5	4	A – 5 K – 4	4	5	A – 27 K – 26
0.1M acetic acid	$3CH_3COOH + Fe(OH)_3 = Fe^{3+} + 3CH_3COO^- + 3H_2O$	A – 1 K – 1	A – 1 K – 1	4	4	A – 1 K – 2	5	4	A – 20 K – 21
0.1 M dithionite	$2FeOOH + Na_2S_2O_4 + 4H^+ = 2Fe^{2+} + 2Na^+ + 2HSO_3^- + 2H_2O$	A – 5 K – 5	A – 5 K – 5	4	4	A – 3 K – 4	5	4	A – 30 K – 31
0.01 M dithionite		A – 2 K – 2	A – 2 K – 2	5	4	A – 3 K – 5	5	4	A – 25 K – 27
0.2 M oxalate	$(NH_4)_2C_2O_4.H_2O + Fe(OH)_3 + 3H^+ = NH_4)_2C_2O_4.H_2O\text{-}Fe^{3+} + 3H_2O$	A – 4 K – 4	A – 3 K – 3	2	2	A – 1 K – 2	2	3	A – 17 K – 18
0.1 M hydroxylamine hydrochloride	$2NH_2OH.HCl + Fe(OH)_3 = Fe^{2+} + N_2O + 4H_2O + 2Cl^-$	A – 1 K – 1	A – 1 K – 1	4	2	A – 2 K – 3	2	3	A – 15 K – 16

a. A = Atlantis; K = KKRWSS

b. Determined from MSDS (Mallinckrodt Baker Inc, 2003 a-d; 2004; 2005a-b) but proper ecotoxicology tests should be done because information on many of the chemicals is limited.

High scores are achieved by Na dithionite which is effective at low concentrations and degrades in groundwater to Na and SO_4^{2-}. The optimisation matrix indicates that the use of certain less kinetically effective reagents over a longer time period may be advantageous in terms of environmental effects e.g., ascorbic acid. More concentrated reagents may be worthwhile as the short time periods required for dissolution could limit the negative side-effects. This matrix is a first attempt at providing a tool for wellfield managers to choose the optimal reagent for their needs.

6.5 Conclusions

Assessment of the chemical rehabilitation of iron encrusted boreholes in the field has revealed that, although the methods used are effective, they could be optimized to maximize rehabilitation and minimize environmental impact. Monitoring of purge water chemistry indicates that concentrated, hazardous reagents in the BCHT method mobilise metals, are a hazard to workers, and are difficult to completely remove from the system, partly due to density settling of the reagent and partly due to the long residence times of the reagent in the borehole. The aquifer hydrology should be used to calculate the optimal volumes and length of time to leave reagents within the borehole. Rehabilitation using "anolyte," a strong oxidizing solution that does not dissolve iron was as effective as rehabilitation using strong acids, implying that simple physical methods may be as effective as strong chemicals at cleaning the borehole.

Testing of commonly used chemical rehabilitation reagents on natural and synthetic samples in the laboratory showed that natural samples are generally more rapidly dissolved than synthetic samples, and Atlantis samples are the most easily dissolved. Of the synthetic iron oxides, FH2 and schwertmannite dissolve most similarly to natural samples, regardless of the mineralogical composition of the natural sample. Dissolution could best be modelled by the Kabai equation, although the β value was close to 1 in many experiments, indicating a first order random nucleation surface-limited dissolution behaviour. The rate of acid dissolution is limited by the concentration of protons on the oxide surface, which is related to the concentration of protons

in solution, i.e., the pH, and the charge density on the mineral surface. The rate of acid dissolution is also inversely related to the amount of iron in the sample, suggesting that the presence of non-iron ions within the crystal matrix cause crystal defects which are more rapidly attacked and dissolved. Dissolution of iron oxides by reducing agents is not affected by the amount of iron in the sample and dissolution rates across the range of samples are similar, suggesting a different limitation to dissolution rates in reducing agents.

Using criteria of rate and extent of dissolution, reagent concentration, toxicity, pH, corrosivity and degradability, reagents were ranked in order of their suitability for chemical rehabilitation of wells. Na dithionite was found to be the most suitable in terms of both dissolution kinetics and environmental safety.

7 Dispersion and dissolution of iron oxide minerals adhered to artificial surfaces

7.1 Introduction

Iron clogging is due to the precipitation or adherence of iron oxide colloids onto the surfaces of the aquifer rocks and borehole equipment, such as pumps and screens. Unattached colloidal material is pumped to the surface and removed in sand filters in the water treatment works, and is not a direct clogging problem. Laboratory investigations of chemical rehabilitation have looked at the dissolution behaviour of unattached, colloidal or particulate iron oxide material (e.g. Houben, 2003b) which may behave differently from iron oxides attached to surfaces. Two materials commonly used in well construction are stainless steel and PVC. There is a tendency in the South African groundwater community to favour PVC over stainless steel (SST) because SST is believed to clog more rapidly (Engelbrecht and Jolly, 2000). As the respective surface charge of the oxide and the screen surface affect the likelihood of adherence, there may be some truth to these beliefs.

This chapter investigates the pH-dependent adherence of a selection of synthetic and natural iron oxides to different surfaces, and then considers the effectiveness of chemical rehabilitation at removing iron oxides from the surfaces. Although there is considerable evidence that bacteria can affect iron oxide adhesion (Warren and Ferris, 1998; Grantham *et al.*, 1997; Grantham and Dove, 1996; Lo *et al.*, 1996; Mills *et al.*, 1994; Ghiorse, 1984; Macrae and Edwards, 1972), this chapter makes no attempt to consider the additional effects of bacteria, and investigates iron oxide adherence from a purely physico-chemical viewpoint.

7.2 Methodology

7.2.1 Attachment of iron oxides to surfaces

The pH-dependent adherence of iron oxide minerals to artificial surfaces was tested using the heterogeneous suspension method of Scheidegger *et al.*, (1993). Surfaces were coated by mixing the substrate with a suspension of the oxide mineral (Scheidegger *et al.*, 1993).

Four different substrates were used: quartz sand, glass, stainless steel and PVC. The quartz sand is rock sampled from the Peninsula Formation and crushed and sieved to grain sizes between 1 and 2 mm. Glass boiling beads of 2 mm diameter were used for the glass surface, and stainless steel ball bearings of 2.5 mm diameter were used for the stainless steel surface. The PVC surface consists of approximately 2 mm thick disks cut from 2 mm diameter PVC rods by a plastics mouldings company. The average thickness of the disks varied considerably, but the thicknesses were found to be normally distributed so the mean thickness is representative. The cut surface of the PVC is rougher than the original sides of the PVC rod. Attempts to measure the surface area of the glass, stainless steel and PVC with BET were unsuccessful because the surface areas are too small, and surface area was calculated geometrically (Table 7.1). Prior to coating, the substrates (referred to from this point as beads) were cleaned with 0.1 M HCl for 30 minutes in an ultrasonicating bath, rinsed repeatedly with deionised water and dried at 60°C.

Table 7.1. Average sizes and surface areas for beads used in iron oxide attachment studies.

	Diameter (mm)	Length (mm)	Area (mm^2)	Method	Mass (mg)	Specific surface area ($x\ 10^{-3}\ m^2/g$)	Repeats
Sand	nd	nr	nd	BET	nd	250.0±34.0	3
Glass	1.962±0.090	nr	12.10±0.91	Geometric	10.71±1.02	1.13±0.14	25
Stainless steel	2.473±0.092	nr	18.87±0.29	Geometric	65.50±1.20	0.29±0.01	20
PVC	3.842±0.294	2.450±0.722	52.89±13.19	Geometric	31.06±15.42	1.77±0.57	125

Nd = no data; nr = not relevant

Synthetic iron oxides (Gt, FH6, and FH2) and four natural iron oxide minerals collected from field sites (A3, K4, H1 and H2) were used to coat the beads. A suspension of 100 mg iron oxide mineral in 30 mL of artificial groundwater (See Chapter 4; ionic strength = 3.2×10^{-3}) was prepared in a 50 mL centrifuge tube. Small amounts of 0.1 M NaOH or HCl were added to adjust the pH to between 3 and 9, and the suspensions allowed to equilibrate overnight, before a final pH reading was taken. The suspensions were placed in an ultrasonicating bath for 15 minutes prior to starting the coating experiments to ensure that the iron oxides were fully dispersed. Substrate beads were added to the tubes, which were placed on a reciprocating shaker for 72 hours. The mass of beads added to the centrifuge tubes was varied for

each substrate in order to maintain roughly equal surface areas for each experiment. On removing the tube from the shaker, the iron oxide suspension was decanted, the coated beads rinsed repeatedly with deionised water, and then soaked in pH 3 1 M KCl for 10 minutes to disperse any oxide that was not securely attached. The beads were again thoroughly rinsed in deionised water, and dried in an oven at 40°C for 10 minutes. Attempts to prepare duplicate coatings were unsuccessful because of difficulties replicating the pH of the suspension. Scheidegger *et al.* (1993) noted that adherence data were noisy around the PZC because of poor suspension of the particles. The samples run as duplicates were added to dataset as additional points.

The amount of iron attached to the beads was determined by dithionite-citrate-acetate (DCA) extraction (Section 3.2.1.2). The initial extractions were found to reach steady-state after 48 hours on a reciprocating shaker, although the coating was not completely removed from PVC surfaces, particularly the rough edges (Table A.37; Figure A.2; Appendix A). All subsequent iron coatings were extracted on a reciprocating shaker for 48 hours before the iron concentration of the supernatant was measured using the phenanthroline method.

7.2.2 Coated surface batch dispersion and dissolution

The potential for using dispersion methods for rehabilitation, and the rate of dissolution of sorbed iron oxides were determined using batch experiments on iron oxide coated PVC and stainless steel surfaces. Beads of PVC and SST were coated with FH2, FH6 and Gt in the same manner as the adherence experiments, except using a 500 mg / 50 mL oxide: artificial groundwater ratio without pH adjustment.

7.2.2.1 Dispersion

The coated beads were initially treated by physicochemical dispersion to ascertain the effectiveness of these methods, and to determine if pre-treatment enhanced or inhibited subsequent chemical dissolution methods. Five pre-treatments were tested:

- no pre-treatment
- shaking for 24 hours in 10 mL 0.1 M NaOH

- shaking for 24 hours in 10 mL 0.001 M Calgon ($Na(PO_4)_6$)
- Ultrasonication of beads in 10 mL MQ water for 30 minutes
- Ultrasonication of beads in 10 mL 0.001 M Calgon solution for 30 minutes

Following the pretreatment, the supernatant was decanted and stored. The beads were rinsed three times with 10 mL deionised water, and each of these aliquots was added to the initial decanted supernatant. The beads were kept for further chemical treatment. One mL concentrated HCl was added to the supernatant suspension to dissolve the colloidal iron. HCl was effective for the ferrihydrite suspensions, but did not dissolve the goethite suspensions which were instead treated with DCA solution. Iron concentrations in the supernatant were measured using ferrozine colorimetry for the HCl extracts and phenanthroline colorimetry for the DCA extracts, and represent the amount of iron dispersed from the surfaces of the beads by the various physicochemical methods. SEM was used to examine the PVC and stainless steel beads before and after the pretreatments.

7.2.2.2 Chemical rehabilitation

Following dispersion, dissolution reagents were added to the untreated and pretreated beads. Reagents were chosen based on their effectiveness at dissolving particulate iron oxide (Chapter 6), and included 0.4 M sulfamic acid, 0.1 M sulphuric acid and 0.1 M buffered dithionite solution. The reagents were added to the beads and shaken for 48 hours. Periodically 1 mL samples were collected, filtered through a 0.2 μm membrane filter, and analysed for iron by ferrozine or phenanthroline colorimetry. The beads were examined by SEM before and after dissolution.

7.3 Results

7.3.1 Adherence or iron oxides to surfaces

The full results of iron oxide adherence experiments are included in Table A.36 (Appendix A) and displayed in graphical form in Figure 7.1. SEM images of uncoated and coated surfaces are given in Figure 7.2 and 7.3.

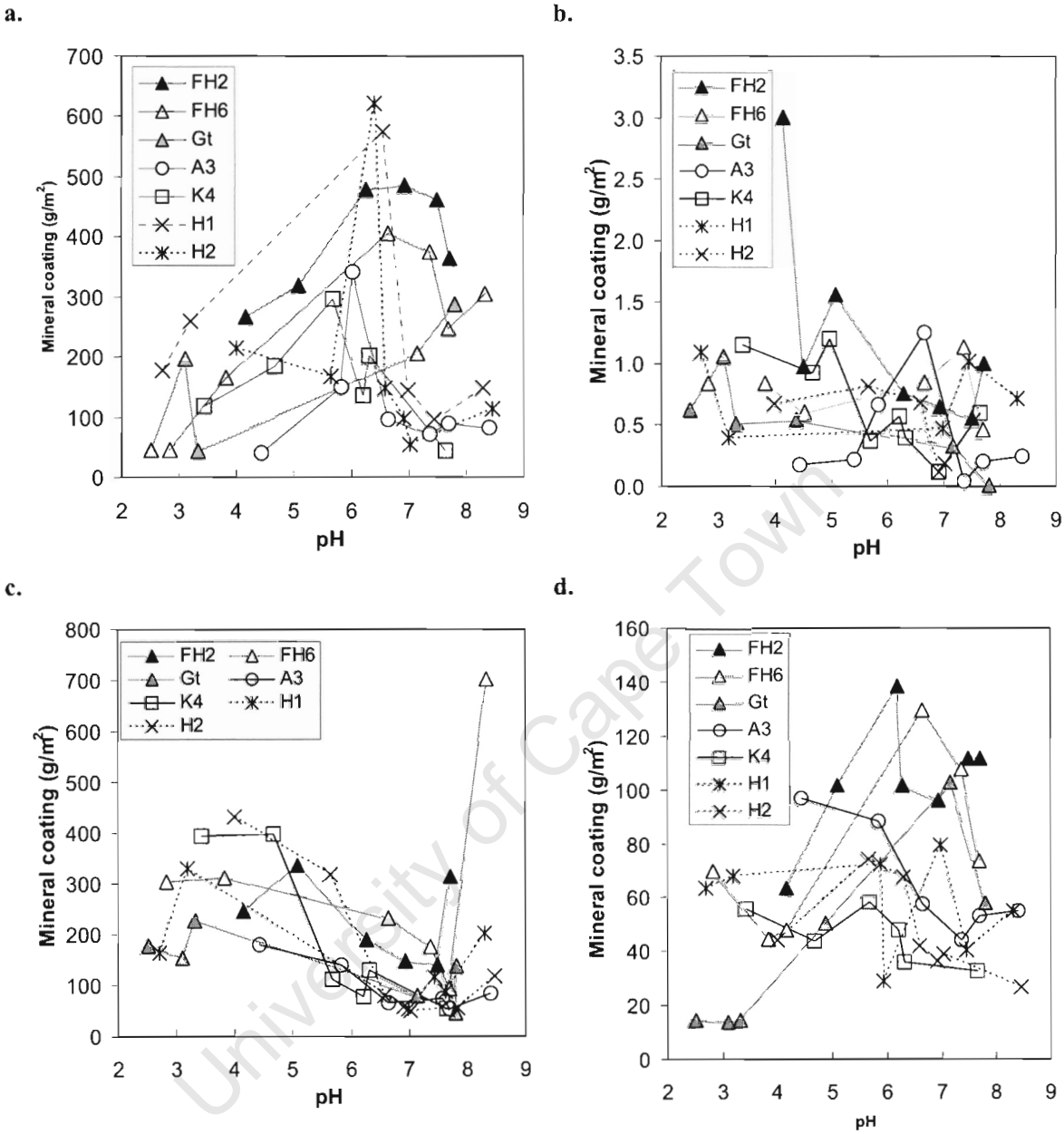

Figure 7.1. Amount of iron oxide coating on a. SST, b. sand, c. PVC and d. glass beads as a function of pH

Most sorption on stainless steel and glass surfaces occurs in the neutral pH-range of 6 – 7 (Figure 7.1). In contrast, for PVC and sand surfaces, least sorption occurs between pH 6.5 - 8, and the bowl-shaped curves indicate that more sorption is occurring at low and high pH. Sample A3 adhesion is opposite to the other samples on glass and sand surfaces. The average amount of mineral adhered to the PVC and stainless steel surfaces is of the

same order of magnitude, whereas less material sorbs onto glass and even less onto sand surfaces. More FH2 adheres to surfaces than FH6, and more FH6 than Gt. No trends in the degree of adherence are observed in the natural samples. The uncoated surfaces of PVC and sand are uneven, with many crevices and edges, whereas the uncoated SST and glass surfaces are comparatively smooth, with few surface defects (Figure 7.2). Ferrihydrite coatings on the SST tend to be uniform with some surface roughness, whereas on PVC the coatings are less even due to the uneven underlying PVC surface (Figure 7.3). The Gt coating on PVC consists of 1-2 μm long needles lying parallel to the surface but not to each other, and covering most of the visible surface, but hardly any Gt is visible on the SST surface.

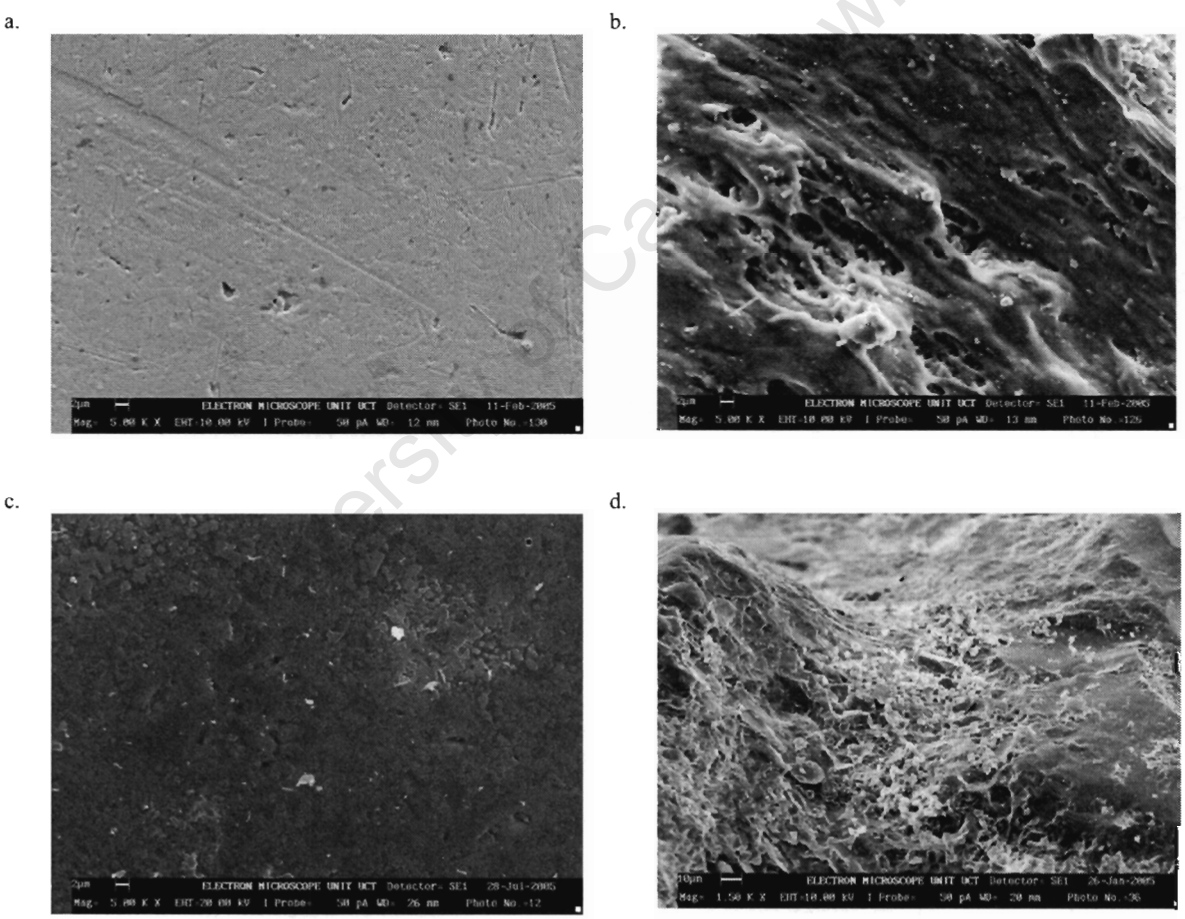

Figure 7.2. Uncoated a. SST, b. PVC, c. glass bead and d. sand surfaces

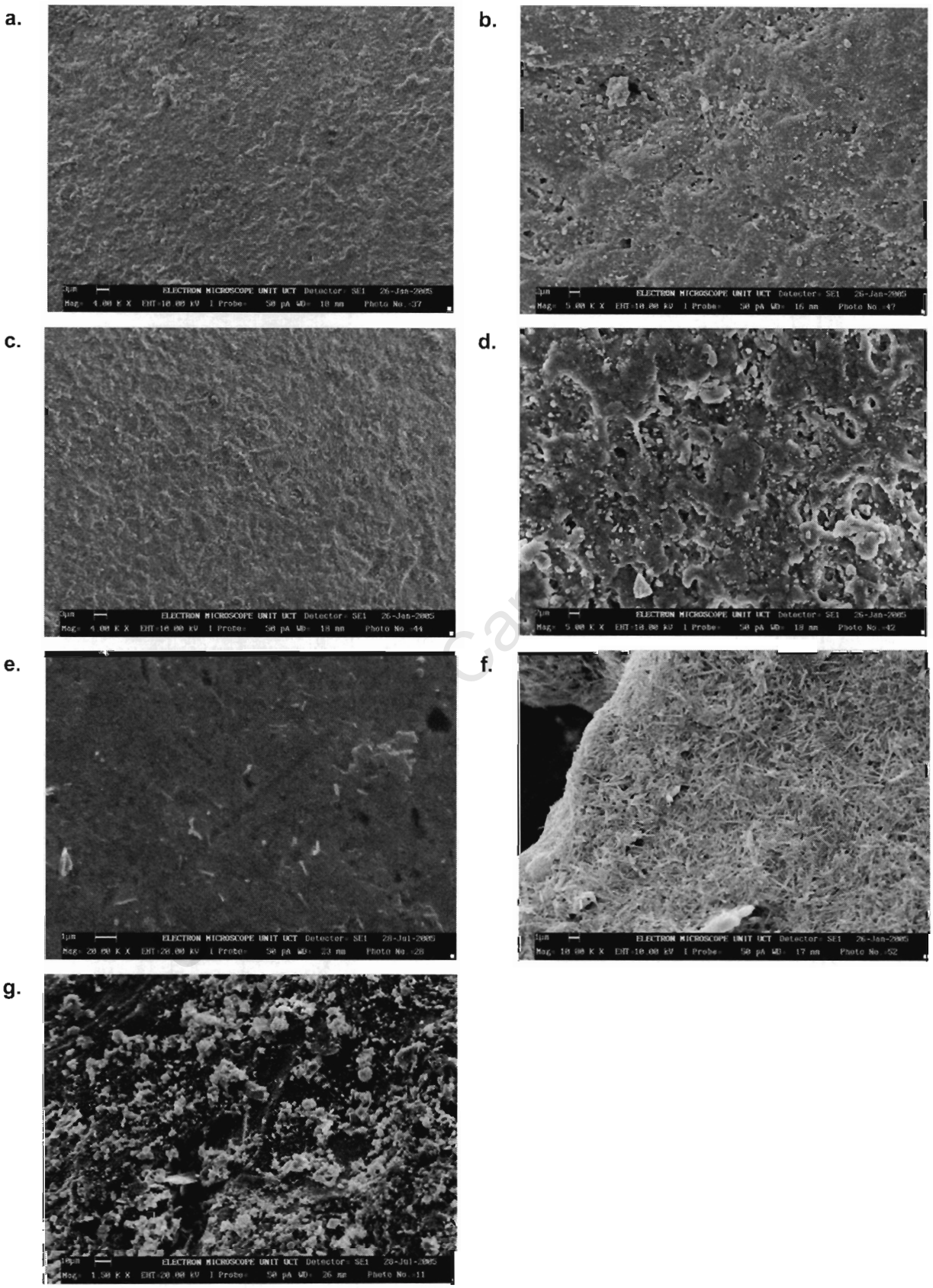

Figure 7.3. Coated bead surfaces a. FH6 coated SST, b. FH6 coated PVC, c. FH2 coated SST, d. FH2 coated PVC, e. Gt coated SST, f. Gt coated PVC, g. FH2 coated sand

7.3.2 Dispersion of attached iron oxides

The percentage of surface coating dispersed by each of the methods from the PVC and SST surfaces is given in Table 7.2. The results for the pretreatments are the average of three replicates which show good repeatability (<10% RSD) for FH6 and FH2 on stainless steel, and greater variability (>20% RSD) for dispersion of goethite from stainless steel and all minerals from PVC (Table B.13, Appendix B). Calgon, with or without ultrasonication, is generally the most effective dispersant, and NaOH and ultrasonication are less effective. FH6 and FH2 are on average more easily dispersed than Gt. The SEM images do not always agree with the chemically determined degree of dispersion (Appendix F). SST appears cleaner than PVC in SEM images, except by ultrasonication, yet this is not reflected in the measured data. The SEM images do tend to agree with the measurements that ultrasonication is the least effective and that calgon is the most effective dispersion method. The development of irregular white-edged craters on SST surfaces following dispersion suggests corrosion by NaOH.

Table 7.2. % mineral coating dispersed from coated surfaces by pretreatments

		FH2	FH6	Gt
Total Fe ($mmol/m^2$)	PVC	2.1	2.2	11.1
	SST	9.9	12.5	10.5
0.1 M NaOH	PVC	5.8	3.6	9.3
	SST	15.3	9.8	16.3
Calgon	PVC	23.6	18.4	17.8
	SST	28.7	23.7	8.3
Ultrasonicator	PVC	20.1	4.6	10.3
	SST	8.0	4.2	3.3
Ultrasonicator and calgon	PVC	24.4	34.1	7.8
	SST	27.0	23.8	9.0

7.3.3 Dissolution of attached iron oxides

Full results of dissolution of mineral coatings with time are given in Tables A.38 to A.43 (Appendix A), and the results are given graphically in Figures 7.4 – 7.6. The y-intercept of the graphs represents the amount of mineral dispersed during the pre-treatment, and the lines on the graphs are dissolution models (see Discussion).

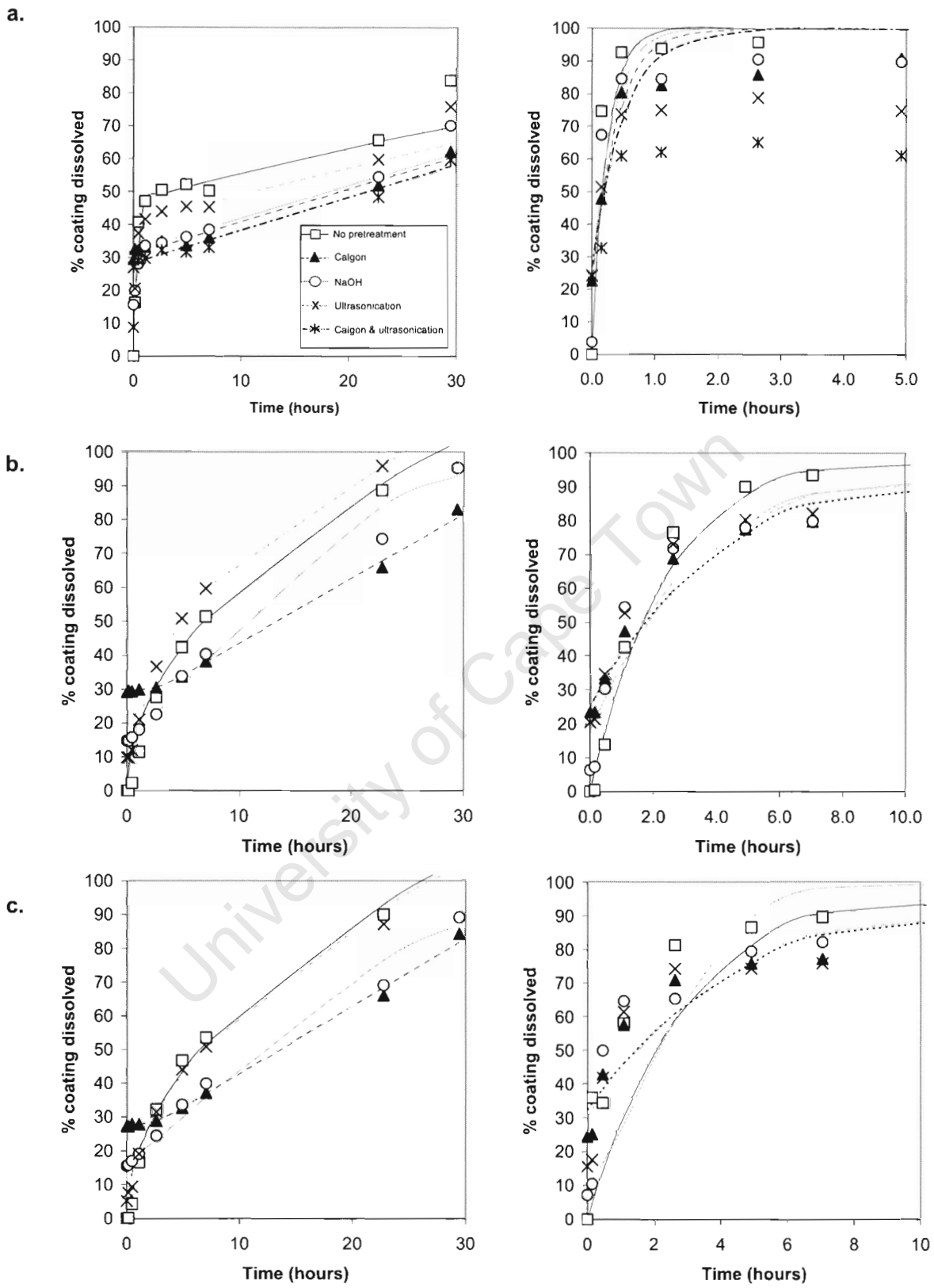

Figure 7.4. Dissolution with time of FH2 coatings from stainless steel (left) and PVC surfaces (right) using a. 0.1 M dithionite, b. 0.4 M sulfamic acid and c. 0.1 M sulphuric acid. Lines on the graphs are fitted rate equations.

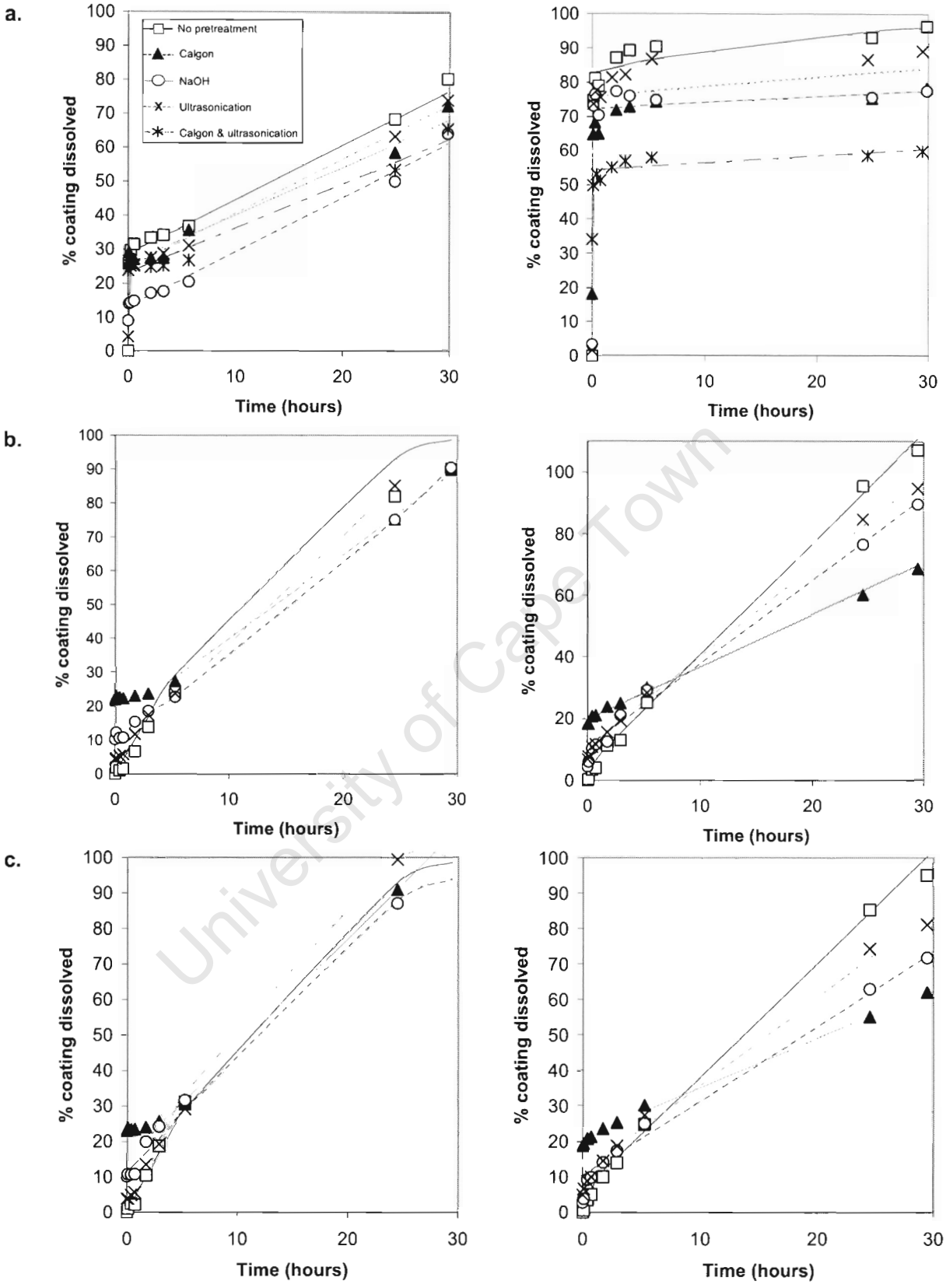

Figure 7.5. Dissolution with time of FH6 coatings from stainless steel (left) and PVC surfaces (right) using a. 0.1 M dithionite, b. 0.4 M sulfamic acid and c. 0.1 M sulphuric acid. Lines on the graphs are fitted rate equations.

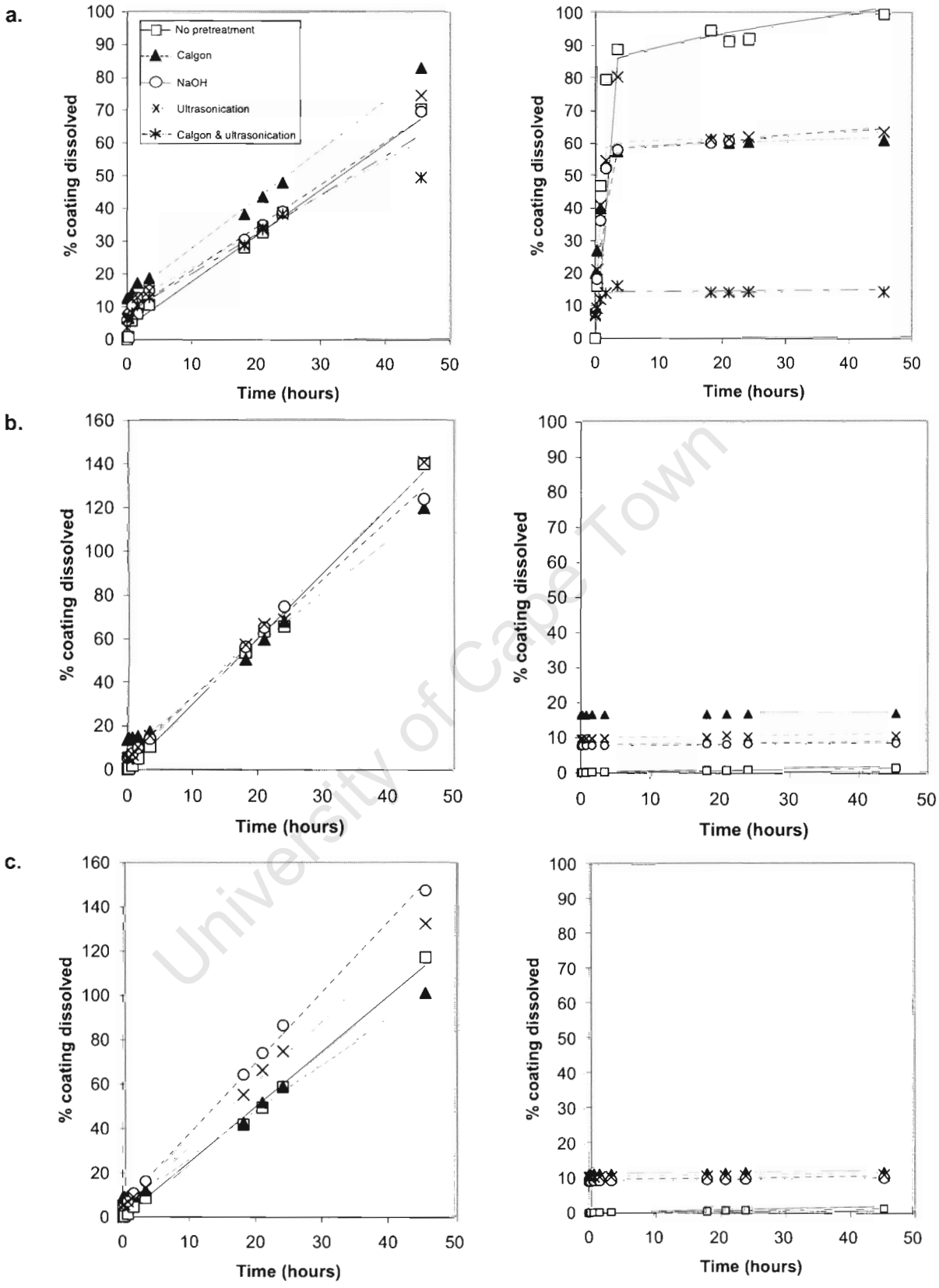

Figure 7.6. Dissolution with time of Gt coatings from stainless steel (left) and PVC surfaces (right) using a. 0.1 M dithionite, b. 0.4 M sulfamic acid and c. 0.1 M sulphuric acid. Lines on the graphs are fitted rate equations.

Dissolution of the minerals from stainless steel shows generally linear behaviour in all reagents, although dissolution is deceleratory when no pre-treatment is used. Dissolution from PVC is commonly deceleratory and differs in acids compared to in dithionite. Dissolution of oxides from surfaces using dithionite often does not reach 100%. FH2 is dissolved more rapidly from PVC surfaces than FH6 or Gt, but the rate of dissolution from SST is more similar between the different synthetic iron oxides. The results for goethite dissolution from stainless steel in acid are surprising because particulate goethite and goethite on PVC do not dissolve in acids, yet in this case dissolution exceeds 100%. The SEM images reveal that not all coating is removed, particularly from the PVC surfaces, following chemical dissolution of iron oxide coatings. Goethite is not well dissolved from SST surfaces. SST surfaces appear damaged after dissolution, with white-edged irregular craters hinting at corrosion.

7.4 Discussion

7.4.1 Controls on sorption of oxides to surfaces

The interaction of suspended colloids with charged surfaces depends on the respective charge of the surfaces and the greatest adherence is expected when the colloids and surfaces are oppositely charged (Saleh and Jones, 1984; Matijevic, 1980; Hogg *et al.*, 1965). The aggregation of oxides onto surfaces is pH-dependent. Aggregation and flocculation are greatest at the PZC where the overall oxide surface charge is lowest (Schwertmann and Taylor, 1992). Based on this information and knowledge of the charge on surfaces, prediction of the pH of greatest adherence should be possible. For example, iron oxides should be attracted to SST surfaces between the PZC of the SST, i.e. pH 5 (Matijevic, 1980), and the PZC of the oxide. Goethite has a PZC of 9, so maximum adherence onto SST would be expected between pH 5 and pH 9. Quartz sand has low negative charge from the PZC at 2.2 to a pH of 6, and becomes increasingly negatively charged above that pH (Grantham *et al.*, 1997; Scheidegger *et al.*, 1993). Goethite adherence to quartz sand should increase below pH 9. Glass surfaces are also negatively charged at all pHs in this study (Ryde *et al.*, 1992; Kolakowski and Matijevic, 1978), and adherence of goethite would be greatest below the PZC of the

oxide. Predicted and observed maximal and minimal adherences are given in Table 7.3. Many of the pH-dependent graphs show a sharp increase at high pH, always defined by a single point. The reason for this is not known, but could be due to dissolution effects or increased ionic strength at high pH. In the following discussion these points are not considered to be part of the more consistent trends with changing pH.

Table 7.3. Predicted and actual adherence of iron oxides to natural and artificial surfaces

		SST		Sand		PVC		Glass	
Sample	**PZC**	**Pred max[a]**	**Act max[b]**	**Pred min[c]**	**Act min[d]**	**Pred min**	**Act min**	**Pred min**	**Act min**
FH2	6.9	5-6.9	6.9	>6.9	7.5	>6.9	6.2	>6.9	4.2
FH6	6.4	5-6.4	6.7	>6.4	7.7	>6.4	6.7	>6.4	3.8
Gt	9.0	5-9	8	>9	7.8	>9.0	7.2	>9.0	3.1
A3	-	<5	6.0	-	Max 6.7	-	Min 7.4	-	7.4
K4	3.6	3.6-5	5.7	>3.6	6.9	>3.6	5.7	>3.6	7.6
H1	4.6	4.6-5	6.4	>4.6	7.0	>4.6	5.9	>4.6	5.9
H2	4.0	4-5	6.6	>4.0	7.0	>4.0	5.7	>4.0	8.5

a. pH of predicted maximum adherence, b. pH of actual maximum adherence, c. pH of predicted minimum adherence, d. pH of actual minimum adherence

In this study, the greatest adhesion of synthetic oxides to SST appears to be at or just above the PZSE, compared to predictions of below the PZC (Figure 7.1). Matijevic (1980) found maximum adhesion of haematite to SST between pH 6.5 and 7.5 just below the haematite PZC of 7.5. Oxide adherence to glass follows a similar behaviour to SST. The most iron oxide attachment to glass occurs in the neutral pH ranges near the PZC with a decline to higher pH. Glass is expected to have similar surface charge behaviour to quartz i.e. zero or negative charge through the pH range (Litton and Olson, 1993), yet the behaviour of iron oxide attachment to glass is inverted compared to the quartz sand.

Adherence to quartz sand and PVC is closer to predicted behaviour with a minimum just above the PZC and an increase in the amount of iron oxide adhered to the surface below that PZC. Scheidegger *et al.*, (1993) found maximum adherence of goethite to quartz sand particles at pH just below the PZC and explained his observations by assuming maximum sorption where the surface charge of the oxide and the substrate neutralise each other. The difference between observed maximal adherence in the experiments of

Scheidegger *et al.*, (1993) and these experiments could be because the sand used in these experiments is not pure quartz and likely contains a small amount of clay. The PZC of illite is < 3 and of muscovite is 3.9, and both have a greater surface charge density than quartz (Hendershot and Lavkulich, 1983). The negative surface charge density of the sand used in this experiment would be increased at low pH compared to pure quartz sand. As pH of the suspension decreases, the charge on oxide surfaces becomes more positive while the charge on clays remains constantly negative, and the difference in charge between the two will increase, resulting in greater adherence. The surface charge dependence of PVC on pH is not known, but as the PVC demonstrates a similar, but more pronounced effect to sand, it is believed that the surface maintains a constant negative charge.

The difference in adherence behaviour between glass and SST, and PVC and sand might be explained by differences in physical surface properties. Glass and SST are even with little surface roughness (Figure 7.2) compared to the PVC and sand surfaces. Oxide flocculation is greatest at the PZC (Schwertmann and Taylor, 1992), so greatest adherence to SST and glass close to the PZC suggests that the oxide is adhering to itself, rather than the surface. Multilayer deposition has been found to follow different behaviour to monolayer deposition because both adhesion of particles to the original surface as well as to already occupied portions of the surface need to be considered (Ryde *et al.*, 1992). The SEM image of coated SST confirms the evenness and completeness of the coating layer (Figure 7.3). Once an initial layer is attached to the surface, additional oxides would adhere to already attached iron oxides. Sand and PVC have rough surfaces, greater surface areas and the exposed surface will take longer to be coated. The coating reaction on PVC and sand is likely to have a greater dependence on the surface charge of the surface to be coated. Matijevic (1980) observed a strong dependence on the surface charge of steel for greatest adherence of iron oxide to the steel, but noted that the stainless steel surface was rough with well pronounced crevices. The surface charge of Hg electrodes has been found to change depending on the amount of coverage by colloidal haematite (Andrade *et al.*, 1994), and the PZC of kaolinite is affected by Fe

oxide coatings (Hendershot and Lavkulich, 1983). It is likely that the PZC of the surface will increasingly tend to the PZC of the coating material as the coating coverage increases. On surfaces with little surface roughness and low surface areas, complete coverage will be reached with less coating than on rough surfaces with large surface areas.

The discussion so far has focussed on synthetic oxides, but natural samples (except A3) are found to behave similarly to synthetic oxides on all surfaces. On SST, maximum attachment of natural samples is between pH 5.5 and 7.0, despite measured PZSE in the range of 3.6 - 4.6. If the natural samples are behaving like the synthetic samples, then greatest adherence should be near the PZSE. However, the maximum adherence is similar to that observed for synthetic samples and is better described by the PZSE of the synthetic analogues of the natural samples. The PZSE of the natural samples without adsorbed anions, i.e. the PPZC (pristine point of zero charge (Dzombak and Morel, 1990)), would probably be in the same range as the synthetic iron oxides. It is possible that the PPZC is a more useful parameter for prediction of natural iron oxide attachment to surfaces than the PZSE.

Comparison between the amount of sorption of different minerals to different surfaces shows few relationships amongst the natural samples, but sorption of synthetic oxides generally decreases in the order FH2>FH6>Gt. Scheidegger *et al.* (1997) also found that amorphous iron hydroxide was more strongly attracted to a quartz surface than goethite. The decrease in sorption corresponds to a decrease in surface area of the oxide. The greatest amount of iron oxide that adheres per surface area is on stainless steel and PVC, with less on glass surfaces and little on sand. There are no distinguishable trends in the degree of adherence of the natural samples, but in general less natural sample is attached to the surface than synthetic samples. The lower iron content of natural samples compared to synthetic samples would result in fewer available variable charge sites, and an overall lower charge density. The amount of iron oxide adhered to PVC is probably significantly over-estimated because of underestimation of the surface area.

In summary, the degree of coating of surfaces by iron oxide minerals is determined by the pH of the suspension, the charge density of the mineral, the PZC of the mineral, the PZC of the surface and the surface roughness. On smooth surfaces, the pH dependence of coating tends towards the PZC of the coating mineral as the surface is rapidly covered and the oxide begins to adhere to itself. On rough surfaces, the pH dependence of coating tends to the PZC of the surface, which takes a long time to coat. The greater the surface charge density of the mineral, the more it adheres to the surface.

7.4.2 Success of physical and chemical dispersion methods

Dispersion of oxides from surfaces is an alternative to chemical dissolution that has the advantage of using no reagents, or less concentrated reagents. However, dispersion was found to be only partially effective. In general, calgon seems to be the best dispersant, but only a maximum of 29% of the iron oxide coating is removed from any surface. Scheidegger *et al.* (1993) observed equally poor dispersion of oxides from quartz surfaces using NaOH and ultrasonication, and concluded Fe-O-Si bonds form between silica surfaces and attached goethite particles (Scheidegger *et al.*, 1993). Matijevic (1980) noted that only a fraction of iron oxide attached to SST was desorbed in NaOH, due to the high energy required. Desorption of iron oxides from surfaces will occur when the double layer repulsion energy exceeds the attractive energy of the van der Waals forces (Matijevic, 1980).

There seems to be little pattern to dispersion behaviour between the different surfaces. Based on measured amounts of iron dispersed, NaOH is more effective at dispersing oxides from SST, and ultrasonication has more effect on PVC coated surfaces, but calgon appears to be equally effective at dispersing oxides from either surface. Matijevic (1980) noted that surface roughness affected the degree of dispersion from a surface, but this does not appear to be the case in this study as dispersion from SST would be expected to be greater than dispersion from PVC. However, SEM images tend to support Matijevic's (1980) observation as the SST surfaces appear clean following dispersion. It is possible that the total oxide coating on SST has

been overestimated due to dissolution of corroded and oxidized stainless steel. If this is the case, the % dispersion will be underestimated, and dispersion of oxides from SST may indeed be more complete than from PVC surfaces.

7.4.3 Effectiveness of dissolution from surfaces

7.4.3.1 Rate of dissolution

The rate of iron oxide dissolution from surfaces was determined by fitting rate equations (Equations 6.5 to 6.11) to dissolution data. Theoretical dissolution curves were calculated for dissolution of iron oxides from surfaces, and are fitted to the data in Figures 7.4 to 7.6. A linear rate model (Equation 6.5) proved effective for most dissolution reactions, however, a single model was often not able to describe the complete dissolution curve for many samples, and two models were used, with an initial rate and a final rate. The model used, calculated apparent rate constants (k), and c values for dissolution equations are given in Tables 7.4 and 7.5. For samples that had been subjected to a pretreament method, the amount dispersed was used as the starting point of the dissolution curve i.e., these samples have a non-zero intercept on a plot of percent dissolved against time. The non-zero intercept was included in the kinetic models as c, the y-intercept. As observed in free oxide dissolution experiments, FH2 dissolves most rapidly, followed by FH6 and the slowest to dissolve is goethite. Fits on PVC are not as good as on SST.

Table 7.4. Kinetic parameters for dissolution of adhered iron oxides by dithionite

	Initial rate			Final rate				Initial rate			Final rate			
Pretreament	Type[a]	k (hr^{-1})	c	Type	k (hr^{-1})	c	r^2	Type	k (hr^{-1})	c	Type	k (hr^{-1})	c	r^2
				Gt-SST							Gt-PVC			
None	L	7.5×10^{-2}	-	L	1.4×10^{-2}	3.7×10^{-2}	1.00	L	0.25	-	L	3.0×10^{-3}	0.88	0.94
Calgon	L	3.0×10^{-2}	8.4×10^{-2}	L	1.5×10^{-2}	5.2×10^{-2}	1.00	L	0.11	0.27	L	7.0×10^{-4}	0.59	0.98
NaOH	L	4.1×10^{-2}	8.8×10^{-2}	L	1.3×10^{-2}	0.11	1.00	L	0.14	0.18	L	1.6×10^{-3}	0.58	0.82
Ultra	L	3.6×10^{-2}	4.0×10^{-2}	L	1.1×10^{-2}	9.8×10^{-2}	0.99	L	0.28	0.12	L	9.0×10^{-4}	0.60	0.95
Ultra+Cal	L	4.0×10^{-2}	9.8×10^{-2}	L	1.2×10^{-2}	0.11	0.98	L	4.1×10^{-2}	7.8×10^{-2}	L	1.2×10^{-4}	0.14	0.96
				FH6-SST							FH6-PVC			
None	L	1.0	-	L	1.6×10^{-2}	0.29	0.97	L	8.5	-	RN	5.0×10^{-2}	1.8	0.99
Calgon	L	1.4×10^{-2}	0.26				0.99	L	0.51	0.41	RN	7.0×10^{-3}	1.3	0.77
NaOH	L	0.61	9.0×10^{-2}	L	1.6×10^{-2}	0.13	1.00	L	6.6	2.7×10^{-2}	RN	7.0×10^{-3}	1.3	1.00
Ultra	L	2.7	4.3×10^{-2}	L	1.6×10^{-2}	0.25	1.00	L	7.2	1.7×10^{-2}	RN	1.4×10^{-2}	1.4	0.99
Ultra+Cal	L	1.3×10^{-2}	0.23				0.99	L	1.6	0.34	RN	2.1×10^{-3}	0.54	0.98
				FH2-SST							FH2-PVC			
None	1D	0.21	-	1D	9.0×10^{-3}	0.22	0.98	RN	4.3					0.95
Calgon	L	1.0×10^{-2}	0.31				0.99	RN	2.6	0.23				0.98
NaOH	L	0.16	0.18	L	1.0×10^{-2}	0.32	0.99	RN	3.2	0.24				0.73
Ultra	L	0.28	0.15	L	8.0×10^{-3}	0.41	0.97	RN	2.0	0.31				0.93
Ultra+Cal	L	1.0×10^{-2}	0.28				0.99	RN	2.0	0.31				0.89

a. L = linear, 1D = 1 dimensional diffusion, RN = random nucleation

Table 7.5. Kinetic parameters for dissolution of adhered iron oxides by sulfamic acid and sulphuric acid

		Initial rate			Final rate				Initial rate			Final rate			
	Pretreament	Type	k (hr^{-1})	c	Type	k (hr^{-1})	c	r^2	Type	k (hr^{-1})	c	Type	k (hr^{-1})	c	r^2
					Gt-SST							**Gt-PVC**			
Sulfamic acid	None	L	3.0×10^{-2}	-				1.00	L	3.6×10^{-4}	-				0.99
	Calgon	L	8.0×10^{-3}	9.8×10^{-2}	L	2.4×10^{-2}	5.2×10^{-2}	1.00	L	1.5×10^{-4}	0.17				0.99
	NaOH	L	2.7×10^{-2}	0.34				1.00	L	2.2×10^{-4}	7.8×10^{-2}				0.97
	Ultra	L	2.9×10^{-2}	2.9×10^{-2}				1.00	L	2.6×10^{-4}	9.8×10^{-2}				0.91
					FH6-SST							**FH6-PVC**			
	None	Sqrt	3.0×10^{-2}	-				1.00	L	8.9×10^{-2}	-	L	3.6×10^{-2}	4.8×10^{-2}	1.00
	Calgon	L	4.3×10^{-3}	0.22	L	2.5×10^{-2}	0.15	1.00	L	1.7×10^{-2}	0.20				1.00
	NaOH	A-E	3.8×10^{-2}	0.33				1.00	L	0.15	4.6×10^{-2}	L	2.7×10^{-2}	0.11	1.00
	Ultra	A-E	4.7×10^{-2}	0.24				1.00	L	0.10	6.8×10^{-2}	L	2.9×10^{-2}	0.11	1.00
					FH2-SST							**FH2-PVC**			
	None	1D	3.6×10^{-2}	-				1.00	RN	0.42					0.99
	Calgon	L	4.8×10^{-3}	0.29	L	1.9×10^{-2}	0.25	1.00	RN	0.23	0.29				0.96
	NaOH	A-E	4.2×10^{-2}	0.40				0.99	RN	0.27	0.20				0.93
	Ultra	1D	4.0×10^{-2}	2.1×10^{-2}				0.99	RN	0.26	0.29				0.96
					Gt-SST							**Gt-PVC**			
	Pretreament	Fit	k	c	Fit	k	c	r2	Fit	k	c	Fit	k	c	r2
Sulphuric acid	None	L	2.5×10^{-2}	-				1.00	L	3.3×10^{-4}	-				0.98
	Calgon	L	8.0×10^{-3}	6.3×10^{-2}	L	2.1×10^{-2}	3.6×10^{-2}	1.00	L	1.7×10^{-4}	0.11				0.96
	NaOH	L	3.2×10^{-2}	7.8×10^{-2}				1.00	L	2.3×10^{-4}	9.4×10^{-2}				0.97
	Ultra	L	2.8×10^{-2}	3.3×10^{-2}				1.00	L	1.8×10^{-4}	0.10				1.00
					FH6-SST							FH6-PVC			
	None	Sqrt	3.0×10^{-2}	-				1.00	L	9.1×10^{-2}	-	L	3.2×10^{-2}	6.1×10^{-2}	1.00
	Calgon	L	7.3×10^{-3}	0.23	L	3.1×10^{-2}	0.15	1.00	L	1.4×10^{-2}	0.21				1.00
	NaOH	A-E	4.5×10^{-2}	0.35				0.99	L	1.7×10^{-1}	2.6×10^{-2}	L	2.1×10^{-2}	0.10	1.00
	Ultra	A-E	8.5×10^{-2}	0.19				0.99	L	6.5×10^{-2}	5.8×10^{-2}	L	2.5×10^{-2}	0.11	1.00
					FH2-SST							FH2-PVC			
	None	1D	3.8×10^{-2}	-				0.99	RN	0.34					0.94
	Calgon	L	5.9×10^{-3}	0.27	L	2.0×10^{-2}	0.23	1.00	RN	0.21	0.39				0.91
	NaOH	A-E	3.4×10^{-2}	0.43				0.99	RN	0.24	0.32				0.87
	Ultra	1D	3.7×10^{-2}	-				1.00	RN	0.22	0.36				0.87

L = linear, 1D = 1 dimensional diffusion, RN = random nucleation, Sqrt = square root, A-E = Avrami-Erofejev

7.4.3.2 Dissolution from stainless steel

Dissolution of iron oxides from stainless steel by dithionite generally follows first order random nucleation deceleratory behaviour or 2 linear dissolution models, describing an initial high rate of dissolution followed by a significant decrease in rate. Dissolution reached completion in 30 hours for FH2 and FH6, but took closer to 50 hours for Gt. The final rate of dissolution for each oxide is similar regardless of the pre-treatment, but the initial rate of dissolution depends on the pre-treatment. The effect of the pre-treatment is much greater on the FH6 and FH2 coated SST beads compared to the Gt coated beads. The greatest initial rates are found where the least material is removed by dispersion, i.e., no pretreatment, ultrasonication and NaOH pre-treatments. The rate of dissolution following ultrasonic pre-treatment of both FH6 and FH2 coated PVC is greater than the rate with no pre-treatment, suggesting that ultrasonication enhances initial dissolution, while more successful pre-treatments suppress initial dissolution rates. Calgon pre-treatment results in a constant dissolution rate throughout the reaction.

The initial rapid rate of dissolution in dithionite is believed to be due to dissolution of loosely attached iron oxides on the surface of the stainless steel. The more of these that are removed by the pre-treatment, the slower the initial rate of dissolution will be. Dissolution of iron oxides firmly attached to each other and to the stainless steel surface will be slower than dissolution of loose oxides on the surface, hence the reduction in rate in samples with effective pre-treatment. The enhancement of dissolution by ultrasonication could be due to formation of surface defects that allow penetration of reagents into the coating. The limited extent of dissolution in dithionite (<100%) suggests that some material is permanently attached.

Dissolution of iron oxide coatings on SST in sulfamic and sulphuric acid is much slower than in dithionite. One rate equation, either deceleratory or linear, was sufficient to describe the dissolution behaviour of most coatings and pretreatments. Dissolution following calgon pre-treatment required two linear rate models because the initial rate was slower than the final rate. The rates of dissolution of oxides from SST are similar in both sulfamic and

sulphuric acid indicating that neither the reagent nor the mineral affect the rate of dissolution, and dissolution is probably limited by the rate of detachment of the oxide from the surface. Although the proton concentration on the iron oxide surface was found to be limiting in proton-promoted dissolution of free oxides (Chapter 6), this is clearly not the case for dissolution of oxides from SST. The pH of sulfamic acid is about 0.2 units lower than sulphuric acid yet dissolution is at the same rate.

Greatest initial dissolution rates in sulfamic and sulphuric acid are observed for no-pretreatment, NaOH and ultrasonication pretreatments, with NaOH and ultrasonication in some cases appearing to enhance dissolution, and calgon pre-treatment inhibiting initial dissolution. The pretreatments do not affect intial dissolution rates to the same extent as observed with dithionite dissolution. The initial rate of dissolution of oxides in acids following calgon pre-treatment is about 3 times slower than the final dissolution rate, and could be explained by the PO_4 present in calgon. Phosphate ions adsorbed to the surface of the iron oxides have been found to inhibit iron oxide dissolution by preventing attachment of the dissolution reagent to the surface (Houben, 2003b; Biber *et al.*, 1994; Borggaard, 1991). In this case, PO_4 could be preventing protonation of the oxide surface.

Dissolution data for removal of Gt from SST once again suggests that iron oxides formed by corrosion of the SST surface are being dissolved rather than goethite, especially because particulate Gt did not dissolve in acid reagents (Chapter 6). SEM images of SST surfaces following chemical dissolution reveal white rims around shallow craters, which are believed to be evidence of corrosion of the steel. These rims are not visible in the untreated stainless steel (Appendix F).

7.4.3.3 Dissolution from PVC

Dissolution of iron oxides from PVC surfaces by dithionite occurs more rapidly than from stainless steel surfaces, reaching steady state within the first 5 hours, suggesting that oxides are not as strongly adhered to PVC. Initial dissolution is rapid, and final rates are about 2 orders of magnitude slower.

Complete dissolution is only achieved for non-pretreated coated beads and the more material initially dispersed, the lower the rate and extent of dissolution in dithionite. Dissolution rates can be modelled, not very successfully, with linear or random nucleation models. Dissolution of FH6 from PVC with sulfamic and sulphuric acids is similar to dissolution of FH6 from stainless steel, but dissolution of FH2 is more rapid from PVC than from SST, and Gt is not dissolved. The lack of dissolution of Gt in the acid reagents supports the theory that measured iron concentrations during Gt dissolution from SST are actually due to dissolution of corroded SST. Again, the extent of initial dispersion determines the rate and extent of dissolution, particularly in sulfamic acid, suggesting that similar processes are happening on PVC as on SST.

7.4.3.4 Comparison with dissolution of free oxides

Initial linear apparent rate constants for dissolution of the synthetic oxides in free form and attached to stainless steel and PVC surfaces are given in Table 7.6. Surprisingly, the initial rate of dissolution of attached oxides is of a similar order of magnitude or even faster than the rate at which free oxides are dissolved.

Table 7.6. Initial linear apparent rate constants (hr^{-1}) for dissolution of FH2, FH6 and Gt by three different reagents in free form and attached to SST and PVC surfaces (no pre-treatment)

	H_2SO_4	Sulfamic	Dithionite
		FH2	
Free	0.48	2.2×10^{-2}	0.32
SST	3.4×10^{-2}	3.4×10^{-2}	0.40
PVC	0.24	8.9×10^{-2}	1.6
		FH6	
Free	5.1×10^{-2}	3.8×10^{-3}	0.32
SST	3.1×10^{-2}	3.1×10^{-2}	1.0
PVC	9.1×10^{-2}	8.9×10^{-2}	8.5
		Gt	
Free	7.1×10^{-5}	2.4×10^{-5}	0.41
SST	2.5×10^{-2}	3.0×10^{-2}	7.5×10^{-2}
PVC	3.3×10^{-4}	3.6×10^{-4}	0.25

The initial rate reflects the dissolution of more soluble oxide material. The more rapid initial dissolution from surfaces compared to particulate oxides may be a function of the coating process. More reactive oxides and smaller,

more highly charged particles in the oxide suspension are likely to attach to the surface, resulting in a natural separation of these more reactive oxides onto the surfaces. These particles will also be more susceptible to dissolution and will dissolve more rapidly, so the higher rate does not mean that the dissolution rate of the oxide is faster, but that the surface area and size fraction of the particles segregating from the main suspension onto the surface are different from the bulk oxide suspension.

7.5 Conclusions

This chapter has investigated the interaction of synthetic iron oxide minerals with artificial surfaces in an attempt to identify whether the material used in well construction has an impact on the degree of clogging. It has been found that the attachment of oxides to surfaces is dependent on the pH of the solution and the surface area/roughness of the surface. PVC has a much greater surface roughness than SST, and the degree of coating is lower on a per m^2 basis. Smooth surfaces are rapidly coated following which further coating is controlled by adherence of the iron oxide to itself. The coatings can be removed to some extent by dispersive techniques using ultrasonication, NaOH and Calgon, but only a maximum of 29% was removed. The pre-treatments had a residual effect on the dissolution of coatings by rehabilitation chemicals because they preferentially removed the more soluble fraction. Initial dissolution rates of oxides from treated beads were therefore slower than initial dissolution rates from non-treated beads. This effect only lasted for a short time. The PO_4 in calgon appeared to inhibit dissolution by occupying iron oxide surface sites. SST is clearly affected by the dissolution chemicals with some corrosion evident by SEM. FH2 on PVC appears to be the easiest to disperse and to remove by chemical means. The initial rate of dissolution of free oxides is of the same order of magnitude and often slower than dissolution from surfaces, possibly because the oxides that attach to surfaces tend to be the more reactive, higher surface area particles which are relatively easy to dissolve. Important results for wellfield managers are that dispersion techniques can remove a reasonable proportion of the oxide, and that PVC is easier to chemically rehabilitate if the encrustation is predominantly 2-line ferrihydrite, and is resistant to corrosion.

8 References

Amirbahman, A., Schönenberger, R., Furrer, G. and Zobrist, J. 2003. Experimental study and steady-state simulation of biogeochemical processes in laboratory columns with aquifer material, *Journal of Contaminant Hydrology*, 64, 169-190.

Andrade, E.M., Molina, F.V., Gordillo, G.J. and Posadas, D. 1994. Adhesion of colloidal haematite onto metallic surfaces: II. Influence of electrode potential, pH, ionic strength, colloid concentration and nature of the electrolyte on the adhesion on mercury, *Journal of Colloid and Interface Science*, 165, 459-466.

Appel, C., Ma, L.Q., Rhue, R.D. and Kennelley, E. 2003. Point of zero charge determination in soils and minerals via traditional methods and detection of electroacoustic mobility, *Geoderma*, 113, 77-93.

Appelo, C.A.J. and de Vet, W.W.J.M 2003. Modeling in situ iron removal from groundwater with trace elements such as As, in Welch, A.H. and Stollenwerk, K.G. *Arsenic in Groundwater*, Kluwer Academic, Boston, 381-401.

Appelo, C.A.J., Drijver, B., Hekkenberg, R. and de Jonge, M. 1999. Modeling in situ iron removal rom ground water, *Ground Water*, 37(6), 811-817.

Appelo, C.A.J. and Postma, D. 1996. *Geochemistry, groundwater and pollution*, A.A. Balkema, Rotterdam.

Appelo, C.A.J., Van der Weiden, M.J.J., Tournassat, C. and Charlet, L. 2002. Surface complexation of ferrous iron and carbonate on ferrihydrite and the mobilization of arsenic, *Environ. Sci. Technol.*, 36, 3096-3103.

Applin, K.R. and Zhao, N. 1989. The kinetics of Fe(II) oxidation and well screen encrustation, *Ground Water*, 27(2), 168-174.

Armon, R., Arbel, T. and Green, M. 1998. A quantitative and qualitative study of biofilm disinfection on glass, metal and PVC surfaces by chlorine, bromine and bromochloro-5,5-dimethylhydantion (BCDMH), *Wat. Sci. Tech.*, 38(12), 175-179.

Baker, K.F. 1976. The determination of organic carbon in soil using a probe-colorimeter, *Laboratory Practice*, 25, 82-83.

Ball, J.W. and Nordstrom, D.K. 1991. *User's manual for WATEQ4F, with revised thermodynamic database and test cases for calculating speciation of major, trace, and redox elements in natural waters*, Open-File Report 91-183, U.S. Geological Survey, Menlo Park, California.

Baveye, P., Vandevivere, P., Hoyle, B.L., DeLeo, P.C. and Sanchez de Lozada, D. 1998. Environmental impact and mechanisms of the biological clogging of saturated soils and aquifer materials, *Critical Reviews in Environmental Science and Technology,* 28(2), 123-191.

Biber, M.V., Dos Santos Afonso, M. and Stumm, W. 1994. The coordination chemistry of weathering: IV. Inhibition of the dissolution of oxide minerals, *Geochimica et Cosmochimica Acta*, 58(9), 1999-2010.

Bigham, J.M., Schwertmann, U., Carlson, L. and Murad, E. 1990. A poorly crystallized oxyhydroxysulfate of iron formed by bacterial oxidation of Fe(II) in acid mine waters, *Geochimica et Cosmochimica Acta*, 54, 2743-2758.

Bishop, R. and Killick, M. 2003. Role of groundwater in meeting Cape Town's water demand, *Borehole Water Journal*, 53, 2-4.

Boochs, P.W. and Barovic, G. 1981. Numerical model describing groundwater treatment by recharge of oxygenated water, *Water Resources Research*, 17(1), 49-56.

Borggaard, O.K. 1991. Effects of phosphate on iron oxide dissolution in ethylenediamine-N,N,N',N'-tetraacetic acid and oxalate, *Clays and Clay Minerals*, 39(3), 324-328.

Brantley, S.L. 2003. Reaction Kinetics of Primary Rock-Forming Minerals under Ambient Conditions, in Drever, J.I. (ed) *Treatise on Geochemistry: Volume 5 Surface and Groundwater, Weathering and Soils*, Elsevier, Netherlands, 74-108.

Braune, E. 2000. Towards comprehensive groundwater resource management in South Africa, in Sililo, O. et al. *Groundwater: Past Achievements and Future Challenges*, Balkema, Rotterdam, 7-15.

Brown, D.A., Beveridge, T.J., Keevil, C.W. and Sherriff, B.L. 1998. Evaluation of microscopic techniques to observe iron precipitation in a natural microbial biofilm, *FEMS Microbiology Ecology*, 26, 297-310.

Brown, D.A., Sherriff, B.L., Sawicki, J.A. and Sparling, R. 1999. Precipitation of iron minerals by a natural microbial consortium, *Geochimica et Cosmochimica Acta*, 63(15), 2163-2169.

Brown, C.J., Schoonen, M.A.A. and Candela, J.L. 2000. Geochemical modeling of iron, sulfur, oxygen and carbon in a coastal plain aquifer, *Journal of Hydrology*, 237, 147-168.

Brunauer, S., Emmett, P.H. and Teller, E. 1938. Adsorption of gases in multimolecular layers, *Journal of the American Chemical Society*, 60, 309-319.

Burke, S.P. and Banwart, S.A. 2002. A geochemical model for removal of iron(II)(aq) from mine water discharges, *Applied Geochemistry*, 17, 431-443.

Canfield, D.E. 1989. Reactive iron in marine sediments, *Geochimica et Cosmochimica Acta*, 53, 619-632.

Carlson, L., Vuorinen, A., Lahermo, P. and Tuovinen, O.H. 1980. Mineralogical, geochemical, and microbiological aspects of iron deposition from groundwater, in P.A., Trudinger and M.R., Waller *Biochemistry of Ancient and Modern Environments*, Australian Academy of Science, Canberra, 355-364.

Carlson, L. and Schwertmann, U. 1981. Natural ferrihydrites in surface deposits from Finland and their association with silica, *Geochimica et Cosmochimica Acta*, 45, 421-429.

Carlson, L. and Schwertmann, U. 1987. Iron and manganese oxides in Finnish ground water treatment plants, *Water Research*, 21(2), 165-170.

Cavé, L.C. and Smith, M.E. 2004. In-borehole measurements of chemical parameters in a wellfield affected by iron biofouling, in Wanty, R.B. and Seal, R.R. *Water Rock Interaction, Volume 2. Proceedings of the 11th International Symposium on WRI, Saratoga Springs, New York, USA*, 27 June - 2 July 2004., A.A. Balkema, Leiden, 1179-1184..

Chapelle, F.H. 1993. *Groundwater microbiology and geochemistry*, J. Wiley & Sons inc., New York.

Chevallier, L., de Beer, C.H. and Fick, T. 1998. *Geological report and structural analysis of the Klein Karoo area with special emphasis on the Kammanassie Mountains*, K8/324, Water Research Commission, Pretoria.

CMC. 2001. *Abridged Report for the Proposal Call for the Feasibility Study and Pilot Project on the Potential for Exploiting the Table Mountain Group Aquifer*, City of Cape Town, Cape Town.

Coleman, M.L., Shephard, T.J., Rouse, J.E. and Moore, G.M. 1982. Reduction of water with zinc for hydrogen isotope analysis, *Analytical Chemistry*, 54, 993-995.

Colvin, C., Cavé, L. and Saayman, I. 2004. *A functional approach to setting resource quality objectives for groundwater*, WRC Report No. 1235/1/04, Water Research Commission, Pretoria.

Cornell, R.M. 1988. The influence of some divalent cations on the transformation of ferrihydrite to more crystalline products, *Clay Minerals*, 23, 329-332.

Cornell, R.M. and Giovanoli, R. 1988. Acid dissolution of akaganéite and lepidocrocite: the effect on crystal morphology, *Clays and Clay Minerals*, 36(5), 385-390.

Cornell, R.M. and Giovanoli, R. 1993. Acid dissolution of hematites of different morphologies, *Clay Minerals*, 28, 223-232.

Cornell, R.M. and Schwertmann, U. 1996. *The Iron Oxides*, Wiley-VCH.

Cullimore, D.R. 1992. *Practical Manual of Groundwater Microbiology*, CRC Press, Florida, 142.

Cullimore, D.R. and McCann, A.E. 1978. The identification, cultivation and control of iron bacteria in ground water, in Skinner, F.A. and Shewan, J.M. (eds) *Aquatic Microbiology*, Academic Press.

Davison, W. and Seed, G. 1983. The kinetics of the oxidation of ferrous iron in synthetic and natural waters, *Geochimica et Cosmochimica Acta*, 47, 67-79.

de Beer, C.H. 2002. The stratigraphy, lithology and structure of the Table Mountain Group, in Pieterson, K. and Parsons, R. (ed's) *A Synthesis of the Hydrogeology of the Table Mountain Group - Formation of a Research Strategy*, WRC Report No TT 158/01, SA, 8-18.

de Swardt, A.M.J. and Rowsell, D.M. 1974. *The relationship between diagenesis and deformation in the Cape Fold-Belt*, Trans. Geol. Soc.S.A., 77, 239-245.

Deng, Y. 1997. Formation of iron(III) hydroxides from homogenous solutions, *Water Research*, 31(6), 1347-1354.

Dold, B. 2003. Dissolution kinetics of schwertmannite and ferrihydrite in oxidized mine samples and their detection by differential X-ray diffraction, *Applied Geochemistry*, 18, 1531-1540.

Drever, J.I. 1997. *The Geochemistry of Natural Waters: Surface and Groundwater Environments (3rd ed.),* Prentice-Hall, New Jersey.

Drever, J.I. and Stillings, L.L. 1997. The role of organic acids in mineral weathering, *Colloids and Surfaces A: Physicochemical and Engineering Aspects*, 120, 167-181.

DWAF. 2004. *National Groundwater Database*, Department of Water Affairs and Forestry, Pretoria.

Dzombak, D.A. and Morel, F.M.M. 1990. *Surface Complexation Modelling: Hydrous Ferric Oxide*, John Wiley & Sons, New York.

Eaton, A.D., Clesceri, L. and Greenberg, A.E. 1995. *Standard Methods for the Examination of Water and Wastewater (19th ed.)*, American Public Health Association, Washington DC.

Emerson, D. 2000. Microbial oxidation of Fe(II) and Mn(II) at circumneutral pH, in Lovley, D.R. *Environmental Microbe-Metal Interactions*, ASM Press, Washington D.C., 31-52.

Emerson, D. and Moyer, C. 1997. Isolation and characterization of novel iron-oxidizing bacteria that grow at circumneutral pH, Applied and *Environmental Microbiology*, 63(12), 4784-4792.

Engelbrecht, P. and Jolly, J. 2000. *Iron precipitation problems in boreholes in the Klein Karoo*, DWAF, Cape Town.

Faure, G. 1992. *Principals and Applications of Inorganic Geochemistry*, Macmillan Publishing Company, New York.

Ferris, F.G., Hallberg, R.O., Lyvén, B. and Pedersen, K. 2000. Retention of strontium, cesium, lead and uranium by bacterial iron oxides from a subterranean environment, *Applied Geochemistry*, 15, 1035-1045.

Flower, P.R. and Bishop, R.C. 2003. *Atlantis water scheme: A case study on borehole clogging and biofouling management initiatives*, Unpublished Report, City of Cape Town.

Furrer, G., von Gunten, U. and Zobrist, J. 1996. Steady-state modelling of biogeochemical processes in columns with aquifer material 1. Speciation and mass balances, *Chemical Geology*, 133, 15-28.

Garrels, R.M. and Mackenzie, F.T. 1967. Origin of the chemical composition of some springs and lakes, in Stumm, W. *Equilibrium Concepts in Natural Water Systems*, Adv. Chem. Series 67 American Chemical Society, Washington, 222-242.

Gehrels, J. and Alford, G. 1990. Application of physico-chemical treatment techniques to a severely biofouled community well in Ontario, Canada, in Howsam, P. (ed) *Groundwater Engineering Conference*, Granfield Institute of Technology.

Ghiorse, W.C. 1984. Biology of iron- and manganese depositing bacteria, *Ann. Rev. Microbiol.*, 38, 515-550.

Glasauer, S., Langley, S. and Beveridge, T.J. 2001. Sorption of Fe (hydr)oxides to the surface of *Shewanella putrefaciens*: Cell-bound fine-grained minerals are not always formed De Novo, Applied and *Environmental Microbiology*, 67(12), 5544-5550.

Gloter, A., Zbinden, M., Guyot, F., Gaill, F. and Colliex, C. 2004. TEM-EELS study of natural ferrihydrite from geological-biological interactions in hydrothermal systems, *Earth and Planetary Science Letters*, 222, 947-957.

Grantham, M.E. and Dove, P.M. 1996. Bacterial-mineral surface interactions: Investigations using Fluid Tapping Mode Atomic Force Microscopy, *Geochimica et Cosmochimica Acta*, 60, 2473-2480.

Grantham, M.C., Dove, P.M. and DiChristina, T.J. 1997. Microbially catalyzed dissolution of iron and aluminum oxyhydroxide mineral surface coatings, *Geochimica et Cosmochimica Acta*, 61(21), 4467-4477.

Greeff, G.J. and Hälbich, I.W. 2000. The structural control of groundwater in the Kammanassie Mountain, Little Karoo, South Africa, *Journal of African Earth Sciences*, Geocongress, 23-24.

Grenthe, I., Stumm, W., Laaksuharju, M., Nilsson, A.-C. and Wikberg, P. 1992. Redox potentials and redox reactions in deep groundwater systems, *Chemical Geology*, 98, 131-150.

Hälbich, I.W. 1983. A tectogenesis of the Cape Fold Belt, *Spec. Publ. geol. Soc. S. Afr,* 12, 165-175.

Hälbich, I.W. and Greef, G.J. 1995. *Final report on a structural analysis of the west plunging nose of the Kammanassie Anticline*, Consulting report to DWAF, Department of Geology, University of Stellenbosch.

Hallbeck, L. and Pedersen, K. 1990. Culture parameters regulating stalk formation and growth rate of *Gallionella ferruginea*, *J. Gen. Microbiol.*, 136, 1675-1680.

Hallberg, R.O. and Martinell, R. 1976. Vyredox - In situ purification of ground water, *Ground Water*, 14(2), 88-93.

Hanert, H.H. 1981. Chapter 40: The Genus *Gallionella*, in Starr, M.P., Stolp, H., Trüper, H.G., Balows, A. and Schlegel, H.G. *The Prokaryotes: A Handbook on Habitats, Isolation and Identification of Bacteria v. VI*, Springer-Verlag, Berlin, 509-515.

Hanert, H.H. 1989. Genus *Gallionella*, in Stanley, J.T., Bryant, M.P., Pfennig, N. and Holt, J.G. *Bergey's Manual of Systematic Bacteriology*, Williams & Wilkins, Baltimore, 1974-1979.

Hanert, H.H. 2002. Bacterial and chemical iron oxide deposition in a shallow bay on Palaea Kameni, Santorini, Greece: Microscopy, electron probe microanalysis, and photometry of in situ experiments., *Geomicrobiology Journal*, 19, 317-342.

Hansel, C.M., Benner, S.G., Neiss, J., Dohnalkova, A., Kukkadapu, R.K. and Fendorf, S. 2003. Secondary mineralization pathways induced by dissimilatory iron reduction of ferrihydrite under advective flow, *Geochimica et Cosmochimica Acta*, 67(16), 2977-2992.

Harris, C. and Diamond, R.E. 2002. The thermal springs of the Table Mountain Group: A stable isotope study, in Pieterson, K. and Parsons, R. (ed's) *A Synthesis of the Hydrogeology of the Table Mountain Group - Formation of a Research Strategy*, WRC Report No TT 158/01, SA, 230-235.

Hartnady, C.J.H., Newton, A.R. and Theron, J.N. 1974. *The stratigraphy and structure of the Malmesbury Group in the southwestern Cape*, Bulletin Precambrian Research Unit, University of Cape Town, 15, 193-123.

Hartnady, C.J.H. and Hay, E.R. 2002. Fracture system and attribute studies in Table Mountain Group groundwater target generation, in Pieterson, K. and Parsons, R. (ed's) *A Synthesis of the Hydrogeology of the Table Mountain Group - Formation of a Research Strategy*, WRC Report No TT 158/01, SA, 89-96.

Hattingh, J. and Goedhart, M.L. 1997. Neotectonic control on drainage evolution in the Algoa Basin, Southeastern Cape Province, *South African Journal of Geology*, 100, 43-52.

Hendershot, W.H. and Lavkulich, L.M. 1983. Effect of sesquioxide coatings on surface charge of standard mineral and soil samples, *Soil Science Society of America Journal*, 47, 1252-1260.

Hill, R.S. 1991. *Lithostratigraphy of the Baviaanskloof Formation (Table Mountain Group), including the Kareedouw Sandstone Member*, Lithostratigraphic Series No. 12, South African Committee for Stratigraphy, Pretoria.

Hogg, R., Healy, T.W. and Fuerstenau, D.W. 1965. Mutual coagulation of colloidal dispersions, *Trans. Faraday Soc.*, 62, 1638-1651.

Houben, G.J. 2003a. Iron oxide incrustations in wells. Part 1: genesis, mineralogy and geochemistry, *Applied Geochemistry*, 18, 927-939.

Houben, G.J. 2003b. Iron oxide incrustations in wells. Part 2: chemical dissolution and modeling, *Applied Geochemistry*, 18, 941-954.

Houben, G.J. 2004. Modeling the buildup of iron oxide encrustations in wells, *Ground Water*, 42(1), 78-82.

Hunter, R.J. 1981. *Zeta potential in colloid science: principals and applications*, Academic Press, Sydney.

Jambor, J.L. and Dutrizac, J.E. 1998. Occurrence and constitution of natural and synthetic ferrihydrite, a widespread iron oxyhydroxide, *Chemical Reviews*, 98, 2549-2585.

Janney, D.E., Cowley, J.M. and Buseck, P.R. 2000a. Transmission electron microscopy of synthetic 2- and 6-line ferrihydrite, *Clays and Clay Minerals*, 48(1), 111-119.

Janney, D.W., Cowley, J.M. and Buseck, P.R. 2000b. Structure of synthetic 2-line ferrihydrite by electron nanodiffraction, *American Mineralogist*, 85, 1180-1187.

Janney, D.E., Cowley, J.M. and Buseck, P.R. 2001. Structure of synthetic 6-line ferrihydrite by electron nanodiffraction, *American Mineralogist*, 86, 327-335.

Jolly, J.L. 2000. Biofouling in boreholes of the Klein Karoo Rural Water Supply Scheme, Oudtshoorn, South Africa, and the effect on well scheme management, in Sililo, O. et al. *Groundwater: Past Achievements and Future Challenges*, Balkema, Rotterdam, 527-531.

Jolly, J., Engelbrecht, P. and Uys, J. 2001. Production Boreholes, *Borehole Water Journal*, 49, 15-17.

Jolly, J.L. and Kotze, J.C. 2002. The Klein Karoo Rural Water Supply Scheme, in Pieterson, K. and Parsons, R. (ed's) *A Synthesis of the Hydrogeology of the Table Mountain Group - Formation of a Research Strategy*, WRC Report No TT 158/01, SA, 198-201.

Kim, J.J., Kim, S.J. and Tazaki, K. 2002. Mineralogical characterization of microbial ferrihydrite and schwertmannite, and non-biogenic Al-sulfate precipitates from acid mine drainage in the Donghae mine area, Korea, *Environmental Geology*, 42, 19-31.

Kirby, C.S., Thomas, H.M., Southam, G. and Donald, R. 1999. Relative contributions of abiotic and biological factors in Fe(II) oxidation in mine drainage, *Applied Geochemistry*, 14, 511-530.

Kolakowski, J.E. and Matijevic, E. 1979. Particle adhesion and removal in model systems: Part I - Monodispersed chromium hydroxide on glass, *Journal of Chemical Society Faraday Transactions*, 75, 65.

Kostka, J.E. and Luther, G.W. III 1994. Partitioning and speciation of solid phase iron in saltmarsh sediments, *Geochimica et Cosmochimica Acta*, 58(7), 1701-1710.

Kostka, J.E. and Nealson, K.H. 1995. Dissolution and reduction of magnetite by bacteria, *Environ. Sci. Technol.*, 29, 2535-2540.

Kostka, J.E., Wu, J., Nealson, K.H. and Stucki, J.W. 1999. The impact of structural Fe(III) reduction by bacteria on the surface chemistry of smectite clay minerals, *Geochimica et Cosmochimica Acta*, 63(22), 3705-3713.

Kotze, J.C. 2001. *Hydrogeology Of The Table Mountain Sandstone Aquifer - Klein Karoo*, Unpublished PhD Thesis, University of the Free State, Bloemfontein.

Kotze, J.C. and Rosewarne, P.N. 1996. *Little Karoo Scheme - Hydrogeological Overview,* SRK Consulting Report No 230827/1, Unpublished consulting report, Cape Town.

Kotze, J.C. and Rosewarne, P.N. 1999. *Klein Karoo Rural Water Supply Scheme Augmentation Study: Groundwater Augmentation Options*, DWAF Report No. PB J000/00/0899, Department of Water Affairs and Forestry, South Africa.

Kotze, J.C., Verhagen, B. Th. and Butler, M.J. 2000. An aquifer model based on chemistry, isotopes and lineament mapping: Little Karoo, South Africa, in Sililo, O. et al. *Groundwater: Past Achievements and Future Challenges*, Balkema, Rotterdam, 539-544.

Kuntze, H. 1982. *Iron Clogging in Soils and Pipes: Analysis and Treatment*, DVWK, Berlin.

Langmuir, D. 1997. *Aqueous Environmental Chemistry*, Prentice-Hall.

Larsen, O. and Postma, D. 2001. Kinetics of reductive bulk dissolution of lepidocrocite, ferrihydrite, and goethite, *Geochimica et Cosmochimica Acta*, 65(9), 1367-1379.

Lee, J. and Beveridge, T. 2001. Interaction between iron and *Pseudomonas aeruginosa* biofilms attached to Sepharose surfaces, *Chemical Geology*, 180, 67-80.

Litton, G.M. and Olson, T.M. 1993. Colloid deposition rates on silica bed media and artifacts related to collector surface preparation methods, *Environ. Sci. Technol.*, 27, 185-193.

Liu, C., Kota, S., Zachara, J.M., Fredrickson, J.K. and Brinkman, C.K. 2001. Kinetic analysis of the bacterial reduction of goethite, *Environ. Sci. Technol.*, 35, 2482-2490.

Lo, W., Nelson, Y.M., Lion, L.W., Shuler, M.L. and Ghiorse, W.C. 1996. Determination of iron colloid size distribution in the presence of suspended cells: Application to iron deposition onto a biofilm surface, *Water Research*, 30(10), 2413-2423.

Loewenthal, R.E., Wiechers, H.N.S. and Marais, G.v.R. 1986. *Softening and stabilization of municipal waters*, Water Research Commission, Pretoria.

Lütters-Czekalla, S. 1990. Lithoautotrophic growth of the iron bacterium *Gallionella ferruginea* with thiosulfate or sulfide as energy source, *Arch Microbiol.*, 154, 417-421.

Maclear, L.G.A. 2001. The hydrogeology of the Uitenhage Artesian Basin with reference to the Table Mountain Group Aquifer, *Water SA*, 27(4), 499-505.

Macrae, I.C. and Edwards, J.F. 1972. Adsorption of colloidal iron by bacteria, *Applied Microbiology*, 24, 819-823.

Malan, J.A. and Theron, J.N. 1989. *Nardouw Subgroup, Catalogue os S. African Lithostratigraphic Units*, SA Committee for Stratigraphy, Pretoria.

Malan, J.A., Theron, J.N. and Hill, R.S. 1989. *Lithostratigraphy of the Goudini Formation (Table Mountain Group)*, Lithostratigraphic series No. 2, South African Committee for Stratigraphy, Pretoria.

Mallinckrodt Baker, Inc 2003a. *Material Safety Data Sheet S7586: Sulfamic Acid*, http://www.jtbaker.com/msds/englishhtml/s7586.htm.

Mallinckrodt Baker, Inc 2003b. *Material Safety Data Sheet A7608: Ascorbic Acid,* http://www.jtbaker.com/msds/englishhtml/a7608.htm.

Mallinckrodt Baker, Inc 2003c. *Material Safety Data Sheet A6072: Ammonium oxalate*, www.jtbaker.com/msds/englishhtml/a6702.htm.

Mallinckrodt Baker, Inc 2003d. *Material Safety Data Sheet H3883: Hydrochloric Acid (Less than 10%)*, www.jtbaker.com/msds/englishhtml/s3883.htm.

Mallinckrodt Baker, Inc 2004. *Material Safety Data Sheet P3973: Phosphoric Acid*, http://www.jtbaker.com/msds/englishhtml/p3973.htm.

Mallinckrodt Baker, Inc 2005a. *Material Safety Data Sheet A0326: Acetic Acid Glacial*, http://www.jtbaker.com/msds/englishhtml/a0326.htm.

Mallinckrodt Baker, Inc 2005b. *Material Safety Data Sheet S8236: Sulfuric Acid, <10%*, http://www.jtbaker.com/msds/englishhtml/s8236.htm.

Malmström, M., Banwart, S., Lewenhagen, J., Duro, L. and Bruno, J. 1996. The dissolution of biotite and chlorite at 25°C in the near-nuetral pH region, *Journal of Contaminant Hydrology*, 21, 201-213.

Mansuy, N., Nuzman, C. and Cullimore, D.R. 1990. Well problem identification and its importance in well rehabilitation, in Howsam, P. *Groundwater Engineering Conference*, Granfield Institute of Technology, Granfield.

Martinez, R.E., Smith, D.S., Pedersen, K. and Ferris, F.G. 2003. Surface chemical heterogeneity of bacteriogenic iron oxides from a subterranean environment, *Environ. Sci. Technol.*, 37, 5671-5677.

Matijevic, E. 1980. Colloidal chemical aspects of corrosion of metals, *Pure and Applied Chemistry*, 52, 1179-1193.

Mayer, T.D. and Jarrell, W.M. 1996. Formation and stability of iron(II) oxidation products under natural concentrations of dissolved silica, *Water Research*, 30(5), 1208-1214.

McBride, M.B. 1994. *Environmental Chemistry of Soils*, Oxford University Press, New York.

McLaughlan, R. 2002. *Managing Water Well Deterioration*, AA Balkema, Lisse, 128.

McLaughlan, R.G. and Knight, M.J. 1989. *Corrosion and incrustation in groundwater bores: A critical review*, Centre for Groundwater Management and Hydrogeology, University of New South Wales.

Meyer, P.S. 1999. *An explanation of the 1:500 000 general hydrogeological map: Oudtshoorn 3320*, Department of Water Affairs and Forestry, Pretoria.

Meyer, P.S. 2001. *An explanation of the 1:500 000 general hydrogeological map: Cape Town 3317*, Department of Water Affairs and Forestry, Pretoria, SA.

Meyer, P.S. 2002. Springs in the Table Mountain Group, with special reference to fault controlled springs, in Pieterson, K. and Parsons, R. (ed's) *A Synthesis of the Hydrogeology of the Table Mountain Group - Formation of a Research Strategy*, WRC Report No TT 158/01, SA, 224-229.

Miller, S.J. 2000. *Geochemistry of Ferruginous Clogging of Karroo Wells*, Unpublished MSc Thesis, UCT, Cape Town.

Mills, A.L., Herman, J.S., Hornberger, G.M. and DeJesús, T.H. 1994. Effect of solution ionic strengths and iron coatings on mineral grains on the sorption of bacterial cells to quartz sand, *Applied and Environmental Microbiology*, 60 (9), 3300-3306.

Mitchell, R. 2005. *An Investigation into the Lithological Source of Iron in the Kammanassie Mountain Aquifer*, Unpublished MSc Thesis, University of Cape Town.

Mogg, J.L. 1972. Practical corrosion and incrustation guidelines for water wells, *Ground Water*, 10, 6-11.

More Water cc 2002. *Atlantis Wellfield Rehabilitation - Consolidation Report Of Phases 1 To 5*, More Water cc, Cape Town.

Mulder, E.G. 1989. Genus Leptothrix, in Stanley, J.T., Bryant, M.P., Pfennig, N. and Holt, J.G. *Bergey's Manual of Systematic Bacteriology*, Williams & Wilkins, Baltimore, 1998-2003.

Mulder, E.G. and Deinema, M.H. 1981. Chapter 27: The Sheathed Bacteria, in Starr, M.P., Stolp, H., Trüper, H.G., Balows, A. and Schlegel, H.G. *The Prokaryotes: A Handbook on Habitats, Isolation and Identification of Bacteria v. VI*, Springer-Verlag, Berlin, 425-440.

Ochs, M. 1996. Influence of humified and non-humified natural organic compounds on mineral dissolution, *Chemical Geology*, 132, 119-124.

Parkhurst, D.L. and Appelo, C.A.J. 1999. *User's Guide to PHREEQC (Version 2)- A computer program for speciation, batch reaction, one dimensional transport, and inverse geochemical calculations*, Water Resources Investigations Report 99-4259, US Geological Survey, Colorado.

Postma, D. 1993. The reactivity of iron oxides in sediments: A kinetic approach, *Geochimica et Cosmochimica Acta*, 57, 5027-5034.

Pullin, M.J. and Cabaniss, S.E. 2003. The effects of pH, ionic strength, and iron-fulvic acid interactions on the kinetics of non-photochemical iron transformations. II. The kinetics of thermal reduction, *Geochimica et Cosmochimica Acta*, 67(21), 4079-4089.

Ralph, D.E. and Stevenson, J.M. 1995. The role of bacteria in well clogging, *Water Research*, 29(1), 365-369.

Rancourt, D.G., Thibault, P., Mavrocordatos, D. and Lamarche, G. 2005. Hydrous ferric oxide precipitation in the presence of nonmetabolizing bacteria: Constraints on the mechanism of a biotic effect, *Geochimica et Cosmochimica Acta*, 69(3), 553-577.

Riekel, Th. and Hintze, G. 2002. *Rehabilitation of wells using electrochemically activated water*, Unpublished report.

Roden, E.E., Urrutia, M.M. and Mann, C.J. 2000. Bacterial reductive dissolution of crystalline Fe(III) oxide in continuous-flow column reactors, *Applied and Environmental Microbiology*, 66(3), 1062-1065.

Roden, E.E. and Zachara, J.M. 1996. Microbial reduction of crystalline iron(III) oxides: influence of oxide surface area and potential for cell growth, *Environ. Sci. Technol.*, 30, 1618-1628.

Rogers, J. 1982. Lithostratigraphy of Cenozoic sediments between Cape Town and Eland's Bay, *Palaeo-ecology of Africa*, 15, 121-137.

Rohde, H. and Keevill, B.A. 1990. Challenges in sustaining water well infrastructure on the Canadian Prairies, *International Association of Hydrology Report*, 217.

Rosenblum, S. and Brownfield, I.K. 1996. *Magnetic susceptibilities of minerals*, US Geological Survey Open-File Report 99-529.

Roychoudhury, A.N. 1998. *Biogeochemical Dynamics in Aquatic Sediments: Novel Laboratory and Field-based Approaches*, Unpublished PhD Thesis, Georgia Institute of Technology, Georgia.

Roychoudhury, A.N., Van Cappellen, P., Kostka, J.E. and Viollier, E. 2003. Kinetics of microbially mediated reactions: dissimilatory sulfate reduction in saltmarsh sediments (Sapelo Island, Georgia, USA), *Estuarine, Coastal and Shelf Science*, 56, 1001-1010.

Roychoudhury, A.N., Viollier, E. and Van Cappellen, P. 1998. A plug flow-through reactor for studying biogeochemical reactions in undisturbed aquatic sediments, *Applied Geochemistry*, 13, 269-280.

Ryde, N., Kihira, H. and Matijevic, E. 1992. Particle adhesion in model systems: 15. Effect of colloid stability in multilayer deposition, *Journal of Colloid and Interface Science*, 151(2), 421-432.

Saleh, A.M. and Jones, A.A. 1984. The crystallinity and surface characteristics of synthetic ferrihydrite and its relationship to kaolinite surfaces, *Clay Minerals*, 19, 745-755.

Sarazin, G., Michard, G. and Prevot, F. 1999. A rapid and accurate spectroscopic method for alkalinity measurements in sea water samples, *Water Research*, 33(1), 290-294.

Scheepers, R. 1995. Geology, geochemistry and petrogenesis of the Late Precambrian S-, I-, and A-type granitoids in the Saldania belt, Western Cape Province, *Journal of African Earth Sciences*, 21(1), 35-58.

Scheidegger, A., Borkovec, M. and Sticher, H. 1993. Coating of silica sand with goethite: preparation and analytical identification, *Geoderma*, 58, 43-65.

Schnitzer, M. and Kodama, H. 1976. The dissolution of micas by fulvic acid, *Geoderma*, 15, 381-391.

Schnoor, J.L. 1990. Kinetics of chemical weathering: A comparison of laboratory and field weathering rates, in Stumm, W. (ed) *Aquatic Chemical Kinetics: Reaction Rates of Processes in Natural Waters*, John Wiley, New York, 475-505.

Schott, J. and Berner, R.A. 1983. X-ray photoelectron studies of the mechanism of iron silicate dissolution during weathering, *Geochimica et Cosmochimica Acta*, 47, 2233-2240.

Schwertmann, U. and Taylor, R.M. 1992. Iron oxides, in Dixon, J.B. and Weed, S.B. (ed) *Minerals in Soil Environments (2nd Ed.),* Soil Science Society of America, Madison, 379-438.

Schwertmann, U. and Thalmann, H. 1976. The influence of [Fe(II)], [Si], and pH on the formation of lepidocrocite and ferrihydrite during oxidation of aqueous $FeCl_2$ solutions, *Clay Minerals*, 11, 189-200.

Segal, M.G. and Sellers, R.M. 1980. Reactions of solid iron(III) oxides with aqueous reducing agents, *J.C.S. Chem. Comm.*, 991-993.

Sidhu, P.S., Gilkes, R.J., Cornell, R.M., Posner, A.M. and Quirk, J.P. 1981. Dissolution of iron oxides and oxyhydroxides in hydrochloric and perchloric acid, *Clays and Clay Minerals*, 29(4), 269-276.

Siever, R. and Woodford, N. 1979. Dissolution kinetics and weathering of mafic minerals, *Geochimica et Cosmochimica Acta*, 43, 717-724.

Smart, M.C. and Tredoux, G. 2002. Groundwater quality and fitness for use, in Pieterson, K. and Parsons, R. (ed's) *A Synthesis of the Hydrogeology of the Table Mountain Group - Formation of a Research Strategy*, WRC Report No TT 158/01, SA, 118-123.

Smit, A.K. 2002. *Geochemistry of a pristine fynbos ecosystem in the Harold Porter National Botanical Gardens and Kogelberg Biosphere Reserve*, Unpublished MSc Thesis, University of Cape Town.

Smith, L.A. 2002. *Iron related bacterial clogging of boreholes in Oudtshoorn, South Africa, and the remediation thereof*, Unpublised report, Directorate of Geohydrology, Department of Water Affairs and Forestry.

Smith, E.J., Davison, W. and Hamilton-Taylor, J. 2002. Methods for preparing synthetic freshwaters, *Water Research*, 36, 1286-1296.

Smith, S.A. and Tuovinen, O.H. 1985. Environmental analysis of iron-precipitating bacteria in ground water and wells, *Ground Water Monitor Rev*, 5(4), 45-53.

Sobolev, D. and Roden, E.E. 2001. Suboxic deposition of ferric iron by bacteria in opposing gradients of Fe(II) and oxygen at circumnuetral pH, *Applied and Environmental Microbiology*, 67(3), 1328-1334.

Socki, R.A., Karlsson, H.R. and Gibson, E.K. 1992. Extraction technique for the determination of oxygen-18 in water using preevacuated glass vials, *Analytical Chemistry*, 64, 829-831.

Sogaard, E.G., Aruna, R., Abraham-Peskir, J. and Koch, C.B. 2001. Conditions for biological precipitation of iron by *Gallionella ferruginea* in a slightly polluted ground water, *Applied Geochemistry*, 16, 1129-1137.

Søgaard, E.G., Medewaldt, R. and Abraham-Peskir, J.V. 2000. Conditions and rates of biotic and abiotic iron precipitation in selected Danish freshwater plants and microscopic analysis of precipitate morphology, *Water Research*, 34(10), 2675-2682.

Stuetz, R.M. and McLaughlan, R.G. 2004. Impact of localised dissolved iron concentrations on the biofouling of environmental wells, *Wat. Sci.* Tech., 49(2), 107-113.

Stumm, W. and Morgan, J.J. 1996. *Aquatic Chemistry: Chemical Equilibria and Rates in Natural Waters* 3rd Ed, John Wiley & Sons, New York.

Stumm, W. and Sulzberger, B. 1992. The cycling of iron in natural environments: Considerations based on laboratory studies of heterogenous redox processes, *Geochimica et Cosmochimica Acta*, 56, 3233-3257.

Sulzberger, B., Suter, D., Siffert, C., Banwart, S. and Stumm, W. 1989. Dissolution of Fe(III)(hydr)oxides in natural waters: laboratory assessment on the kinetics controlled by surface coordination, *Marine Chemistry*, 28, 127-144.

Sung, W. and Morgan, J.L. 1980. Kinetics and products of ferrous iron oxygenation in aqueous systems, *Environ. Sci. Technol.*, 14, 561-568.

Sverjensky, D.A. 2005. Prediction of surface charge on oxides in salt solutions: Revisions for 1:1 (M+L-) electrolytes, *Geochimica et Cosmochimica Acta*, 69(2), 225-257.

Tamura, H., Goto, K. and Nagayama, M. 1976. The effect of ferric hydroxide on the oxygenation of ferrous ions in neutral solutions, *Corrosion Science*, 16, 197-207.

Tapscott, C. and Ellis, W. 1999. *Klein Karoo Rural Water Supply Scheme Augmentation Study: Socio-Economic Assessment*, DWAF Report No. PB J000/00/0599, Department of Water Affairs and Forestry, SA.

Taylor, S.W., Lange, C.R. and Lesold, E.A. 1997. Biofouling of contaminated groundwater recovery wells: Characterization of microorganisms, *Groundwater*, 35(6), 973-981.

Taylor, R.M. and Schwertmann, U. 1974. Maghemite in soils and it's origin: II. Maghemite syntheses at ambient temperature and pH 7, *Clay Minerals*, 10, 299-310.

Thamm, A.G. 1988. *Contributions to the geology of the Table Mountain Group*, Unpublished MSc Thesis, University of Cape Town.

Theis, T.L. and Singer, P.C. 1974. Complexation of iron(II) by organic matter and its effect on iron(II) oxygenation, *Environ. Sci. Technol.*, 8(6), 569-573.

Theron, J.N., Malan, J.A. and Hill, R.S. 1989. *Lithostratigraphy of the Skurweberg Formation (Table Mountain Group),* Lithostratigraphic Seris No. 3, South African Committee for Stratigraphy, Pretoria.

To, T., Nordstrom, D.K., Ball, J.W. and McCleskey, R.B. 1999. New method for the direct determination of dissolved Fe(III) concentration in acid mine waters, *Environ. Sci. Technol.*, 33, 807-813.

Todar, K. 2002. *Todar's Online Textbook of Bacteriology*, www.textbookofbacteriology.net.

Tredoux, G. and Cavé, L. 2002. *Atlantis Aquifer: A status report on 20 years of groundwater management at Atlantis*, ENV-S-C 2002-069, CSIR, Stellenbosch.

Tuhela, L., Carlson, L. and Tuovinen, O.H. 1992. Ferrihydrite in water wells and bacterial enrichment cultures, *Water Research*, 26(9), 1159-1162.

Tuhela, L., Carlson, L. and Tuovinen, O. 1997. Biogeochemical transformations of iron and manganese in oxic groundwater and well water environments, *Journal of Environmental Science and Health*, A32(2), 407-427.

Tyrrel, S.F. and Howsam, P. 1997. Aspects of the occurrence and behaviour of iron bacteria in boreholes and aquifers, *Quaterly Journal of Engineering Geology*, 30, 161-169.

Urrutia, M.M., Roden, E.E. and Zachara, J.M. 1999. Influence of aqueous and solid-phase Fe(II) complexants on microbial reduction of crystalline iron(III) oxides, *Environ. Sci. Technol.*, 33, 4022-4028.

van Hees, P.A.W., Lundström, U.S. and Mörth, C.-M. 2002. Dissolution of microcline and labradorite in a forest O horizon extract: the effect of naturally occurring organic acids, *Chemical Geology*, 189, 199-211.

van Oorschot, I.H.M. and Dekkers, M.J. 1999. Dissolution behaviour of fine-grained magnetite and maghemite in the citrate-bicarbonate-dithionite extraction method, *Earth and Planetary Science Letters*, 167, 283-195.

Vegter, J.R. 1995. *An explanation of a set of national groundwater maps*, Department of Water Affairs, South Africa.

Viollier, E., Inglett, P.W., Hunter, K., Roychoudhury, A.N. and Van Cappellen, P. 2000. The ferrozine method revisited: Fe(II)/Fe(III) determination in natural waters, *Applied Geochemistry*, 15, 785-790.

Visser, H.N. and Schoch, A.E. 1973. *The Geology and Mineral Resources of the Saldanha Bay Area*, Memoir 63, Dept. of Mines Geological Survey, Pretoria.

von Gunten, U. and Furrer, G. 2000. Steady-state modelling of biogeochemical processes in columns with aquifer material: 2. Dynamics of iron-sulfur interactions, *Chemical Geology*, 167, 271-284.

Von Gunten, U. and Schneider, W. 1991. Primary products of the oxygenation of iron(II) at an oxic-anoxic boundary: nucleation, aggregation, and aging, *Journal of Colloid and Interface Science*, 145(1), 127-139.

Von Gunten, U. and Zobrist, J. 1993. Biogeochemical changes in groundwater-infiltration systems: column studies, *Geochimica et Cosmochimica Acta*, 57, 3895-3906.

Vuorinen, A., Carlson, L., Seppänen, H. and Hatva, T. 1988. Chemical, mineralogical and microbiological factors affecting the precipitation of Fe and Mn from groundwater, *Wat. Sci. Tech.*, 20(3), 249.

Walter, D.A. 1997. *Geochemistry and mirobiology of iron-related well-screen encrustation and aquifer biofouling in Suffolk County, Long Island, New York*, Water-Resources Investigations Report 97-4032, US Geological Survey, New York.

Warren, L.A. and Ferris, F.G. 1998. Continuum between sorption and precipitation of Fe(III) on microbial surfaces, *Environ. Sci. Technol.*, 32, 2331-2337.

Weaver, J.M.C. 1992. *Groundwater Sampling: A comprehensive guide for sampling methods.*, WRC Project No. 339 TT 54/92, Water Research Commission, Pretoria.

Weaver, J. and Talma, S. 1999. *Field studies of CFC's as a groundwater dating tool in fractured rock aquifers*, Report No. 731/1/99, WRC, SA.

Wen, C.Y. and Fan, L.T. 1975. *Models for Flow Systems and Chemical Reactors*. Marcel Dekker, New York.

White, A.F. 2003. Reaction Kinetics of Primary Rock-Forming Minerals under Ambient Conditions, in Drever, J.I. (ed) *Treatise on Geochemistry: Volume 5 Surface and Groundwater, Weathering and Soils*, Elsevier, Netherlands, 134-164.

White, A.F. and Yee, A. 1985. Aqueous oxidation-reduction kinetics associated with coupled electron-cation transfer from iron-containing silicates at 25°C, *Geochimica et Cosmochimica Acta*, 49, 1263-1275.

Wieland, E. and Stumm, W. 1992. Dissolution kinetics of kaolinite in acidic aqueous solutions at 25°C, *Geochimica et Cosmochimica Acta*, 56, 3339-3355.

Wightman, P.G. and Fein, J.B. 2005. Iron adsorption by *Bacillus subtilis* bacterial cell walls, *Chemical Geology*, 216, 177-189.

Wolthoorn, A., Temminghoff, E.J.M. and van Riemsdijk, W.H. 2004a. Colloid formation in groundwater by subsurface aeration: characterisation of the geo-colloids and their counterparts, *Applied Geochemistry*, 19, 1391-1402.

Wolthoorn, A., Temmingshoff, E.J.M., Weng, L. and van Riemsdijk, W.H. 2004b. Colloid formation in groundwater: effect of phosphate, manganese, silicate and dissolved organic matter on the dynamic heterogenous oxidation of ferrous iron, *Applied Geochemistry*, 19, 611-622.

Yeld, J. 2002. Man vs. nature in a drying landscape, *Cape Argus*, Thursday July 25.

Zachara, J.M., Fredrickson, J.K., Li, S., Kennedy, D.W., Smith, S.C. and Gassman, P.L. 1998. Bacterial reduction of crystalline Fe3+ oxides in single phase suspensions and subsurface materials, *American Mineralogist*, 83, 1426-1443.

Appendix A Additional Data

A.1 Historical groundwater quality Data

A.1.1 Full historical groundwater quality dataset

The full set of historical groundwater quality data is included in Table A1. The sources used for the data are as follows:

1. Hazenjagt (DWAF, 1998)
2. National Groundwater Database (2004)
3. Kotze and Rosewarne (1999)
4. WRC/1998 from Kotze (2001)
5. WRC/1997 from Kotze (2001)
6. WRC/1996 from Kotze (2001)
7. ADD/1997 from Kotze (2001)
8. Simonic from Kotze (2001)
9. This study
10. WRC/mar98/re from Kotze (2001)
11. Simonic/Issar from Kotze (2001)
12. Engelbrecht and Jolly (1999)
13. Kotze and Rosewarne (1996) (SRK report #230827)
14. Miller (2000)
15. Kotze, Verhagen and Butler (2000)
16. Weaver and Talma (1999)
17. Vermaaks River wellfield monitoring data

Abbreviations used in the table are as follows:

Group		Fm (Formation)	
BOK	Bokkeveld Group	BOK	Bokkeveld
TMG	Table Mountain Group	BAV	Baviaanskloof
TMG-N	Nardouw Subgroup	SKW	Skurweberg
TMG-P	Peninsula Formation	GOUD	Goudini
		PEN	Peninsula
		HS	Hotspring
		SUR	Surface
		UNK	Unknown

Sample names consist of the borehole name followed by the number of that sample from that particular well.

Table A.1. Historical groundwater quality data for TMG. Data in mg/L unless otherwise specified.

Borehole	Source	Group	Fm	EC	pH	Na	Mg	Ca	Cl	SO4	TAL (mg/L CaCO3)	Si	K	Fe	Al	Mn	δD	$\delta^{18}O$	DO	Temp	Charge
				mS/m													‰	‰	mg/L	°C	Bal %
22/3	1	BOK	BOK	199.0	7.3	195.0	44.7	115.3	320.8	269.2	518.9	6.8	7.3								-16.1
22/4	1	BOK	BOK	150.0	7.9	131.9	31.1	98.2	239.8	145.1	440.8	8.1	11.0								-15.9
98274	2	BOK	BOK	152.0	8.2	154.4	48.9	95.4	474.3	37.6	86.1	14.1	6.3								-0.7
99773	2	BOK	BOK	51.9	6.6	46.4	12.7	15.0	100.1	25.7	35.6	5.2	14.4								1.3
160064	2	BOK	BOK	100.0	7.8	120.2	14.7	58.5	144.7	79.9	172.3	13.3	13.0								2.7
163/1	1	BOK	BOK	149.0	7.8	150.0	47.1	73.3	215.7	79.3	764.4	11.5	2.9								-23.9
HE3	3	BOK	BOK	397.0	7.9	601.0	85.0	163.0	889.0	463.0	354.0	7.8	14.7								-0.2
HSD1	3	BOK	BOK	204.0	7.7	430.0	69.0	180.0	662.0	332.0	437.0	9.8	3.1								-1.3
KK1	3	BOK	BOK	60.0	7.7	70.0	10.0	40.0	72.0	20.0	164.0	11.5	1.0								1.4
KK2	3	BOK	BOK	140.0	7.8	167.0	37.0	117.0	244.0	158.0	296.0	9.7	2.5								0.4
KN1	3	BOK	BOK	118.9	7.0	79.0	38.0	107.0	98.0	355.0	105.0	12.8	17.0								0.3
KN2	3	BOK	BOK	385.0	7.8	524.0	108.0	175.0	668.0	579.0	500.0	10.2	26.9	0.10							0.3
KN3	3	BOK	BOK	1350.0	7.8	1792.0	533.0	662.0	3738.0	2205.0	233.0	8.0	31.7								-0.1
KT1	3	BOK	BOK	341.0	7.2	435.0	86.0	181.0	694.0	415.0	304.0	9.9	4.2								1.2
OK1	3	BOK	BOK	40.1	6.9	32.0	5.0	31.0	51.0	34.0	76.0	7.6	0.8			0.69					-4.2
OR1	3	BOK	BOK	215.0	7.4	274.0	67.0	156.0	367.0	382.0	362.0	10.8	3.9								-0.4
SBH1	4	BOK	BOK	50.8	6.0	62.9	7.8	7.7	130.6	10.5	37.7	9.2	7.6			3.09	-49.5	-7.0			-8.1
SBH2	4	BOK	BOK	25.5	5.9	30.8	4.1	2.9	56.2	5.6	12.7	5.6	2.6	0.01	0.06	0.25	-38.4	-5.6			-1.7
BADEN	11	TMG	HS	7.7	7.5	7.0	2.0	4.0	11.0		42.5	13.2	3.0				-40.0	-6.8			-21.7
BATHS	11	TMG	HS	9.1	7.1	8.2	2.0	2.9	12.8	1.5	32.0	11.1	0.3				-25.0	-4.9			-20.9
BRAND	11	TMG	HS	7.7	7.4	8.0	2.0	3.0	11.0		37.5	18.6	2.5				-33.0	-5.7			-18.6
CHS-5	10	TMG	HS	22.8	7.1	17.6	3.4	9.2	26.8	12.0	108.1	17.8	7.9	0.51		2.50					-29.5
GDN1	11	TMG	HS	7.9	7.2	5.4	1.8	6.2	8.4	10.5	48.2	15.3	1.6				-28.0	-4.8			-31.9
GDN2	11	TMG	HS	7.1	7.1	5.4	1.7	5.7	8.9	2.1	43.7	14.5	1.4				-28.0	-4.5			-25.4
GDN3	11	TMG	HS	6.5	7.5	5.4	1.5	5.1	8.6	0.7	42.0	12.5	1.3				-28.0	-4.5			-25.9
MONT	11	TMG	HS	25.3	8.3	15.8	3.6	23.8	24.1	8.5	163.3	14.3	0.5				-37.0	-6.5			-30.7
m-vnotch-1	6	TMG	SUR	11.5	7.1	16.0	2.0	2.0			17.5	4.1	1.6				-45.8	-7.2			48.3
m-vnotch-2	5	TMG	SUR	16.1	7.1	20.0	2.6	2.1	31.4	14.8	31.0	4.4	1.0	0.12	0.12		-54.8	-7.8			-19.6
m-vnotch-3	7	TMG	SUR	11.0	6.5	15.0	3.0	2.0	28.0	7.0	12.5	3.9	0.6	0.14	0.09						-7.5
VR Notch-1	9	TMG	SUR	19.1	6.0	29.1	3.4	2.6	42.4	8.9		5.6	0.4			0.01	-43.0	-7.9			9.8
VR Notch-2	6	TMG	SUR	17.5	7.0	25.0	3.0	3.0			22.5	5.0	2.2	0.19			-46.2	-7.3		13.4	55.0
VR Notch-3	10	TMG	SUR	18.9	7.0	24.8	2.0	3.8	33.8	7.6	33.7	5.7	0.3	0.01			-55.3	-7.8			-10.6
VR Notch-4	7	TMG	SUR	12.8	6.1	20.0	2.0	2.0	32.0	8.0	10.0	4.7	0.6	0.13	0.27						-4.7
PKBG	11	TMG	UNK	30.5	8.2	12.3	3.8	39.5	21.5	3.4	244.5	4.5	4.1				-22.0	-4.1			-31.1

Table A.1. cont. Historical groundwater quality Data

Borehole	Source	Group	Fm	EC	pH	Na	Mg	Ca	Cl	SO4	TAL (mg/L CaCO3)	Si	K	Fe	Al	Mn	δD	$\delta^{18}O$	DO	Temp	Charge
				mS/m													‰	‰	mg/L	°C	Bal %
PKBGB	11	TMG	UNK	32.0	4.8	35.5	9.5	4.9	44.9	0.8	12.2	4.1	0.9				-23.0	-3.8			25.9
PLM	11	TMG	UNK	14.5	6.5	15.8	3.4	2.7	26.4	6.5	30.0	5.5	1.2				-17.0	-3.0			-13.2
TM27	8	TMG	UNK	11.3	6.0	12.8	2.3	1.8	24.3	12.7	14.5	3.6	0.5				-16.0	-4.0			-18.7
TM28	8	TMG	UNK	6.3	6.0	8.1	1.6	0.7	15.2	6.3	11.0	3.6					-18.0	-4.3			-20.1
TM29	8	TMG	UNK	8.1	6.1	10.2	1.9	0.6	19.4	4.4	8.2	3.4					-18.0	-4.5			-12.1
TM30	8	TMG	UNK	8.4	6.8	10.7	2.1	0.8	20.1	3.7	9.0	3.6					-25.0	-5.3			-9.7
TM31	8	TMG	UNK	22.5	7.3	33.1	3.9	2.9	63.9	7.0	11.2	4.7	0.3				-34.0	-6.1			-6.4
TM32	8	TMG	UNK	18.4	7.8	19.0	6.0	4.0	39.0	6.0	67.4	5.1	3.6				-34.0	-6.3			-23.0
TM33	8	TMG	UNK	16.9	7.3	23.0	5.0	1.0	44.0	7.0	32.5	3.5					-16.0	-4.0			-16.4
TM34	8	TMG	UNK	3.4	7.8	3.0			6.0		15.0	1.4					-18.0	-4.3			-56.4
TM35	8	TMG	UNK	3.6	7.3	3.0			5.0		17.5	0.9					-18.0	-4.5			-58.0
TM36	8	TMG	UNK	3.1	7.2	2.0		1.0	5.0		17.5	1.4					-25.0	-5.3			-56.4
TM37	8	TMG	UNK	4.4	7.8	5.0		2.0	7.0	5.0	15.0	0.6					-34.0	-6.1			-30.9
99779	2	TMG-N	BAV	57.2	7.4	60.0	9.7	14.1	108.0	27.5	60.3	5.2	15.6								-3.4
145578	2	TMG-N	BAV	18.5	6.8	21.2	3.2	4.4	34.1	11.3	18.7	4.5	2.3								-3.5
180475	2	TMG-N	BAV	27.5	6.5	34.2	4.5	3.0	71.1	4.6	10.6	5.4	1.3								-6.2
Boer	12	TMG-N	BAV	19.0	5.5	24.0	3.3	2.6	44.0	7.5	5.3		2.0	0.20		0.44			3.8		0.0
DL13-1	13	TMG-N	BAV	49.5	7.2	66.0	8.0	12.0	115.0	24.0	147.3	5.3	16.2	0.57			-42.7	-7.0			-18.9
DL13-2	2	TMG-N	BAV	17.9	8.3	7.2	2.3	25.7	6.1	9.4	80.6	3.1	1.0	0.36		0.49	-48.2	-7.2		20.0	-4.1
DL13-3	9	TMG-N	BAV	95.0	7.5	173.0	40.1	37.3				3.1	26.4	0.93	0.14	0.66			7.0	16.6	100.0
DL13-4	9	TMG-N	BAV	27.4	6.4	57.5	7.2	11.8	86.0	18.9		5.2	14.5	4.79		0.52	-37.0	-6.8		24.7	19.9
DL13-6	8	TMG-N	BAV	62.6	7.3	70.6	11.3	15.7	131.3	26.9	155.8	5.5	15.9				-39.0	-6.4			-17.4
DL15-1	13	TMG-N	BAV	44.5	7.2	37.0	10.0	12.0	90.0	20.0	89.9	4.5	14.2	3.41							-14.9
DL15-2	10	TMG-N	BAV	46.1	7.0	43.0	10.1	13.3	89.5	14.7	106.4	5.2	14.8			0.58					-13.9
DL15-3	7	TMG-N	BAV	51.9	6.6	46.0	13.0	15.0	100.0	26.0	89.9	5.2	14.4	0.02		0.83					-10.4
DL16-1	13	TMG-N	BAV	46.7	7.3	47.0	9.0	12.0	91.0	20.0	124.9	4.9	14.3	3.75							-17.0
DL16-2	2	TMG-N	BAV	48.0	7.0	50.9	8.1	10.9	90.9	26.4	37.0	6.7	12.9	0.16		0.34	-46.5	-6.6		20.4	-1.2
DL16-3	15	TMG-N	BAV	48.6	6.9	57.3	8.6	13.2	94.2	22.5	54.8	5.8	15.2			0.32	-32.4	-6.6			0.3
DL16-4	2	TMG-N	BAV	45.1	6.8	46.0	8.2	11.3	79.3	10.7	55.9	5.3	13.9			0.42					0.3
DL16-5	12	TMG-N	BAV	41.0	6.4	46.0	8.5	11.7	81.0	14.0	54.0		15.7	4.70		0.42			2.0		2.6
DL16-6	9	TMG-N	BAV	48.0	6.2	63.4	11.7	10.6			20.2	3.4	14.8	0.75	0.01	0.48			3.5	19.0	84.0
DL16-7	9	TMG-N	BAV	52.2	6.3	54.4	8.5	13.7	90.6	18.9		5.6	14.7	6.12		0.46	-40.0	-7.1	0.6	22.8	19.1
DL17-1	14	TMG-N	BAV	49.0	5.7	44.2	11.4	27.4	93.3	27.0	75.1	5.2	14.8	3.55						17.6	0.4
DL17-2	15	TMG-N	BAV	50.9	6.7	47.9	11.9	15.7	98.9	24.6	42.7	5.7	14.4				-32.2	-6.6			0.7

Table A.1. cont. Historical groundwater quality Data

Borehole	Source	Group	Fm	EC	pH	Na	Mg	Ca	Cl	SO4	TAL (mg/L CaCO3)	Si	K	Fe	Al	Mn	δD	$\delta^{18}O$	DO	Temp	Charge
				mS/m													‰	‰	mg/L	°C	Bal %
DL17-3	2	TMG-N	BAV	40.2	6.5	44.4	10.9	14.3	92.1	24.7	36.9	5.7	13.4	0.74		0.27	-46.4	-6.6			0.8
DL17-4	12	TMG-N	BAV	44.0	6.2	42.0	11.2	14.0	93.0	19.0	40.0		14.7	2.60		0.68			1.2		1.3
DL17-5	9	TMG-N	BAV	56.6	7.2	62.2	17.2	17.8				3.3	17.1	4.08	0.02	1.75			4.5	20.3	100.0
DL17-6	9	TMG-N	BAV	58.2	6.1	30.6	21.9	28.9	73.7	27.2		6.4	7.5	13.0		2.18		-6.9		22.5	32.8
DL17-7	8	TMG-N	BAV	38.6	7.2	36.2	8.2	11.6	80.6	14.8	109.1	4.9	13.1				-37.0	-6.5			-20.2
DP12-1	13	TMG-N	BAV	22.2	6.4	32.0	4.0	5.0	41.0	16.0	47.5	5.0	4.3				-47.3	-6.6			-7.9
DP12-2	12	TMG-N	BAV	26.0	6.1	28.0	4.5	8.5	42.0	40.0	6.8		6.1	4.00		1.06			3.4		3.5
DP15-1	13	TMG-N	BAV	30.2	3.7	21.0	3.0	3.0	32.0	60.0	10.0	5.0	3.7				-47.8	-7.7			-25.2
DP15-10	2	TMG-N	BAV	9.5	6.0	10.6	2.0	2.4	20.0			4.5	0.4								14.5
DP15-11	2	TMG-N	BAV	9.3	6.0	10.4	1.9	1.7	18.3			4.6	0.4								15.3
DP15-12	2	TMG-N	BAV	9.6	6.4	9.6	1.7	1.7	16.6			4.5	0.4								16.3
DP15-2	16	TMG-N	BAV	29.0	3.7	20.0	3.7	3.3	46.0	46.0		4.7	2.2	1.34			-41.9	-7.4	0.5		-21.9
DP15-3	9	TMG-N	BAV	25.5	3.6	22.6	3.7	2.9				2.2	2.7	5.29	2.23	0.60			6.1	22.2	100.0
DP15-4	9	TMG-N	BAV	22.9	4.1	22.3	3.5	4.0	38.1	41.8	10.0	6.0	2.9	3.43		0.66			0.1	19.5	-13.0
DP15-5	9	TMG-N	BAV	19.8	4.3	22.9	3.6	3.7	34.6	38.2	10.0	6.0	2.9	3.10		0.67	-42.0	-7.8	2.7	18.5	-8.7
DP15-6	2	TMG-N	BAV	20.7	4.4	19.1	3.7	3.6	34.7	19.1		5.6	2.1								-0.2
DP15-7	2	TMG-N	BAV	55.2	3.3	20.8	5.4	6.5	30.5	98.4		6.7	2.5								-25.2
DP15-8	2	TMG-N	BAV	22.0	3.4	20.7	3.6	3.6	35.3	30.3		5.8	2.1								-6.4
DP15-9	2	TMG-N	BAV	9.4	5.9	10.2	1.9	1.7	19.5	4.6		4.6	0.5								3.8
DP25-1	12	TMG-N	BAV	128.0	3.5	24.0	14.8	20.4	37.0	548.0			3.9	89.10		4.60			1.4		-30.9
DP25-2	11	TMG-N	BAV	17.8	6.0	19.7	4.2	3.8	32.4	27.8	12.0	5.3	2.8				-44.0	-7.3			-8.4
DP28-1	13	TMG-N	BAV	18.0	5.9	22.0	3.0	3.0	39.0	18.0	22.5	5.4	3.6	0.65	3.67	1.80	-48.6	-7.9			-13.4
DP28-2	16	TMG-N	BAV	17.5	5.1	20.0	3.6	3.2	34.0	17.4	3.5	4.7	2.2	1.41			-39.8	-7.4	0.6		1.5
DP28-3	14	TMG-N	BAV	57.0	3.1	22.7	13.1	22.8	26.6	209.3		7.4	3.9	15.41							-14.0
DP28-4	12	TMG-N	BAV	38.0	4.2	23.0	8.9	8.4	35.0	84.0			2.8	2.50		1.50			0.7		-8.4
DP28-5	12	TMG-N	BAV	74.0	3.2	28.0	18.0	18.0	34.0	210.0			1.1	20.60		3.00					-10.0
DP28-6	9	TMG-N	BAV	19.1	5.4	21.8	2.4	2.4	37.4	8.9	22.4	5.0	2.3	3.76		0.43	-42.0	-7.0	2.9	18.5	-7.3
DP28-7	7	TMG-N	BAV	26.9	4.1	21.0	5.0	5.0	28.0	38.0		5.2	2.2		0.35	0.80					1.6
DP29-1	13	TMG-N	BAV	20.8	6.4	25.0	4.0	5.0	36.0	14.0	37.5	4.9	4.2		1.61	0.58	-48.9	-7.7		23.3	-7.4
DP29-2	16	TMG-N	BAV	19.0	5.5	21.0	4.4	4.9	35.0	13.9	13.8	4.5	2.8	0.76			-43.9	-7.7	0.2		2.1
DP29-3	12	TMG-N	BAV	21.0	6.0	25.0	4.3	5.6	40.0	19.0	12.0		3.1	2.00		0.70	-50.8	-7.9	3.4		3.0
DP29-4	9	TMG-N	BAV	18.4	6.7	25.3	3.8	4.3			16.8	1.8	3.4	1.26	0.00	0.63			1.5	20.8	67.9
DP29-5	9	TMG-N	BAV	22.6	5.5	25.8	3.5	5.7	40.8	19.6	30.0	5.4	2.9	2.13		0.66	-45.0	-7.8	3.1	19.2	-7.9
DP29-8	7	TMG-N	BAV	19.6	6.0	25.0	4.0	6.0	38.0	21.0	32.5	5.0	2.6			0.73					-9.5

Table A.1. cont. Historical groundwater quality Data

Borehole	Source	Group	Fm	EC	pH	Na	Mg	Ca	Cl	SO4	TAL (mg/L CaCO3)	Si	K	Fe	Al	Mn	δD	$\delta^{18}O$	DO	Temp	Charge
				mS/m													‰	‰	mg/L	°C	Bal %
G40174 147M	17	TMG-N	BAV	22.7	7.3	20.8	3.1	12.2	32.2	10.6	79.2	4.7	1.9				-37.5	-6.7			-19.7
G40177	2	TMG-N	BAV	45.0	6.9	40.4	7.1	17.7	85.3	39.1	33.2	2.1	14.1								-4.0
G40177	2	TMG-N	BAV	37.6	7.6	40.9	6.9	17.7	85.6	37.8	33.9	2.1	14.6								-3.7
G40177 92M	17	TMG-N	BAV	45.0	6.9	40.4	7.1	17.7	85.3	39.1	82.9	2.1	14.1			2.14	-45.0	-7.3			-15.3
G40177B 150M	17	TMG-N	BAV	37.6	7.6	40.9	6.9	17.7	85.6	37.8	84.7	2.1	14.6			1.74	-40.2	-7.3			-15.2
G40178	2	TMG-N	BAV	109.9	6.9	135.2	27.6	37.0	230.1	115.4	73.7	15.2	4.9								-1.2
G40178	2	TMG-N	BAV	155.0	7.9	232.8	43.1	73.4	395.2	220.5	88.8	13.9	9.7								0.2
G40178 120M	17	TMG-N	BAV	155.0	7.9	232.8	43.1	73.4	395.2	220.5	221.8	13.9	9.7			7.20	-42.0	-7.3			-6.9
G40178 54M	17	TMG-N	BAV	109.9	6.9	135.2	27.6	37.0	230.1	115.4	184.0	15.2	4.9			3.44	-40.7	-7.0			-10.8
KOUTF	4	TMG-N	BAV	10.7	6.7	11.8	2.1	2.1	15.2	19.3	16.0	7.3	2.9	0.01	0.06		-43.5	-7.2			-14.1
LA1	3	TMG-N	BAV	30.5	7.0	23.0	4.0	23.0	38.0	46.0	26.0	8.1	6.4								1.8
SL2-1	13	TMG-N	BAV	54.4	7.0	49.0	11.0	36.0	136.0	26.0	142.3	10.3	14.2				-41.4	-6.4			-16.3
SL2-2	13	TMG-N	BAV	83.7	6.2	54.9	19.9	57.4	126.7	158.6	85.2	13.5	13.2			2.60	-47.4	-6.9			-8.5
VG1-1	12	TMG-N	BAV	24.0	5.5	28.0	3.5	3.5	53.0	12.0	7.2		6.3	3.20		3.50			2.6		1.8
VG1-2	12	TMG-N	BAV	24.0	5.7	29.0	3.6	6.1	54.0	11.0	4.3		5.9	5.30		0.38					9.0
VG2-1	14	TMG-N	BAV	33.0	5.6	22.3	4.1	17.0	49.6	16.6	52.9	7.5	7.1	1.04							-8.3
VG2-2	12	TMG-N	BAV	32.0	6.3	31.0	4.7	13.4	60.0	26.0	26.0		10.1	0.20		4.70			1.0		-1.5
VG2-3	12	TMG-N	BAV	30.0	6.6	28.0	4.5	11.0	53.0	20.0	27.0		9.1	13.10		3.10					7.3
VG3-1	16	TMG-N	BAV	19.5	4.5	26.0	3.7	1.8	46.0	6.2	1.0	4.1	0.8	0.01			-43.5	-7.9	4.4		3.3
VG3-2	15	TMG-N	BAV	15.5	5.0	23.0	3.0	2.0	40.0	5.0	10.0	4.4	0.7		0.05	0.23	-51.8	-7.9			-2.4
VG3-3	12	TMG-N	BAV	21.0	4.9	27.0	3.6	2.3	48.0	8.1	4.3		0.9	0.30		0.42	-57.1	-7.7	2.6		0.3
VG3-4	9	TMG-N	BAV	21.0	5.3	33.6	4.1	1.9			9.1	0.1	0.9	0.01	0.06	0.21			5.9	16.5	82.7
VG3-5	2	TMG-N	BAV	20.3	5.4	26.7	2.6	2.3	41.3	10.2		5.0	0.6								4.4
VG3-5	11	TMG-N	BAV	18.3	6.3	23.0	3.0	2.0	37.4	8.1	17.2	5.4	0.9		0.04	0.22	-49.0	-7.4		15.0	-6.7
VG3-6	2	TMG-N	BAV	20.6	5.2	23.6	3.3	2.4	38.9	18.3		4.7	0.8								-1.4
VG3-6	10	TMG-N	BAV	20.3	5.4	26.7	2.6	2.3	41.3	10.2	5.2	5.0	0.6		0.03	0.14	-57.1	-7.7			0.8
VG3-7	4	TMG-N	BAV	20.6	5.2	23.6	3.3	2.4	38.9	18.3	1.5	4.7	0.8			0.95	-55.1	-8.0			-2.4
VSBH	4	TMG-N	BAV	26.4	6.6	17.7	6.7	5.7	36.8	13.9	91.6	6.4	12.5			0.80	-50.6	-8.1			-24.3
VSS	4	TMG-N	BAV	37.7	6.9	53.5	7.0	3.2	80.2	22.6	71.7	0.3	1.0			0.58	-32.6	-3.2			-14.9
WK3	15	TMG-N	BAV	17.4	5.8	23.8	3.4	2.6	39.8	24.1	15.2	5.1	1.6				-50.6	-7.2			-13.0
WN2	13	TMG-N	BAV	25.9	6.2	35.0	5.0	9.0	55.0	40.0	30.0	7.5	8.5				-50.4	-7.8			-6.9
WN3	15	TMG-N	BAV	25.1	5.8	30.1	4.6	8.7	50.8	31.6	21.2	7.7	6.5			0.18	-53.2	-7.7			-4.7
180473	2	TMG-N	GOUD	8.8	6.5	8.7	1.6	1.7	20.4		6.1	3.2	0.7								-6.5
WK4	15	TMG-N	GOUD	26.0	5.5	31.3	4.4	3.5	58.0	13.6	13.5	5.0	1.1				-50.9	-7.2			-6.4

Table A.1. cont. Historical groundwater quality Data

Borehole	Source	Group	Fm	EC	pH	Na	Mg	Ca	Cl	SO4	TAL (mg/L CaCO3)	Si	K	Fe	Al	Mn	δD	$\delta^{18}O$	DO	Temp	Charge
				mS/m													‰	‰	mg/L	°C	Bal %
CHS-1	9	TMG-N	HS	19.6	6.8	16.3	2.8	10.0	32.0	5.3		18.5	8.9	0.83		2.61				52.0	25.1
CHS-2	13	TMG-N	HS	21.5	7.3	17.0	4.0	9.0	34.0	9.0	104.9	17.7	9.4	0.28		2.85	-46.6	-7.5			-29.4
CHS-3	3	TMG-N	HS	21.0	7.1	17.0	4.0	10.0	32.0	8.0	42.0	18.1	7.4	0.01		2.90		-7.1			-4.1
CHS-4	3	TMG-N	HS	18.8	7.0	16.0	4.0	10.0	30.0	6.0	41.0	17.8	7.6			2.68	-49.7	-7.4			-2.0
CHS-6	11	TMG-N	HS	22.3	7.7	15.2	5.0	10.0	26.0	5.3	113.4	19.1	8.4				-44.0	-7.1			-27.0
WBG-1	6	TMG-N	HS	23.9	7.3	23.0	3.0	15.0	28.0	4.0	154.8	21.4	9.6				-46.0	-7.6			-27.8
WBG-2	11	TMG-N	HS	23.9	7.3	23.0	3.0	15.0	28.0		154.8	21.4	9.6	0.90	0.02	0.96	-43.0	-7.1			-26.1
99772	2	TMG-N	SKW	9.2	5.5	10.1	1.5	1.3	17.8	14.9		4.2	0.6								-11.6
180474	2	TMG-N	SKW	17.7	6.4	20.7	2.9	1.8	38.6	6.5	6.4	4.6	0.9								-3.8
DG110-1	14	TMG-N	SKW	17.0	5.4	20.6	3.6	5.4	46.5	9.9	27.0	3.9	1.4	11.7							-3.5
DG110-10	2	TMG-N	SKW	18.6	6.7	21.2	3.4	3.1	37.6	7.9		5.6	2.1								7.0
DG110-11	2	TMG-N	SKW	19.5	6.6	22.0	3.5	4.1	39.1	8.4		5.6	2.1								8.1
DG110-12	2	TMG-N	SKW	22.0	5.5	24.6	3.9	4.0	47.5	10.2	8.1	5.0	1.3								-2.7
DG110-13	2	TMG-N	SKW	20.3	5.5	21.3	4.0	3.6	42.8	10.5	5.6	5.3	1.3	0.82		0.31					-1.3
DG110-14	2	TMG-N	SKW	21.5	5.7	25.3	2.9	3.8	42.6	8.6		4.6	0.8	0.13		3.23					5.9
DG110-2	15	TMG-N	SKW	22.0	5.5	24.6	3.9	4.0	47.5	10.2	20.2	5.0	1.3				-49.5	-7.7			-9.3
DG110-3	12	TMG-N	SKW	21.0	5.6	23.0	3.7	3.0	47.0	10.0	4.0		1.4	8.40		3.30					5.2
DG110-4	9	TMG-N	SKW	18.9	4.8	20.8	3.4	3.6				4.8	1.7	8.89		3.94					100.0
DG110-5	2	TMG-N	SKW	22.0	5.2	16.1	3.9	4.3	45.1	9.5		3.9	1.5								-7.3
DG110-6	2	TMG-N	SKW	21.0	6.2	19.0	4.0	4.2	44.8	6.2		4.9	1.2								0.1
DG110-7	2	TMG-N	SKW	21.1	6.6	20.1	3.9	4.2	44.9	6.5		5.0	1.2								1.2
DG110-8	2	TMG-N	SKW	37.6	3.4	22.3	4.2	5.8	35.0	8.0		5.9	2.2								18.0
DG110-9	2	TMG-N	SKW	19.3	6.1	21.2	3.5	3.4	38.3	8.0		5.6	2.0								6.9
DR2	4	TMG-N	SKW	32.3	6.9	25.9	4.8	26.2	43.5	45.8	123.1	9.6	9.7				-46.5	-7.0			-20.3
KG1-1	15	TMG-N	SKW	39.9	6.7	38.1	8.1	12.0	78.6	11.2	82.9	5.2	9.6	0.25		1.11	-27.7	-6.3		22.4	-12.8
KG1-2	12	TMG-N	SKW	38.0	6.4	33.0	9.5	14.8	79.0	8.1	40.0		11.1	6.10		1.60			1.4		3.9
KG1-3	12	TMG-N	SKW	40.0	6.4	37.0	10.0	13.0	80.0	22.0	31.0		10.0	7.40		1.30					3.9
KG1-4	9	TMG-N	SKW	43.9	6.1	44.7	10.8	11.7			24.3	1.0	10.1	5.37	0.01	1.69			3.2	21.5	77.8
KG1-5	9	TMG-N	SKW	31.8	5.9	36.3	9.0	15.6	85.7	48.8		5.1	10.7	18.4		0.19	-39.0	-7.2	2.3	24.2	8.0
KG1-6	8	TMG-N	SKW	42.4	7.2	41.8	9.2	11.7	92.4	20.6	69.9	4.7	8.4				-37.0	-6.1			-13.6
LD2-1	13	TMG-N	SKW	14.3	6.0	21.0	2.0	3.0	31.0	4.0	22.5	4.1	1.1				-44.5	-7.4			-5.7
LD2-2	15	TMG-N	SKW	13.9	5.8	18.6	2.2	2.4	27.5	3.2	25.2	4.7	0.4				-50.3	-7.4			-9.2
LD2-3	10	TMG-N	SKW	13.5	6.2	18.5	1.4	2.2	26.4	4.1	7.7	4.1	0.4								2.8
RF2-1	13	TMG-N	SKW	11.9	5.7	17.0	2.0	2.0	25.0	4.0	15.0	4.3	0.5				-44.0	-7.1			-3.4

Table A.1. cont. Historical groundwater quality Data

Borehole	Source	Group	Fm	EC	pH	Na	Mg	Ca	Cl	SO4	TAL (mg/L CaCO3)	Si	K	Fe	Al	Mn	δD	$\delta^{18}O$	DO	Temp	Charge
				mS/m													‰	‰	mg/L	°C	Bal %
RF2-2	5	TMG-N	SKW	12.4	5.7	16.4	1.9	2.0	25.8	6.0	31.5	4.5	0.3				-50.3	-7.6			-20.5
RF2-3	10	TMG-N	SKW	13.1	7.0	16.7	1.3	3.0	22.6	3.6	11.7	4.3	0.7								2.7
RF2-4	7	TMG-N	SKW	12.6	5.3	16.0	1.0	2.0	27.0	14.0		4.2	0.5								-8.3
RF8	15	TMG-N	SKW	10.4	5.3	14.8	1.6	1.7	19.9	15.7	9.7	4.7	0.6	0.03	0.09		-40.8	-7.2			-10.5
TM21	8	TMG-N	SKW	10.8	6.6	13.0	2.2	1.5	25.2	10.2	12.7	4.7	0.0				-44.0	-6.8			-17.8
TM24	8	TMG-N	SKW	10.3	6.6	12.5	2.2	1.0	24.4	7.0	9.5	2.7					-28.0	-5.4			-13.8
TM25	8	TMG-N	SKW	9.9	7.4	11.8	1.9	1.4	21.9	5.1	12.5	2.6					-20.0	-3.8			-13.7
TM5	8	TMG-N	SKW	15.6	6.3	18.9	2.1	2.2	36.6	5.3	15.2	3.7					-46.0	-7.0			-13.4
TM6	8	TMG-N	SKW	7.3	6.1	8.2	1.3	0.9	14.3	3.0	10.7	2.2					-36.0	-4.4			-14.5
YR2	15	TMG-N	SKW	18.1	5.6	19.4	3.1	7.0	31.5	20.1	21.7	7.3	4.7	0.01	0.20		-50.6	-7.2			-5.2
97161	2	TMG-N	UNK	23.4	6.7	27.3	4.1	7.4	42.4	19.4	17.6	6.2	3.0								0.4
97161	2	TMG-N	UNK	19.5	5.3	19.1	4.5	5.4	36.5	10.7	12.6	5.4	3.1								1.5
97161	2	TMG-N	UNK	20.8	6.4	24.5	3.8	5.0	36.2	13.7	15.4	4.9	4.2								3.6
97161	2	TMG-N	UNK	19.6	6.0	24.6	3.9	5.6	38.1	20.6	12.7	5.0	2.6								-0.6
TM2	8	TMG-N	UNK	11.2	5.8	12.4	1.8	1.3	23.1	4.6	8.0	2.4					-19.0	-4.6			-9.3
TM3	8	TMG-N	UNK	24.1	6.3	31.0	3.6	2.8	54.9	5.5	26.7	3.1					-22.0	-4.9			-10.4
TM4	8	TMG-N	UNK	38.7	6.4	48.6	5.9	7.7	99.7	6.9	37.5	3.3					-25.0	-5.2			-10.8
TM7	8	TMG-N	UNK	15.5	6.6	16.3	2.5	3.9	32.0	4.7	30.2	3.7	0.1				-19.0	-4.4			-18.1
TM8	8	TMG-N	UNK	17.3	6.2	18.0	3.1	2.5	37.7	3.5	24.2	3.7	2.8				-19.0	-4.6			-13.5
T/W	3	TMG-P	HS	17.2	7.0	12.0	4.0	15.0	24.0		48.0	15.5	6.1	1.44		1.51		-7.2			5.0
T/W-1	6	TMG-P	HS	16.5	7.0	14.0	4.0	11.0	22.0	4.0	149.8	15.1	7.9				-48.0	-7.1			-37.3
T/W-2	10	TMG-P	HS	22.5	6.8	15.4	3.2	10.9	24.6	11.9	117.6	15.1	9.3	0.11		1.74					-31.4
145262	2	TMG-P	PEN	17.4	7.5	18.2	2.0	7.9	27.7	10.8	30.6	4.4	1.7								-7.4
145262	2	TMG-P	PEN	26.3	7.6	15.7	2.1	30.4	24.6	14.0	77.9	9.4	0.8								-3.0
BPT1	1	TMG-P	PEN	2.6	6.5	2.1	1.0	0.8	4.5	5.4	9.5	1.4	0.3								-32.1
G40171	2	TMG-P	PEN	13.6	6.6	14.3	2.1	3.8	20.6	5.6	12.9	4.4	0.6	0.14			-41.8	-7.2			2.5
G40172	2	TMG-P	PEN	13.3	6.5	15.6	2.3	2.5	21.6	8.3	9.4	4.4	0.7	0.14			-41.6	-7.3			2.3
G40173	2	TMG-P	PEN	12.9	6.3	14.6	2.0	2.2	20.5	5.6	8.2	4.0	0.7	0.25		0.16	-45.2	-7.7			4.4
G40175	7	TMG-P	PEN	10.5	5.2	13.0	2.0	3.0	23.0	8.0		4.6	0.9			0.17					5.1
G40175 51M	17	TMG-P	PEN	17.7	7.0	14.5	1.8	9.8	21.9	11.7	67.4	4.6	1.1			0.11	-40.5	-7.0			-26.0
G40175A	2	TMG-P	PEN	13.2	6.2	13.6	2.4	2.4	19.7	10.8	5.1	4.6	1.0			0.19	-42.2	-7.3			2.8
G40175A 23M	17	TMG-P	PEN	16.8	7.1	15.2	1.6	9.7	22.5	14.8	63.2	4.5	1.1	0.31	0.07	0.14	-38.5	-7.1			-25.3
G40175A 27M	17	TMG-P	PEN	14.1	6.8	13.5	2.3	3.2	22.0	8.7	52.2	4.4	1.4			0.09	-39.3	-7.2			-30.9
G40175A 60M	17	TMG-P	PEN	12.1	6.7	11.9	1.5	3.5	16.9	9.8	53.9	2.3	2.6			0.31	-38.7	-7.2			-33.3

Table A.1. cont. Historical groundwater quality Data

Borehole	Source	Group	Fm	EC	pH	Na	Mg	Ca	Cl	SO4	TAL (mg/L CaCO3)	Si	K	Fe	Al	Mn	δD	$\delta^{18}O$	DO	Temp	Charge
				mS/m													‰	‰	mg/L	°C	Bal %
G40175A 84M	17	TMG-P	PEN	11.0	6.6	12.7	2.1	3.5	21.3	12.1	26.5	4.2	1.8			0.51	-38.3	-7.0			-18.7
G40175B 115M	17	TMG-P	PEN	11.8	6.2	13.8	1.6	2.0	20.9	8.6	17.7	4.4	1.1			0.17	-39.5	-7.0			-13.3
G40175C 126M	17	TMG-P	PEN	12.4	6.6	13.4	1.7	2.3	20.8	9.6	21.7	4.6	1.2	0.07		0.20	-40.4	-7.0			-16.8
G40176	2	TMG-P	PEN	13.5	6.4	13.7	2.4	2.9	19.1	7.0	9.0	4.6	0.8			0.01	-44.3	-7.4			5.2
G40176A 42M	17	TMG-P	PEN	14.2	7.0	14.1	2.0	2.9	23.2	7.3	34.7	2.6	1.1			0.50	-42.8	-7.5			-22.5
G40176A 119M	17	TMG-P	PEN	18.2	7.4	15.5	2.2	10.1	22.7	12.3	88.9	5.0	3.0				-42.7	-7.3			-30.1
G40176B 150M	17	TMG-P	PEN	19.0	7.2	15.1	2.2	11.2	21.5	8.1	98.1	5.0	2.7	0.22		0.02	-45.5	-7.3			-30.0
HRIV1	4	TMG-P	PEN	9.7	7.3	11.2	1.8	1.3	15.0	8.0	20.7	3.0	0.4			0.04	-39.9	-6.5			-17.2
HRIVN	4	TMG-P	PEN	9.3	7.2	10.9	1.6	1.1	13.8	4.7	2.7	3.1	0.5				-43.3	-6.7			10.8
HRIVS	4	TMG-P	PEN	9.6	6.7	10.5	2.4	2.4	11.1	23.5	14.0	3.2	1.2			0.42	-42.6	-6.6			-14.7
MPOORT	4	TMG-P	PEN	3.0	6.8	3.6	0.6	0.6	4.1	2.7	0.2	1.5	0.2				-39.3	-5.8			15.6
NM1	3	TMG-P	PEN	13.4	6.0	12.0	4.0	6.0	25.0	4.0	12.0	8.4	1.8	1.12							9.2
Parshall -Ver	5	TMG-P	PEN	12.9	6.2	16.1	2.5	2.1	24.2	3.9	22.0	4.7	0.6				-51.2	-7.7			-7.9
RF1	13	TMG-P	PEN	13.3	5.9	22.0	2.0	2.0	33.0	4.0	25.0	4.7	1.7								-8.9
Spring	9	TMG-P	PEN	14.1	5.9	20.1	2.4	2.1	32.0	6.1		4.7	0.6			0.01					7.2
SPZ1	1	TMG-P	PEN	4.0	7.3	3.0	1.1	2.5	5.1	2.8	14.7	1.5	0.3								-17.0
SPZ3	1	TMG-P	PEN	2.8	6.3	2.0	0.9	0.4	4.5	3.4	9.0	1.4	0.2								-33.7
T/W-3	8	TMG-P	PEN	19.3	6.9	11.6	3.4	10.1	21.5	5.0	113.9	13.9	7.0				-41.0	-6.8			-34.1
TM1	8	TMG-P	PEN	48.5	5.9	64.8	10.3	2.7	124.6	16.4	22.7	4.3	1.9				-19.0	-4.4			-5.6
TM10	8	TMG-P	PEN	17.9	7.1	9.9	5.6	13.3	15.0	14.7	118.6	2.3	0.2				-34.0	-5.8			-33.1
TM11	8	TMG-P	PEN	2.8	7.5	1.9	0.8	0.9	4.1	5.6	11.7	1.0					-34.0	-6.1			-41.4
TM12	8	TMG-P	PEN	2.6	6.9	1.5	0.9	1.1	3.7	6.3	9.5	0.7					-29.0	-5.3			-37.3
TM14	8	TMG-P	PEN	10.1	4.7	10.8	2.0	2.0	21.1	11.7	12.2	2.0					-15.0	-3.6			-19.2
TM15	8	TMG-P	PEN	10.0	5.2	11.4	2.2	1.0	22.8	8.2	12.2	3.0					-16.0	-3.9			-18.6
TM16	8	TMG-P	PEN	11.1	6.0	13.0	2.3	1.2	26.6	5.1	8.7	2.7					-20.0	-4.6			-11.7
TM17	8	TMG-P	PEN	11.6	6.2	13.1	2.2	2.3	24.4	5.1	26.7	3.9	0.3				-43.0	-7.2			-20.7
TM22	8	TMG-P	PEN	8.8	7.0	8.8	2.7	1.4	20.8	5.8	10.0	2.4					-29.0	-4.8			-14.7
TM23	8	TMG-P	PEN	3.6	6.6	2.8	1.1	1.3	5.8	2.8	16.2	3.7					-36.0	-6.7			-32.7
TM26	8	TMG-P	PEN	5.3	5.7	4.7	1.0	4.7	11.2	96.9	43.0	1.5					-18.0	-3.9			-71.9
UKK1	1	TMG-P	PEN	2.9	6.7	2.9	1.0	0.9	5.2	3.8	15.7	1.5	0.3								-34.9
VR11-1	13	TMG-P	PEN	9.5	5.9	11.0	2.0	1.0	19.0	4.0	17.5	4.4	1.6				-35.5	-7.1		18.8	-13.8
VR11-2	16	TMG-P	PEN	9.0	4.3	11.0	1.9	1.0	20.0	2.5	3.5	3.7	0.5				-42.1	-7.1	5.8		0.8
VR11-3	15	TMG-P	PEN	7.5	6.7	10.9	1.0	1.3	14.6	2.1	8.5	4.3	0.4				-51.1	-7.2			0.4
VR11-4	12	TMG-P	PEN	9.0	4.9	10.0	1.6	1.3	19.0	2.8	3.0		0.6	0.10					5.6		-0.3

Table A.1. cont. Historical groundwater quality Data

Borehole	Source	Group	Fm	EC	pH	Na	Mg	Ca	Cl	SO4	TAL (mg/L CaCO3)	Si	K	Fe	Al	Mn	δD	$\delta^{18}O$	DO	Temp	Charge
				mS/m													‰	‰	mg/L	°C	Bal %
VR11-5	9	TMG-P	PEN	27.1	6.2						12.7								0.5	16.7	-100.0
VR11-6	7	TMG-P	PEN	9.2	5.5	10.0	2.0	1.0	18.0	15.0		4.1	0.6			0.00					-10.5
VR6-1	13	TMG-P	PEN	11.5	6.0	14.0	2.0	2.0	21.0	4.0	22.5	4.0	1.2	0.18			-48.1	-7.7			-10.5
VR6-2	16	TMG-P	PEN	10.4	4.5	14.0	1.9	1.3	23.0	2.3	5.0	3.5	0.4				-43.4	-7.4	5.0		2.7
VR6-3	15	TMG-P	PEN	11.5	6.0	14.0	2.0	2.0	21.0	4.0	22.5	4.0	1.2				-48.1	-7.7			-10.9
VR6-4	14	TMG-P	PEN	9.0	6.2	11.9	2.0	5.1	19.6	2.7	11.0	3.5	0.8								7.1
VR6-5	9	TMG-P	PEN	8.9	5.8	14.3	1.4	1.2			6.3	1.8	0.3	0.08		0.00				16.1	73.3
VR6-6	12	TMG-P	PEN	10.0	5.0	13.0	1.5	1.7	22.0	2.2	4.3	0.4	0.10			0.05			4.8		2.3
VR6-7	9	TMG-P	PEN	10.0	4.3	11.8	1.3	1.6	21.8	1.8		4.1	0.7			0.00	-40.0	-7.4			4.6
VR6-8	11	TMG-P	PEN	10.9	6.6	12.2	2.0	2.3	20.0	2.4	21.5	5.0	2.0				-41.0	-7.3			-9.6
VR6-9	7	TMG-P	PEN	10.1	6.3	11.0	2.0	2.0	20.0		12.5	3.9	0.4								-3.9
VR7-1	13	TMG-P	PEN	9.5	6.2	12.0	2.0	2.0	18.0	4.0	22.5	3.7	1.2	0.18			-45.2	-7.6			-11.6
VR7-2	16	TMG-P	PEN	8.8	4.5	11.0	1.8	1.2	19.0	2.3	5.8	3.6	0.3	0.05			-44.2	-7.3	5.6		-0.3
VR7-3	15	TMG-P	PEN	9.0	5.5	9.0	2.0	2.0	17.0	1.0	15.0	4.6	0.3				-45.2	-7.6			-9.3
VR7-4	12	TMG-P	PEN	8.0	5.1	11.0	1.4	1.5	19.0	1.6	4.5		0.3	0.10					5.6		1.5
VR7-5	9	TMG-P	PEN	8.8	4.2	10.5	1.2	1.6	18.8	1.5		4.1	0.5			0.01	-42.0	-8.1			6.9
VR7-6	2	TMG-P	PEN	14.1	7.2	13.6	1.6	5.4	19.4	4.5	14.4	4.1	1.7								5.5
VR7-6	11	TMG-P	PEN	10.8	6.6	13.4	2.5	2.5	19.3	18.9	31.0	4.8	0.3				-42.0	-7.2		20.3	-25.7
VR7-7	2	TMG-P	PEN	9.0	5.5	9.4	1.8	2.1	17.3		6.0	4.6	0.3								4.9
VR7-7	10	TMG-P	PEN	14.1	7.2	13.6	1.6	5.4	19.4	4.5	36.0	4.1	1.7				-52.7	-7.7			-13.5
VR8-1	13	TMG-P	PEN	8.9	5.9	9.0	2.0	2.0	22.0	8.0	10.0	3.8	1.2	0.21							-17.4
VR8-2	16	TMG-P	PEN	8.6	5.0	10.0	1.8	1.2	19.0	2.4	4.8	3.8	0.5				-40.1	-7.2	4.9		-1.9
VR8-3	12	TMG-P	PEN	8.0	4.8	10.0	1.5	1.3	18.0	2.4	2.0		0.6	0.10					4.7		3.6
VR8-4	9	TMG-P	PEN	9.4	3.7	8.4	1.0	1.3	17.3	2.4		4.3	0.5			0.01					-1.1
VR8-5	11	TMG-P	PEN	8.3	7.0	10.8	1.9	2.3	16.9	1.9	18.2	4.9	0.2				-39.0	-7.1		22.7	-8.3
VR8-6	7	TMG-P	PEN	8.9	5.4	10.0	1.0	2.0	17.0			4.2	0.6				-49.7	-7.3			13.7

A.1.2 Rock chemistry

Table A.2. Results (mol %) of microanalysis of rocks and tentative mineralogy

Sample	Si	Al	K	Fe	O	Si:O	Si:Al	(Si+Al):O	Fe:O	K:O	Mineral
C1	20.7	9.9	4.7	3.1	61.6	0.3	2.1	0.5	0.1	0.1	Ca-Fs
C1	27.1	4.6	2.8	1.5	64.0	0.4	5.9	0.5	0.0	0.0	Ca-Fs
B1	28.6	3.9	2.3	0.5	64.7	0.4	7.4	0.5	0.0	0.0	Ca-Fs
G1	13.6	17.1	0.1	2.3	60.9	0.2	0.8	0.5	0.0	0.0	Chlorite
G1	16.7	18.9	0.8	0.6	62.8	0.3	0.9	0.6	0.0	0.0	Chlorite
G1	15.9	11.6	1.2	8.5	60.6	0.3	1.4	0.5	0.1	0.1	Chlorite-Fe
C1	16.6	9.5	1.9	8.9	60.3	0.3	1.7	0.4	0.1	0.1	Chlorite-Fe
C2	20.2	9.3	1.0	6.3	62.1	0.3	2.2	0.5	0.1	0.0	Chlorite-Fe
G1	1.4	1.1	0.1	45.9	51.1	0.0	1.3	0.0	0.9	0.0	Fe
G1	0.7	0.7	0.1	47.9	50.6	0.0	1.1	0.0	0.9	0.0	Fe
P1	11.2	0.4	0.7	32.1	55.5	0.2	25.1	0.2	0.6	0.1	Fe
G1	3.4	0.5	1.2	43.4	51.5	0.1	6.5	0.1	0.8	0.4	Fe
G1	2.2		0.4	46.4	51.0	0.0		0.0	0.9	0.0	Fe
P1	9.9		1.3	34.2	54.6	0.2		0.2	0.6	0.0	Fe
P1	8.3		0.0	37.6	54.1	0.2		0.2	0.7	0.0	Fe
G1	9.0	6.6	1.1	27.4	55.9	0.2	1.4	0.3	0.5	0.0	Fe
G1	9.7	4.4	1.3	28.8	55.6	0.2	2.2	0.3	0.5	0.0	Fe
G1	9.2	3.5	1.0	31.1	55.2	0.2	2.7	0.2	0.6	0.0	Fe
G1	25.8	5.1	3.0	2.2	63.5	0.4	5.0	0.5	0.0	0.0	Feldspar
G1	23.0	6.9	2.4	5.2	62.6	0.4	3.3	0.5	0.1	0.1	Feldspar
C2	19.6	8.7	6.7	2.9	60.9	0.3	2.3	0.5	0.0	0.3	Feldspar
C2	19.8	9.3	6.1	2.2	61.3	0.3	2.1	0.5	0.0	0.3	Feldspar
B1	26.0	6.0	3.7	0.7	63.6	0.4	4.3	0.5	0.0	0.1	Feldspar
B1	28.7	3.6	2.6	0.6	64.6	0.4	8.0	0.5	0.0	0.1	Feldspar
G1	19.6	11.2	6.3	1.8	61.0	0.3	1.8	0.5	0.0	0.3	Feldspar
C1	19.7	10.7	5.9	2.6	61.0	0.3	1.8	0.5	0.0	0.3	Feldspar
G1	20.2	10.7	5.3	2.2	61.5	0.3	1.9	0.5	0.0	0.1	Feldspar
G1	21.0	10.5	5.7	1.0	61.7	0.3	2.0	0.5	0.0	0.1	Feldspar
G1	15.5	13.6	7.5	3.3	59.3	0.3	1.1	0.5	0.1	0.1	Musc
G1	15.0	12.0	6.0	7.1	59.0	0.3	1.3	0.5	0.1	0.1	Musc
G1	16.7	13.4	6.6	1.4	60.2	0.3	1.2	0.5	0.0	0.1	Musc
G1	16.2	13.6	7.9	1.8	59.6	0.3	1.2	0.5	0.0	0.1	Musc
G1	16.4	16.6	3.6	1.5	61.4	0.3	1.0	0.5	0.0	0.1	Musc
G1	15.8	15.7	7.1	0.6	60.1	0.3	1.0	0.5	0.0	0.1	Musc
G1	15.6	16.2	6.2	0.3	60.2	0.3	1.0	0.5	0.0	0.1	Musc
G1	15.8	15.6	6.5	0.4	60.2	0.3	1.0	0.5	0.0	0.1	Musc
G1	16.6	10.8	7.9	5.8	59.0	0.3	1.5	0.5	0.1	0.1	Musc
G1	32.2	0.9	0.6	0.1	66.2	0.5	37.3	0.5	0.0	0.0	Quartz
G1	33.2	0.0	0.0	0.1	66.6	0.5	675.5	0.5	0.0	0.0	Quartz
G1	33.3	0.0	0.0	0.0	66.6	0.5		0.5	0.0	0.0	Quartz
S1	32.4	0.6	0.5	0.2	66.2	0.5	55.3	0.5	0.0	0.0	Quartz
P1	32.3	0.7	0.6	0.3	66.1	0.5	49.6	0.5	0.0	0.0	Quartz
P1	30.6	2.4	1.3	0.3	65.5	0.5	12.9	0.5	0.0	0.0	Quartz
C1	31.7		0.8	1.3	65.9	0.5		0.5	0.0	0.0	Quartz
C1	33.1		0.0	0.4	66.5	0.5		0.5	0.0	0.0	Quartz
P1	32.9	0.3	0.4	0.1	66.4	0.5	123.9	0.5	0.0	0.0	Quartz
G1	30.5		1.3	0.6	65.2	0.5		0.5	0.0	0.0	Quartz
B1	32.9	0.3	0.3	0.1	66.4	0.5	103.7	0.5	0.0	0.0	Quartz
S1	33.1		0.2	0.3	66.5	0.5		0.5	0.0	0.0	Quartz
P1	33.1		0.2	0.3	66.5	0.5		0.5	0.0	0.0	Quartz
C2	31.7	1.3	0.6	0.3	66.0	0.5	23.8	0.5	0.0	0.0	Quartz
B1	33.2	0.0	0.2	0.1	66.5	0.5		0.5	0.0	0.0	Quartz
S1	17.5	0.0	0.1	23.6	58.7	0.3		0.3	0.4	0.0	Qtz coated?

Table A.3. Full dataset of rock geochemistry as determined by XRF (all except TC from Mitchell, 2005)

Sample	P1	P2	P3	P4	P5	P6	C1	C2	C3	C4	C5	
SiO_2	97.39	95.58	96.74	96.23	93.26	98.06	61.91	59.64	57.27	57.63	72.26	
Al_2O_3	1.27	2.27	1.70	1.97	2.91	0.88	15.66	19.03	21.96	19.47	13.17	
TiO_2	0.04	0.11	0.06	0.10	0.16	0.28	0.86	0.96	0.90	1.02	0.72	
Fe_2O_3	0.39	0.53	0.49	0.47	0.90	0.59	6.82	6.44	6.50	6.81	5.44	
MnO	0.02	0.02	0.02	0.02	0.03	0.02	0.07	0.04	0.14	0.04	0.06	
MgO	0.17	0.28	0.22	0.22	0.27	0.19	1.84	2.61	1.67	2.22	1.22	
CaO	0.01	0.02	0.02	0.02	0.02	0.02	1.40	0.03	0.02	0.25	0.05	
Na_2O	0.17	0.12	0.13	0.10	0.21	0.17	0.30	0.79	0.28	0.31	0.23	
K_2O	0.23	0.60	0.45	0.49	0.73	0.18	3.96	4.94	5.34	5.86	3.23	
P_2O_5	0.01	0.01	0.01	0.01	0.03	0.02	1.23	0.12	0.12	0.42	0.05	
SO_3	0.00	0.00	0.02	0.00	0.02	0.00	0.00	0.00	0.00	0.00	0.02	
Cr_2O_3	0.01	0.01	0.01	0.01	0.01	0.01	0.02	0.02	0.03	0.02	0.02	
NiO	0.00	0.00	0.00	0.00	0.01	0.00	0.01	0.00	0.01	0.01	0.00	
H_2O-	0.07	0.03	0.04	0.04	0.05	0.06	0.84	0.44	0.93	0.37	0.24	
LOI	0.22	0.37	0.25	0.28	0.53	0.18	4.45	4.26	4.45	4.71	3.26	
Total	**100.01**	**99.96**	**100.16**	**99.95**	**99.15**	**100.67**	**99.35**	**99.32**	**99.63**	**99.15**	**99.98**	
S (ppm)	4.08	4.53	3.54	9.89	21.60	2.75	49.75	21.63	23.26	165.50	43.30	
TC	0.073	0.059	0.082	0.041	nd	nd	0.137	0.177	0.209	0.306	0.083	

Sample	G1	G2	G3	G4	S1	S2	S3	B4	B6	B7	B1	B2
SiO_2	60.81	97.16	78.92	83.15	93.32	97.26	98.33	88.78	92.70	91.33	71.37	67.58
Al_2O_3	20.20	1.06	11.99	5.22	3.11	1.67	0.79	6.18	3.41	5.03	13.82	16.68
TiO_2	0.92	0.33	0.59	0.57	0.20	0.11	0.16	0.10	0.26	0.16	1.16	0.96
Fe_2O_3	6.54	0.67	1.62	6.47	0.60	0.43	0.45	0.60	0.73	0.60	3.38	2.75
MnO	0.04	0.02	0.02	0.05	0.02	0.02	0.02	0.03	0.02	0.02	0.02	0.03
MgO	0.83	0.21	0.65	0.54	0.22	0.16	0.16	0.33	0.36	0.35	0.86	1.80
CaO	0.02	0.03	0.04	0.02	0.02	0.03	0.02	0.02	0.02	0.10	0.14	0.23
Na_2O	0.43	0.28	0.26	0.38	0.18	0.19	0.14	0.22	0.16	0.19	0.41	0.98
K_2O	5.84	0.20	3.85	0.62	0.79	0.08	0.03	1.95	0.79	1.70	5.65	4.07
P_2O_5	0.04	0.02	0.05	0.04	0.01	0.02	0.01	0.01	0.01	0.01	0.08	0.08
SO_3	0.01	0.00	0.00	0.02	0.00	0.00	0.00	0.00	0.00	0.00	0.01	0.00
Cr_2O_3	0.02	0.01	0.02	0.01	0.01	0.01	0.01	0.01	0.01	0.01	0.02	0.02
NiO	0.01	0.00	0.01	0.01	0.00	0.03	0.00	0.00	0.00	0.07	0.00	0.00
H_2O-	0.11	0.07	0.03	0.12	0.08	0.04	0.02	0.06	0.24	0.07	0.66	0.72
LOI	3.22	0.20	2.02	1.78	0.56	0.29	0.16	1.00	1.00	0.71	2.68	3.75
Total	**99.06**	**100.27**	**100.08**	**99.00**	**99.13**	**100.34**	**100.31**	**99.29**	**99.71**	**100.36**	**100.27**	**99.68**
S (ppm)	101.5	1.6	22.5	193.1	3.4	136.9	53.5	59.5	13.6	29.1	426.4	90.2
TC	0.126	0.057	0.081	0.061	nd	nd	nd	0.093	0.126	0.219	nd	0.088

A.2 Leach data

Table A.4. Leach data for aerobic leaching experiments (Fe in mmol/kg dry mass rock)

	DL17			pH 3 Organic			pH 5 Organic		
Time	Fe	pH	pe	Fe	pH	pe	Fe	pH	pe
Sample B1									
24	0.97	5.00	7.96	6.92	3.12	7.68	1.90	4.97	7.53
120	0.86	5.01	7.99	4.28	3.14	8.13	1.56	5.01	7.79
216	1.50	5.01	8.01	2.13	3.15	8.40	1.79	5.01	7.75
374	0.57	5.01	8.28	0.52	3.16	8.42	0.60	5.01	8.04
710	0.91	5.00	8.66	2.25	3.18	8.91	1.66	5.00	8.35
1214	0.16	5.04	8.87	2.03	3.24	9.35	1.33	5.04	8.51
1958	0.26	5.03	8.25	1.59	3.26	8.53	0.58	5.02	7.79
2726	0.05	5.13	8.45	1.57	3.26	9.54	0.21	5.11	8.74
Sample B2									
24	0.37	5.00	8.23	3.14	3.21	8.30	0.69	5.00	7.99
120	0.34	5.02	8.35	2.33	3.32	8.27	0.77	5.02	8.08
216	1.16	5.03	7.89	1.37	3.35	8.37	0.85	5.03	7.41
374	0.36	5.02	8.70	1.19	3.42	8.23	0.20	5.02	8.20
710	2.93	5.02	8.72	1.64	3.50	7.85	2.39	5.02	8.31
1214	0.17	5.01	8.99	1.54	3.63	7.77	0.18	5.08	8.44
1958	0.16	4.97	8.25	0.68	3.74	8.04	0.24	4.99	7.72
2726	0.01	5.06	7.80	0.35	3.73	8.83	0.13	5.13	8.54
Sample B4									
24	0.09	5.00	8.77	13.13	3.10	7.42	0.56	4.99	8.16
120	0.25	5.01	10.06	7.10	3.10	7.97	1.01	5.01	8.00
216	0.65	5.01	8.31	3.62	3.08	8.40	1.04	5.00	7.55
374	0.60	5.00	8.65	2.29	3.08	8.56	0.71	5.00	7.97
710	0.63	4.99	8.82	2.79	3.14	8.92	0.78	4.99	8.13
1214	0.25	5.03	9.04	2.33	3.19	9.59	1.00	5.035	8.36
1958	0.18	4.97	8.33	2.08	3.14	8.66	0.75	4.96	7.92
2726	0.04	5.04	8.45	2.24	3.125	9.91	0.33	5.05	8.72
Sample B7									
24	1.13	5.00	8.13	11.80	3.19	7.49	1.61	4.99	7.77
120	1.16	5.01	8.10	7.30	3.10	7.97	1.71	5.02	7.72
216	1.14	5.01	7.82	4.89	3.07	8.39	1.66	5.00	7.27
374	1.30	5.01	7.91	1.04	3.08	8.65	1.30	5.01	7.67
710	1.07	5.00	8.13	2.88	3.11	8.89	1.27	5.00	7.84
1214	0.83	5.03	8.27	2.54	3.15	9.26	0.84	5.04	8.08
1958	0.55	4.98	8.28	2.18	3.16	8.58	0.83	4.99	7.75
2726	0.30	5.04	8.21	2.43	3.14	9.37	0.54	5.08	8.55
Sample C1									
24	0.00	5.01	9.67	2.50	3.15	10.28	0.25	5.00	9.59
120	0.03	5.02	9.20	2.25	3.23	9.61	0.53	5.02	9.19
216	1.59	5.01	8.70	1.21	3.27	8.85	1.23	4.99	8.55
374	0.08	5.00	9.08	0.38	3.33	8.96	0.15	4.99	8.92
710	0.73	5.01	9.26	1.45	3.41	9.24	0.44	4.98	9.25
1214	0.52	5.06	9.25	1.69	3.51	9.80	0.40	5.03	9.20
1958	0.40	5.00	8.39	1.37	3.58	8.46	1.58	4.97	8.03
2726	0.01	5.07	8.84	0.54	3.66	10.05	0.04	5.06	8.98
Sample C2									
24	0.03	5.00	9.06	4.01	3.20	7.70	0.23	5.00	8.90
120	0.05	5.01	8.89	3.00	3.30	7.75	0.14	5.02	8.59
216	0.13	5.00	8.44	2.40	3.33	7.87	0.20	5.01	7.87
374	0.11	5.00	8.65	0.42	3.40	7.94	0.20	5.01	8.23
710	0.16	5.01	8.74	1.00	3.50	8.28	0.30	5.00	8.43
1214	0.08	5.06	8.85	0.62	3.70	8.53	0.26	5.05	8.53
1958	0.09	5.01	8.27	0.32	3.98	7.99	0.34	4.99	7.75
2726	0.05	5.1	8.38	0.15	4.23	9.10	0.05	5.08	8.67

Table A.4 cont. Leach data for aerobic leaching experiments (Fe in mmol/kg dry mass of rock)

		DL17			pH 3 Organic			pH 5 Organic	
Time	Fe	pH	pe	Fe	pH	pe	Fe	pH	pe
Sample G1									
24	0.41	5.01	8.25	7.35	3.12	7.48	0.78	4.96	8.00
120	1.62	5.02	7.76	3.24	3.17	8.10	1.17	5.02	7.67
216	1.62	5.01	7.74	1.60	3.18	8.46	1.24	5.01	7.58
374	1.17	5.00	7.91	0.49	3.17	8.61	0.80	5.00	7.81
710	1.12	5.00	8.07	2.12	3.19	8.86	0.78	4.99	8.07
1214	0.51	5.03	8.26	2.09	3.23	9.64	0.41	5.04	8.25
1958	0.26	4.97	8.36	1.53	3.22	8.61	0.53	4.97	8.02
2726	0.10	5.04	8.71	1.54	3.255	10.03	0.09	5.03	8.89
Sample G2									
24	0.00	5.00	9.85	12.03	3.08	7.42	0.25	4.99	8.99
120	0.10	5.00	9.68	6.77	3.10	8.01	0.23	5.01	8.99
216	0.33	5.01	8.66	2.68	3.08	8.37	0.25	5.00	8.59
374	0.37	5.00	9.01	0.99	3.13	8.78	0.17	4.99	8.78
710	0.18	4.99	9.17	2.86	3.08	9.13	0.32	4.99	9.03
1214	0.06	5.03	9.23	2.41	3.14	9.97	0.33	5.03	8.83
1958	0.09	4.96	8.34	2.24	3.17	8.71	0.43	4.98	7.99
2726	0.01	5.05	8.71	2.49	3.12	10.02	0.10	5.06	8.86
Sample P1									
24	0.66	5.01	8.27	14.27	3.13	7.15	0.82	4.99	7.97
120	0.73	5.01	8.25	6.84	3.12	7.92	0.85	5.01	7.96
216	1.11	5.01	8.08	4.36	3.11	8.42	0.96	5.01	7.92
374	1.12	5.01	8.22	0.85	3.10	8.75	0.71	4.99	8.11
710	0.97	5.00	8.25	2.63	3.12	9.00	0.84	4.99	8.16
1214	0.77	5.03	8.39	2.18	3.16	9.51	0.67	5.04	8.77
1958	0.60	4.96	8.32	2.03	3.17	8.61	0.68	4.96	7.96
2726	0.40	5.05	8.66	2.02	3.16	9.97	0.50	5.05	8.72
Sample P3									
24	0.32	5.01	8.53	14.54	3.17	7.10	0.65	5.00	8.23
120	0.44	5.01	8.27	6.91	3.12	7.96	1.00	5.01	7.82
216	0.91	5.01	8.44	4.33	3.12	8.34	0.99	5.00	7.92
374	0.84	5.00	8.51	0.96	3.10	8.73	0.87	4.99	8.08
710	0.84	4.98	8.52	2.54	3.10	8.96	1.09	4.98	8.16
1214	0.61	5.02	8.56	2.24	3.14	9.54	0.78	5.03	8.20
1958	0.40	4.98	8.42	1.90	3.15	8.73	0.79	4.98	8.04
2726	0.26	5.03	8.83	2.00	3.16	10.16	0.56	5.06	8.76
Sample S1									
24	0.52	5.00	8.23	13.85	3.12	6.93	0.98	4.99	7.92
120	0.72	5.00	8.27	7.20	3.11	7.91	1.05	5.01	8.03
216	0.93	4.99	8.13	4.64	3.10	8.42	1.04	4.99	7.85
374	0.99	4.99	8.30	0.92	3.08	8.71	0.86	4.99	8.08
710	0.73	4.99	8.38	2.43	3.10	9.12	0.94	5.00	8.18
1214	0.56	5.02	8.49	2.09	3.14	9.83	0.75	5.04	8.25
1958	0.50	4.96	8.32	1.88	3.15	8.58	0.77	4.97	7.92
2726	0.29	5.03	8.67	1.95	3.14	9.90	0.55	5.05	8.74
Sample S2									
24	0.04	5.00	9.63	16.00	3.14	7.22	0.39	4.99	8.25
120	0.06	4.99	9.32	8.29	3.10	7.80	0.60	5.01	8.06
216	0.35	4.99	9.18	4.88	3.11	8.27	0.71	4.98	8.23
374	0.26	4.99	9.47	1.13	3.07	8.73	0.52	4.99	8.28
710	0.27	4.98	9.66	2.50	3.08	9.00	0.68	4.98	8.26
1214	0.10	5.03	9.52	2.09	3.12	9.59	0.47	5.04	8.25
1958	0.12	4.97	8.39	1.96	3.13	8.71	0.45	5.00	8.03
2726	0.03	5.03	8.86	2.02	3.13	10.11	0.36	5.08	8.88

Table A.5. Leach data for anaerobic leaching experiments (Fe in mmol/kg dry mass of rock)

		DL17			pH 3 Organic			pH 5 Organic	
Time	Fe	pH	pe	Fe	pH	pe	Fe	pH	pe
Sample B1									
24	5.83	4.95	0.17	8.86	3.11	4.71	5.79	4.97	-0.40
120	5.75	4.96	0.61	8.45	3.14	5.29	5.54	4.97	0.55
216	3.81	4.96	0.03	7.97	3.14	6.36	4.60	4.98	-0.04
374	4.40	4.95	-0.80	8.16	3.54	2.92	4.32	4.96	0.63
710	5.13	4.96	-0.50	8.03	3.11	4.23	5.41	4.97	-0.53
1214	4.44	4.99	-0.42	7.46	3.26	5.21	4.77	5.03	-1.28
1958	4.09	4.95	1.59	7.24	3.23	6.32	4.37	4.97	2.56
2726	4.64	5.00	-3.46	7.65	3.27	4.30	4.46	5.01	-3.47
Sample B2									
24	1.23	nd	nd	4.28	3.22	5.19	1.31	4.98	-0.85
120	1.03	4.97	0.12	3.45	3.33	5.81	1.22	5.00	-0.06
216	1.17	4.96	-1.24	0.80	3.39	5.83	0.23	4.99	0.60
374	0.87	4.95	-1.45	1.04	3.45	3.55	0.90	4.97	2.20
710	0.90	4.97	-1.00	2.06	3.56	-0.09	0.94	4.99	-0.81
1214	0.80	5.00	-1.59	1.85	3.67	1.70	0.79	5.02	0.96
1958	0.67	4.95	0.63	1.72	3.76	6.39	0.85	4.98	3.23
2726	0.72	5.01	-3.44	1.32	3.86	3.55	0.93	5.03	-3.30
Sample B4									
24	1.97	nd	nd	16.74	3.06	4.05	5.38	4.97	-0.67
120	15.93	4.98	-0.30	18.57	3.11	5.78	17.22	5.00	-0.33
216	14.26	4.99	0.06	15.64	3.10	5.97	14.12	4.99	0.54
374	14.01	4.96	-2.22	14.60	3.08	5.32	15.64	4.97	-0.07
710	15.72	4.97	-0.75	17.07	3.12	4.18	16.44	4.98	-0.65
1214	15.31	5.00	-1.49	16.51	3.155	4.97	14.75	5.03	-0.24
1958	14.48	4.96	0.83	15.82	3.17	6.36	14.70	4.97	2.33
2726	13.69	5.01	-3.46	14.68	3.185	3.90	14.05	5.02	-3.45
Sample B7									
24	12.08	nd	nd	20.48	3.10	2.95	16.45	4.97	-1.48
120	17.58	4.97	0.89	19.40	3.10	4.09	18.11	5.00	1.32
216	14.43	4.96	0.03	15.24	3.11	5.96	14.40	4.99	0.32
374	14.76	4.94	-1.45	16.00	3.08	5.12	14.31	4.97	0.89
710	16.21	4.98	-1.37	17.89	3.11	2.93	16.52	4.98	-0.83
1214	14.09	5.00	-0.45	16.75	3.16	3.81	14.56	5.01	-0.13
1958	14.49	4.96	0.85	16.52	3.18	6.74	14.79	4.98	2.90
2726	13.85	5.00	-3.46	15.77	3.18	5.26	14.20	5.04	-3.44
Sample C1									
24	0.14	nd	nd	2.52	3.11	6.35	0.11	4.96	0.10
120	0.22	4.97	-0.84	1.37	3.23	7.02	0.52	4.98	0.73
216	0.75	4.97	-0.13	1.47	3.29	6.37	0.56	4.99	0.06
374	0.10	4.94	-2.80	0.46	3.36	5.94	0.13	4.96	-0.84
710	0.48	4.96	-1.29	2.56	3.54	4.47	0.47	4.97	-0.04
1214	0.99	4.98	0.13	3.72	3.765	4.04	1.52	5.01	-0.33
1958	0.29	4.96	0.82	4.74	4.02	4.90	0.64	4.97	1.58
2726	0.04	5.00	-3.45	5.50	4.24	-1.60	0.04	5.01	-3.46
Sample C2									
24	0.20	nd	nd	7.62	3.22	5.21	0.21	4.95	1.51
120	0.18	4.97	-0.73	13.82	3.38	3.09	0.26	4.99	2.14
216	0.21	4.96	0.17	13.75	3.45	3.16	0.38	4.98	0.34
374	0.29	4.95	-1.11	15.56	3.13	5.67	0.45	4.95	0.58
710	0.63	4.95	-0.33	26.11	3.77	-1.34	0.73	4.96	-0.47
1214	0.51	4.97	-0.04	28.37	4	-0.21	0.73	5.01	-0.01
1958	0.68	4.94	0.96	30.71	4.23	5.29	0.91	4.99	2.80
2726	0.63	4.99	-3.44	30.33	4.38	-0.19	0.98	5.02	-3.47

Table A.5 cont. Leach data for anaerobic leaching experiments (Fe in mmol/kg dry mass of rock)

		DL17			pH 3 Organic			pH 5 Organic	
Time	Fe	pH	pe	Fe	pH	pe	Fe	pH	pe
Sample G1									
24	8.24			10.49	3.18	4.49	7.88	4.96	-0.36
120	9.94	4.96	-0.75	10.12	3.18	5.48	8.58	4.98	0.37
216	6.99	4.97	0.20	8.91	3.18	5.81	7.35	4.99	0.25
374	6.68	4.95	-1.67	8.64	3.16	5.38	6.64	4.96	-1.51
710	7.90	4.96	-1.35	9.41	3.22	4.14	6.22	4.97	-0.81
1214	7.43	4.98	-1.58	11.44	3.25	4.85	7.69	5.01	-1.24
1958	7.07	4.96	0.85	9.13	3.28	5.95	7.54	4.98	1.71
2726	6.89	5.01	-3.47	7.77	3.36	2.40	7.01	5.01	-3.47
Sample G2									
24	0.11			18.97	3.06	5.64	0.21	4.96	0.46
120	0.04	4.95	-0.64	16.88	3.09	6.44	0.32	4.97	1.73
216	0.37	4.95	-0.14	14.42	3.09	6.41	0.59	4.97	0.03
374	0.17	4.93	-2.41	13.45	3.07	6.08	0.91	4.95	-0.35
710	0.21	5.02	0.08	16.02	3.10	6.01	19.12	4.99	-0.19
1214	0.14	4.98	0.12	15.62	3.13	5.86	18.02	5.03	-0.26
1958	0.11	4.94	1.10	15.04	3.15	6.22	16.84	4.99	1.87
2726	0.06	4.99	-3.44	14.17	3.21	4.13	16.11	5.02	-3.49
Sample P1									
24	0.73			33.11	3.13	3.98	1.09	4.95	-0.21
120	1.03	4.95	-0.92	28.18	3.16	5.64	18.60	5.00	0.44
216	1.33	4.96	-0.45	16.59	3.16	5.72	25.57	5.00	0.03
374	2.81	4.93	-3.07	21.41	3.13	5.36	23.87	4.98	-1.83
710	30.38	4.95	-0.60	28.32	3.17	3.99	28.49	4.99	-0.21
1214	28.47	5.01	-0.40	26.53	3.21	4.55	26.48	5.03	-1.07
1958	26.4	4.98	0.61	25.72	3.23	6.15	25.21	5.00	1.97
2726	25.51	5.02	-3.49	23.30	3.23	4.06	24.39	5.03	-3.51
Sample P3									
24	0.77			16.84	3.12	3.47	1.54	4.96	0.48
120	16.65	4.98	-0.42	35.55	3.15	5.50	39.20	5.00	0.65
216	34.23	4.99	0.06	19.71	3.16	5.77	33.45	5.02	1.37
374	33.65	4.93	-3.01	24.80	3.13	5.64	35.14	4.98	-1.23
710	38.84	4.99	-1.22	34.91	3.17	5.19	36.48	5.00	-0.62
1214	34.64	5.01	-2.50	34.73	3.26	5.12	34.86	5.04	-0.40
1958	33.15	4.97	1.22	33.55	3.27	5.72	33.02	5.00	1.97
2726	31.59	5.01	-3.47	32.33	3.21	2.88	32.47	5.04	-3.47
Sample S1									
24	0.71			16.64	3.12	3.40	0.99	4.95	0.36
120	1.30	4.96	2.57	32.47	3.14	5.36	8.47	4.97	1.41
216	0.96	4.95	0.12	20.46	3.15	5.77	31.17	5.01	0.94
374	1.21	4.94	1.51	23.52	3.12	5.31	31.75	4.98	-1.83
710	1.24	4.95	0.63	31.85	3.16	3.51	35.64	5.00	-0.53
1214	1.20	4.97	0.67	32.66	3.18	4.26	32.77	5.02	-1.33
1958	33.0	4.98	0.27	30.94	3.21	6.24	31.57	5.01	2.18
2726	32.89	5.01	-3.44	29.15	3.21	4.23	30.15	5.04	-3.47
Sample S2									
24	1.16			17.05	3.10	4.00	1.02	4.95	0.10
120	0.82	4.96	-0.90	32.59	3.13	5.55	5.97	4.97	0.37
216	0.88	4.95	0.30	20.28	3.14	5.81	33.60	5.00	0.44
374	1.05	4.91	-3.05	25.73	3.11	5.65	34.48	4.98	-1.40
710	1.22	4.94	-1.30	36.22	3.12	5.29	36.95	5.00	-0.65
1214	1.48	4.97	-1.66	35.29	3.16	5.36	35.33	5.03	-0.11
1958	33.7	4.98	0.27	33.54	3.20	5.89	33.25	4.99	1.59
2726	34.24	5.01	-3.46	31.02	3.19	3.02	32.41	5.01	-3.47

A.3 Column reactor data

A.3.1 Breakthrough curves

The E(t) curve was calculated by integrating the F-curve for each time interval i.e.:

$$E(t) = \frac{F_{t2} - F_{t1}}{t_2 - t_1}$$

This E(t) curve was then normalised to a sum of 1, and then each point on the curve is multiplied by t and then by t^2. The mean of E(t)*t divided by the number of datapoints gives the mean residence time, which is then used with $E(t)*t^2$ to calculate the second moment about the mean:

$$\sigma_{\lambda}^2 = \frac{((\sum Et^2) - \bar{t}^2)}{\bar{t}^2}$$

The longitudinal Peclet number, 2M is solved by iteration of equation x given in section x, and is used to calculate D_T using equation x.

(Roychoudhury, 1998).

The following abbreviations are used in the tables:

C = concentration of tracer in outflow

C_o = concentration of tracer in inflow

$\bar{t}$ = Mean residence time

σ = Second moment about the mean

M = longitudinal Peclet number

D_T = hydrodynamic dispersion coefficient

Table A.6. Breakthrough curve calculations for flow rate of 0.011 m/hr

Time Hrs	C mS/cm	F C/C_0	E Derivative	E Corrected	E*t	E*t*t
0.00	0	0.000	0.000	0.000	0.000	0.000
7.10	0.00	0.000	0.000	0.000	0.000	0.000
7.57	0.00	0.000	0.000	0.000	0.000	0.000
8.05	0.00	0.000	0.000	0.000	0.000	0.000
8.52	0.00	0.000	0.000	0.000	0.000	0.000
8.99	0.00	0.000	0.014	0.007	0.060	0.541
9.47	0.06	0.007	0.077	0.037	0.348	3.297
9.94	0.39	0.043	0.329	0.156	1.551	15.421
10.41	1.79	0.199	0.589	0.280	2.914	30.343
10.89	4.30	0.478	0.425	0.202	2.197	23.915
11.36	6.11	0.679	0.369	0.175	1.988	22.587
11.83	7.68	0.853	0.150	0.071	0.844	9.991
12.31	8.32	0.924	0.056	0.027	0.329	4.052
12.78	8.56	0.951	0.019	0.009	0.114	1.457
13.73	8.72	0.969	0.000	0.000	0.000	0.000
14.20	8.64	0.960	0.019	0.009	0.127	1.798
14.67	8.72	0.969	0.059	0.028	0.409	6.001
15.15	8.97	0.997	0.000	0.000	0.000	0.000
SUM			**2.1056**	**1.0000**		
C_o (mS/cm)	9.00					
$\bar{t}$ (hr)	10.8819		**D_T (m^2/hr)**		3.02E-05	
σ	0.008338		**D_T (cm^2/s)**		8.38E-05	
M	119.4300		**Dispersivity (m)**		0.0018	

Table A.7. Breakthrough curve calculations for flow rate of 0.021 m/hr

Time hrs	C mS/cm	F C/C_0	E Derivative	E Corrected	E*t	E*t*t
0.00	0	0.0000	0.0000	0.0000	0.0000	0.0000
4.50	0	0.0000	0.0000	0.0000	0.0000	0.0000
4.72	0	0.0000	0.0000	0.0000	0.0000	0.0000
4.93	0	0.0000	0.0103	0.0022	0.0109	0.0536
5.15	0.02	0.0022	0.0821	0.0176	0.0907	0.4674
5.37	0.18	0.0200	0.2923	0.0628	0.3369	1.8080
5.58	0.75	0.0833	0.7846	0.1685	0.9408	5.2528
5.80	2.28	0.2533	1.1846	0.2544	1.4756	8.5582
6.02	4.59	0.5100	0.9026	0.1938	1.1662	7.0168
6.23	6.35	0.7056	0.5692	0.1222	0.7620	4.7498
6.45	7.46	0.8289	0.3231	0.0694	0.4475	2.8865
6.67	8.09	0.8989	0.1692	0.0363	0.2423	1.6153
6.88	8.42	0.9356	0.0923	0.0198	0.1365	0.9393
7.10	8.6	0.9556	0.0000	0.0000	0.0000	0.0000
7.32	8.42	0.9356	0.1795	0.0385	0.2820	2.0635
7.53	8.77	0.9744	0.0359	0.0077	0.0581	0.4375
7.75	8.84	0.9822	0.0308	0.0066	0.0512	0.3969
7.97	8.9	0.9889	0.0000	0.0000	0.0000	0.0000
SUM			**4.6564**	**1.0000**		
C_o (mS/cm)	9.00					
$\bar{t}$ (hr)	6.0007		**D_T (m^2/hr)**		4.32E-05	
σ	0.006593		**D_T (cm^2/s)**		1.20E-04	
M	151.1800		**Dispersivity (m)**		0.0019	

Table A.8. Breakthrough curve calculations for flow rate of 0.039 m/hr

Time hrs	C mS/cm	F C/C_0	E Derivative	E Corrected	E*t	E*t*t
0.00	0	0.0000	0.0000	0.0000	0.0000	0.0000
2.84	0	0.0000	0.0000	0.0000	0.0000	0.0000
2.96	0	0.0000	0.0529	0.0079	0.0233	0.0689
3.08	0.04	0.0065	0.4629	0.0688	0.2120	0.6537
3.21	0.39	0.0636	0.0000	0.0000	0.0000	0.0000
3.33	0.08	0.0131	0.4762	0.0707	0.2355	0.7843
3.45	0.44	0.0718	1.2301	0.1827	0.6310	2.1789
3.58	1.37	0.2235	1.9840	0.2947	1.0540	3.7699
3.70	2.87	0.4682	1.6005	0.2377	0.8796	3.2544
3.95	5.29	0.8630	0.2778	0.0413	0.1628	0.6426
4.07	5.5	0.8972	0.6481	0.0963	0.3918	1.5947
4.19	5.99	0.9772	0.0000	0.0000	0.0000	0.0000
4.32	5.96	0.9723	0.0000	0.0000	0.0000	0.0000
4.44	6.1	0.9951	0.0000	0.0000	0.0000	0.0000
4.56	6.1	0.9951	0.0000	0.0000	0.0000	0.0000
SUM			**6.7325**	**1.0000**		
C_o (mS/cm)	6.13					
$\bar{t}$ (hr)	3.5900		**D_T (m^2/hr)**		5.04E-05	
σ	0.004603		**D_T (cm^2/s)**		1.40E-04	
M	216.7500		**Dispersivity (m)**		0.0013	

Table A.9. Breakthrough curve calculations for flow rate of 0.061 m/hr

Time hrs	C mS/cm	F C/C_0	E Derivative	E Corrected	E*t	E*t*t
0	0	0.0000	0.0000	0.0000	0.0000	0.0000
2.00	0	0.0000	0.0000	0.0000	0.0000	0.0000
2.08	0	0.0000	0.2189	0.0187	0.0389	0.0811
2.17	0.11	0.0182	0.2786	0.0238	0.0515	0.1116
2.25	0.25	0.0415	1.2537	0.1070	0.2407	0.5415
2.33	0.88	0.1459	2.2289	0.1902	0.4437	1.0353
2.42	2	0.3317	3.0050	0.2564	0.6196	1.4973
2.50	3.51	0.5821	1.6517	0.1409	0.3523	0.8807
2.58	4.34	0.7197	1.6517	0.1409	0.3640	0.9404
2.67	5.17	0.8574	0.5771	0.0492	0.1313	0.3501
2.75	5.46	0.9055	0.2388	0.0204	0.0560	0.1541
2.83	5.58	0.9254	0.3383	0.0289	0.0818	0.2317
2.92	5.75	0.9536	0.2786	0.0238	0.0693	0.2022
3.00	5.89	0.9768	0.0000	0.0000	0.0000	0.0000
3.08	5.88	0.9751	0.0000	0.0000	0.0000	0.0000
SUM			**11.7214**	**1.0000**		
C_o (mS/cm)	6.03					
$\bar{t}$ (hr)	2.4491		**D_T (m^2/hr)**		7.49E-05	
σ	0.004667		**D_T (cm^2/s)**		2.08E-04	
M	213.7500		**Dispersivity (m)**		0.0013	

Table A.10. Breakthrough curve calculations for flow rate of 0.078 m/hr

Time hrs	C mS/cm	F C/C0	E Derivative	E Corrected	E*t	E*t*t
0.00	0	0.0000	0.0000	0.0000	0.0000	0.0000
1.54	0	0.0000	0.0000	0.0000	0.0000	0.0000
1.60	0	0.0000	0.0883	0.0054	0.0087	0.0139
1.67	0.03	0.0054	0.4709	0.0289	0.0482	0.0802
1.73	0.19	0.0345	1.3244	0.0814	0.1405	0.2426
1.79	0.64	0.1162	2.8548	0.1754	0.3137	0.5610
1.85	1.61	0.2922	1.8541	0.1139	0.2108	0.3899
1.91	2.24	0.4065	4.7089	0.2893	0.5531	1.0574
1.97	3.84	0.6969	2.6782	0.1646	0.3247	0.6408
2.04	4.75	0.8621	1.4127	0.0868	0.1766	0.3595
2.10	5.23	0.9492	0.1766	0.0108	0.0227	0.0477
2.16	5.29	0.9601	0.6769	0.0416	0.0898	0.1937
2.22	5.52	1.0018	0.0294	0.0018	0.0040	0.0089
2.28	5.53	1.0036	0.0000	0.0000	0.0000	0.0000
2.34	5.51	1.0000	0.0000	0.0000	0.0000	0.0000
SUM			**16.2751**	**1.0000**		
C_o (mS/cm)	5.51					
$\bar{t}$ (hr)	1.8928		**D_T (m^2/hr)**		7.43E-05	
σ	0.003580		**D_T (cm^2/s)**		2.06E-04	
M	278.8000		**Dispersivity (m)**		0.0010	

Table A.11. Breakthrough curve calculations for flow rate of 0.100 m/hr

Time hrs	C mS/cm	F C/C_0	E Derivative	E Corrected	E*t	E*t*t
0	0.00	0.00	0.0000	0.0000	0.0000	0.0000
1.20	0.00	0.00	0.0000	0.0000	0.0000	0.0000
1.25	0.00	0.00	0.1958	0.0097	0.0121	0.0152
1.30	0.06	0.01	0.7830	0.0388	0.0505	0.0656
1.35	0.30	0.05	2.1533	0.1068	0.1442	0.1946
1.40	0.96	0.16	3.6542	0.1812	0.2537	0.3552
1.45	2.08	0.34	4.5677	0.2265	0.3285	0.4763
1.50	3.48	0.57	3.3279	0.1650	0.2476	0.3714
1.55	4.50	0.73	2.3817	0.1181	0.1831	0.2838
1.60	5.23	0.85	1.5987	0.0793	0.1269	0.2030
1.65	5.72	0.93	1.4029	0.0696	0.1148	0.1894
1.70	6.15	1.00	0.0000	0.0000	0.0000	0.0000
1.75	6.10	1.00	0.0979	0.0049	0.0085	0.0149
1.80	6.13	1.00	0.0000	0.0000	0.0000	0.0000
1.85	6.13	1.00	0.0000	0.0000	0.0000	0.0000
SUM			**20.1631**	**1.0000**		
C_o (mS/cm)	6.15					
$\bar{t}$ (hr)	1.47		**D_T (m^2/hr)**		1.11E-04	
σ	0.004160		**D_T (cm^2/s)**		3.09E-04	
M	239.90		**Dispersivity (m)**		0.0011	

A.3.2 Iron flowthrough curves

Table A.12. Iron concentrations measured at column outlet using a pH 5 buffered input solution

DL17 groundwater						Artificial groundwater					
Time (days)	FeT mg/L	Fe^{2+} mg/L	C/C_o FeT	C/C_o Fe^{2+}	pH	Time (days)	FeT mg/L	Fe^{2+} mg/L	C/C_o FeT	C/C_o Fe^{2+}	pH
0.33	0.29	0.22	0.02	nd	5.03	0.31	0.18	0.08	0.01	0.01	4.79
0.42	0.32	0.19	0.02	0.01	nd	0.34	0.15	0.01	0.01	0.00	4.82
0.44	0.43	0.27	0.03	0.02	4.41	0.37	0.14	0.20	0.01	0.02	4.79
0.47	1.92	0.42	0.15	0.03	4.79	0.39	0.48	0.41	0.04	0.03	4.76
0.50	3.62	3.60	0.27	0.27	4.85	0.42	1.79	1.56	0.14	0.12	4.67
0.53	4.16	0.83	0.32	0.06	5.03	0.45	3.06	1.13	0.24	0.09	4.67
0.56	4.63	nd	0.35	nd	5.02	0.48	4.97	3.63	0.40	0.29	4.7
0.58	5.41	5.66	0.41	0.43	4.32	0.50	6.48	2.44	0.52	0.19	4.73
0.61	7.22	6.37	0.55	0.48	4.83	0.53	7.41	4.15	0.59	0.33	4.77
0.64	7.50	7.22	0.57	0.55	4.87	0.56	7.63	2.80	0.61	0.22	4.73
0.67	7.50	7.87	0.57	0.60	4.93	0.59	8.80	4.24	0.70	0.34	4.7
0.69	7.41	8.61	0.56	0.65	4.60	0.62	8.97	4.87	0.71	0.39	4.71
0.72	7.85	8.39	0.60	0.64	4.76	0.64	10.84	4.70	0.86	0.37	4.73
0.75	8.30	8.92	0.63	0.68	4.83	0.67	9.46	4.51	0.75	0.36	4.79
0.78	8.51	8.98	0.65	0.68	4.82	0.70	9.47	3.81	0.75	0.30	4.65
0.81	9.20	9.21	0.70	0.70	4.23	0.73	10.21	7.77	0.81	0.62	4.82
0.83	8.16	9.25	0.62	0.70	4.77	0.75	11.35	5.96	0.90	0.47	4.84
0.86	8.34	9.36	0.63	0.71	4.80	0.78	11.62	8.13	0.92	0.65	nd
0.89	8.18	9.46	0.62	0.72	4.79	0.82	10.68	6.60	0.85	0.52	4.19
0.92	8.41	9.16	0.64	0.69	4.17	0.89	11.09	4.76	0.88	0.38	4.52
1.04	9.92	9.41	0.75	0.71	4.25	0.96	11.97	5.45	0.95	0.43	4.86
1.11	10.03	9.91	0.76	0.75	4.68	1.03	11.53	5.92	0.92	0.47	4.88
1.18	9.96	9.94	0.76	0.75		1.07	12.37	9.87	0.98	0.79	4.47
1.25	9.99	7.12	0.76	0.54	4.49	1.14	11.55	6.82	0.92	0.54	4.44
1.32	9.98	9.86	0.76	0.75	4.75	1.21	11.68	5.42	0.93	0.43	4.63
1.39	9.95	9.84	0.76	0.75	4.75	1.28	12.73	6.57	1.01	0.52	4.64
1.46	9.85	9.90	0.75	0.75	4.78	1.31	13.08	8.82	1.04	0.70	4.77
1.53	9.83	9.83	0.75	0.75	4.83	1.38	11.68	10.11	0.93	0.80	4.74
1.76	9.94	9.88	0.75	0.75		1.45	11.79	7.87	0.94	0.63	4.68
1.83	10.03	9.77	0.76	0.74	4.71	1.52	12.74	6.75	1.01	0.54	4.71
1.90	9.98	9.87	0.76	0.75	4.75	1.56	11.55	5.68	0.92	0.45	4.77
1.97	10.02	9.92	0.76	0.75	4.60	1.63	11.59	6.00	0.92	0.48	4.72
2.04	10.01	9.78	0.76	0.74	4.71	1.73	11.21	10.83	0.89	0.86	4.04
2.11	9.94	8.12	0.75	0.62	4.68	1.80	11.09	7.52	0.88	0.60	4.36
2.18	9.90	9.72	0.75	0.74	4.68	1.87	11.63	5.87	0.93	0.47	4.66
2.25	10.05	9.88	0.76	0.75	4.73	1.94	11.81	6.51	0.94	0.52	4.43
2.32	10.02	9.84	0.76	0.75	4.61	2.01	11.93	6.84	0.95	0.54	4.8
2.38	9.94	9.92	0.75	0.75	4.73	2.08	11.36	8.04	0.90	0.64	nd
2.15	9.76	9.75	0.74	0.74	4.75						
2.22	9.98	9.82	0.76	0.74	4.84						
2.28	9.86	9.47	0.75	0.72	4.66						
2.35	9.43	9.77	0.72	0.74	4.57						
2.42	8.76	9.80	0.66	0.74	4.69						
2.49	8.79	9.74	0.67	0.74	4.70						
2.56	9.91	9.80	0.75	0.74	4.49						
2.63	9.95	9.55	0.76	0.72	4.57						
2.70	8.18	9.69	0.62	0.74	4.69						
2.77	9.83	8.35	0.75	0.63	4.70						
3.01	9.93	7.89	0.75	0.60	4.49						

Table A.13. Iron concentrations measured at column outlet using a pH 6 buffered input solution

DL17						Artificial groundwater					
Time (days)	FeT mg/L	Fe^{2+} mg/L	C/C_o FeT	C/C_o Fe^{2+}	pH	Time (days)	FeT mg/L	Fe^{2+} mg/L	C/C_o FeT	C/C_o Fe^{2+}	pH
0.07	<0.01	nd	-	-	6.02	0.07	0.27	nd	0.02	-	4.01
0.21	0.01	nd	<0.01	-	5.94	0.14	0.25	nd	0.01		5.43
0.26	0.01	nd	<0.01	-	5.95	0.21	0.17	nd	0.01		6.50
0.32	<0.01	nd	-	-	5.94	0.24	0.17	nd	0.01		6.53
0.38	0.05	nd	<0.01	-	5.97	0.27	0.30	nd	0.01		6.38
0.43	0.01	nd	<0.01	-	5.94	0.30	0.27	nd	0.01		6.22
0.49	0.05	nd	<0.01	-	5.93	0.32	0.29	nd	0.01		6.14
0.57	0.01	0.02	<0.01	0.00	5.85	0.35	0.31	nd	0.01		6.06
0.61	0.64	0.64	0.06	0.06	5.8	0.38	0.39	nd	0.02		5.94
0.64	1.10	1.10	0.10	0.10	5.71	0.41	0.53	nd	0.02		5.78
0.67	3.31	3.19	0.29	0.28	5.42	0.49	1.59	nd	0.11	0.04	5.72
0.70	5.60	5.39	0.49	0.47	5.5	0.56	3.27	nd	0.22	0.09	5.68
0.85	7.71	7.69	0.68	0.67	5.51	0.63	4.75	nd	0.31	0.12	5.65
0.92	8.47	8.41	0.74	0.73	5.64	0.76	6.57	nd	0.43	0.13	5.21
0.99	8.40	8.36	0.74	0.73	5.62	0.83	7.13	nd	0.48	0.18	5.41
1.04	8.73	8.64	0.76	0.75	5.66	0.90	7.56	nd	0.52	0.21	5.45
1.11	8.83	8.76	0.77	0.76	5.67	0.97	7.82	nd	0.54	0.22	5.62
1.18	9.17	9.09	0.80	0.79	5.68	1.02	7.80	7.87	0.58	0.50	5.03
1.25	9.40	9.31	0.82	0.81	5.73	1.09	7.93	7.93	0.59	0.52	5.18
1.31	9.74	9.67	0.85	0.84	5.74	1.16	7.81	7.75	0.61	0.53	5.35
1.38	10.02	9.92	0.88	0.86	5.77	1.23	8.10	8.04	0.62	0.57	5.20
1.45	10.20	10.17	0.89	0.88	5.77	1.30	8.18	8.11	0.68	0.59	5.53
1.52	10.34	10.27	0.91	0.89	5.79	1.37	8.42	8.27	0.67	0.57	5.60
1.59	10.41	10.38	0.91	0.90	5.81	1.44	8.41	8.33	0.67	0.62	5.58
1.69	10.69	10.56	0.94	0.92	5.7	1.50	8.40	8.39	0.67	0.60	5.63
1.76	9.76	9.73	0.86	0.84	5.72	1.57	8.43	8.42	0.70	0.64	5.64
1.83	9.45	9.58	0.83	0.83	5.73	1.64	8.56	8.54	0.70	0.62	5.70
1.89	9.88	9.89	0.87	0.86	5.72	1.68	8.14	6.60	0.67	0.45	5.23
1.96	10.11	10.08	0.89	0.87	5.77	1.75	8.24	7.14	0.67	0.46	5.57
2.03	10.02	9.97	0.88	0.86	5.79	1.82	8.29	8.10	0.68	0.54	5.59
2.10	10.26	10.17	0.90	0.88	5.81	1.89	8.27	8.39	0.66	0.57	5.52
2.17	9.78	9.69	0.86	0.84	5.83	1.96	8.36	8.38	0.69	0.63	5.65
2.24	9.98	9.92	0.87	0.86	5.83	2.00	7.08	6.43	0.66	0.59	5.42
2.31	10.19	10.14	0.89	0.88	5.85	2.14	7.64	6.29	0.67	0.58	5.54
2.80	10.19	11.01	0.89	0.95		2.21	7.83	6.96	0.69	0.61	5.16
2.87	10.45	10.40	0.92	0.90		2.28	7.73	6.92	0.64	0.54	5.55
2.94	10.59	10.55	0.93	0.92		2.35	7.93	7.39	0.65	0.57	5.55
3.01	10.83	10.79	0.95	0.94		2.83	8.52	7.99	0.68	0.63	5.5
3.08	10.96	11.02	0.96	0.96		2.90	8.55	8.63	0.69	0.66	5.41

Table A.14. Iron concentrations measured at column outlet using a pH 6.0 buffered input solution in a column inoculated with iron precipitates from a clogged borehole with and without $HgCl_2$ inhibition

Not inhibited						Inhibited with $HgCl_2$					
Time (days)	FeT mg/L	Fe^{2+} mg/L	C/C_o FeT	C/C_o Fe^{2+}	pH	Time (days)	FeT mg/L	Fe^{2+} mg/L	C/C_o FeT	C/C_o Fe^{2+}	pH
0.03	0.07	0.08	0.01	0.01	6.46	0.23	8.20	7.41	0.68	0.62	5.63
0.31	0.08	0.06	0.01	0.01	6.56	0.28	8.15	7.54	0.68	0.63	5.74
0.45	0.03	0.06	0.00	0.01	6.49	0.34	8.08	7.60	0.67	0.63	5.70
0.59	0.03	0.09	0.00	0.01	6.46	0.42	7.69	7.22	0.64	0.60	5.55
0.73	0.08	0.12	0.01	0.01	6.42	0.48	7.68	7.38	0.64	0.61	5.41
0.86	0.12	0.20	0.01	0.02	6.38	0.51	7.08	6.81	0.59	0.57	5.38
1.00	0.19	0.25	0.02	0.02	6.34	0.53	6.27	5.89	0.52	0.49	5.32
1.03	0.19	0.24	0.02	0.02	6.28	0.56	4.72	4.58	0.39	0.38	5.22
1.17	0.29	0.32	0.02	0.03	6.25	0.59	3.55	3.49	0.30	0.29	5.49
1.31	0.30	0.41	0.02	0.03	6.23	0.62	2.02	1.99	0.17	0.17	5.31
1.45	0.25	0.40	0.02	0.03	6.18	0.65	0.96	1.03	0.08	0.09	5.13
1.59	0.34	0.45	0.03	0.04	6.13	0.67	0.34	0.42	0.03	0.04	5.14
1.73	0.39	0.56	0.03	0.05	6.09	0.70	0.13	0.20	0.01	0.02	5.14
1.86	0.44	0.63	0.04	0.05	6.05	0.73	0.10	0.17	0.01	0.01	5.18
2.00	0.55	0.73	0.04	0.06		0.76	0.05	0.00	0.00	0.00	5.29
2.03	0.69	0.82	0.06	0.07	6.12	0.78	0.10	0.17	0.01	0.01	5.23
2.17	0.60	0.88	0.05	0.07	6.05	0.81	0.15	0.21	0.01	0.02	5.22
2.23	0.50	0.78	0.04	0.06	6.00	0.84	0.15	0.24	0.01	0.02	
2.31	0.68	1.01	0.05	0.08	6.03	0.87	0.00	0.38	<0.01	0.03	
2.36	0.62	0.71	0.05	0.06	5.98	1.10	0.12		0.01	<0.01	5.40
2.45	0.80	0.70	0.06	0.06	6.00	1.24	<0.01	<0.01	<0.01	<0.01	5.43
2.50	0.68	0.70	0.05	0.06	5.82	1.66	<0.01	<0.01	<0.01	<0.01	5.37
2.59	1.03	0.92	0.08	0.07	5.98	2.07	<0.01	<0.01	<0.01	<0.01	5.34
2.64	0.79	0.77	0.06	0.06	5.96	2.65	0.01	<0.01	<0.01	<0.01	4.91
2.73	0.99	0.91	0.08	0.07	5.74	3.07	<0.01	<0.01	<0.01	<0.01	4.80
2.78	0.92	0.88	0.07	0.07	5.95	3.79	<0.01	<0.01	<0.01	<0.01	4.32
2.86	1.17	1.22	0.09	0.10	5.89						
2.92	1.07	1.10	0.09	0.09	5.93						
3.00	1.28	1.35	0.10	0.11	5.52						
3.06	1.32	1.43	0.11	0.12	5.92						
3.20	1.33	1.44	0.11	0.12	5.72						
3.34	1.45	1.57	0.12	0.13	5.45						
3.39		1.70		0.14	5.76						
3.48	1.56	1.67	0.13	0.14	5.63						
3.53		1.77		0.14	5.74						
3.61	1.66	1.75	0.13	0.14	5.46						
3.67		1.90		0.15	5.71						
3.75	1.78	1.84	0.14	0.15	5.85						
3.89	1.78	1.88	0.14	0.15	5.67						

Table A.15. Iron concentrations measured at column outlet using a pH 6.5 buffered input solution

DL17						Artificial groundwater					
Time (days)	FeT mg/L	Fe^{2+} mg/L	C/C_o FeT	C/C_o Fe^{2+}	pH	Time (days)	FeT mg/L	Fe^{2+} mg/L	C/C_o FeT	C/C_o Fe^{2+}	pH
0.39	0.11	0.06	0.01	0.01	4.30	0.07	nd	0.34	0.03	-	6.44
0.42	0.06	0.05	0.01	0.01	4.30	0.14	0.25	0.38	0.04	0.02	6.52
0.45	0.20	0.06	0.01	0.01	4.30	0.21	nd	0.18	0.02	-	6.52
0.48	0.06	0.06	0.01	0.01	4.30	0.24	nd	0.22	0.02	-	6.53
0.51	0.32	0.06	0.02	0.01	4.30	0.26	nd	0.30	0.03	-	6.50
0.53	0.16	0.17	0.01	0.01	3.22	0.29	nd	0.31	0.03	-	6.53
0.55	0.04	0.06	0.01	0.01	4.30	0.32	nd	0.13	0.01	-	6.48
0.58	0.11	0.12	0.01	0.02	4.24	0.35	nd	0.06	0.01	-	6.38
0.61	0.39	0.41	0.03	0.03	4.24	0.38	nd	0.08	0.01	-	6.30
0.64	0.86	0.89	0.06	0.07	4.23	0.40	nd	0.06	0.01	-	6.24
0.67	1.63	1.57	0.12	0.12	4.22	0.49	nd	0.17	0.02	-	6.23
0.70	2.26	2.29	0.16	0.17	4.22	0.56	nd	0.19	0.02	-	6.25
0.73	3.00	3.01	0.22	0.24	4.21	0.63	nd	0.30	0.03	-	6.23
0.77	3.55	3.50	0.28	0.29	4.21	0.71	nd	0.34	0.03	-	6.21
0.80	4.14	4.11	0.32	0.34	4.20	0.78	0.49	0.54	0.05	0.05	6.22
0.83	5.05	5.09	0.41	0.43	4.20	0.85	0.71	0.77	0.07	0.07	6.23
0.86	5.21	5.23	0.43	0.45	4.19	0.92	1.17	1.24	0.12	0.11	6.24
0.89	5.60	5.39	0.46	0.47	4.19	0.99	1.33	1.41	0.13	0.12	6.23
0.92	5.83	5.71	0.48	0.50	4.20	1.00	1.65	1.68	0.16	0.15	6.23
0.95	6.28	6.18	0.51	0.53	4.13	1.07	2.18	2.23	0.21	0.20	6.18
0.99	6.11	6.06	0.51	0.54	4.19	1.14	2.56	2.56	0.24	0.24	6.24
1.02	5.57	6.09	0.41	0.50	nd	1.21	3.01	3.02	0.28	0.28	6.20
1.05	5.56	6.16	0.47	0.50	4.13	1.28	3.21	3.28	0.31	0.30	6.25
1.08	5.66	5.39	0.41	0.44	3.17	1.35	3.34	3.51	0.33	0.31	6.26
1.11	5.66	5.49	0.51	0.50	4.17	1.42	3.82	3.83	0.36	0.36	6.26
1.14	6.18	5.59	0.45	0.46	3.18	1.49	3.87	3.95	0.37	0.36	6.29
1.18	5.80	5.80	0.50	0.50	4.16	1.56	4.09	4.07	0.38	0.38	6.29
1.21	5.89	6.79	0.43	0.55	3.14	1.63	4.15	4.11	0.38	0.39	6.29
1.24	6.30	6.23	0.52	0.52	4.14	1.76	2.81	4.48	0.42	0.26	6.02
1.27	6.40	6.15	0.47	0.50	3.13	1.83	3.34	4.52	0.42	0.31	5.88
1.30	6.28	6.07	0.50	0.51	4.16	1.90	3.80	4.71	0.44	0.36	6.08
1.33	6.24	6.18	0.45	0.51	3.18	1.97	3.84	4.63	0.43	0.36	5.90
1.36	6.47	6.42	0.51	0.52	4.16	2.04	4.10	4.84	0.45	0.38	5.83
1.40	6.43	6.35	0.47	0.52	3.16	2.11	4.22	4.82	0.45	0.40	6.08
1.43	6.96	6.92	0.51	0.57	3.13	2.18	4.21	4.90	0.46	0.39	5.27
1.46	6.63	6.51	0.51	0.54	4.15	2.25	4.13	5.00	0.47	0.39	6.16
1.49	6.76	6.91	0.49	0.56	3.19	2.32	4.27	5.03	0.47	0.40	
1.52	6.65	6.56	0.52	0.54	3.16	2.39	4.50	5.19	0.49	0.42	
1.55	6.62	6.66	0.48	0.54	3.19	5.74	6.33	6.43	0.60	0.59	6.21
1.58	6.76	6.70	0.51	0.54	4.18	5.81	6.23	6.43	0.60	0.58	6.30
1.61	6.90	6.73	0.50	0.55	3.20	5.88	6.35	6.38	0.60	0.59	6.33

Table A.16. Iron concentrations measured at column outlet using a pH 7.0 buffered input solution

DL17						Artificial			
Time (days)	FeT mg/L	Fe^{2+} mg/L	C/C_o FeT	C/C_o Fe^{2+}	pH	Time (days)	FeT mg/L	C/C_o FeT	pH
0.18	<0.01	0.03	<0.01	0.00	7.00	0.07	0.11	0.01	6.88
0.31	<0.01	0.02	<0.01	0.14	6.96	0.14	0.18	0.01	6.98
0.45	<0.01	0.01	<0.01	0.04	6.88	0.22	0.04	<0.01	7.06
0.59	<0.01	0.05	<0.01	0.12	6.86	0.25	0.04	<0.01	7.06
0.73	<0.01	0.05	<0.01	0.09	6.85	0.27	0.31	0.02	7.04
0.87	0.01	0.07	0.00	0.10	6.85	0.30	0.04	<0.01	6.94
1.00	0.03	0.07	0.00	0.09	6.84	0.33	0.04	<0.01	6.86
1.35	0.04	0.10	0.00	0.10	6.80	0.36	0.06	<0.01	6.85
1.69	<0.01	0.06	<0.01	0.05	6.84	0.39	0.03	<0.01	6.83
4.89	0.10	0.06	0.01	0.04	6.82	0.41	0.12	0.01	6.75
						0.50	0.06	<0.01	6.83
						0.57	0.07	<0.01	6.85
						0.64	0.06	<0.01	6.84
						0.70	0.12	0.01	6.83
						0.77	0.20	0.01	6.79
						0.84	0.05	<0.01	6.84
						0.89	0.07	<0.01	6.78
						0.96	0.05	<0.01	6.81
						1.03	0.07	<0.01	6.83
						1.10	0.07	<0.01	6.87
						1.17	0.07	<0.01	6.82
						1.20	0.11	0.01	6.82
						1.27	0.09	0.01	6.82
						1.34	0.07	<0.01	6.83
						1.41	0.10	0.01	6.87
						1.48	0.08	0.01	6.88
						1.61	0.06	<0.01	6.85
						1.68	0.03	<0.01	6.83
						1.82	0.09	0.01	6.89

A.4 Field rehabilitation data

Table A.17. Field rehabilitation data for borehole KG1 (concentrations in mg/L unless otherwise stated)

	Date	Time	Field pH	Field EC mS/cm	DO mg/l	Temp °C
A-1	24-Jul	17h45	5.8	2.7	2.8	22.5
A-2	24-Jul	17h50	6.1	2.6	2.0	23.0
A-3	24-Jul	18h00	6.1		1.3	23.0
A-4	24-Jul	18h25	6.1	2.5	0.2	23.1
B-1	25-Jul	11h15	5.9	3.2	2.3	24.2
C-1	27-Jul	16h00	2.1	nd	6.0	22.7
C-1.5	27-Jul	16h30	2.0	nd	3.1	25.0
C-2	27-Jul	17h00	2.5	nd	1.9	22.1
C-2.5	27-Jul	17h30	2.6	nd	2.4	22.8
C-3	27-Jul	18h00	2.5	nd	1.4	22.3
C-3.5	27-Jul	18h35	2.6	nd	1.9	22.3
C-4	27-Jul	20h30	Nd	nd	nd	nd
D-1	30-Jul	08h30	6.1	nd	nd	21.6
D-2	30-Jul	08h40	3.1	nd	1.1	22.6
D-3	30-Jul	08h50	5.6	nd	0.8	22.9
D-4	30-Jul	12h55	nd	nd	3.4	nd

Stage in rehabilitation

A	Calibration test
B	Step test
C	Purge
D	Final step test

Borehole properties

Pump depth	100 m
Water depth	30.33 m
Borehole depth	

Table A.18. Laboratory rehabilitation data for borehole KG1 (concentrations in mg/L unless otherwise stated)

	Lab	Lab	Unfiltered		Filtered									
	pH	EC	Fe2+	FeT	Fe2+	FeT	Cl	NO_2	SO_4	Na	NH_4	K	Mg	Ca
A-1	6.3	0.36	9.60	10.2	10.1	10.3	77.8	bdl	23.5	34.4	10.8	10.4	8.35	15.1
B-1	5.8	0.40	17.3	20.1	16.3	18.4	85.7	bdl	48.8	36.3	1.00	10.7	9.00	15.6
C-1	2.3	13.2	3665	nd	3085	3325	503	66.5	6124	646	1071	40.7	16.4	229
C-2	2.6	2.67	168	380	132	367	211	34.0	2039	768	276	24.4	17.4	77.7
C-3	2.8	4.37	167	481	70.3	163	146	20.2	1403	555	174	24.9	17.0	50.7
C-4	3.0	2.97	95.8	134	Nd	Nd	141	13.7	1103	300	91.3	11.9	37.9	20.6
D-1	4.3	1.40	145	171	134	136	102	6.59	502	129	29.3	10.7	26.7	21.6
D-4	4.63	0.98	bdl	77.3	48.3	63.0	92.9		264	100	22.4	11.5	23.5	16.5

	Al	Si	Ti	Mn	Ni	Co	Cu	Zn	Br	Sr	Pb	Th	U
	µg/L		µg/L	µg/L	µg/L	µg/L	µg/L	µg/L	µg/L	µg/L	µg/L	µg/L	µg/L
A-1	19.8	5.00	20.6	2134	26.6	8.45	4.01	422	788	139	0.75		0.14
B-1	8.1	5.15	4.12	191	1.90	1.26	1.04	33.2	102	7.54	0.084	0.025	0.16
C-1	849	23.0	366	1797	139	20.3	348	844	3980	162	116	6.46	11.9
C-2	6756	9.20	237	2238	140	82.4	677	3975	1031	225	619	236	103
C-3	8157	7.53	185	1964	262	112	449	4734	1005	278	486	263	94.7
C-4	6630	7.68	118	1678	262	115	293	4918	641	285	290	229	75.0
D-1	1067	6.18	67.0	2165	110	63.4	63.0	2599	*nd*	210	10.6	0.96	6.49
D-4	295	6.49	48.6	1611	109	39.7	36.7	1997	202	131	1.89	0.20	7.51

Table A.19. Field rehabilitation data for borehole DP28 (concentrations in mg/L unless otherwise stated)

	Date	Time	Pumping rate (l/s)	Field pH	Field EC (mS/cm)	DO	Temp
A1	15-Aug	02h35		6.0	0.2	3.1	18.5
A2	15-Aug	03h35		5.4	0.2	2.9	18.5
B1	15-Aug	15h15	0.88	3.5	5.5	2.9	16.8
B1.5	15-Aug	15h45	0.86	6.5	0.4	2.9	18.7
B2	15-Aug	16h15	5.52	5.7	0.3	2.6	20.1
B2.5	15-Aug	16h45		5.3	0.2	1.6	19.2
B3	15-Aug	17h15	11.1	5.3	0.3	1.6	19.1

Stage in rehabilitation

A	Pump test
B	Final pump test

Borehole properties

Water depth	100
Pump depth	140

Table A.20. Laboratory rehabilitation data for borehole DP28 (concentrations in mg/L unless otherwise stated)

	Lab	Lab EC	Unfiltered		Filtered										
	pH	mS/cm	Fe2+	FeT	Fe_{2+}	FeT	Cl	NO_3	SO_4	HCO_3	Na	NH_4	K	Mg	Ca
A1	6.2	0.2	11.0	12.6	11.5	10.9	39.2	0.35	25.7	14.9	22.0	0.75	3.27	3.35	4.64
A2	6.2	0.2	4.07	3.95	3.74	3.76	37.4	0.06	8.94	13.6	21.8		2.27	2.40	2.39
B1	3.8	6.1	0.72	4.59	0.01	0.62	2043	1.46	32.7	-64.7	1424	12.2	3.42	3.20	13.3
B2	5.8	0.3	2.76	2.79	2.83	2.60	72.3	0.03	7.68	13.9	46.9		2.21	2.45	2.93
B3	5.5	0.3	2.24	2.31	2.23	2.28	72.1	0.05	17.3		47.9	0.25	2.37	3.15	3.71

	Al	Si	Ti	Mn	Ni	Co	Cu	Zn	Br	Sr	Pb	U
	µg/L		µg/L	µg/L	µg/L	µg/L	µg/L	µg/L	µg/L	µg/L	µg/L	µg/L
A1		4.05	6.02	1031	57.3	24.4	0.87	468	217	48.1		0.29
A2	10.7	5.01	1.89	427	14.4	8.87	0.37	130	207	12.0	0.07	0.64
B1	64.1	3.07	27.7	49.7	43.3	7.09	58.0	193		149	16.6	12.1
B2	26.0	5.11	3.76	343	12.4	7.68	1.03	107		13.6	0.09	1.12
B3	133	5.38	4.11	503	26.3	15.7	2.83	261	229	22.7	3.66	8.81

Table A.21. Field rehabilitation data for borehole DL16 (concentrations in mg/L unless otherwise stated)

	Date	Time	Pumping rate (l/s)	Field pH	Field EC mS/cm	DO	Temp °C
A1	26-Jul	13h40		6.1	5.67	4.5	23.9
A1.5	26-Jul	13h45		6.2	5.08	3.0	22.5
A2	26-Jul	13h50		6.2	4.15	2.5	22.7
A3	26-Jul	14h00	5.92	6.2	3.86	1.6	23.1
A4	26-Jul	14h05		6.3	3.96	0.9	23.2
A5	26-Jul	14h15		6.2	3.97	0.8	23.3
A6	26-Jul	14h37	18.4	6.3	3.91	0.4	23.3
A7	26-Jul	14h45		6.3	4.23	0.4	23.1
B1	27-Jul	12h30		6.3	5.22	0.6	22.8
C1	01-Aug	18h45		Nd	11.1	nd	nd
C1.5	01-Aug	19h00		Nd	10.6	nd	nd
C2	01-Aug	19h15		Nd	10.6	nd	nd
C3	02-Aug	08h30		6.6	1.23	nd	22
D1	17-Aug	13h40		6.2	0.848	3.2	19.9
D1.1	17-Aug	13h47		5.7	4.08	4.1	19.9
D1.2	17-Aug	13h58		5.6	5.58	3.6	20.2
D1.3	17-Aug	14h05		nd	2.99	3.5	19.4
D1.4	17-Aug	14h15	2.07	5.7	2.48	3.3	20.4
D1.5	17-Aug	14h33		6.0	1.92	2.8	20.9
D2	17-Aug	14h40	4.95	6.4	1.47	2.4	20.1
D2.1	17-Aug	14h55		6.4	1.39	2.4	21.0
D2.2	17-Aug	15h10		6.6	1.20	2.1	20.5
D2.3	17-Aug	15h25		6.6	1.09	1.6	22.3
D3	17-Aug	15h40		6.7	1.01	1.6	nd
D3.1	17-Aug	15h55		6.6	0.929	1.4	20.7
D3.2	17-Aug	16h10		6.7	0.836	1.4	20.0
D3.3	17-Aug	16h25		6.6	0.849	1.1	20.3
D4	17-Aug	16h40	10.0	6.6	0.796	1.2	20.5
D4.1	17-Aug	16h55		6.6	0.758	1.6	20.1
D4.2	17-Aug	17h10		6.7	0.723	0.7	21.1
D5	17-Aug	17h25		6.6	0.736	0.8	20.3

	Stage in rehabilitation
A	Calibration test
B	Pump test
C	Pump to waste
D	Final pump test

Table A.22. Laboratory rehabilitation data for borehole DL16 (concentrations in mg/L unless otherwise stated)

	Lab	Lab EC	Unfiltered		Filtered									
	pH	mS/cm	Fe^{2+}	FeT	Fe^{2+}	FeT	Cl	SO_4	HCO_3	Na	NH_4	K	Mg	Ca
A1	7.0	0.52	1.83	3.69	2.12	3.00	109	41.7	Nd	66.9	bdl	15.5	11.2	16.6
A2	6.8	0.45	5.29	7.55	2.26	2.76	92.8	24.0	Nd	60.3	0.50	15.4	8.30	13.6
B1	6.7	0.42	5.41	5.97	5.01	6.12	90.6	18.9	Nd	54.4	1.10	14.7	8.50	13.7
C1	2.1	10.6	89.0	170	89.0	210	202	3437	Nd	706	573	95.1	20.9	128
C2	2.2	9.65	66.4	164	73.2	188	220	3780	Nd	673	520	42.5	19.8	127
C3	6.9	1.12	5.05	4.30	4.90	3.85	117	292	nd	186	34.4	21.3	9.25	18.3
D1	6.6	0.84	8.94	25.2	8.05	8.73	205	57.5	47.6	143	bdl	14.8	10.8	13.5
D2	7.0	1.44	1.33	4.55	0.68	0.70	308	136	87.1	208	18.1	15.0	9.55	20.8
D3	7.0	0.92	2.14	2.34	1.91	2.11	141	108	114	136	10.1	17.1	7.55	15.9
D4	6.9	0.74	3.39	3.51	3.22	3.45	103	100	114	118	10.1	16.6	8.18	14.7
D5	7.1	0.69	3.60	4.20	3.74	4.12	95.6	88.9	112	101	8.80	16.6	8.50	13.3

	Al	Si	Ti	Mn	Ni	Co	Cu	Zn	Br	Sr	Pb	U
	µg/L		µg/L	µg/L	µg/L	µg/L	µg/L	µg/L	µg/L	µg/L	µg/L	µg/L
A1	10.0	5.45	20.2	1722	24.7	5.91	1.76	76.7	364	99.2	0.50	0.12
A2	6.79	6.36	15.7	649	*Bdl*	2.02	1.30	15.8	131	72.5	0.49	0.063
B1	3.13	5.61	15.5	462	*Bdl*	0.46	0.31	24.5	239	68.9	0.036	0.070
C1	1976	15.4	342	2635	130	25.7	332	7617	1526	167	202	44.9
C2	1912	14.8	336	3576	111	28.8	323	6469	*nd*	177	196	47.9
C3	1.36	5.42	43.9	536	2.72	1.81	2.15	384	1389	81.8	*nd*	1.27
D1	2.11	4.00	20.4	670	23.2	5.69	1.97	83.7	1228	94.3	0.082	0.98
D2	44.0	4.85	35.9	550	5.77	2.31	6.27	143	494	90.5	nd	0.45
D3	0.28	4.68	24.8	399	*Bdl*	0.73	1.63	64.6	610	72.4	0.16	1.52
D4	5.67	4.88	24.4	430	Bdl	0.57	1.69	71.8	199	77.2	0.25	1.89
D5	*bdl*	4.95	21.2	450	*bdl*	0.46	0.59	61.5	338	81.8	*nd*	1.96

A.5 Batch dissolution results

Table A.23. Dissolution data for 0.4 M sulfamic acid

Time	T (hrs)	Fe (mol/kg)	Fe (%)	T (hrs)	Fe (mol/kg)	Fe (%)	T (hrs)	Fe (mol/kg)	Fe (%)	T (hrs)	Fe (mol/kg)	Fe (%)	T (hrs)	Fe (mol/kg)	Fe (%)	T (hrs)	Fe (mol/kg)	Fe (%)	T (hrs)	Fe (mol/kg)	Fe (%)
		K1			K2			K3			K4			K5			H1			H2	
1	0.1	0.57	6.58	0.1	0.08	0.94	0.1	0.15	2.04	0.1	0.68	9.04	0.1	0.12	1.96	0.1	0.15	1.94	0.1	0.26	3.03
2	0.2	1.44	16.8	0.4	0.44	5.23	0.4	0.91	12.1	0.2	2.09	27.6	0.4	1.75	29.2	0.2	0.39	4.93	0.2	0.67	7.76
3	0.5	1.87	21.8	1.2	1.62	19.3	1.2	3.16	42.3	0.5	2.43	32.2	1.2	5.92	98.3	0.5	0.73	9.33	0.6	1.35	15.7
4	1.0	4.77	55.4	2.4	4.83	57.7	2.5	5.19	69.4	1.0	7.09	93.9	2.4	6.64	110	1.0	2.84	36.4	1.0	6.22	72.4
5	2.4	6.46	75.0	4.1	4.95	59.0	4.1	6.15	82.2	2.4	8.38	111	4.1	7.50	125	2.4	5.85	74.9	2.3	9.17	107
6	4.6	7.33	85.1	6.1	5.83	69.6	6.1	7.16	95.8	4.5	7.59	101	6.1	6.65	111	4.6	7.18	91.8	4.6	8.92	104
7	6.6	7.40	85.9	8.4	6.44	76.8	8.4	6.21	83.0	6.6	6.91	91.5	8.4	5.58	92.6	6.6	7.24	92.5	6.6	8.09	94.0
8	23.5	9.57	111	23.7	8.30	99.0	23.7	6.67	89.2	23.5	6.52	86.3	23.7	5.58	92.8	23.5	8.66	111	23.5	7.92	92.1
9	30.5	7.79	90.5	31.2	7.81	93.2	31.2	5.72	76.4	30.5	6.06	80.3	31.2	4.84	80.3	30.5	6.76	86.5	30.5	6.93	80.6
TOTAL		8.61			8.38			7.48			7.55			6.02			7.82			8.60	
		A1			A2			A3			A4			A5			A6				
1	0.1	2.37	37.4	0.1	2.19	33.1	0.1	1.47	25.8	0.2	1.40	22.5	0.2	2.12	37.2	0.2	1.55	24.9			
2	0.2	4.00	63.0	0.4	5.20	78.6	0.4	3.74	65.6	0.4	4.15	66.8	0.4	4.54	79.5	0.4	3.65	58.7			
3	0.5	3.80	59.8	1.2	6.99	106	1.2	5.29	92.8	1.2	5.76	92.7	1.2	5.75	101	1.2	4.86	78.2			
4	1.0	5.61	88.4	2.4	6.42	97.1	2.4	5.36	94.1	2.5	5.99	96.5	2.5	5.43	95.1	2.5	4.83	77.6			
5	2.3	5.80	91.3	4.1	6.03	91.2	4.1	5.16	90.5	4.2	5.55	89.4	4.2	5.13	89.8	4.2	4.76	76.6			
6	4.6	5.63	88.6	6.2	5.76	87.2	6.1	4.46	78.3	6.1	5.28	85.0	6.1	4.85	84.9	6.1	4.63	74.5			
7	6.6	5.41	85.2	8.4	5.47	82.8	8.4	5.23	91.8	8.4	5.14	82.7	8.4	4.64	81.2	8.4	4.42	71.0			
8	23.5	5.13	80.9	23.7	5.34	80.8	23.7	4.91	86.1	23.7	5.07	81.6	23.7	4.63	81.1	23.7	4.69	75.4			
9	30.5	4.99	78.6	31.2	5.11	77.2	31.2	4.40	77.3	31.2	4.69	75.5	31.2	4.20	73.6	31.2	4.23	68.0			
TOTAL		6.35			6.61			5.70			6.21			5.71			6.22				
		FH2			FH6			Gt			Sch			S1			S2				
1	0.2	0.39	4.34	0.1	0.27	2.67	0.1	0.00	0.02	0.2	0.39	5.11	0.1	0.38	4.46	0.2	1.41	23.5			
2	0.4	3.57	39.9	0.2	0.43	4.20	0.2	0.01	0.05	0.5	4.49	59.3	0.2	1.12	13.3	0.5	4.52	75.4			
3	1.2	7.56	84.4	0.5	0.49	4.78	0.5	0.01	0.05	1.2	7.66	101	0.5	1.67	19.9	1.3	6.85	114			
4	2.5	7.59	84.7	1.0	1.42	13.9	1.0	0.01	0.09	2.5	7.44	98.3	1.0	4.33	51.5	2.5	6.07	101			
5	4.2	7.36	82.2	2.4	2.33	22.7	2.4	0.01	0.07	4.2	6.94	91.7	2.4	6.91	82.3	4.2	5.62	93.9			
6	6.1	6.97	77.8	4.5	3.42	33.5	4.5	0.01	0.08	6.1	6.66	88.0	4.6	7.73	92.0	6.1	5.36	89.5			
7	8.4	6.65	74.2	6.6	4.63	45.3	6.5	0.01	0.08	8.4	6.37	84.2	6.6	7.07	84.1	8.4	5.14	85.7			
8	23.7	6.52	72.7	23.5	13.78	135	23.5	0.03	0.27	23.7	6.92	91.4	23.5	9.24	110	23.7	4.94	82.6			
9	31.2	6.13	68.4	30.5	10.67	104	30.5	0.02	0.18	31.2	6.13	81.0	30.5	7.10	84.5	31.2	4.61	77.0			
TOTAL		8.96			10.2			10.9			7.57			8.40			5.99				

Table A.24. Dissolution data for 0.1 M sulfamic acid

Time	T (hrs)	Fe (mol/kg)	Fe (%)	T (hrs)	Fe (mol/kg)	Fe (%)	T (hrs)	Fe (mol/kg)	Fe (%)	T (hrs)	Fe (mol/kg)	Fe (%)	T (hrs)	Fe (mol/kg)	Fe (%)	T (hrs)	Fe (mol/kg)	Fe (%)	T (hrs)	Fe (mol/kg)	Fe (%)
		K1			K2			K3			K4			K5			S1			S2	
1	0.20	0.10	1.12	0.20	0.03	0.36	0.10	0.02	0.28	0.18	0.05	0.69	0.11	0.01	0.15	0.12	0.04	0.54	0.11	0.10	1.73
2	0.50	0.20	2.30	0.50	0.07	0.85	0.40	0.06	0.75	0.48	0.16	2.11	0.41	0.04	0.65	0.42	0.12	1.48	0.41	0.34	5.68
3	1.43	0.53	6.16	1.44	0.16	1.87	1.33	0.13	1.76	1.41	0.51	6.77	1.34	0.16	2.69	1.35	0.33	3.90	1.35	1.04	17.4
4	2.57	1.01	11.8	2.57	0.25	2.95	2.47	0.23	3.10	2.55	1.07	14.1	2.47	0.56	9.25	2.48	0.63	7.46	2.48	1.91	31.8
5	4.28	1.80	20.9	4.29	0.42	4.97	4.18	0.47	6.28	4.26	1.78	23.6	4.19	1.16	19.2	4.20	1.08	12.9	4.20	3.21	53.6
6	22.6	6.88	80.0	22.6	2.90	34.6	22.5	3.89	52.1	22.6	5.51	73.0	22.5	4.99	82.9	22.5	4.80	57.1	22.48	9.65	161
7	48.6	7.04	81.8	48.6	5.52	65.9	48.5	5.86	78.4	48.6	7.14	94.6	48.5	7.01	116	48.5	5.99	71.3	48.51	9.28	155
TOTAL		8.61			8.38			7.48			7.55			6.02			8.40			5.99	
		A1			A2			A3			A4			A5			A6				
1	0.19	0.22	3.44	0.21	0.38	5.79	0.18	0.39	6.79	0.18	0.21	3.38	0.18	0.64	11.2	0.18	0.43	6.87			
2	0.49	0.72	11.3	0.51	1.11	16.9	0.48	1.15	20.2	0.48	0.67	10.9	0.48	1.92	33.7	0.48	1.36	21.9			
3	1.43	1.63	25.7	1.44	2.96	44.8	1.41	2.57	45.1	1.41	2.18	35.2	1.41	4.22	74.0	1.41	2.86	46.0			
4	2.56	2.04	32.2	2.58	3.70	56.0	2.55	3.08	54.0	2.55	3.16	50.9	2.54	4.84	84.8	2.55	3.27	52.6			
5	4.28	2.59	40.8	4.29	4.15	62.8	4.26	3.43	60.1	4.26	3.76	60.6	4.26	4.69	82.2	4.26	3.16	50.8			
6	22.6	4.97	78.3	22.6	6.18	93.5	22.6	5.61	98.4	22.6	6.89	111	22.5	6.24	109	22.6	4.36	70.0			
7	48.6	4.85	76.4	48.6	6.49	98.1	48.6	5.59	98.1	48.6	6.62	107	48.6	6.67	117	48.6	4.75	76.3			
TOTAL		6.35			6.61			5.70			6.21			5.71			6.22				
		FH2			FH6			Gt			Sch			H1			H2				
1	0.15	0.06	0.63	0.15	0.04	0.39	0.17	0.00	0.00	0.16	0.04	0.47	0.19	0.04	0.50	0.18	0.06	0.70			
2	0.45	0.15	1.65	0.45	0.09	0.86	0.47	0.01	0.08	0.46	0.13	1.74	0.49	0.09	1.18	0.48	0.13	1.57			
3	1.38	0.35	3.87	1.39	0.17	1.70	1.40	0.01	0.07	1.39	0.43	5.62	1.42	0.32	4.14	1.41	0.38	4.45			
4	2.52	0.45	5.03	2.52	0.23	2.27	2.54	0.01	0.07	2.53	1.03	13.7	2.55	0.65	8.29	2.55	0.81	9.38			
5	4.23	0.67	7.45	4.24	0.43	4.17	4.25	0.01	0.09	4.24	2.62	34.6	4.27	1.15	14.7	4.26	1.79	20.8			
6	22.5	4.41	49.3	22.5	1.14	11.2	22.5	0.01	0.12	22.5	9.52	126	22.6	5.15	65.9	22.6	10.8	126			
7	48.6	9.81	110	48.6	1.90	18.6	48.6	0.02	0.15	48.6	10.0	133	48.6	6.51	83.2	48.6	11.1	129			
TOTAL		8.96			10.2			10.9			7.57			7.82			8.60				

Table A.25. Dissolution data for 0.05 M ascorbic acid

	Time (hrs)	Fe (mol/kg)	Fe (%)	Time (hrs)	Fe (mol/kg)	Fe (%)	Time hrs)	Fe (mol/kg)	Fe (%)	Time (hrs)	Fe (molkg)	Fe (%)	Time hrs)	Fe (mol/kg)	Fe (%)	Time (hrs)	Fe (mol/kg)	Fe (%)	Time (hrs)	Fe (mmol/g)	Fe (%)
		K1			K2			K3			K4			K5			H1			H2	
1	0.28	0.11	1.24	0.16	0.05	0.60	0.18	0.15	2.01	0.27	0.14	1.83	0.17	0.03	0.44	0.28	0.02	0.28	0.28	0.05	0.59
2	0.65	0.16	1.89	0.59	0.09	1.13	0.60	0.33	4.42	0.64	0.28	3.66	0.59	0.05	0.78	0.65	0.03	0.34	0.65	0.09	1.00
3	1.53	0.27	3.17	1.44	0.15	1.84	1.45	0.50	6.71	1.52	0.63	8.29	1.45	0.11	1.77	1.53	0.03	0.44	1.53	0.15	1.71
4	3.37	0.46	5.31	3.30	0.27	3.16	3.31	0.72	9.69	3.36	1.50	19.9	3.31	0.23	3.80	3.37	0.05	0.70	3.37	0.24	2.76
5	5.64	0.67	7.83	5.54	0.34	4.11	5.56	0.86	11.5	5.63	2.04	27.0	5.55	0.38	6.38	5.64	0.07	0.85	5.64	0.31	3.60
6	7.31	0.74	8.65	7.24	0.34	4.10	7.25	1.26	16.9	7.30	2.15	28.5	7.25	0.49	8.20	7.31	0.07	0.89	7.31	0.35	4.12
7	22.9	3.57	41.5	22.9	0.96	11.5	22.9	3.90	52.2	22.9	4.74	62.9	22.9	2.76	45.8	22.9	0.20	2.60	22.9	2.52	29.3
8	32.1	3.61	41.9	32.0	0.98	11.7	32.1	3.95	52.8	32.1	5.87	77.7	32.0	3.84	63.8	32.1	0.45	5.72	32.1	3.87	45.0
9	55.2	4.17	48.5	55.2	1.43	17.0	55.2	4.32	57.7	55.2	5.68	75.3	55.2	4.01	66.6	55.2	1.01	12.9	55.2	4.53	52.6
10	96.2	4.33	50.3	96.2	2.57	30.7	96.2	3.88	51.9	96.2	4.99	66.1	96.2	3.77	62.7	96.2	3.69	47.1	96.2	4.99	58.0
TOTAL		8.61			8.38			7.48			7.55			6.02			7.82			8.60	
		A1			A2			A3			A4			A5			A6				
1	0.25	0.03	0.498	0.15	0.07	1.11	0.25	0.095	1.66	0.29	0.07	1.07	0.19	0.10	1.81	0.19	0.085	1.36			
2	0.63	0.13	2.12	0.58	0.21	3.13	0.63	0.25	4.34	0.66	0.15	2.38	0.61	0.31	5.38	0.60	0.24	3.79			
3	1.50	0.43	6.69	1.43	0.65	9.89	1.50	0.75	13.1	1.53	0.42	6.69	1.46	0.97	16.9	1.46	0.87	13.9			
4	3.35	1.19	18.8	3.30	2.10	31.8	3.35	2.25	39.5	3.37	0.90	14.5	3.32	2.53	44.3	3.32	2.63	42.2			
5	5.61	1.66	26.2	5.53	2.62	39.7	5.61	2.63	46.1	5.64	1.27	20.5	5.57	3.61	63.2	5.56	2.77	44.5			
6	7.29	1.88	29.5	7.23	2.36	35.7	7.29	2.51	44.0	7.31	1.52	24.4	7.26	3.33	58.3	7.25	3.18	51.2			
7	22.9	4.20	66.2	22.9	4.34	65.6	22.9	4.73	82.9	23.0	4.53	72.9	22.9	5.38	94.2	22.9	4.30	69.1			
8	32.1	4.78	75.2	32.0	4.74	71.8	32.1	4.65	81.5	32.1	4.78	76.9	32.1	5.19	90.9	32.1	4.21	67.7			
9	55.2	4.30	67.6	55.2	4.34	65.7	55.2	4.39	77.0	55.2	4.81	77.4	55.2	4.44	77.7	55.2	3.93	63.2			
10	96.2	4.41	69.4	96.2	4.23	63.9	96.2	4.74	83.1	96.2	4.67	75.2	96.2	4.16	72.9	96.2	3.97	63.8			
TOTAL		6.35			6.61			5.70			6.21			5.71			6.22				
		FH2			FH6			Gt			Sch			S1			S2				
1	0.21	0.021	0.231	0.21	0.024	0.231	0.20	0.008	0.070	0.22	0.019	0.248	0.28	0.078	0.929	0.16	0.078	1.31			
2	0.61	0.030	0.330	0.62	0.037	0.362	0.61	0.007	0.064	0.62	0.020	0.265	0.65	0.13	1.51	0.59	0.15	2.57			
3	1.47	0.042	0.474	1.48	0.046	0.450	1.47	0.003	0.025	1.48	0.023	0.310	1.52	0.20	2.37	1.44	0.34	5.60			
4	3.33	0.070	0.781	3.33	0.15	1.48	3.33	0.006	0.052	3.34	0.033	0.432	3.37	0.32	3.80	3.31	0.63	10.6			
5	5.58	0.081	0.901	5.58	0.094	0.923	5.57	0.004	0.035	5.59	0.038	0.504	5.63	0.46	5.50	5.54	1.15	19.3			
6	7.27	0.090	1.01	7.27	0.10	0.993	7.26	0.004	0.035	7.28	0.041	0.535	7.31	0.46	5.41	7.24	1.51	25.2			
7	22.9	0.27	2.97	22.9	0.22	2.11	22.9	0.009	0.079	22.9	0.16	2.07	22.9	1.65	19.6	22.9	4.40	73.3			
8	32.1	0.33	3.69	32.1	0.23	2.23	32.1	0.010	0.091	32.1	0.26	3.36	32.1	1.80	21.4	32.0	4.95	82.6			
9	55.2	0.64	7.14	55.2	0.34	3.31	55.2	0.011	0.098	55.2	0.69	9.17	55.2	2.44	29.1	55.2	4.32	72.1			
10	96.2	1.90	21.2	96.2	0.42	4.06	96.2	0.013	0.118	96.2	2.23	29.4	96.2	nd	Nd	96.2	3.82	63.8			
TOTAL		8.96			10.2			10.9			7.57			8.40			5.99				

Table A.26. Dissolution data for 0.1 M sodium dithionite

	Time (hrs)	Fe (mol/kg)	Fe (%)	Time (hrs)	Fe (mol/kg)	Fe (%)	Time (hrs)	Fe (mol/kg)	Fe (%)	Time (hrs)	Fe (mol/kg)	Fe (%)	Time (hrs)	Fe (mol/kg)	Fe (%)	Time (hrs)	Fe (mol/kg)	Fe (%)	Time (hrs)	Fe (mol/kg)	Fe (%)
		K1			**K2**			**K3**			**K4**			**K5**			**H1**			**H2**	
1	0.22	2.25	26.1	0.18	2.65	31.6	0.11	2.59	34.9	0.21	2.96	39.2	0.11	2.81	46.7	0.20	0.35	4.46	0.16	1.20	14.0
2	0.50	5.27	61.2	0.45	6.38	76.1	0.38	4.19	56.0	0.43	4.71	62.3	0.38	5.36	89.1	0.46	3.25	41.5	0.42	4.71	54.8
3	0.76	7.15	83.1	0.77	7.72	92.2	0.69	5.23	69.9	0.64	5.53	73.2	0.68	5.52	91.7	0.77	5.34	68.3	0.73	6.40	74.5
4	1.43	7.85	91.1	1.59	7.83	93.5	1.52	6.79	90.8	1.41	7.00	92.7	1.52	5.54	92.0	1.61	6.87	87.9	1.56	8.25	96.0
5	2.54	8.71	101	2.82	8.45	101	2.76	7.62	102	2.53	7.73	102	2.75	6.33	105	2.84	7.77	99.4	2.80	9.05	105
6	4.73	8.85	103	5.09	8.40	100	5.02	7.57	101	4.72	7.77	103	5.02	6.19	103	5.11	8.08	103	5.06	9.00	105
7	6.70	8.67	101	6.67	8.48	101	6.61	7.70	103	6.69	7.94	105	6.60	6.13	102	6.69	8.02	103	6.65	9.09	106
TOTAL		8.61			8.38			7.48			7.55			6.02			7.82			8.60	
		A1			**A2**			**A3**			**A4**			**A5**			**A6**				
1	0.20	1.05	16.6	0.18	1.96	29.6	0.20	1.61	28.2	0.20	1.49	24.0	0.16	2.00	35.0	0.17	1.10	17.7			
2	0.46	3.43	54.0	0.44	4.78	72.3	0.48	3.33	58.4	0.47	3.92	63.2	0.43	4.61	80.8	0.44	3.83	61.5			
3	0.77	4.11	64.7	0.75	5.79	87.6	0.72	4.13	72.5	0.71	4.76	76.6	0.74	5.03	88.1	0.74	4.86	78.1			
4	1.61	5.47	86.2	1.58	7.74	117	1.41	4.83	84.8	1.40	5.48	88.2	1.57	5.61	98.3	1.58	5.50	88.4			
5	2.84	6.45	102	2.82	6.66	101	2.53	5.58	97.9	2.52	6.05	97.4	2.81	5.75	101	2.81	6.09	97.9			
6	5.11	6.68	105	5.08	6.47	97.9	4.72	5.63	98.8	4.71	6.10	98.2	5.07	5.75	101	5.08	6.20	99.6			
7	6.69	6.69	105	6.67	6.49	98.2	6.68	5.72	100	6.68	6.09	98.1	6.66	5.85	102	6.66	6.16	99.1			
TOTAL		6.35			6.61			5.70			6.21			5.71			6.22				
		FH2			**FH6**			**Gt**			**Sch**			**S1**			**S2**				
1	0.20	2.05	22.8	0.19	3.03	29.6	0.20	0.73	6.71	0.15	1.43	18.8	0.10	3.68	43.8	0.10	5.28	88.2			
2	0.48	5.44	60.7	0.46	7.97	77.9	0.48	1.84	16.8	0.41	5.98	79.0	0.36	6.25	74.3	0.37	5.89	98.3			
3	0.73	7.60	84.8	0.74	9.32	91.1	0.73	4.96	45.5	0.72	7.13	94.2	0.67	7.31	87.1	0.68	6.07	101			
4	1.41	8.05	90.0	1.46	9.91	96.9	1.41	7.48	68.6	1.56	7.00	92.5	1.51	8.09	96.3	1.51	5.87	98.0			
5	2.52	8.99	100	2.62	10.4	101	2.52	11.2	103	2.80	7.52	99.3	2.74	8.47	101	2.74	6.71	112			
6	4.71	8.98	100	4.84	10.3	100	4.71	10.7	98.1	5.06	7.72	102	5.01	8.74	104	5.01	6.61	110			
7	6.68	8.91	99.4	6.67	10.4	102	6.68	11.1	102	6.64	7.76	102	6.59	8.53	102	6.59	6.74	112			
TOTAL		8.96			10.2			10.9			7.57			8.40			5.99				

Table A.27. Dissolution data for 0.01 M sodium dithionite

	Time (hrs)	Fe (mmol/g)	Fe (µmol/m2)	Fe (%)	Time (hrs)	Fe (mmol/g)	Fe (µmol/m2)	Fe (%)
Sample			**K1**				**K4**	
1	0	0	0	0	0	0	0	0
2	0.10	2.53	8.80	8.80	0.09	2.73	29.7	32.6
3	0.27	3.30	11.5	11.5	0.26	2.88	31.3	34.4
4	0.65	3.50	12.1	12.1	0.64	4.11	44.6	49.0
5	1.58	3.76	13.1	13.1	1.58	4.34	47.2	51.8
6	2.67	3.91	13.6	13.6	2.66	4.53	49.2	54.1
7	4.53	4.22	14.6	14.6	4.53	4.90	53.2	58.4
8	22.1	5.27	18.3	18.3	22.1	6.32	68.7	75.4
TOTAL		8.61				8.38		
Surface area		288				92.0		
			A3				**A4**	
1	0	0	0	0	0	0	0	0
2	0.09	1.35	7.66	23.7	0.11	1.08	4.77	17.4
3	0.26	2.05	11.6	35.9	0.28	1.86	8.21	30.0
4	0.64	2.31	13.2	40.6	0.66	2.03	8.96	32.8
5	1.58	2.60	14.8	45.6	1.59	2.31	10.2	37.1
6	2.66	2.81	16.0	49.3	2.68	2.43	10.7	39.2
7	4.53	3.11	17.7	54.6	4.54	2.71	11.9	43.6
8	22.1	4.82	27.4	84.5	22.1	4.21	18.5	67.8
TOTAL		5.70				6.21		
Surface area		176				227		
			FH2				**FH6**	
1	0	0	0	0	0	0	0	0
2	0.12	1.52	4.85	17.0	0.09	1.77	8.98	17.3
3	0.28	2.63	8.37	29.3	0.26	3.48	17.7	34.0
4	0.67	2.81	8.96	31.4	0.64	3.78	19.2	37.0
5	1.60	2.95	9.38	32.9	1.57	3.82	19.4	37.4
6	2.68	2.95	9.41	33.0	2.66	3.80	19.3	37.2
7	4.55	3.01	9.60	33.6	4.52	3.84	19.5	37.5
8	22.1	3.48	11.1	38.8	22.1	4.04	20.5	39.5
TOTAL		8.96				10.2		
Surface area		314				197		
			Gt					
1	0	0	0	0				
2	0.12	0.32	10.9	2.90				
3	0.29	0.80	27.7	7.38				
4	0.67	1.12	38.7	10.3				
5	1.61	1.01	34.6	9.22				
6	2.69	1.01	34.9	9.30				
7	4.56	1.04	35.7	9.53				
8	22.1	1.07	36.8	9.82				
TOTAL		10.9						
Surface area		29.1						

Table A.28. Dissolution data for 0.1 M acetic acid

	Time (hrs)	Fe (mmol/g)	Fe (µmol/m^2)	Fe (%)	Time (hrs)	Fe (mmol/g)	Fe (µmol/m^2)	Fe (%)
Sample		**K1**				**K4**		
1	0	0	0	0.00	0	0	0	0.00
2	0.3	0.004	0.01	0.05	0.3	0.002	0.03	0.03
3	0.5	0.010	0.04	0.12	0.5	0.011	0.12	0.14
4	1.3	0.025	0.09	0.29	1.3	0.026	0.28	0.34
5	2.3	0.035	0.12	0.41	2.3	0.040	0.43	0.53
6	4.5	0.052	0.18	0.60	4.4	0.052	0.56	0.68
7	6.8	0.061	0.21	0.71	6.7	nd	nd	nd
8	25.6	0.094	0.33	1.09	25.6	0.100	1.09	1.33
9	47.5	0.117	0.41	1.36	47.5	0.118	1.29	1.57
TOTAL		8.61				7.55		
Surface area (m^2/g)		288.00				92.00		
Time		**A3**				**A4**		
1	0	0	0	0.00	0	0	0	0.00
2	0.3	0.014	0.08	0.25	0.3	0.005	0.02	0.08
3	0.5	0.029	0.17	0.51	0.5	0.012	0.05	0.20
4	1.3	0.040	0.23	0.70	1.3	0.025	0.11	0.40
5	2.3	0.060	0.34	1.06	2.3	0.037	0.16	0.60
6	4.5	0.089	0.50	1.56	4.5	0.092	0.40	1.48
7	6.8	0.105	0.60	1.85	6.8	0.074	0.32	1.19
8	25.6	0.168	0.96	2.95	25.6	0.117	0.51	1.88
9	47.5	0.213	1.21	3.73	47.5	0.149	0.66	2.40
TOTAL		5.70				6.21		
Surface area (m^2/g)		176.00				227.00		
Time		**FH2**				**FH6**		
1	0	0	0.00	0.00	0	0	0.00	0.00
2	0.3	0.002	0.01	0.03	0.27	0.017	0.09	0.17
3	0.5	0.008	0.02	0.09	0.47	0.009	0.05	0.09
4	1.3	0.030	0.10	0.34	1.24	0.013	0.07	0.13
5	2.3	0.039	0.12	0.44	2.24	0.017	0.09	0.17
6	4.5	0.058	0.18	0.65	4.44	0.016	0.08	0.16
7	6.8	0.068	0.22	0.76	6.74	0.032	0.16	0.31
8	25.6	0.110	0.35	1.23	25.61	0.047	0.24	0.46
9	47.5	0.143	0.46	1.60	47.49	0.065	0.33	0.63
TOTAL		8.96				10.2		
Surface area (m^2/g)		314.00				197.00		
Time		**Gt**						
1	0	0	-	0.00				
2	0.3	0.013	0.45	0.12				
3	0.5	0.003	0.09	0.02				
4	1.2	bdl	bdl	bdl				
5	2.2	0.000	0.00	0.00				
6	4.4	0.004	0.12	0.03				
7	6.7	0.011	0.36	0.10				
8	25.6	0.006	0.21	0.06				
9	47.5	0.012	0.42	0.11				
TOTAL		10.9						
Surface area (m^2/g)		29.10						

Table A.29. Dissolution data for 0.1 M phosphoric acid

Sample	Time (hrs)	Fe (mmol/g)	Fe (μmol/m^2)	Fe (%)	Time (hrs)	Fe (mmol/g)	Fe (μmol/m^2)	Fe (%)
		K1				**K4**		
1	0	0	0	0	0	0	0	0
2	0.14	0.44	1.54	5.14	0.14	0.66	7.20	8.78
3	0.47	0.93	3.24	10.8	0.47	0.74	8.02	9.77
4	1.24	1.12	3.87	13.0	1.24	1.25	13.6	16.6
5	2.29	2.59	9.01	30.1	2.29	3.81	41.4	50.5
6	4.44	3.60	12.5	41.8	4.44	4.12	44.8	54.6
7	6.79	4.00	13.9	46.5	6.79	4.52	49.1	59.8
8	25.7	4.86	16.9	56.5	25.7	5.19	56.4	68.7
9	47.5	5.69	19.7	66.0	47.5	6.36	69.2	84.3
TOTAL		8.61				7.55		
Surface area (m^2/g)		288				92		
		A3				**A4**		
1	0	0	0	0	0	0	0	0
2	0.15	0.724	4.11	12.7	0.14	0.535	2.36	8.61
3	0.48	1.17	6.63	20.5	0.48	1.15	5.07	18.5
4	1.25	1.22	6.92	21.4	1.24	1.16	5.12	18.7
5	2.30	3.00	17.1	52.6	2.29	3.32	14.6	53.4
6	4.45	4.11	23.4	72.2	4.44	4.12	18.2	66.3
7	6.80	4.32	24.6	75.8	6.79	4.46	19.6	71.8
8	25.7	4.67	26.5	8.84	25.7	4.79	21.1	77.1
9	47.6	5.24	29.8	91.9	47.5	5.36	23.6	86.4
TOTAL		5.70				6.21		
Surface area (m^2/g)		176				227		
		FH2				**FH6**		
1	0	0	0	0	0	0	0	0
2	0.13	0.21	0.67	2.34	0.12	0.16	0.81	1.55
3	0.47	0.60	1.91	6.69	0.46	0.26	1.34	2.58
4	1.23	0.80	2.55	8.93	1.22	0.45	2.28	4.38
5	2.28	1.93	6.14	21.5	2.27	0.89	4.50	8.67
6	4.43	2.63	8.36	29.3	4.42	1.35	6.84	13.2
7	6.78	2.89	9.20	32.2	6.77	1.61	8.18	15.8
8	25.7	3.48	11.1	38.8	25.6	2.77	14.1	27.1
9	47.5	4.07	13.0	45.4	47.5	3.20	16.2	31.3
TOTAL		8.96				10.2		
Surface area (m^2/g)		314				197		
		Gt						
1	0.00	0.00	0.00	0.00				
2	0.13	0.01	0.43	0.12				
3	0.46	0.01	0.43	0.12				
4	1.23	0.02	0.55	0.15				
5	2.28	0.02	0.70	0.19				
6	4.43	0.02	0.75	0.20				
7	6.78	0.02	0.83	0.22				
8	25.64	0.04	1.22	0.33				
9	47.53	0.04	1.49	0.40				
TOTAL		10.9						
Surface area (m^2/g)		29.1						

Table A.30. Dissolution data for 0.1 M hydroxylamine hydrochloride

Sample	Time (hrs)	Fe (mmol/g)	Fe (μmol/m^2)	Fe (%)	Time (hrs)	Fe (mmol/g)	Fe (μmol/m^2)	Fe (%)
Time			K1				K4	
1	0	0	0	0	0	0	0	0
2	0.21	0.01	0.02	0.07	0.20	0.01	0.06	0.07
3	0.49	0.03	0.10	0.35	0.49	0.03	0.37	0.45
4	1.01	0.07	0.23	0.78	1.00	0.07	0.72	0.88
5	2.16	0.16	0.55	1.85	2.15	0.17	1.90	2.31
6	4.11	0.30	1.06	3.54	4.10	0.35	3.79	4.62
7	7.54	0.50	1.74	5.83	7.54	0.64	7.00	8.53
8	23.8	1.50	5.21	17.4	23.8	1.66	18.1	22.0
9	49.9	2.52	8.77	29.3	49.9	2.17	23.5	28.7
TOTAL		8.61				7.55		
Surface area (m^2/g)		288				92.0		
Time			A3				A4	
1	0	0	0	0	0	0	0	0
2	0.22	0.04	0.20	0.62	0.21	0.01	0.05	0.20
3	0.50	0.11	0.60	1.85	0.49	0.05	0.23	0.82
4	1.02	0.23	1.32	4.06	1.01	0.12	0.55	2.01
5	2.17	0.51	2.89	8.92	2.16	0.31	1.35	4.94
6	4.12	0.84	4.77	14.7	4.11	0.57	2.49	9.10
7	7.55	1.14	6.51	20.1	7.54	0.87	3.85	14.1
8	23.8	1.81	10.3	31.8	23.8	1.72	7.59	27.7
9	49.9	2.23	12.7	39.1	49.9	2.38	10.5	38.4
TOTAL		5.70				6.21		
Surface area (m^2/g)		176				227		
Time			FH2				FH6	
1	0	0	0	0	0	0	0	0
2	0.20	0.00	0.01	0.02	0.19	0.00	0.00	0.01
3	0.48	0.02	0.07	0.25	0.47	0.01	0.05	0.09
4	1.00	0.06	0.19	0.66	0.99	0.02	0.12	0.23
5	2.15	0.15	0.47	1.65	2.14	0.06	0.31	0.59
6	4.10	0.27	0.85	2.98	4.09	0.11	0.57	1.10
7	7.53	0.46	1.47	5.15	7.52	0.16	0.82	1.58
8	23.8	1.42	4.52	15.8	23.8	0.43	2.19	4.22
9	49.9	2.16	6.89	24.1	49.8	0.70	3.57	6.88
TOTAL		8.96				10.2		
Surface area (m^2/g)		314				197		
Time			Gt					
1	0	0	0	0				
2	0.20	0.004	0.13	0.03				
3	0.48	0.002	0.06	0.02				
4	1.00	Bdl						
5	2.15	0.001	0.05	0.01				
6	4.10	0.002	0.06	0.02				
7	7.53	0.001	0.04	0.01				
8	23.8	0.004	0.13	0.03				
9	49.9	0.007	0.25	0.07				
TOTAL		10.9						
Surface area (m^2/g)		29						

Table A.31. Dissolution data for 0.1 M HCl

Sample	Time (hrs)	Fe (mmol/g)	Fe (μmol/m²)	Fe (%)	Time (hrs)	Fe (mmol/g)	Fe (μmol/m²)	Fe (%)
Time		**K1**				**K4**		
1	0	0	0	0	0	0	0	0
2	0.16	0.05	0.18	0.60	0.15	0.03	0.34	0.41
3	0.44	0.26	0.90	3.02	0.44	0.20	2.13	2.60
4	0.96	0.61	2.11	7.06	0.95	0.55	5.96	7.26
5	2.11	1.90	6.60	22.1	2.10	1.73	18.8	22.9
6	4.06	4.34	15.1	50.4	4.05	3.60	39.1	47.6
7	7.49	6.22	21.6	72.2	7.49	5.13	55.8	68.0
8	23.8	8.06	28.0	93.6	23.8	8.44	91.7	112
9	49.8	7.80	27.1	90.6	49.8	9.20	100	123
TOTAL		8.61				7.55		
Surface area (m^2/g)		288				92.0		
Time		**A3**				**A4**		
1	0	0	0	0	0	0	0	0
2	0.17	0.38	2.14	6.62	0.16	0.12	0.53	1.96
3	0.45	1.23	7.01	21.6	0.44	0.88	3.88	14.2
4	0.97	2.16	12.3	37.9	0.96	2.12	9.36	34.2
5	2.12	3.88	22.0	68.0	2.11	4.25	18.7	68.4
6	4.07	5.12	29.1	89.9	4.06	5.76	25.4	92.8
7	7.50	5.80	33.0	102	7.49	6.30	27.7	101
8	23.8	6.20	35.2	109	23.8	6.79	29.9	109
9	49.8	5.79	32.9	102	49.8	6.27	27.6	101
TOTAL		5.70				6.21		
Surface area (m^2/g)		176				227		
Time		**FH2**				**FH6**		
1	0.00	0.00	0.00	0.00	0.00	0.00	0.00	0.00
2	0.15	0.06	0.18	0.64	0.14	0.03	0.18	0.34
3	0.43	0.29	0.91	3.19	0.42	0.11	0.57	1.09
4	0.95	0.62	1.98	6.93	0.94	0.20	1.03	1.98
5	2.10	1.56	4.96	17.4	2.09	0.38	1.93	3.72
6	4.05	5.17	16.5	57.7	4.04	0.63	3.20	6.16
7	7.48	9.19	29.3	103	7.47	1.02	5.16	9.94
8	23.8	12.3	39.2	138	23.8	2.71	13.8	26.5
9	49.8	9.10	29.0	102	49.8	4.59	23.3	44.9
TOTAL		8.96				10.2		
Surface area (m^2/g)		314.00				197		
Time		**Gt**						
1	0.00	0.000	0.000	0.000				
2	0.14	0.000	0.000	0.000				
3	0.43	0.000	0.000	0.000				
4	0.94	0.002	0.056	0.015				
5	2.09	0.001	0.018	0.005				
6	4.04	0.001	0.034	0.009				
7	7.48	0.001	0.037	0.010				
8	23.76	0.003	0.098	0.026				
9	49.79	0.004	0.129	0.034				
TOTAL		10.9						
Surface area (m^2/g)		29.1						

Table A.32. Dissolution data for 0.1 M H_2SO_4

Sample	Time (hrs)	Fe (mmol/g)	Fe (μmol/m²)	Fe (%)	Time (hrs)	Fe (mmol/g)	Fe (μmol/m²)	Fe (%)
Time		**K1**				**K4**		
1	0	0	0	0	0	0	0	0
2	0.17	0.38	1.32	4.41	0.17	0.67	7.23	8.81
3	0.46	1.95	6.77	22.6	0.45	2.11	22.9	27.9
4	0.97	3.42	11.9	39.8	0.97	4.40	47.8	58.3
5	2.12	6.07	21.1	70.6	2.12	7.08	76.9	93.7
6	4.07	7.48	26.0	86.9	4.07	8.16	88.7	108
7	7.51	8.68	30.2	101	7.50	8.19	89.0	109
8	23.8	10.9	37.7	126	23.8	7.88	85.6	104
9	49.8	9.79	34.0	114	49.8	7.81	84.9	103
TOTAL		8.61				7.55		
Surface area (m^2/g)		288				92.0		
Time		**A3**				**A4**		
1	0	0	0	0	0	0	0	0
2	0.18	1.56	8.84	27.3	0.18	1.56	6.88	25.1
3	0.47	3.43	19.5	60.2	0.46	3.96	17.4	63.7
4	0.98	4.61	26.2	80.9	0.98	4.75	20.9	76.6
5	2.13	5.76	32.7	101	2.13	6.27	27.6	101
6	4.08	5.78	32.8	101	4.08	6.28	27.7	101
7	7.52	5.79	32.9	102	7.51	6.21	27.4	100
8	23.8	5.88	33.4	103	23.8	6.23	27.5	100
9	49.8	5.80	33.0	102	49.8	6.25	27.5	101
TOTAL		5.70				6.21		
Surface area (m^2/g)		176				227		
Time		**FH2**				**FH6**		
1	0	0	0	0	0	0	0	0
2	0.17	0.55	1.76	6.16	0.16	0.12	0.60	1.16
3	0.45	3.16	10.1	35.3	0.44	0.45	2.27	4.38
4	0.97	6.54	20.8	73.0	0.96	0.85	4.30	8.29
5	2.12	8.87	28.2	99.0	2.11	1.80	9.15	17.6
6	4.07	8.29	26.4	92.6	4.06	3.21	16.3	31.4
7	7.50	7.96	25.3	88.8	7.49	5.18	26.3	50.6
8	23.8	8.09	25.8	90.3	23.8	12.5	63.4	122
9	49.8	8.09	25.8	90.3	49.8	17.0	86.4	166
TOTAL		8.96				10.2		
Surface area (m^2/g)		314				197		
Time		**Gt**						
1	0	0	0	0				
2	0.16	0.00	0.08	0.021				
3	0.44	0.00	0.08	0.021				
4	0.96	0.00	0.04	0.010				
5	2.11	0.00	0.10	0.026				
6	4.06	0.01	0.22	0.058				
7	7.49	0.01	0.39	0.105				
8	23.8	0.03	0.95	0.253				
9	49.8	0.04	1.29	0.345				
TOTAL		10.9						
Surface area (m^2/g)		29.1						

Table A.33. Rate constants and correlation coefficients for iron oxide dissolution by sulfamic acid and phosphoric acid

	Square-root law		Cube root-law		1st order random nucleation		Avrami-Erofejev 2D law		Avrami-Erofejev 3D law		Kabai		
	r^2	k	r^2	k	r^2	k	r^2	k	r^2	k	r^2	k	β
0.1 M Sulfamic Acid													
FH2	0.99	0.011	0.99	0.007	0.97	0.030	**1.00**	0.033	0.98	0.031	0.97	0.019	0.89
FH6	0.98	0.002	0.98	0.001	0.98	0.004	0.87	0.008	0.79	0.009	**1.00**	0.002	0.69
Gt	0.64	1.2×10^{-5}	0.64	8.1×10^{-6}	0.64	2.4×10^{-5}	0.51	5.2×10^{-4}	0.46	1.4×10^{-3}	**0.85**	2.1×10^{-9}	0.17
Sch	0.49	0.039	0.93	0.026	0.99	0.927	**1.00**	0.144	**1.00**	0.156	**1.00**	0.101	1.32
A1	0.80	0.015	0.81	0.010	**0.90**	0.064	0.75	0.043	0.62	0.035	0.89	0.100	0.76
A2	0.89	0.075	0.66	0.050	0.83	0.080	0.67	0.213	0.41	0.192	**0.98**	0.196	0.74
A3	0.74	0.018	0.74	0.012	0.95	0.178	0.73	0.075	0.67	0.051	**0.99**	0.272	0.80
A4	0.86	0.075	0.82	0.015	**0.99**	0.230	0.95	0.215	0.90	0.197	0.99	0.267	1.08
A5	0.84	0.168	0.53	0.112	0.95	0.447	0.79	0.504	0.68	0.413	**0.95**	0.823	1.06
A6	0.78	0.104	0.55	0.069	0.84	0.748	0.40	0.305	0.32	0.291	**0.91**	0.089	0.48
K1	0.94	0.018	0.94	0.012	0.96	0.039	0.77	0.027	0.58	0.022	**0.98**	0.060	1.06
K2	**1.00**	0.007	1.00	0.005	0.99	0.022	0.96	0.021	0.87	0.019	**1.00**	0.018	1.04
K3	0.98	0.009	0.99	0.006	**0.99**	0.032	0.93	0.025	0.80	0.022	0.99	0.024	1.06
K4	0.96	0.010	0.96	0.007	**1.00**	0.060	0.91	0.033	0.74	0.025	1.00	0.060	1.08
K5	**1.00**	0.019	1.00	0.012	0.98	0.080	0.98	0.057	0.98	0.047	0.99	0.067	1.35
H1	0.95	0.009	0.96	0.006	**0.99**	0.038	0.87	0.027	0.71	0.022	**0.99**	0.041	1.10
H2	0.94	0.032	0.98	0.021	0.98	0.075	1.00	0.124	**1.00**	0.138	0.97	0.050	1.08
S1	0.95	0.008	0.95	0.005	0.98	0.027	0.83	0.022	0.68	0.019	**0.99**	0.029	0.94
S2	0.94	0.064	0.91	0.042	0.96	0.180	0.98	0.194	**0.99**	0.186	0.97	0.165	1.03
0.4 M Sulfamic acid													
FH2	0.97	0.359	0.97	0.239	**0.99**	1.607	0.97	1.112	0.90	0.945	0.93	1.283	1.88
FH6	0.94	0.016	0.94	0.011	**1.00**	0.089	0.89	0.102	0.76	0.098	0.94	0.070	0.77
Gt	**0.85**	0.000	**0.85**	0.000	**0.85**	0.001	0.66	0.022	0.55	0.066	0.83	3.17E-06	0.56
Sch	0.91	0.417	0.91	0.278	0.93	7.718	**0.99**	2.495	0.99	1.657	0.95	1.862	2.81
A1	0.59	0.149	0.59	0.099	0.81	0.978	0.63	0.513	0.50	0.392	**0.91**	2.595	0.54
A2	0.81	0.407	0.84	0.272	**1.00**	4.015	0.92	2.997	0.83	2.675	0.93	4.013	1.00
A3	0.86	0.361	0.86	0.241	**1.00**	2.228	0.89	1.233	0.76	0.973	0.95	2.355	1.00
A4	0.69	0.175	0.69	0.117	**0.91**	1.386	0.79	0.664	0.68	0.492	0.91	1.808	0.98
A5	0.78	0.369	0.78	0.246	**0.98**	6.230	0.98	2.123	0.89	1.422	0.93	3.512	1.35
A6	0.83	0.294	0.83	0.196	**0.94**	1.212	0.80	0.882	0.68	0.770	0.90	1.480	0.89
K1	0.82	0.093	0.82	0.062	0.94	0.433	0.82	0.274	0.70	0.217	**0.97**	0.542	0.91
K2	0.85	0.049	0.85	0.032	0.93	0.182	0.83	0.140	0.76	0.120	**0.96**	0.243	1.28
K3	0.90	0.081	0.90	0.054	**0.99**	0.498	0.94	0.273	0.85	0.209	0.96	0.429	1.30
K4	0.86	0.237	0.86	0.158	0.86	2.593	0.94	1.458	0.90	1.151	**0.92**	1.526	1.33
K5	0.86	0.243	0.86	0.162	0.94	3.683	**1.00**	1.763	0.99	1.329	0.93	1.599	2.27
H1	0.92	0.109	0.92	0.072	**0.99**	0.570	0.94	0.344	0.87	0.270	0.97	0.463	1.37
H2	0.93	0.245	0.93	0.163	0.85	1.218	**0.96**	1.033	0.95	0.937	0.95	0.867	1.61
S1	0.85	0.105	0.85	0.070	0.97	0.584	0.85	0.070	0.78	0.254	**0.96**	0.599	1.10
S2	0.97	0.824	0.97	0.549	0.91	3.081	**1.00**	2.572	0.98	2.414	0.91	2.537	2.16
0.1 M Phosphoric													
FH2	0.60	0.004	0.66	0.003	0.74	0.011	0.48	0.012	0.40	0.011	**0.89**	0.016	0.55
FH6	0.86	0.003	0.85	0.002	0.81	0.008	0.66	0.010	0.55	0.010	**0.97**	0.005	0.57
Gt	0.68	3.2×10^{-5}	0.77	3.2×10^{-5}	0.77	6.4×10^{-5}	0.61	3.2×10^{-5}	0.53	1.6×10^{-3}	**0.98**	2.1×10^{-3}	0.22
A3	0.52	0.008	0.56	0.005	0.68	0.047	0.41	0.024	0.31	0.018	**0.93**	0.158	0.54
A4	0.50	0.007	0.55	0.005	0.86	0.037	0.39	0.022	0.30	0.016	**0.91**	0.121	0.55
K1	**0.94**	0.006	0.69	0.004	0.72	0.021	0.51	0.016	0.41	0.013	0.94	0.038	0.53
K4	0.53	0.007	0.63	0.005	0.70	0.034	0.48	0.021	0.39	0.016	**0.91**	0.082	0.56

Table A.34. Rate constants and correlation coefficients for iron oxide dissolution by ammonium oxalate, ascorbate and acetic acid

	Square-root law		Cube root-law		1st order random nucleation		Avrami-Erofejev 2D law		Avrami-Erofejev 3D law		Kabai		
	r^2	k	r^2	k	r^2	k	r^2	k	r^2	k	r^2	k	β
0.2 M Oxalate													
FH2	0.85	0.099	0.85	0.066	**0.88**	0.395	0.55	0.138	0.74	0.256	0.84	0.254	1.41
FH6	0.93	0.119	0.92	0.079	0.92	0.307	0.70	0.153	0.96	0.328	**0.98**	0.349	2.51
Sch	0.86	0.110	0.86	0.073	**0.86**	0.500	0.49	0.147	0.72	0.278	**0.86**	0.331	1.63
A1	**0.85**	0.104	**0.85**	0.069	0.84	0.371	0.47	0.143	0.71	0.269	0.83	0.306	1.74
A3	0.89	0.090	**0.89**	0.060	0.81	0.283	0.41	0.132	0.62	0.241	0.77	0.269	1.67
A4	0.88	0.093	0.87	0.062	0.92	0.305	0.70	0.135	0.87	0.251	**0.93**	0.257	1.73
A5	**0.84**	0.093	**0.84**	0.062	0.83	0.308	0.47	0.135	0.67	0.245	0.81	0.274	1.50
A6	0.86	0.103	0.85	0.069	0.89	0.378	0.58	0.141	0.78	0.265	**0.89**	0.306	1.59
K1	0.89	0.117	0.89	0.078	0.86	0.506	0.56	0.152	0.84	0.305	**0.92**	0.345	2.03
K2	0.81	0.118	0.81	0.079	**0.83**	0.486	0.50	0.151	0.74	0.308	0.82	0.327	2.03
K3	0.88	0.112	0.87	0.075	0.86	0.457	0.57	0.147	0.84	0.291	**0.89**	0.297	1.70
K4	0.86	0.108	0.86	0.072	0.86	0.411	0.47	0.146	0.71	0.275	**0.87**	0.350	1.76
K5	**0.84**	0.103	**0.84**	0.068	0.84	0.364	0.47	0.141	0.69	0.264	0.83	0.308	1.62
H1	0.90	0.115	0.89	0.077	0.85	0.510	0.74	0.151	0.97	0.328	**0.97**	0.339	3.17
H2	0.87	0.117	0.87	0.078	0.86	0.488	0.53	0.152	0.82	0.309	**0.91**	0.381	2.50
S1	0.91	0.120	0.90	0.080	0.89	0.473	0.66	0.154	0.92	0.321	**0.96**	0.352	2.19
S2	**0.83**	0.107	**0.83**	0.072	0.83	0.489	0.47	0.145	0.69	0.270	0.77	0.255	1.46
0.05 M Ascorbate													
FH2	0.93	9.8×10^{-4}	0.92	9.8×10^{-4}	0.91	3.7×10^{-3}	**0.99**	5.1×10^{-3}	0.97	5.1×10^{-3}	0.85	4.0E-04	0.70
FH6	0.89	2.0×10^{-4}	0.55	2.0×10^{-4}	0.89	7.0×10^{-4}	0.68	1.2×10^{-2}	0.56	2.4×10^{-3}	**0.97**	1.3E-05	0.47
Gt	**0.63**	4.6×10^{-6}	**0.63**	4.6×10^{-6}	0.63	1.8×10^{-5}	0.48	3.5×10^{-2}	0.39	5.1×10^{-4}	0.62	7.2E-27	0.13
Sch	0.89	1.4×10^{-3}	0.88	1.4×10^{-3}	0.88	3.2×10^{-3}	**1.00**	5.1×10^{-3}	0.99	6.2×10^{-3}	0.82	5.1E-04	0.77
A1	0.85	1.2×10^{-2}	0.84	8.0×10^{-3}	0.94	4.4×10^{-2}	0.82	3.4×10^{-2}	0.68	2.9×10^{-2}	**0.95**	5.3E-02	1.14
A2	0.72	1.1×10^{-2}	0.71	7.3×10^{-3}	0.83	3.9×10^{-2}	0.65	3.1×10^{-2}	0.51	2.6×10^{-2}	**0.90**	5.7E-02	0.92
A3	0.80	1.8×10^{-2}	0.83	1.2×10^{-2}	0.94	7.6×10^{-2}	0.81	4.4×10^{-3}	0.73	4.2×10^{-2}	**0.95**	8.2E-02	0.98
A4	0.91	1.3×10^{-2}	0.89	8.6×10^{-3}	0.92	4.9×10^{-2}	0.89	1.7×10^{-3}	0.77	3.0×10^{-2}	**0.96**	4.8E-02	1.06
A5	0.64	2.0×10^{-2}	0.70	1.3×10^{-2}	0.92	1.2×10^{-1}	0.72	2.0×10^{-4}	0.62	5.1×10^{-2}	**0.94**	1.4E-01	1.09
A6	0.69	1.5×10^{-2}	0.66	9.8×10^{-3}	0.77	5.1×10^{-2}	0.60	4.2×10^{-2}	0.52	3.6×10^{-2}	**0.88**	8.9E-02	1.00
K1	0.79	3.0×10^{-3}	0.80	2.0×10^{-3}	0.84	8.5×10^{-3}	0.54	8.7×10^{-3}	0.38	7.9E-03	**0.90**	9.8E-03	0.79
K2	**0.98**	1.7×10^{-3}	**0.98**	1.1×10^{-3}	0.98	4.1×10^{-3}	0.89	5.8×10^{-3}	0.79	5.9E-03	0.96	1.6E-03	0.63
K3	0.86	1.1×10^{-2}	0.85	7.3×10^{-3}	0.83	3.1×10^{-2}	0.86	3.2×10^{-2}	0.77	3.0E-02	**0.89**	1.4E-02	0.67
K4	0.85	1.2×10^{-2}	0.83	7.9×10^{-3}	0.94	4.5×10^{-2}	0.83	3.4×10^{-2}	0.69	2.8E-02	**0.94**	4.7E-02	0.92
K5	0.84	7.1×10^{-3}	0.84	4.8×10^{-3}	**0.91**	2.3×10^{-2}	0.77	2.1×10^{-2}	0.59	1.8E-02	0.89	2.0E-02	1.06
H1	0.87	2.2×10^{-3}	0.86	1.4×10^{-3}	0.84	5.7×10^{-3}	0.95	7.4×10^{-3}	**0.99**	7.5E-03	0.83	1.3E-03	0.85
H2	0.89	3.5×10^{-3}	0.89	2.4×10^{-3}	0.93	1.0×10^{-2}	0.69	1.0×10^{-2}	0.51	9.4E-03	**0.93**	1.0E-02	0.95
S1	0.96	2.8×10^{-3}	0.91	2.8×10^{-3}	0.97	6.5×10^{-3}	0.81	1.2×10^{-2}	0.65	1.0E-02	**0.98**	4.4E-02	0.96
S2	0.86	1.4×10^{-2}	**0.97**	1.4×10^{-2}	0.93	5.6×10^{-2}	0.81	3.5×10^{-2}	0.73	3.2E-02	0.73	3.6E-03	0.70
0.1 M Acetic acid													
FH2	0.80	1.6×10^{-4}	0.85	1.0×10^{-4}	0.85	3.2×10^{-4}	0.69	2.1×10^{-3}	0.60	3.6×10^{-3}	**0.92**	1.3×10^{-4}	0.72
FH6	0.80	5.8×10^{-5}	0.89	3.9×10^{-5}	0.56	1.2×10^{-4}	0.76	1.1×10^{-3}	0.68	2.2×10^{-3}	**0.93**	2.2×10^{-9}	0.33
Gt	0.05	7.6×10^{-6}	**0.25**	7.6×10^{-6}	0.25	1.5×10^{-5}	0.24	6.7×10^{-6}	0.22	1.1×10^{-3}	0.24	9.6×10^{-9}	0.20
A3	0.79	3.6×10^{-4}	0.79	2.4×10^{-4}	0.86	7.3×10^{-4}	0.69	3.0×10^{-3}	0.60	4.3×10^{-3}	**0.98**	4.4×10^{-5}	0.51
A4	0.82	2.5×10^{-4}	0.85	1.7×10^{-4}	0.85	5.1×10^{-4}	0.71	2.6×10^{-3}	0.61	4.2×10^{-3}	**0.88**	8.0×10^{-5}	0.62
K1	0.78	1.3×10^{-4}	0.82	8.8×10^{-5}	0.82	2.7×10^{-4}	0.65	1.8×10^{-3}	0.56	3.2×10^{-3}	**0.94**	2.9×10^{-5}	0.60
K4	0.84	1.6×10^{-4}	0.85	1.0×10^{-4}	0.85	3.2×10^{-4}	0.69	2.1×10^{-3}	0.58	3.5×10^{-3}	**0.92**	6.8×10^{-5}	0.65

Table A.35. Rate constants and correlation coefficients for iron oxide dissolution by dithionite, HCl, H_2SO_4 and hydroxylamine hydrochloride

	Square-root law		Cube root-law		1st order random nucleation		Avrami-Erofejev 2D law		Avrami-Erofejev 3D law		Kabai		
	r^2	k	r^2	k	r^2	k	r^2	k	r^2	k	r^2	k	β
0.1 M Dithionite													
FH2	0.67	0.177	0.66	0.118	0.88	4.249	0.88	1.203	0.67	0.750	**0.99**	1.882	1.37
FH6	0.54	0.158	0.54	0.105	0.96	1.919	0.63	0.754	0.44	0.522	**0.98**	2.355	0.98
Gt	0.94	0.204	0.92	0.136	0.75	2.502	0.81	**0.964**	0.94	0.669	0.94	0.963	1.80
Sch	0.45	0.142	0.53	0.095	0.83	1.136	0.51	0.543	0.39	0.403	**0.94**	2.091	0.89
A1	0.71	0.156	0.79	0.104	0.99	1.139	0.82	0.565	0.69	0.422	**0.99**	1.154	1.04
A2	0.57	0.137	0.54	0.063	**0.99**	2.418	0.59	0.616	0.47	0.376	0.96	2.328	0.96
A3	0.73	0.168	0.73	0.112	0.98	1.461	0.76	0.668	0.61	0.488	**0.99**	1.616	0.92
A4	0.55	0.170	0.67	0.113	0.96	1.421	0.70	0.662	0.54	0.486	**0.98**	1.696	0.97
A5	0.52	0.137	0.53	0.091	0.89	1.365	0.55	0.588	0.40	0.421	**0.98**	2.766	0.77
A6	0.68	0.153	0.68	0.102	0.96	1.328	0.70	0.606	0.55	0.441	**0.98**	1.573	1.00
K1	0.55	0.172	0.68	0.115	0.98	1.563	0.74	0.700	0.56	0.508	**0.99**	1.645	1.04
K2	0.53	0.140	0.54	0.093	0.95	1.822	0.60	0.694	0.44	0.476	**0.98**	2.473	0.90
K3	0.73	0.150	0.73	0.100	0.96	2.855	0.85	0.906	0.71	0.581	**0.98**	2.373	0.88
K4	0.59	0.159	0.69	0.106	0.97	1.372	0.72	0.629	0.58	0.459	**1.00**	1.914	0.81
K5	0.44	0.124	0.45	0.083	0.89	2.183	0.51	0.734	0.39	0.484	**0.98**	4.525	0.64
H1	0.70	0.169	0.81	0.113	**0.98**	1.165	0.84	0.603	0.70	0.458	0.96	0.978	1.53
H2	0.75	0.166	0.75	0.111	**0.99**	1.839	0.83	0.745	0.67	0.518	**0.99**	1.471	1.20
S1	0.30	0.130	0.54	0.087	0.84	1.164	0.53	0.527	0.40	0.383	**1.00**	3.820	0.55
S2	0.28	0.097	0.31	0.064	0.59	1.414	0.32	0.532	0.48	0.371	**0.98**	21.910	0.38
0.1 M HCl													
FH2	0.91	0.030	0.96	0.030	0.94	0.205	0.97	0.215	0.97	0.206	**0.98**	0.182	1.41
FH6	1.00	0.005	**1.00**	0.005	**1.00**	0.012	0.90	0.014	0.90	0.014	0.98	0.011	0.86
Gt	0.73	0.000	0.73	0.000	0.82	0.000	0.68	0.000	0.68	0.001	**0.97**	0.000	0.35
A3	0.59	0.020	0.66	0.020	0.98	0.564	0.95	0.341	0.91	0.269	**1.00**	0.537	1.08
A4	0.59	0.021	0.66	0.021	**1.00**	0.656	0.97	0.386	0.93	0.304	0.99	0.525	1.49
K1	0.83	0.020	0.85	0.013	0.97	0.118	0.75	0.066	0.69	0.051	**1.00**	0.138	1.26
K4	0.91	0.013	0.93	0.013	**0.99**	0.158	0.98	0.142	0.97	0.128	0.86	0.172	1.46
0.1 M H_2SO_4													
FH2	0.74	0.239	0.96	0.239	0.94	2.202	0.96	0.984	0.85	0.716	**0.99**	1.219	1.67
FH6	0.99	0.017	**1.00**	0.017	0.96	0.095	0.95	0.103	0.95	0.099	0.96	0.098	1.04
Gt	0.94	3.6E-05	0.95	3.5E-05	0.94	7.1E-05	0.78	1.0E-03	0.69	2.3E-03	**0.98**	9.5E-07	0.59
A3	0.80	0.214	0.89	0.214	**1.00**	2.348	0.94	1.213	0.89	1.058	1.00	1.844	1.10
A4	0.79	0.212	0.88	0.212	0.99	2.457	0.92	1.145	0.86	1.018	**0.99**	1.837	1.11
K1	0.71	0.023	0.91	0.015	0.92	0.897	0.93	0.326	0.86	0.263	**0.97**	0.531	1.18
K4	0.88	0.134	0.95	0.134	0.97	1.326	0.98	0.743	0.93	0.581	**1.00**	0.974	1.34
0.1 M Hydroxylamine Hydrochloride													
FH2	0.98	0.003	**0.99**	0.004	0.98	0.006	0.86	0.010	0.76	0.011	0.97	0.010	1.19
FH6	**0.98**	0.001	**0.98**	0.001	**0.98**	0.001	0.86	0.005	0.77	0.007	0.97	0.003	1.13
Gt	0.76	5.5E-06	0.76	5.9E-06	**0.77**	1.1E-05	0.76	3.6E-04	0.72	1.1E-03	0.43	5.8E-31	0.12
A3	0.84	0.004	0.86	0.004	0.87	0.010	0.65	0.012	0.54	0.012	**0.94**	0.014	0.79
A4	0.94	0.004	0.95	0.004	0.95	0.010	0.78	0.013	0.67	0.013	**0.97**	0.015	0.98
K1	0.99	0.003	0.99	0.002	**1.00**	0.007	0.89	0.011	0.80	0.012	0.99	0.010	1.09
K4	0.94	0.003	0.95	0.003	**0.95**	0.007	0.78	0.011	0.67	0.012	0.95	0.012	1.09
0.01 M Dithionite													
FH2	0.24	0.004	0.24	0.004	0.15	0.011	0.16	0.012	0.16	0.012	**0.97**	0.169	0.41
FH6	0.47	0.253	0.55	0.253	0.37	0.649	0.42	0.855	0.48	0.921	**0.97**	0.367	0.46
Gt	0.41	0.075	0.33	0.075	0.13	0.159	0.37	0.436	0.43	0.597	**0.72**	0.094	0.77
A3	0.66	0.013	0.68	0.013	0.52	0.070	0.53	0.039	0.53	0.030	**0.97**	0.173	0.31
A4	0.65	0.010	0.66	0.010	0.50	0.040	0.52	0.028	0.52	0.023	**0.97**	0.049	0.29
K1	0.38	0.007	0.39	0.005	0.27	0.027	0.28	0.020	0.28	0.017	**0.99**	0.025	0.17
K4	0.46	0.011	0.47	0.011	0.32	0.061	0.33	0.034	0.33	0.026	**0.99**	0.351	0.25

A.6 Iron oxide adherence and dissolution data

Table A.36. Full data for iron oxide adherence experiments

	PVC			GLASS			SAND			STAINLESS STEEL		
	Fe g/m^2	pH	Oxide g/m^2	Fe g/m^2	pH	Oxide g/m^2	Fe g/m^2	pH	Oxide g/m^2	Fe (g/m^2)	pH	Oxide g/m^2
H2	214.46	3.99	431.49	21.89	3.99	44.05	0.34	3.99	0.67	106.75	3.99	214.78
	158.44	5.65	318.78	36.97	5.65	74.39	0.41	5.65	0.82	82.84	5.65	166.67
	39.94	6.58	80.35	33.51	6.30	67.43	0.34	6.58	0.68	308.73	6.41	621.16
	28.45	6.91	57.24	20.87	6.58	41.99	0.06	6.91	0.12	73.17	6.58	147.22
	25.26	7.02	50.82	18.13	6.91	36.47	0.09	7.02	0.18	48.38	6.91	97.33
	27.61	7.83	55.55	19.45	7.02	39.14	1.91	8.46	3.84	26.83	7.02	53.99
	58.29	8.46	117.28	13.36	8.46	26.87				56.34	8.46	113.36
K5	167.61	3.43	394.91	23.58	3.43	55.55	0.49	3.43	1.15	50.09	3.43	118.01
	169.06	4.67	398.34	18.55	4.67	43.70	0.39	4.67	0.92	78.25	4.67	184.36
	47.87	5.68	112.78	24.80	5.68	58.44	0.51	4.98	1.20	125.43	5.68	295.53
	33.27	6.21	78.39	20.26	6.21	47.74	0.16	5.68	0.37	57.88	6.21	136.38
	54.83	6.31	129.20	15.29	6.31	36.03	0.24	6.21	0.57	86.06	6.31	202.77
	26.80	7.64	53.91	13.80	7.64	32.51	0.17	6.31	0.39	18.66	7.64	43.96
							0.05	6.91	0.12			
							0.25	7.64	0.60			
FH2	133.81	4.15	246.26	34.50	4.15	63.50	1.63	4.15	3.01	144.57	4.15	266.07
	182.80	5.08	336.43	55.37	5.08	101.90	0.53	4.51	0.98	173.42	5.08	319.15
	102.90	6.27	189.37	75.28	6.18	138.53	0.85	5.08	1.56	259.79	6.27	478.11
	80.64	6.93	148.41	55.29	6.27	101.75	0.41	6.27	0.76	264.37	6.93	486.53
	75.89	7.49	139.66	52.27	6.93	96.20	0.35	6.93	0.65	250.51	7.49	461.03
	171.04	7.71	314.78	60.69	7.49	111.68	0.30	7.49	0.55	197.38	7.71	363.25
				60.64	7.71	111.60	0.54	7.71	1.00	445.92	7.72	820.65
FH6	172.00	2.83	304.94	39.39	2.83	69.84	0.47	2.83	0.84			
	176.07	3.82	312.17	25.03	3.82	44.38	0.47	3.82	0.84	25.50	2.83	45.21
	131.09	6.65	232.41	26.93	4.15	47.75	0.34	4.53	0.61	92.92	3.82	164.74
	98.88	7.36	175.31	73.08	6.65	129.56	0.48	6.65	0.85	228.99	6.65	405.98
	53.01	7.69	93.98	60.76	7.36	107.73	0.64	7.36	1.13	211.42	7.36	374.83
	395.74	8.33	701.63	41.48	7.69	73.54	0.26	7.69	0.46	139.48	7.69	247.28
				97.25	8.33	172.41	0.99	8.33	1.76	171.82	8.33	304.63
Gt	109.43	2.51	178.14	8.85	2.51	14.40	0.38	2.51	0.62	28.26	2.51	46.00
	94.02	3.10	153.06	8.39	3.10	13.66	0.65	3.10	1.06	121.11	3.10	197.16
	139.51	3.32	227.11	8.97	3.32	14.61	0.32	3.32	0.52	27.21	3.32	44.29
	48.84	7.15	79.50	30.99	4.87	50.45	0.34	4.39	0.55	126.45	7.15	205.85
	27.76	7.80	45.19	63.12	7.15	102.75	0.20	7.15	0.33	176.91	7.80	287.98
	84.64	7.81	137.79	35.48	7.80	57.75	0.00	7.80	0.01			
A3	59.49	4.43	180.55	31.97	4.43	97.02	0.06	4.43	0.18	13.14	4.43	39.87
	46.39	5.83	140.79	29.13	5.83	88.40	0.07	5.41	0.22	49.10	5.83	149.01
	21.43	6.65	65.05	18.98	6.65	57.61	0.22	5.83	0.66	112.18	6.02	340.48
	24.38	7.58	73.99	14.53	7.36	44.09	0.41	6.65	1.25	31.72	6.65	96.27
	17.61	7.69	53.44	17.49	7.69	53.10	0.01	7.36	0.05	23.53	7.36	71.42
	27.76	8.40	84.24	18.04	8.40	54.76	0.07	7.69	0.20	29.36	7.69	89.10
							0.08	8.40	0.24	26.94	8.40	81.77
H1	72.95	2.70	163.28	28.38	2.70	63.53	0.49	2.70	1.09	79.56	2.70	178.08
	147.78	3.19	330.79	30.28	3.19	67.78	0.18	3.19	0.40	115.88	3.19	259.37
	24.13	6.98	54.01	32.35	5.88	72.41	0.21	6.98	0.47	256.61	6.56	574.38
	51.51	7.44	115.30	13.01	5.93	29.12	0.45	7.44	1.01	64.79	6.98	145.01
	39.24	7.62	87.83	35.57	6.98	79.62	0.32	8.30	0.71	42.51	7.44	95.15
	89.84	8.30	201.10	18.09	7.44	40.50				65.96	8.30	147.63
				24.63	8.30	55.12						

Table A.37. Time-dependent dissolution of adhered oxides (note that samples of same name are not duplicates but adherence experiments performed at different pH)

Time Minutes	FH2 Glass	FH2 Glass	FH6 SST	K4 SST	K4 SST	H2 SST
5	0.4	97.2	6.0	90.9	40.6	45.3
10	4.3	115.3	11.1	73.9	39.0	44.0
20	13.8	299.2	25.4	80.0	42.4	61.5
40	30.8	365.8	51.7	85.3	84.5	129.4
80	59.6	92.9	348.2	117.6	88.1	110.7
160	72.4	101.8	324.0	117.7	111.3	145.3
320	75.9	107.6	340.1	145.0	115.4	149.9
480	73.9	99.4	349.2	150.2	124.2	150.6
1440	71.3	93.4	340.3	147.4	127.5	170.9
1830	69.0			151.3		
4680		93.7				174.9

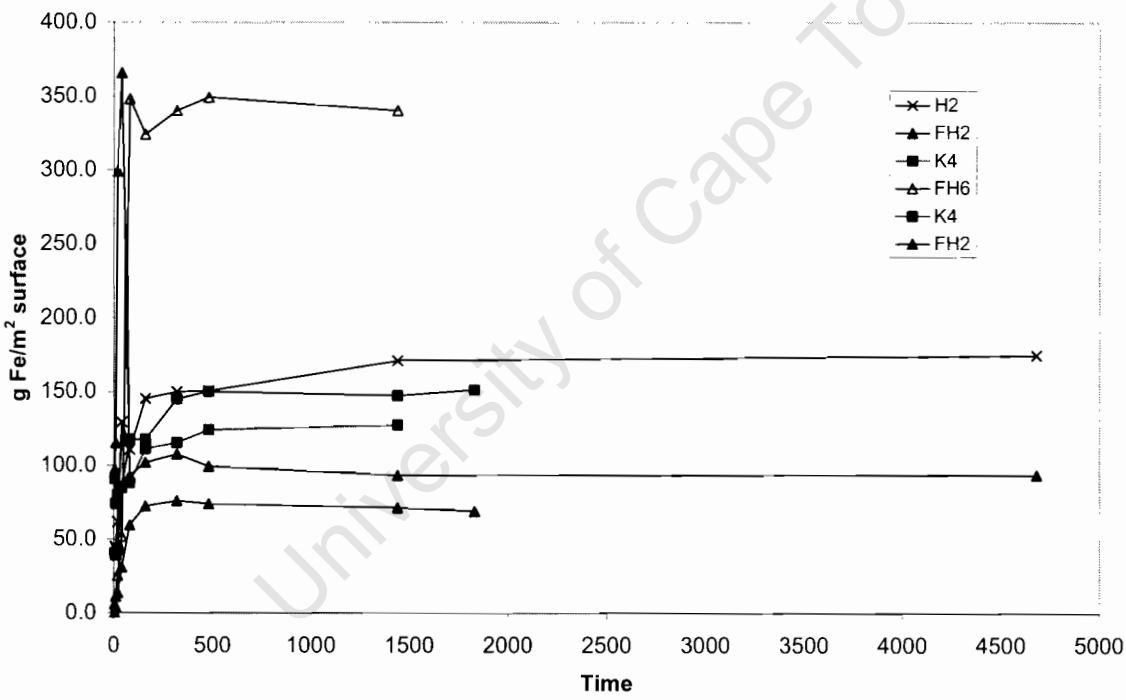

Figure A.1. Time dependence of dithionite dissolution of iron from bead surfaces

Table A.38. Dissolution of ferrihydrite-2 from coated stainless steel surfaces

		Time (hrs)	mmol/m^2 Dithionite	%	Time (hrs)	mmol/m^2 Sulfamic acid	%	Time (hrs)	mmol/m^2 Sulfuric acid	%
No pretreatment	T0	0.00	0.00	0.00	0.00	0.00	0.00	0.00	0.00	0.00
	T1	0.15	1.61	16.31	0.15	0.00	0.00	0.15	0.01	0.15
	T2	0.47	4.03	40.76	0.47	0.23	2.29	0.47	0.43	4.32
	T3	1.10	4.67	47.21	1.10	1.14	11.55	1.10	1.65	16.67
	T4	2.63	5.00	50.57	2.63	2.74	27.66	2.63	3.18	32.19
	T5	4.92	5.17	52.30	4.92	4.19	42.33	4.92	4.63	46.79
	T6	7.05	4.98	50.39	7.05	5.08	51.40	7.05	5.30	53.57
	T7	22.78	6.50	65.73	22.78	8.78	88.79	22.78	8.91	90.04
	T8	29.47	8.29	83.87	29.47	10.21	103.23	29.47	10.58	106.94
	T9	120.63	8.65	87.43	120.63	10.34	104.56	120.63	10.68	107.95
Pretreated with Calgon	T0	0.00	2.92	29.50	0.00	2.88	29.13	0.00	2.70	27.31
	T1	0.15	3.22	32.59	0.15	2.92	29.51	0.15	2.69	27.25
	T2	0.47	3.19	32.24	0.47	2.90	29.36	0.47	2.76	27.94
	T3	1.10	3.30	33.32	1.10	2.95	29.87	1.10	2.75	27.85
	T4	2.63	3.46	35.03	2.63	3.02	30.50	2.63	2.86	28.90
	T5	4.92	3.33	33.69	4.92	3.34	33.73	4.92	3.24	32.73
	T6	7.05	3.58	36.15	7.05	3.78	38.21	7.05	3.68	37.16
	T7	22.78	5.15	52.09	22.78	6.52	65.93	22.78	6.54	66.12
	T8	29.47	6.16	62.29	29.47	8.22	83.09	29.47	8.34	84.38
	T9	120.63	6.31	63.81	120.63	8.40	84.96	120.63	8.58	86.72
Pretreated with NaOH	T0	0.00	1.55	15.64	0.00	1.47	14.82	0.00	1.54	15.57
	T1	0.15	1.97	19.93	0.15	1.46	14.75	0.15	1.57	15.87
	T2	0.47	2.78	28.11	0.47	1.56	15.80	0.47	1.68	16.98
	T3	1.10	3.33	33.66	1.10	1.79	18.11	1.10	1.89	19.10
	T4	2.63	3.42	34.54	2.63	2.24	22.64	2.63	2.42	24.48
	T5	4.92	3.59	36.33	4.92	3.35	33.85	4.92	3.33	33.64
	T6	7.05	3.82	38.59	7.05	3.99	40.34	7.05	3.95	39.96
	T7	22.78	5.40	54.57	22.78	7.36	74.39	22.78	6.84	69.16
	T8	29.47	6.94	70.19	29.47	9.43	95.39	29.47	8.82	89.21
	T9	120.63	7.24	73.18	120.63	9.53	96.33	120.63	8.92	90.16
Pretreated by ultrasonication	T0	0.00	0.87	8.78	0.00	0.97	9.84	0.00	0.52	5.22
	T1	0.15	2.04	20.59	0.15	0.97	9.84	0.15	0.75	7.60
	T2	0.47	3.70	37.41	0.47	1.19	12.06	0.47	0.93	9.36
	T3	1.10	4.13	41.73	1.10	2.08	21.04	1.10	1.89	19.11
	T4	2.63	4.36	44.08	2.63	3.63	36.66	2.63	3.11	31.50
	T5	4.92	4.51	45.55	4.92	5.03	50.89	4.92	4.36	44.08
	T6	7.05	4.49	45.45	7.05	5.90	59.69	7.05	5.04	50.92
	T7	22.78	5.92	59.81	22.78	9.49	95.93	22.78	8.62	87.20
	T8	29.47	7.51	75.94	29.47	10.87	109.94	29.47	10.64	107.62
	T9	120.63	7.84	79.24	120.63	11.00	111.23	120.63	10.72	108.37
Pretreated with Calgon and ultrasonication	T0	0.00	2.67	27.00						
	T1	0.15	2.98	30.11						
	T2	0.47	2.89	29.19						
	T3	1.10	2.95	29.79						
	T4	2.63	3.20	32.34						
	T5	4.92	3.14	31.72						
	T6	7.05	3.28	33.18						
	T7	22.78	4.80	48.49						
	T8	29.47	5.91	59.74						
	T9	120.63	6.07	61.37						

Table A.39. Dissolution of ferrihydrite-2 from coated PVC surfaces

		Time (hrs)	mmol/m^2 Dithionite	%	Time (hrs)	mmol/m^2 Sulfamic acid	%	Time (hrs)	mmol/m^2 Sulfuric acid	%
No pretreatment	T0	0.00	0.00	0.00	0.00	0.00	0.00	0.00	0.00	0.00
	T1	0.15	1.59	74.68	0.15	0.01	0.45	0.15	0.77	36.05
	T2	0.47	1.97	92.72	0.47	0.30	13.95	0.47	0.73	34.46
	T3	1.10	2.00	93.89	1.10	0.91	42.63	1.10	1.24	58.16
	T4	2.63	2.04	95.91	2.63	1.63	76.63	2.63	1.73	81.43
	T5	4.92	2.17	101.91	4.92	1.92	90.11	4.92	1.85	86.72
	T6	7.05	1.98	92.75	7.05	1.99	93.50	7.05	1.91	89.74
	T7	22.78	1.99	93.21	22.78	2.04	95.69	22.78	1.93	90.77
	T8	29.47	2.19	102.99	29.47	2.11	99.05	29.47	2.02	94.92
	T9	120.63	2.24	105.37	120.63	2.15	100.73	120.63	2.01	94.33
Pretreated with Calgon	T0	0.00	0.48	22.64	0.00	0.50	23.52	0.00	0.52	24.53
	T1	0.15	1.02	47.80	0.15	0.50	23.52	0.15	0.54	25.19
	T2	0.47	1.71	80.40	0.47	0.71	33.41	0.47	0.92	42.99
	T3	1.10	1.76	82.68	1.10	1.01	47.34	1.10	1.23	57.74
	T4	2.63	1.83	85.89	2.63	1.46	68.76	2.63	1.51	71.02
	T5	4.92	1.94	91.12	4.92	1.65	77.55	4.92	1.62	75.98
	T6	7.05	1.77	83.01	7.05	1.70	79.80	7.05	1.65	77.35
	T7	22.78	1.77	83.32	22.78	1.75	82.35	22.78	1.67	78.33
	T8	29.47	1.85	86.88	29.47	1.82	85.55	29.47	1.73	81.25
	T9	120.63	1.88	88.08	120.63	1.92	90.06	120.63	1.73	81.24
Pretreated with NaOH	T0	0.00	0.08	3.87	0.00	0.14	6.37	0.00	0.15	7.18
	T1	0.15	1.44	67.39	0.15	0.16	7.36	0.15	0.22	10.50
	T2	0.47	1.80	84.63	0.47	0.65	30.33	0.47	1.07	50.07
	T3	1.10	1.80	84.62	1.10	1.16	54.46	1.10	1.38	64.80
	T4	2.63	1.93	90.63	2.63	1.53	71.84	2.63	1.39	65.49
	T5	4.92	1.92	89.95	4.92	1.66	77.97	4.92	1.70	79.58
	T6	7.05	1.23	57.92	7.05	1.70	79.89	7.05	1.75	82.35
	T7	22.78	1.21	56.75	22.78	1.73	81.32	22.78	1.74	81.92
	T8	29.47	1.30	61.02	29.47	1.82	85.51	29.47	1.81	85.01
	T9	120.63	1.28	59.95	120.63	1.85	87.05	120.63	1.81	85.07
Pretreated by ultrasonication	T0	0.00	0.51	24.16	0.00	0.44	20.52	0.00	0.33	15.65
	T1	0.15	1.09	51.38	0.15	0.46	21.37	0.15	0.38	17.61
	T2	0.47	1.57	73.73	0.47	0.74	34.68	0.47	0.89	41.94
	T3	1.10	1.60	75.03	1.10	1.12	52.76	1.10	1.31	61.62
	T4	2.63	1.68	78.87	2.63	1.56	73.13	2.63	1.59	74.42
	T5	4.92	1.60	74.97	4.92	1.71	80.37	4.92	1.59	74.46
	T6	7.05	1.61	75.46	7.05	1.75	82.17	7.05	1.62	76.08
	T7	22.78	1.57	73.81	22.78	1.79	83.96	22.78	1.65	77.28
	T8	29.47	1.70	79.76	29.47	1.87	87.68	29.47	1.72	80.76
	T9	120.63	1.68	78.78	120.63	1.89	88.72	120.63	1.72	80.83
Pretreated with Calgon and ultrasonication	T0	0.00	0.52	24.37						
	T1	0.15	0.70	32.71						
	T2	0.47	1.30	60.97						
	T3	1.10	1.32	62.15						
	T4	2.63	1.39	65.16						
	T5	4.92	1.30	61.26						
	T6	7.05	1.31	61.35						
	T7	22.78	1.34	63.07						
	T8	29.47	1.38	64.89						
	T9	120.63	1.44	67.83						

Table A.40. Dissolution of ferrihydrite-6 from coated stainless steel surfaces

		Time (hrs)	mmol/m^2	%	Time (hrs)	mmol/m^2	%	Time (hrs)	mmol/m^2	%
			Dithionite			Sulfamic acid			Sulfuric acid	
No pretreatment	T0	0.00	0.00	0.00	0.00	0.00	0.00	0.00	0.00	0.00
	T1	0.08	3.27	26.06	0.10	0.24	1.93	0.10	0.13	1.03
	T2	0.25	3.71	29.58	0.40	0.13	1.03	0.40	0.31	2.51
	T3	0.57	3.94	31.46	0.73	0.20	1.58	0.73	0.28	2.20
	T4	2.13	4.19	33.41	1.75	0.84	6.69	1.75	1.32	10.50
	T5	3.32	4.28	34.17	2.93	1.75	13.92	2.93	2.35	18.76
	T6	5.67	4.61	36.81	5.28	3.03	24.14	5.28	3.92	31.23
	T7	24.92	8.56	68.32	24.53	10.28	81.99	24.53	15.00	119.62
	T8	29.87	10.06	80.22	29.48	11.30	90.16	29.48	16.25	129.62
Pretreated with Calgon	T0	0.00	3.24	25.86	0.00	2.77	22.09	0.00	2.90	23.14
	T1	0.08	3.65	29.14	0.10	2.90	23.10	0.10	3.00	23.92
	T2	0.25	3.38	26.94	0.40	2.84	22.67	0.40	2.93	23.37
	T3	0.57	3.39	27.05	0.73	2.80	22.36	0.73	2.94	23.46
	T4	2.13	3.44	27.44	1.75	2.90	23.11	1.75	3.02	24.06
	T5	3.32	3.44	27.44	2.93	2.98	23.79	2.93	3.22	25.69
	T6	5.67	4.47	35.65	5.28	3.44	27.46	5.28	3.84	30.60
	T7	24.92	7.33	58.48	24.53	9.44	75.29	24.53	11.40	90.96
	T8	29.87	9.05	72.19	29.48	11.27	89.93	29.48	13.39	106.80
	T9	121.00	9.30	74.18	120.62	11.86	94.64	120.62	13.87	110.62
Pretreated with NaOH	T0	0.00	1.12	8.95	0.00	1.29	10.26	0.00	1.28	10.19
	T1	0.08	1.76	14.03	0.10	1.53	12.22	0.10	1.36	10.83
	T2	0.25	1.80	14.36	0.40	1.33	10.64	0.40	1.34	10.70
	T3	0.57	1.86	14.81	0.73	1.35	10.78	0.73	1.36	10.81
	T4	2.13	2.15	17.16	1.75	1.94	15.44	1.75	2.51	19.99
	T5	3.32	2.21	17.64	2.93	2.33	18.62	2.93	3.04	24.25
	T6	5.67	2.57	20.49	5.28	2.85	22.77	5.28	3.97	31.68
	T7	24.92	6.27	49.99	24.53	9.43	75.19	24.53	10.92	87.13
	T8	29.87	8.03	64.04	29.48	11.35	90.56	29.48	14.16	112.96
	T9	121.00	8.38	66.85	120.62	11.81	94.17	120.62	14.61	116.53
Pretreated by ultrasonication	T0	0.00	0.54	4.27	0.00	0.56	4.47	0.00	0.49	3.88
	T1	0.08	3.33	26.54	0.10	0.58	4.64	0.10	0.49	3.88
	T2	0.25	3.32	26.45	0.40	0.67	5.35	0.40	0.62	4.95
	T3	0.57	3.15	25.15	0.73	0.73	5.81	0.73	0.71	5.67
	T4	2.13	3.46	27.60	1.75	1.47	11.75	1.75	1.70	13.53
	T5	3.32	3.61	28.78	2.93	2.18	17.42	2.93	2.42	19.32
	T6	5.67	3.90	31.07	5.28	2.99	23.87	5.28	3.66	29.18
	T7	24.92	7.92	63.20	24.53	10.68	85.22	24.53	12.47	99.48
	T8	29.87	9.27	73.91	29.48	12.75	101.68	29.48	14.65	116.83
	T9	121.00	9.42	75.10	120.62	13.00	103.66	120.62	14.65	116.83
Pretreated with Calgon and ultrasonication	T0	0.00	2.99	23.84						
	T1	0.08	3.30	26.33						
	T2	0.25	3.14	25.06						
	T3	0.57	3.19	25.48						
	T4	2.13	3.11	24.81						
	T5	3.32	3.16	25.19						
	T6	5.67	3.36	26.81						
	T7	24.92	6.70	53.43						
	T8	29.87	8.20	65.43						

Table A.41. Dissolution of ferrihydrite-6 from coated PVC surfaces

		Time (hrs)	mmol/m^2	%	Time (hrs)	mmol/m^2	%	Time (hrs)	mmol/m^2	%
			Dithionite			Sulfamic acid			Sulfuric acid	
No pretreatment	T0	0.00	0.00	0.00	0.00	0.00	0.00	0.00	0.00	0.00
	T1	0.08	1.66	74.86	0.10	0.01	0.39	0.10	0.02	0.69
	T2	0.25	1.80	81.26	0.40	0.08	3.43	0.40	0.08	3.58
	T3	0.57	1.75	78.96	0.73	0.09	4.07	0.73	0.11	5.11
	T4	2.13	1.93	87.24	1.75	0.25	11.26	1.75	0.22	10.14
	T5	3.32	1.98	89.35	2.93	0.29	13.03	2.93	0.31	14.04
	T6	5.67	2.01	90.53	5.28	0.56	25.22	5.28	0.55	24.94
	T7	24.92	2.07	93.23	24.53	2.12	95.59	24.53	1.89	85.39
	T8	29.87	2.14	96.57	29.48	2.38	107.23	29.48	2.11	95.23
Pretreated with Calgon	T0	0.00	0.40	18.17	0.00	0.41	18.28	0.00	0.42	18.86
	T1	0.08	1.44	64.81	0.10	0.41	18.38	0.10	0.43	19.51
	T2	0.25	1.51	68.30	0.40	0.46	20.84	0.40	0.46	20.92
	T3	0.57	1.44	64.97	0.73	0.47	21.16	0.73	0.47	21.37
	T4	2.13	1.60	71.93	1.75	0.53	23.96	1.75	0.53	23.69
	T5	3.32	1.62	72.94	2.93	0.56	25.09	2.93	0.57	25.49
	T6	5.67	1.65	74.31	5.28	0.67	30.05	5.28	0.67	30.33
	T7	24.92	1.67	75.37	24.53	1.34	60.22	24.53	1.23	55.25
	T8	29.87	1.74	78.48	29.48	1.53	68.82	29.48	1.38	62.17
	T9	121.00	1.69	76.04	120.62	2.23	100.41	120.62	1.74	78.45
Pretreated with NaOH	T0	0.00	0.08	3.41	0.00	0.10	4.54	0.00	0.06	2.86
	T1	0.08	2.51	113.21	0.10	0.14	6.12	0.10	0.09	3.94
	T2	0.25	2.64	118.83	0.40	0.23	10.40	0.40	0.21	9.36
	T3	0.57	2.50	112.95	0.73	0.26	11.67	0.73	0.22	9.99
	T4	2.13	2.76	124.63	1.75	0.28	12.58	1.75	0.31	14.20
	T5	3.32	2.77	125.07	2.93	0.47	21.14	2.93	0.39	17.42
	T6	5.67	1.86	84.10	5.28	0.65	29.23	5.28	0.56	25.06
	T7	24.92	1.88	84.89	24.53	1.70	76.64	24.53	1.40	63.07
	T8	29.87	1.93	86.86	29.48	1.99	89.73	29.48	1.59	71.88
	T9	121.00	1.92	86.63	120.62	2.62	118.01	120.62	2.12	95.42
Pretreated by ultrasonication	T0	0.00	0.04	1.66	0.00	0.15	6.91	0.00	0.11	5.10
	T1	0.10	1.63	73.69	0.10	0.17	7.74	0.10	0.15	6.88
	T2	0.40	1.72	77.74	0.40	0.24	10.94	0.40	0.20	8.91
	T3	0.73	1.68	75.70	0.73	0.26	11.77	0.73	0.22	10.13
	T4	1.75	1.81	81.52	1.75	0.35	15.62	1.75	0.32	14.64
	T5	2.93	1.83	82.31	2.93	0.43	19.45	2.93	0.42	18.84
	T6	5.28	1.93	86.86	5.28	0.63	28.44	5.28	0.61	27.50
	T7	24.53	1.92	86.77	24.53	1.88	84.87	24.53	1.65	74.42
	T8	29.48	1.98	89.28	29.48	2.10	94.86	29.48	1.80	81.23
	T9	120.62	1.97	88.62	120.62	2.55	114.82	120.62	2.15	97.05
Pretreated with Calgon and ultrasonication	T0	0.00	0.76	34.09						
	T1	0.10	1.11	49.87						
	T2	0.40	1.18	53.10						
	T3	0.73	1.14	51.30						
	T4	1.75	1.22	55.13						
	T5	2.93	1.26	56.96						
	T6	5.28	1.29	58.01						
	T7	24.53	1.30	58.63						
	T8	29.48	1.33	59.99						

Table A.42. Dissolution of goethite from coated stainless steel surfaces

		Time (hrs)	mmol/m^2 Dithionite	%	Time (hrs)	mmol/m^2 Sulfamic acid	%	Time (hrs)	mmol/m^2 Sulfuric acid	%
No pretreatment	T0	0.00	0.00	0.00	0.00	0.00	0.00	0.00	0.00	0.00
	T1	0.25	0.08	0.81	0.25	0.05	0.44	0.25	0.04	0.35
	T2	0.78	0.59	5.65	0.78	0.19	1.76	0.78	0.13	1.28
	T3	1.63	0.82	7.80	1.63	0.54	5.16	1.63	0.48	4.59
	T4	3.45	1.11	10.58	3.45	1.11	10.57	3.45	0.91	8.71
	T5	18.17	2.95	28.07	18.17	5.65	53.84	18.17	4.40	41.92
	T6	21.03	3.43	32.70	21.03	6.68	63.60	21.03	5.21	49.67
	T7	24.12	4.08	38.82	24.12	6.91	65.78	24.12	6.18	58.89
	T8	45.55	7.40	70.49	45.55	14.73	140.29	45.55	12.34	117.54
	T9	117.08	7.43	70.76	117.08	15.36	146.28	117.08	12.77	121.58
Pretreated with Calgon	T0	0.00	0.93	8.82	0.00	1.01	9.61	0.00	0.66	6.30
	T1	0.25	0.93	8.82	0.25	1.07	10.17	0.25	0.69	6.60
	T2	0.78	1.09	10.35	0.78	1.09	10.39	0.78	0.72	6.87
	T3	1.63	1.42	13.52	1.63	1.16	11.03	1.63	0.80	7.63
	T4	3.45	1.57	14.97	3.45	1.39	13.23	3.45	0.99	9.45
	T5	18.17	3.62	34.47	18.17	4.88	46.52	18.17	4.22	40.18
	T6	21.03	4.19	39.86	21.03	5.85	55.76	21.03	5.18	49.33
	T7	24.12	4.64	44.20	24.12	6.72	63.98	24.12	5.94	56.56
	T8	45.55	8.32	79.23	45.55	12.19	116.05	45.55	10.37	98.76
	T9	117.08	8.68	82.70	117.08	12.73	121.27	117.08	10.80	102.90
Pretreated with NaOH	T0	0.00	0.86	8.15	0.00	3.52	33.56	0.00	0.75	7.14
	T1	0.25	1.06	10.08	0.25	3.60	34.24	0.25	0.84	7.97
	T2	0.78	1.34	12.74	0.78	3.72	35.42	0.78	0.96	9.11
	T3	1.63	1.59	15.12	1.63	3.99	37.97	1.63	1.36	12.92
	T4	3.45	1.81	17.28	3.45	4.43	42.20	3.45	1.92	18.33
	T5	18.17	3.46	32.92	18.17	8.88	84.61	18.17	6.98	66.50
	T6	21.03	3.92	37.38	21.03	9.81	93.42	21.03	8.01	76.31
	T7	24.12	4.36	41.50	24.12	10.82	103.02	24.12	9.32	88.79
	T8	45.55	7.57	72.07	45.55	16.00	152.34	45.55	15.73	149.85
	T9	117.08	7.55	71.94	117.08	17.05	162.36	117.08	16.10	153.33
Pretreated by ultrasonication	T0	0.00	0.27	2.53	0.00	0.38	3.59	0.00	0.39	3.71
	T1	0.25	0.56	5.36	0.25	0.42	4.01	0.25	0.42	3.97
	T2	0.78	1.18	11.28	0.78	0.56	5.30	0.78	0.57	5.46
	T3	1.63	1.24	11.76	1.63	0.90	8.60	1.63	0.80	7.62
	T4	3.45	1.45	13.80	3.45	1.45	13.83	3.45	1.24	11.78
	T5	18.17	2.94	28.05	18.17	5.86	55.79	18.17	5.65	53.85
	T6	21.03	3.49	33.28	21.03	6.85	65.26	21.03	6.82	64.99
	T7	24.12	3.92	37.30	24.12	7.07	67.37	24.12	7.72	73.48
	T8	45.55	7.72	73.57	45.55	14.66	139.62	45.55	13.77	131.16
	T9	117.08	7.75	73.77	117.08	15.27	145.43	117.08	14.08	134.14
Pretreated with Calgon and ultrasonication	T0	0.00	0.94	8.98						
	T1	0.25	0.99	9.45						
	T2	0.78	1.12	10.65						
	T3	1.63	1.36	13.00						
	T4	3.45	1.62	15.43						
	T5	18.17	3.29	31.35						
	T6	21.03	3.81	36.26						
	T7	24.12	4.30	40.97						
	T8	45.55	5.48	52.15						
	T9	117.08	5.46	52.03						

Table A.43. Dissolution of goethite from coated PVC surfaces

		Time (hrs)	mmol/m^2 Dithionite	%	Time (hrs)	mmol/m^2 Sulfamic acid	%	Time (hrs)	mmol/m^2 Sulfuric acid	%
No pretreatment	T0	0.00	0.00	0.00	0.00	0.00	0.00	0.00	0.00	0.00
	T1	0.25	2.00	18.08	0.25	0.02	0.17	0.25	0.01	0.10
	T2	0.78	5.82	52.60	0.78	0.02	0.19	0.78	0.02	0.17
	T3	1.63	9.87	89.28	1.63	0.03	0.28	1.63	0.03	0.25
	T4	3.45	11.02	99.65	3.45	0.04	0.33	3.45	0.04	0.35
	T5	18.17	11.75	106.28	18.17	0.10	0.90	18.17	0.07	0.64
	T6	21.03	11.33	102.46	21.03	0.10	0.94	21.03	0.10	0.95
	T7	24.12	11.41	103.19	24.12	0.12	1.08	24.12	0.11	1.03
	T8	45.55	12.39	112.04	45.55	0.20	1.77	45.55	0.17	1.58
	T9	117.08	11.83	106.99	117.08	0.27	2.47	117.08	0.23	2.07
Pretreated with Calgon	T0	0.00	2.48	22.43	0.00	2.04	18.45	0.00	1.37	12.42
	T1	0.25	3.35	30.26	0.25	2.05	18.52	0.25	1.38	12.49
	T2	0.78	4.96	44.86	0.78	2.05	18.56	0.78	1.38	12.52
	T3	1.63	6.63	59.91	1.63	2.06	18.62	1.63	1.39	12.58
	T4	3.45	7.14	64.55	3.45	2.06	18.60	3.45	1.39	12.55
	T5	18.17	7.61	68.84	18.17	2.09	18.86	18.17	1.42	12.84
	T6	21.03	7.47	67.55	21.03	2.09	18.88	21.03	1.43	12.90
	T7	24.12	7.50	67.80	24.12	2.10	18.96	24.12	1.46	13.18
	T8	45.55	7.59	68.59	45.55	2.13	19.28	45.55	1.47	13.29
	T9	117.08	7.94	71.77	117.08	2.18	19.68	117.08	1.49	13.48
Pretreated with NaOH	T0	0.00	0.98	8.89	0.00	0.95	8.57	0.00	1.14	10.34
	T1	0.25	2.26	20.41	0.25	0.96	8.67	0.25	1.16	10.46
	T2	0.78	4.49	40.57	0.78	0.97	8.80	0.78	1.17	10.58
	T3	1.63	6.48	58.58	1.63	0.98	8.82	1.63	1.18	10.64
	T4	3.45	7.20	65.08	3.45	0.98	8.82	3.45	1.18	10.66
	T5	18.17	7.47	67.51	18.17	1.03	9.35	18.17	1.23	11.10
	T6	21.03	7.55	68.29	21.03	1.02	9.25	21.03	1.23	11.12
	T7	24.12	5.17	46.70	24.12	1.04	9.40	24.12	1.24	11.23
	T8	45.55	5.32	48.13	45.55	1.08	9.73	45.55	1.28	11.58
	T9	117.08	5.39	48.73	117.08	1.13	10.23	117.08	1.32	11.95
Pretreated by ultrasonication	T0	0.00	0.92	8.34	0.00	1.20	10.82	0.00	1.28	11.58
	T1	0.25	2.62	23.66	0.25	1.21	10.92	0.25	1.29	11.67
	T2	0.78	5.08	45.89	0.78	1.21	10.98	0.78	1.30	11.74
	T3	1.63	6.79	61.36	1.63	1.22	11.02	1.63	1.30	11.75
	T4	3.45	9.98	90.20	3.45	1.22	11.07	3.45	1.30	11.79
	T5	18.17	7.59	68.65	18.17	1.27	11.45	18.17	1.34	12.09
	T6	21.03	7.62	68.92	21.03	1.34	12.10	21.03	1.34	12.12
	T7	24.12	7.71	69.67	24.12	1.29	11.67	24.12	1.35	12.19
	T8	45.55	7.90	71.44	45.55	1.34	12.09	45.55	1.39	12.57
	T9	117.08	8.08	73.08	117.08	1.40	12.67	117.08	1.43	12.93
Pretreated with Calgon and ultrasonication	T0	0.00	0.86	7.77						
	T1	0.25	1.15	10.39						
	T2	0.78	1.49	13.44						
	T3	1.63	1.73	15.62						
	T4	3.45	2.00	18.05						
	T5	18.17	1.76	15.91						
	T6	21.03	1.76	15.91						
	T7	24.12	1.79	16.16						
	T8	45.55	1.79	16.18						
	T9	117.08	2.02	18.22						

Appendix B Data Quality

B.1 General data quality for field and laboratory work

Table B.1. Bias and precision for water chemistry measured in selected boreholes from the Klein Karoo

	Method	n	Bias	n	Precision	Uncertainty
Na	IC	2	0.2	10	19.5	19.7
Mg	AA	2	-1.7	10	12.3	14.0
Ca	AA	2	2.3	10	8.2	10.5
K	IC	2	-3.8	12	52.5	56.2
Si	Colorimetry	1	18.1	9	4.1	22.2
Fe	Colorimetry	6	18.2	37	5.2	23.5
Fe	ICP-MS	1	-34.1	9	29.7	63.8
Cl	IC	2	-1.2	10	12.7	13.8
SO_4	IC	2	-10.1	11	18.6	28.8

Table B.2. Comparison of laboratory and field data for iron measurements (Fe, DO in mg/L, T in °C)

Borehole	Field	Lab	Field	Field	Field unfilt		Field filtered		Lab filtered		Lab acidified		ICP-MS
	pH	pH	DO	Temp	Fe^{2+}	Fe^{T}	Fe^{2+}	Fe^{T}	Fe^{2+}	Fe^{T}	Fe^{2+}	Fe^{T}	Fe^{T}
CHS-1		6.8		52.0	0.69	1.11	0.65	0.83	0.05	0.02	0.69	1.10	0.87
DL13-4	6.4	6.6	Bdl	24.7	5.39	6.55	4.53	4.79	0.10	0.13	4.68	4.73	3.56
DL17-6	6.1	6.1	bdl	22.5	12.29	14.25	10.75	13.03	1.00	1.03	13.73	15.62	14.12
DP15-4	4.1	4.1	0.1	19.5	3.53	3.49	3.35	3.43	3.25	3.39	3.08	4.91	3.28
DP15-5	4.3	4.1	2.7	18.5	2.80	3.28	2.80	3.10	1.10	1.56	1.24	1.80	2.94
DP29-5	5.5	6.1	3.1	19.2	2.20	2.08	2.21	2.13	0.64	0.60	2.87	2.71	2.01
DP28-6	5.4	6.2	2.9	18.5	4.07	3.95	3.74	3.76	3.24	3.18	0.16	0.09	3.04
KG1-5	5.9	5.8	2.3	24.2	17.3	20.1	16.3	18.4	4.7	4.9	12.0	20.1	2.0
DL16-7	6.3	6.7	0.6	22.8	5.41	5.97	5.01	6.12	0.43	0.43	4.68	5.35	0.26

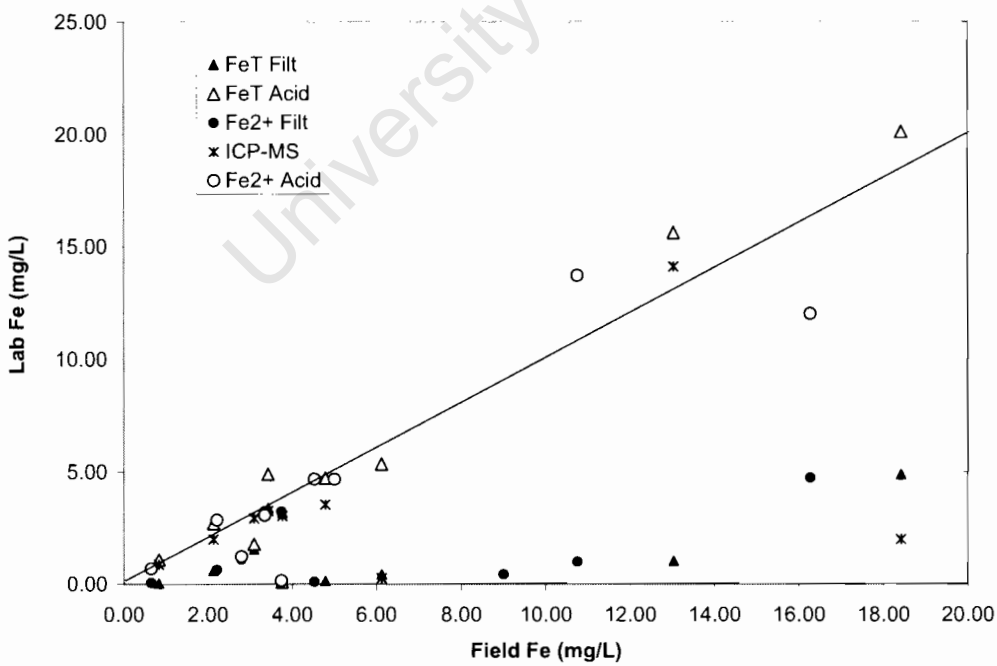

Figure B.1. Comparison between iron measured colorimetrically in the field on filtered sample (0.45 μm) and iron measured colorimetrically in the laboratory on filtered but unacidified samples, filtered and acidified samples, and by ICP-MS on filtered acidified samples. Line on the graph is 1:1.

Table B.3. Duplicate analyses of total carbon in rock and iron precipitate samples (* is iron oxide)

	Total Carbon (wt %)			
Sample ID	Dup 1	Dup 2	Diff	%RSD
B2	0.084	0.092	0.008	6.4
C2	0.178	0.176	0.002	0.9
C5	0.086	0.08	0.006	5.1
G1	0.121	0.131	0.010	5.6
P1	0.069	0.077	0.008	7.7
P2	0.064	0.053	0.011	13.3
P4	0.044	0.037	0.007	12.2
K4*	0.658	0.718	0.060	6.2
A1*	4.688	4.714	0.026	0.4
A4*	3.931	3.953	0.022	0.4

Table B.4. Duplicate analyses of ascorbate and dithionite extracts of iron from rock and iron precipitate samples (* is iron oxide)

	Ascorbate (mmol/g)				Dithionite (mmol/g)			
Sample	Dup 1	Dup 2	Difference	%RSD	Dup 1	Dup 2	Difference	%RSD
B2	0.005	0.005	0.0	2.4	0.034	0.035	0.0	1.1
B7	0.021	0.021	0.0	0.6	0.026	0.027	0.0	3.1
G1	0.013	0.013	0.0	1.3	0.666	0.575	0.1	10.3
A1*	5.700	5.471	0.2	2.9	6.540	6.388	0.2	1.7
H2*	7.589	7.084	0.5	4.9	8.966	8.780	0.2	1.5
A3*	5.425	5.216	0.2	2.8	5.852	5.931	0.1	0.9
S1*	6.090	6.236	0.1	1.7	7.732	8.538	0.8	7.0
H1*	4.648	4.803	0.2	2.3	7.894	8.188	0.3	2.6
Gt*	0.010	0.012	0.0	16.4	10.908	11.128	0.2	1.4

Table B.5. Duplicate leach data for leaching experiments (Fe^T in mmol/kg dry mass of rock)

Sample	Leachate	AEROBIC				ANAEROBIC			
24 hours		**Repeat 1**	**Repeat 2**	**Difference**	**%RSD**	**Repeat 1**	**Repeat 2**	**Difference**	**%RSD**
B4	O3	11.06	15.20	4.14	91.02	20.34	13.13	7.20	158.40
B4	O5	0.55	0.57	0.02	0.40	5.97	4.78	1.19	26.16
B4	D5	0.09	0.09	0.00	0.03	1.27	2.67	1.40	30.88
G1	O3	7.15	7.54	0.40	8.69	11.30	9.68	1.62	35.57
G1	O5	0.77	0.80	0.04	0.84	7.96	7.81	0.15	3.36
G1	D5	0.51	0.32	0.19	4.08	8.10	8.39	0.29	6.41
C1	O3	2.67	2.33	0.35	7.60	2.49	2.56	0.08	1.65
C1	O5	0.24	0.26	0.03	0.59	0.11	0.11	0.00	0.11
C1	D5	bdl	bdl			0.18	0.11	0.07	1.51
120 hours									
B4	O3	7.31	6.89	0.42	9.17	18.75	18.40	0.35	7.71
B4	O5	0.95	1.03	0.08	1.75	17.54	16.91	0.63	13.96
B4	D5	0.23	0.28	0.05	1.10	15.75	16.10	0.35	7.71
G1	O3	3.94	2.53	1.41	31.10	10.32	9.92	0.40	8.76
G1	O5	1.11	1.22	0.11	2.39	8.62	8.53	0.10	2.10
G1	D5	1.83	1.41	0.43	9.41	8.49	11.40	2.90	63.84
C1	O3	2.42	2.07	0.35	7.78	0.75	1.99	1.24	27.25
C1	O5	0.71	0.35	0.36	7.95	0.62	0.42	0.20	4.46
C1	D5	0.03	0.02	0.01	0.23	0.09	0.36	0.27	5.89
216 hours									
B4	O3	4.71	2.46	2.25	49.43	15.49	15.65	0.16	3.47
B4	O5	1.01	1.11	0.10	2.21	14.03	14.39	0.36	7.94
B4	D5	0.60	0.62	0.02	0.37	13.87	14.78	0.91	19.93
G1	O3	1.59	1.54	0.06	1.24	9.25	8.78	0.48	10.46
G1	O5	1.34	1.17	0.17	3.80	7.45	7.16	0.29	6.46
G1	D5	1.68	1.49	0.19	4.18	7.00	7.05	0.05	1.10
C1	O3	1.52	0.83	0.69	15.08	0.80	2.12	1.32	28.98
C1	O5	2.19	0.30	1.89	41.67	0.57	0.49	0.08	1.71
C1	D5	2.05	1.06	0.99	21.66	0.86	0.68	0.17	3.84
374 hours									
B4	O3	3.65	0.93	2.72	59.83	13.97	15.23	1.26	27.76
B4	O5	0.74	0.68	0.06	1.41	15.59	15.69	0.10	2.19
B4	D5	0.55	0.65	0.10	2.14	13.40	14.62	1.22	26.77
G1	O3	0.54	0.43	0.11	2.37	8.54	8.74	0.20	4.29
G1	O5	0.79	0.82	0.04	0.82	6.91	6.36	0.54	11.92
G1	D5	1.23	1.10	0.13	2.81	6.47	6.89	0.41	9.11
C1	O3	0.50	0.25	0.25	5.54	0.42	0.50	0.08	1.77
C1	O5	0.19	0.12	0.07	1.44	0.14	0.11	0.03	0.68
C1	D5	0.09	0.07	0.01	0.30	0.11	0.08	0.02	0.54
710 hours									
B4	O3	2.90	2.68	0.22	4.80	16.69	17.45	0.76	16.73
B4	O5	0.76	0.80	0.03	0.76	15.98	16.90	0.92	20.31
B4	D5	0.74	0.53	0.21	4.53	15.82	15.62	0.20	4.37
G1	O3	2.08	2.15	0.07	1.46	9.49	9.34	0.15	3.37
G1	O5	0.79	0.78	0.01	0.23	7.29	5.14	2.15	47.24
G1	D5	0.86	1.38	0.52	11.53	7.86	7.95	0.09	1.89
C1	O3	1.36	1.54	0.18	3.92	2.25	2.87	0.63	13.80
C1	O5	0.44	nd			0.54	0.39	0.15	3.30
C1	D5	0.90	0.55	0.35	7.65	0.42	0.53	0.11	2.41

Table B.5. cont. Duplicate leach data for leaching experiments (Fe^T in mmol/kg dry mass of rock)

Sample	Leachate	AEROBIC				ANAEROBIC			
1214 hours		**Repeat 1**	**Repeat 2**	**Difference**	**RSD**	**Repeat 1**	**Repeat 2**	**Difference**	**RSD**
B4	O3	2.35	2.31	0.04	0.81	16.50	16.52	0.02	0.37
B4	O5	0.48	1.53	1.04	22.97	14.69	14.81	0.12	2.68
B4	D5	0.29	0.21	0.09	1.88	15.29	15.32	0.02	0.47
G1	O3	1.81	2.38	0.57	12.58	9.23	13.65	4.42	97.16
G1	O5	0.46	0.37	0.08	1.85	7.70	7.69	0.01	0.21
G1	D5	0.51	0.51	0.00	0.11	7.05	7.80	0.75	16.45
C1	O3	1.56	1.81	0.26	5.61	3.31	4.12	0.82	17.94
C1	O5	0.40	nd			1.02	2.02	1.00	22.05
C1	D5	0.62	0.42	0.19	4.21	0.58	1.40	0.82	18.12
1958 hours									
B4	O3	2.12	2.03	0.09	1.98	16.08	15.57	0.51	11.28
B4	O5	0.89	0.60	0.29	6.46	14.33	15.06	0.73	16.04
B4	D5	0.19	0.16	0.03	0.68	14.44	14.53	0.08	1.79
G1	O3	1.54	1.52	0.02	0.54	9.10	9.15	0.05	1.05
G1	O5	0.50	0.55	0.05	1.04	7.31	7.76	0.45	9.84
G1	D5	0.25	0.27	0.01	0.28	6.94	7.20	0.26	5.81
C1	O3	1.63	1.11	0.52	11.41	4.46	5.02	0.56	12.36
C1	O5	1.58	nd			0.87	0.41	0.47	10.29
C1	D5	0.32	0.49	0.17	3.72	0.26	0.33	0.07	1.43
2726 hours									
B4	O3	2.24	2.25	0.01	0.33	14.82	14.54	0.28	6.17
B4	O5	0.40	0.26	0.14	2.99	13.96	14.14	0.18	3.93
B4	D5	0.04	0.03	0.01	0.16	13.69	nd		
G1	O3	1.59	1.49	0.11	2.40	7.28	8.26	0.98	21.54
G1	O5	0.11	0.08	0.02	0.49	7.10	6.91	0.19	4.14
G1	D5	0.09	0.11	0.02	0.42	6.81	6.97	0.16	3.53
C1	O3	0.61	0.47	0.15	3.24	4.92	6.09	1.16	25.58
C1	O5	0.04	nd		0.00	0.06	0.03	0.04	0.78
C1	D5	0.01	0.00	0.01	0.28	0.03	0.04	0.01	0.11
2726 hours Fe^{2+}									
B4	O3	0.11	0.11	0.00	0.08	14.24	14.42	0.17	3.82
B4	O5	0.40	0.25	0.15	3.31	14.00	14.24	0.24	5.17
B4	D5	0.12	0.08	0.03	0.75	13.85	nd		
G1	O3	0.09	0.08	0.00	0.00	7.42	8.03	0.61	13.39
G1	O5	0.14	0.13	0.01	0.31	7.13	7.10	0.03	0.69
G1	D5	0.14	0.17	0.03	0.70	6.85	7.00	0.15	3.19
C1	O3	0.07	0.06	0.01	0.18	4.75	5.96	1.21	26.59
C1	O5	0.12	nd			0.07	0.03	0.04	0.93
C1	D5	0.02	0.06	0.04	0.87	0.03	0.03	0.00	0.01

Table B.6. Duplicate C/C_o total iron values determined during repeat flow-through experiments at pH 6.0 and pH 6.5

pH 6.5					pH 6.0					
Time (days)	C/C_o 1	C/C_o 2	Average	Std dev	Time	C/C_o 1	C/C_o 2	C/C_o 3	Average	Stdev
0.39	0.02	0.01	0.01	0.62	0.42	0.01	0.04		0.02	2.61
0.42	0.01	0.00	0.01	0.63	0.50	0.08	0.13		0.11	3.04
0.45	0.01	0.01	0.01	0.35	0.57	0.17	0.26		0.22	6.47
0.48	0.02	0.00	0.01	0.84	0.64	0.24	0.38		0.31	9.75
0.50	0.01	0.02	0.02	0.84	0.75	0.33	0.53		0.43	13.99
0.56	0.01	0.00	0.01	0.58	0.82	0.39	0.57		0.48	12.73
0.59	0.02	0.01	0.01	0.89	0.89	0.43	0.60		0.52	12.19
0.61	0.03	0.03	0.03	0.05	0.96	0.45	0.63		0.54	12.07
0.64	0.07	0.06	0.06	0.29	1.06	0.52	0.62	0.58	0.58	4.97
0.67	0.12	0.12	0.12	0.17	1.13	0.54	0.63	0.58	0.59	4.59
0.70	0.16	0.16	0.16	0.19	1.19	0.57	0.62	0.62	0.61	3.28
0.73	0.23	0.22	0.22	0.87	1.26	0.59	0.65	0.63	0.62	2.71
0.75	0.30	0.26	0.28	2.95	1.33	0.71	0.65	0.67	0.68	3.01
0.78	0.34	0.30	0.32	2.92	1.40	0.67	0.67		0.67	0.01
0.84	0.45	0.37	0.41	5.59	1.47	0.65	0.67	0.68	0.67	1.68
0.86	0.49	0.38	0.43	7.58	1.54	0.67	0.67		0.67	0.07
0.89	0.52	0.41	0.46	7.68	1.61	0.68	0.67	0.74	0.70	3.68
0.92	0.54	0.43	0.48	8.01	1.68	0.72	0.68		0.70	2.46
0.95	0.56	0.46	0.51	7.42	1.70	0.68	0.65		0.67	2.08
0.98	0.58	0.45	0.51	9.67	1.77	0.68	0.66		0.67	1.60
1.05	0.53	0.41	0.47	8.59	1.84	0.69	0.66		0.68	2.23
1.11	0.60	0.41	0.51	13.13	1.91	0.65	0.66		0.66	0.82
1.16	0.57	0.42	0.50	10.30	1.98	0.67	0.67	0.74	0.69	4.23
1.23	0.59	0.46	0.52	9.00	2.05	0.66	0.57	0.75	0.66	8.99
1.30	0.54	0.46	0.50	6.14	2.12	0.64	0.61	0.75	0.67	7.54
1.37	0.55	0.47	0.51	5.69	2.19	0.66	0.63	0.80	0.69	9.09
1.44	0.53	0.48	0.51	3.38	2.26	0.66	0.62		0.64	2.93
1.51	0.56	0.48	0.52	5.66	2.33	0.66	0.63		0.65	1.63
1.58	0.54	0.49	0.51	3.05	2.83	0.68	0.68		0.68	0.00
1.65	0.54	0.45	0.50	6.46	2.90	0.70	0.68		0.69	1.10
1.72	0.54	0.49	0.51	3.06						

Table B.7. Comparison of CHN and Walkley-Black analysis of organic carbon in iron precipitate samples

Sample	Walkley Black			CHN			Difference	RSD
	Dup 1	Dup 2	Average	Dup 1	Dup 2	Average	WB-CHN	%
A1	3.74	4.01	3.87	3.63		3.63	-0.244	4.6
H1	bdl	0.08	0.08	1.09		1.09	1.009	122.7
H2	bdl			0.62	0.41	0.52	0.517	
K1	0.66		0.66	0.45	0.38	0.41	-0.242	32.1
K4	0.12		0.12	0.45		0.45	0.338	84.0
S1	0.92		0.92	0.43		0.43	-0.497	51.9
A3	3.56		3.56	4.03		4.03	0.473	8.8

Table B.8. Duplicate analyses for XRF analysis of iron oxide samples (concentrations in wt %)

Sample	Dup 1	Dup 2	RSD	Dup 1	Dup 2	RSD	Dup 1	Dup 2	RSD
Analyte		SiO_2			Al_2O_3			Na_2O	
Hm	0.06	0.04	23.2	0.33	0.35	4.6	0.13	0.13	0.1
FH2	0.18	0.82	89.8	0.32	0.37	10.8	0.32	0.33	1.2
H2	9.33	9.46	0.9	0.30	0.30	0.3	0.08	0.12	24.0
K1	3.91	4.01	1.7	0.51	0.48	3.0	0.09	0.15	38.5
A1	4.66	4.70	0.6	2.21	2.22	0.3	0.60	0.66	6.9
		MnO			MgO			Cr_2O_3	
Hm	0.04	0.04	10.3	0.16	0.15	3.9	0.02	0.02	0.1
FH2	0.02	0.03	14.5	0.13	0.16	13.6	0.01	0.01	8.4
H2	1.08	1.14	3.5	0.18	0.19	5.1	0.01	0.01	7.3
K1	0.12	0.13	3.4	0.17	0.15	11.8	0.01	0.01	20.8
A1	0.09	0.09	<0.1	0.22	0.23	1.3	0.02	0.02	3.7
		K_2O			P_2O_5			CaO	
Hm	0.00	0.00	0.1	bdl	bdl		0.02	0.02	11.0
FH2	0.02	0.89	136.4	bdl	bdl		0.02	0.03	36.3
H2	0.02	0.02	4.8	3.09	3.07	0.5	0.39	0.39	0.3
K1	0.05	0.05	0.6	4.49	4.46	0.4	0.23	0.23	0.1
A1	0.07	0.07	1.3	6.20	6.02	2.1	4.18	4.18	<0.1
		TiO_2			Fe_2O_3			SO_3	
Hm	0.03	0.04	9.6	98.78	98.77	0.0	0.05	0.04	15.8
FH2	0.03	0.04	28.1	71.08	70.17	0.9	0.02	0.04	45.6
H2	0.03	0.03	15.4	65.82	65.63	0.2	0.02	0.01	14.2
K1	0.04	0.04	2.1	67.80	67.71	0.1	0.01	0.01	19.0
A1	0.05	0.06	6.1	49.14	49.20	0.1	0.11	0.11	0.5

B.2 Batch dissolution experiments

B.2.1 Calculation of repeatability

Because duplicate batch dissolution samples were not prepared and sampled simultaneously, there is often a time difference between sampling of the two duplicates. As the concentration of iron is time dependent, the time delay will lead to differences in the iron concentration that are not due to analytical error or sample inhomogeneity. To overcome this problem, the instantaneous rates at each duplicate point were calculated i.e. the concentration of iron in mol/kg of dry weight, divided by the time elapsed. The standard deviation of the duplicate rates was calculated, then converted back to an error in concentration units by multiplying by the average time elapsed of the two duplicates. The error for the time period is divided by the average concentration of iron to obtain a relative standard deviation, which is listed in the tables below.

Table B.9 Duplicate analysis of batch dissolution of sample K4 by a number of reagents

DUPLICATE 1			DUPLICATE 2				
Time (days)	**mol/kg**	**Rate**	**Time (days)**	**mol/kg**	**Rate**	**SD of rate**	**SD at mean time**
			0.1 M ACETIC ACID				
0.01	0.002	0.14	0.01	0.003	0.27	0.09	0.001
0.02	0.008	0.40	0.02	0.013	0.64	0.17	0.003
0.05	0.021	0.42	0.05	0.030	0.56	0.10	0.005
0.09	0.039	0.42	0.09	0.041	0.43	0.01	0.001
				Relative mean SD			14.10
			0.1 M PHOSPHORIC ACID				
0.01	0.77	118.64	0.00	0.56	114.45	2.96	0.02
0.02	0.64	31.36	0.02	0.84	44.64	9.39	0.18
0.05	1.32	25.25	0.05	1.18	23.33	1.35	0.07
0.10	3.85	40.03	0.09	3.77	39.94	0.07	0.01
0.19	3.71	20.01	0.18	4.53	24.63	3.26	0.60
0.28	4.71	16.62	0.28	4.32	15.34	0.90	0.26
1.07	5.04	4.71	1.07	5.34	5.00	0.20	0.22
1.98	6.32	3.19	1.98	6.41	3.24	0.03	0.06
				Relative mean SD			5.31
			0.1M HCL				
0.01	0.03	4.06	0.01	0.03	5.86	1.28	0.01
0.02	0.19	10.18	0.02	0.20	11.49	0.93	0.02
0.04	0.57	14.11	0.04	0.52	13.48	0.44	0.02
0.09	1.80	20.31	0.09	1.66	19.15	0.82	0.07
0.17	3.61	21.25	0.17	3.59	21.35	0.07	0.01
0.31	5.13	16.39	0.31	5.14	16.52	0.09	0.03
0.99	8.87	8.95	0.99	8.01	8.09	0.61	0.60
2.08	9.13	4.40	2.07	9.27	4.47	0.05	0.10
				Relative mean SD			2.98
			0.1 M HYDROXYLAMINE HCL				
0.01	0.00	0.56	0.01	0.01	0.73	0.12	0.00
0.02	0.03	1.75	0.02	0.03	1.58	0.12	0.00
0.04	0.07	1.65	0.04	0.07	1.54	0.08	0.00
0.09	0.16	1.82	0.09	0.19	2.08	0.18	0.02
0.17	0.35	2.07	0.17	0.35	2.01	0.04	0.01
0.31	0.64	2.05	0.31	0.65	2.06	0.01	0.00
0.99	1.68	1.70	0.99	1.64	1.65	0.03	0.03
2.08	2.19	1.05	2.08	2.14	1.03	0.02	0.03
				Relative mean SD			1.94
			0.1 M H2SO4				
0.01	0.37	59.45	0.01	0.96	121.84	44.11	0.31
0.02	2.21	122.27	0.02	2.01	102.25	14.16	0.27
0.04	4.58	115.80	0.04	4.22	102.40	9.48	0.38
0.09	7.29	83.35	0.09	6.86	76.94	4.53	0.40
0.17	8.46	50.15	0.17	7.86	46.16	2.82	0.48
0.31	8.00	25.65	0.31	8.38	26.75	0.78	0.24
0.99	7.77	7.84	0.99	7.98	8.05	0.14	0.14
2.08	7.61	3.67	2.08	8.01	3.86	0.13	0.28
				Relative mean SD			5.42
			0.01M DITHIONITE				
0.00	2.50	721.16	0.00	2.96	673.89	33.43	0.13
0.01	3.79	363.54	0.01	1.98	174.38	133.75	1.46
0.03	4.18	158.34	0.03	4.03	147.69	7.53	0.20
0.07	4.41	67.56	0.07	4.27	64.47	2.18	0.14
0.11	4.67	42.33	0.11	4.38	39.38	2.09	0.23
0.19	4.95	26.30	0.19	4.84	25.61	0.49	0.09
0.92	6.51	7.08	0.92	6.12	6.65	0.31	0.28
				Relative mean SD			8.52

Table B.10. Duplicate analysis of batch dissolution of a selection of samples by ascorbic acid.

Duplicate 1			Duplicate 2				
Time (days)	mol/kg	Rate	Time (days)	mol/kg	Rate	SD of rate	SD at mean time
				SAMPLE A1			
0.01	0.06	5.81	0.01	0.00	0.00	4.11	0.04
0.03	0.15	5.46	0.03	0.12	4.71	0.54	0.01
0.06	0.51	8.10	0.06	0.34	5.44	1.88	0.12
0.14	1.58	11.30	0.14	0.81	5.79	3.89	0.54
0.23	2.03	8.65	0.23	1.30	5.58	2.17	0.51
0.30	2.12	6.98	0.30	1.63	5.36	1.14	0.35
0.96	3.94	4.13	0.95	4.46	4.68	0.39	0.37
1.34	4.58	3.42	1.34	4.98	3.73	0.21	0.29
2.30	3.90	1.69	2.30	4.69	2.04	0.24	0.56
4.01	4.16	1.04	4.01	4.65	1.16	0.09	0.35
				Relative mean SD			13.64
				SAMPLE H2			
0.01	0.05	5.06	0.01	0.05	3.85	0.86	0.01
0.03	0.09	3.30	0.03	0.08	3.03	0.19	0.01
0.06	0.15	2.32	0.06	0.15	2.30	0.02	0.00
0.14	0.24	1.74	0.14	0.23	1.64	0.08	0.01
0.23	0.34	1.44	0.24	0.28	1.19	0.18	0.04
0.30	0.37	1.21	0.31	0.34	1.12	0.07	0.02
0.96	2.85	2.99	0.96	2.19	2.29	0.50	0.47
1.34	4.13	3.09	1.34	3.61	2.70	0.28	0.38
2.30	4.68	2.03	2.30	4.38	1.90	0.09	0.21
4.01	5.53	1.38	4.01	4.45	1.11	0.19	0.76
				Relative mean SD			11.22
				SAMPLE K4			
0.01	0.16	12.15	0.01	0.12	12.59	0.31	0.00
0.03	0.30	10.79	0.03	0.25	9.72	0.76	0.02
0.06	0.68	10.52	0.06	0.57	9.25	0.89	0.06
0.14	1.60	11.34	0.14	1.41	10.13	0.86	0.12
0.24	1.79	7.57	0.23	2.29	9.81	1.59	0.37
0.31	2.06	6.76	0.30	2.24	7.37	0.43	0.13
0.96	4.90	5.13	0.95	4.59	4.80	0.23	0.22
1.34	5.09	3.81	1.34	6.64	4.97	0.82	1.10
2.30	5.52	2.40	2.30	5.85	2.54	0.10	0.24
4.01	4.82	1.20	4.01	5.16	1.29	0.06	0.24
				Relative mean SD			8.93
				SAMPLE K1			
0.01	0.11	8.77	0.01	0.11	9.45	0.48	0.01
0.03	0.17	6.07	0.03	0.16	5.93	0.10	0.00
0.06	0.28	4.42	0.06	0.26	4.15	0.20	0.01
0.14	0.48	3.44	0.14	0.43	3.08	0.26	0.04
0.24	0.68	2.91	0.23	0.66	2.83	0.05	0.01
0.31	0.81	2.67	0.30	0.68	2.22	0.32	0.10
0.96	3.92	4.10	0.96	3.23	3.38	0.51	0.49
1.34	3.73	2.78	1.34	3.49	2.61	0.12	0.16
2.30	4.20	1.82	2.30	4.15	1.80	0.01	0.03
4.01	4.14	1.03	4.01	4.52	1.13	0.07	0.27
				Relative mean SD			6.15

Table B.11. Duplicate analysis of batch dissolution of a selection of samples by Na dithionite.

Duplicate 1			Duplicate 2				
Time (days)	mol/kg	Rate	Time (days)	mol/kg	Rate	SD of rate	SD at mean time
				Sample FH2			
0.01	2.75	263.77	0.01	1.34	210.92	37.37	0.31
0.02	5.73	257.76	0.02	5.15	294.48	25.96	0.52
0.05	7.59	145.66	0.07	8.50	130.68	10.59	0.62
0.09	8.65	92.26	0.12	9.33	80.09	8.61	0.90
0.18	8.82	48.48	0.21	9.13	43.31	3.66	0.72
0.28	8.65	30.90	0.28	9.17	33.11	1.56	0.44
				Relative mean SD			8.27
				Sample Gt			
0.01	0.35	34.64	0.01	1.11	168.33	94.53	0.79
0.02	1.94	88.28	0.02	1.73	97.90	6.80	0.14
0.05	5.93	114.38	0.07	9.03	138.40	16.98	0.99
0.09	10.02	107.08	0.12	12.35	105.83	0.88	0.09
0.18	10.00	55.05	0.21	11.40	54.00	0.74	0.15
0.28	10.94	39.14	0.28	11.27	40.69	1.10	0.31
				Relative mean SD			5.73
				Sample A4			
0.01	1.19	218.50	0.01	1.79	164.79	37.98	0.31
0.02	3.61	218.18	0.02	4.23	186.62	22.32	0.44
0.06	5.51	85.95	0.05	5.44	103.58	12.46	0.73
0.12	6.16	53.30	0.09	5.94	63.05	6.90	0.72
0.21	6.20	29.53	0.18	6.00	32.87	2.36	0.46
0.28	6.19	22.42	0.28	6.00	21.39	0.73	0.20
				Relative mean SD			9.83
				Sample A3			
0.01	2.08	187.14	0.01	1.14	192.42	3.73	0.03
0.02	3.62	157.89	0.02	3.04	178.45	14.54	0.29
0.05	4.68	88.64	0.06	4.99	77.23	8.07	0.47
0.09	5.44	57.54	0.12	5.71	49.27	5.85	0.62
0.18	5.50	30.11	0.21	5.77	27.40	1.91	0.38
0.28	5.56	19.81	0.28	5.88	21.28	1.04	0.29
				Relative mean SD			7.78
				Sample H2			
0.00	1.56	409.47	0.01	0.84	91.47	224.86	1.46
0.01	4.12	276.09	0.02	5.29	261.41	10.38	0.18
0.03	6.20	223.03	0.03	6.61	199.72	16.48	0.50
0.06	8.17	130.71	0.07	8.33	122.89	5.53	0.36
0.11	9.12	80.08	0.12	8.98	75.34	3.35	0.39
0.21	9.02	43.30	0.21	8.98	42.04	0.89	0.19
0.27	9.08	33.11	0.28	9.10	32.54	0.41	0.11
				Relative mean SD			6.69
				Sample A1			
0.01	0.65	80.92	0.01	1.46	172.71	64.90	0.53
0.02	3.47	181.71	0.02	3.39	173.14	6.06	0.12
0.03	4.09	127.88	0.03	4.13	127.55	0.23	0.01
0.07	5.38	80.69	0.07	5.56	82.86	1.54	0.10
0.12	6.48	54.92	0.12	6.41	54.09	0.59	0.07
0.21	6.63	31.18	0.21	6.73	31.58	0.28	0.06
0.28	6.69	24.04	0.28	6.68	23.94	0.07	0.02
				Relative mean SD			2.69

Table B.12. Duplicate analysis of batch dissolution of a selection of samples by ammonium oxalate.

Duplicate 1			Duplicate 2				
Time (days)	mol/kg	Rate	Time (days)	mol/kg	Rate	SD of rate	SD at mean time
				Sample K1			
0.01	0.07	7.61	0.01	0.03	4.01	2.54	0.02
0.02	0.25	11.01	0.02	0.32	14.39	2.39	0.05
0.04	0.43	11.63	0.04	0.49	13.59	1.39	0.05
0.06	1.45	22.48	0.06	1.44	22.53	0.04	0.00
0.09	5.54	63.44	0.09	5.50	63.23	0.15	0.01
0.17	7.42	43.66	0.17	7.33	43.22	0.31	0.05
0.89	7.24	8.15	0.89	7.05	7.94	0.15	0.13
				Relative mean SD			1.46
				Sample FH6			
0.01	0.02	2.25	0.01	0.01	1.45	0.57	0.00
0.02	0.11	4.68	0.02	0.10	4.80	0.09	0.00
0.04	0.39	10.45	0.03	0.28	8.15	1.62	0.06
0.06	2.15	33.15	0.06	1.55	24.95	5.80	0.37
0.09	5.39	61.55	0.09	5.01	58.81	1.94	0.17
0.17	9.41	55.27	0.17	8.87	52.89	1.68	0.28
0.89	9.93	11.19	0.89	10.19	11.51	0.23	0.21
				Relative mean SD			4.08
				Sample H2			
0.01	0.01	0.67	0.01	0.01	1.48	0.58	0.00
0.02	0.26	12.25	0.02	0.30	12.83	0.41	0.01
0.04	0.37	10.53	0.04	0.60	16.16	3.99	0.14
0.06	1.37	21.74	0.06	1.64	25.25	2.48	0.16
0.09	5.78	67.24	0.09	5.96	67.93	0.49	0.04
0.17	7.27	43.11	0.17	7.16	41.99	0.79	0.13
0.89	7.18	8.10	0.89	6.95	7.83	0.19	0.17
				Relative mean SD			2.94
				Sample Sch			
0.01	0.11	18.01	0.01	0.13	13.27	3.35	0.03
0.02	0.24	11.92	0.02	0.35	14.96	2.16	0.05
0.03	0.45	13.12	0.04	0.80	21.47	5.90	0.21
0.06	1.53	24.72	0.07	1.47	22.56	1.53	0.10
0.08	5.36	63.29	0.09	5.33	60.65	1.86	0.16
0.17	5.93	35.45	0.17	5.91	34.65	0.57	0.10
0.88	6.01	6.79	0.89	5.84	6.58	0.15	0.13
				Relative mean SD			3.89
				Sample S2			
0.01	0.23	25.73	0.01	0.05	6.21	13.80	0.11
0.02	0.35	15.60	0.02	0.25	11.58	2.84	0.06
0.04	0.35	9.62	0.04	0.30	8.38	0.88	0.03
0.06	1.04	16.18	0.06	0.81	12.82	2.38	0.15
0.09	4.32	49.50	0.09	4.18	48.45	0.74	0.06
0.17	4.70	27.66	0.17	4.47	26.49	0.83	0.14
0.89	4.61	5.20	0.89	4.42	4.99	0.15	0.13
				Relative mean SD			4.64
				Sample A1			
0.01	0.08	8.52	0.01	0.07	8.73	0.14	0.00
0.02	0.17	7.49	0.02	0.21	9.62	1.50	0.03
0.04	0.44	12.06	0.04	0.35	9.80	1.59	0.06
0.06	1.08	16.66	0.06	1.06	16.70	0.03	0.00
0.09	4.22	48.26	0.09	4.16	48.26	0.00	0.00
0.17	4.70	27.61	0.17	4.67	27.67	0.04	0.01
0.89	4.71	5.30	0.89	4.49	5.07	0.16	0.14
				Relative mean SD			1.61

B.3 Dissolution of oxide from coated surfaces

Table B.13. Repeat analysis of iron coating released during pretreatments

		Stainless Steel					PVC				
		Repeats			Average	RSD		Repeats		Average	RSD
	Calgon	25.9	22.1	23.1	23.7	8.2	18.2	18.3	18.9	18.4	2.0
FH6	NaOH	9.0	10.3	10.2	9.8	7.5	3.4	4.5	2.9	3.60	23.7
	Ultrasonic	4.3	4.5	3.9	4.2	7.1	1.7	6.9	5.1	4.56	58.5
	Calgon	29.5	29.1	27.3	28.7	4.1	22.6	23.5	24.5	23.6	4.0
FH2	NaOH	15.6	14.8	15.6	15.3	3.0	3.9	6.4	7.2	5.81	29.7
	Ultrasonic	8.8	9.8	5.2	8.0	30.5	24.2	20.5	15.7	20.1	21.2
	Calgon	10.6	11.6	9.0	10.4	12.8	29.9	23.8	17.1	23.6	27.2
Gt	NaOH	5.6		3.9	4.8	24.9	23.6	23.5	28.4	25.2	11.0
	Ultrasonic	3.3	4.3	4.7	4.1	17.7	10.9	15.7	18.5	15.0	25.4

Appendix C Mössbauer Report

^{57}Fe Mössbauer-effect Spectroscopy

Determination of Fe(II)/Fe(III) ratio and iron speciation in rock samples from Klein Karoo Region.

from Meris Smith

Department of Geological Sciences

UCT

fax: #27 (0)21 650 3783

ph: #27 (0)21 650 2913

e-mail : smithm@geology.uct.ac.za

Report, ***Merisuct1***, compiled by

Dr G.R. Hearne, Dr. V. Pischedda,

N. Jackson and M. Manzi.

Mössbauer Lab, School of Physics @ WITS

SEPTEMBER 2004

PO#654440

REPORT

Four rock samples from the Klein Karoo Region were received from Meris Smith of the Department of Geological Sciences at UCT to ascertain the Fe^{+2}/Fe^{+3} ratio and the iron- oxide precipitate content. The four samples received are described below:

- **G1** Colour: orange/brown;
  Mineralogy: quartz, muscovite, amorphous iron oxides, feldspar;
  Total wgt % Fe: 4.58
- **C2** Colour: grey;
  Mineralogy: quartz, Fe-bearing chlorite, feldspar, magnetite;
  Total wgt % Fe: 4.51
- **B4** Colour: white/yellow;
  Mineralogy: quartz, feldspar, sericite;
  Total wgt % Fe: 0.42
- **P1** Colour: white;
  Mineralogy: quartz, feldspar, sericite, minor magnetite;
  Total wgt % Fe: 0.42

^{57}Fe Mössbauer spectroscopy measurements at room temperature have been performed in the Mössbauer Laboratory of the School of Physics at WITS in Johannesburg.

Samples were received in powdered form and Mössbauer spectra were recorded in the normal transmission geometry. A WISSEL constant acceleration motor was used to scan the velocity range of interest, with a ^{57}Co(Rh) *"point"* source (~10mCi) at room temperature. The absorbers (samples of interest) were thoroughly mixed with an organic buffer to form a homogeneous disk of uniform thickness of about 140mg/cm^2 in powder-clamp sample holders, except for sample P1 where the thickness was about 280mg/cm^2 because of the low Fe concentration. Samples G1 and C2 were measured for 48 and 32 hrs, respectively. Instead sample B4 required 16 days of data collection. Velocity calibration was obtained by measuring the spectrum of a 25μm thick Fe foil at room temperature. This gave a linewidth of Γ = 0.32 mm/s. For our convenience,

sample P1 was recorded on a separate Mössbauer spectrometer (conventional $^{57}Co(Rh)$ source ~30mCi) for 10 days. Velocity calibration was obtained from the spectrum of powder Fe_2O_3 (linewidth of Γ = 0.32mm/s) at room temperature.

Each spectrum was recorded in 1024 channels to ensure at least 10^5 counts in each channel. Prior to fitting, each spectrum was folded to remove geometrical base-line curvature.

Each spectrum comprising 512 channels was analysed using the non-linear least squares fitting program NORMOS-90 (distributed by *Wissenschaftliche Elektronik GmbH*-Germany).

In the analysis spectra were fitted with a combination of sextets and doublets. Distinct Fe-bearing phases are identified in theoretical fits to the spectrum at room temperature through the hyperfine interaction parameters of each spectral component: isomer (centroid) shift IS, quadrupole (doublet) splitting QS, (sextet) magnetic hyperfine field B_{hf} and linewidth Γ.

Mössbauer spectroscopy only detects Fe-bearing phases. Each spectrum may be comprised of a superposition of sub-spectra (sextets, doublets, singlets or even a distribution of sextets) which represent different Fe-bearing phases in the sample.

Characteristic Mössbauer parameters of paramagnetic (doublet) ferrous (Fe^{2+}) species are *IS*~1 mms^{-1} and *QS* ~1.5 – 3.0 mms^{-1} ; and ferric (Fe^{3+}) species have *IS*~ 0.3 mms^{-1} and *QS* ~0.5 mms^{-1}.

The integrated area under each sub-spectrum yields *at. %* of iron in that particular phase. Fe-phase abundance's are obtained from the integrated area under each of the spectral components.

Percentage abundance's of the various minerals phases found in each sample are tabulated below the corresponded plot. Typical **relative errors** in the abundances are ~10% for all minerals detected with appreciable intensities.

The magnetic hyperfine fields (sextets) of hematite or iron metal have been found to be present in some of the samples. The presence of paramagnetic or non-magnetic Fe^{2+} and Fe^{3+} of unidentified parentage has been detected.

A tabulation of the hyperfine interaction parameters and abundances of each phase or site is presented in tables that accompany each spectrum.

Sample G1

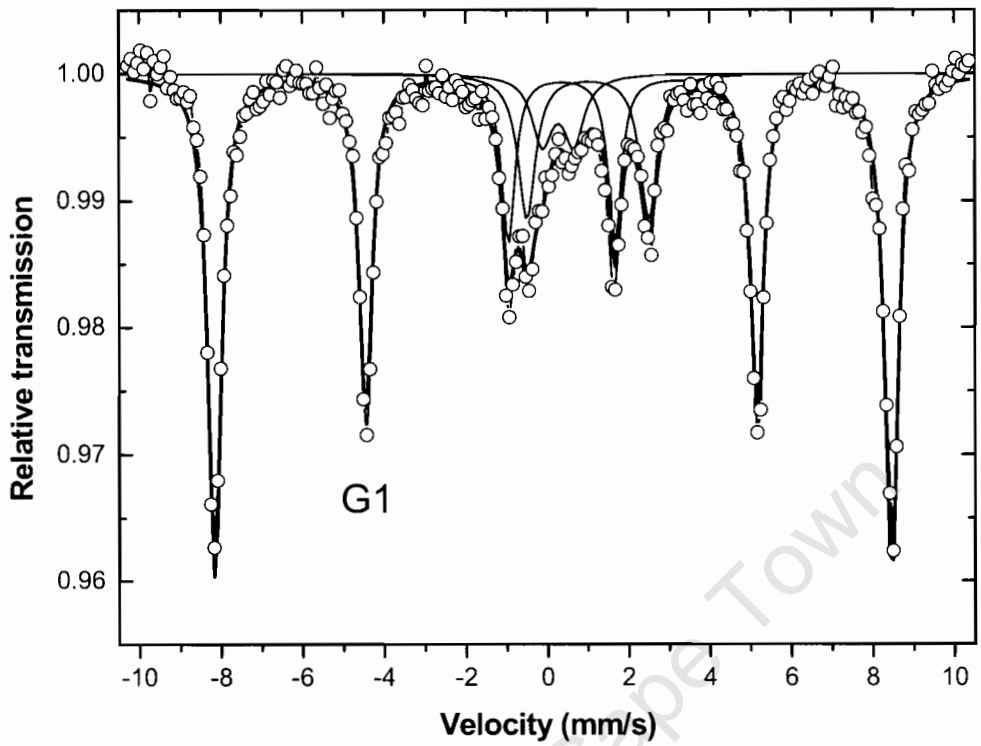

Figure 1: *Mössbauer spectrum of sample* **G1**. *The overall fit to the spectrum is the solid line through the data points represented as open circles. The spectrum is fitted with one sextet (six-line pattern) and two doublets. The sextet represents hematite, the central doublets are unidentified* Fe^{3+} *and* Fe^{2+} *species.*

Table 1: Hyperfine interaction parameters of the spectral components in the spectrum of sample G1, see Figure 1.

SAMPLE	Spectral Component	Γ, Linewidth (mm/s)	δ/Fe (mm/s)	QS (mm/s)	B_{hf} (T)	¥Abundance %
G1	Hematite (Fe_2O_3)	0.39	0.36	-0.20	51.5	77
	Fe^{3+}	0.52	0.37	0.78	-	8
	Fe^{2+}	0.60#	1.11	3.00	-	15

¥ From the integrated area under the sub-spectrum.

These parameters were fixed to be consistent with literature values so as to allow a sensible fit to the data.

Comments

G1: This spectrum is fitted with two crystalline components, a sextet and two doublets. This six-line pattern is assigned to hematite which has a characteristic negative value for QS~-0.2mm/s and a comparatively narrow linewidth Γ~0.34 mm/s indicative of good crystallinity and near-stoichiometry. The central doublets have been used to represent unidentified Fe^{2+} and Fe^{3+} species.

Sample C2

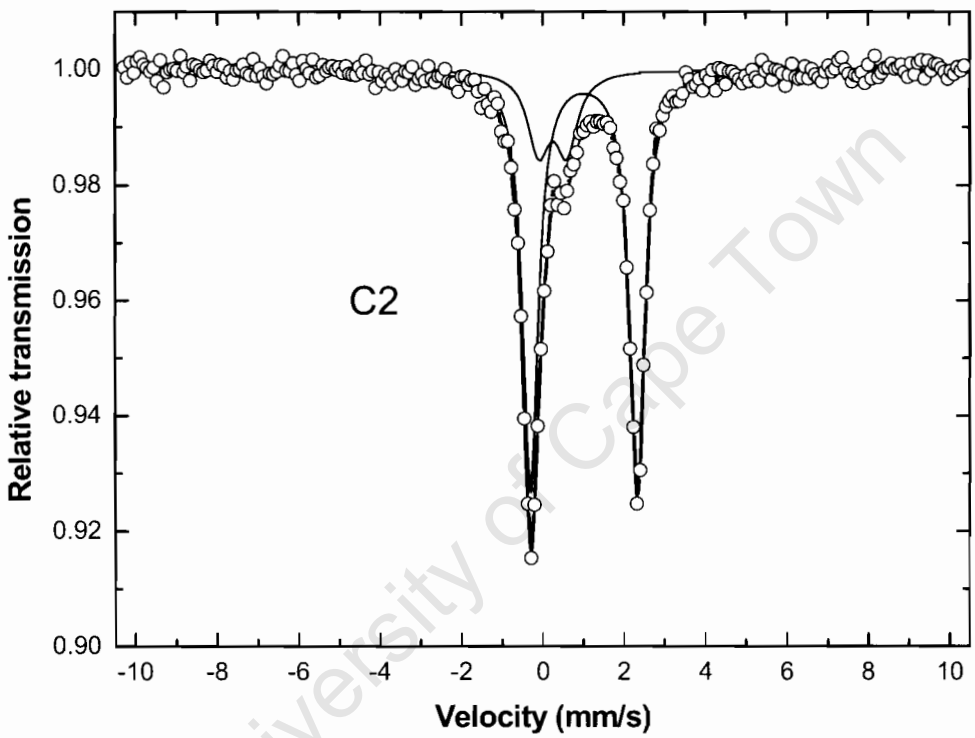

Figure 2: *Mössbauer spectrum of sample* **C2**. *The overall fit to the spectrum is the solid line through the data points represented as open circles. The spectrum is fitted with two doublets. The central doublets represent unidentified Fe^{3+} and Fe^{2+} species.*

Table 2: Hyperfine interaction parameters of the spectral components in the spectrum of sample C2, see Figure 2.

SAMPLE	Spectral Component	Γ, Linewidth (mm/s)	δ/Fe (mm/s)	QS (mm/s)	B_{hf} (T)	¥Abundance %
C2	Fe^{3+}	0.64	0.38	0.69	-	21
	Fe^{2+}	0.45	1.12	2.63	-	79

¥ From the integrated area under the sub-spectrum.

Comments

C2: This spectrum is fitted with two doublets, they are as yet unidentified Fe^{2+} and Fe^{3+} species.

Sample B4

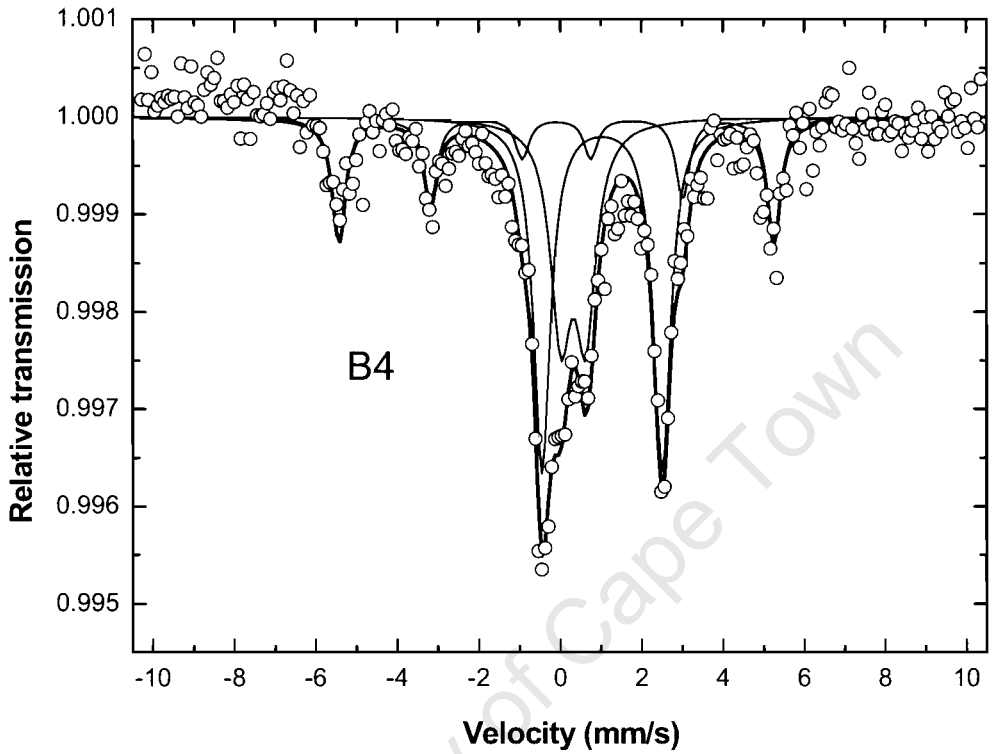

Figure 3: *Mössbauer spectrum of sample* **B4**. *The overall fit to the spectrum is the solid line through the data points represented as open circles. The spectrum is fitted with one sextet (six-line pattern) and two doublets. The sextet represents iron metal; the central doublets are unidentified* Fe^{3+} *and* Fe^{2+} *species.*

Table 3: Hyperfine interaction parameters of the spectral components in the spectrum of sample B4, see Figure 3.

SAMPLE	Spectral Component	Γ, Linewidth (mm/s)	δ/Fe (mm/s)	QS (mm/s)	B_{hf} (T)	¥Abundance %
B4	Iron metal (Fe^0)	0.4#	-0.07	0.0#	33.1	25
	Fe^{3+}	0.50	0.44	0.61	-	30
	Fe^{2+}	0.40#	1.13	2.94	-	45

¥ From the integrated area under the sub-spectrum.

These parameters were fixed to be consistent with literature values for Fe-metal so as to allow a sensible fit to the data.

Comments

B4: This spectrum is fitted with a sextet and two doublets. The central doublets represent unidentified Fe^{2+} and Fe^{3+} species, the sextet represents iron metal Fe^{0}.

Sample P1

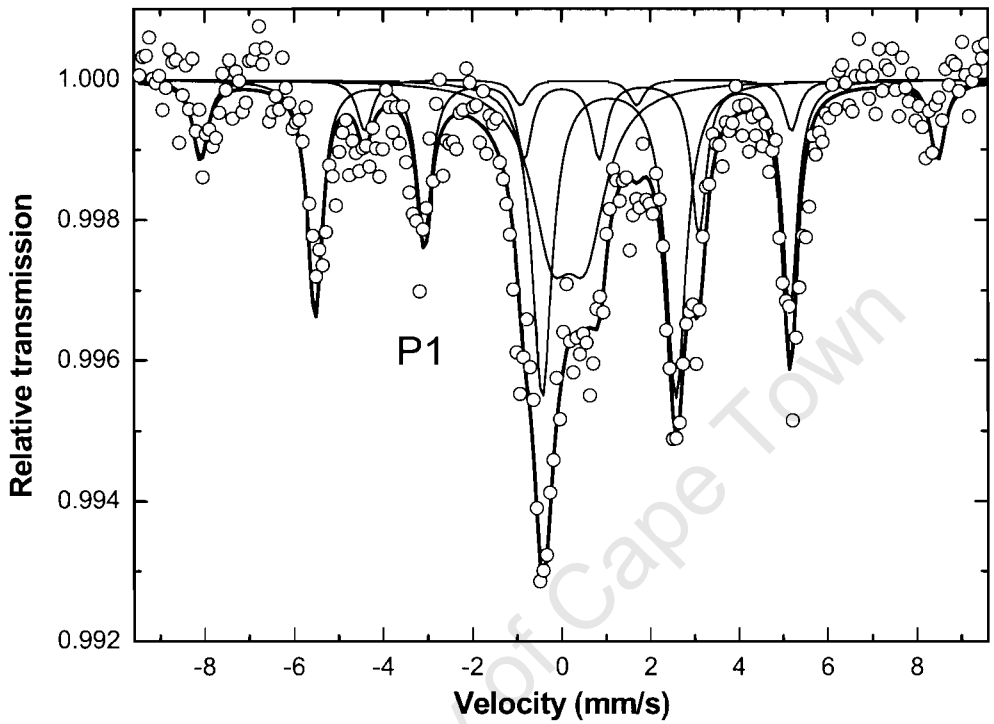

Figure 4 : *Mössbauer spectrum of sample* **P1**. *The overall fit to the spectrum is the solid line through the data points represented as open circles. The spectrum is fitted with two sextets (six-line pattern) and two doublets. The sextets represent iron metal and hematite; the central doublets are unidentified* Fe^{3+} *and* Fe^{2+} *species.*

Table 4: Hyperfine interaction parameters of the spectral components in the spectrum of sample P1, see Figure 4.

SAMPLE	Spectral Component	Γ, Linewidth (mm/s)	δ/Fe (mm/s)	QS (mm/s)	B_{hf} (T)	¥Abundance %
P1	Iron metal Fe^{0}	0.4#	-0.08	0	33.1	32
	Fe^{3+}	1.08	0.27	0.76	-	27
	Fe^{2+}	0.54	1.18	3.02	-	30
	Hematite (Fe_2O_3)	0.40#	0.40	-0.20#	51.4	11

[¥] From the integrated area under the sub-spectrum.

[#] These parameters were fixed to allow for a sensible fit consistent with reports on iron metal and hematite.

Comments

P1: This spectrum is fitted with two sextets and two doublets. The six-line pattern is assigned to hematite which has a characteristic negative value for QS~-0.2mm/s and a comparatively narrow linewidth Γ~0.34 mm/s indicative of good crystallinity and near-stoichiometry. The other sextet is assigned to iron metal, Fe^0. The central doublets are unidentified Fe^{2+} and Fe^{3+} species.

Concluding Remarks

- Because of the very low iron content (< 0.5 wgt %) in some of the sample (B4 and P1) data acquisition was effected for several days to reduce statistical scatter. To reduce statistical scatter even further would require measuring times of a few weeks. It is in these low iron content samples that the Mössbauer data shows evidence of iron-metal (Fe^0) species.
- Spectra of all samples each have two separate doublets which are unidentified Fe^{2+} and Fe^{3+} species. This ferrous and ferric content *either* represents different crystallographic sites in the same mineral phase or they originate from different mineral phases in the same sample.

References

- O. Lahav, G. Ritvo, I. Slijper, G. Hearne, M. Cochva (2004) . The potential of using iron-oxide-rich soils for minimizing the detrimental effects of H_2S in freshwater acquaculture systems. ***Acquaculture 238: 263-281.***

- G. M. Bancroft (1969). Quantitative site populations in silicate minerals by the Mössbauer effect. ***Chem. Geol. 5, 255-258.***

- E. Murad (1985). In : W. Stucki, B.A. Goodman, U. Schwertmann (Eds), Iron in Soils and Clays. ***Proceedings of the NATO Advanced Study Institute on Iron in Soils and Clay Minerals***, held in Bad Windsheim, FRG, July 1-13.

Appendix D XRD Scans

D.1 Kammanassie Rocks

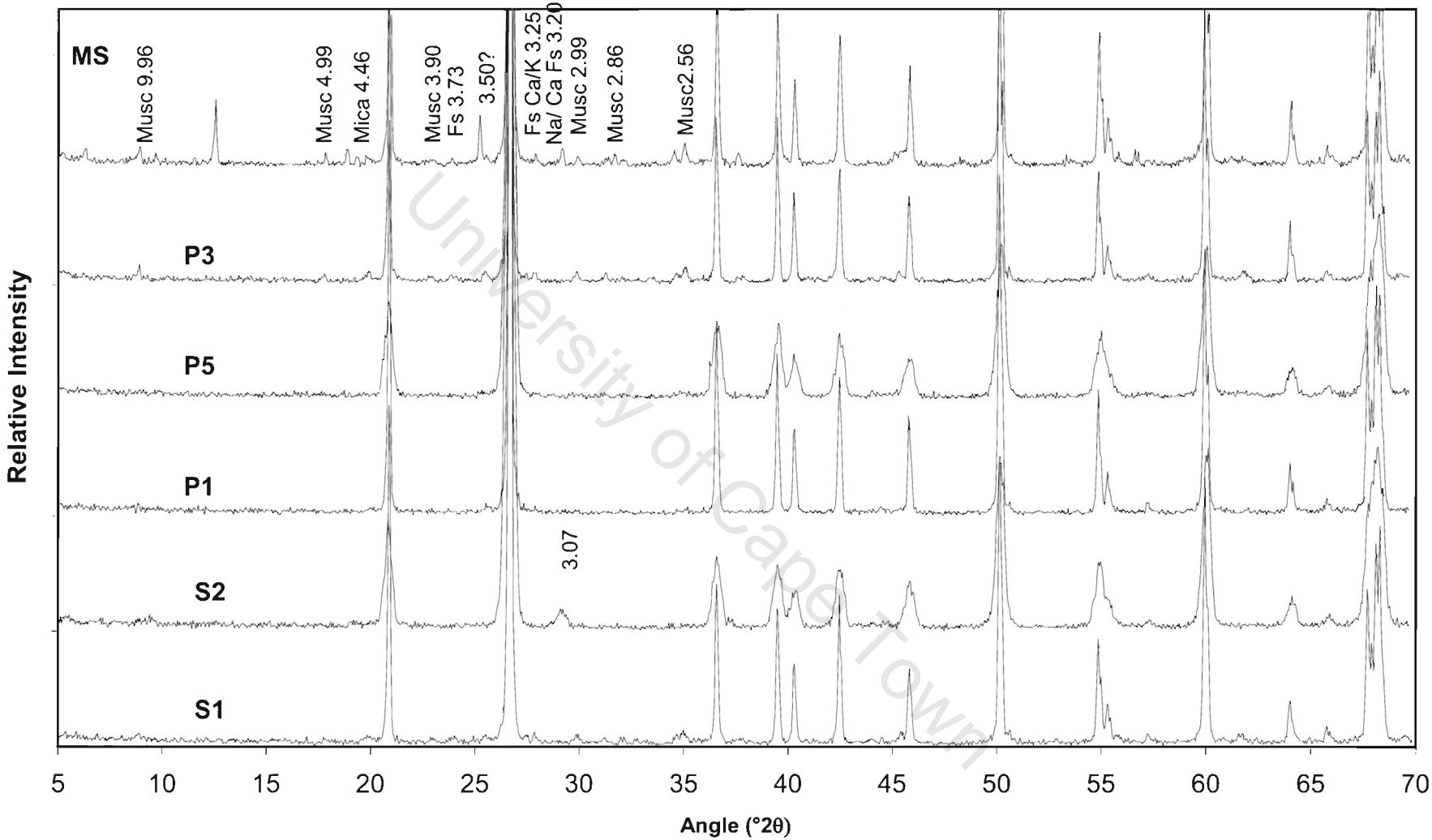

Figure D.1. XRD scan of samples from the Peninsula and Skurweberg Formations (MS = magnetic separate from Peninsula)

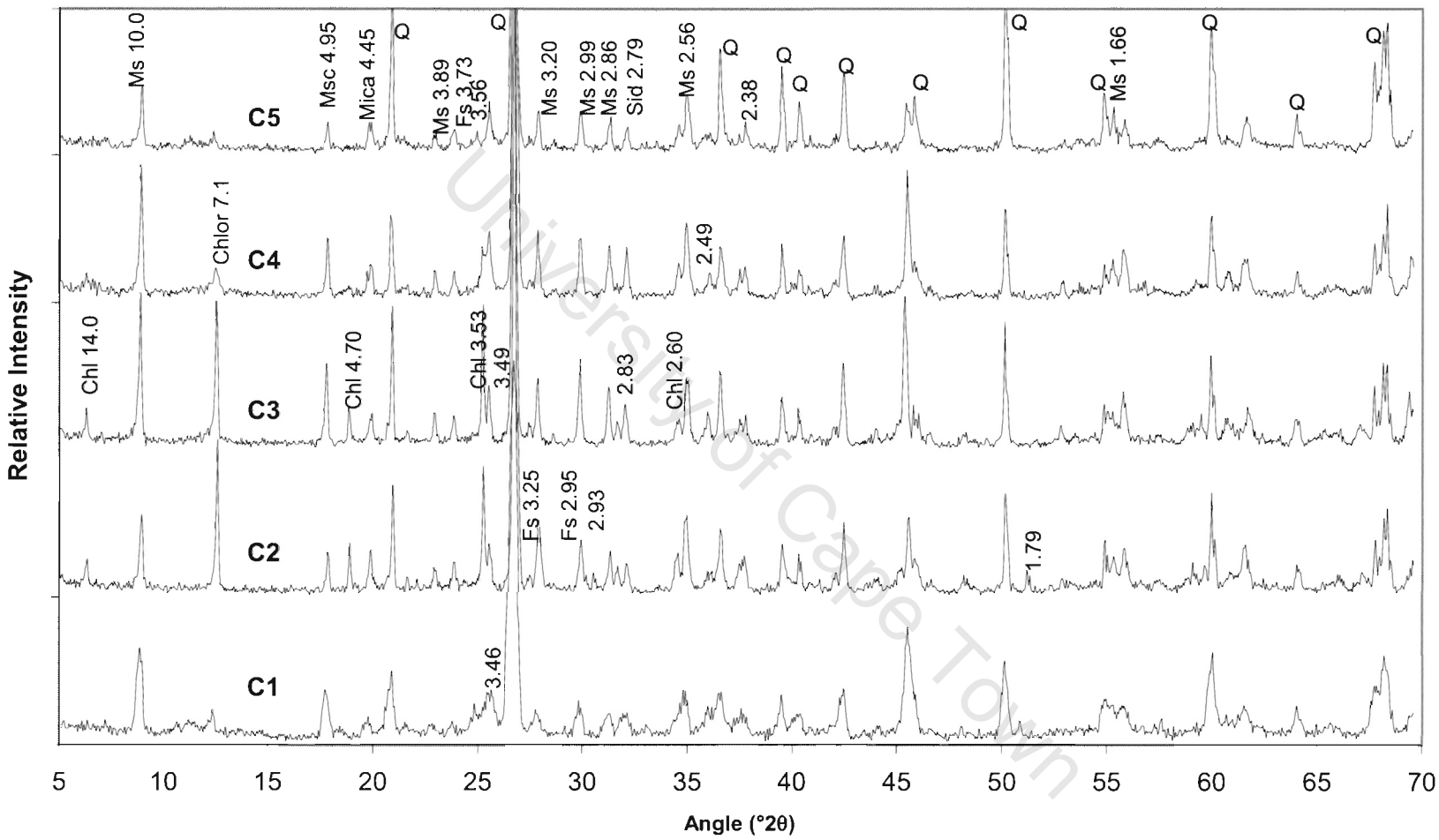

Figure D.2. XRD scan of samples from the Cedarberg Shale Formation

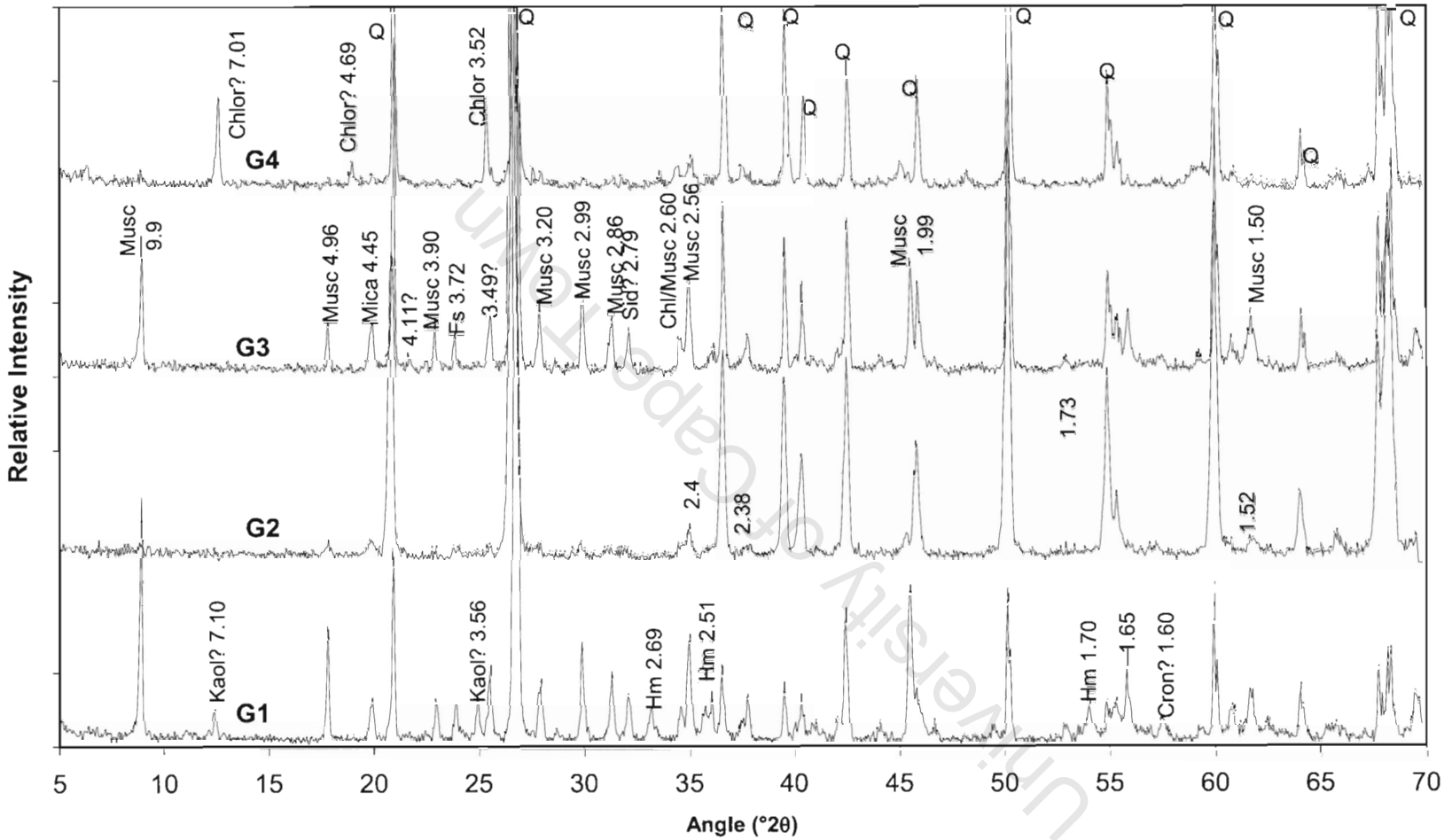

Figure D.3. XRD scan of samples from the Goudini Formation

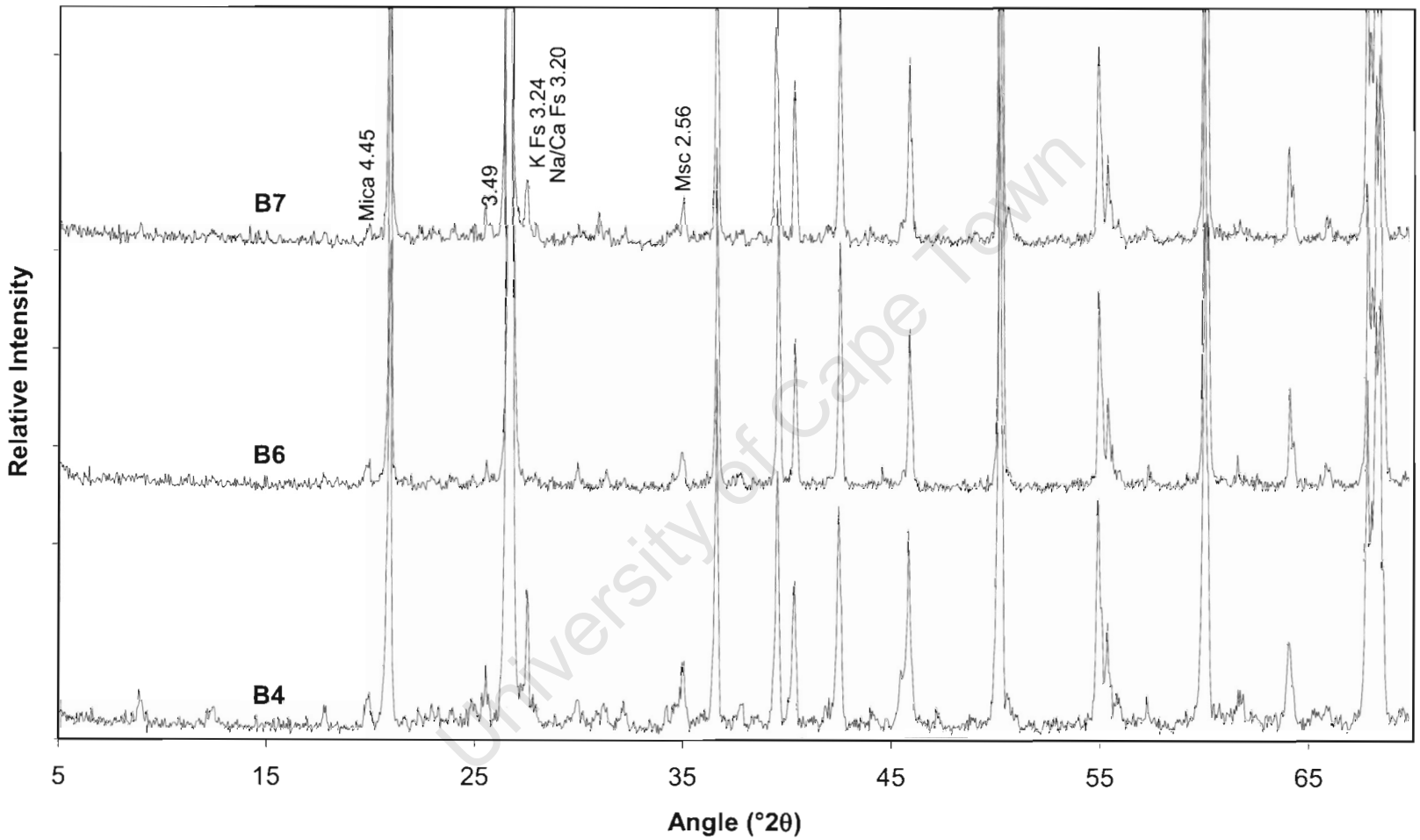

Figure D.4. XRD scan of samples from the Baviaanskloof Formation

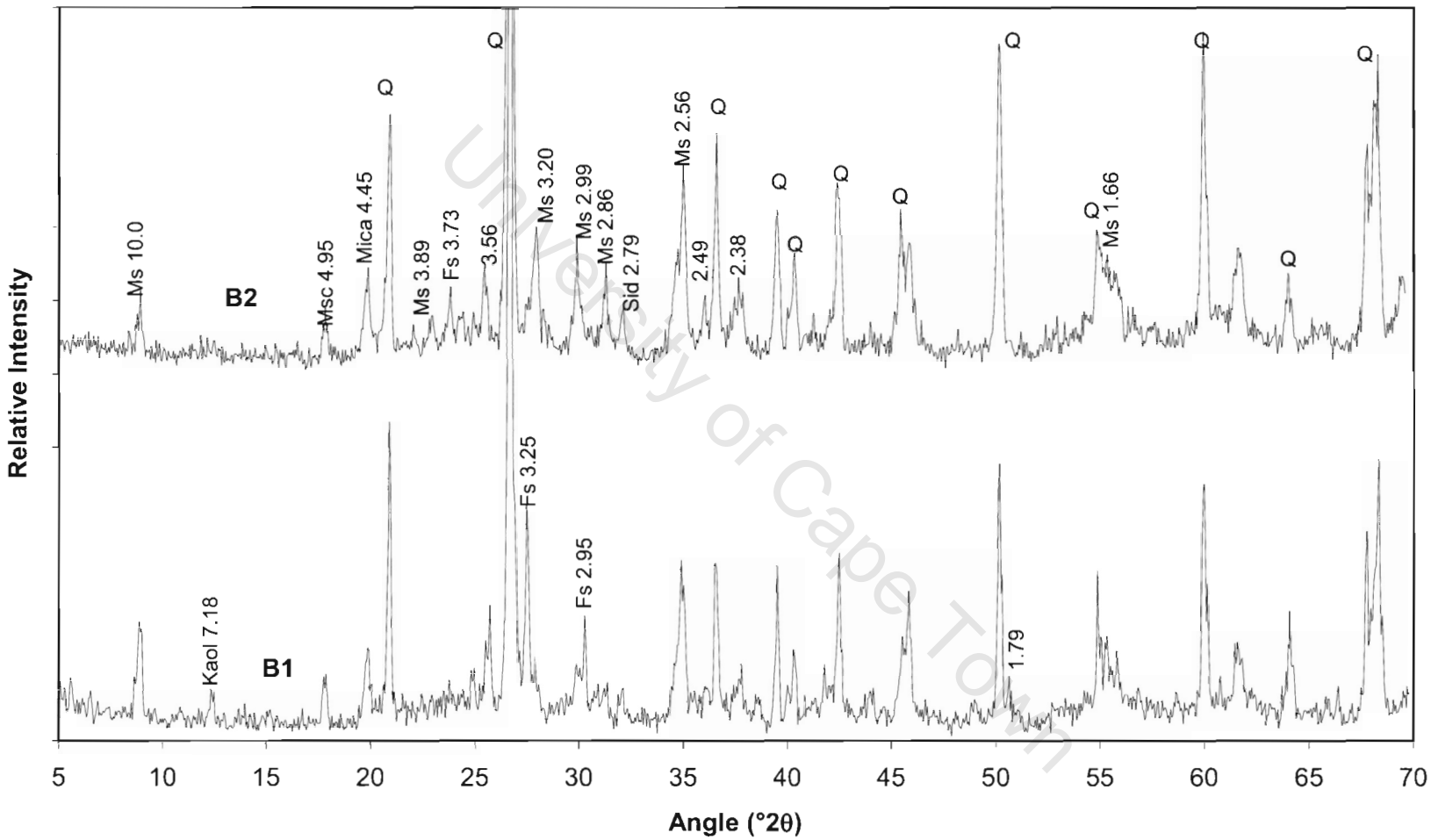

Figure D.5. XRD scan of samples from the Bokkeveld Formation

D.2 Iron oxide precipitate XRD scans

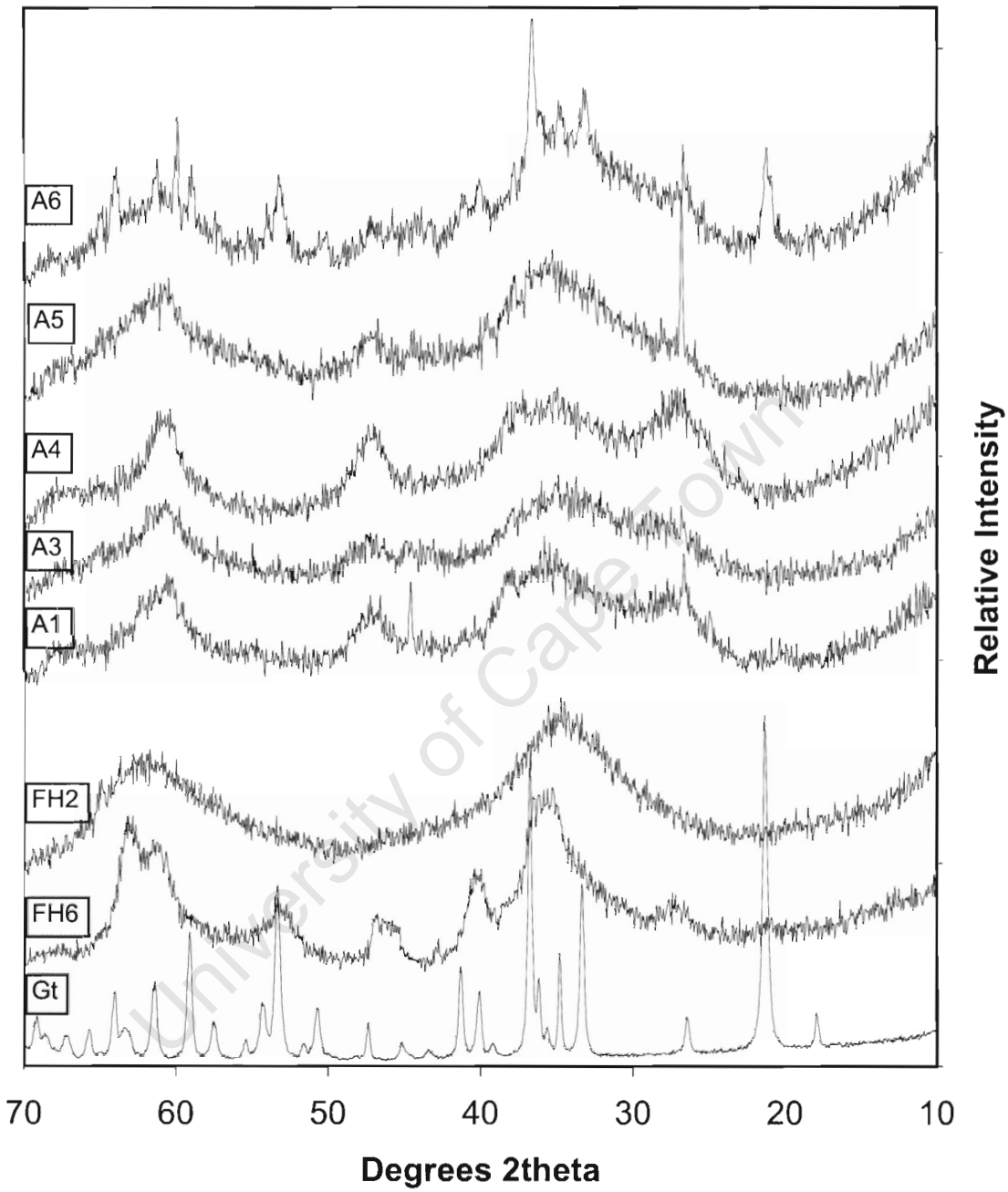

Figure D.6. XRD scans of iron hydroxide precipitates from the Atlantis wellfield

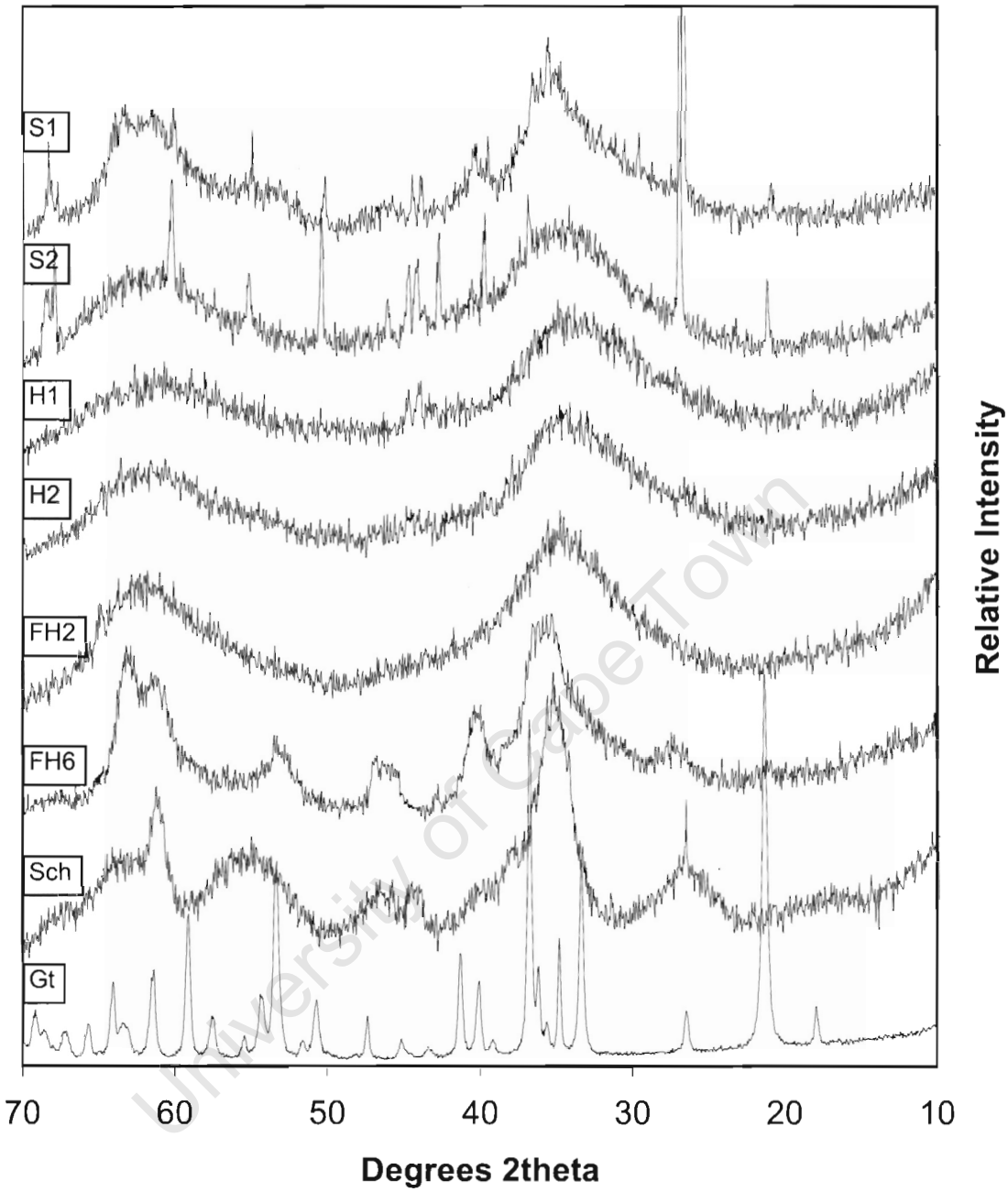

Figure D.7. XRD scans of iron hydroxide precipitates from springs

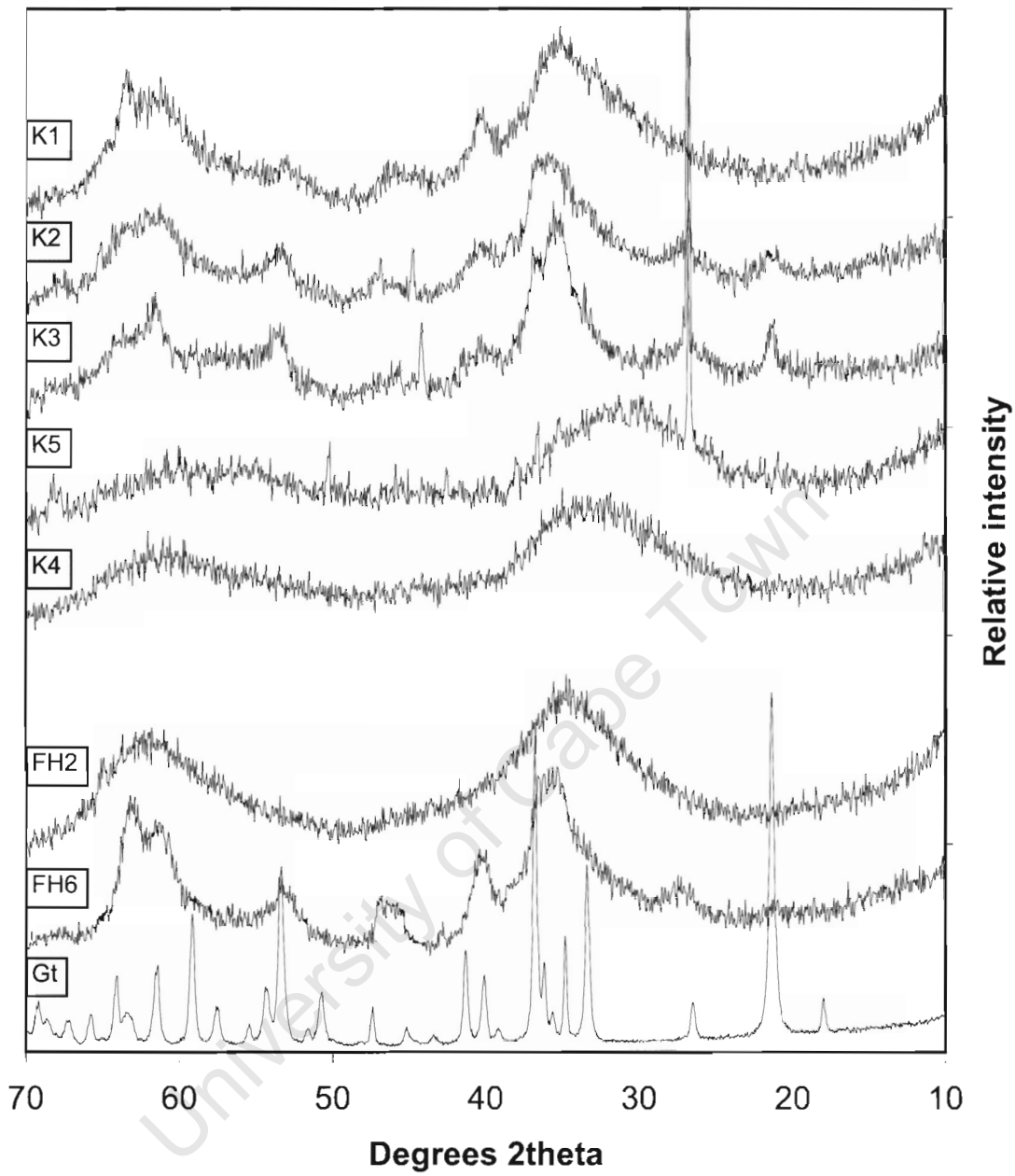

Figure D.8. XRD scans of iron hydroxide precipitates from KKRWSS boreholes

Appendix E Phreeqci Modelling

E.1 Additions to the Wateq4f database

The modification and additions to the Wateq4f database as input into Phreeqci are given in Table E.1. Fe_di (Fe^{2+}) and Fe_tri (Fe^{3+}) were added to the database to enable kinetic calculations and surface speciation. The two iron species were added in the SOLUTION_MASTER_SPECIES keyword and the reactions they are involved in were defined in the SOLUTION_SPECIES keyword, following the method of Appelo *et al.* (1999). The phases goethite, ferrihydrite, siderite, haematite, maghemite and amorphous $Fe(OH)_3$ were also added to the database to allow calculation of the saturation indices of these minerals and equilibration of the solution with them if necessary. The equilibrium constants for all of the above species and phases were sourced from the Wateq4f database (Ball and Nordstrom, 1991) except for ferrihydrite equilibrium constant which was in Appelo and de Vet (2003).

Table E.1. Modification and additions to the Wateq4f database

```
SOLUTION_MASTER_SPECIES
Fe_di               Fe_di+2    0.0     Fe_di              55.847
Fe_tri              Fe_tri+3   0.0     Fe_tri             55.847

SOLUTION_SPECIES
Fe_di+2 = Fe_di+2
        log_k   0.0
Fe_tri+3 = Fe_tri+3
        log_k   0.0
#
# Fe+2 species
#
Fe_di+2 + H2O = Fe_diOH+ + H+
        log_k   -9.5
        delta_h 13.20   kcal
#
#... and also other Fe+2 species
#
Fe_di+2 + Cl- = Fe_diCl+
        log_k   0.14
Fe_di+2 + CO3-2 = Fe_diCO3
        log_k   4.38
Fe_di+2 + HCO3- = Fe_diHCO3+
        log_k   2.0
Fe_di+2 + SO4-2 = Fe_diSO4
        log_k   2.25
        delta_h 3.230   kcal
Fe_di+2 + HSO4- = Fe_diHSO4+
        log_k   1.08
```

```
Fe_di+2 + 2HS- = Fe_di(HS)2
        log_k   8.95
Fe_di+2 + 3HS- = Fe_di(HS)3-
        log_k   10.987
Fe_di+2 + HPO4-2 = Fe_diHPO4
        log_k   3.6
Fe_di+2 + H2PO4- = Fe_diH2PO4+
        log_k   2.7
Fe_di+2 + F- = Fe_diF+
        log_k   1.0
#
# Fe+3 species
#
Fe_tri+3 + H2O = Fe_triOH+2 + H+
        log_k   -2.19
        delta_h 10.4    kcal
#
#... and also other Fe+3 species
#
Fe_tri+3 + 2H2O = Fe_tri(OH)2+ + 2H+
        log_k   -5.67
        delta_h 17.1    kcal
Fe_tri+3 + 3H2O = Fe_tri(OH)3 + 3H+
        log_k   -12.56
        delta_h 24.8    kcal
Fe_tri+3 + 4H2O = Fe_tri(OH)4- + 4H+
        log_k   -21.6
        delta_h 31.9    kcal
2Fe_tri+3 + 2H2O = Fe_tri2(OH)2+4 + 2H+
        log_k   -2.95
        delta_h 13.5    kcal
3Fe_tri+3 + 4H2O = Fe_tri3(OH)4+5 + 4H+
        log_k   -6.3
        delta_h 14.3    kcal
Fe_tri+3 + Cl- = Fe_triCl+2
        log_k   1.48
        delta_h 5.6     kcal
Fe_tri+3 + 2Cl- = Fe_triCl2+
        log_k   2.13
Fe_tri+3 + 3Cl- = Fe_triCl3
        log_k   1.13
Fe_tri+3 + SO4-2 = Fe_triSO4+
        log_k   4.04
        delta_h 3.91    kcal
Fe_tri+3 + HSO4- = Fe_triHSO4+2
        log_k   2.48
Fe_tri+3 + 2SO4-2 = Fe_tri(SO4)2-
        log_k   5.38
        delta_h 4.60    kcal
Fe_tri+3 + HPO4-2 = Fe_triHPO4+
        log_k   5.43
        delta_h 5.76    kcal
Fe_tri+3 + H2PO4- = Fe_triH2PO4+2
        log_k   5.43
Fe_tri+3 + F- = Fe_triF+2
        log_k   6.2
        delta_h 2.7     kcal
Fe_tri+3 + 2F- = Fe_triF2+
        log_k   10.8
        delta_h 4.8     kcal
Fe_tri+3 + 3F- = Fe_triF3
```

```
        log_k   14.0
        delta_h 5.4     kcal


PHASES
Goethite
        Fe_triOOH + 3H+ = Fe_tri+3 + 2H2O
        log_k   -1.0
Ferrihydrite
        Fe_triOO2H3 + 3H+ = Fe_tri+3 + 3H2O
        log_k    2.0
Siderite(d)
        Fe_diCO3 = Fe_di+2 + CO3-2
        log_k    -10.45
Hematite
        Fe_tri2O3 + 6H+ =2Fe_tri+3 + 3H2O
        log_k    -4.008
Maghemite
        Fe_tri2O3 + 6H+ =2Fe_tri+3 + 3H2O
        log_k    6.386
Fe(OH)3(a)
        Fe_tri(OH)3 + 3H+ = Fe_tri+3 + 3H2O
        log_k     4.891
```

E.2 Breakthrough curves

E.2.1 Input file

The breakthrough curves were modelled using an input solution of pH 5 pure water containing 0.1 M K^+ (Solution 0) and an existing pH 5 pure water solution in each of the cells in the column (Solution 1-10) (Table E.2). The TRANSPORT keyword was used to model the concentration of K exiting the column at time intervals. The column was theoretically divided into 10 cells, each with a residence time equal to 1/10 the residence time of the column. Because the TRANSPORT keyword calculates the solution concentration at the midpoint of the cells, a half-cell has to be added to the column to determine the solution concentration at the outflow point. This was done by starting the experimental calculations at a time equal to half a cell residence time. The different flow rates on the pump were modelled by changing the residence time. The *Shifts* keyword describes the number of times a solution in each cell moves to the next cell. In this case 20 shifts were required to reach equilibrium. The default diffusion coefficient of 0.3 x 10^{-9} m^2/s was used and in this example a dispersivity of 0.0025 m was required to fit the model to the data.

Table E.2. Input and background solutions and transport keyword used to calculate breakthrough curves for a flow velocity of 0.11 m/hr.

```
SOLUTION 0  Input solution
        units mg/kgw
        pH              5
        Cl              3910
        K               3910
SOLUTION 1-10     Background solution
        units mg/kgw
        pH              5

TRANSPORT
-cells                  10
-shifts                 20          #No of cell transfers
-time_step              3744        #Time, in seconds, of each shift time)
-length                 0.02792     #Length of each cell in m
-flow_direction         forward
-boundary_conditions    flux  flux
-dispersivity           0.0025      #In m
-diffusion_coefficient  0.3e-9      #In m2/s (used default)
-initial_time           1872
-correct_disp           True
END
```

E.2.2 Results

The output files from Phreeqci are extremely long and rather than give the full output, the relevant data have been tabulated (Table E.3)

Table E.3. Calculated F-curve (C/C_0) of K in outflow of column at different flow rates

Flow rate (m/hr)											
0.011		0.021		0.039		0.061		0.078		0.100	
Time (hrs)	F	Time (hrs)	F	Time (hrs)	F	Time (hrs)	F	Time (hrs)	F	Time (hrs)	F
0.52	0	0.30	0	0.18	0	0.12	0	0.09	0	0.07	0
1.56	0	0.90	0	0.54	0	0.37	0	0.28	0	0.22	0
2.60	0	1.50	0	0.90	0	0.61	0	0.47	0	0.37	0
3.64	0	2.10	0	1.26	0	0.86	0	0.66	0	0.51	0
4.68	0	2.70	0	1.62	0	1.10	0	0.85	0	0.66	0
5.72	1.6×10^{-5}	3.30	2.8×10^{-8}	1.97	2.6×10^{-8}	1.35	2.6×10^{-8}	1.04	2.6×10^{-8}	0.81	2.5×10^{-8}
6.76	1.4×10^{-3}	3.90	1.2×10^{-5}	2.33	1.2×10^{-5}	1.59	1.2×10^{-5}	1.23	1.1×10^{-5}	0.96	1.1×10^{-5}
7.80	2.2×10^{-2}	4.50	8.3×10^{-4}	2.69	8.1×10^{-4}	1.84	8.0×10^{-4}	1.42	8.0×10^{-4}	1.10	7.9×10^{-4}
8.84	0.13	5.10	2.0×10^{-2}	3.05	2.0×10^{-2}	2.08	2.0×10^{-2}	1.61	1.9×10^{-2}	1.25	1.9×10^{-2}
9.88	0.38	5.70	0.20	3.41	0.20	2.33	0.20	1.79	0.20	1.40	0.20
10.92	0.67	6.30	0.81	3.77	0.81	2.57	0.81	1.98	0.81	1.54	0.81
11.96	0.84	6.90	0.97	4.13	0.97	2.82	0.97	2.17	0.97	1.69	0.97
13.00	0.95	7.50	1.00	4.49	1.00	3.06	1.00	2.36	1.00	1.84	1.00
14.04	0.99	8.10	1.00	4.85	1.00	3.31	1.00	2.55	1.00	1.98	1.00
15.08	1.00	8.70	1.00	5.20	1.00	3.55	1.00	2.74	1.00	2.13	1.00
16.12	1.00	9.30	1.00	5.56	1.00	3.80	1.00	2.93	1.00	2.28	1.00
17.16	1.00	9.90	1.00	5.92	1.00	4.04	1.00	3.12	1.00	2.42	1.00
18.20	1.00	10.50	1.00	6.28	1.00	4.29	1.00	3.31	1.00	2.57	1.00
19.24	1.00	11.10	1.00	6.64	1.00	4.53	1.00	3.49	1.00	2.72	1.00
20.28	1.00	11.70	1.00	7.00	1.00	4.78	1.00	3.68	1.00	2.87	1.00
21.32	1.00	12.30	1.00	7.36	1.00	5.02	1.00	3.87	1.00	3.01	1.00

E.3 Modelled iron flow-through curves

E.3.1 Homogenous iron oxidation

E.3.1.1 Non-buffered

The input file for calculating the outflow concentration of iron from the column when using a non-buffered inflow solution and pure iron oxidation is given in Table E.4. Only the input file for pH 6 is given. The column is divided into 100 cells each with its own background solution. The input (SOLUTION 0) and background solutions for each cell (SOLUTION 1-100) are the same except for the presence of iron in the input solution. To generate the dissolved oxygen gradient along the column, the solution in each cell is equilibrated with $O_2(g)$ at a different partial pressure. For example, SOLUTION 1, in cell 1, is equilibrated with EQUILIBRIUM_PHASES 1 i.e., $O_2(g)$ at a partial pressure of $10^{-2.54}$. The solution in each cell is also held in equilibrium with FH. "*Ferrihydrite 0.0 0.0*" means that the solution must be maintain a saturation index of 0.0 with respect to FH (by precipitating whatever Fe^{3+} is present in excess of the saturation index). The second 0.0 is the amount of FH that the solution is allowed to dissolve to achieve saturation if it is undersaturated with respect to FH, in this case none.

The kinetically controlled oxidation of Fe^{2+} is calculated using the RATES and KINETICS keywords. RATES calculates the number of moles of Fe^{3+} generated by oxidation of Fe^{2+} under the chemical conditions in each cell. The calculation is specified by the user and in this case is the rate law governing iron oxidation (Equation 2.7) using the rate constant from Tamura *et al.* (1976). The KINETICS keyword tells Phreeqci how to use the "moles" value generated in RATES, in this case, subtract "moles" from Fe^{2+} and add "moles" to Fe^{3+}.

All of the above calculations are repeated for each cell for each time-step as specified in the TRANSPORT keyword. The variables used in the TRANSPORT keyword are the same as discussed for the breakthrough curves (Section E.2).

Table E.4. Input file for modelling oxidation of iron in the flow-through column

```
SOLUTION 0  Input solution
        units mg/kgw
        pH              6
        Alkalinity      1.46
        Na              28.5
        Cl              60
        Ca              9.34
        K               4.65
        Mg              0.64
```

```
        S(6)            30
        Fe_di           12.7
SOLUTION 1-50     Background solution
        units mg/kgw
        pH              6
        Alkalinity      1.46
        Na              28.5
        Cl              60
        Ca              9.34
        K               4.65
        Mg              0.64
        S(6)            30

EQUILIBRIUM_PHASES 0
      Ferrihydrite 0.0 0.0
      O2(g)       -2.54
EQUILIBRIUM_PHASES 1-5
      Ferrihydrite 0.0 0.0
      O2(g)       -2.16
EQUILIBRIUM_PHASES 6-10
      Ferrihydrite 0.0 0.0
      O2(g)       -1.97
EQUILIBRIUM_PHASES 11-15
      Ferrihydrite 0.0 0.0
      O2(g)       -1.83
EQUILIBRIUM_PHASES 16-20
      Ferrihydrite 0.0 0.0
      O2(g)       -1.73
EQUILIBRIUM_PHASES 21-25
      Ferrihydrite 0.0 0.0
      O2(g)       -1.64
EQUILIBRIUM_PHASES 26-30
      Ferrihydrite 0.0 0.0
      O2(g)       -1.57
EQUILIBRIUM_PHASES 31-35
      Ferrihydrite 0.0 0.0
      O2(g)       -1.51
EQUILIBRIUM_PHASES 36-40
      Ferrihydrite 0.0 0.0
      O2(g)       -1.46
EQUILIBRIUM_PHASES 41-45
      Ferrihydrite 0.0 0.0
      O2(g)       -1.41
EQUILIBRIUM_PHASES 46-50
      Ferrihydrite 0.0 0.0
      O2(g)       -1.37

RATES
Fe_di_ox
-start
10  Fe_di = TOT("Fe_di")
20  if (Fe_di <= 0) then goto 200
30  p_o2 = 10^(SI("O2(g)"))
40  O2aq = 1.26e-3 * p_o2
50  moles = 2.3e14 * (ACT("OH-"))^2 * O2aq * Fe_di * TIME
200 SAVE moles
-end
KINETICS
Fe_di_ox
        -formula  Fe_di  -1.0  Fe_tri  1.0
```

```
TRANSPORT
-cells                  50
-shifts                 350          #No of cell transfers
-time_step              748          #Time, in seconds, of each shift time)
-length                 0.005584     #Length of each cell in m
-flow_direction         forward
-boundary_conditions    flux  flux
-dispersivity           0.0025       #In m
-diffusion_coefficient  0.3e-9       #In m2/s (used default)
-initial_time           374
-correct_disp           True
```

E.3.1.2 Buffered

The input file for the buffered iron oxidation system is almost identical to the non-buffered system but for the addition of an additional equilibrium phase. The phase pH_fix is used to specify that the pH (in this case) should be kept at 6 by the dissolution or addition of HCl (Table E.5). The pH_fix equilibration is performed for every EQUILIBRIUM_PHASES keyword.

Table E.5. Modifications to the input file to enable buffering of pH during iron oxidation in the iron flow-through column

```
PHASES
      pH_fix
        H+ = H+
        log_k     0.0

EQUILIBRIUM_PHASES 0
      Ferrihydrite 0.0 0.0
      O2(g)        -2.54
      pH_fix       -6     HCl   10
```

E.3.2 Autocatalytic oxidation of iron

To model autocatalytic oxidation, the RATES keyword must change to include the additional term for autocatalytic oxidation (Table E.7). Equations 4.7 - 4.9 are used, with the rate constants from Tamura *et al.* (1976). The solid-phase iron concentration required in the equation was obtained from the amount of FH in the system, which increased as precipitation of FH occurred following oxidation. Outflow concentrations were modelled at different background concentrations of FH from 0 M to 0.01 M pre-existing FH.

Table E.7. RATES keyword used for modelling autocatalytic oxidation of Fe^{2+}

```
RATES
#From Tamura et al., 1976
Fe_auto_ox
-start
10 Fe_di = TOT("Fe_di")
20 FeIIIs = EQUI("Ferrihydrite")*55.845*1000
30 if (Fe_di <= 0) then goto 200
40 k0 = 2.3e14
50 p_o2 = 10^(SI("O2(g)"))
60 ks0 = 73
70 K = 10^-9.6
80 k1 = 6.7e-5 * p_o2
90 ks = ks0 * MOL("O2")
100 k_prime = ks * K
110 Fe_ox = k0 * Fe_di * MOL("O2") * (ACT("OH-"))^2 * TIME
120 Fe_auto = Fe_di * k_prime*FeIIIs*p_o2/(ACT("H+")) * TIME
130 moles = Fe_ox + Fe_auto
200 SAVE moles
-end
KINETICS 1-100
Fe_auto_ox
        -formula  Fe_di  -1.0  Fe_tri  1.0
```

E.3.3 Surface complexation of iron to ferrihydrite surfaces

Strong and weak surface sites on hydrous ferric oxide were defined using the SURFACE_SPECIES keyword, with equilibrium constants from Appelo and de Vet (2003) and Appelo *et al.* (2002; Table E.8). The SURFACE keyword is used to specify which surface sites exist in the experiment (Hfo_wOH and HfO_sOH), the mineral on which they exist (Ferrihydrite), and the number of sites per mol on that particular mineral (0.2 for HfO_wOH and 5 x 10^{-3} for HfO_sOH).

Table E.8. RATES keyword used for modelling autocatalytic oxidation of Fe^{2+}

```
SURFACE_SPECIES
#From Appelo and de Wet, 2003
Hfo_sOH + Fe_di+2 = Hfo_sOFe_di+ + H+
      log_k -0.95
Hfo_wOH + Fe_di+2 = Hfo_wOFe_di+ + H+
      log_k -2.98
Hfo_wOH + CO3-2 + H+ = Hfo_wOCO2- + H2O
      log_k +12.56
Hfo_wOH + CO3-2 + 2H+ = Hfo_wOCO2H + H2O
      log_k +20.62
Hfo_wOH + Fe_di+2 + H2O = Hfo_wOFe_diOH + 2H+
      log_k -11.55

SURFACE 1-100
Hfo_wOH  Ferrihydrite  eq_phase 0.2  3.2e4 #weak sites, eq_phase,
sites/mol,m2/mol
Hfo_sOH Ferrihydrite  eq_phase  5e-3       #strong sites, moles
-equil 1
```

Appendix F SEM Images

F.1 Dispersion and dissolution of iron oxides from coated surfaces

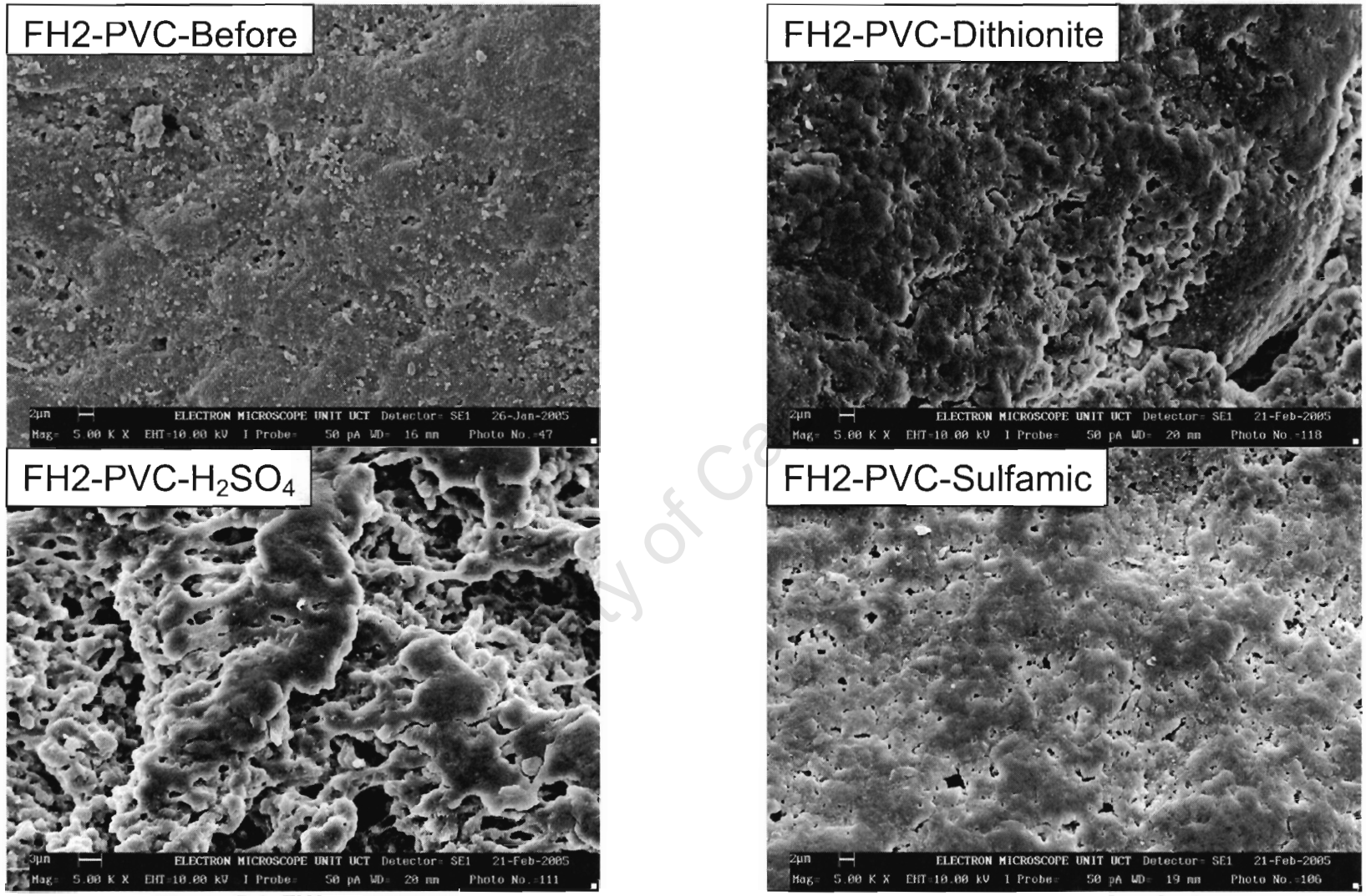

Figure F.1. FH2 coated PVC beads with no-pretreatment after dissolution in various chemicals

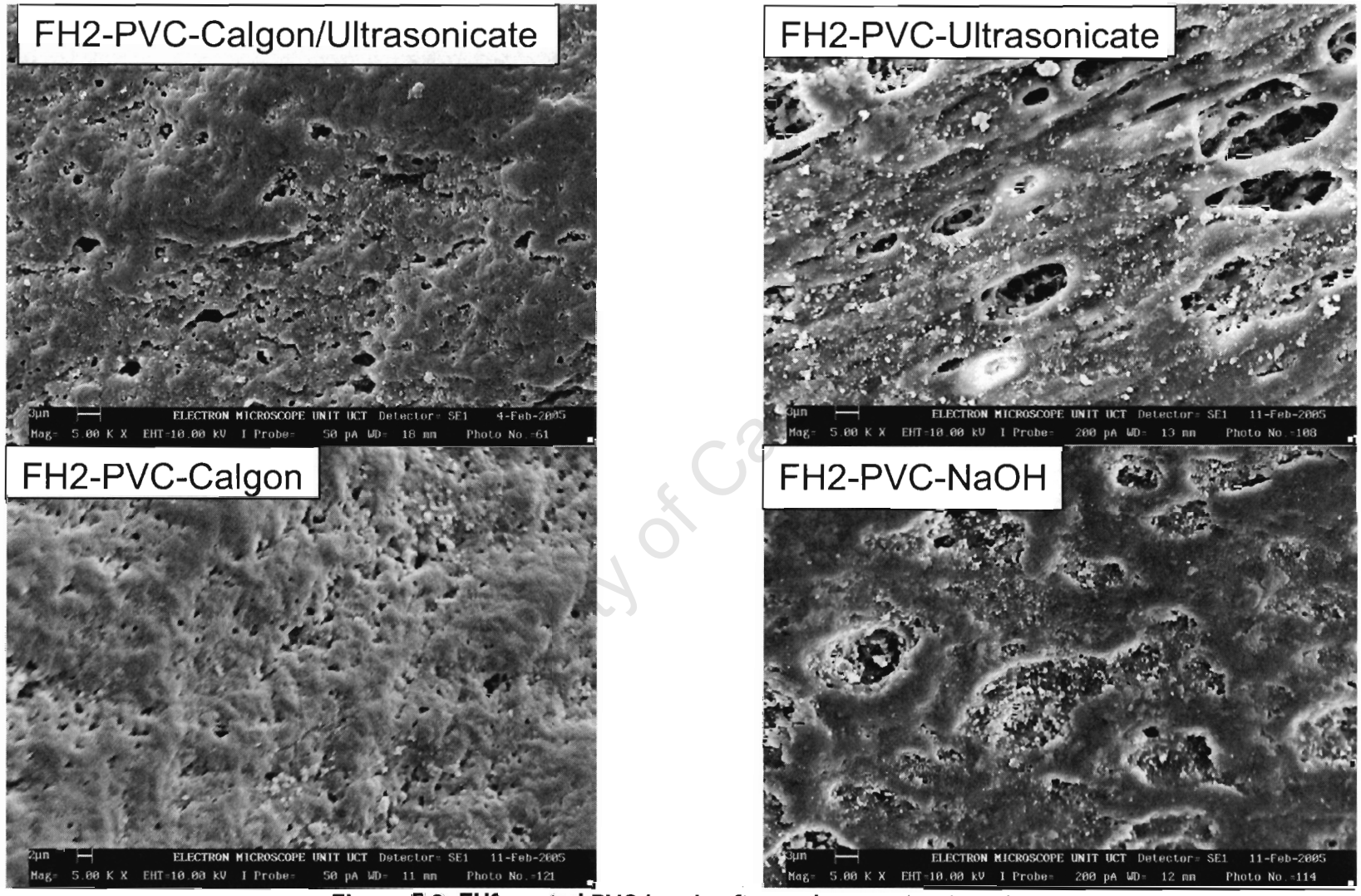

Figure F.2. FH2 coated PVC beads after various pretreatments

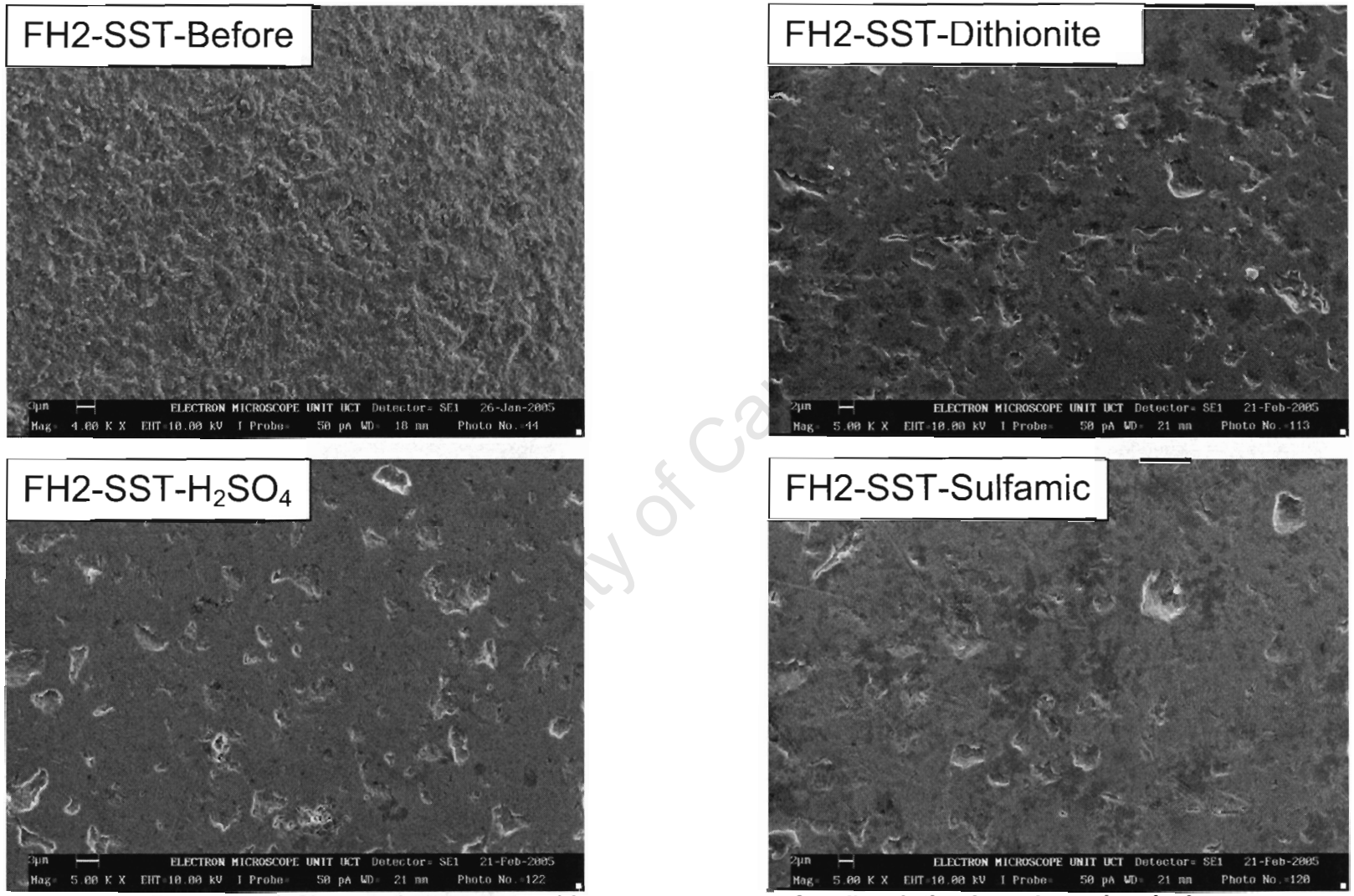

Figure F.3. FH2 coated SST beads with no-pretreatment after dissolution in various chemicals

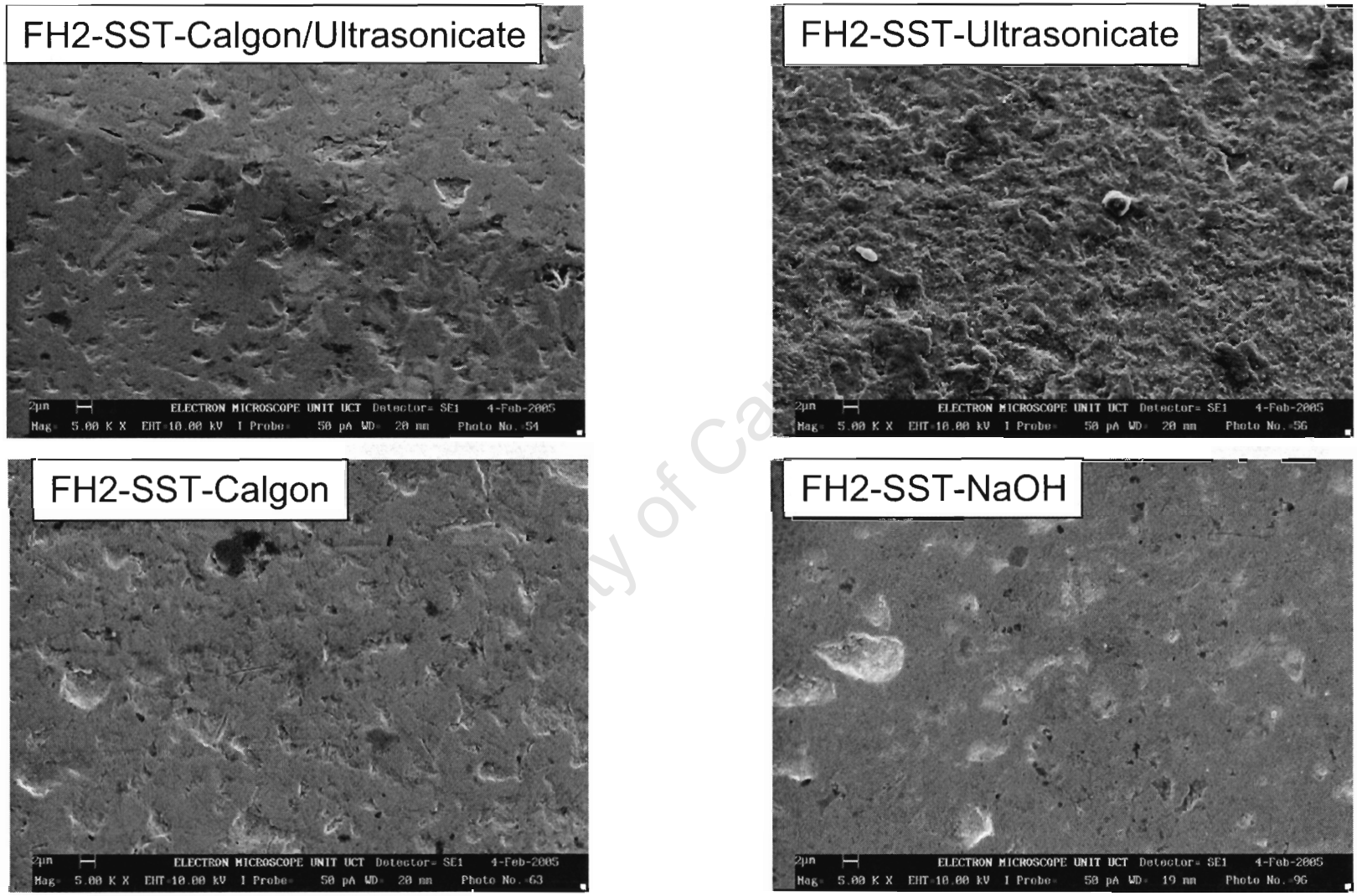

Figure F.4. FH2 coated SST beads after various pretreatments

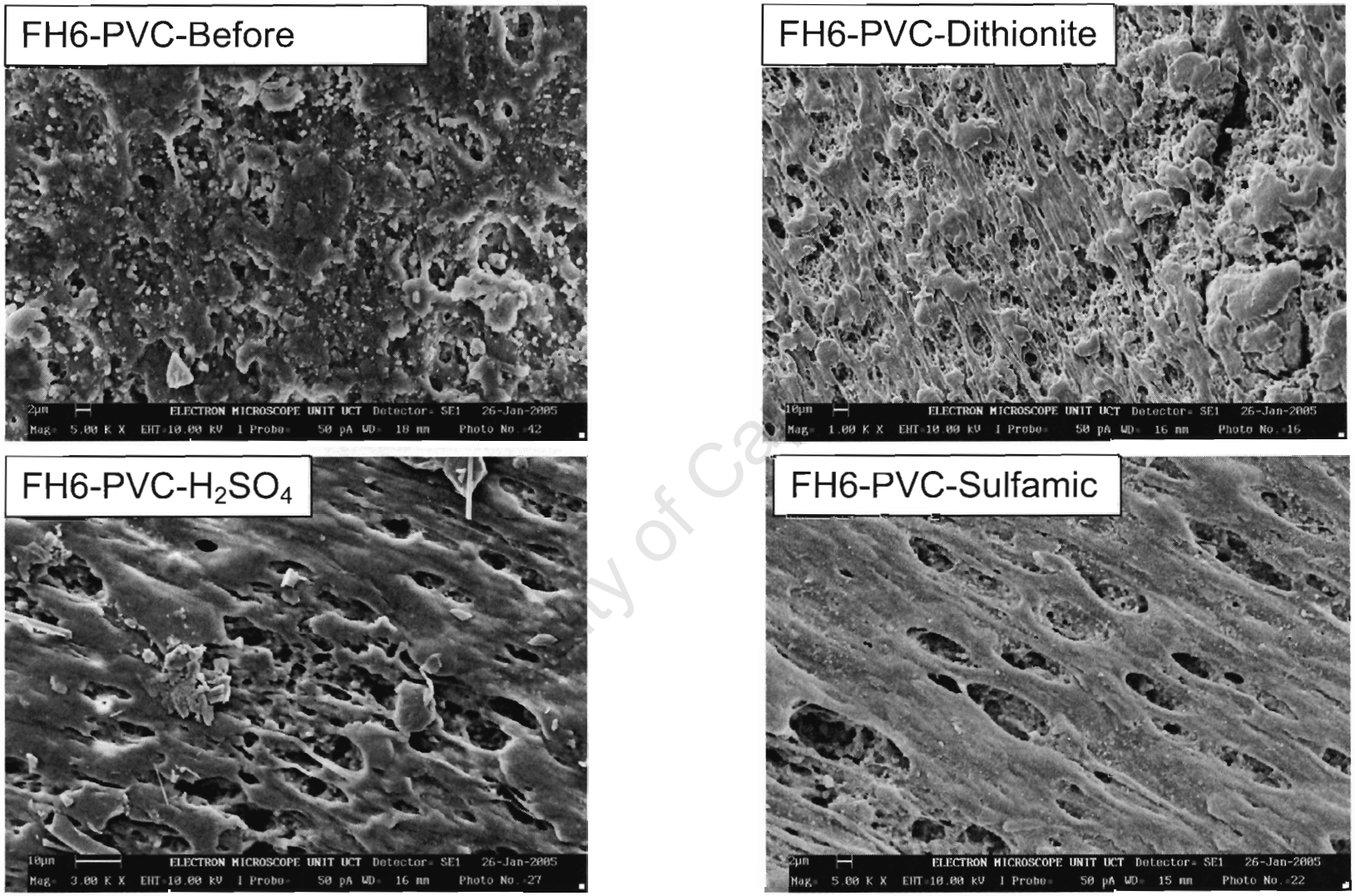

Figure F.5. FH6 coated PVC beads with no-pretreatment after dissolution in various chemicals

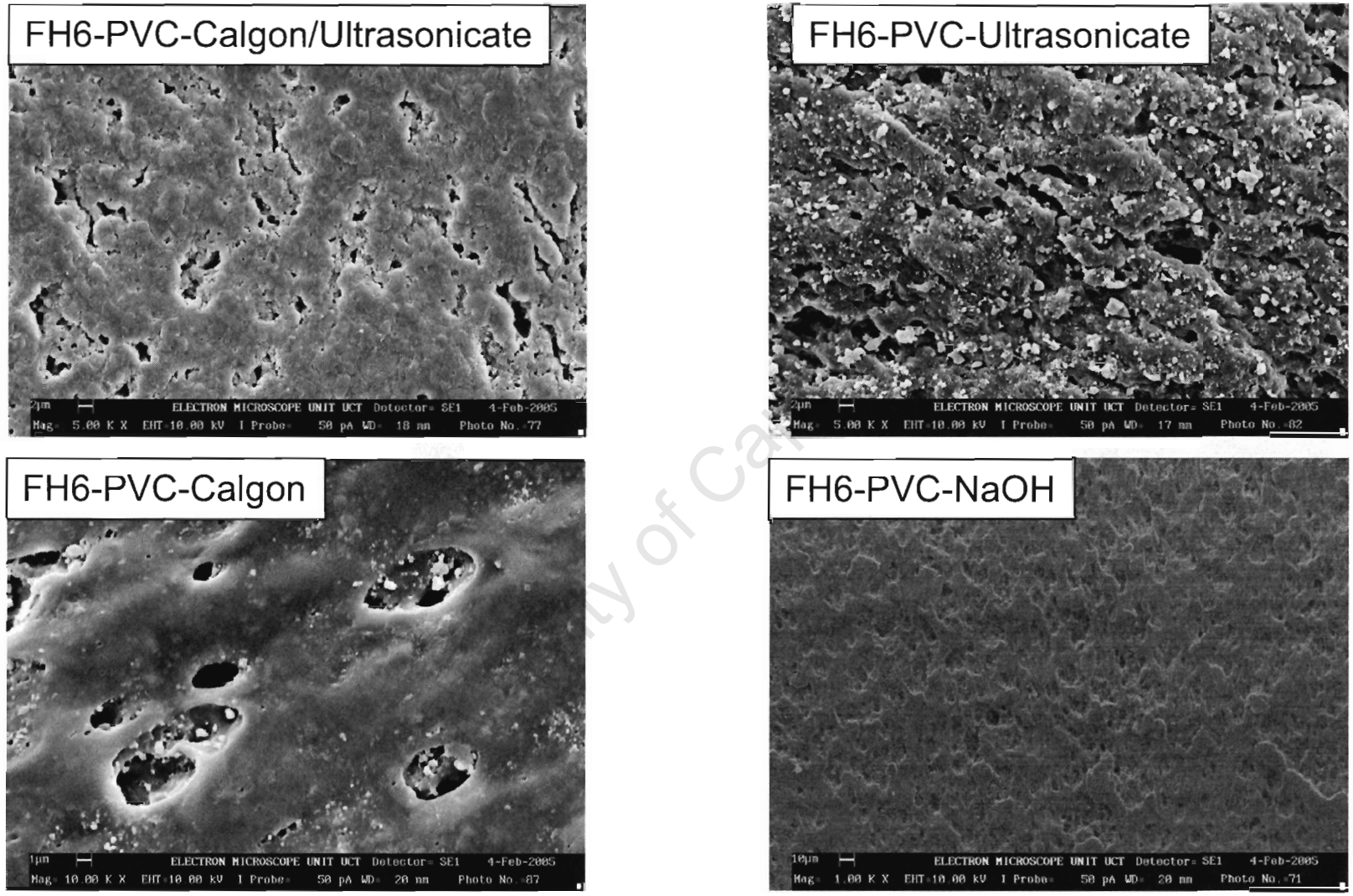

Figure F.6. FH6 coated PVC beads after various pretreatments

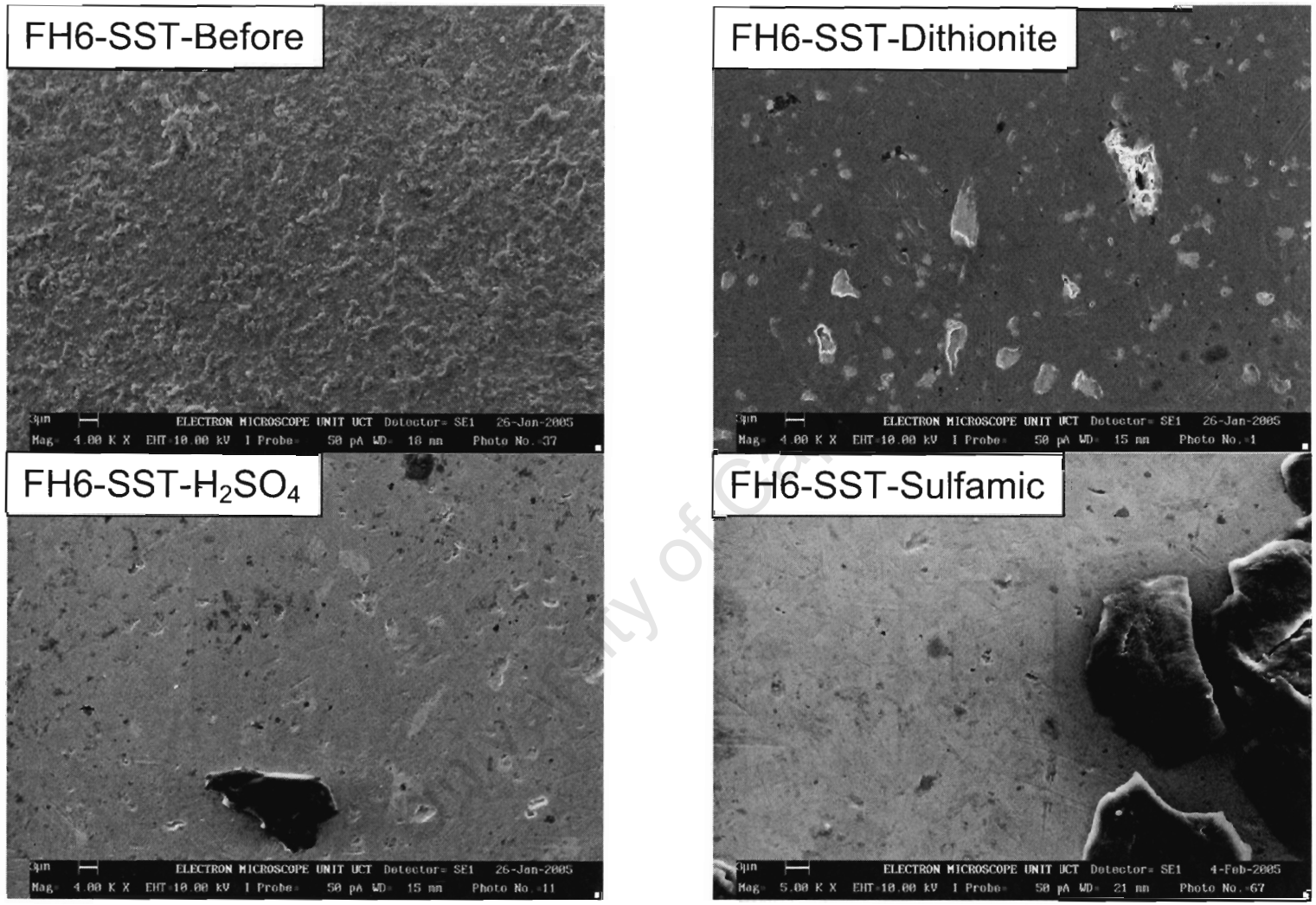

Figure F.7. FH6 coated SST beads with no-pretreatment after dissolution in various chemicals

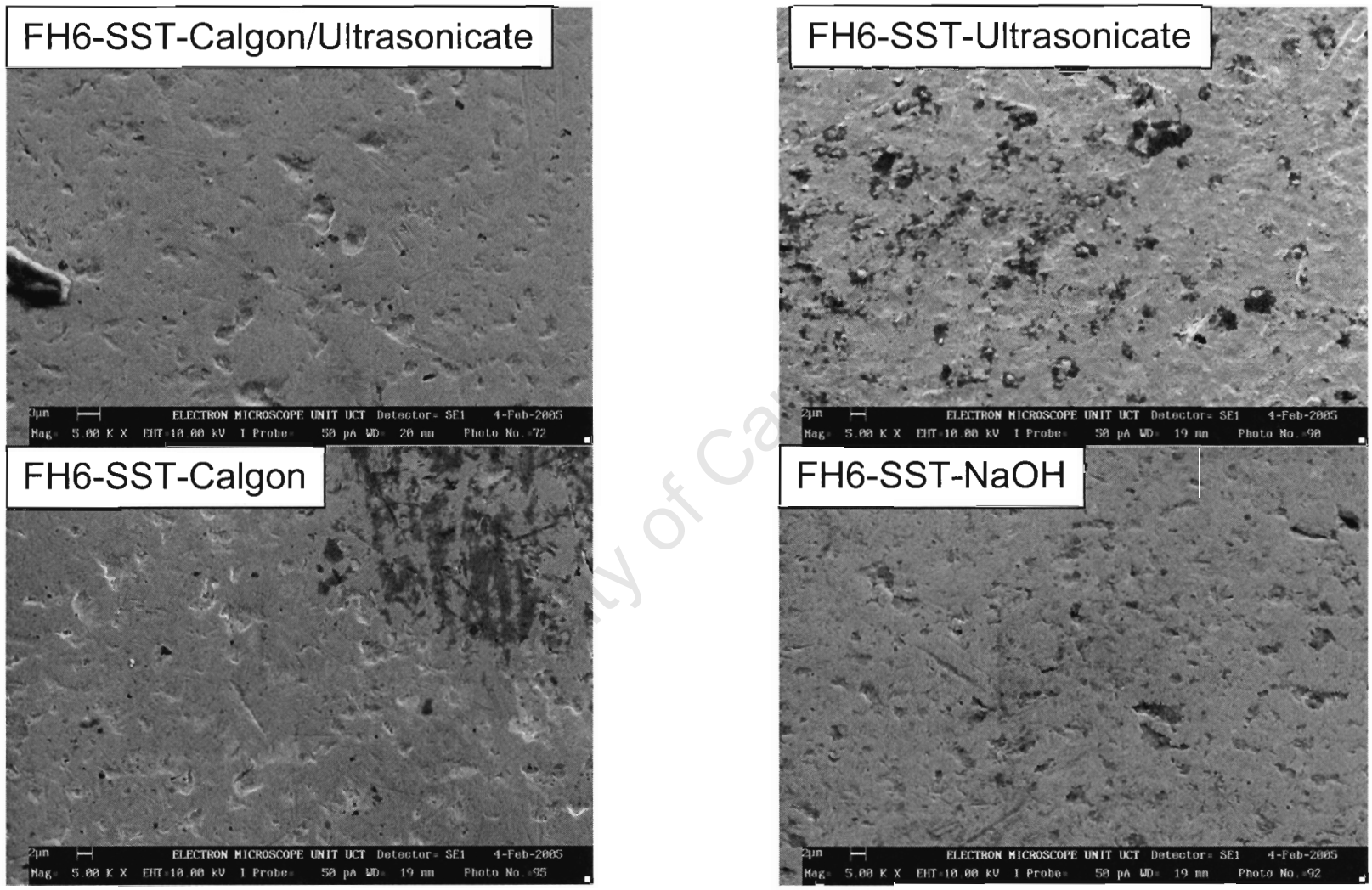

Figure F.8. FH6 coated PVC beads after various pretreatments

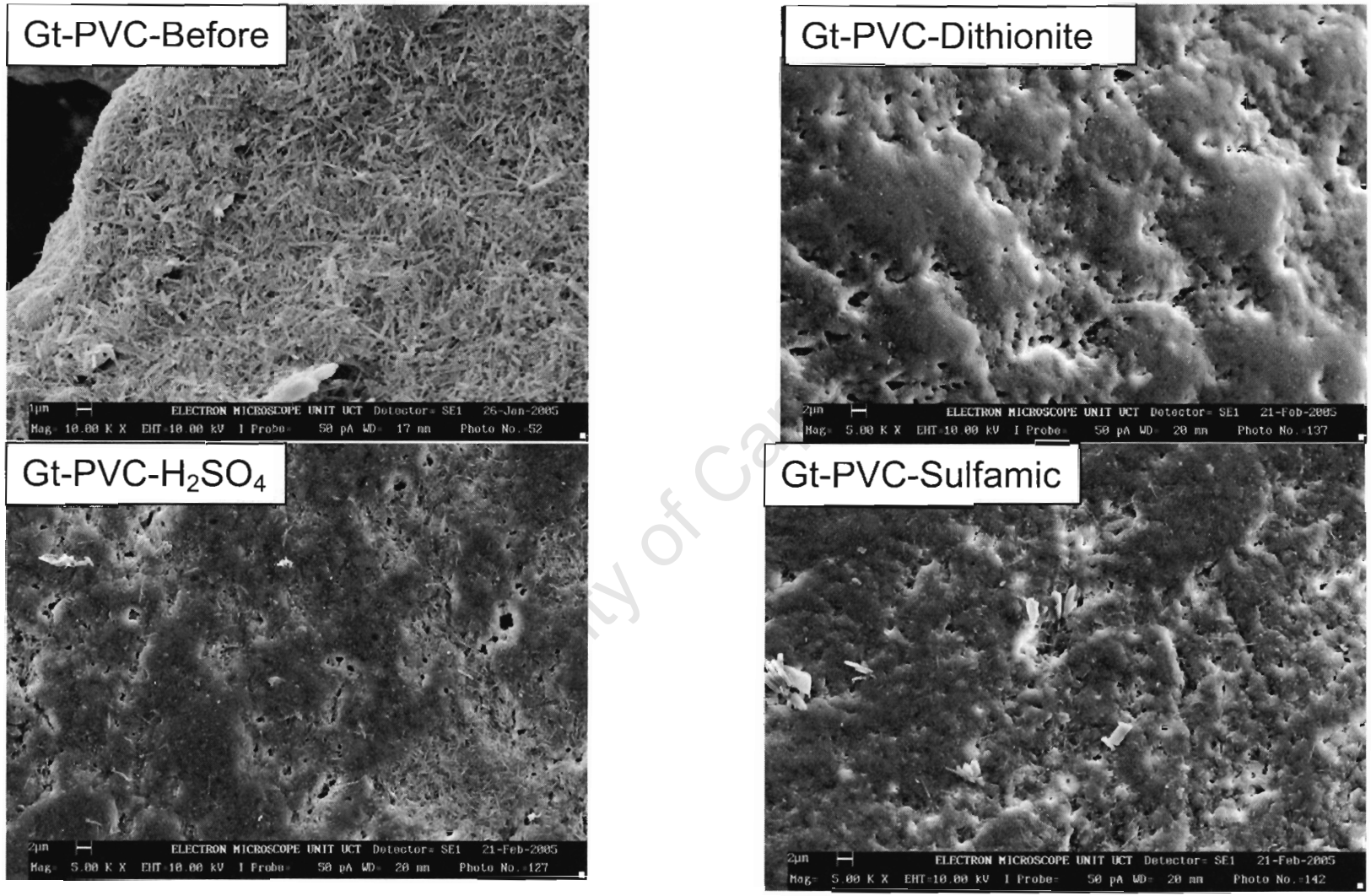

Figure F.9. Gt coated PVC beads with no-pretreatment after dissolution in various chemicals

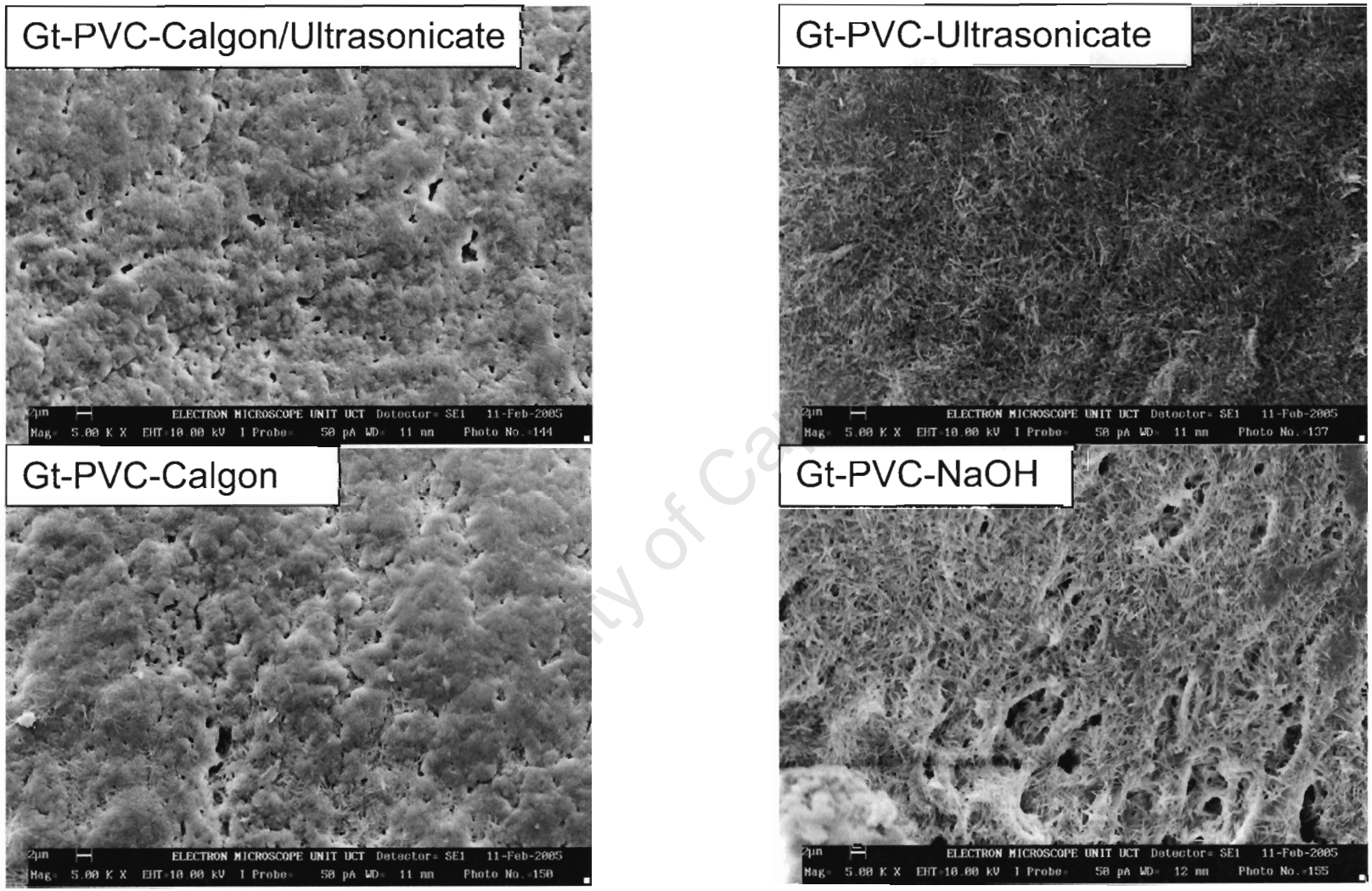

Figure F.10. Gt coated PVC beads after various pretreatments

Appendix G PZC Graphs

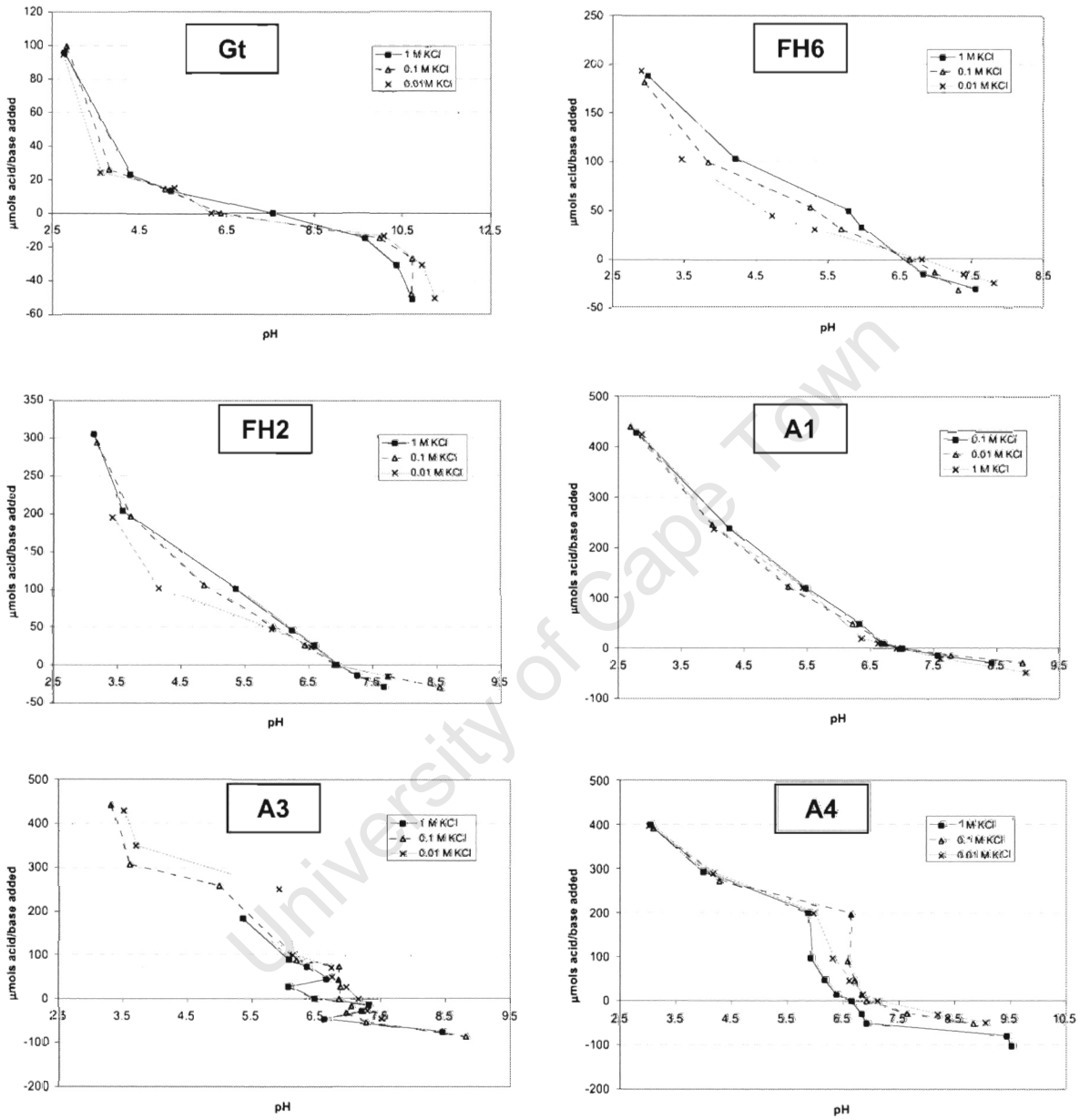

Figure G.1. PZSE graphs for iron oxide samples from two aquifers

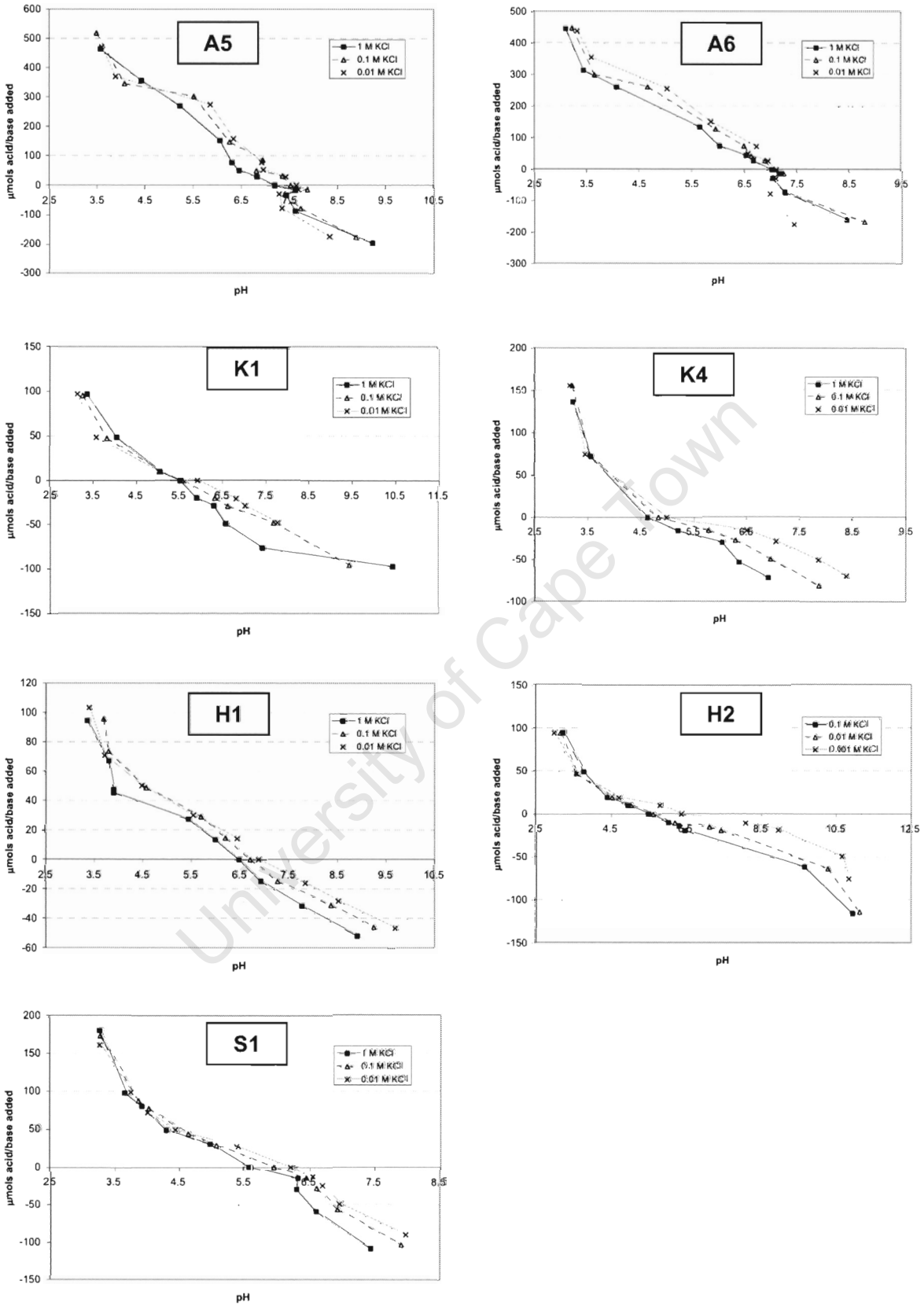

Figure G.2. PZSE graphs for iron oxide samples from two aquifers

Appendix H FT-IR

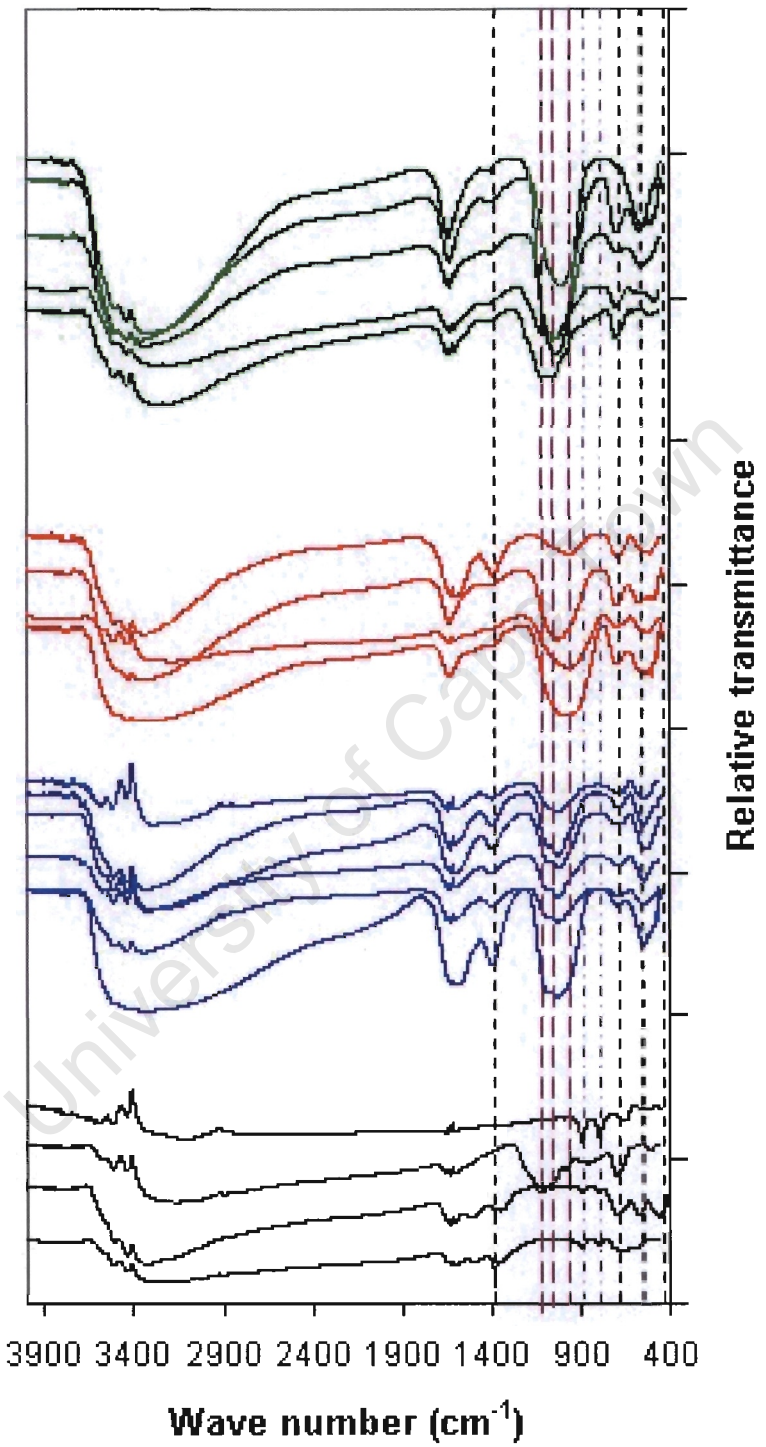

Figure H.1. All FT-IR scans. Black scans at the base are synthetic samples in order from base of graph FH2, FH6, Sch and Gt. Blue scans are Atlantis samples, red are springs and green are Klein Karoo. Scans are shown in more detail in following figures. Black dashed vertical lines trace the FH peaks, blue dot-dash lines follow goethite peaks and red long dash lines indicate schwertmannite peaks.

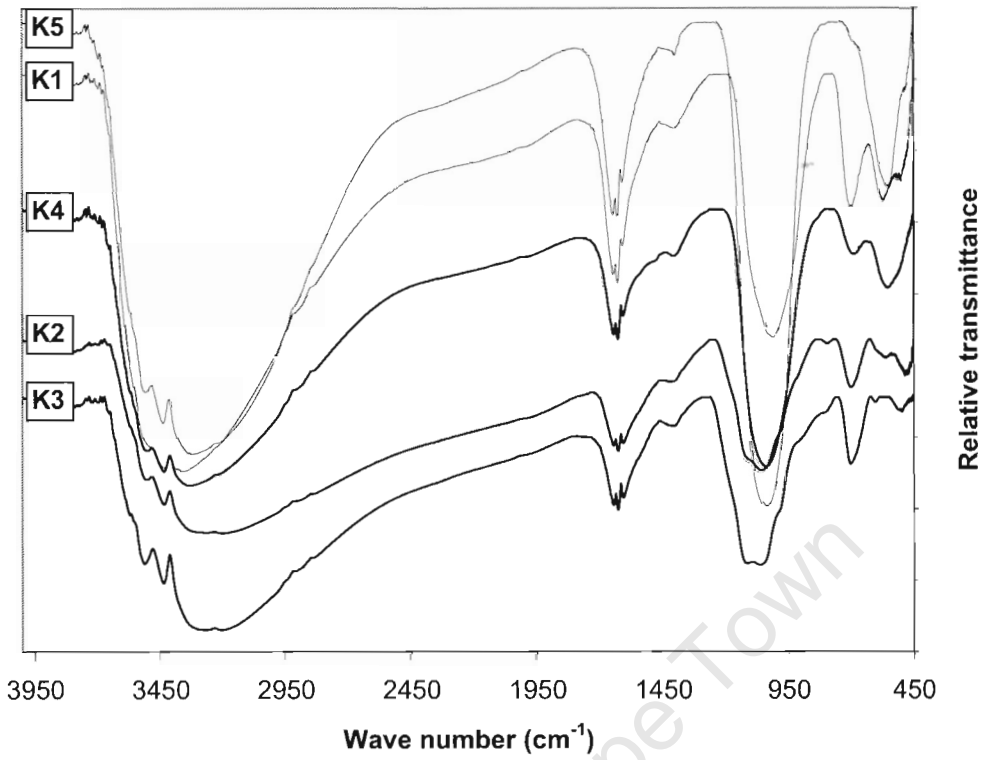

Figure H.2. FT-IR scans of samples from the KKRWSS

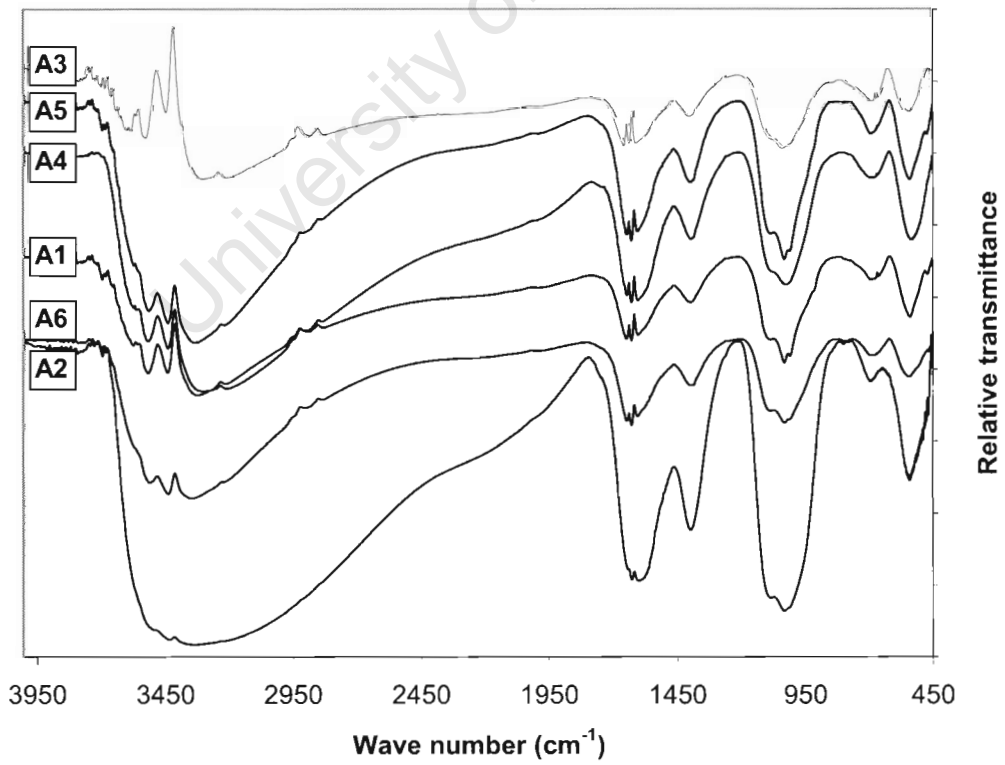

Figure H.3. FT-IR scans of samples from Atlantis

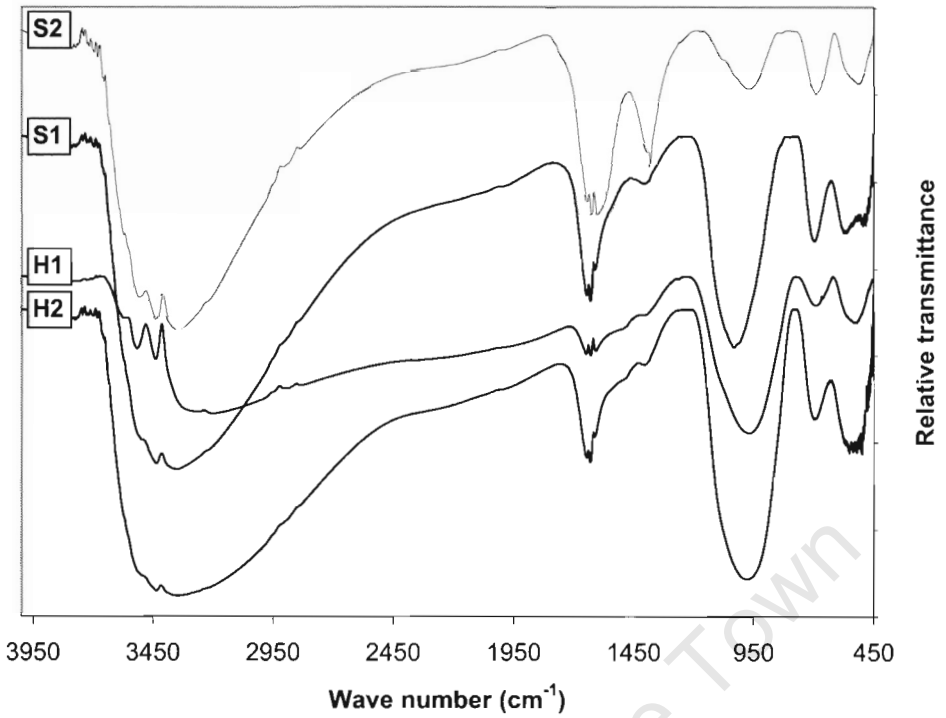

Figure H.4. FT-IR scans of spring samples

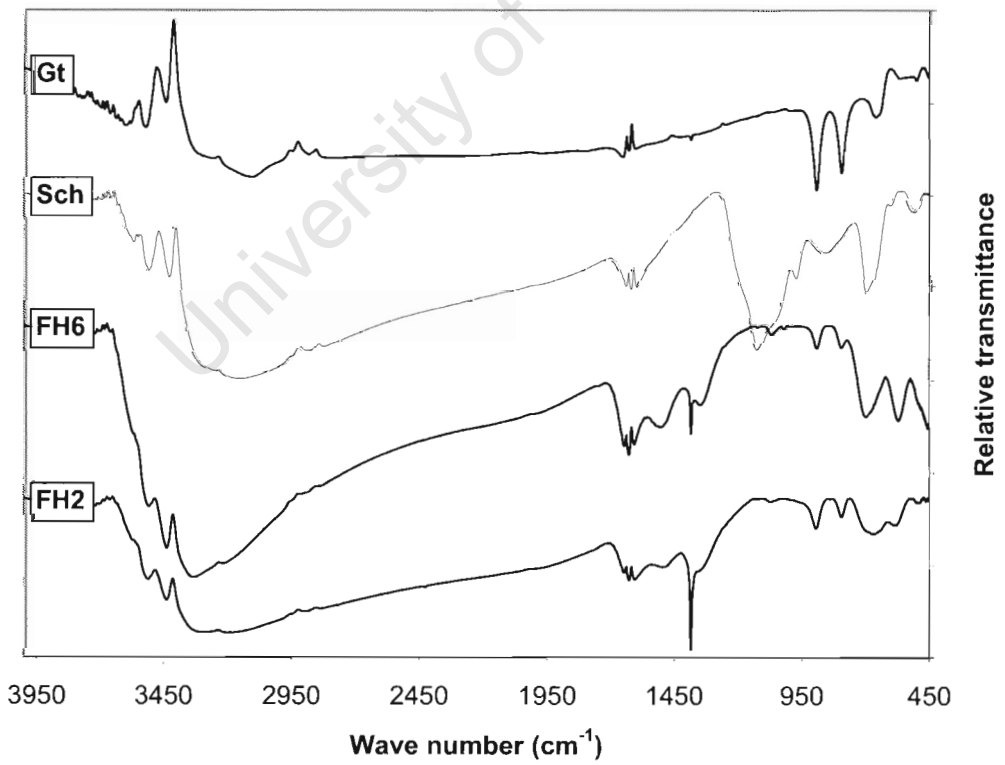

Figure H.5. FT-IR scans of synthetic samples

Appendix I

Cavé and Smith (2004) from WRI Conference Proceedings

This paper is included as an Appendix purely for reference purposes. The paper was published in a conference proceedings book that may not be readily available to readers of the thesis. The work presented within the paper is not intended to be part of the thesis, or to be examined, although the field work was undertaken as part of the larger project on iron encrustation in collaboration with the CSIR.

In-borehole measurements of chemical parameters in a wellfield affected by iron fouling

L.C.Cavé
Division of Water, Environment and Forestry Technology, CSIR, South Africa

M.E.Smith
Department of Geological Sciences, University of Cape Town, South Africa

ABSTRACT: Variations in temperature, electrical conductivity, pH, pe and dissolved oxygen with depth were used to investigate controls on iron biofouling in boreholes of the Calitzdorp wellfield, South Africa. Zones of inflow and chemical reaction in the standing water column were identified. Trends in pH and pe in the upper part of the boreholes correlate well with expected conditions for the equilibrium between dissolved ferrous iron and amorphous ferric oxyhydroxide precipitates. The depth of the oxidation zone suggests that it is virtually impossible to control iron fouling by management of drawdown in this wellfield. In-borehole measurements have proved a useful tool for improving understanding of the iron fouling phenomenon.

1 INTRODUCTION

Changes in pH, ionic strength, redox potential, CO_2 partial pressure, dissolved O_2 or dissolved organic compounds in the vicinity of a borehole may trigger the precipitation of ferric oxyhydroxides when dissolved iron is present in groundwater. Microorganisms in the aquifer are often actively or passively involved in precipitation (MacLaughlan & Knight 1989, Tyrrel & Howsam 1997). Many water supply boreholes worldwide have been affected by iron encrustation and biological fouling arising from these biogeochemical processes (Howsam 1990, Walter 1997, MacLaughlan 2002).

Water within the casing of boreholes differs in composition from that of the aquiferdue tochemical reactions, biological processes, convective mixing, evaporation, leaking and vertical groundwater flow (Robbins & Martin-Hayden 1991). Most groundwater studies are designed to assess the quality of aquifer water, and sampling protocols involve purging stagnant water from the borehole. Iron fouling, however, is closely linked to processes that occur in the standing water column and routine sampling of the aquifer is likely to miss important information. Our study has focused on the in-borehole chemistry of the water column in boreholes affected by iron fouling, with the aim of understanding of the underlying chemical reactions.

2 STUDY SITE

The Klein Karoo Rural Water Supply Scheme (KKRWSS) is located near the towns of Oudtshoorn and Calitzdorp in the Western Cape Province. The scheme consists of 18 boreholes drilled into fractured sandstones of the Table Mountain Group. Over the last decade, iron fouling has occurred in most of the boreholes. Extensive resources have been directed at rehabilitation by physical, chemical and electrochemical treatment methods to restore lost yields. The Calitzdorp wellfield, one of the most severely affected areas, targets 100-200 m deep water-bearing fractures in the quartzitic sandstones of the Nardouw Subgroup. Water-rock interactions are expected to be responsible for the presence of iron in the groundwater through the dissolution of iron-bearing minerals in shales and mudstones along the flowpath (Smith et al. 2002). Moderate levels of mixed anaerobic and aerobic bacteria have been found in groundwater samples from the Calitzdorp wellfield, including iron-related, slime forming and some sulphate reducing bacteria (Jolly, 2000).

3 FIELD INVESTIGATIONS

Vertical logs of hydrochemical parameters were collected for affected boreholes at the Calitzdorp wellfield using a Minisonde® 4a water quality multiprobe (Hydrolab) during August 2002. The multiprobe is fitted with glass pH electrode,

platinum redox (Eh) electrode and reference electrode, permeable membrane dissolved oxygen (DO) sensor, electrical conductivity (EC) cell, temperature (T) sensor and depth/pressure sensor. Data were collected at 2 m increments to just above the bottom of the hole. Logs of T, EC, pH, Eh (converted to pe) and DO concentrations were downloaded from the multiprobe after retrieval from the borehole. Recent closed circuit camera logs of the boreholes were obtained from the Department of Water Affairs and Forestry (DWAF). Field measurements of pH, EC, and iron speciation using a ferrozine colorimetric method were made at the same time. There was also a considerable historical record of water quality data from KKRWSS monitoring available for the study.

4 RESULTS

Data obtained from the hydrochemical logging is shown for boreholes DL15 and DL16 in the Calitzdorp wellfield (Fig.1). Both boreholes are cased with PVC casing and fitted with short sections of stainless steel Johnson screens. The location of the screens is indicated by the shaded areas of the graphs in Figure 1. DL15 was drilled to 137 m and is cased and screened for the entire length, while DL16, which is 165 m deep, has an open hole section after 149 m. DL15 had been standing for several months without pumping, while DL16 was logged 4 days after a intensive pumping, during which the water samples were collected. DL16 data have a higher degree of scatter than DL15 (see, for example, the EC logs), possibly due to the pumping test. The lowering of the multiprobe through the water column may also cause a small amount of physical mixing. Table 1 shows analytical data for DL16 from the start (DL16a) and end (DL16b) of the 24 hour pumping test together with mean values from the monitoring records for DL16 (DL16m) and DL15 (DL15m). Historical records show that total dissolved iron concentrations in the KKRWSS boreholes tend to fluctuate widely (<0.1 to 15.4 $mg.l^{-1}$, mean 3.3 $mg.l^{-1}$; Smith et al. 2002). Jolly (2000) attributed the concentration changes to iron oxide precipitation and cycles of sloughing of iron-rich biofilm in the holes. Iron measurements in boreholes affected by iron clogging are therefore not believed to be a good representation of dissolved iron concentrations in the aquifer. Iron speciation measurements show that approximately half the iron in the standing borehole water (DL16a) is present in colloidal form (>0.45 µm), while the dominant species in the aquifer (DL16b) is dissolved Fe^{2+}.

The camera logs showed extensive encrustation and biofilm development inside the boreholes, especially around the screens and casing joints, but decreasing with depth. Floating orange/brown flocs occur in the standing water column above the top screen at 33 m in DL15 and throughout the length of the water column in DL16 (could this not reflect the disturbance of the pumping test?). The casing of DL15 is clean for about 8 m between the two lowest screens, until black, presumably sulphidic solids and anaerobic bacterial colonies start to flourish at the base of the lowest screen (131 m).

Table 1. Chemical data for boreholes DL16 and DL15.

Parameter	DL16a	DL16b	DL16m	DL15m
Temp °C	23.1	22.8	-	-
pH	6.2	6.3	6.5	6.2
DO $mg.l^{-1}$	1.8	0.6	-	-
Na	63.6	54.4	50.3	37.0
K	15.4	14.7	14.1	14.2
Ca	16.8	14.8	11.9	12
Mg	10.9	8.4	8.5	10
Cl	101	91	89	90
SO_4	32.9	18.9	19.9	20
HCO_3	83#	83#	83	110
Si	5.7	5.0	5.7	4.5
Fe^{2+}	2.1	5.0	-	-
Fe_T (<0.45µm)*	3.0	6.1	3.0	4.0-
Fe_T (>0.45µm)[1]	3.7	6.0	-	

Estimated value. * Total dissolved Fe^{2+} + Fe^{3+}
[1] Total dissolved + colloidal Fe

5 DISCUSSION

5.1 *Inflow from the aquifer*

The hydrochemical logs all show perturbations relating to the inflow of groundwater through the screens. Most of the water in the boreholes appears to originate from the lower screens, below 100 m, where stronger yielding fractures occur in the aquifer and the screens are less clogged. Above the uppermost screen in each borehole is a zone of stagnant water that is isolated from the aquifer, but exposed to the atmosphere at the water table.

The temperature gradient in each borehole is disrupted by the inflow of cooler water at the lower set of screens. The local thermal gradient of the sandstones is reflected in the background temperature profile of DL16, which increases with depth at a rate of $1.4°C.km^{-1}$. Water at the top of each column has been cooled by contact with the atmosphere. The constant temperature and EC in the middle of the profiles suggest vertical mixing of groundwater occurs between the main screened sections. The EC logs show that inflow water is very slightly fresher water than water in the hole, especially in the open hole section of DL16. The low EC at the surface of borehole DL15 is likely affected by direct leakage of rainwater.

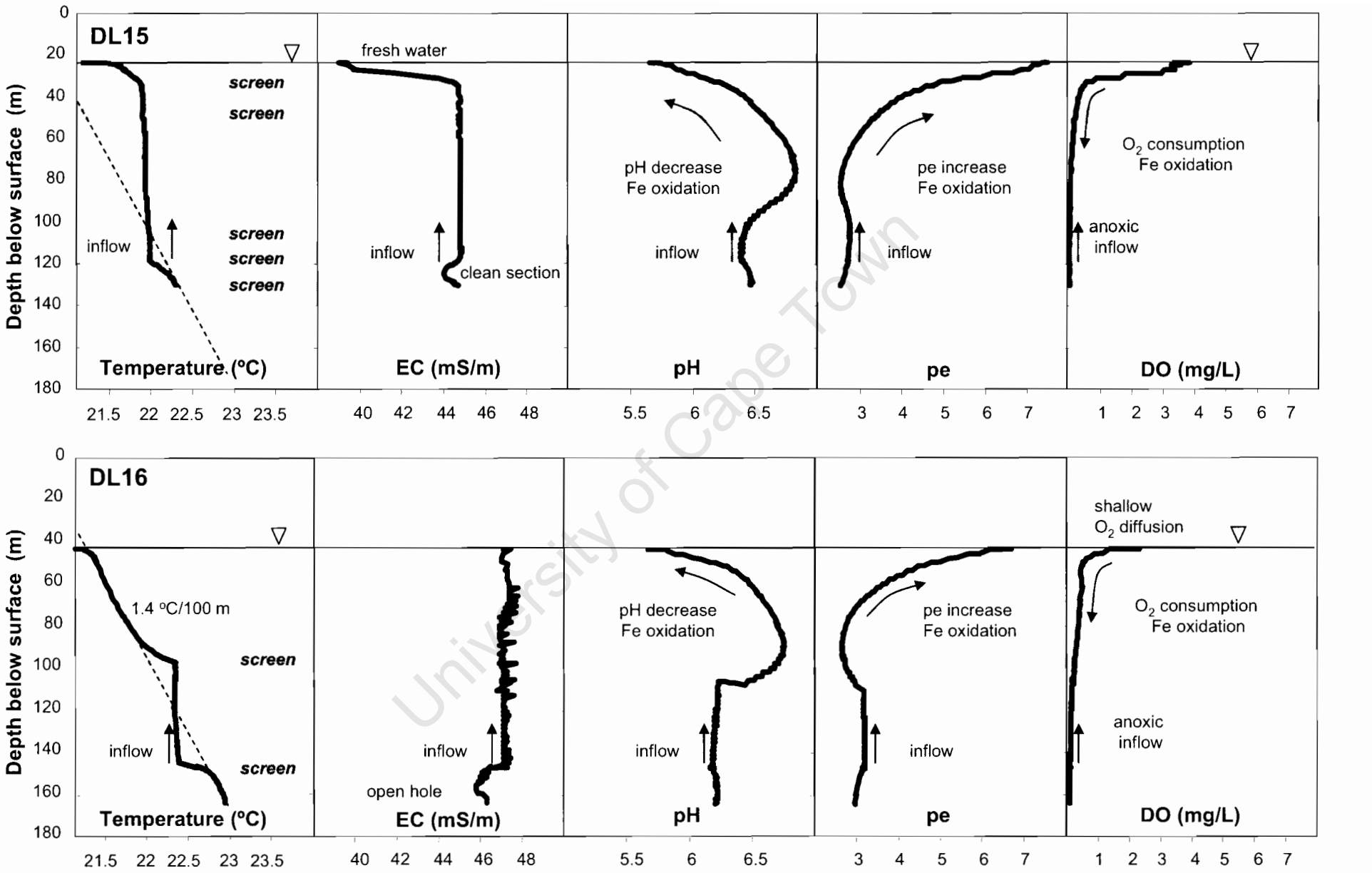

Figure 1. In-borehole profiles of temperature, EC, pH, pe and DO for two boreholes in the KKRWSS affected by iron fouling problems.

5.2 *Dissolved oxygen*

The inflowing groundwater is anoxic at depth with oxygen in the recharge waters being consumed by redox reactions along the flowpath to the borehole. Oxygen may also be consumed by the bacterial biomass in the aquifer and boreholes. DO is introduced through the exposed water table in the borehole, where atmospheric oxygen dissolves and diffuses at the air-water interface. This is probably a major trigger for the precipitation of iron in the stagnant water above the upper screens.

5.3 *Iron oxidation and precipitation*

pH and pe display opposing trends in the borehole profiles. The trend of upward decreasing pH and increasing pe occurs over a region of the boreholes in which there is limited or no inflow, especially in DL16, where this is above the screens. This trend is believed to arise from a redox-controlled, acidifying reaction in the standing water column. Plotting the logging data on a stability data for the system $Fe\text{-}O_2\text{-}H_2O\text{-}CO_2$ (Fig.3), shows that the conditions in the upper section of each profile closely follows the boundary controlled by the equilibrium between ferrous iron and ferric hydroxide:

$$2Fe^{2+} + \tfrac{1}{2} O_2 + 5H_2O \leftrightarrow 2Fe(OH)_3 + 4H^+ \qquad (1)$$

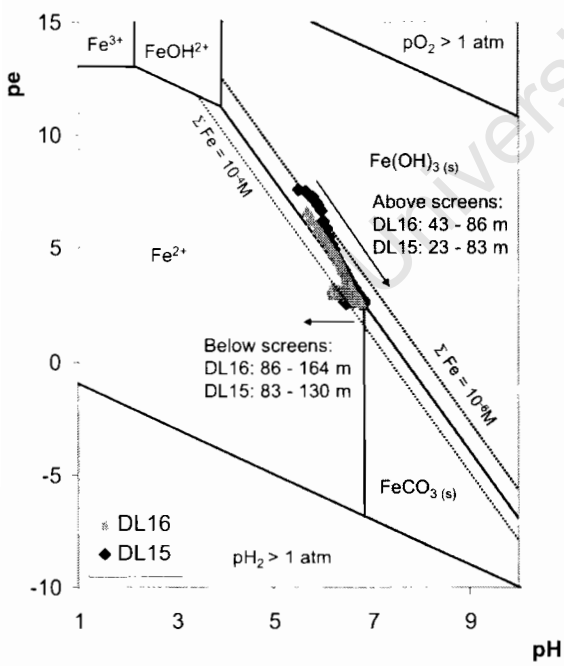

Figure 3. In-borehole pe vs pH data for DL15 and DL16 plotted on a stability diagram for the system $Fe\text{-}O_2\text{-}H_2O\text{-}CO_2$. The stability boundaries are shown for $\Sigma Fe = 10^{-5}$ M and $\Sigma CO_2 = 2\times10^{-3}$ M.

Below the screens, the water chemistry falls within the Fe^{2+} stability field, indicating that dissolved iron is the stable species in the fresh groundwater inflow. A gradual increase in pH with little change in pe is observed within this region, before the system abruptly equilibrates with $Fe(OH)_3$. This increase in pH is probably caused by microbially catalysed oxidation of iron at low concentrations of DO (<0.5. mg/L, Ralph and Stevenson, 1995).:

$$2Fe^{2+} + \tfrac{1}{2} O_2 + 2H^+ = 2Fe^{3+} + H_2O \qquad (2)$$

Despite the apparent presence of sulphide minerals in the depths of DL15, the sulphide stability field is not approached.

6 CONCLUSIONS

Hydrochemical conditions within the borehole casing differ significantly from those in the aquifer, particularly in the stagnant water zone above the screens. Dissolved ferrous iron in the Klein Karoo groundwater is relatively stable as the dominant form of iron in the water entering the borehole, but oxygen in the upper part of the water column triggers iron oxidation and precipitation as ferric oxyhydroxides inside the borehole. Microbial catalysis allows this reaction to occur at low levels of dissolved oxygen. This chemical reaction controls pH and pe trends in the standing water column.

Vertical logging of hydrochemical parameters inside the boreholes, supported by video logs, has been useful in pinpointing problem areas. The logs show that the iron reaction zone extends for 60 m or more below the water table in the Calitzdorp boreholes. It is impossible to prevent oxygen ingress by managing pumping regimes and iron fouling problems are likely to arise even if water levels are not lowered down to the screens. Abstraction control at KKRWSS has met with little success in managing iron fouling. Regular cleaning of boreholes, including disinfection to control bacteria, appears to be a necessity at this stage.

In the long term alternative approaches could be considered, such as *in situ* oxidation of iron in the aquifer before it reaches the production borehole. This has been used successfully in primary aquifers (Braester & Martinell 1988), but to our knowledge, application in fractured rock has yet to be attempted.

ACKNOWLEDGEMENTS

We would like to thank Johan Uys, manager of the KKRWSS and Lukas Smith of the Department of Water Affairs and Forestry (DWAF) for logistical help and provision of historical data. Field sampling and literature review were ably assisted by Sumaya Clarke and video camera logs for the boreholes recorded by Barry Smit of DWAF. We are grateful to the National Research Foundation of South Africa for funding groundwater sampling and analysis, and your funding?

REFERENCES

Braester, C. & Martinell, R. 1988. The Vyredox and Nitredox method *in situ* treatment of groundwater. *Wat. Sci. Tech.* 20(3): 149-163. Howsam, P. (ed.) 1990. *Water wells. Monitoring, maintenance and rehabilitation. Proc. intern. groundwater eng. conf.*, Cranfield. London: E.& F.N. Spon.

Jolly, J.L. 2000. Biofouling in boreholes of the Klein Karoo Rural Water Supply Scheme, Oudtshoorn, South Africa, and the effect on well scheme management. In Sililo et al. (eds.), *Groundwater: Past achievements and future challenges. Proc. XXX IAH congress, Cape Town, 26 Nov-1 Dec 2000.* Rotterdam: Balkema.

MacLaughlan, R.G. 2002. *Managing water well deterioration. IAH Intern. contrib.. hydrogeol. 22.* Lisse: Balkema.

MacLaughlan, R.G. & Knight, M.J. 1989. *Corrosion and incrustation in groundwater boreholes. A critical review. Research publ. 1/89, CGMH.* Kensington: Univ. New South Wales.

Ralph, D.E. and Stevenson, J.M. 1995. The role of bacteria in well clogging. *Wat.Res.* 29: 365-369.

Robbins, G.A. & Martin-Hayden, J.M. 1991. Mass balance evaluation of monitoring well purging. *J. Contam. Hydrol.* 8: 203-224.

Smith, M.E., Cavé, L.C. & Clarke, S. 2002. Chemical evolution of Table Mountain Group groundwater and the source of iron. In *Tales of a hidden treasure. Proc. regional. groundwater conf., Somerset West, 16 Sept. 2002.* Groundwater Division, Geol. Soc. S. Afr.

Tyrrel, S.F. & Howsam, P. 1997. Aspects of the occurrence and behaviour of iron bacteria in boreholes and aquifers. *Quarterly J. Eng. Geol.* 30: 161-169.

Walter, D.A. 1997. Geochemistry and microbiology of iron-related well-screen encrustation and aquifer biofouling in Suffolk County, Long Island, New York. Water-res. invest. rep. 97-4032. Coram, NY: US Geological Survey.